NUREG/CP-0119
Vol. 3

Proceedings of the U.S. Nuclear Regulatory Commission

Nineteenth Water Reactor Safety Information Meeting

Volume 3
- Structural Engineering
- Advanced Reactor Research
- Advanced Passive Reactors
- Human Factors Research
- Human Factors Issues Related to Advanced Passive LWRs
- Thermal Hydraulics
- Earth Sciences

Held at
Bethesda Marriott Hotel
Bethesda, Maryland
October 28–30, 1991

U.S. Nuclear Regulatory Commission

Office of Nuclear Regulatory Research

Proceedings prepared by
Brookhaven National Laboratory

Available from

Superintendent of Documents
U.S. Government Printing Office
P.O. Box 37082
Washington D.C. 20013-7082

and

National Technical Information Service
Springfield , VA 22161

NUREG/CP-0119
Vol. 3
R1,R2,R3,R4,R5,R9,
RD,RF,RM,RV,RW,RX

Proceedings of the U.S. Nuclear Regulatory Commission

Nineteenth Water Reactor Safety Information Meeting

Volume 3
- Structural Engineering
- Advanced Reactor Research
- Advanced Passive Reactors
- Human Factors Research
- Human Factors Issues Related to Advanced Passive LWRs
- Thermal Hydraulics
- Earth Sciences

Held at
Bethesda Marriott Hotel
Bethesda, Maryland
October 28–30, 1991

Manuscript Completed: April 1992

Compiled by: Allen J. Weiss

Office of Nuclear Regulatory Research
U.S. Nuclear Regulatory Commission
Washington, DC 20555

Proceedings prepared by
Brookhaven National Laboratory

ABSTRACT

This three-volume report contains 83 papers out of the 108 that were presented at the Nineteenth Water Reactor Safety Information Meeting held at the Bethesda Marriott Hotel, Bethesda, Maryland, during the week of October 28-30, 1991. The papers are printed in the order of their presentation in each session and describe progress and results of programs in nuclear safety research conducted in this country and abroad. Foreign participation in the meeting included 14 different papers presented by researchers from Canada, Germany, France, Japan, Sweden, Taiwan, and USSR. The titles of the papers and the names of the authors have been updated and may differ from those that appeared in the final program of the meeting.

PROCEEDINGS OF THE
19th WATER REACTOR SAFETY INFORMATION MEETING

October 28-30, 1991

Published in Three Volumes

GENERAL INDEX

VOLUME 1

VOLUME 2

VOLUME 3

REGISTERED ATTENDEES(NON NRC)
19th WATER REACTOR SAFETY INFORMATION MEETING

D. ACKER
CEA FRENCH ATOMIC ENERGY COMMISSION
CEB SACLAY DMT/SEMT
GIF SUR YVETTE, 91191
FRANCE

S. ADDITON
TENERA/ARSAP
7272 WISCONSIN AVE., SUITE 300
BETHESDA, MD 20814
USA

T. AJIMA
NUPEC-NUCLEAR POWER ENG. TEST CENTER
3-17,1-CHOME,TORANOMON,MINATO-KU
TOKYO, 105
JAPAN

R. ALLEN
WESTINGHOUSE SAVANNAH RIVER COMPANY
P.O. BOX 616
AIKEN, SC 29802
USA

R. ALLEN
BATTELLE-PACIFIC NORTHWEST LABS.
P.O. BOX 999
RICHLAND, WA 99352
USA

C. ALLISON
EG&G IDAHO, INC.
P.O. BOX 1625
IDAHO FALLS, ID 83404
USA

A. ALONSO
MADRID POLYTECHNICAL UNIVERSITY
JOSE GUTIERREZ ABASCAL, 2
MADRID, 28006
SPAIN

H. AMARASOORIYA
SCIENTECH, INC.
11921 PARKLAWN DRIVE
ROCKVILLE, MD 20852
USA

T. ANDREYCHUK
WESTINGHOUSE ELECTRIC
PO BOX 355
PITTSBURGH, PA 15230
USA

F. ARAYA
JAPAN ATOMIC ENERGY RES. INST
TOKAI-MURA, NAKA-GUN
IBARAKI-KEN, 319-11
JAPAN

R. ARCHULETA
UNIVERSITY OF CALIFORNIA, SANTA BARBARA
DEPT. OF GEOLOGICAL SCIENCES
SANTA BARBARA, CA 93106
USA

W. ARCIERI
EG&G
11426 ROCKVILLE PIKE, SUITE 300
ROCKVILLE, MD 20852
USA

N. ARNE
KOREA ELECTRIC POWER CORP., NY OFFICE
270 SYLVAN AVENUE
ENGLEWOOD CLIFFS, NJ 07632
USA

V. ASMOLOV
I.V. KURCHATOV INST. OF ATOMIC ENERGY
KURCHATOV SQUARE
MOSCOW, 123182
USSR

M. AZARM
BROOKHAVEN NATIONAL LABORATORY
BUILDING 130
UPTON, NY 11973
USA

S. BALL
OAK RIDGE NATIONAL LABORATORY
P.O. BOX 2008
OAK RIDGE, TN 37831-6010
USA

A. BARATTA
PENN STATE UNIVERSITY
231 SAKETT BLDG.
UNIVERSITY PARK, PA 16802
USA

R. BARI
BROOKHAVEN NATIONAL LABORATORY
BUILDING 197C
UPTON, NY 11973
USA

G. BAROIS
FRAMATOME
TOUR FIAT CEDEX 16
PARIS-LA-DEFENSE, 92084
FRANCE

J. BASSELIER
BELGONUCLEAIRE
AVENUE ARIANE 4,
BRUSSELS, 1200
BELGIUM

J. BAST
STRATEGIC BUSINESS SYSTEMS
6 MOUNTAINVIEW TERRACE
BALLSTON LAKE, NY 12019
USA

J. BASURTO
CNSNS-MEXICO
AV. INSURGENTES SUR, 1778
MEXICO CITY, 01030
MEXICO

G. BAUMGARTNER
BASLER & HOFMANN
FORCHSTRASSE 395
ZURICH, 8029
SWITZERLAND

R. BEATY
SCIENCE & ENGINEERING ASSOCIATES, INC.
1421 PRINCE STREET, SUITE 300
ALEXANDRIA, VA 22314
USA

L. BELL
OAK RIDGE NATIONAL LABORATORY
P.O. BOX 2009, MS-8063
OAK RIDGE, TN 37831
USA

R. BELL
NUMARC
1776 EYE STREET NW., SUITE 300
WASHINGTON, DC 20006
USA

G. BERNA
EG&G IDAHO, INC.
P.O. BOX 1625
IDAHO FALLS, ID 83404
USA

R. BEYER
WESTINGHOUSE
206 NAVAJO ROAD
W. PGH, PA 15241
USA

D. BHARGAVA
VIRGINIA POWER
5001 DOMINION BLVD.
GLEN ALLEN, VA 23060
USA

J. BICKEL
EG&G IDAHO, INC.
P.O. BOX 1625, MS 2405
IDAHO FALLS, ID 83415-2406
USA

W. BINNER
RES. CTR. SIEBERSDORF
KRAMERGASSE 1
VIENNA, A 010
AUSTRIA

D. BLAHNIK
BATTELLE-PACIFIC NORTHWEST LABS.
P.O. BOX 999
RICHLAND, WA 99352
USA

M. BOHN
SANDIA NATIONAL LABORATORIES
P.O. BOX 5800, DIVISION 6419
ALBUQUERQUE, NM 87185
USA

R. BOSCH
FOSTER WHEELER ENERGY GROUP
8 PEACH TREE HILL ROAD
LIVINGSTON, NJ 07021
USA

E. BOUCHERON
SANDIA NATIONAL LABORATORIES
P.O. BOX 5800, DIVISION 6418
ALBUQUERQUE, NM 87185-5800
USA

M. BOWMAN
BALTIMORE GAS & ELECTRIC CO.
P.O. BOX 1535
LUSBY, MD 20657
USA

B. BOYACK
LOS ALAMOS NATIONAL LABORATORY
P.O. BOX 1663, MS K551
LOS ALAMOS, NM 87545
USA

R. BOYD
WESTINGHOUSE SAVANNAH RIVER COMPANY
SAVANNAH RIVER SITE
AIKEN, SC 29808
USA

U. BREDOLT
ABB ATOM
BOX 53
VASTERAS, 72163
SWEDEN

C. BUCHHOLZ
GE NUCLEAR ENERGY
175 CURTNER AVE, M/C 754
SAN JOSE, CA 95125
USA

R. BUDNITZ
FUTURE RESOURCES ASSOCIATES INC
2000 CENTER STREET, SUITE 418
BERKELEY, CA 94704
USA

J. BUTLER
NUMARC
1776 EYE STREET NW, SUITE 300
WASHINGTON, DC 20006
USA

N. BUTTERY
NUCLEAR ELECTRIC PLC
PWR PROJECT GROUP, BOOTHS HALL
KNUTSFORD, CHESHIRE WA168QP
UK

A. CAMP
SANDIA NATIONAL LABORATORIES
P.O. BOX 5800, DIVISION 6412
ALBUQUERQUE, NM 87185
USA

J. CAREW
BROOKHAVEN NATIONAL LABORATORY
BUILDING 475B
UPTON, NY 11973
USA

D. CASADA
OAK RIDGE NATIONAL LABORATORY
P.O. BOX 2009
OAK RIDGE, TN 37831-8063
USA

R. CHAMBERS
EG&G IDAHO, INC.
P.O. BOX 1625
IDAHO FALLS, ID 83415-1560
USA

F. CHANG
ARGONNE NATIONAL LABORATORY
9700 S. CASS AVENUE
ARGONNE, IL 60439
USA

S. CHAVEZ
EG&G IDAHO, INC.
P.O. BOX 1625 MS-2509
IDAHO FALLS, ID 83404
USA

C. CHEN
GILBERET/COMMONWEALTH
P.O. BOX 1498
READING, PA 19603
USA

S. CHENG
INSTITUTE OF ENERGY RESEARCH, AEC
P.O. BOX 3-3
LUNG-TAN 32500
TAIWAN

R. CHEVERTON
OAK RIDGE NATIONAL LABORATORY
P.O. BOX 2009, BLDG 9204-1
OAK RIDGE, TN 37831-8047
USA

O. CHOPRA
ARGONNE NATIONAL LABORATORY
9700 S. CASS AVENUE
ARGONNE, IL 60439
USA

S. CHOW
STONE & WEBSTER ENG. CORP.
#3 EXECUTIVE CAMPUS, ROUTE 70
CHERRY HILL, NJ 08003
USA

L. CHU
BROOKHAVEN NATIONAL LABORATORY
BUILDING 130
UPTON, NY 11973
USA

R. COLE, JR.
SANDIA NATIONAL LABORATORIES
P.O. BOX 5800, DIVISION 6418
ALBUQUERQUE, NM 87185-5800
USA

M. CONFLANT
DIRECTORATE SAFETY INSTALLATION NUCLEAR
CEN/FAR DRSN BP NO. 6
FONTENAY-AUX-ROSES, 92265
FRANCE

C. COOPER
AEA TECHNOLOGY, WINFRITH
WINFRITH TECHNOLOGY CENTRE
DORCHESTER, DORSET DT2 8DH
UK

J. COOPER
MPR ASSOCIATES, INC
1050 CONNECTICUT AVE, NW
WASHINGTON, DC 20036
USA

W. COPELAND
WESTINGHOUSE SAVANNAH RIVER COMPANY
SAVANNAH RIVER SITE
AIKEN, SC 29808
USA

E. CORUS
SANDIA NATIONAL LABORATORIES
41 EAGLE,TR
TIJERAS, NM 87059
USA

P. CORTICELLI
ENEA
VIO MARTIRI DI MONTESOLE
BOLOGNA 40100
ITALY

W. CORWIN
OAK RIDGE NATIONAL LABORATORY
P.O. BOX 2008, BLDG 4500S
OAK RIDGE, TN 37831-6151
USA

D. COX
OAK RIDGE NATIONAL LABORATORY
P.O. BOX 2009
OAK RIDGE, TN 37831-8038
USA

K. COZENS
NUMARC
1776 EYE STREET NW, SUITE 300
WASHINGTON, DC 20006
USA

D. CRAMER
WESTINGHOUSE SAVANNAH RIVER COMPANY
SAVANNAH RIVER SITE
AIKEN, SC 29808
USA

R. CURTIS
JUPITER CORPORATION
15909 WHITE ROCK RD.
GAITHERSBURG, MD 20878
USA

D. DAHLGREN
SANDIA NATIONAL LABORATORIES
P.O. BOX 5800, DIVISION 6410
ALBUQUERQUE, NM 87185
USA

R. DAIL
APTECH ENGINEERING SERVICES, INC
9872 PENNSYLVANIA AVE
UPPER MARLBORO, MD 20772
USA

R. DALLMAN
UNC ANALYTICAL SERVICES
P.O. BOX 5400
ALBUQUERQUE, NM 87185
USA

P. DAMERELL
MPR ASSOCIATES, INC
1050 CONNECTICUT AVE, NW
WASHINGTON, DC 20036
USA

J. DANKO
UNIV. OF TENNESSEE
COLLEGE OF ENGINEERING, PERKINS HALL
KNOXVILLE, TN 37996-2000
USA

N. DAVIES
AEA TECHNOLOGY
RISLEY
WARRINGTON, CHESHIRE WA3 6AT
UK

M. DAVISTER
U.S. DEPARTMENT OF ENERGY, DP-621
19901 GERMANTOWN ROAD
GERMANTOWN, MD 20874
USA

B. DE L'EPINOIS
DIRECTORATE SAFETY INSTALLATION NUCLEAR
CEN/FAR DRSN BP NO. 6
FONTENAY-AUX-ROSES, 92265
FRANCE

R. DE WIT
NAT'L INST. OF STANDARDS & TECHNOLOGY
ROOM B144, MATERIALS BLDG.
GAITHERSBURG, MD 20899
USA

J. DEBOR
SCIENCE APPLICATIONS INTL. CORP
1710 GOODRIDGE DRIVE
MCLEAN, VA 22102
USA

R. DENNING
BATTELLE COLUMBUS
505 KING AVE.
COLUMBUS, OHIO 43201
USA

J. DEVOS
CEA FRENCH ATOMIC ENERGY COMMISSION
CEB SACLAY DMT/SEMT
GIF SUR YVETTE, 91190
FRANCE

K. DEWALL
EG&G IDAHO, INC.
P.O. BOX 1625
IDAHO FALLS, ID 83404
USA

H. DIETERSHAGEN
KNOLLS ATOMIC POWER LAB, GENERAL ELEC.
P.O. BOX 1072
SCHENECTADY, NY 12301-1072
USA

M. DIMARZO
UNIVERSITY OF MARYLAND
M.E. DEPT.
COLLEGE PARK, MD 20742
USA

C. DIPALO
SCIENCE APPLICATIONS INTL. CORP.
1710 GOODRIDGE DRIVE
MCLEAN, VA 22102
USA

S. DOCTOR
BATTELLE-PACIFIC NORTHWEST LABS.
P.O. BOX 999
RICHLAND, WA 99352
USA

M. DROUIN
SCIENCE APPLICATIONS INTL. CORP.
2109 AIR PARK RD., S. E.
ALBUQUERQUE, NM 87106
USA

R. DUFFEY
BROOKHAVEN NATIONAL LABORATORY
BUILDING 197C
UPTON, NY 11973
USA

R. DURANTE
AECL TECHNOLOGIES
15400 CALHOUN DRIVE, SUITE 100
ROCKVILLE, MD 20855
USA

K. DWIVEDY
VIRGINIA POWER
5000 DOMINION BLVD.
GLEN ALLEN, VA 23060
USA

J. EAST
WESTINGHOUSE SAVANNAH RIVER COMPANY
SAVANNAH RIVER SITE
AIKEN, SC 29808
USA

K. EBISAWA
JAPAN ATOMIC ENERGY RES. INST.
TOKAI-MURA, NAKA-GUN
IBARAKI-KEN, 319-11
JAPAN

J. EDSON
EG&G IDAHO, INC.
P.O. BOX 1625
IDAHO FALLS, ID 83415-2406
USA

Z. ELAWAR
ARIZONA PUBLIC SERVICE
P.O. BOX 52034
PHOENIX, AZ 85029
USA

P. EMAIN
ÉLECTICITÉ DE FRANCE
12-14, AVENUE DUTRIEVOZ
VILLEURBANNE, 69628
FRANCE

G. EMBLEY
GENERAL ELECTRIC
P.O. BOX 1072
SCHENCTADY, NY 12301
USA

B. ETTINGER
MPR ASSOCIATES, INC.
1050 CONNECTICUT AVE, NW
WASHINGTON, DC 20036
USA

B. EVANS
NUMARC
1776 EYE STREET NW, SUITE 300
WASHINGTON, DC 20006
USA

R. FAKORY
S3 TECHNOLOGIES
8930 STANFORD BLVD.
COLUMBIA, MD 21045
USA

M. FELTUS
PENN STATE UNIVERSITY
231 SAKETT BLDG.
UNIVERSITY PARK, PA 16802
USA

R. FERCH
ATOMIC ENERGY CONTROL BOARD
P.O.BOX 1046, STATION B
OTTAWA, ONTARIO K1P 5S9
CANADA

M. FISCHER
SIEMENS-KWU
LAMPERNBUHL 45
ERLANGEN, W8520
GERMANY

S. FLEGER
SCIENCE APPLICATIONS INTL. CORP.
1710 GOODRIDGE DRIVE
MCLEAN, VA 22102
USA

M. FONTANA
OAK RIDGE NATIONAL LABORATORY
P.O. BOX 2009
OAK RIDGE, TN 37831-8063
USA

T. FORTUNATO
BETTIS ATOMIC POWER LABORATORY
P.O. BOX 79
WEST MIFLIN, PA 15122
USA

E. FOX
OAK RIDGE NATIONAL LABORATORY
P.O. BOX 2009
OAK RIDGE, TN 37831-8063
USA

W. FRID
SWEDISH NUCLEAR POWER INSPECTORATE
P.O. BOX 27106
STOCKHOLM, S-102 52
SWEDEN

T. FUNAHASHI
TOSHIBA CORPORATION
8, SHINSUGITA-CHO, ISOGO-KU
YOKOHAMA, 235
JAPAN

H. FUNEJIKAWA
HITACH WORKS, HITACHI LTD.
1-1, 3-CHOME, SAIWAI-CHO
HITACHI-SHI, IBARAKI-KEN 317
JAPAN

R. GAMBLE
SARTREX CORP.
1700 ROCKVILLE PIKE, STE. 400
ROCKVILLE, MD 20852
USA

D. GERTMAN
EG&G IDAHO, INC.
P.O. BOX 1625 MS-2405
IDAHO FALLS, ID 83404
USA

B. GILBERT
EG&G IDAHO, INC.
P.O. BOX 1625 MS-2405
IDAHO FALLS, ID 83404
USA

J. GLEASON
WYLE LABORATORIES
P.O. BOX 07-7777
HUNTSVILLE, AL 35807-7777
USA

M. GOMOLINSKI
CEA FRENCH ATOMIC ENERGY COMMISSION
321 RUE DE CHAVEVTON
PARIS, 75012
FRANCE

W. GRANT
MPR ASSOCIATES, INC.
1050 CONNECTICUT AVE. NW
WASHINGTON, DC 20036
USA

R. GREENE
OAK RIDGE NATIONAL LABORATORY
P.O. BOX 2009
OAK RIDGE, TN 37831-8038
USA

E. GROUNDWATER
SCIENCE APPLICATIONS INTL. CORP.
1710 GOODRIDGE DRIVE
MCLEAN, VA 22102
USA

E. GROVE
BROOKHAVEN NATIONAL LABORATORY
BUILDING 130
UPTON, NY 11973
USA

T. HAKE
SANDIA NATIONAL LABORATORIES
P.O. BOX 5800, DIVISION 6412
ALBUQUERQUE, NM 87185
USA

R. HALL
BROOKHAVEN NATIONAL LABORATORY
BUILDING 130
UPTON, NY 11973
USA

R. HAMMERSLEY
FAUSKE & ASSOCIATES
16W070 W. 83RD ST.
BURR RIDGE, IL 60521
USA

S. HAQ
BECHTEL
9801 WASHINGTON BLVD.
GAITHERSBURG, MD 20878-5356
USA

F. HARPER
SANDIA NATIONAL LABORATORIES
P.O. BOX 5800, DIVISION 6413
ALBUQUERQUE, NM 87185-5800
USA

C. HARRISON
ATOMIC ENERGY CONTROL BOARD
270 ALBERT ST.
OTTAWA, ONTARIO K1P 5S9
CANADA

L. HARROP
HM NUCLEAR INSTALLATIONS INSPECTORATE
ST. PETERS HOUSE, BALLIOL ROAD
BOOTLE, MERSEYSIDE L20 3LZ
UK

E. HARVEGO
EG&G IDAHO, INC.
P.O. BOX 1625
IDAHO FALLS, ID 83415-2406
USA

R. HARVEY
YANKEE ATOMIC ELECTRIC CO.
580 MAIN ST.
BOLTON, MA 01740
USA

H. HASHEMIAN
AMS CORPORATION
9111 CROSS PARK DRIVE
KNOXVILLE, TN 37923
USA

M. HASSAN
BROOKHAVEN NATIONAL LABORATORY
BUILDING 130
UPTON, NY 11973
USA

J. HAWTHORNE
MATERIALS ENGINEERING ASSOCIATES
9700-B MARTIN L. KING, JR. HWY
LANHAM, MD 20706
USA

N. HAYASHI
NUPEC-NUCLEAR POWER ENG. TEST CENTER
3-17,1-CHOME,TORANOMON,MINATO-KU
TOKYO, 105
JAPAN

G. HEDRICK
DUKE ENGINEERING & SERVICES, INC.
P.O. BOX 1004, MS ST02A
CHARLOTTE, NC 28201-1004
USA

S. HENRY
BALTIMORE GAS & ELECTRIC CO.
P.O. BOX 1535
LUSBY, MD 20657
USA

H. HEPER
UNIVERSITY OF MARYLAND
9314 CHERRY HILL ROAD #217
COLLEGE PARK, MD 20740
USA

D. HIDINGER
GENERAL ELECTRIC
P.O. BOX 1072
SCHENCTADY, NY 12301
USA

J. HIGGINS
BROOKHAVEN NATIONAL LABORATORY
BUILDING 130
UPTON, NY 11973
USA

P. HILL
PENNSYLVANIA POWER & LIGHT
TWO NORTH NINTH STREET
ALLENTOWN, PA 18101
USA

R. HOBBINS
EG&G IDAHO, INC.
P.O. BOX 1625
IDAHO FALLS, ID 83415
USA

N. HOBSON
HM NUCLEAR INSTALLATIONS INSPECTORATE
ST. PETERS HOUSE, BALLIOL ROAD
BOOTLE, MERSEYSIDE L20 7LZ
UK

L. HOCHREITER
WESTINGHOUSE ELECTRIC
PO BOX 355
PITTSBURGH, PA 15230
USA

S. HODGE
OAK RIDGE NATIONAL LABORATORY
P.O. BOX 2009
OAK RIDGE, TN 37831-8057
USA

P. HOFMANN
KERNFORSCHUNGSZENTRUM KARLSRUHE
P.O. BOX 3640
KARLSRUHE, W-7500
GERMANY

C. HOFMAYER
BROOKHAVEN NATIONAL LABORATORY
BUILDING 475C
UPTON, NY 11973
USA

P. HOLDEN
AEA TECHNOLOGY
RISLEY
WARRINGTON, CHESHIRE WA3 6ZRQ
UK

H. HOLMSTRÖM
OECD/NUCLEAR ENERGY AGENCY
38, BOULEVARD SUCHET
PARIS, F-75016
FRANCE

R. HOPPE
BETTIS ATOMIC POWER LABORATORY
P.O. BOX 79
WEST MIFLIN, PA 15122
USA

Y. HORIKAWA
THE KANSAI ELECTRIC POWER CO., INC.
1100 17TH STREET, N.W., SUITE 500
WASHINGTON, DC 20036
USA

D. HORSCHEL
SANDIA NATIONAL LABORATORIES
P.O. BOX 5800, DIVISION 6473
ALBUQUERQUE, NM 87185-5800
USA

T. HSU
VIRGINIA POWER
5000 DOMINION BLVD.
GLEN ALLEN, VA 23060
USA

F. HSU
BROOKHAVEN NATIONAL LABORATORY
BUILDING 130
UPTON, NY 11973
USA

Y. HUANG
INSTITUTE OF ENERGY RESEARCH, AEC
P.O. BOX 3-3
LUNG-TAN, 32500
TAIWAN

T. HUNT
GULF STATES UTILITIES
P.O. BOX 220
ST. FRANCISVILLE, LA 70775
USA

T. HUNT
EG&G IDAHO, INC.
P.O. BOX 1625
IDAHO FALLS, ID 83415-2406
USA

S. HYTEN
WYLE LABORATORIES
P.O. BOX 07-7777
HUNTSVILLE, AL 35807-7777
USA

S. INAMDAR
ONTARIO HYDRO
700 UNIVERSITY AVE.
TORONTO, ONTARIO M5G 1X6
CANADA

L. INNES
ATOMIC ENERGY CONTROL BOARD
270 ALBERT ST.
OTTAWA, ONTARIO K1P 5S9
CANADA

J. IRELAND
LOS ALAMOS NATIONAL LABORATORY
P.O. BOX 1663, MS K561
LOS ALAMOS, NM 87545
USA

H. ISBIN
NRC NSRRC
2815 MONTEREY PKWY
ST. LOUIS PARK, MN 55416
USA

J. ISHIGURO
JAPAN NUS
910 CLOPPER ROAD
GAITHERSBURG, MD 20877
USA

R. JACOBS
PENN STATE UNIVERSITY
DEPARTMENT OF PSYCHOLOGY
UNIVERSITY PARK, PA 16802
USA

M. JACOBUS
SANDIA NATIONAL LABORATORIES
P.O. BOX 5800, DIVISION 6419
ALBUQUERQUE, NM 87185
USA

J. JANSKY
BTB JANSKY
GERUNGER STRASSE 151
LEONBERG, 7250
GERMANY

D. JARRELL
BATTELLE-PACIFIC NORTHWEST LABS.
P.O. BOX 999
RICHLAND, WA 99352
USA

J. JARVIS
BECHTEL
9801 WASHINGTON BLVD.
GAITHERSBURG, MD 20878-5356
USA

A. JIMENEZ
CSN
JUSTO DORADO 11
MADRID, 28040
SPAIN

G. JOHNSON
EG&G IDAHO, INC.
P.O. BOX 1625
IDAHO FALLS, ID 83404
USA

B. JOHNSON
BATTELLE-PACIFIC NORTHWEST LABS.
P.O. BOX 999
RICHLAND, WA 99352
USA

J. JONES
OAK RIDGE NATIONAL LABORATORY
P.O. BOX 2009
OAK RIDGE, TN 37831-8063
USA

K. JONES
EG&G IDAHO, INC.
P.O. BOX 1625 MS-2508
IDAHO FALLS, ID 83404
USA

C. JUPITER
JUPITER CORPORATION
SUITE 503 WHEATON PLAZA N, 2730 UNIVERSITY BLVD. WEST
WHEATON, MD 20902
USA

K. KARWAT
TECHN. UNIV. MUNICH
FORSCHUNGSAREA
GARCHING, BAVARIA W8046
GERMANY

W. KASTENBERG
UCLA
48-121 ENGINEER IV
LOS ANGELES, CA 90[illegible]
USA

S. KATANISHI
JAPAN ATOMIC ENERGY RES. INST.
TOKAI-MURA, NAKA-GUN
IBARAKI-KEN, 319-11
JAPAN

W. KATO
BROOKHAVEN NATIONAL LABORATORY
BUILDING 197C
UPTON, NY 11973
USA

S. KAWAKAMI
NUPEC-NUCLEAR POWER ENG. TEST CENTER
3-13,4-CHOME,TORANOMON,MINATO-KU
TOKYO, 105
JAPAN

K. KAWANISHI
MITSUBISHI HEAVY INDUSTRIES, LTD.
2-1-1, SHINHAMA, ARAI-CHO
TAKASAGO-SHI, HYOGO-KEN 676
JAPAN

D. KELLY
EG&G IDAHO, INC.
P.O. BOX 1625 MS-2405
IDAHO FALLS, ID 83404
USA

J. KELLY
SANDIA NATIONAL LABORATORIES
P.O. BOX 5800, DIVISION 6401
ALBUQUERQUE, NM 87185-5800
USA

M. KHATIB-RAHBAR
ENERGY RESEARCH, INC.
PO BOX 2034
ROCKVILLE, MD 20847
USA

HHO KIM
KOREA INSTITUTE OF NUCLEAR SAFETY
P.O. BOX 16 DAEDUK-DANJI
DAEJON, 305353
KOREA

H. KIM
KAERI
P.O. BOX 7 DAEDUK-DANJI
DAEJON,
KOREA

I. KIM
BROOKHAVEN NATIONAL LABORATORY
BUILDING 130
UPTON, NY 11973
USA

S. KINNERSLY
AEA TECHNOLOGY, WINFRITH
WINFRITH TECHNOLOGY CENTRE
DORCHESTER, DORSET DT2 8DH
UK

E. KINTNER
NRC/RAC
P.O. BOX 882
NORWICH, VT 05055
USA

P. KLOEG
KEMA
UTRECHTSEWEG 310
ARNHEM, 6812 AR
THE NETHERLANDS

G. KLOPP
COMMONWEALTH EDISON
1400 OPUS PLACE, SUITE 400
DOWNERS GROVE, IL 60515
USA

L. KMETYK
SANDIA NATIONAL LABORATORIES
P.O. BOX 5800, DIVISION 6418
ALBUQUERQUE, NM 87185-5800
USA

S. KOBAYASHI
ISHIKAWAJIMA-HARIMA HEAVY INDUSTRIES
1,SHIN-NAKAHARA-CHO, ISOGO-KU
YOKOHAMA, 235
JAPAN

T. KODAMA
MITSUBISHI HEAVY INDUSTRIES, LTD.
2-1-1, SHINHAMA, ARAI-CHO
TAKASAGO-SHI, HYOGO-KEN 676
JAPAN

E. KOHN
ONTARIO HYDRO
700 UNIVERSITY AVE.
TORONTO, ONTARIO M5A
CANADA

C. KOT
ARGONNE NATIONAL LABORATORY
9700 S. CASS AVENUE
ARGONNE, IL 60439
USA

P. KRISHNASWAMY
BATTELLE COLUMBUS
505 KING AVE.
COLUMBUS, OHIO 43201
USA

P. KUAN
EG&G IDAHO, INC.
P.O. BOX 1625 MS-1560
IDAHO FALLS, ID 83404
USA

T. KUBOKOYA
TOSHIBA CORPORATION
8, SHINSUGITA -CHO, ISOGO-KU
YOKOHAMA, 235
JAPAN

Y. KUKITA
JAPAN ATOMIC ENERGY RES. INST.
TOKAI-MURA, NAKA-GUN
IBARAKI-KEN, 319-11
JAPAN

M. KUROHARA
MITSUBISHI HEAVY INDUSTRIES, LTD.
4-1, 2 CHOME, SHIBAKOUEN, MINATO-KU
TOKYO, 105
JAPAN

Y. KUSAMA
JAERI, TAKASAKI RAD. CHEM. RES. INST.
1233 WATANUKI-MACHI
TAKASAKI, GUNMA, 370-12
JAPAN

K. KUSSMAUL
MPA STUTTGART
P.O. BOX 2009
STUTTGART 80, D-7000
GERMANY

J. LAKE
EG&G IDAHO, INC.
P.O. BOX 1625 MS-2507
IDAHO FALLS, ID 83415-1560
USA

M. LAMBERT
ELECTICITE DE FRANCE
12-14, AVENUE DUTRIEVOZ
VILLEURBANNE, 69628
FRANCE

F. LANDY
PENN STATE UNIVERSITY
RESEARCH BLDG. D
UNIVERSITY PARK, PA 16802
USA

D. LEAVER
TENERA
1340 SARATOGA-SUNNYVALE ROAD
SAN JOSE, CA 95129
USA

C. LECOMTE
CEA-FRENCH ATOMIC ENERGY COMMISSION
CENTAR DRSN BP NO. 6
FONTENAY-AUX-ROSES, 92265
FRANCE

J. LEE
KOREA INSTITUTE OF NUCLEAR SAFETY
P.O. BOX 16 DAEDUK-DANJI
DAEJON, 305353
KOREA

S. LEE
FAUSKE & ASSOCIATES
16W070 W. 83RD ST.
BURR RIDGE, IL 60521
USA

J. LEHNER
BROOKHAVEN NATIONAL LABORATORY
BUILDING 130
UPTON, NY 11973
USA

R. LIN
LOS ALAMOS NATIONAL LABORATORY
P.O. BOX 1663, MS K557
LOS ALAMOS, NM 87545
USA

M. LINDQUIST
WESTINGHOUSE HANFORD CO.
BOX 1970
RICHLAND, WA 99352
USA

M. LIVOLANT
CEA FRENCH ATOMIC ENERGY COMMISSION
CENTAR DRSN BP NO. 6
FONTENAY-AUX-ROSES, 92265
FRANCE

R. LOFARO
BROOKHAVEN NATIONAL LABORATORY
BUILDING 130
UPTON, NY 11973
USA

J. LOPEZ-MONTERO
MADRID POLYTECHNICAL UNIVERSITY
JOSE GUTIERREZ ABASCAL, 2
MADRID, 28006
SPAIN

F. LOSS
MATERIALS ENGINEERING ASSOCIATES
9700-B MARTIN L. KING, JR. HWY
LANHAM, MD 20706
USA

K. LYNCH
GROVE ENGINEERING
15215 SHADY GROVE RD., STE. 202
ROCKVILLE, MD 20850
USA

P. MacDONALD
EG&G IDAHO, INC.
P.O. BOX 1625
IDAHO FALLS, ID 83415-2406
USA

A. MacKINNEY
NUMARC
1776 EYE STREET NW, SUITE 300
WASHINGTON, DC 20006
USA

I. MADNI
BROOKHAVEN NATIONAL LABORATORY
BUILDING 130
UPTON, NY 11973
USA

D. MAGALLON
CEC-JRC ISPRA
JRC EURATUM ISPRA
ISPRA, VARESE 21020
ITALY

H. MAGLEBY
EG&G IDAHO, INC.
P.O. BOX 1625
IDAHO FALLS, ID 83415-2406
USA

M. MANAHAN
PENN STATE UNIVERSITY
231 SACKETT
UNIVERSITY PARK, PA 16802
USA

P. MANBECK
BALTIMORE GAS & ELECTRIC CO.
P.O. BOX 632
LUSBY, MD 20657
USA

R. MANDL
SIEMENS/KWU
HAMMERBACHENSTR 12
ERLANGEN,
GERMANY

J. MARRINUCCI
GILBERT/COMMONWEALTH
P.O. BOX 1498
READING, PA 19603
USA

P. MARSILI
ENEA-DISP
VIA V. BRANCATI, 48
ROME, 00144
ITALY

I. MASAOKA
HITACHI RESEARCH LABORATORY
3-1, SAIWAI-CHO
HITACHI-SHI, IBARAKI-KEN 317
JAPAN

H. MASSIE
DNF SAFETY BOARD
625 INDIANA AVENUE, SUITE 700
WASHINGTON, DC 20004
USA

A. MATSUMOTO
JAPAN ATOMIC ENERGY RES. INST
TOKAI-MURA, NAKA-GUN
IBARAKI-KEN, 319-11
JAPAN

B. MAVKO
J. STEFAN INSTITUTE
JAMOVA 39
LJUBLJANA, 61000
SLOVENIA

B. MAVKO
J. STEFAN INSTITUTE
JAMOVA 39
LJUBLJANA, 61000
SLOVENIA

E. McCRAW
DUKE ENGINEERING & SERVICES, INC
P.O. BOX 1004, M/S ST02A
CHARLOTTE, NC 28201-1004
USA

W. McCURDY
MPR ASSOCIATES, INC
1050 CONNECTICUT AVE, NW
WASHINGTON, DC 20036
USA

D. McMULLAN
KNOLLS ATOMIC POWER LAB. / GENERAL ELEC.
P.O. BOX 1072
SCHENECTADY, NY 12301-1072
USA

C. MEDICH
SIET
VIA NINO BIXIO N. 27
PIACENZA, 29100
ITALY

J. MEINCKE
CONSUMERS POWER COMPANY
27780 BLUE STAR HIGHWAY
COVERT, MI 49043
USA

B. MENKE
MATERIALS ENGINEERING ASSOCIATES
9700-B MARTIN L. KING, JR. HWY
LANHAM, MD 20706
USA

J. METCALF
STONE & WEBSTER ENG. CORP.
245 SUMMER STREET
BOSTON, MA 02107
USA

Y. MEYZAUD
FRAMATOME
TOUR FIAT CEDEX 16
PARIS-LA-DEFENSE, 92084
FRANCE

L. MILLER
SCIENCE APPLICATIONS INTL. CORP.
1710 GOODRIDGE DR.
MC LEAN, VA 22102
USA

S. MIRSKY
SCIENCE APPLICATIONS INTL. CORP.
1710 GOODRIDGE DRIVE
MCLEAN, VA 22102
USA

D. MODEEN
NUMARC
1776 EYE STREET NW, SUITE 300
WASHINGTON, DC 20006
USA

S. MOORE
EG&G IDAHO, INC.
4417 S. HOLMES AVE.
IDAHO FALLS, ID 83404
USA

K. MOKHTARIAN
CBI TECHNICAL SERVICES
2700 JORIE BL. RD.
OAK BROOK, IL 60521
USA

F. MOODY
GE NUCLEAR ENERGY
175 CURTNER AVENUE
SAN JOSE, CA 95125
USA

N. MORAY
UNIVERSITY OF ILLINOIS
DEPT. OF MECH. & IE
URBANA, IL 61801
USA

D. MORRISON
MITRE CORPORATION
7525 COLSHIRE DRIVE
MCLEAN, VA 22102
USA

V. MUBAYI
BROOKHAVEN NATIONAL LABORATORY
BUILDING 130
UPTON, NY 11973
USA

M. MUHLHEIM
OAK RIDGE NATIONAL LABORATORY
P.O. BOX 2009, MS-8065
OAK RIDGE, TN 37831-8065
USA

M. MURASE
HITACHI LTD.
1168 MORIYAMA-CHO
HITACHI-SHI, IBARAKI 316
JAPAN

K. MURATA
SANDIA NATIONAL LABORATORIES
P.O. BOX 5800
ALBUQUERQUE, NM 87185-5800
USA

S. NAFF
EG&G IDAHO, INC.
P.O. BOX 1625
IDAHO FALLS, ID 83415
USA

H. NAGASAKI
NUPEC-NUCLEAR POWER ENG. TEST CENTER
3-17,1-CHOME,TORANOMON,MINATO-KU
TOKYO, 105
JAPAN

T. NAKAYAMA
HITACHI WORKS, HITACHI LTD.
1-1, 3-CHOME, SAIWAI-CHO
HITACHI-SHI, IBARAKI-KEN 317
JAPAN

K. NAMATAME
JAPAN ATOMIC ENERGY RES. INST
TOKAI-MURA, NAKA-GUN
IBARAKI-KEN, 319-11
JAPAN

H. NARAI
UNIVERSITY OF TSUKUBA
1 CHOME, TENNODAI
TSUKUBA-SHI, IBARAKI-KEN 305
JAPAN

D. NAUS
OAK RIDGE NATIONAL LABORATORY
P.O. BOX 2009
OAK RIDGE, TN 37831-8063
USA

C. NEGIN
GROVE ENGINEERING
15218 SHADY GROVE RD., STE. 202
ROCKVILLE, MD 20850
USA

A. NELSON
US GEOLOGICAL SURVEY
P.O. BOX 25046
DENVER, CO 80225
USA

W. NELSON
EG&G IDAHO, INC.
PO BOX 1625
IDAHO FALLS, ID 83415
USA

S. NESSIT
DUKE ENGINEERING & SERVICES, INC
600 MARYLAND AVE., SW, SUITE 890
WASHINGTON, DC 20024
USA

J. NESTELL
MPR ASSOCIATES, INC
1050 CONNECTICUT AVE, NW
WASHINGTON, DC 20036
USA

MAW NI
ATOMIC ENERGY COUNCIL
67 LANE 144 KEELUNG RD, SECT 4
TAIPEI, TAIWAN
ROC

M. NICHOLS
UNIVERSITY OF MINNESOTA
271 19TH AVE SOUTH
MINNEAPOLIS, MN 55455
USA

T. NISHIMOTO
JAPAN ELEC. POWER INFORMATION CENTER
1726 M ST., NW, STE. 403
WASHINGTON, DC 20036
USA

H. NIU
ATOMIC ENERGY COUNCIL
67 LANE 144 KEELUNG RD SECT 4
TAIPEI, TAIWAN 10772
ROC

A. NONAKA
NUPEC-NUCLEAR POWER ENG. TEST CENTER
3-13,4-CHOME,TORANOMON,MINATO-KU
TOKYO, 105
JAPAN

H. NOURBAKHSH
BROOKHAVEN NATIONAL LABORATORY
BUILDING 130
UPTON, NY 11973
USA

J. O'BRIEN
EG&G IDAHO, INC.
301 RANCH DR.
IDAHO FALLS, ID 83404
USA

D. O'MALLEY
TITAN CORP.
4201 CATHEDRAL AVE, NW APT 1410W
WASHINGTON, DC 20016
USA

S. OBERMEIRER
US GEOLOGICAL SURVEY
422 NATIONAL CENTER
RESTON, VA 22092
USA

Y. OCHI
COMPUTER SOFTWARE DEVELOPMENT
2-4-1,SHIBA KOEN
TOKYO, MINATO-KU 105
JAPAN

R. ODETTE
UNIVERSITY OF CALIFORNIA, SANTA BARBARA
DEPT. OF CHEM. & NUCLEAR ENGINEER
SANTA BARBARA, CA 93106
USA

B. OLAND
OAK RIDGE NATIONAL LABORATORY
P.O. BOX 2009
OAK RIDGE, TN 37831-8063
USA

R. [illegible]
ATOMIC ENERGY OF CANADA RESEARCH
CHALK RIVER LABORATORY
CHALK RIVER, ONTARIO K0J1J0
CANADA

R. OLSON
BALTIMORE GAS & ELECTRIC CO.
P.O. BOX 1535
LUSBY, MD 20657
USA

A. ONYEMAECHI
S3 TECHNOLOGIES
8930 STANFORD BLVD.
COLUMBIA, MD 21045
USA

M. ORTIZ
EG&G IDAHO, INC.
P.O. BOX 1625 M/S 2404
IDAHO FALLS, ID 83415-2402
USA

L. OTT
OAK RIDGE NATIONAL LABORATORY
P.O. BOX 2009
OAK RIDGE, TN 37831-8057
USA

N. PAL
PAL CONSULTANTS, INC.
1885 THE ALAMEDA STREET 100H
SAN JOSE, CA 95126
USA

D. PALMROSE
EG&G IDAHO, INC.
P.O. BOX 1625 M/S 2404
IDAHO FALLS, ID 83415-2412
USA

F. PANISKO
BATTELLE-PACIFIC NORTHWEST LABS
P.O. BOX 999
RICHLAND, WA 99352
USA

M. PARADIES
SYSTEM IMPROVEMENTS, INC.
238 PETERS ROAD,SUITE 301
KNOXVILLE, TN 37923
USA

S. PARISH
COUNCIL FOR NUCLEAR SAFETY
P.O. BOX 7106
HENNOPSMEER, 0046
SOUTH AFRICA

M. PARKS
SANDIA NATIONAL LABORATORIES
P.O. BOX 5800, DIVISION 6473
ALBUQUERQUE, NM 87185-5800
USA

W. PASEDAG
U.S. DEPARTMENT OF ENERGY
NE-42
WASHINGTON, DC 20585
USA

M. PATTERSON
SCIENTECH, INC
11821 PARKLAWN DRIVE
ROCKVILLE, MD 20852
USA

P. PAUL
DUKE POWER CO
P.O. BOX1006
CHARLOTTE, NC 28201
USA

A. PAYNE, JR.
SANDIA NATIONAL LABORATORIES
P.O. BOX 5800, DIVISION 6412
ALBUQUERQUE, NM 87185-5800
USA

W. PENNELL
OAK RIDGE NATIONAL LABORATORY
P.O. BOX 2009
OAK RIDGE, TN 37831-8056
USA

K. PEREIRA
ATOMIC ENERGY CONTROL BOARD
P.O.BOX 1046, STATION B
OTTAWA, ONTARIO K1P 5S9
CANADA

G. PEREZ
CNSNS-MEXICO
AV. INSURGENTES SUR 1778
MEXICO CITY, 01030
MEXICO

G. PETRANGELI
ENEA-DISP
VIA V. BRANCATI, 48
ROME, 00144
ITALY

J. PHILLIPS
EG&G IDAHO, INC.
P.O. BOX 1625 MS-2406
IDAHO FALLS, ID 83415-1560
USA

L. PHILPOT
GILBERET/COMMONWEALTH
P.O. BOX 1498
READING, PA 19603
USA

B. PIKUL
MITRE CORPORATION
7525 COLSHIRE DRIVE
MCLEAN, VA 22102
USA

G. PINO
ENEA DISP
VIA V. BRANCATI, 48
ROME, 00144
ITALY

M. PODOWSKI
RPI, TROY NEW YORK
DEPT. OF NUCLEAR ENGINEERING
TROY, NY 12180-3592
USA

S. POPE
HALLIBURTON NUS
18804 LINDENHOUSE RD.
GAITHERSBURG, MD 20879
USA

L. PRICE
EG&G IDAHO, INC.
P.O. BOX 1625
IDAHO FALLS, ID 83415-2406
USA

J. PUGA
UNESA
PLO. GERVAS 3
MADRID, 28020
SPAIN

C. PUGH
OAK RIDGE NATIONAL LABORATORY
P.O. BOX 2009, MS 8063
OAK RIDGE, TN 37922
USA

D. RAKOVICH
ONTARIO HYDRO
700 UNIVERSITY AVE.
TORONTO, ONTARIO M5G 1X6
CANADA

J. RANTAKIVI
FINNISH CENTRE FOR RAD. & NUCL. SAFETY
P.O. BOX 268
HELSINKI, SF-00101
FINLAND

W. REECE
EG&G IDAHO, INC.
P.O. BOX 1625 MS-2405
IDAHO FALLS, ID 83404
USA

J. REMPE
EG&G IDAHO, INC.
P.O. BOX 1625 MS-2508
IDAHO FALLS, ID 83404
USA

M. RIOCREUX
CEA FRENCH ATOMIC ENERGY COMMISSION
CEN CADARACHE DRS/SEMAR
ST PAUL LEZ DURANCE, 13108
FRANCE

W. RETTIG
U.S. DEPARTMENT OF ENERGY
785 DOE PLACE
IDAHO FALLS, ID 83402
USA

L. RIB
ABCL TECHNOLOGIES
15400 CALHOUN DRIVE, SUITE 100
ROCKVILLE, MD 20855
USA

M. RIGHTLEY
SANDIA NATIONAL LABORATORIES
P.O. BOX 5800, DIVISION 6463
ALBUQUERQUE, NM 87185-5800
USA

G. ROBINSON
PENN STATE UNIVERSITY
731 SAKETT BLDG.
UNIVERSITY PARK, PA 16802
USA

U. ROHATGI
BROOKHAVEN NATIONAL LABORATORY
BUILDING 475B
UPTON, NY 11973
USA

G. ROMBOLD
NUMARC
1776 EYE STREET NW, SUITE 300
WASHINGTON, DC 20006
USA

A. ROOSBOOM
SZW/NUCLEAR SAFETY DEPARTMENT
KERSENGAARDE 215
VOORBURG, 2270ND
THE NETHERLANDS

E. ROTH
WESTINGHOUSE
1310 BEULAH ROAD
PITTSBURGH, PA 15217
USA

H. RYALS
BETTIS ATOMIC POWER LABORATORY
P.O. BOX 79
WEST MIFLIN, PA 15122
USA

B. SAFFELL
BATTELLE COLUMBUS
505 KING AVE.
COLUMBUS, OH 43201
USA

R. SALIZZONI
WESTINGHOUSE SAVANNAH RIVER COMPANY
SAVANNAH RIVER SITE
AIKEN, SC 29802
USA

P. SAMANTA
BROOKHAVEN NATIONAL LABORATORY
BUILDING 130
UPTON, NY 11973
USA

R. SAMMATARO
GENERAL DYNAMICS
75 EASTERN POINT ROAD
GROTON, CT 06340
USA

J. SANCHEZ
CSN
JUSTO DORADO 11
MADRID, 28040
SPAIN

O. SANDERVAG
SWEDISH NUCLEAR POWER INSPECTORATE
P.O. BOX 27106
STOCKHOLM, S-102 52
SWEDEN

L. SANTOMA
CSN
JUSTO DORADO 11
MADRID, 28040
SPAIN

M. SARRAM
UNITED ENGINEERS
30 S. 17TH ST.
PHILADELPHIA, PA 19101
USA

K. SATO
HITACHI,LTD
3-1-1 SAIWAI-CHO
HITACHI-SHI, IBARAKI-KEN 317
JAPAN

R. SCHMIDT
BATTELLE COLUMBUS
505 KING AVE.
COLUMBUS, OHIO 43201
USA

R. SCHNEIDER
ABB/C-E
1000 PROSPECT HILL ROAD
WINDSOR, CT 06095
USA

G. SCHUECKTANZ
UNIVERSAL TESTING LABORATORIES
5959 SHALLOWFORD RD., SUITE 531
CHATANOOGA, TN 37421
USA

E. SCHULTZ
INDUSTRIAL POWER CO. LTD. IVO
27160 OLKILUOTO
SUOMI, SF-27160
FINLAND

G. SCHWARZ
ATOMIC ENERGY CONTROL BOARD
270 ALBERT ST.
OTTAWA, ONTARIO K1P 5S9
CANADA

W. SEUCON
HM NUCLEAR INSTALLATIONS INSPECTORATE
ST. PETERS HOUSE, BALLIOL ROAD
BOOTLE, MERSEYSIDE L20 3LZ
UK

B. SEHGAL
ELECTRIC POWER RESEARCH INSTITUTE
3412 HILLVIEW AVE. P.O. BOX 10412
PALO ALTO, CA 94303
USA

S. SERKAN
GUBERETY/COMMONWEALTH
P.O. BOX 1498
READING, PA 19603
USA

S. SETH
MITRE CORPORATION
7525 COLSHIRE DRIVE
MCLEAN, VA 22102
USA

W. SHA
ARGONNE NATIONAL LABORATORY
9700 S. CASS AVENUE
ARGONNE, IL 60439
USA

W. SHACK
ARGONNE NATIONAL LABORATORY
9700 S. CASS AVENUE, BLDG 212
ARGONNE, IL 60439
USA

R. SHARMA
AMERICAN ELECTRIC POWER
ONE RIVERSIDE PLAZA
COLUMBUS, OHIO 43215
USA

A. SHARON
QUANTUM TECHNOLOGIES
2625 BUTTERFIELD RD.
OAKBROOK, IL 60521
USA

K. SHIBA
JAPAN ATOMIC ENERGY RES. INST
TOKAI-MURA, NAKA-GUN
IBARAKI-KEN, 319-11
JAPAN

J. SHIN
EBASCO SERVICES, INC.
TWO WORLD TRADE CENTER
NEW YORK, NY 10048
USA

J. SIENICKI
ARGONNE NATIONAL LABORATORY
9700 S. CASS AVENUE, BLDG 206
ARGONNE, IL 60439
USA

F. SIMONOM
BATTELLE-PACIFIC NORTHWEST LABS.
P.O. BOX 999
RICHLAND, WA 99352
USA

A. SIMPKINS
WESTINGHOUSE SAVANNAH RIVER COMPANY
SAVANNAH RIVER SITE
AIKEN, SC 29808
USA

C. SLATER
EG&G IDAHO, INC.
P.O. BOX 1625
IDAHO FALLS, ID 83404
USA

G. SLAUGHTER
OAK RIDGE NATIONAL LABORATORY
P.O. BOX 2008, BLDG 4500S
OAK RIDGE, TN 37831-6152
USA

S. SLOAN
EG&G IDAHO, INC.
PO BOX 1625
IDAHO FALLS, ID 83415
USA

G. SLOVIK
BROOKHAVEN NATIONAL LABORATORY
BUILDING 475B
UPTON, NY 11973
USA

L. SMITH
LOS ALAMOS NATIONAL LABORATORY
P.O. BOX 1663, MS E561
LOS ALAMOS, NM 87544
USA

K. SODA
JAPAN ATOMIC ENERGY RES. INST
TOKAI-MURA, NAKA-GUN
IBARAKIKEN, 319-11
JAPAN

M. SOEJIMA
MITSUBISHI HEAVY INDUSTRIES, LTD.
1-1,1-CHOME,WADASAKI-CHO,HYOGO-KU
KOBE-SHI, 652
JAPAN

C. SORRELL
VIRGINIA POWER
5000 DOMINION BLVD.
GLEN ALLEN, VA 23060
USA

W. SPEZIALETTI
WESTINGHOUSE SAVANNAH RIVER COMPANY
37 VARDEN DRIVE
AIKEN, SC 29803
USA

K. STAHLKOPF
ELECTRIC POWER RESEARCH INSTITUTE
3412 HILLVIEW AVE, P.O. BOX 10412
PALO ALTO, CA 94303
USA

R. STAROK
MPR ASSOCIATES, INC
1050 CONNECTICUT AVE, NW
WASHINGTON, DC 20036
USA

M. STRAND
JUPITER CORPORATION
2750 UNIVERSITY BLVD. WEST, #403
WHEATON, MD 020902
USA

D. STRAWSON
MPR ASSOCIATES, INC
1050 CONNECTICUT AVE, NW
WASHINGTON, DC 20036
USA

E. STUBBE
TRACTEBEL
AV. ARIANE 7
BRUSSELS, B-1200
BELGIUM

M. SUBUDHI
BROOKHAVEN NATIONAL LABORATORY
BUILDING 130
UPTON, NY 11973
USA

K. SUH
FAUSKE & ASSOCIATES
16W070 W. 83RD ST.
BURR RIDGE, IL 60521
USA

R. SUMMERS
SANDIA NATIONAL LABORATORIES
P.O. BOX 5800, DIVISION 6418
ALBUQUERQUE, NM 87185-5800
USA

J. SUN
ARGONNE NATIONAL LABORATORY
9700 S. CASS AVENUE
ARGONNE, IL 60439
USA

M. TAEB
S3 TECHNOLOGIES
8930 STANFORD BLVD.
COLUMBIA, MD 21045
USA

H. TAKEDA
NUPEC-NUCLEAR POWER ENG. TEST CENTER
3-13,4-CHOME,TORANOMON,MINATO-KU
TOKYO, 106
JAPAN

K. TAKUMI
NUPEC-NUCLEAR POWER ENG. TEST CENTER
3-13,4-CHOME,TORANOMON,MINATO-KU
TOKYO, 106
JAPAN

J. TAYLOR
BROOKHAVEN NATIONAL LABORATORY
BUILDING 130
UPTON, NY 11973
USA

T. THEOFANOUS
UNIVERSITY OF CALIFORNIA, SANTA BARBARA
6740 CORTONE DR.
SAN GOLETA, CA 93117
USA

W. THOMAS
QUANTUM TECHNOLOGY, INC.
2625 BUTTERFIELD RD.
OAK BROOK, IL 60521
USA

S. THOMPSON
SANDIA NATIONAL LABORATORIES
P.O. BOX 5800, DIVISION 6418
ALBUQUERQUE, NM 87185-5800
USA

H. THORNBURG
ABB ATOM, INC.
901 S. WARFIELD DRIVE
MT. AIRY, MD 21771
USA

J. TILLS
JACK TILLS & ASSOCIATES, INC.
PO BOX 549
SANDIA PARK, NM 87047
USA

D. TONG
AEA TECHNOLOGY, SRD
WIGSHAW LANE
CULCHETH, CHESHIRE WA3 4NE
UK

T. TRAN
WESTINGHOUSE SAVANNAH RIVER COMPANY
SAVANNAH RIVER SITE
AIKEN, SC 29808
USA

P. TROY
NEWMAN & HOLTZINGER
1615 L STREET, N.W.
WASHINGTON, DC 20036
USA

J. TUCCIARONE
WESTINGHOUSE SAVANNAH RIVER COMPANY
SAVANNAH RIVER SITE
AIKEN, SC 29808
USA

M. TUTTLE
LAMONT-DOHERTY GEOLOGICAL OBS.
COLUMBIA UNIVERSITY
PALISADES, NY 10964
USA

K. UMEKI
NUPEC-NUCLEAR POWER ENG. TEST CENTER
3-13,4-CHOME,TORANOMON,MINATO-KU
TOKYO, 105
JAPAN

L. UNGER
SYSTEM IMPROVEMENTS
238 PETERS BLVD., SUITE 351
KNOXVILLE, TN 37923
USA

R. VALENTIN
ARGONNE NATIONAL LABORATORY
9700 S. CASS AVENUE, BLDG 308
ARGONNE, IL 60439
USA

S. VAN HEMEL
STAR MOUNTAIN, INC.
113 CLERMONT AVENUE
ALEXANDRIA, VA 22304
USA

J. VEEDER
AECL RESEARCH
CHALK RIVER LABORATORY
CHALK RIVER, ONTARIO K0J1J0
CANADA

R. VOGEL
CONSULTANT
2081 ROBIN HOOD LANE
LOS ALTOS, CA 94024
USA

W. VON RIESEMANN
SANDIA NATIONAL LABORATORIES
P.O. BOX 5800, DIVISION 6473
ALBUQUERQUE, NM 87185-5800
USA

R. VOSS
WESTINGHOUSE SAVANNAH RIVER COMPANY
SAVANNAH RIVER SITE
AIKEN, SC 29808
USA

B. WALSH
SCIENCE & ENGINEERING ASSOCIATES, INC.
6100 UPTOWN BLBD., NE
ALBUQUERQUE, NM 87110
USA

D. WALTERS
NUMARC
1776 EYE STREET NW, SUITE 300
WASHINGTON, DC 20006
USA

S. WANG
INSTITUTE OF ENERGY RESEARCH, AEC
P.O. BOX 5-3
LUNG-TAN, 32500
TAIWAN

L. WARD
EG&G
11426 ROCKVILLE PIKE, SUITE 300
ROCKVILLE, MD 20852
USA

K. WASHINGTON
SANDIA NATIONAL LABORATORIES
P.O. BOX 5800, DIVISION 6429
ALBUQUERQUE, NM 87185-5800
USA

R. WATSON
SANDIA NATIONAL LABORATORIES
P.O. BOX 5800, DIVISION 6473
ALBUQUERQUE, NM 87185-5800
USA

J. WERNER
U.S. DEPARTMENT OF ENERGY
785 DOE PLACE
IDAHO FALLS, ID 83402
USA

P. WHEATLEY
EG&G IDAHO, INC.
P.O. BOX 1625 M/S 2412
IDAHO FALLS, ID 83415-2412
USA

D. WHITEHEAD
SANDIA NATIONAL LABORATORIES
P.O. BOX 5800, DIVISION 6412
ALBUQUERQUE, NM 87185
USA

B. WHITESEL
NUMARC
1776 EYE STREET NW, SUITE 300
WASHINGTON, DC 20006
USA

K. WHITT
SOUTHERN NUCLEAR
40 INVERNESS CENTER PARKWAY
BIRMINGHAM, AL 35201
USA

G. WILKOWSKI
BATTELLE COLUMBUS
505 KING AVE.
COLUMBUS, OHIO 43201
USA

K. WILLIAMS
SCIENCE APPLICATIONS INTL. CORP.
2109 AIR PARK RD., S. E.
ALBUQUERQUE, NM 87106
USA

J. WILSON
AEA TECHNOLOGY
HARWELL LABORATORY
DIDCOT, OXFORDSHIRE OX11 0RA
UK

H. WINGO
WESTINGHOUSE SAVANNAH RIVER COMPANY
SAVANNAH RIVER SITE
AIKEN, SC 29808
USA

G. WIRE
WESTINGHOUSE
5890 KEY STONE DR.
BETHEL PARK, PA 15102
USA

F. WITT
WESTINGHOUSE
P.O. BOX 2728
PITTSBURGH, PA 15230-2728
USA

M. W[illegible] J.
LAWRENCE LIVERMORE NATIONAL LAB
P.O. BOX 808, L-196
LIVERMORE, CA 94550
USA

L. WOLF
KIK/PMDR, BATTELLE-EUROPE
POSTFACH 900160,AM ROMERHOF 35
FRANKFURT AM MAIN 90, 6000
GERMANY

[illegible] WOLF
NATIONAL ACADEMY OF SCIENCE
2101 CONSTITUTION AVENUE NW
WASHINGTON, DC 20418
USA

N. WOODY
WESTINGHOUSE SAVANNAH RIVER COMPANY
SAVANNAH RIVER SITE
AIKEN, SC 29808
USA

W. WULFF
BROOKHAVEN NATIONAL LABORATORY
BUILDING 475B
UPTON, NY 11973
USA

M. YOKOTA
TOKYO ELECTRIC POWER
1901 L ST N.W. SUITE 720
WASHINGTON, DC 20036
USA

K. YOON
B&W NUCLEAR SERVICE
PO BOX 10935
LYNCHBURG, VA 24503
USA

R. YOUNGBLOOD
BROOKHAVEN NATIONAL LABORATORY
BUILDING 130
UPTON, NY 11973
USA

G. ZIGLER
SCIENCE & ENGINEERING ASSOCIATES, INC.
6100 UPTOWN BLBD., NE
ALBUQUERQUE, NM 87110
USA

F. ZIKRIA
HALLIBURTON NUS CORP
910 KLOPPER ROAD
GAITHERSBURG, MD 20877
USA

P. ZMOLA
C & P ENGINEERING
5409 NEWINGTON ROAD
BETHESDA, MD 20816
USA

H. ZOGRAN
MPR ASSOCIATES, INC.
1050 CONNECTICUT AVE, NW
WASHINGTON, DC 20036
USA

P. ZWICKY
BASLER & HOFMANN
FORCHSTRASSE 395
ZURICH, [illegible] 29
SWITZERLAND

PROCEEDINGS OF THE
NINETEENTH WATER REACTOR SAFETY INFORMATION MEETING
October 28-30, 1991

CONTENTS - VOLUME 3

CONTENTS - VOLUME 3 (Cont'd)

Studies Performed in Support of the Proposed Revision of Engineering Design Aspects of 10CFR100, Appendix A

Monika Witte and Pete Prassinos*, **
Lawrence Livermore National Laboratory

Abstract

Part 100 of Title 10 of the code of Federal Regulations (10CFR100) describes criteria which guide the commission in its evaluation of the suitability of proposed sites for nuclear power plants. Appendix A of this part describes seismic and geologic siting criteria for nuclear power plants. Some engineering design aspects of nuclear power plants are also addressed in Appendix A. These include: definitions of the Operating Basis Earthquake (OBE) and the Safe Shutdown Earthquake (SSE), definitions of safety related structures, systems and components, ratio of OBE to SSE, identification of acceptable analytical methods, and definition of vibratory ground motion. In fact, the seismic design requirements for nuclear power plants in the U.S. were established with the publication of Appendix A to 10CFR100, pertinent Regulatory Guides, and the Standard Review Plan.

One of the interpretations of the regulations on the selection of the two earthquake design levels, the SSE and OBE, was that the SSE would control the design of all safety related systems while the OBE would be applied to the remaining systems required for continued power operation. In practice, however, with load factors, damping, and service limits, the OBE, rather than the SSE, has controlled the design for some systems.

Lawrence Livermore National Laboratory, under contract to the U.S. Nuclear Regulatory Commission, will assist the staff in developing the technical basis to support engineering related changes to Appendix A. Included in this effort are investigations of the impact of removing the OBE from design considerations with regard to safety options and review of possible strategies regarding the definition and requirements of the OBE for future reactors.

This paper will report on the status and results of studies performed to date in support of this project. These include a study to identify components that are important to plant safety and also are affected by OBE designs, a study to evaluate the impact on ASME BPVC Section III Division I of eliminating the OBE; and a study to evaluate the impact on seismic design margins if the OBE is eliminated from design. This paper addresses the engineering design aspects of Appendix A only.

* Presently employed at the Department of Energy, Albuquerque Field Office
** We appreciate the input and support of Roger Kenneally and Nilesh Chokshi of the NRC

Introduction

The NRC is in the process of revising Title 10, Part 100 of the Code of Federal Regulations, which describes reactor site criteria. Appendix A to 10CFR Part 100 describes the seismic and geologic siting criteria for nuclear power plants.

In the existing regulation, the Operating Basis Earthquake (OBE) is associated with functionality, likelihood of occurrence, and a minimum fraction of the Safe Shutdown Earthquake (SSE). Three distinct definitions in the regulation have led to sometimes conflicting objectives in the use of the OBE in design. The definition which has controlled the level of the OBE is the "minimum fraction of the SSE", which has resulted in seismic criteria for which the design of a number of components is governed by the OBE, significantly increasing the level of effort required for analysis, without significantly adding safety.

Evaluation of the Design Impact of the OBE

LLNL, under contract to the NRC, is in the process of evaluating the impact of removing the OBE from seismic design. Two studies have been undertaken: the first was a survey of utilities, engineering consulting firms, AE's, code organizations, and utility consortiums in order to obtain feedback on the feasibility of eliminating the requirement for design associated with the OBE. The second is a risk study which has identified components which might be affected by a change in the OBE design criteria, and generic categories of components which are potential seismic risk contributors based on previous Probabilistic Risk Assessments. This study will determine components for which the design is governed* by the load combination equation which include OBE load, and will evaluate the effect (if any) on component capacity for the hypothetical condition of no OBE design analysis. The study will determine the effect on seismic risk, if the capabilities are reduced, and will suggest changes to the component design process if there is an increase in the seismic risk.

Some broad, general conclusions may be drawn from the survey, and the portions of the risk study which are complete at this time. The survey results are qualitative, and occasionally contradictory. First, the impact of removing the OBE from design will depend to a large extent on the current philosophy of the designers. Two examples of this are that some designers use different damping to generate response spectrum for SSE and OBE. Some use only OBE damping for both the OBE and SSE since the determination has been made that the OBE may govern anyway. Another example is that in-line components are frequently designed for SSE loads, and then compared to OBE allowables. A second conclusion is that streamlining the design process is a worthy goal, and a third is that the OBE might govern the design of the following components:

- Concrete frames including walls, floors, and roofs in auxiliary building, fuel handling building etc.
- Piping and piping support systems
- Spherical steel containments and heads on cylindrical steel containments
- Containment penetration reinforcement
- Reactor vessel and steam generator internal components
- Large bore component support snubbers
- Embedment plates

* Governed by the OBE in this case means that the total upset load, including the OBE load, divided by the upset allowable, is greater than the total faulted load, including the SSE load, divided by the faulted allowable.

We have obtained detailed design data for thirty two components of thirteen component types. The data is preliminary, however it does indicate that it is difficult to make the statement that removing the OBE will have no effect on design, and likewise that removing the OBE will make the plant less safe. More work is still required, both in obtaining more data, and in analyzing the results. The data from both studies is summarized in Tables 1 to 7.

In addition to these two efforts, a third study has been completed to evaluate the required changes to Codes and Standards, if the OBE were eliminated from design. The following documents have been reviewed:

Sections of ASME BPVC Section III

ACI 349-85 and 349.1R-80

ANSI/AISC N690-1991

ASCE 1-82 N-725 and ASCE 4-86

IEEE 323 and IEEE 344

Suggested changes are fairly minor, and include definitions, references to dual earthquake loads and other minor wording changes, and a necessity to include fatigue and seismic anchor movement loads in the design.

Summary

The work in progress will develop the technical basis to support engineering related changes to Appendix A. This paper has reported on the status and results of studies performed to date in support of this project.

It is anticipated that the revised regulation and supporting regulatory guides will be released for public comment in early 1992.

Table 1: In-Line Components

Summary of Comments from Utilities and Designers

- How to evaluate impact of eliminating OBE? Require operability proof at SSE for active valves. Show elastic or do a detailed analysis for passive valves.
- Valves might fail because of binding.
- All kinds of possible problems:
  - *corrosion*
  - *wear*
  - *material degradation*
- Problems not really related to design:
  - *might be cleanliness*
  - *might be improper selection or misuse, perhaps used as a control valve when not designed for it.*
- Components and equipment items are not as much influenced by OBE/SSE since they may be attached to stiffer portion of the building.
- Steam generator internal components and reactor vessel internal components are typically governed by the OBE.
- Fatigue effects in equipment qualifications should be accounted for by considering an appropriate number of seismic events of a lesser magnitude corresponding to stress levels that are a specified fraction of the SSE values (e.g. 50%).

Results from First Phase of Risk Study

Valves	What governs design?	Margins* Large/Small
Globe Valve, 1"	SSE loads compared to OBE allowable	Usually pass with substantial margin
Main Feedwater Valve		
14" Bezel Gear Gate Valve		
16" M.D. Gate Valve		(High stress in valve body, still pass with OBE allowable)

Comments

- Idea of valve design is to stay elastic, even at SSE
- If g's on operator are higher than manufacturer's analysis, then either resupport pipe and/or valve or redo analysis—either pipe or valve.
- Valves not designed so much for seismic. Valve body and bonnet really controlled by pressure design.
- Yoke and bolts which hold yoke to bonnet and operator to bonnet might be controlled by seismic.

* Margin is with respect to design allowables for whichever earthquake controls

Table 2: Concrete Containment

Summary of Comments from Utilities and Designers

- Penetration reinforcement may be governed by localized OBE loads on the vessel.
- For concrete containment and internal structures, OBE is not the dominant load, even with the 1.9 factor. Accident loads (such as accident pressures, pipe break effects) govern.

Results from First Phase of Risk Study

Containment Penetration	What governs design?	Margins Large/Small
Plant 1 -elevation 11' below grade	OBE load (upset) combinations typically control design, but this could be due to thermal expansion or other stresses	Sometimes quite small
Plant 2 -elevation 109'-6" above grade	OBE load comb (upset) typically governs, in a few locations, the faulted bounding load governs	Medium

Comments

- Gut feeling is that seismic contribution is not that much.
- NB-3600 does not include shear and axial loading. NB-3200 does include shear and axial, and has higher allowables
- SSE usually not explicitly included. Instead, faulted condition uses bounding loads from pipe break analysis.
- Penetration is designed to be stronger than the pipe. The penetration anchorage is designed to be stronger than the penetration itself.
- Penetration is supplied by C.V. liner supplier. It is an M.C. (metal containment) component.
- OBE loads acting on the penetration are primarily piping OBE loads from dynamic analysis.

Table 3: Concrete Framing (Including Walls, Floors, Roofs)

Summary of Comments from Utilities and Designers

- OBE currently governs concrete framing design (including walls, floors, roofs) due to 1.9 load factor specified in ACI. This is for balance of plant structures: i.e. aux bldg., fuel handling buildings. This was changed in 1974. Formerly 1.7.
- For concrete safety structures (e.g. reactor bldg. and aux bldg.) typically don't design reinforcing pattern to minimize steel; instead try to minimize labor costs so use worst case reinforcing pattern in repeated locations.
- OBE controls if structure in flexible range. SSE controls or tends to have a greater importance if structure in rigid range. Must go through two complete sets of analyses to determine which governs.

Results from First Phase of Risk Study

Shear Walls	What governs design?	Margins Large/Small
Plant 1 Aux Building -elevation 25' above grade	SSE	Medium
Plant 1 Aux Building -elevation at grade	SSE	Small
Plant 2 Aux Building -elevation 76'-6" above grade	SSE	Horizontal reinforcement: large margin Vertical reinforcement: small margin
Plant 2 Aux Building -elevation 39' above grade	SSE (barely)	Horizontal reinforcement: large margin Vertical reinforcement: small margin

Comments

- SSE governed Plant 1, both walls with L.F. = 1.9
- SSE governed one Plant 2 case even with load factor = 1.9
- OBE would govern other Plant 2 case if load factor would be 1.9

Table 4: Pipe Supports

Summary of Comments from Utilities and Designers

- Piping support systems are typically governed by the OBE.

Results from First Phase of Risk Study

Piping Support Systems	What governs support design?	Margins Large/Small
Plant 1 16" O.D. Class 2	4 out of 6 governed by SSE	Some very small
Plant 1 2" O.D. Class 1	5 out of 6 governed by SSE	Medium to large
Plant 2 12" O.D. Class 1	10 out of 14 governed by SSE	Medium to large
Plant 2 2" O.D.	16 out of 18 governed by SSE	Some small

Comments

- Usually SSE governs support design, not always. Here 44 supports were reviewed from 4 pipe systems; 9 of these were governed by OBE.

Table 5: Piping

Summary of Comments from Utilities and Designers

- Typically piping is too rigid; there is too much reliance on snubbers. If eliminate OBE, this will help a little bit.
- ASME code change in progress: seismic stress removed as a primary stress and made a secondary stress. The numbers of supports will go way down, due to higher allowables for secondary loads. (Pending NRC approval).
- Presently, the seismic design requires 50 times more analysis for piping than other components/equipment.
- If remove OBE from design, then we'll require fatigue evaluation for SSE and must consider seismic anchor motions for SSE.
- OBE does not enhance safety, if additional efforts are put on SSE, safety will be enhanced.
- If PVRC damping is used for design, then OBE results will no longer govern.

Results from First Phase of Risk Study

Piping Systems	What governs design?	Margins Large/Small
Plant 1 16" O.D. Class 2	OBE	Medium
Plant 1 2" O.D. Class 1	OBE	Large
Plant 2 12" O.D. Class 1	OBE	Small
Plant 2 2" O.D.	OBE	Small

Comments

- All four systems reviewed use PVRC damping (since reanalyzed at time of snubber reduction program.)
- OBE governs all four cases we reviewed, even with PVRC damping.
- General comment: If earthquake is a large percentage of the total load, then SSE governs. But, if earthquake is a small percentage of the total load, then OBE tends to govern.

Table 6: Steel Containment

Summary of Comments from Utilities Designers
• For spherical steel containments and for heads on cylindrical steel containments, OBE can introduce stresses which are additive to the stresses due to pressure, requiring a greater thickness. • For steel containment vessels, shell thickness is governed by design pressure. Longitudinal and shear stresses due to OBE are small relative to the pressure stress. • Perhaps only 1000 psi OBE in total upset allowable of 19000 psi load, so proportionately small amount, but still pivotal. • If design thickness of shell right up to allowable in tension, then even a small earthquake could be a problem. • Want the S.C.V. thickness small enough so that post weld heat treatment is not required. (About 1 1/2 inches) • In external pressure case, compressive (hence buckling stress) is the issue. External pressure brings vessel right up to margin of what basic allowable would be in the code. • In some vessels buckling due to seismic overturning governs, then earthquake load is significant. • Some vessels have a corrosion allowance (perhaps 1/16"), some do not. New vessels will pay more attention to corrosion allowance. • Level of effort of OBE for steel containment design is not that high. The advantage of eliminating the OBE is not worth it. • If eliminate OBE from design could have a small decrease in safety. If buckling controls, ignoring OBE could be significant.

Results from First Phase of Risk Study		
Steel Containment Vessel	What governs design?	Margins Large/Small
(No detailed calculations reviewed yet for steel containments.)		

Table 6: Steel Containment (con't)

Summary of Comments from Utilities and Designers
• The contribution of earthquake induced stress to the total stress is minimum when tensile stress governs the steel containment vessel design. However, when buckling governs the design (much lower allowable), the earthquake contribution will be significant. • When tension governs, Service level C allowable = 2 times (Service level B). When earthquake stress is only a small portion of the total stress, increase of earthquake stress due to SSE will not have a significant impact such that Service level B design (including OBE) will govern the design. • When compression governs, Service level C allowable = 1.2 times (Service level B). Increase in stress due to SSE will have more significant impact when compression governs. With the combination of higher stresses and 20% higher allowable, Service level C (including SSE) will govern the containment design.

Table 7: Structures: Steel Design

Summary of Comments from Utilities and Designers

- Steel design typically governed by SSE.
- Component supports are mostly steel, governed by SSE.
- Large bore component support snubbers governed by OBE.

Results from First Phase of Risk Study

Auxilliary steel (large component supports)	What governs design?	Margins Large/Small
Plant 2 Mechanical component support Containment gallery Elevation 97'-4" above grade	SSE	Large
Plant 2 Mechanical component support Containment gallery Elevation 97'-4" above grade	OBE	Large
Plant 1 Containment building Elevation 1' below grade	SSE	Small

Enhancing the Seismic Margin Review Methodology to Obtain Risk Insights *

Robert J. Budnitz

Future Resources Associates, Inc.
2000 Center Street, Suite 418
Berkeley, California 94704

ABSTRACT

This paper will discuss methods for obtaining risk insights from the seismic margin review (SMR) methodology. The SMR methodology was originally developed in 1984-1987 with the objective of analyzing an individual nuclear power plant to ascertain whether the plant has the ability to withstand earthquakes substantially beyond the design-basis earthquake without suffering a core-damage accident. Recently, in the context of NRC's IPEEE program, the SMR methodology has been developed further by NRC to allow plants to identify plant-specific "vulnerabilities" (in the IPEEE sense) to seismic events. Among the important enhancements of the SMR methodology is a method to obtain risk insights. The enhanced methodology consists of several "steps" that an analyst should carry out, beyond those already specified in either the NRC-type or the EPRI-type SMR methodology. In this paper, the steps involved in the enhanced methodology will be discussed, with emphasis on their rationale.

1. INTRODUCTION

A new technique known as the seismic margin review methodology has recently been developed that enables the 'seismic margin' of a specific nuclear power plant to be analyzed. Two different variants of this methodology have been developed, one by the U.S. Nuclear Regulatory Commission, NRC (Ref. NUREG/CR-4334, 1985;

---

* This short paper is a summary of part of an NRC report, NUREG/CR-5679, to be published soon as a full report of the work that is summarized here. The authors of NUREG/CR-5679, besides the author of this short paper, are David L. Moore and Jeffry A. Julius, both of NUS Corporation, Kent, Washington. The work has been sponsored by the Office of Nuclear Regulatory Research of the U.S. Nuclear Regulatory Commission. It is referred to here as (Ref. Budnitz, Moore, and Julius, 1992).

NUREG/CR-4482, 1986) and the other by the Electric Power Research Institute, EPRI (Ref. EPRI-Margins, 1988). Starting with an earthquake level chosen for margin review, the new technique determines whether the plant can or cannot withstand the review-level earthquake without a core-damage accident: here 'withstand' means 'withstand with a high confidence of a low probability of failure', called 'HCLPF'. This HCLPF-based method can develop a lower bound on a plant's 'seismic margin' without undertaking a costly full-scope PRA.

In three trial applications (to the Maine Yankee, Catawba, and Hatch nuclear power plants), some limitations in the methodologies have been revealed (Ref. NRC-Maine Yankee, 1987; EPRI-Catawba, 1989; Georgia Power, 1991; APG, 1991). One of these limitations is the subject of this paper. The limitation can be stated as follows:

> The current methodology only analyzes plants up to "level I" as defined in standard PRA methodology --- that is, the methodology only analyzes accident sequences up to the onset of core damage. There is no analysis of plant damage states and of the potential of a given sequence to lead to large radiological releases.

The broad goal of the project that this paper summarizes has been to develop the HCLPF-based margin methodology further. The objective has been to provide recommendations for enhancements to the margin methodologies. These enhancements will enable seismic-margin analysts to obtain risk insights concerning the potential for large radiological releases.

The significance of the problem being addressed is as follows: the seismic-margins methodology has been developed to a mature state, and may become a standard method used for reviewing many nuclear power plants, especially in the context of NRC's IPE (Individual Plant Examination) program. The fact that NRC is endorsing the seismic-margins methodology as one way to accomplish the IPE objectives for earthquake-initiated accidents will encourage many utilities to use seismic-margin methods for the IPE (Ref. NRC-IPEEE Generic Letter, 1991). Also, most of the older U.S. plants will be doing seismic reviews of equipment soon to satisfy the requirements of resolving NRC Unresolved Safety Issue A-46, "Seismic Qualification of Equipment in Operating Plants." The resources (person-years and dollars) to be devoted to such reviews will be very substantial in the next few years. If limitations in the seismic-margin methodologies are better understood and partially remedied, these resources will be more effectively applied, and the engineering insights will be more technically sound.

Furthermore, it is anticipated that the cost of applying the

proposed enhanced methodology should be only slightly greater (in the 10% to 15% range) than the cost of applying the existing seismic margin methodology, if a level-I seismic PRA or level-I IPE internal-initiators evaluation is available. If there is no PRA or IPE to fall back on, then the effort will be greater. This is because in this case it is necessary to develop information anew about containment systems and functions and so on. This extra effort could be very large.

2. TECHNICAL APPROACH

The project's technical approach has been to demonstrate the feasibility of the proposed enhanced methodology by applying it in two actual cases:

(1) by revisiting the completed Maine Yankee trial margin study, which used the NRC-type margin approach; and (2) by studying the application at Hatch of both the EPRI-type and the NRC-type approaches together. An attempt was made to revisit the Catawba trial application of the EPRI-type seismic-margin methodology, but not enough information was available to provide useful methodological insights.

The seismic-margin approach stays away from dealing with overall earthquake-initiated risk directly. Indeed, one major benefit of a seismic margins review is the fact that the methodology does not rely at all on input concerning the seismic hazard. Rather, the margins approach begins by defining a peak ground acceleration level and spectrum (the "review-level earthquake") against which the specific plant is to be reviewed. Both the NRC method and the EPRI method then review the plant to determine whether the plant's seismic capacity is, or is not, above the review-level earthquake. The plant's capacity is expressed in terms of its "HCLPF capacity value", as defined in the methodology documents. If the plant HCLPF value is above the review-level earthquake, then the statement can be made that "there is a high confidence of a low probability of failure if the plant were subjected to an earthquake smaller or equal in 'size' to the review-level earthquake".

There are important strengths to the HCLPF-based approach, which uses as its main tool the proposition that it is feasible to develop, for each component, structure, or equipment item at a plant, the so-called "HCLPF value" ---- defined as that value of peak ground acceleration at which analysts can agree that for that component there is "a high confidence of a low probability of failure". If this HCLPF value for every plant component and structure is known, then it is possible to develop a HCLPF value for key accident sequences, including combinations of seismic-induced failures of various components and structures. The HCLPF value of a given sequence is obtained by combining properly the

HCLPF values of the various items whose failures contribute to that sequence.

In principle, this method can be used as a means of determining the HCLPF value for <u>each</u> accident sequence, and hence by proper analysis for "the plant-as-a-whole". Unfortunately, such a complete analysis would require an effort nearly as extensive as that required for a full-scope PRA. The great value of the newly-developed seismic margins approach is that it avoids this large effort by judiciously using conservative screening methods to reduce the number of components requiring detailed analysis.

In the NRC-supported approach, such screening is done within both the systems-analysis part and the fragilities-analysis part of the methodology, and involves eliminating (screening out) many components (Ref. NUREG/CR-4334, 1985; NUREG/CR-4482, 1986). The fragilities screening eliminates components based on screening guidelines whenever it can be established that their capacities are, with high confidence, well above the review-level earthquake being used in the analysis. Systems screening is done to eliminate components which are parts of systems not needed for certain functions. This set of simplifications is coupled with eliminating the seismic hazard evaluation: the question of how probable might be the earthquake-initiated accidents of interest is simply not asked.

In the EPRI-supported approach (Ref. EPRI-Margins, 1988), the screening is done by the judicious selection, early in the analysis, of one or more "success paths" that represent a methods whereby the plant can reach a safe shutdown condition after the occurrence of the postulated review-level earthquake. The analysis team then examines each selected success path in detail, determining the HCLPF capacity values for the functions, systems, and components required to operate successfully after the earthquake.

3. EVALUATION OF THE FEASIBILITY OF THE ENHANCEMENTS

Based on the work described, the authors' evaluation is that the recommended methodological enhancements are indeed fully feasible. A summary of that evaluation is as follows:

The authors believe that it is fully feasible to obtain insights using the seismic-margin methodologies concerning whether specific earthquake-caused faults, leading to core-threatening accident scenarios, are or are not associated with potential large radiological releases. A proposed methodology to accomplish this is specified in the body of the report.

The principal limitation is that the insights obtained are only approximate. This is mainly because the categorization of

success paths or cutsets into accident sequences, and further into plant damage states and radiological-release "bins", can only be approximate in light of shortcuts taken in the early part of the seismic-margin methodology. In the authors' view, these shortcuts can only be overcome by carrying out a full-scope level-II PRA. Some of these shortcuts involve how non-seismic failures and human errors are treated, even using the enhanced methodology that is recommended in this report. Other shortcuts involve the compromises intrinsic in the quasi-quantitative features of the margin-review approach. To repeat, the authors believe that only a full level-II PRA can overcome these difficulties.

A further limitation of the EPRI-type success-path margin method, which is absent when using the NRC-type fault-space method, is that one group of accident sequences will be missed entirely. These are postulated sequences in which the initiating event would be earthquake-caused loss of offsite power, but core damage would occur with no other seismic faults (due only to subsequent non-seismic faults or human errors). If seismic-caused failures were to occur in the containment or in containment systems, which could lead to potential large radiological releases, the existence of these would be an important insight that the EPRI-type methodology simply cannot identify.

Despite all of the limitations just discussed, it is the authors' overall evaluation that the enhanced methodology is well worth undertaking.

The recommendations here are considered enhancements of the guidance contained in the standard reports supporting the NRC and EPRI seismic margin review methodologies. It will not be possible to understand how to apply the enhancements here without reference to these original methodology reports.

4. DESCRIPTION OF THE STEPS IN THE ENHANCED METHODOLOGY

The broad structure of each of the enhanced methodologies can be found in the body of the report, NUREG/CR-5679 (Ref. Budnitz, Moore and Julius, 1992). Here, only the summary tables will be displayed, showing the several Steps in both the NRC and EPRI margin-review methodologies, with enhancements. The analyst should note that it is not necessary to perform these Steps in the order listed. Indeed, it is probably more efficient to carry out certain Steps concurrently with others. An example is the systems-analysis work in Step C of the NRC-type methodology. Another example is the seismic-capacity assessment work in NRC Step G, or alternatively in EPRI Step G.

Enhanced NRC Seismic Margin Methodology: The original NRC methodology guidance provides for 8 Steps. The enhanced guidance

recommends 9 more Steps to consider the potential for large radiological releases. The structure is summarized in Table 1.

Enhanced EPRI Seismic Margin Methodology: The original EPRI methodology guidance provides for 7 Steps. The enhanced guidance recommends 9 more Steps to consider the potential for large radiological releases. The structure is summarized in Table 2.

The enhanced methodology consists of 9 additional steps, and is somewhat different depending on whether the EPRI-type success path approach or the NRC-type fault-space approach has been selected. The differences are in the first two additional steps; the last 7 additional steps are very similar.

The assumption is made that a seismic-margin review has been completed, using either the EPRI-type or the NRC-type methodology, and following the guidance in the appropriate EPRI or NRC methodology reports.

It is also assumed that either a level-I PRA or an internal-initiators IPE analysis has been accomplished, or is being accomplished in parallel with this analysis. While this is not an essential assumption, if it is not true a considerable amount of extra effort will be required to complete the work here.

The 9-step enhanced methodological guidance can be briefly described as follows:

EPRI-type seismic-margin methodology, Steps A and B

Step A_{EPRI} Determine if any success path has a HCLPF capacity less than the SME. If there are none, the methodology stops.

Step B_{EPRI} For each low-HCLPF success path identified in Step A, determine the one or more accident sequences associated with that postulated low-HCLPF situation.

NRC-type seismic-margin methodology, Steps A and B

Step A_{NRC} Identify each cutset whose HCLPF capacity is less than the SME. If there are none, the methodology stops. Also, identify relevant non-seismic failures, human errors above the screening cutoffs, and opportunities for recovery.

Step B_{NRC} For each cutset identified in Step A, determine the one or more accident sequences associated with that postulated low-HCLPF cutset.

EPRI-type or NRC-type seismic-margin methodology, Steps C to I

Step C — For each accident sequence identified in Step B, use the event-tree method to extend that sequence to one or more plant-damage states. The use of internal-initiator event trees should generally be satisfactory for this purpose.

Step D — Perform a binning of the plant damage states identified in Step C, into bins corresponding to types/sizes/severities of radiological release, with emphasis on large, early releases and intermediate-sized releases.

Step E — For each large-release and intermediate-release bin identified in Step D, determine the containment systems and functions and the operator actions called on by plant procedures as the sequences associated with that bin evolve in time.

Step F — For each large-release and intermediate-release bins identified in Step D, determine the containment systems and functions and the operator actions available for recovery as the sequences associated with that bin evolve in time.

Step G — Assess the HCLPF capacity of each containment system/function identified in either Step E or Step F.

Step H — Assess the likelihood of operator error associated with those necessary operator actions identified in Step E, and the likelihood of success for those operator-initiated recovery actions identified in Step F.

Step I — Document the results and insights derived from earlier Steps.

A more extended description of the 9 steps can be found in the full report, NUREG/CR-5679 (Ref. Budnitz, Moore, and Julius, 1992).

5. ALTERNATIVES TO THE 9 STEPS DESCRIBED ABOVE

The 9-step methodology just discussed is the recommended approach for obtaining insights about the potential for large radiological releases. However, it is not the only way to obtain the engineering insights. Here, some alternative ways to approach

these issues will be discussed.

Alternative A. Perform HCLPF capacity review for ALL containment systems: The recommended methodology, as structured, has as one objective that not all containment functions and systems need be examined for their seismic HCLPF capacity --- the HCLPF capacity work need be done only for those which are involved in the accident sequences/plant damage states surviving the screening. This can be a great simplification, reducing cost, effort, and complexity.

The price paid for this simplification is that significant systems-analysis work is required in Steps B, C, D, E, and F. This systems work would not be necessary if the following four items could be accomplished successfully:

(1) all containment functions and systems were reviewed and found to have high HCLPF capacities, above the SME;

(2) this was also found to be true of all support systems necessary for the minimum configuration of front-line containment systems to perform the needed functions;

(3) no spatial systems-interaction issues or other unusual ways were identified that could compromise these containment functions; and

(4) the operator actions required were reviewed and found to be acceptable in terms of susceptibility for error.

This approach could be an acceptable alternative to the 9-step process outlined earlier.

Alternative B. Reduced program --- a systematic containment-function walkdown, but without calculations: An abbreviated alternative, not as satisfactory as "Alternative A" but perhaps acceptable in some cases --- especially in regions of low seismicity, such as along the U.S. Gulf Coast --- could be a reduced program. Such a reduced program would emphasize a thorough walkdown, but would not necessarily emphasize HCLPF capacity calculations.

This reduced-program approach is suggested in the spirit of the NRC's suggested reduced-program guidelines for the seismic-margin methodology for the IPE. The NRC's recent guidance on this subject should be referred to for further background information (Ref. NRC-IPEEE Generic Letter, 1991).

6. REFERENCES

APG, 1991: D. Orvis and P. Moieni, "Seismic Margin Review of Plant Hatch Unit 1, Systems Analysis", Accident Prevention Group, Inc., Report NUREG/CR-5632, prepared for Lawrence Livermore National Laboratory and U.S. Nuclear Regulatory Commission (1991)

EPRI-Catawba, 1989: NTS Engineering, RPK Consulting, Pickard Lowe & Garrick, Woodward Clyde Consultants, and Duke Power Company, "Seismic Margin Assessment of the Catawba Nuclear Station", in 2 volumes, Electric Power Research Institute Report EPRI NP-6359 (1989)

EPRI-Margins, 1988: NTS Engineering, RPK Structural and Mechanics Consulting, Pickard Lowe & Garrick, Woodward Clyde Consultants, and Duke Power Company, "A Methodology for Assessment of Nuclear Power Plant Seismic Margin", Electric Power Research Institute, Report EPRI NP-6041 (1988)

Georgia Power, 1991: Georgia Power Company, Southern Company Services, RPK Structural Mechanics Consulting, Woodward-Clyde Consultants, and EQE Inc., "Seismic Margin Assessment of Edwin I. Hatch Nuclear Plant - Unit 1", EPRI Report NP-7217-M, Electric Power Research Institute, in 3 volumes (1991)

NRC-IPEEE Generic Letter, 1991: U.S. Nuclear Regulatory Commission, Generic Letter 88-20, Supplement 4, "Individual Plant Examination for Severe Accident Vulnerabilities Due to External Events" (1991). This Generic Letter is supplemented with additional guidance in Report NUREG-1407, "Procedural and Submittal Guidance for the Individual Plant Examination of External Events (IPEEE) for Severe Accident Vulnerabilities" (1991).

NRC-Maine Yankee, 1987: P.G. Prassinos, R.C. Murray, G.E. Cummings, M.K. Ravindra, G.S. Hardy, P.S. Hashimoto, M.J. Griffin, D.L. Moore, D.M. Jones, M.D. Quilici, and J. Young, "Seismic Margin Review of the Maine Yankee Atomic Power Station", Lawrence Livermore National Laboratory and U.S. Nuclear Regulatory Commission, Report NUREG/CR-4826, in 3 volumes (1987)

NUREG/CR-4334, 1985: R.J. Budnitz, P.J. Amico, C.A. Cornell, W.J. Hall, R.P. Kennedy, J.W. Reed, and M. Shinozuka, "An Approach to the Quantification of Seismic Margins in Nuclear Power Plants", Lawrence Livermore National Laboratory and U.S. Nuclear Regulatory Commission Report NUREG/CR-4334 (1985)

NUREG/CR-4482, 1986: P.G. Prassinos, M.K. Ravindra, and J.B. Savy, "Recommendations to the NRC on Trial Guidelines for Seismic Margin Reviews of Nuclear Power Plants", Lawrence Livermore National Laboratory and U.S. Nuclear Regulatory Commission, draft report NUREG/CR-4482, published for comment (1986)

TABLE 1

ENHANCED NRC SEISMIC MARGIN METHODOLOGY

Step	Description
Original NRC Step 1	Select Seismic Margin Earthquake
Original NRC Step 2	Initial Systems Review
Original NRC Step 3	Component Grouping by HCLPF
Original NRC Step 4	First Plant Walkdown
Original NRC Step 5	System Modeling
Original NRC Step 6	Second Plant Walkdown
Original NRC Step 7	Determine Minimal Cutsets
Original NRC Step 8	Finalize Plant-Level HCLPF
New NRC Step A	Identify Cutsets with HCLPF < SME and NSF, HE, OFR
New NRC Step B	Determine Accident Sequence for Each low-HCLPF Cutset
New Step C	Extend each Sequence to Plant Damage States
New Step D	Bin Plant Damage States by Radiological Release Potential
New Step E	Determine Needed Containment Systems and Functions and Operator Actions Called on by Procedures
New Step F	Determine Containment Systems and Functions and Operator Actions Available for Recovery
New Step G	Assess HCLPF for each Containment System/Function
New Step H	Assess Likelihood of Operator Error or Operator Recovery Actions
New Step I	Document Results and Insights

TABLE 2

ENHANCED EPRI SEISMIC MARGIN METHODOLOGY

Step	Description
Original EPRI Step 1	Select Seismic Margin Earthquake
Original EPRI Step 2	Select Assessment Team
Original EPRI Step 3	Pre-Walkdown Preparatory Work
Original EPRI Step 4	Systems and Element Selection Walkdown
Original EPRI Step 5	Seismic Capability Walkdown
Original EPRI Step 6	Subsequent Walkdowns
Original EPRI Step 7	Seismic Margin Assessment Work
New EPRI Step A	Determine if any Success Path has HCLPF < SME
New EPRI Step B	Determine Accident Sequences for Each low-HCLPF Success Path
New Step C	Extend each Sequence to Plant Damage States
New Step D	Bin Plant Damage States by Radiological Release Potential
New Step E	Determine Needed Containment Systems and Functions and Operator Actions Called on by Procedures
New Step F	Determine Containment Systems and Functions and Operator Actions Available for Recovery
New Step G	Assess HCLPF for each Containment System/Function
New Step H	Assess Likelihood of Operator Error or Operator Recovery Actions
New Step I	Document Results and Insights

Large-Scale Seismic Test Program at Hualien, Taiwan

H.T. Tang
Electric Power Research Institute

H.L. Graves
U.S. Nuclear Regulatory Commission

P.C. Chen
Taiwan Power Company

Abstract

The Large-Scale Seismic Test (LSST) Program at Hualien, Taiwan, is a follow-on to the Soil-Structure Interaction (SSI) experiments at Lotung, Taiwan. The planned SSI experiment will be conducted at a stiff soil site in Hualien, Taiwan, that historically has had slightly more destructive earthquakes in the past than Lotung. The LSST is a joint effort among many interested parties. The Electric Power Research Institute (EPRI) and the Taiwan Power Company (Taipower) are the organizers of the program and have the lead in planning and managing the program. Other organizations cofunding and cost-sharing the LSST Program are the U.S. Nuclear Regulatory Commission (NRC), the Central Research Institute of Electric Power Industry (CRIEPI), the Tokyo Electric Power Company (TEPCO), the Commissariat A L'Energie Atomique (CEA), the Electricite de France (EdF), Framatome, the Korea Electric Power Corporation (KEPCO), the Korea Institute of Nuclear Safety (KINS) and the Korea Power Engineering Company (KOPEC).

The LSST was initiated in January 1990, and is envisioned to be five years in duration. Based on the assumption of stiff soil and confirmed by soil boring and geophysical results, the test model was designed to provide data needed for SSI studies covering: free-field input, nonlinear soil response, non-rigid body SSI, kinematic interaction, spatial incoherency and other effects. Some specific questions raised by LSST members concerning model design were on embedment effects, model stiffness, base shear and openings for equipment. This paper describes progress in site preparation, design and construction of the model and development of an instrumentation plan.

Introduction and Background

EPRI, in 1985, with the cooperation of Taipower, designed and constructed two scaled (1/4-scale and 1/12-scale) reinforced cylindrical concrete containment models in Lotung, Taiwan, for studying SSI under strong ground motion earthquakes (Tang, H.T., 1987). The soft soil site conditions at Lotung were ideal for invoking significant SSI, particularly for reduced scale models. The Lotung experiment was extensively instrumented to record free-field, SSI and structural response data (Tang, H.T., et al., 1987). Before the deployment of instruments, the U.S. NRC also cosponsored some low-level forced vibration tests (FVT) to evaluate dynamic characteristics of the soil-structure system (Tang, Y.K., et al., 1987).

Because of its extreme soft soil conditions, the Lotung experiment is limited in addressing certain SSI issues, such as effects of structural deformation, foundation uplifting, and particularly, the stiff soil conditions (EPRI, 1989 and Tang, H.T., et al., 1990). To confirm and expand the findings and analytical validations achieved in the Lotung program for more prototypical stiffer soil site applications, a stiff soil site experiment is needed. Specifically, one would like to establish a basis to address the following questions:

- Have Lotung results captured all key SSI behaviors directly applicable to prototypical nuclear power plants?
- Are conservatisms identified based on soft soil site data equally valid for stiff soil sites based on extrapolation using qualified analytical methods but lacking actual stiff soil data confirmation?
- How do soil property uncertainties affect SSI?
- Can one quantify uncertainties and resolve inconsistencies among different laboratory and in-situ soil characterization techniques?

Additionally, associated with the U.S. Standard Review Plan revision, resolution of Unresolved Safety Issue (USI) A-40, NRC raised several questions specifically pertaining to the Lotung results. Stiff site data and analysis can further substantiate answers to these questions.

With the cooperation of Taipower, a site meeting the desired stiff soil conditions was identified in Hualien, Taiwan. An international consortium has subsequently been formed to implement the LSST Program at Hualien for SSI research.

EPRI and Taipower are the organizers of the program and have the lead in planning and managing the program. Other organizations cofunding and cost-sharing the Hualien LSST Program are NRC, CRIEPI, TEPCO, CEA, EdF, Framatome, KEPCO, KINS and KOPEC.

Objectives

The objectives of the Hualien project can be summarized as follows:

- To obtain earthquake-induced SSI data at a stiff soil site having similar prototypical nuclear power plant soil conditions.
- To confirm the findings and methodologies previously qualified against the Lotung soft soil SSI data for prototypical plant site applications.
- To quantify results which were not available or lacked resolution in the Lotung study, such as structural deformation, torsional response, spatial incoherency effects and others.
- To quantify uncertainties and resolve inconsistencies among different laboratory and in-situ soil characterization techniques.
- To further validate and improve the technical basis for realistic SSI analysis approaches.
- To further support the resolution of USI A-40 issue, and provide a basis for improved and rational seismic design.

Site Conditions

The general geology in Hualien consists of massive unconsolidated, poorly bedded conglomerative composed of pebbles varying in diameters from 10 to 20 centimeters. Scoping geophysical and boring tests conducted in 1989 by Taipower and the Institute of Earth Sciences show that the shear wave velocity for the top layer of 100-meter depth is around 400 m/sec and for the layer below (up to about 7 km depth) is 1500 m to 1850 m/sec. The 50 m boring revealed that the top 5 m is of silty sand and the layer below consists of gravels of diameters varying from 3 cm to 7 cm.

Subsequent more detailed in-situ boring and geophysical testing by CRIEPI further confirmed the general geological formation and geotechnical behavior observed in the scoping investigation. Undisturbed samples cored from frozen soil ground are being tested in the CRIEPI laboratory for characterization of soil constitutive properties under both infinitesimal and finite strain conditions.

Test Model Design

The test model designed for the Hualien LSST program is almost a replica of the Lotung model, except that, for the purpose of lowering the soil-structure system frequency to 3 to 5 Hz because of the stiff soil foundation condition, the roof slab is enlarged and thickened to increase the mass. This similarity will make the comparison of results between the two experiments more compatible. Because of the stiffer foundation, the Hualien model is expected to experience slightly more deformation response than the Lotung case, although rocking will remain the dominant model dynamic response component.

Some additional criteria considered in the design of the model include:

- Embedment to be 25-30% with the model founding on the gravel layer.
- Design level ground motion to be 0.25 g with a synthesized spectrum based on local earthquake characteristics and wave propagation path conditions.
- Model response to be elastic at the design level ground motion.
- Model to be as heavy as possible to enhance soil foundation behavior investigation.

Instrumentation Layout

The instrumentation layout in Hualien is very similar to the one in Lotung. In the following, the layout of each category of instrument is briefly described.

Free-Field Instrumentation

For the free-field instrumentation, the layout is shown in Figure 1. There will be five three-component (EW horizontal, NS horizontal and vertical) accelerometers located on the ground surface along each arm. The first accelerometer will be located close to the outside wall of the containment model, with the next three located approximately 1/2, 1-1/2 and 2-1/2 diameters away, respectively. The fifth triaxial accelerometer will be about 5 diameters from the model wall. Because of site constraints, not all instruments may be lined along a straight arm. Nonetheless, orientation of each accelerometer component will be properly aligned.

There will be three downhole arrays as shown in Figure 1. All three will consist of four triaxial accelerometers with one at the interface of alluvium and gravel layers (~5m depth) and the others at depths of 1-1/2, 2-1/2 and 5 diameters from the ground surface. One of the downholes will be on the north-west arm (arm 1) below the most distant surface unit from the model and the second one will be below the most distant surface unit on the south-east arm (arm 2). The third downhole array

will be either directly under the model or at the edge of the model (in this case, under either arm 1, arm 2 or arm 3 gage depending on actual site conditions).

Soil-Structure Interface Instrumentation

Interface behavior between the containment model and the soil will be monitored:

- To determine soil bonding at the structure interface,
- To detect gaps at the interface due to uplift or rocking, and
- To investigate the maximum soil stress beneath the foundation.

Twenty-eight total pressure transducers will be installed on the model. The locations of these instruments are shown in Figures 2 and 3. Out of the nine pressure cells which will be placed under the foundation, eight will be placed forty-five degrees apart, just inboard of the containment shell perimeter, and the ninth one will be at the center of the foundation. Nineteen pressure cells will be placed on the outer surface of the containment shell at different depths of the embedded portion along five directions, north, south, east, west and north-west.

Structural Response Instrumentation

The containment model will be instrumented with triaxial accelerometers at locations shown in Figure 4 to record model response data. Four accelerometers along the east, west, south and north directions will respectively be placed on the basemat inside the containment adjacent to the containment shell and four will be on the roof top inward of the edge. Along the same directions, at mid-height between the ground level and the bottom of the roof, four accelerometers will be placed on the inner surface of the containment shell, and at the height of the ground level, two accelerometers will be placed 90° apart. One additional accelerometer will be installed on the rooftop near an opening designed for equipment transportation in and out of the containment.

Pore Pressure and Ground Settlement Measurement

Although liquefaction potential at Hualien is relatively low, pore pressure variation during earthquakes will nonetheless be measured to provide full understanding of site characteristics and ground response. Ground settlement will also be monitored to provide information for evaluating dynamic and static soil loading bearing characteristics.

CRIEPI will deploy four pore pressure gages, seven settlement gages and two inclinometers, according to the layout as shown in Figures 5 to 7. Also shown in the figures are four additional pore pressure gages, which will be installed to assure sufficient redundancy because of past high failure rates of pore pressure gages at

Lotung. The four additional pore pressure gages will be installed near the downhole accelerometers closest to the ground surface (1/2-diameter depth), two near the structure model along Arm 1 and Arm 3 and two away from the model at the end of Arm 1 and Arm 2 (5-diameter distance away from the model edge.)

Coordination With SMART-2

The layout of the Hualien free-field instrumentation as shown in Figure 1 is designed with the primary focus on SSI research only. Sensors deployed a distance away from the test model will furnish the "free-field" data in the sense that the data is not contaminated by the presence of the test model. The "free-field" data is normally used to define the control motion for SSI analysis. For those sensors in the close proximity of the test model, they provide data to evaluate the SSI effects on the "free-field" motion due to the presence of the test model. The recorded data serves as part of the technical basis in qualifying SSI analysis for defining foundation input motion. The Figure 1 layout also allows one to obtain data required for studying spatial incoherence of wave motions in a domain having the dimension of the order of magnitude of several test model foundation diameters. Furthermore, not only the surface spatial incoherence can be studied because of data from the three surface arms, the three downhole arrays will also yield data for evaluating spatial incoherence at depth.

However, to quantify and characterize strong motion characteristics which include source mechanism, wave attenuation, and spatial incoherence, strong motion network with larger spacing between instruments such as the ones in the SMART-1 array (Bolt et al., 1982) is required. Since SMART-2, a second strong motion array in Taiwan, is going to be deployed at Hualien by the Institute of Earth Sciences, Academia Sinica, coordination between the LSST array and the SMART-2 array has been established for mutual benefit.

Summary

The LSST program is moving along according to plan with a slight schedule delay because of lengthy process involved in obtaining construction permit for the test model. The facility is now scheduled for full operation in the fourth quarter of 1992.

References

- Bolt, B.A., Loh, C.H., Penzien, J., Tsai, Y.B., and Yeh, Y.T. (1982) Preliminary Report on the SMART-1 Strong-Motion Array in Taiwan. Report No. UCB/EERC-82/13. Earthquake Engineering Research Center, College of Engineering, University of California, Berkeley.

- EPRI (1989), Proceedings: EPRI/NRC/TPC Workshop on Seismic Soil-Structure Interaction Analysis Techniques Using Data From Lotung, Taiwan, Volumes 1 and 2, EPRI NP-6154.

- Tang, H.T., (1987) Large-Scale Soil-Structure Interaction. EPRI NP-5513-SR.

- Tang, H.T., et al (1987), A Large-Scale Soil Structure Interaction Experiment: Part I-Design and Construction, SMiRT 9, Vol. K2, pp. 177-182.

- Tang, H.T., et al. (1990), Lotung Large-Scale Seismic Experiment and Soil-Structure Interaction Method Validation, Nuclear Engineering and Design 123, pp. 397-412.

- Tang, Y.K., et al. (1987), A Large-Scale Soil-Structure Interaction Experiment: Part II-EPRI/NRC Research Program on Method Validation, SMiRT 9, Vol. K2, pp. 183-188.

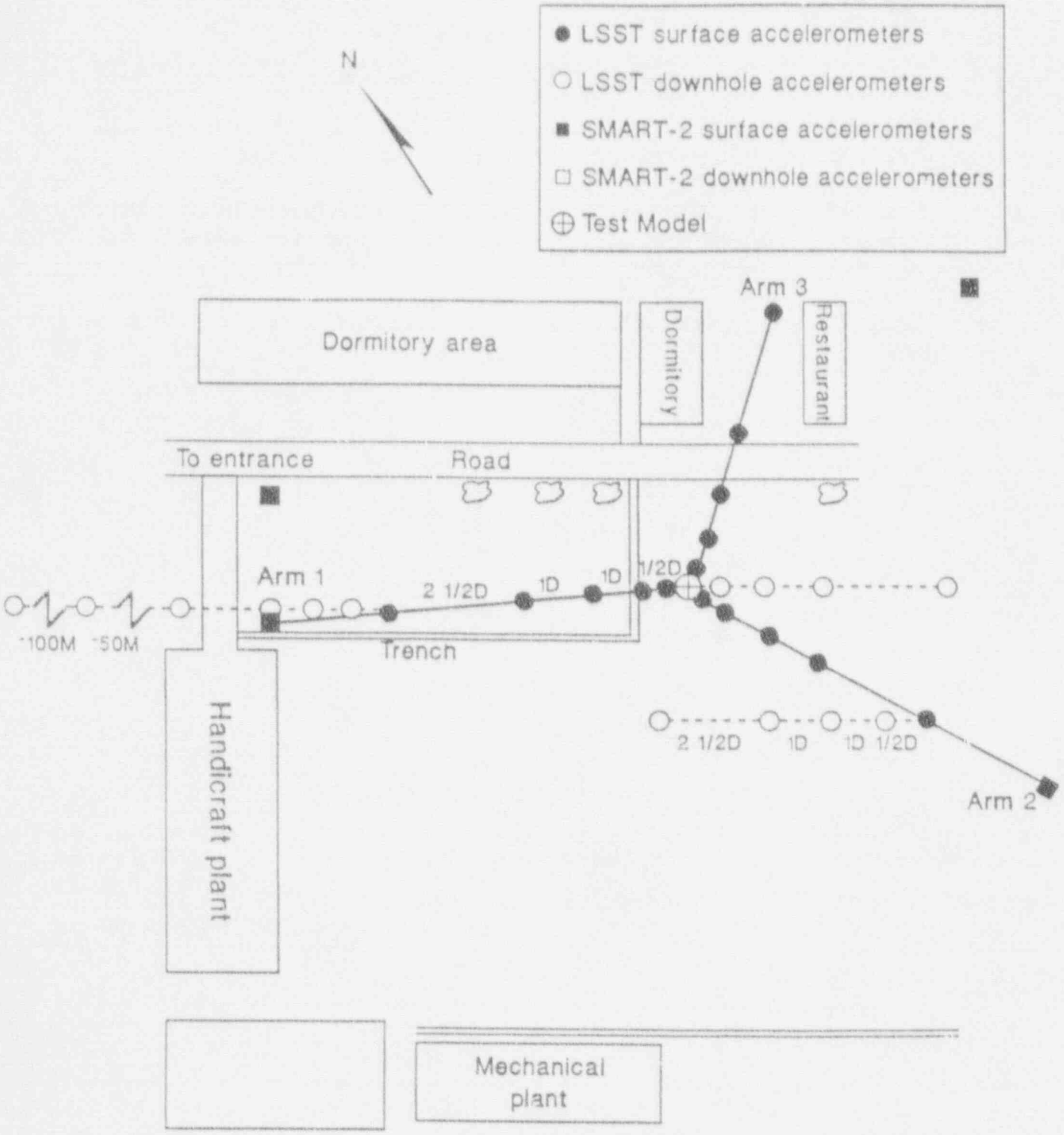

Figure 1. Free-Field Instrumentation Layout for the Hualien LSST Project.

0771.06

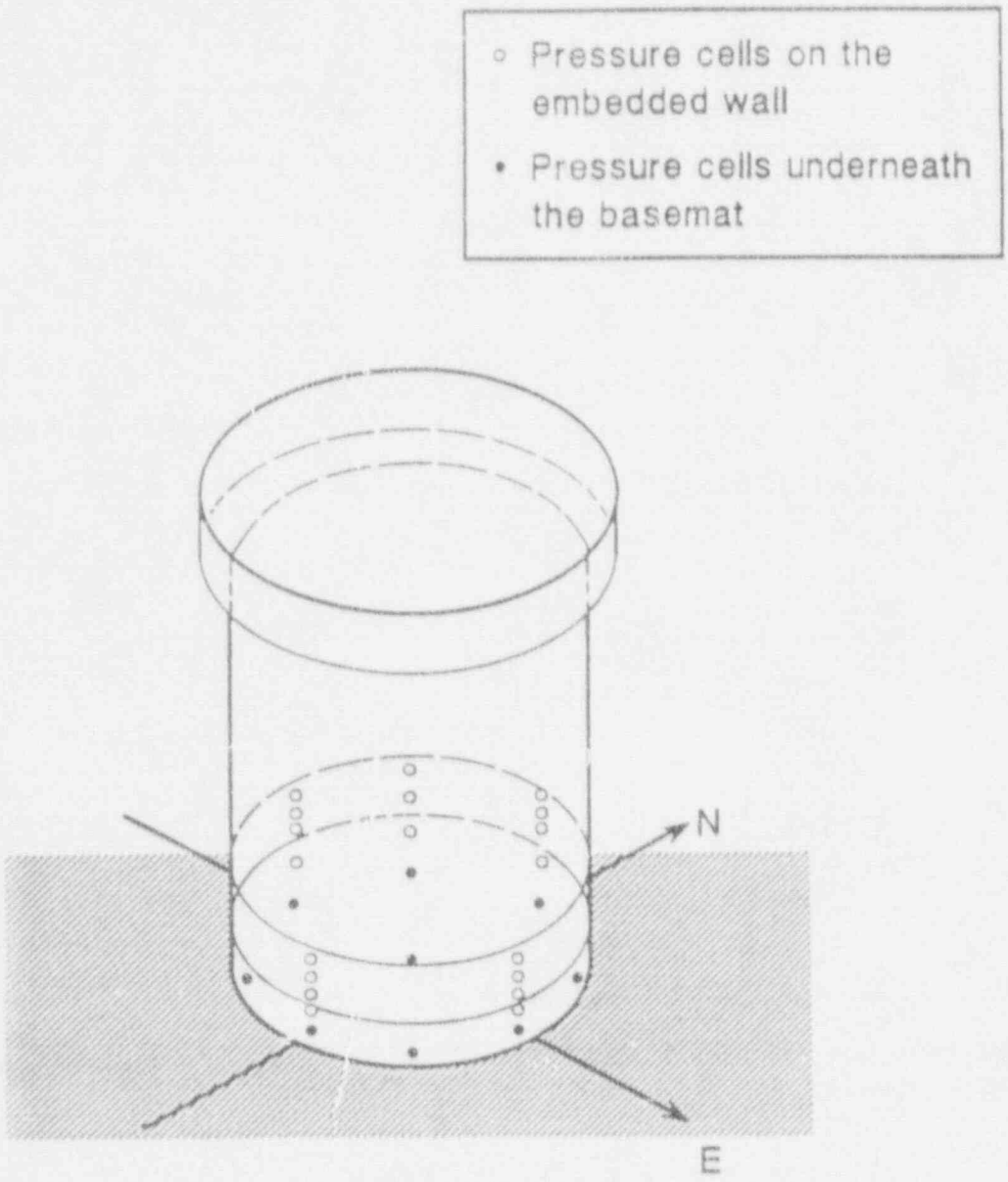

Figure 2. Location of Pressure Cells on the Hualien Containment Model.

0771.02

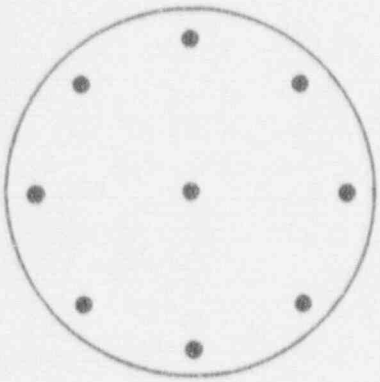

(a) Pressure transducers at the bottom of the foundation

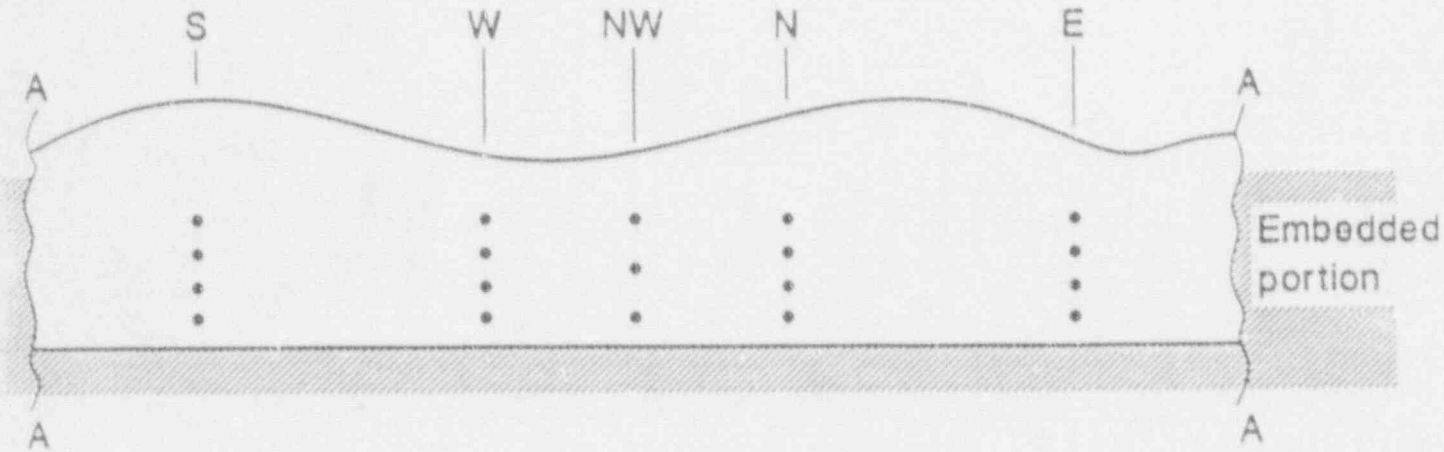

(b) Pressure transducers on the embedded portion of the cylindrical wall

Figure 3. Pressure Transducers Layout.

0771.01

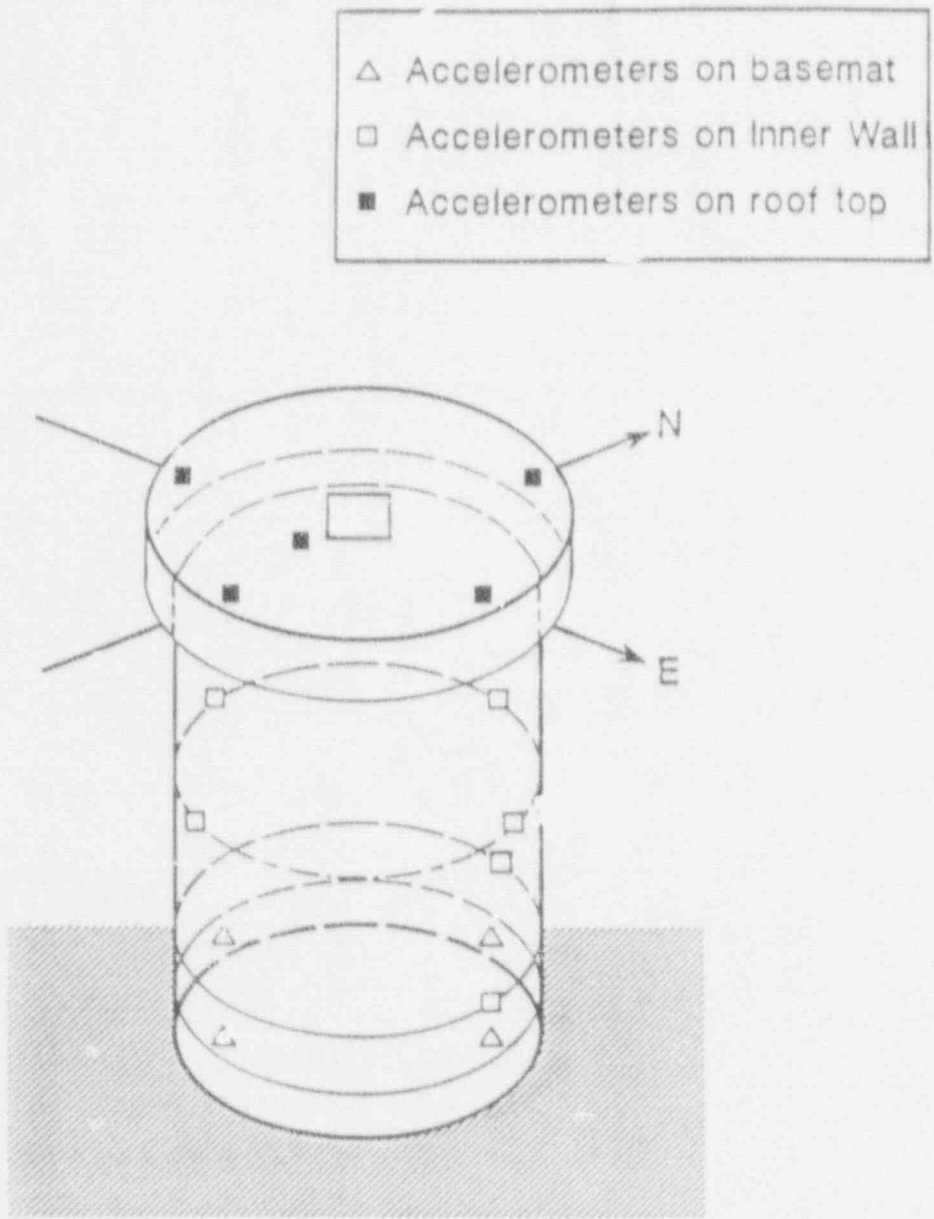

Figure 4. Location of Triaxial Accelerometers on the Hualien Containment Model.

0771.03

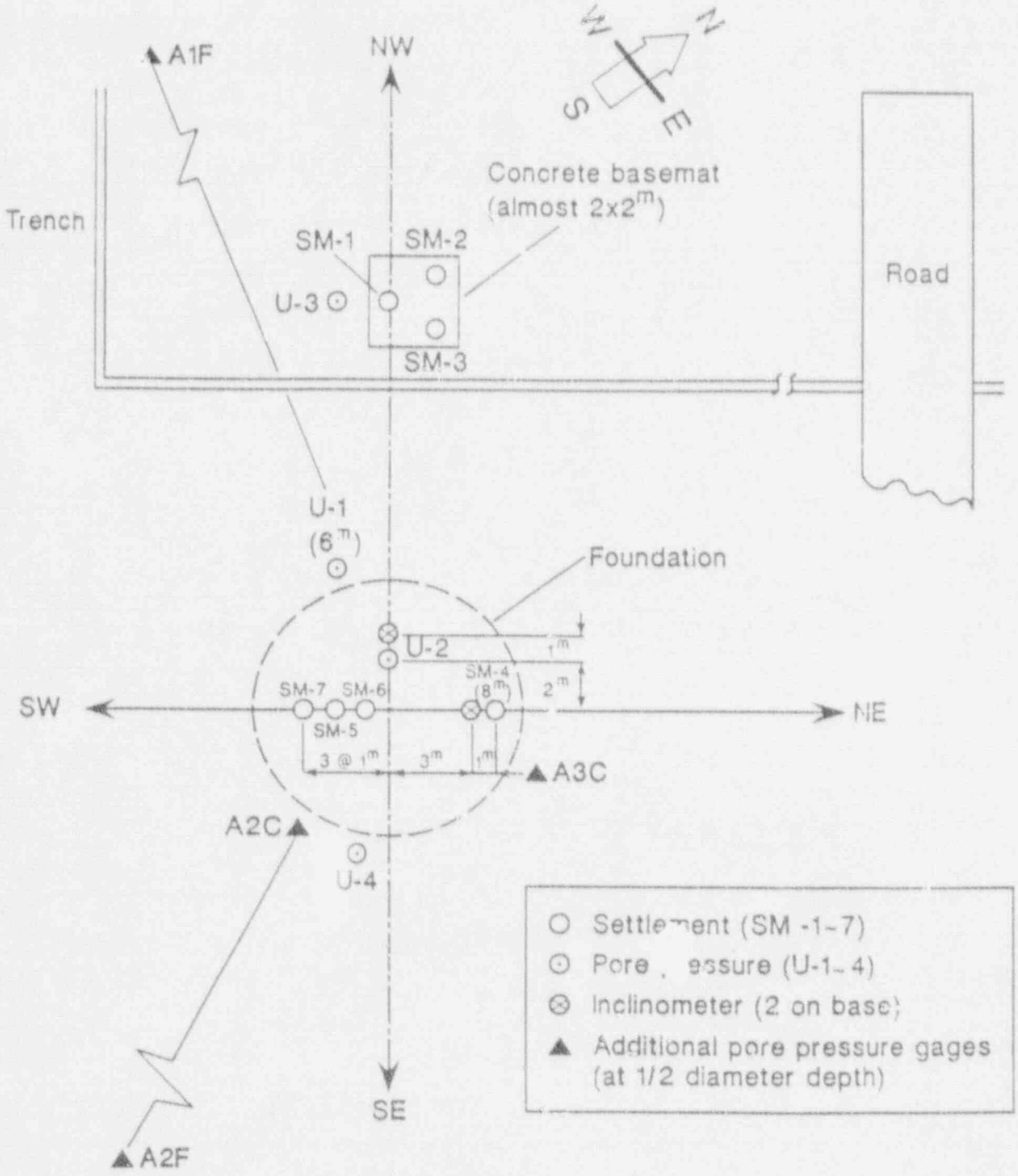

Figure 5. Plane View of Pore Pressure and Settlement Gages Layout.

0771.05

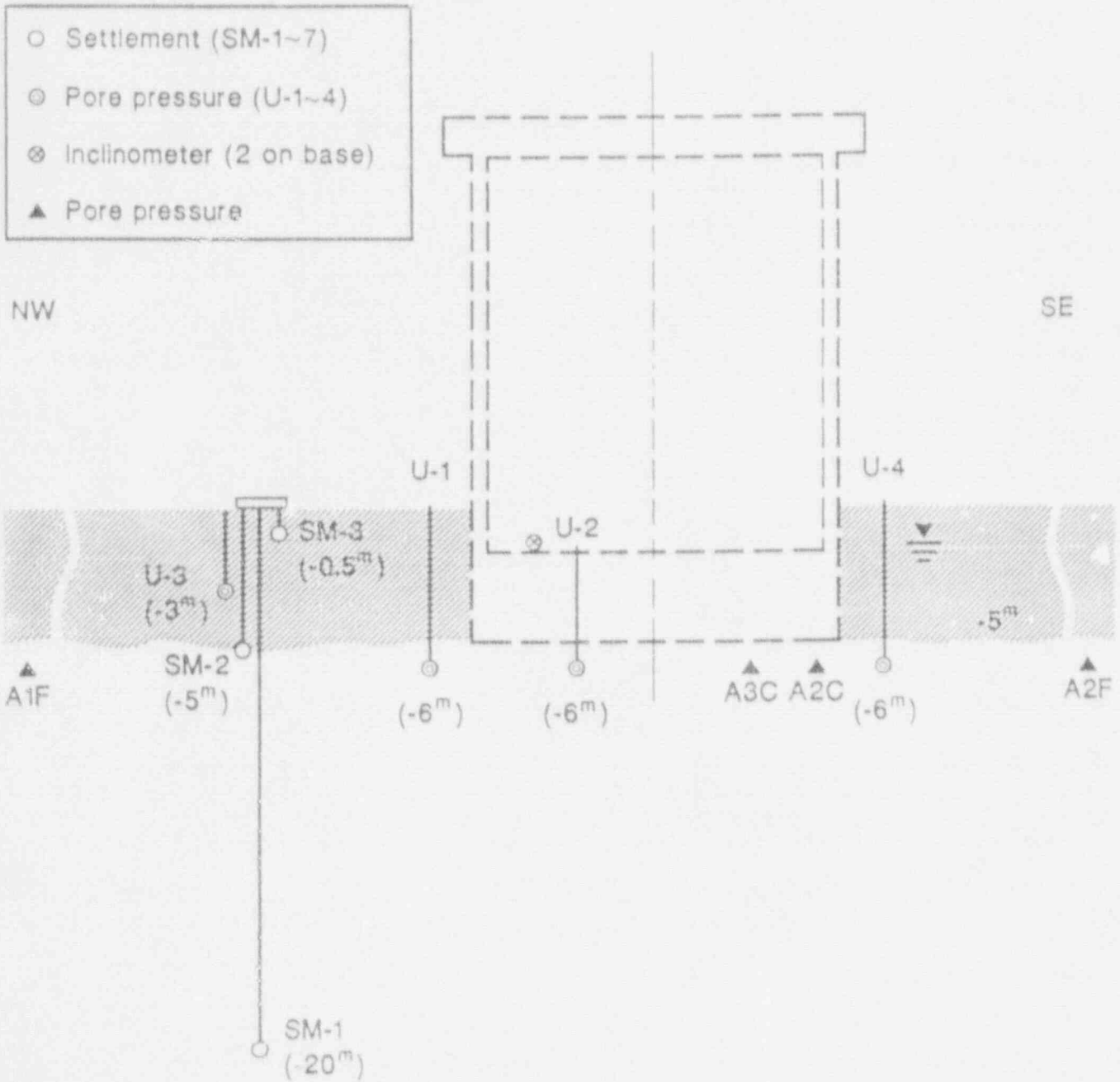

Figure 6. NW - SE Cross-Sectional View of Pore Pressure and Settlement Gages.

0771.04

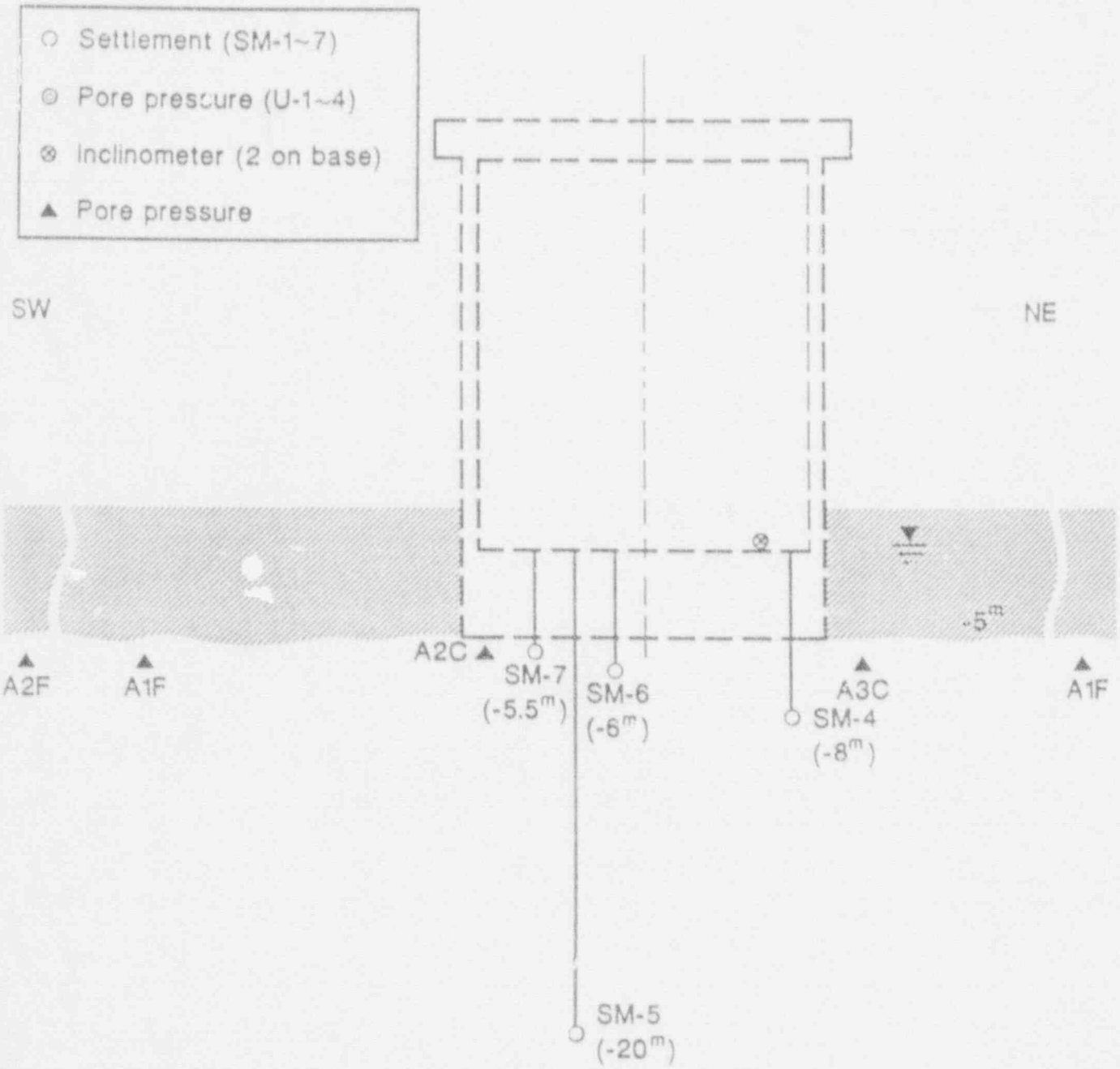

Figure 7. SW - NE Cross-Sectional View of Pore Pressure and Settlement Gages.

0771.04A

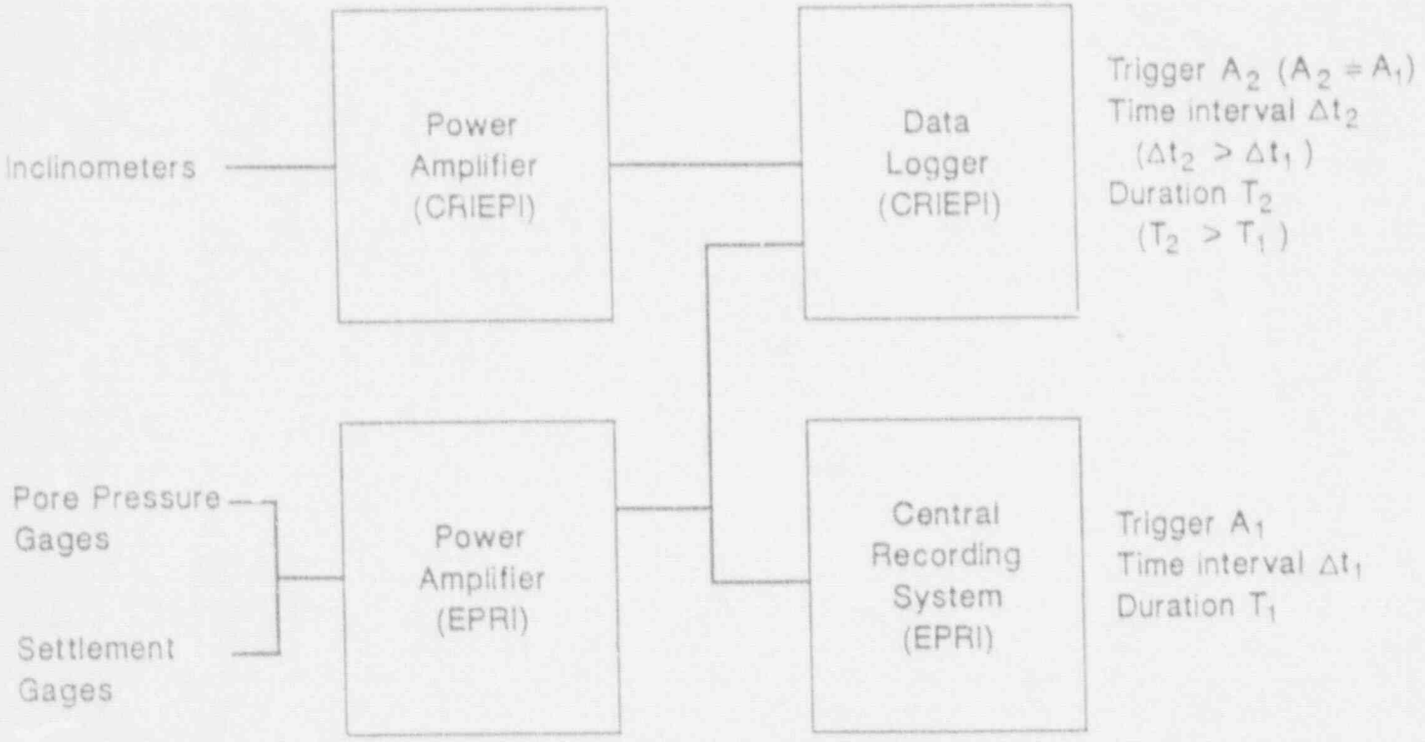

Figure 8. Data Recording Arrangement for Pore Pressure Gages, Settlement Gages and Inclinometers.

0771.07

CONTAINMENT PERFORMANCE EXPERIMENTS UNDER SEVERE ACCIDENT LOADINGS[1]

M. B. Parks
B. L. Spletzer
L. D. Lambert
J. R. Weatherby

Sandia National Laboratories
Albuquerque, NM 87185

Abstract

This paper provides a summary and status report for two ongoing experimental programs. The purpose of each program is to determine the behavior of certain components of the containment pressure boundary when subjected to severe accident conditions. The first program is investigating the effect of various parameters on tearing of the steel liner in reinforced concrete containments. The second will attempt to determine if worst-case containment loading conditions are capable of causing leakage through piping penetration bellows. The liner test program is almost complete; however, the bellows tests have not yet begun. Therefore, the emphasis of the paper is on the liner experiments. The research activities described herein are a part of the Containment Integrity Programs, which are managed by Sandia National Laboratories for the U.S. Nuclear Regulatory Commission.

1.0 INTRODUCTION

The performance of the containment building in a nuclear power plant is a critical factor in determining the consequences of a severe accident. As an example, the consequences of the Three Mile Island accident may be compared to that at Chernobyl. Because of the importance of the containment, the Nuclear Regulatory Commission began a series of programs about ten years ago to investigate containment integrity under severe accident conditions. These programs are collectively known as the Containment Integrity Programs. The main goal of this work is to develop a complete set of validated methods for estimating the pressure capacity, at elevated temperatures, of light water reactor containment buildings.

To accomplish this goal, a series of scale model containment buildings have been tested to failure by internal overpressurization at ambient temperature. A 1:8-scale steel containment model [1] and a 1:6-scale model of a reinforced concrete containment [2] have been tested at Sandia. Also, a 1:10-scale prestressed concrete containment model has been tested in the United Kingdom under a cooperative agreement between the NRC, UKAEA, and others [3].

---

[1] This work was supported by the U. S. Nuclear Regulatory Commission and performed at Sandia National Laboratories, which is operated by the U.S. Department of Energy under contract number DE-AC04-76DP00789.

All of the models were heavily instrumented so that the test results could be compared to pre- and posttest analyses. In this way, the adequacy of existing analytical methods to predict containment behavior has been assessed, and improvements have been made [4-9].

The number and size of penetrations included in the containment models were limited by their scale so an adequate representation of the wide variety of penetration designs could not be included in the containment models. Therefore, several other research programs have been undertaken to better understand the behavior of penetrations under severe accident conditions. These programs have included tests of a full-size personnel airlock [10] and electrical penetration assemblies (EPAs) [11], a 1:6-scale pressure unseating equipment hatch [12], compression seals and gaskets [13], and inflatable seals [14].

As a continuation of the Containment Integrity Programs, there are two ongoing research activities. One program includes a series of experiments to better understand the effects of various parameters on tearing of steel liners in reinforced and prestressed concrete containments. Pretest analyses have been conducted for these tests. The predicted results are being compared to those observed in the tests in order to determine the adequacy of existing analytical methods to predict liner tearing.

The other ongoing program is investigating the performance of containment penetration bellows when subjected to severe accident loadings. Bellows are used at the piping penetrations of steel containments to minimize the loadings imposed on the containment shell that are caused by differential movement between the pipe and the wall of the containment. These types of bellows are an integral part of the containment pressure boundary. During accident conditions, the bellows may be subjected to combinations of axial compression, lateral offset, internal pressure, and elevated temperatures. The purpose of the test program is to determine the types of load combinations necessary to cause leakage past typical containment penetration bellows.

The liner tearing experiments are almost complete at the time of writing; however, the bellows tests have not yet begun. Therefore, the remainder of this paper will be devoted to the liner tearing experiments.

2.0 EXPERIMENTS TO INVESTIGATE LINER TEARING IN CONCRETE CONTAINMENTS

2.1 Motivation For Test Program

A 1:6-scale reinforced concrete containment model has been internally pressurized to failure at Sandia as a part of the Containment Integrity Programs. A cross-section of the model is shown in Figure 1. As is typical in reinforced concrete containments in the U.S., a steel liner on the inside of the wall formed the containment pressure boundary. Studs were welded to the outside of the liner and embedded in the concrete wall to anchor the liner to the wall.

The design pressure for the model was 46 psig. During the test, the internal pressure was slowly increased using nitrogen gas up to a maximum pressure of 145 psig. At that point, leakage through tears in the steel liner became so large that the internal pressure could not be increased further. The rate of leakage grew very rapidly from almost no leakage at 138 psig to the maximum amount at 145 psig. At the maximum test pressure, the rate of leakage was in excess of 4000 scfm, which is 40% of the model's volume per minute.

The relative location of the tears in the liner are shown in Figure 2. Note that all of the tears are adjacent to penetrations along the circumference. This is because the highest strains in an internally pressurized cylinder occur in the circumferential direction. Posttest examination also revealed that each tear was directly associated with a stud.

The primary liner tear occurred adjacent to a thickened insert plate at a piping penetration. The majority of the leakage was caused by this tear. A photograph of the tear is shown in Figure 3. The tear was approximately 22 inches in length and passed through the first row of studs in the liner adjacent to the insert plate. The actual location of the tear was along the edge of the studs on the insert plate side.

Figure 4 shows a horizontal section of the wall through the area in which the tear occurred. For simplification, only the circumferential (hoop) reinforcement is shown in this figure. The figure shows the thickened insert plate (3/16"), the liner plate (1/16"), and the relative location of the studs that are attached to both the insert plate and liner. The shank diameter of the studs is approximately 0.15 inches and they are about 3/4 of an inch in length.

It is believed that the liner tear at this location was caused by two factors. One is the difference in thickness between the insert plate and the liner plate. The other is the load imposed on the liner by the studs that are located near the thickness discontinuity.

As the model was pressurized, the walls moved radially outward and were stretched in the hoop direction. Because the insert plate is thicker, it tends to stretch much less than the thinner liner. The hoop reinforcement is continuous through this region, so it stretches uniformly. As a result, there is a natural "slippage" between the liner and the concrete wall. The studs, which are embedded in the concrete, want to follow the motion of the concrete wall. However, because the base of the studs is welded to the liner, the studs resist this slippage and by doing so impose a local "point" load on the liner at their base. It is believed that this additional liner load caused by the studs is the main reason for the liner tear at this location.

Before the test of the 1:6-scale containment model, several organizations conducted pretest analyses to determine the expected model response and the expected failure mode [6]. Although liner tearing was postulated as a possible mode of failure by some organizations, no one predicted the above mechanism that led to the primary liner tear. Many, if not most, experts felt that the large amount of total elongation of the liner (about 25%) would be sufficient to prevent extensive liner tearing before another mode of failure was realized.

After the test, additional detailed analyses of the region around the main liner tear were conducted. These analyses were able to reproduce the mechanism that caused this tear. In Reference [5], strains as high as 26% (about 15 times the free-field strain of 1.5-2.0%) were computed at the base of the studs for the maximum pressure level of 145 psig. This type of strain concentration is much higher than would be caused solely by the change in thickness between the liner and insert plate and clearly shows the importance of the studs in causing the principal liner tear.

A plane stress finite element method was used in this analysis to model the behavior of the liner anchorage system. Because of the good agreement with the test result, it was felt that the parameters of primary importance could be adequately represented using a plane stress model. However, there was only one data point, the 1:6-scale model, that could be used to validate the analytical method. For this reason, a series of "separate effects" tests were designed and are now being conducted.

The purpose of these tests is to further investigate the effect of various parameters on liner tearing and to provide additional data that can be used for validating analytical methods. The final objective of this program is to develop a validated method to predict the initiation of liner tearing for reinforced and prestressed concrete containments with differing anchorage and discontinuity details.

An outline of the test program, as well as a brief description of the available test results, is provided below. Because the tests have only been recently completed, a detailed presentation of the results will be deferred to later publications for this program.

2.2 Description of Liner Test Program

The liner tearing test program consists of two phases. The primary purpose of the Phase 1 tests is to determine the effect of preload in the liner on liner tearing. The main objective of the Phase 2 tests is to further examine the mechanism that caused liner tearing in the 1:6-scale reinforced concrete containment model using uniaxial test specimens.

Because the dominant strains at failure in the 1:6-scale model were in the hoop direction, it was felt that the important liner tearing parameters could be adequately investigated using uniaxial tensile specimens. Therefore, all of the liner specimens were or will be tested in uniaxial tension. It is much easier and less expensive to conduct uniaxial tests than trying to reproduce the actual bi-axial strain state that was present in the 1:6-scale model.

Pretest analyses, using the same plane stress approach as previously applied to the 1:6-scale containment model, have been performed for each of the liner tests. The results of these analyses are being compared to the test results to further determine the adequacy of plane stress methods for predicting liner tearing.

2.2.1 Phase 1 Tests

Prior to the test of the 1:6-scale containment model, it was generally accepted that the studs used on the liner of reinforced concrete containments were not strong enough to tear the liner. This conclusion was based on the results of construction tests of stud anchorage systems.

During construction, what is known as a "hammer" test is normally performed to determine the adequacy of the connection of the stud to the liner. For this test, a stud is welded to the liner and a hammer is used to bend the stud. In all known tests of this type, the liner is never torn. If a failure occurs, it is in the connection of the stud to the liner.

Stud shear tests were also conducted at Sandia during construction of the 1:6-scale model to determine the shear stiffness and total shear strength of the studs. In these tests, studs were welded to the liner material and then the studs were embedded in a fixed block of concrete. A tensile load was applied to the liner which induced a shear load on the studs at their connection to the liner. The liner load was increased until failure of the specimens. In every one of these tests, the studs failed in shear without tearing the liner.

There is one critical difference between the above construction tests and the test of the 1:6-scale model. That difference is that a substantial liner preload existed in the 1:6-scale model at the time of the liner tear; however, there was no preload in the liner for the construction tests. The preload in the 1:6-scale model was produced primarily by the overall "free-field" hoop strain, which was about 1.5 to 2.0% when the main liner tear occurred. As shown in Figure 6, this

amount of strain is sufficient to yield the liner material.

The purpose of the phase 1 test series was to further demonstrate the importance of liner preload on liner tearing and also to determine the adequacy of plane stress finite element methods to predict liner tearing.

The test specimen configuration used for these tests is shown in Figure 5. The overall length of the specimen is 60 inches. Liner segments are used on each side of the specimen for symmetry. A "dog-bone" shape is used to ensure that the maximum stress will occur at the location of the studs while minimizing the strain concentration caused by the reduced section. The liner width varies from 24" at the ends to a minimum of 8" at mid length. The sides of the liner are cut at a radius of 45". A single row of four studs is attached to each liner segment at mid length. The spacing between the studs is 2", the same as used around penetrations in the 1:6-scale model. These studs are embedded in a common block of concrete, which is 10" thick. The specimens are constructed of the same types of materials as used in the 1:6-scale model. The liner thickness (1/16") and stud size is also the same as in the 1:6-scale model.

A total of five Phase 1 tests were conducted. In the first test, no liner preload was applied. In the remaining four tests, uniaxial tension was initially applied to the specimens to induce preload in the liner. A constant amount of preload was maintained throughout each of these tests. After the desired amount of preload was applied, shear loads were imposed on the studs by pulling on the concrete block. The stud loading was slowly increased until either the studs failed in shear or the liner was torn by the studs.

A summary of the applied liner preloads and resulting failure modes is provided in Table 1. The first tests without liner preload were similar to the previous shear tests conducted at Sandia. As expected, the studs failed in shear without tearing the liner. The next four tests were conducted with liner preloads ranging from in engineering stress from 60 to 70 ksi. An engineering stress-strain curve for the liner is shown in Figure 6 for reference purposes. The yield stress for the liner is about 52 ksi and the ultimate strength is approximately 74 ksi. Thus, the applied preloads were all well into the inelastic range for this material.

Referring to Table 1, the test results indicate that a liner preload in the range of 63 to 65 ksi is required in order for the studs to be "strong enough" to tear the liner. At preloads of 65 ksi or more, the liner was torn by the studs before they failed in shear. However, for preloads of 63 ksi or less, the studs failed in shear before tearing the liner. Again, for these preloads, the studs were not strong enough to tear the liner.

Before the tests, plane stress analyses were conducted to attempt to predict the amount of liner preload necessary to enable the studs to tear the liner. Plane stress continuum elements were used to model the liner. The studs were idealized as simple spring elements. The spring stiffness was based on the previous stud shear tests that were conducted at Sandia. The predicted failure modes from these analyses are also shown in Table 1.

Note that three different stud strengths were assumed for the analyses. A range of stud strengths was used since previous stud tests had indicated considerable scatter in the stud strength data. The mean stud strength from the previous tests is about 1450 pounds.

The analyses indicated that, if a stud strength of 1300 pounds is assumed, the studs will not be strong enough to tear the liner, even at the maximum tested preload of 70 ksi. For a stud strength of 1450 pounds, the transition from stud failure to liner tearing was predicted to be between 65 and 70 ksi. Finally, this transition is expected to occur between liner preloads of 60 and 65 ksi, if a stud strength of 1600 pounds is assumed.

When comparing the observed failure modes to those predicted by analyses, it appears that the pretest analyses were reasonably accurate. In fact, if the actual stud strength was 1600 pounds, the predicted failure modes are in excellent agreement with the test results.

In summary, these tests and associated analyses have shown the importance and sensitivity of stud strength and liner preload on liner tearing. If larger diameter and thus stronger studs were used, it would be expected that less liner preload would be required for the studs to be able to tear the liner. Of course, smaller and weaker studs would require more liner preload.

The difference is significant in the consequences of liner tearing and stud failure. If the studs fail in shear, it is of little consequence to the containment integrity; however, if the liner is torn, the leak integrity of the containment will be compromised. As was the case for the 1:6-scale model, it is possible that the ultimate failure mode of the containment pressure boundary could be leakage through liner tears.

2.2.2 Phase 2 Tests

Phase 2A Tests

The sole purpose of the Phase 2A tests was to investigate the effect of the change in thickness and the weld between the liner and insert plate on the capacity of the liner. Immediately after the 1:6-scale model test, some experts speculated that the primary reason for the main liner tear was the strain concentration caused by the change in thickness. Also, it was postulated that the heat affected zone associated with the weld could have been a factor in causing the main liner tear.

The configuration of the Phase 2A test specimens is shown in Figure 7. In order to isolate the effects of the change in thickness and the weld, only the liner and insert plate are included in these specimens. The same types of materials and welding methods are used for these specimens as used in the 1:6-scale model. The overall length of the specimen is 52". It is composed of 17"-long segments of insert plate on each end welded to a common 18"-long liner section. The width of the specimen is 10".

A total of three tests were conducted. During the tests, the specimens were pulled in uniaxial tension until a tear occurred in the liner. Failure initiated in the liner near the weld in some of the specimens and near mid-length of the specimen, well away from the weld, in others. However, the observed tensile strength of the liner and the total elongation were very similar for all of the tests. The liner elongation and strength properties from these tests were also very similar to those obtained from tensile coupon tests for the liner material.

Based on these test results, it can be concluded that the change in thickness between the liner and insert plate does not significantly reduce the capacity of the liner. Also, the weld that connects the insert and liner plates does not affect the liner capacity. This conclusion further supports the theory that the studs were an essential contributor to the main liner tear.

Phase 2B Tests

The objective of the Phase 2B tests was to determine if the mechanism that caused the main liner tear in the 1:6-scale model could be reproduced using a uniaxial tensile specimen. The Phase 2B specimen represents a circumferential slice of the model, ignoring curvature, through the location where the main liner tear occurred. Thus, the tensile stress applied to the specimen represents the hoop stress in the 1:6-scale model.

The specimen design that was used for these tests is shown in Figure 8. Liner/insert plate sections are used on both sides of the specimen for symmetry. The overall specimen length is 44". The insert plates are 14-1/2" in length and are welded to a common 15"-long section of liner material. The width of the liner and insert plate and the remainder of the specimen is 10 inches. The total depth of the specimen is 15 inches.

Studs are attached to the liner and insert plate at the same spacing (2" in both directions) as in the 1:6-scale model. The studs are embedded in a common block of reinforced concrete. Ten No. 6 reinforcing bars are included in the concrete. This amount of reinforcement provides the same ratio of liner to reinforcing bar area as in the 1:6-scale model. Also, the same types of materials and welding methods are used in the Phase 2B specimens as in the 1:6-scale model.

During the tests, the reinforcing bars and liner/insert plate are pulled uniformly in uniaxial tension. The applied tension is slowly increased until failure of the specimen. At the time of writing, two of the planned three tests have been conducted. In each of the completed tests, failure occurred as a result of a tear in the liner at the first row of studs adjacent to the insert plate. This is the same relative location as the main liner tear in the 1:6-scale model. Thus, it appears that these initial tests have been successful in reproducing the mechanism that caused the tear in the 1:6-scale model.

Pretest finite element analyses were also conducted for these specimens. A plane stress approach was again employed with the liner and insert plate modeled with plane stress continuum elements. The studs were idealized as spring elements with one end connected to the liner or insert plate and the other connected directly to the reinforcing bar. In this way, it is assumed that the concrete is 100% effective in forcing the head of the studs to follow the motion of the reinforcement as the specimen deforms. This is perhaps a conservative assumption for predicting liner tearing, but it is necessary to allow a relatively simple analysis of this complex problem.

Because the tests were only recently completed, there has not yet been time to make a detailed comparison of the test results to the pretest analyses. However, early comparisons indicate that there is relatively good agreement between the predicted and observed results. The total specimen load required to cause a liner tear is about 15% higher than predicted. One possible explanation is that, in the actual test specimen, the concrete is not 100% effective in forcing the head of the studs to follow the movement of the reinforcement. If this is the case, it would explain why more specimen load would be required than was predicted to produce enough slippage to cause the liner tear.

More detailed comparisons between the predicted and observed response will be conducted and, if necessary, improvements will be made in the analytical method.

Phase 2C Tests

The final series of tests will investigate the effect of containment pressure on the mechanism that caused the main liner tear in the 1:6-scale model. To accomplish this, the same specimen design and test procedure as used for the Phase 2B tests will be used. In addition, uniform pressure will be applied to the liner surface on each side of the specimen. The pressure will be increased during the tests such that the relationship between containment pressure and hoop strain is the same as that which occurred during the 1:6-scale model test.

It has been speculated that the containment pressure will increase the amount of friction between the liner and concrete wall and, thus, reduce the amount of load transfer that is carried by the studs. If this is true, then the total amount of specimen load required to tear the liner

should be larger than for the 2B specimens.

The Phase 2C tests will be conducted after completion of the 2B tests. Completion of the 2C tests will mark the end of the currently planned liner tearing tests.

3.0 SUMMARY

Results of the completed liner tearing tests have successfully extended the understanding of the effect of various parameters on liner tearing. The Phase 1 tests verified the importance of initial liner preload on liner tearing. These tests showed that significant initial liner strain (or preload), well into the inelastic strain range, is necessary for the studs used in the 1:6-scale model to be "strong enough" to tear the liner in that model. If the studs had been significantly weaker, the mode of failure could have been changed from liner tearing, which caused the failure of the 1:6-scale model, to stud failure, which would not cause any leakage through the liner. Also, plane stress finite element analyses were successful in indicating the approximate amount of liner preload required to enable the studs to tear the liner.

The Phase 2A tests proved that the change in thickness and the weld between the insert plate and liner, acting alone, do not appreciably reduce the liner's total elongation or tensile capacity. Thus, it was further confirmed that the studs are an essential ingredient in causing the liner tear. Finally, the Phase 2B tests have successfully shown that the mechanism that caused the main liner tear in the 1:6-scale model can be reproduced in a uniaxial tensile specimen. This is significant in that it seems to indicate that only in-plane phenomena are significant and that out-of-plane factors do not have to be included in analytical models used to predict this type of mechanism. This is further demonstrated by the relatively good agreement between pretest plane stress analyses for the 2B specimens and the test results.

4.0 REFERENCES

[1] *Koenig, L. N., "Experimental Results for a 1:8-Scale Steel Model Nuclear Power Plant Containment Pressurized to Failure," NUREG/CR-4216, SAND85-0790, Sandia National Laboratories, Albuquerque, NM, December 1986.*

[2] *Horschel, D. S., "Experimental Results from Pressure Testing a 1:6-Scale Nuclear Power Plant Containment," NUREG/CR-5121, SAND88-0906, Sandia National Laboratories, Albuquerque, NM, December 1991.*

[3] *Palfrey, J. and Smith, J. C. W., "Ultimate Load Test of a 1/10th Scale Model Prestressed Concrete Containment, Transactions of the Eleventh International Conference on Structural Mechanics in Reactor Technology, Volume H10/6, Tokyo, Japan, August 1991.*

[4] *Clauss, D. B., "Comparison of Analytical Predictions and Experimental Results for a 1:8-Scale Steel Containment Model Pressurized to Failure", NUREG/CR-4209, SAND85-0679, Sandia National Laboratories, Albuquerque, NM, July 1985.*

[5] *Weatherby, J. R., "Posttest Analysis of a 1:6-Scale Reinforced Concrete Reactor Containment Building," NUREG/CR-5476, SAND89-2603, Sandia National Laboratories, Albuquerque, NM, February 1990.*

[6] Clauss, D. B., (ed.), "Round Robin Pretest Analyses of a 1:6-Scale Reinforced Concrete Containment Model Subject to Static Internal Overpressurization," NUREG/CR-4913, SAND87-0891, Sandia National Laboratories, Albuquerque, NM, April 1987.

[7] Clauss, D. B., (ed.), "Round-Robin Analysis of the Behavior of a 1:6-Scale Reinforced Concrete Containment Model to Failure: Posttest Evaluations," NUREG/CR-5341, SAND89-0349, Sandia National Laboratories, Albuquerque, NM, October 1989.

[8] Wilkes, M., "Finite Element Analysis of a 1/10 Scale Prestressed Concrete Reactor Containment Vessel Subject to Overpressurization," Proceedings of the Second International Conference on Containment Design and Operation, Toronto, Canada, 1990.

[9] Dameron, R. A., Rashid, Y. R., Sullaway, M. F., "Pretest Predictions of a 1:10-Scale Model Test of the Sizewell B Containment," NUREG/CR-5671, SAND90-7117, Sandia National Laboratories, Albuquerque, NM, (to be published).

[10] Julien, J. T., and Peters, S. W., "Leak and Structural Test of Personnel Airlock for LWR Containments Subjected to Pressures and Temperatures Beyond Design Limits," NUREG/CR-5118, SAND88-7155, Sandia National Laboratories, Albuquerque, NM, May 1989.

[11] Clauss, D. B., "Severe Accident Testing of Electrical Penetration Assemblies," NUREG/CR-5334, SAND89-0327, Sandia National Laboratories, Albuquerque, NM, November 1989.

[12] Parks, M. B., Walther, H. P., and Lambert, L. D., "Evaluation of the Leakage Behavior of Pressure-Unseating Equipment Hatches," Proceedings of the 18th Water Reactor Safety Meeting, NUREG/CP-0114, Washington, DC, 1990.

[13] Brinson, D. A., and Graves, G. A., "Evaluation of Seals for Mechanical Penetrations of Containment Buildings," NUREG/CR-5096, SAND88-7016, Sandia National Laboratories, Albuquerque, NM, August 1988.

[14] Parks, M. B., "Evaluation of the Leakage Behavior of Inflatable Seals Subject to Severe Accident Conditions," NUREG/CR-5394, SAND89-1454, Sandia National Laboratories, Albuquerque, NM, November 1989.

Table 1
Predicted and Observed Results
of the Phase 1 Tests

	Stud Strength (lbs)	Liner Preload (ksi)				
		None	60	63	65	70
Predicted Failure Mode	1300	Stud	Stud	----	Stud	Stud
	1450	Stud	Stud	----	Stud	Liner
	1600	Stud	Stud	----	Liner	Liner
Observed Failure Mode	------	Stud	Stud	Stud	Liner	Liner

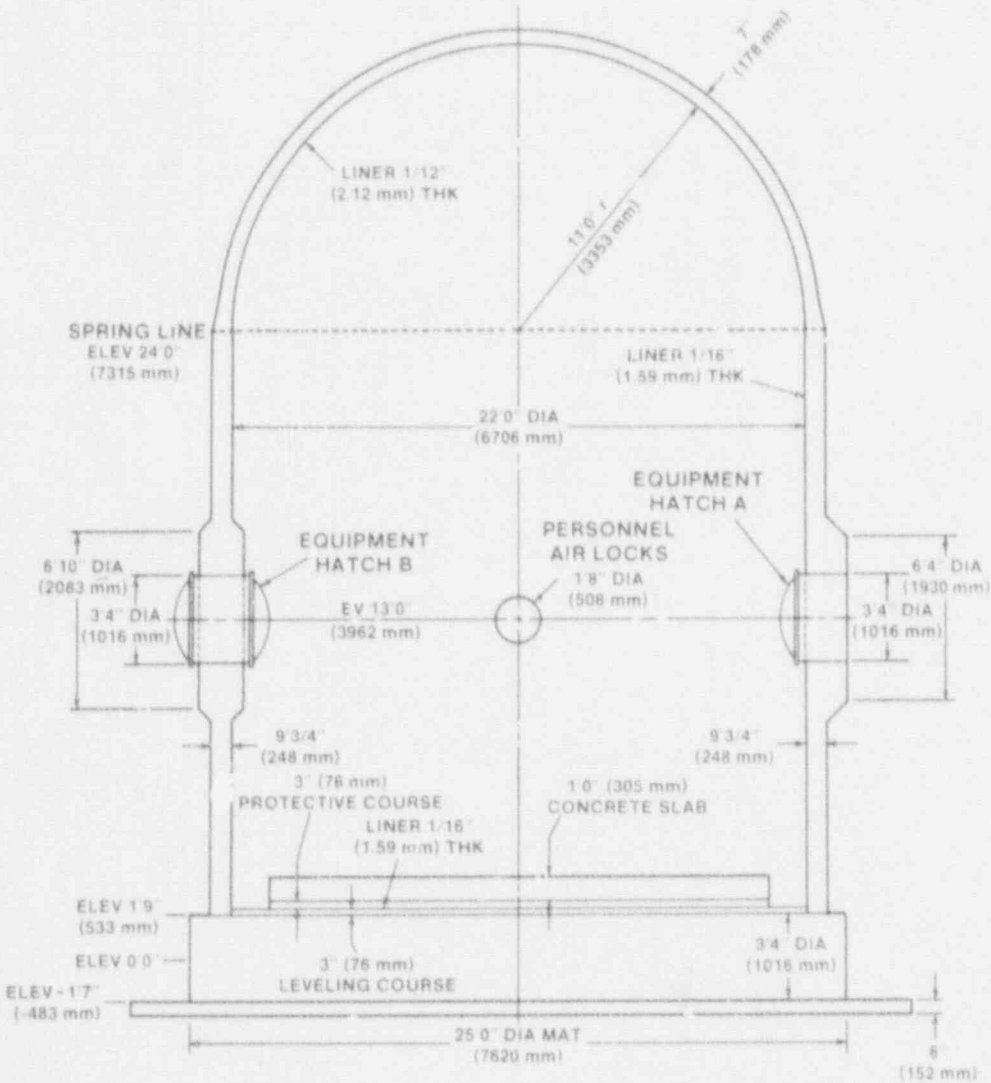

Figure 1. 1:6-Scale Reinforced Concrete Containment Model

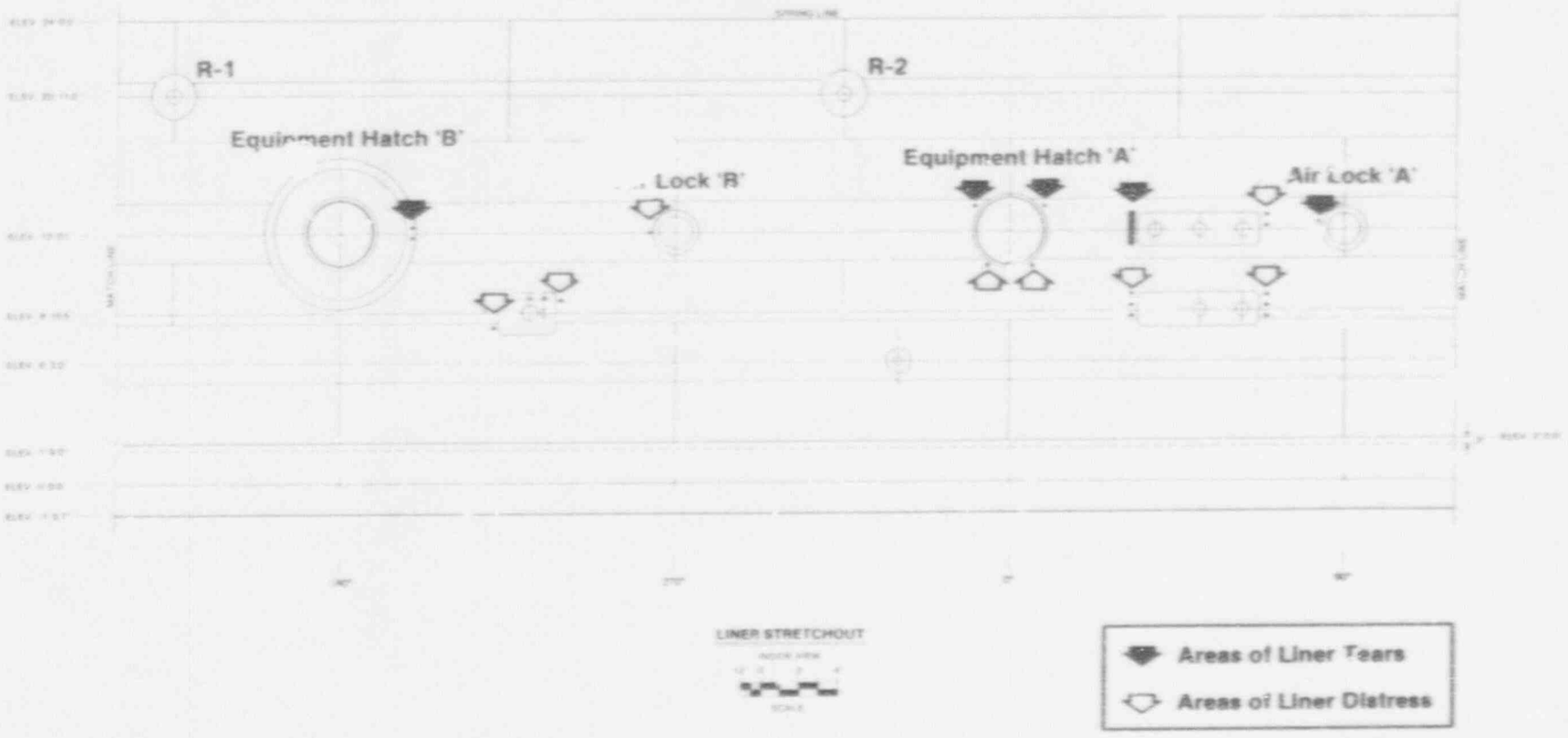

Figure 2. Location of Liner Tears in 1:6-Scale Model

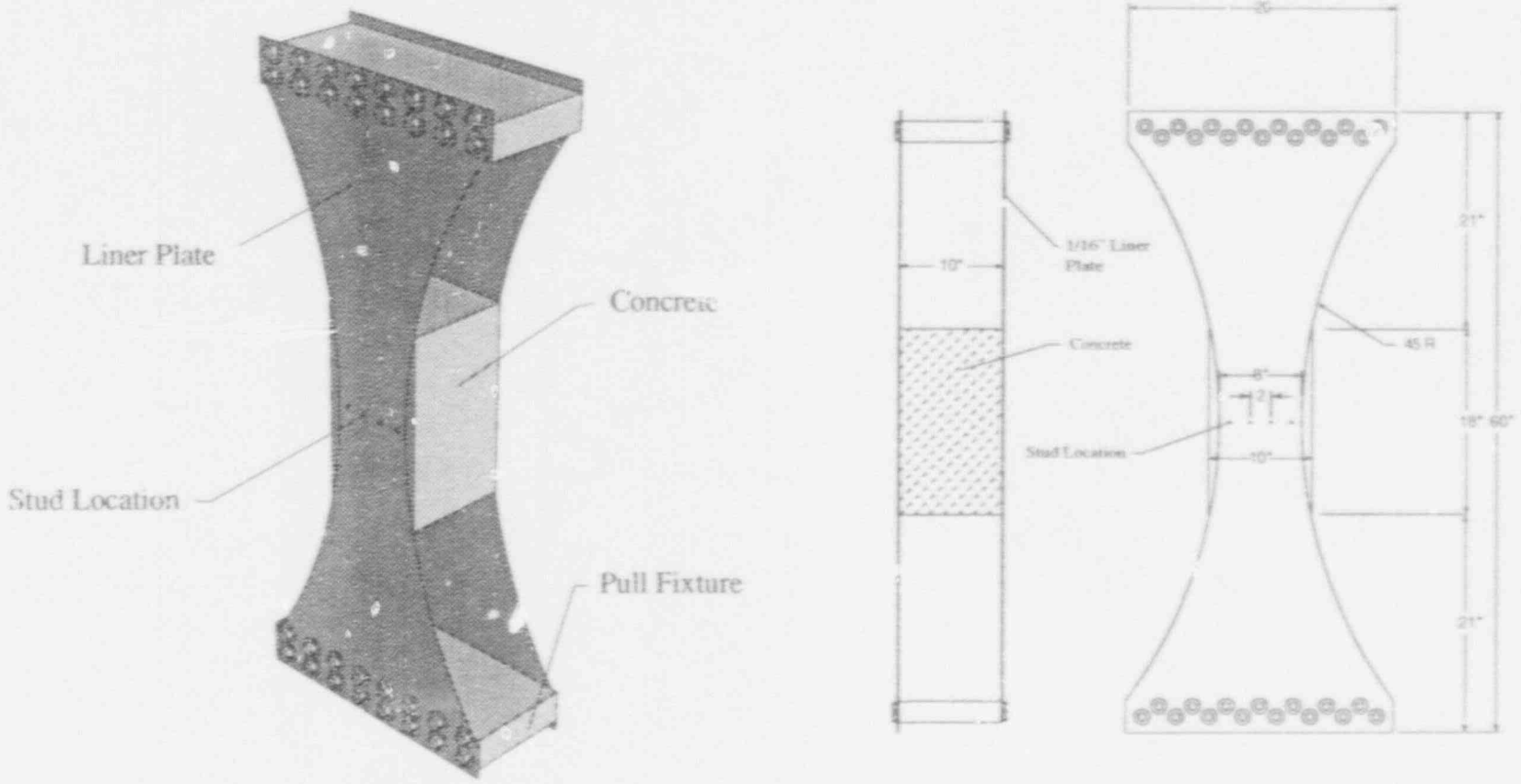

Figure 5. Specimen For Separate Liner/Stud Loading (Phase 1)

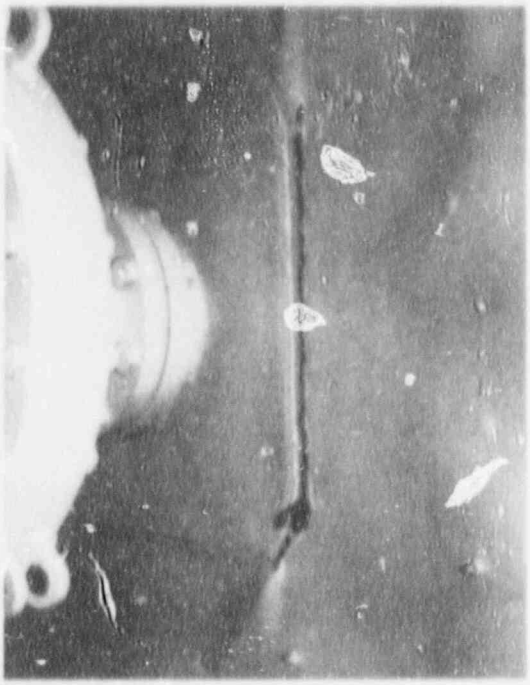

Figure 3. Photo of Primary Liner Tear

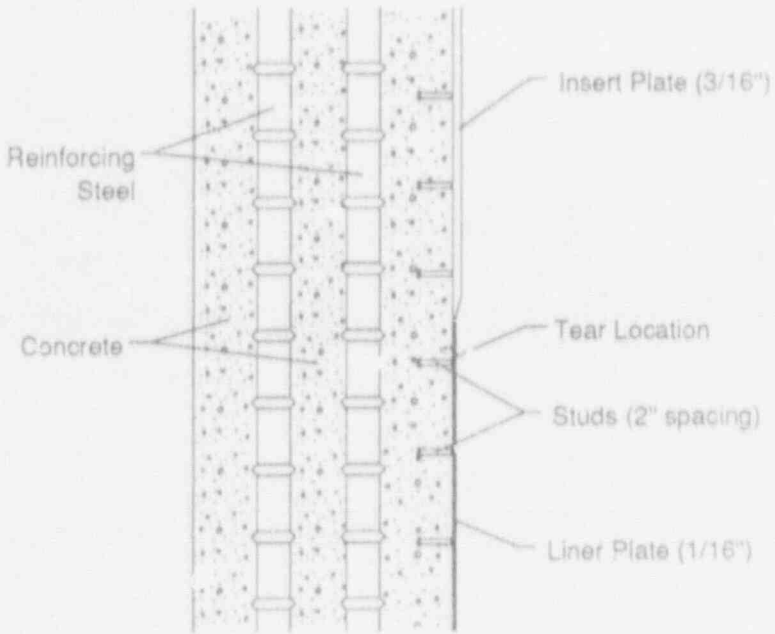

Figure 4. Top View of Cross-Section Through Reinforced Concrete Wall

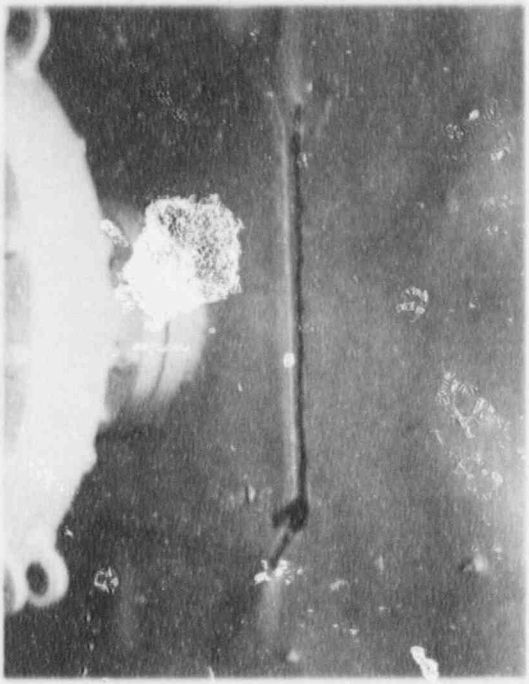

Figure 3. Photo of Primary Liner Tear

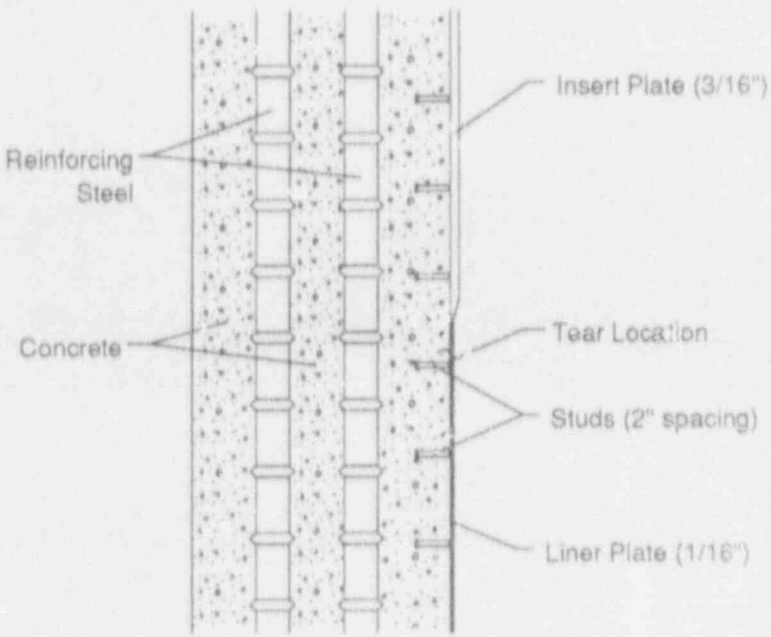

Figure 4. Top View of Cross-Section Through Reinforced Concrete Wall

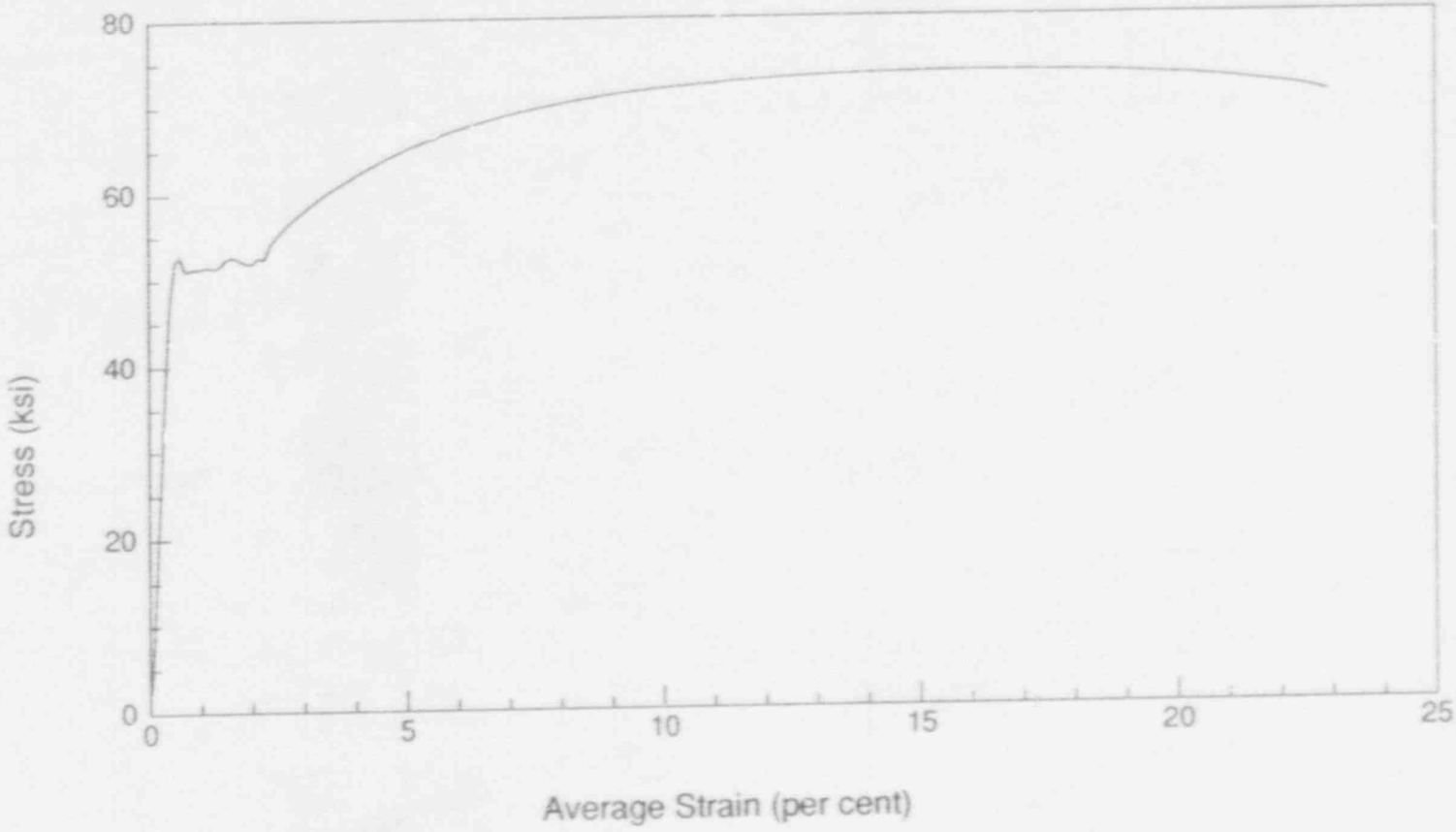

Figure 6. Response of Liner Plate Material

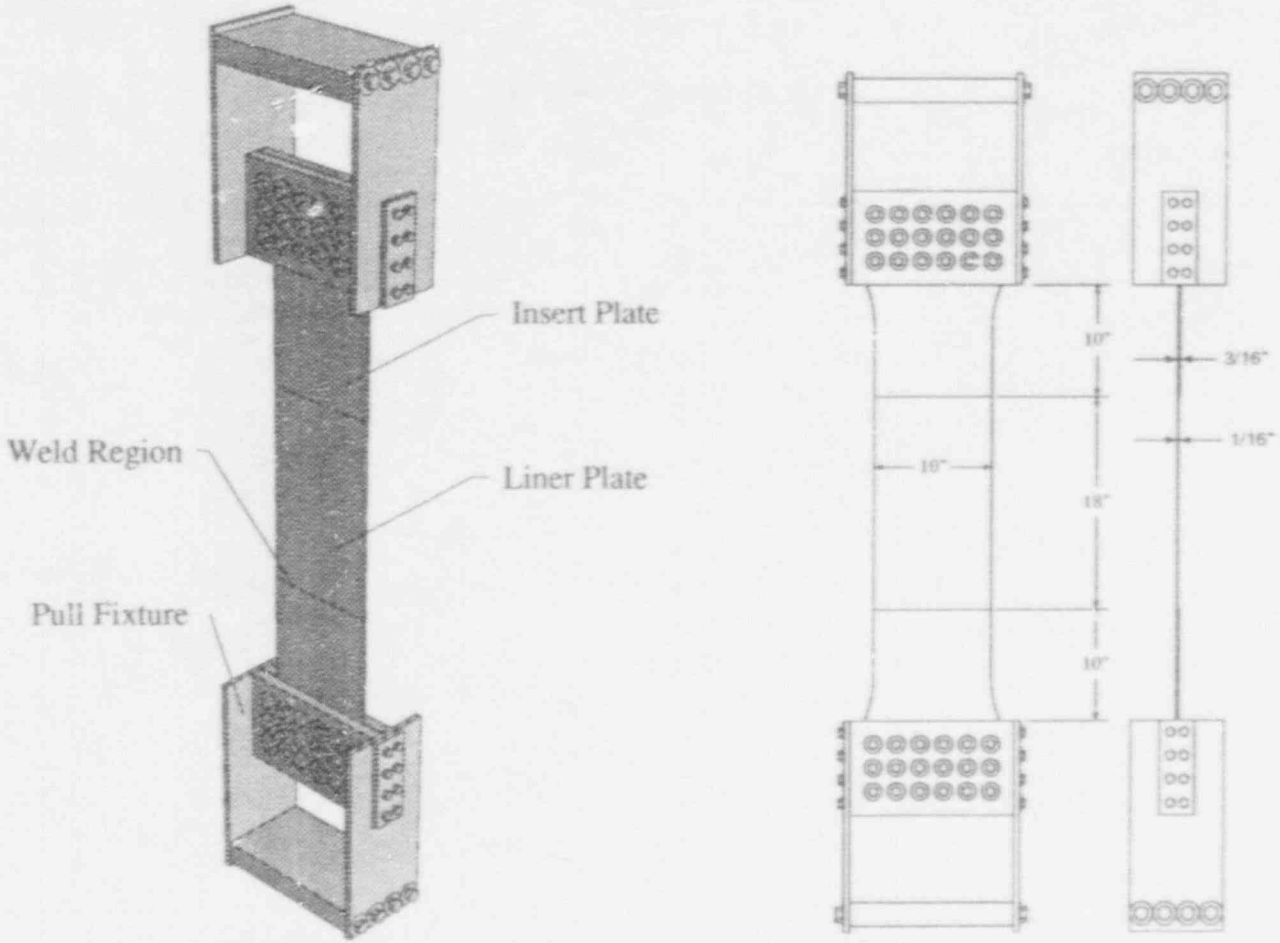

Figure 7. Specimen For Weld Effects Testing (Phase 2A)

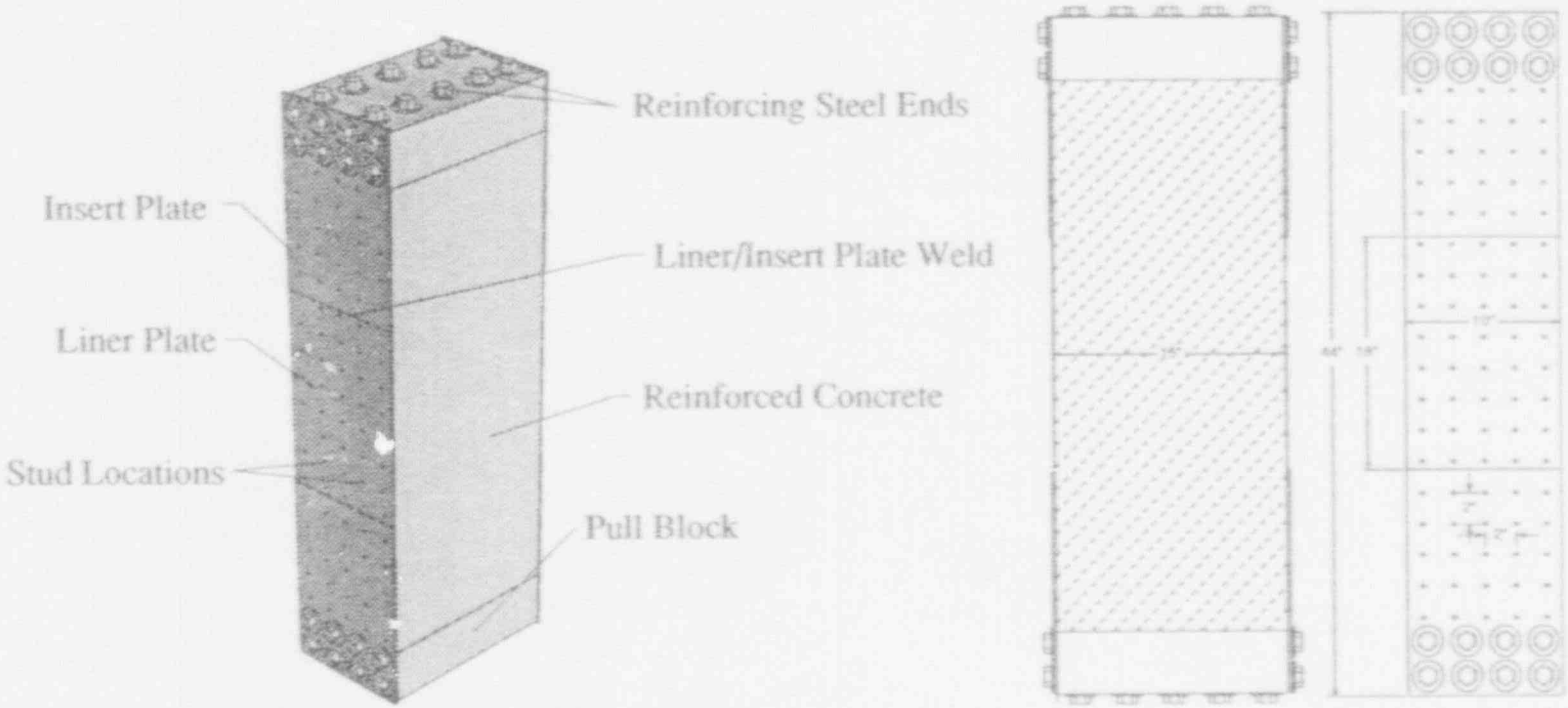

Figure 8. Simulated 1:6-Scale Wall Specimen (Phase 2B)

High Level Seismic/Vibrational Tests at the HDR – An Overview

by
C. A. Kot, M. G. Srinivasan, B. J. Hsieh, Argonne National Laboratory;
D. Schrammel, L. Malcher, Kernforschungszentrum Karlsruhe, FRG;
H. Steinhilber, Fachhochschule Giessen – Friedberg, FRG;
J. F. Costello, U.S. Nuclear Regulator Commission, Office of Research

ABSTRACT

As part of the Phase II testing at the HDR Test Facility in Kahl/Main, FRG two series of high-level seismic/vibrational experiments were performed. In the first of these (SHAG) a coast-down shaker, mounted on the reactor operating floor and capable of generating 1000 tonnes of force, was used to investigate full-scale structural response, soil-structure interaction (SSI), and piping/equipment response at load levels equivalent to those of a design basis earthquake. The HDR soil/structure system was tested to incipient failure exhibiting highly nonlinear response. In the load transmission from structure to piping/equipment significant response amplifications and shifts to higher frequencies occurred. The performance of various pipe support configurations was evaluated. This latter effort was continued in the second series of tests (SHAM), in which an in-plant piping system was investigated at simulated seismic loads (generated by two servo-hydraulic actuators each capable of generating 40 tonnes of force), that exceeded design levels manifold and resulted in considerable pipe plastification and failure of some supports (snubbers). The evaluation of six different support configurations demonstrated that proper system design (for a given spectrum) rather than number of supports or system stiffness is essential to limiting pipe stresses. Pipe strains at loads exceeding the design level eightfold were still tolerable, indicating that pipe failure even under extreme seismic loads is unlikely inspite of multiple support failures. Conservatively, an excess capacity (margin) of at least four was estimated for the piping system, and the pipe damping was found to be 4%. Comparisons of linear and nonlinear computational results with measurements showed that analytical predictions have wide scatter and do not necessarily yield conservative responses, underpredicting, in particular, peak support forces.

1. Introduction

The Heissdampfreaktor (HDR) Test Facility is located in Kahl/Main in the Federal Republic of Germany, 40 km east of Frankfurt/Main. It was built as a prototypical Superheated Steam Reactor in the period of 1965 to 1969 and shut down in 1971 after only 2000 hours of operation. After extensive decommissioning and conversion work it has been used since 1974 by the HDR Safety Project (PHDR) of the Kernforschungszentrum Karlsruhe (KfK) to perform vibrational/seismic, thermal hydraulic, blowdown, and other experiments related to the safety and design of nuclear power plants.

The overall objective of the HDR project is the experimental verification of calculational methods and procedures for use in reactor design and safety analysis, as well as the generation of experimental data and information that can be directly applied to power reactors. While the KfK, on behalf of German Federal Ministry of Research and Technology (BMFT), is responsible for the performance of the experiments, data acquisition, comparisons and evaluations, the efforts are, in general, carried out in collaboration with many industrial and government institutions both within

Germany and abroad. Specifically, the U.S. NRC Office of Research has collaborated with KfK in many of the research efforts at the HDR.

During the first phase of HDR testing in the time frame from 1975 to 1983, low and intermediate level vibrational experiments were performed on the HDR structures and equipment, using eccentric mass shakers, explosives, impact and snapback techniques [1]. In the second phase of HDR testing seismic margins tests of the reactor building, called SHAG, were carried out in 1986 using a large coast-down shaker located on the reactor operating floor. These were followed by failure and seismic margins tests of piping, called SHAM, which were performed in 1988. The U.S. NRC Office of Research through its contractors, Argonne National Laboratory (ANL) and Idaho National Engineering Laboratory (INEL), collaborated extensively in these latter two test series under a special agreement between KfK/BMFT and NRC for the HDR Phase II testing. In this paper interest is limited to the full-scale high-level seismic tests of the HDR building and piping, i.e., to the SHAG and SHAM tests. The following provides a brief description of the HDR Test Facility, the SHAG and SHAM tests, an overview of the results obtained from these experiments and related analyses, and discussions/conclusions emphasizing the implications for nuclear reactor safety and design.

2. HDR Test Facility

The HDR reactor building, Fig. 1, is a reinforced concrete and steel structure approximately 52 m high. It is embedded to a depth of 13 m giving the building an overall height of 65 m. The outer diameter is 22.4 m. The internal concrete structure consists of 2 concentrical cylinders interconnected by numerous walls and floors separating compartments for the mechanical equipment. The reactor pressure vessel is located at the center. It is 10 m in height, and has an inner diameter of 3.0 m and a wall thickness of 14.2 cm.

A steel containment with a wall thickness of approximately 3 cm encloses the inner structure, separated from it by a 2 cm thick styrofoam layer. The steel cylinder extends to a height of 40 m, where a polar crane is located (10 m above the operating floor) and is topped with the hemispherical steel dome. Personnel and equipment hatches are connected to the steel containment shell. The third part of the building, the external containment built out of reinforced concrete, is also a cylindrical shell with a hemispherical dome. The wall thickness is 60 cm and has little reinforcement because the HDR was not designed against external loads other than wind loads.

Finally, the basement consists of the foundation slab and a massive inner cylinder that forms an egg-cup like support for the inner structure. Structurally, this can be regarded as the only connection between inner steel containment and concrete containment. The two shells are independent of each other at all other points. The annulus between concrete and steel shells is 60 cm wide and is accessible. On one side of the reactor building is the crane and equipment tower and on the other side the operations building (Fig. 1). Because the site was previously used for brown coal mining activities, the soil characteristics were improved before construction by vibration injection of gravel columns down to the solid clay layers at 20 m depth. The ground water table is located 6 m below the surface.

An electrically heated boiler of 4 MW, permits the simulation of boiling water as well as pressurized water reactor conditions in the mechanical equipment and piping. Besides that, extensive facilities for measurement and data acquisition were installed, 400 fast (4 kHz) and 200 slow (2.5 Hz) measuring channels can be sampled simultaneously. This measurement/data acquisition system is connected through a data link with a data base at the PHDR/KfK in Karlsruhe. In addition to the experimental data, this data base also contains the results of calculations, which are performed for all experiments. This provides a sound basis for data evaluation and for the

verification of codes, mathematical modeling practices and assumptions (parameters and boundary conditions).

3. SHAG Experiments - Test Series T40

The centerpiece of the Phase II seismic/vibrational testing at the HDR was the high-level shaker test series (SHAG) which was performed in June and July of 1986 [1, 2, 3]. These tests in which the NRC/RES and many other organizations participated provided the culmination of the seismic testing of the reactor building that progressed through low and intermediate level testing in Phase I. The purpose was to investigate full-scale structural response, soil/structure interaction, and piping and equipment response under strong excitation conditions, i.e., under excitation levels that induce significant strains in the structure and soil and produce nonlinear effects in the soil/structure system and piping. As with all HDR experiments, the primary intent of the SHAG tests was to verify and validate calculational procedures and analysis methods. At the same time, the experimental data provide direct information on the response and performance of structural systems, piping, and equipment under high dynamic loading; such information may have direct applicability to understanding the behavior of nuclear power plant systems. Examples of this were the evaluation of various pipe support configurations in an in-plant piping system and the investigation of the performance of a typical U.S. gate valve under seismic loading.

3.1 Test Description

The excitation in the SHAG experiment was provided by a large eccentric-mass coastdown shaker designed by ANCO Engineers, Inc., capable of generating forces in excess of 1000 tons (metric) which was mounted on the operating floor of the HDR building as shown schematically in Fig. 2. The shaker was designed to develop maximum accelerations in the HDR building on the order of 5 m/s^2 and maximum displacements of about ± 7 cm. Test starting frequencies ranged from 1.6 to 8.0 Hz. Details of the shaker operation have been described previously [2, 3]. As the shaker revolutions (frequency) slow down and building resonances are traversed, the shaker energy is transferred to the building and the interior components. The increase in building response when the shaker reaches one of its resonances can clearly be seen in Fig. 3.

The primary purpose of the SHAG experiments was to subject the HDR Reactor Building, which was not designed for earthquake loads, to vibrational excitation up to incipient failure, where local damage could occur but global failure would be excluded. Other objectives included the study of load transmission through the structures and equipment, and the investigation of full-scale equipment and piping response. In particular the response of an in-plant piping system, called the Versuchskreislauf (VKL) with different multiple support configurations was evaluated.

A total of 460 channels of instrumentation was used during the SHAG tests to measure all important response parameters, including the safety aspects of the HDR and neighboring facilities [3]. In planning the SHAG tests, it was intended that the loading of the HDR facility not be limited by the excitation system but rather by the capacity of the building itself. Nearly all tests were designed to generate nominally the same peak force of 10^4 kN, at different starting frequencies of the shaker. Higher shaker frequencies (4.5 to 8.0 Hz) were intended primarily for piping excitation, while the lower frequencies (1.6, 2.1, and 3.1 Hz) were intended primarily to challenge the soil/structure system. A total of 25 experiments were performed, 10 of these were for the investigation of soil/structure system response, the remaining 15 served to study the VKL piping behavior. Of the latter, 5 tests were performed at pressurized water reactor conditions (210°C, 70 kN).

3.2 Reactor Building, Soil and Free Field - Result Overview

The HDR Reactor Building was essentially designed for dead weight and operational loads, with the only external load considered being the horizontal wind load. Hence, the building is very lightly reinforced particularly in the outer concrete containment (shield building). Prior to the tests extensive safety calculations were undertaken [4, 5]. These indicated that the reactor building could only be subjected to relatively low shaker eccentricities (about 10^4 kgm). Therefore, a procedure was established requiring that each test be accompanied by calculational safety evaluations and an immediate assessment of critical test measurements before proceeding with the next test.

During the preliminary shaker functionability tests it was established that the load distribution in the building is quite different from that assumed in the static safety calculations, and that a large share of the load (about 60%) is carried by the inner shell structure and the walls which are normally neglected in static calculations. Taking these aspects into account it was estimated that shaker tests with eccentricities of up to 10^5 kgm could be undertaken.

While the safety calculations predicted that the concrete foundation region would experience the highest stresses, it was found during the functionability tests, and confirmed by more refined calculations [5], that the greatest challenge to the building was in the outer concrete structure. Specifically, locations where floors are coupled to the outer structure (shell) and the embedded region of the outer shell were determined to be weak points. Therefore, these regions were extensively instrumented and samples were taken to determine the characteristics of the concrete. In the actual experiments masses of up to 25 tons per shaker arm were used, with the starting frequencies as planned between 8.0 and 1.6 Hz and eccentricities between 4,700 and 67,000 kgm. Peak forces of more than 10^4 kN (1000 tonnes) were reached as shown in Fig. 4.

3.2.1 Maximum Building Responses

As anticipated the highest stresses in the reactor building occurred in the outer containment (shield building) due to vertical membrane forces in the lower portion of the shell between the elevations of 0 and -11 m. This region is only minimally reinforced. The tensile forces which can be sustained by the reinforcement are less than those allowed for the concrete proper. Based on the measured cracking strength of the concrete the highest allowable membrane tensile stress was determined to be 0.5 MN/m^2. Obviously credit could also be taken for a compression stress of 1.1 MN/m^2 due to the dead weight of the concrete shell. The maximum allowable membrane stress was slightly exceeded in the tests.

There was extensive cracking of some interior floors, shifting and collapse of some masonry walls, and impact with neighboring structures. Nevertheless, the HDR-Reactor Building sustained no significant global damage. This, inspite of the fact that the building was not seismically designed and was subjected to peak accelerations of 0.4 g and displacements of ±5.0 cm, which correspond to an earthquake excitation of an intensity 7-8 on the Mercali scale. A comparison of the maximum building responses in the SHAG tests and a maximum credible earthquake in Central Europe is given in Fig. 5.

3.2.2 Reactor Building Frequencies and Damping

In earlier experiments [6] it had been clearly established that the reactor building response is dominated by rocking modes, nominally at about 1.5 Hz, and out-of-phase bending modes, at around 2.5 Hz, in which the outer concrete containment shell moves in the opposite direction to the inner steel shell containment. Both rocking and out-of-phase bending are associated with two very closely spaced modes, one in each of the horizontal directions (x and z).

A detailed system identification analysis indicates, that as the loads in the SHAG experiments were increased (from 4,700 to 8,200 kgm) the frequencies of the out-of-phase bending modes decreased by about 4% while the modal damping increased by about 30%. The latter consists primarily of structural damping in the concrete structures in the foundation region where the inner structure and the outer shell are coupled. The effect was even more dramatic for the two rocking modes, where as the load increased (from 4,700 to 67,000 kgm) the frequencies dropped by about 40% to around 1.0 Hz. At the same time the damping increased by about 50% to values as high as 9% of critical (see Fig. 6). This damping is composed of concrete structural damping, radiation damping, and hysteretic damping in the soil. However, the large frequency shifts are primarily caused by the reduction in shear stiffness which is associated with large shear deformations.

3.2.3 Load/Vibration Transmission

One of the objectives of the SHAG experiments was to investigate the transmission of vibrational energy from the shaker to the building, its large components and piping, the surrounding soil and adjacent structures. As shown in Fig. 3, the load transmission to various parts of the reactor building was primarily effected by energy transfer during the traversal of the various building resonances.

It is interesting to note that while the shaker excitation was limited to relatively low frequencies (8 Hz maximum), significantly higher frequency vibrations were measured at many locations throughout the building and particularly at mechanical components. Thus in the VKL piping, frequencies as high as 10-12 Hz were strongly excited. This is due primarily to nonlinear effects, such as impacts.

Response amplification was also in evidence at many locations and was particularly pronounced for the VKL piping. Here, velocities and accelerations were as much as 20 times higher than those in building proper. This is partially due to the fact that the VKL was not only attached to the building walls, but also to a large vessel (the HDU). The opportunity for double amplification of the motion, via nonlinear effects, was thus established. Other equipment which exhibited response amplification include the polar crane (factor of 3-4), the material lock (factor of 2), and the external crane structure (factor of 5-6) which was primarily excited during the traversal of the rocking mode. Because of its unique stiff mounting, only the reactor pressure vessel did not show any response amplification relative to the reactor building.

The operations building is adjacent to the reactor building and is connected to it by a bridge structure. During the SHAG tests this structure was coupled to the two buildings predominantly by friction and was displaced only by a few millimeters. The operations building proper, which has its dominant vibration mode at 3.1 Hz, experienced only very minor damage during the tests.

3.2.4 Foundation, Soil and Free Field Response

Using acceleration measurements and assuming rigid body behavior, it was determined that the foundation slab experienced only minimal torsional and vertical motions. The horizontal translational motions are essentially zero when bending resonance is traversed. On the other hand, there are significant rotational motions about the horizontal axes. Based on the relationship between the horizontal translations and the rotations, the center of rotation during the traversal of the rocking mode is determined to lie 15 m below the foundation slab.

Assuming no tensile stresses could be transmitted at the foundation–soil interface, nonlinear pretest calculations [7] indicated that considerable basemat liftoff would occur at the

highest possible shaker load. Based on the measurements in the experiment with maximum shaker eccentricity (67,000 kgm), there was no indication of liftoff. This was substantiated by post-test calculations [8] which show that properly reducing the soil stiffness and adjusting the damping to match the test results leads to considerable margin against basemat liftoff.

A pretest safety assessment of the possibility of soil liquefaction and building instability was performed by comparing the expected dynamic shear stresses with the normal stresses due to building and overburden loads. The estimates indicated that even for shaker loads in excess of those planned, there would be no danger of soil liquefaction. These conclusions were substantiated by pore pressure measurements during the SHAG tests, and extrapolation of the results confirm that the simple approach, used in safety regulations for estimating possible soil liquefaction, is valid [8].

A rotationally symmetric nonlinear finite difference model of the soil was coupled to a simple beam model of the HDR building [8] to predict the free field response in the SHAG experiments. It was found that even for shaker loads much larger than those planned, the free field vibrations at all neighboring installations would be very benign. During the tests actual loads were only about one half of those used in the safety assessments. The maximum measured vibration amplitudes in the free field occurred at higher frequencies during the rocking mode and were primarily horizontal responses. During the bending mode traversal, vertical responses were dominant.

3.2.5 Comparison of Calculated and Measured Soil-Structure Interaction Response

In addition to the safety assessments a number of predictive calculations were performed by German investigators for the soil-structure interaction response of the reactor building [9]. A best-estimate pretest safety prediction was also performed by Weidlinger Associates [10]. In the latter the site is represented by a fully 3-D finite element model with a nonlinear constitutive relation, and the containment building is represented by a beam model with the structure assumed as linear elastic. The structural beam model is coupled to the continuum site model at the soil-structure interface, and separation and recontact at the interface are included in the model. Lastly the shaker is modeled by the appropriate nonlinear rigid body dynamics equations which are coupled to the beam superstructure. The process of shaker arm closure, contact and energy transfer between shaker and structure are simulated.

Calculations using this model were performed with the FLEX Computer Code [10] to simulate the soil-structure interaction for two of the planned SHAG experiments with starting frequencies of 1.6 and 3.1 Hz respectively. The results of these computations were then used as input to a detailed finite-element analysis of the foundation and embedded region of the reactor building to determine the expected internal forces/moments and stresses. Since these calculations were performed for eccentricity values and/or shaker starting frequencies that were larger than those used in the actual tests, a direct comparison with measured values is not possible. However, qualitatively the predictions for both the soil-structure interaction and the detailed response in the embedded region are quite correct. Thus, no soil failure and no significant basemat liftoff were predicted. The maximum moments in the outer containment wall due to membrane tensions were also correctly shown to exceed the allowable moments.

The computational models used by German investigators included the following [8, 9]:

Model BHZ - Beam model with elastic coupling between between inner and outer structure; nonlinear soil-springs derived from a preliminary soil-structure interaction analysis.

Model CER - Beam model with elastic coupling between inner and outer structure; linear soil-springs.

Model IMB - Shell model of outer structure rigidly coupled to a beam model of the inner structure; linear soil-springs.

Model KUH - Beam model with elastic coupling of inner and outer structure; nonlinear soil-springs, decoupled in the two directions (CKUH) for pretest calculations and coupled (DKUH) in post-test calculations.

Model KWU - Rotationally symmetric shell model; linear soil springs.

In Fig. 7 the measured vibrational response (displacement) at the top of the outer containment is compared with the corresponding calculational results. Shown are the displacement amplitude envelopes as a function of shaker frequency which starts at 1.6 Hz and then decays. To understand the results it is essential to recall the test process. The excitation of the building starts during the closure of the shaker arms and the force increases until the arms are completely coupled at a frequency just above the building resonance frequency. As the displacement and soil deformation increase the soil stiffness and hence the resonance frequency decrease, i.e., the resonance frequency tends to decrease ahead of the excitation frequency. Since the excitation force decreases with the frequency, there is very little increase in the displacements until the actual traversal of the resonance frequency occurs (see Fig. 7).

The deviations of the calculational results from the experimental behavior seen in Fig. 7, can be directly related to the model characteristics and the selected parameters. It is thus possible to draw conclusions as to the advantages and disadvantages of the various approaches in representing the nonlinear building responses.

Qualitatively the nonlinear pretest calculations (BBHZ) and blind post-test calculations (CBHZ, CKUH) are similar to the test response. In particular they provide a good estimate of the actual resonance frequency. However, they overestimate the building response, because the damping used in all three cases was too low.

A linear simulation of the soil-structure response does not properly capture the actual behavior (see Fig. 7). Using a good estimate of the reduction in soil stiffness with increase in load as well as the appropriate damping, one can obtain good agreement with the experiment at the time of resonance traversal (Model CIMB). However, above the resonance frequency the building response is significantly underpredicted. If a soil stiffness is used that corresponds to a lower level of excitation and a lower damping value is selected (Model CKWU), the calculated resonance occurs at higher frequency and higher excitation forces, resulting in turn in higher response amplitudes than those measured. The erratic behavior around 1.5 Hz that is in evidence for two of the pretest calculations (BBHZ and BCER) can be traced to the fact that in these simulations the full peak shaker force is applied instantaneously, completely ignoring the transition phase during shaker arm closure. Based on the foregoing it can be stated that nonlinear modeling of soil-structure interaction is required in order to represent, at least qualitatively, the building response during the high level SHAG tests.

The SHAG tests also provided an opportunity to evaluate models and approaches used in probabilistic structural mechanics which take into account the uncertainties in structural and loading parameters by treating them as random variables [11]. In the current application, the shaker loading was assumed to be given (deterministic), while the masses, stiffnesses, damping values, and concrete strength parameters of a structural model were treated as random variables. The parameters of the probability distributions were estimated on the basis of experimental data and values from the literature. The structural responses were determined by the Response Surface Method. Possible failure locations were postulated in the outer containment shell and foundation slab, and the exceedance of the concrete strength was used as the failure criterion. The failure probability was estimated using the Importance-Sampling Approach.

The analysis gave a failure probability of 2.2% for the foundation slab and 16.0% for the outer containment shell. Comparing these results with the usually accepted values of 10^{-6} for the probability of collapse or 10^{-3} for the loss of building functionality confirms that the HDR building was indeed tested up to incipient failure in the SHAG experiments, without inducing global damage.

3.3 Evaluation of the VKL Piping Responses in SHAG Tests

The VKL piping as used in the SHAG Experiments (Fig. 8), consists of a number of pipe runs ranging in nominal size from 100 to 250 mm. The piping is attached to the HDU vessel and associated manifolds and forms part of the experimental piping system at the HDR facility. The top of the pipe runs at about 28 m above ground level, just under the HDR operating floor (where the shaker is located). The original HDR hanger system provided primarily vertical dead weight support and consisted of six spring and constant-force hangers and one threaded rod. To avoid possible permanent damage to the VKL piping, two rigid struts, adjacent to the spherical tee (Fig. 8), were added to the support system. The intent in the SHAG tests was to compare the performance of this very flexible conventional support system (HDR system) with the behavior of hanger configurations designed for seismic loading and to evaluate their relative responses under indirect (through the building) loading at levels of excitation of a design basis earthquake.

The evaluation concentrated on five support configurations. These included the very flexible HDR system, the flexible KWU configuration with five struts (designed by KWU, Offenbach), the stiff NRC configuration with six struts and six snubbers (designed by INEL), the EPRI/EA configuration with three plastic dampers replacing the snubbers (designed by Bechtel Power Corp.), and the EPRI/SS configuration in which the six snubbers were replaced by seismic stops (designed by R. L. Cloud and Associates). Two additional configurations that used viscous dampers were tested each in a single experiment only. These were the GERB configuration and the ANCO configuration (designed by ANCO Engineers, Inc.). Support locations are indicated in Fig. 8 and the support arrangements used in each configuration are given in Fig. 9.

For each of the five evaluated configurations, three experiments were performed with nominally the same loading, i.e., the same shaker eccentricity and starting frequency. However, a direct comparison of the measured responses for the different configurations is not meaningful because of the dependence of shaker force on frequency. This results in higher loadings at higher frequencies. Hence, the more flexible (lower frequency) support configurations are less challenged in the tests. Therefore, the individual experiments were normalized by multiplying the measured responses by factors corresponding to the ratios of the maxima in the building response spectra (for each test) to the maximum value of a reference spectrum with a peak at 40 m/s^2 [3, 8].

The comparison of normalized peak responses (Fig. 10) does not indicate any advantages for a stiff support system (NRC) relative to a reasonably designed flexible (KWU) system. However, the very flexible HDR configuration, which was not designed seismically, results in unacceptably high displacements and stresses. The snubber replacement configurations, i.e., energy absorbers and seismic stops, proved themselves in that they performed as well as the NRC configuration. However, the seismic stops resulted in some local high level impact loads [3, 8].

A number of comparison calculations for the VKL response in the SHAG tests were undertaken by German and U.S. investigators [8, 12]. In general, the computational predictions showed considerable deviations from the experimental results. These discrepancies can be partially attributed to modeling; i.e., differences in masses, stiffnesses, and representation of supports; and partially to the idealization of the excitation in the calculational models. However,

the dominant factor for the lack of agreement between measured and calculated results can be attributed to the poor definition of boundary conditions of the VKL piping in the SHAG tests. In the experiments the VKL piping was not properly isolated or disconnected from other piping and the stiffnesses of anchors were not defined. These effects strongly contributed to the response of the VKL piping, but could not be represented in the computational modeling.

4. SHAM Experiments - Test Series T41

As the last series of tests in Phase II of the HDR Safety Program, high-level seismic experiments, designated SHAM, were performed on an in-plant piping system during April and May 1988. The objectives of the SHAM experiments were to (i) study the response of piping subjected to seismic excitation levels that exceed design levels manifold and which may result in failure/plastification of pipe supports and pipe elements; (ii) provide data for the validation of linear and nonlinear pipe response analyses; (iii) compare and evaluate, under identical loading conditions, the performance of various dynamic support systems, ranging from very flexible to very stiff support configurations; (iv) establish seismic margins for piping, dynamic pipe supports, and pipe anchorages; and (v) investigate the response, operability, and fragility of dynamic supports and of a typical U.S. gate valve under extreme levels of seismic excitation.

The SHAM experiments were conducted as a cooperative effort among a number of organizations in Europe and the USA. These included KfK/PHDR, with the participation of the Fraunhofer Institut für Betriebsfestigkeit (LBF), Darmstadt, FRG, and the Kraftwerk Union (KWU), Offenbach, FRG; the Central Electricity Generating Board (CEGB), UK; the Electric Power Research Institute (EPRI), Palo Alto, California, with the participation of Bechtel Power Corp. and R. L. Cloud & Associates; and the U.S. Nuclear Regulatory Commission, Office of Research (NRC/RES), which supported the efforts of Argonne National Laboratory (ANL) and Idaho National Engineering Laboratory (INEL).

4.1 Description of the SHAM Experiments

The test object in the SHAM experiments was again the VKL piping system that was already extensively tested in the SHAG experiments. In the latter tests, excitation of the piping resulted from the shaking of the HDR containment building. In the SHAM experiments, direct, high-level shaking of the VKL piping was used. Therefore, some significant modification of the test loop was necessary. An isometric sketch of the VKL piping as used in the SHAM testing is shown in Fig. 11. The VKL consists of multiple stainless steel pipe branches ranging from 100 to 300 mm in diameter, with the main two flow loops connected to the HDU vessel and the DF16 manifold. A third major branch connects the DF16 manifold to the DF15 manifold. Aside from the pipe hangers and dynamic supports, the only points of fixity for the entire system, including the HDU and manifolds, are the supports at the bottom of the HDU and the nearly rigid attachment of the DF15 manifold. All extraneous piping leading to other flow systems in the HDR were disconnected for the SHAM tests. As in the earlier tests, the test loop again included an 8" U.S. gate valve from the decommissioned Shippingport Atomic Power Station. (For details see Ref. 13, 14, and 15.)

The VKL piping was excited directly by means of two servohydraulic actuators rated at 40 tonnes (metric) of force each. As shown in Fig. 11, both actuators were acting in the horizontal x-direction at hanger location H5 and at location H25 (DF16 manifold). The excitation system was designed and furnished by LBF-Darmstadt, FRG, and included a computer-controlled hydraulic actuating/control system to provide predetermined displacement-time histories. Extensive pretest design calculations indicated that the hydraulic shakers would be capable of producing up to 6 g acceleration for the VKL piping, with a maximum displacement (stroke) of ± 125 mm [14].

Six different dynamic support systems were designed for the VKL piping by the various participants in the SHAM testing. These ranged from the very stiff NRC system with rigid struts and snubbers, designed by INEL, to a very flexible HDR system with essentially only dead-weight supports. The supports of the NRC system were designed as weak as possible to permit the investigation of support failures. Two support configurations, provided by EPRI in collaboration with industrial partners, contained snubber replacement devices. The first of these, designed by Bechtel Power Corp., uses Energy Absorber (EA) devices, in which a set of specially designed steel plates is plastically deformed to dissipate energy and restrict pipe motion under seismic loading. The second snubber replacement system, designed by R. L. Cloud & Associates, Inc., includes Seismic Stops (SS). In their current design, these stops are simple telescoping-tube devices with preset internal gaps that allow a certain amount of motion to accommodate thermal effects. During seismic excitation, the motion is restricted/stopped by impacting on disc spring pads. Two other support configurations, designed by KWU and CEGB, rely only on rigid struts for dynamic restraint and attempt to optimize the number of supports. Figure 12 shows an overview of all the support configurations with the location and type of dynamic support clearly indicated. All configurations used the same dead-weight hanger system shown in Fig. 11. Similarly, all configurations employed the same rigid struts at locations H4 and H23. These are horizontal struts in the z-direction and their primary function is to stabilize the input motions of the actuators, at H5 and H25 respectively, so that they move only in the x-direction. The components of these supports were sized for the highest loads anticipated.

All dynamic support systems, except the CEGB configuration, were designed for the common HDR spectrum shown in Fig. 13. The actuators were displacement controlled, and the basic earthquake displacement history used was an artificially generated displacement-time function of 15 seconds duration fitted to the preselected common Safe Shutdown Earthquake (SSE)-floor-response spectrum with a 0.6 g peak acceleration (ZPA), shown in Fig. 13. The CEGB hanger system was designed for the Sizewell B spectrum (Fig. 13) which peaks at lower frequency than the common HDR spectrum.

Nearly 300 channels of data were recorded, with major measurements being strains, accelerations, displacements, and forces. Details of the instrumentation and data acquisition have been reported elsewhere [13, 14, and 15].

Fifty-one individual experiments were performed with the VKL piping and the six different pipe support configurations (see Fig. 14). Two random excitation tests of 120-s duration, with each of the hydraulic actuators singly and separately (H5 and H25) were performed for each hanger configuration. These tests provided dynamic characterization of the systems in the frequency range from 2 to 40 Hz.

For all but the CEGB configuration, earthquake experiments were then performed at the low to intermediate level, i.e., at excitation levels ranging from one SSE (0.6 g ZPA) to three/four SSE. These experiments were carried out with the 15-s duration displacement history based on the common HDR spectrum scaled to the proper SSE level. The two hydraulic actuators (at H5 and H25) were operated together and in phase; both were programmed to provide identical displacement histories. The purpose of these tests was to study the behavior of piping systems at load levels exceeding the design load and to compare the performance of different support configurations. These tests were also intended to provide seismic-margin information for dynamic supports, and data for the validation of linear analyses.

Two configurations, namely the KWU system and a modified NRC system [16], were then tested to high levels of excitation (up to 800% SSE) again with scaled-up displacement histories and both actuators operating in phase. The purpose of the high-level tests was to obtain information on possible pipe failure/plastification, seismic margins for piping, and pipe supports, and to provide data for the validation of nonlinear analysis methods.

The CEGB configuration was subjected to its own test program. Low- and intermediate-level earthquake tests were performed with displacement histories of 20-s duration derived from Sizewell B spectrum and an Allsites spectrum [Fig. 13]. Intermediate- and high-level tests were also performed with sine burst histories near the piping resonance, with a duration of 7.0 s and maximum displacement of 60 mm. Finally, to provide a comparison with the other configurations, a 100% SSE earthquake test was performed with the displacement history derived from the common HDR spectrum.

4.2 Highlights of SHAM Experimental Results

Detailed result overviews and discussions have been provided in earlier publications [13, 16]. Following the system identification tests with random excitation, simulated earthquake experiments were performed with all support configurations. The overall sequence of events during these tests and the approach are best illustrated on the basis of the strain measurements at cross-section 7 close to the "Tee" shown in Fig. 15. In this figure the range of strains between the upper and lower limits for each test is given by the bold vertical bar. The thinner horizontal connecting lines between those bars give the permanent strains remaining after each test. The sequence of bars from left to right corresponds to the test sequence.

In the first series of experiments with the HDR-spectrum the excitations were limited to such levels so as not to exceed the nominal support forces by more than a factor of four and to limit the strains in straight pipe sections to 0.2% and in elbows to 0.4%. For all the configurations designed for this spectrum, loads up to 300% SSE could be sustained without significant problems except for the malfunctioning of two snubbers. These were replaced by snubbers of different design but similar capacity.

Comparison tests were then performed with the 100% SSE HDR spectrum loading for the HDR and CEGB configurations. The latter was then tested at 100% and 300% of its design spectrum (Sizewell B) and at 50% and 200% loading corresponding to the Allsites Spectrum. The second series of tests was concluded with a 200% SSE (HDR Spectrum) test of the HDR support configuration.

The modified NRC configuration [13] was then subjected to loads up to eight times of the design earthquake. At 600% SSE three snubbers failed due to overload, these were not replaced. At 800% SSE an additional snubber failed without damage to the piping or excessive pipe deformation. These tests also caused the failure and/or loosening of some typical support anchors.

The purpose of the following sine-burst experiments with the CEGB configuration was to induce the so called "ratcheting" phenomenon, through the combined action of the static loads (internal pressure and dead weight) and the dynamic vibration excitation. This effect can be clearly seen in Fig. 15, where the permanent strains grow monotonically from test to test, on the top side of the pipe as tensile strains and on the bottom side as compressive strains. The resulting global deformation of the piping remained quite limited. Therefore, it was possible to perform the tests with the KWU configuration at 400%, 600% and 800% SSE loading (HDR-spectrum) without repairing the piping. Again in these tests the piping did not fail.

4.2.1 Piping Stresses/Strains

An impression of stresses/strain levels in the SHAM experiments can be obtained from Figures 16 and 17. The fictitious elastic bending stresses at cross-section 7 (see Fig. 15) in the small diameter pipe reached 600 MPa (Fig. 16), far into the plastic regime, with the permanent

strains exceeding 1%. Similarly, the amplitudes of the local strains at Elbow 1 (see Fig. 15)also reached about 1% (Fig. 17).

Comparisons of the response of the VKL piping with the various support configurations, at design level loading (100% SSE), were extensively discussed in References 13 and 16. Of primary interest are the stresses in the piping. Examining the maximum values of the bending stresses which are dominant under dynamic loading, it was found (see Figures 10 and 11 of Reference 13), that at most locations the stiff NRC-configuration had the lowest stresses. However, the differences relative to the KWU-configuration and the two EPRI configurations was insignificant. The pipe region in the vicinity of the excitation point at the DF16 manifold exhibited relatively high stresses for all configurations. In the remainder of the 200 mm piping the peak stress values were all quite low (10-40 MPa).

None of the configurations designed for the HDR spectrum demonstrated any particular advantage or disadvantage relative to stress levels. On the other hand the HDR configuration, which was not seismically designed, and the CEGB configuration, which was designed for another spectrum, exhibited much higher stresses in the 100/125 mm piping.

A direct link between the number of dynamic supports and the piping stresses could not be established. A similar conclusion was already reached in the SHAG tests in which the piping was subjected to indirect excitation through the building. Hence, it can be reiterated that of primary importance to the stress levels in the piping is the proper design of the support system for the actual loading spectrum, and not the number and type of supports or the overall stiffness of the support configuration.

The stress allowables used in the design process for earthquake loading are based on nominal (minimum) material strength parameters. Actual material strengths are usually significantly higher than those values. This approach is used to prevent the plastification of substantial regions of the piping and thus to avoid pipe collapse or ratcheting. For the very tough steels used currently in reactor construction these stress allowables are set much lower than is necessary in order to avoid crack formation during seismic excitation.

This is clearly illustrated in Fig. 18 which gives the allowable strain for the austenitic steel (DIN 1.1961 - German Norms) for Level D conditions as well as fatigue cycle curve for the material based on the German Standard KTA 3201.2. It can be seen that the material can sustain up to 10^4 cycles at the allowable strain level. A comparison of the actual strain amplitude frequencies experienced in the SHAM tests at two highly stressed locations and the fatigue cycle curve can also be made on hand of Fig. 18. The differences between these curves indicate that the entire SHAM test series would have to be repeated approximately 40 times in order to reach the fatigue life of the material. This provides clear evidence that a single earthquake event has no influence on the fatigue life of piping components. For the very few high level vibration cycles experienced in a typical earthquake excitation, the stress allowables used in the design procedures are thus very conservative.

4.2.2 Support Loads and Response

The dynamic supports used in the SHAM experiments included struts, snubbers, energy absorbers and seismic stops. The other supports, such as spring and constant force hangers, carry primarily the static loads and do not influence the dynamic behavior. In the tests each of the support types was separately investigated in at least one support configuration.

Intuitively, one would expect support loads to decrease with an increase in their number. However, it is actually possible to increase the loads by the introduction of additional supports, i.e., there is no direct correlation between the number of supports and the magnitude of the

loads. The design of a particular configuration is much more important than the number and type of supports. Similarly the failure of supports during the tests did not necessarily lead to increased loads at other supports or increased stresses in the piping. In particular, the failure of snubbers under overload occurred as individual events without having a direct effect on neighboring supports (no "Zipper Effect").

The snubber replacement devices again performed very satisfactorily. The impact forces in the current seismic stops with disc-spring impact pads were significantly reduced and were hardly greater than those occurring during snubber lock-up.

Twelve different struts were used in the experiments (2 manufactures, 3 sizes). None of them failed in spite of the fact that some of them repeatedly were subjected to loads exceeding the expected fourfold margins. A total of 15 snubbers were used. In contrast to the struts, 4 out of 9 snubbers, that experienced overloads, failed outright. In addition, at least two additional snubbers malfunctioned in that they allowed excessive travel and had a reduced load bearing capacity. Not all snubbers were able to sustain the expected threefold margin (relative to their nominal capacity). All snubbers failed under overload without any external signs of damage. In all cases the failed snubbers lost their capacity to transmit loads and their motion was unrestricted until internal impact occurred (behavior similar to seismic stops).

4.3 Damping

Damping values currently used in the design of nuclear piping are chosen very conservatively. They take account of external damping effects by allowing larger damping values for larger diameter pipes. The effect of load level on internal damping is accounted for by using higher damping values for the SSE than for the OBE. Because in most vibrational investigations of piping, the damping values have been found to be higher than those typically specified in design codes (1-2%), damping has been a subject of much debate. Recently it has been proposed both in the USA [17, 18] as well as in Germany [19] that more realistic damping values be introduced into the design process for nuclear piping systems.

The motivation for this is that conservative damping values lead to stiff piping system designs under seismic loading, and this, in turn, leads to significant disadvantages in accommodating normal operational loads. Also, there exists a considerable amount of earthquake experience indicating that flexible piping systems do not fail under seismic loading. Lastly the evidence of the SHAM experiments show that the flexible KWU configuration performed as well as the very stiff NRC system under extreme seismic loading without sustaining any damage.

Because of this background it was important that the damping in the SHAM experiments be evaluated very carefully, in particular, since the SHAM tests offered many advantages over other piping vibrational tests. These are: (i) a fairly prototypical piping system (branches, nozzle connections to vessels, different pipe diameters), (ii) the excitation was earthquake-like, (iii) the loads/stresses were increased stepwise far beyond the yield point, and (iv) the same piping system was investigated with different support configurations. Hence, the procedures used in the damping evaluation were also much more sophisticated than the typical single-degree-of-freedom approaches. Parameter identification techniques were directly applied to the measured data of the random tests with curve fitting over all modal frequencies and measurement locations done simultaneously. For the seismic experiments parameter variation calculations were used to fit the individual modal damping values at different loading levels.

Figure 19 presents the damping values as a function of frequency for three support configurations (HDR, KWU, NRC) as derived by parameter identification from the random test data. On the average these results show a tendency for the damping to increase with the number of dynamic supports. However, the difference in the mean damping value between the flexible

KWU system (3.92%) and the stiff NRC configuration (4.15%) is fairly minimal. Note that there are individual modes with either very weak (0.9%) or very strong damping (9.5%).

The dependence of damping on the loading magnitude, as obtained by parameter-variation calculations for individual modes in the earthquake experiments with the KWU configuration, is presented in Fig. 20. These results are compared with damping values used in existing regulatory codes or proposed in new standards. For most of the presented modes there is an increase in damping as the loads increase from 300% to 400% SSE. However, inspite of a modal stress of 500 MPa the damping does not increase for Mode 2. No correlation seems to exist between the calculated modal stresses and the damping values. On the other hand there is a correlation between the system damping (average of six relevant modes) and load level, namely damping decreases as the load increases from 100% to 200% (3.2 to 3%), then remains constant as the load increases from 200% to 300%, and then increases more rapidly (to 3.7%) as the load increases to 400%.

Qualitatively this behavior is in agreement with earlier experience and is due to the fact that there are damping mechanisms for which the damping force is independent of the vibration amplitude (e.g., friction forces). These decrease proportionally with increasing amplitude, while other damping mechanisms (e.g., material damping) come only into play at higher amplitudes. However, it is surprising that the latter effect only became effective in the earthquake tests at loading levels at which stress allowables for Level D were exceeded at a number of locations and the yield point was exceeded at many other points in the piping system.

Comparing the derived damping values with the standards, it is seen that existing codes such as the German KTA Standard are very conservative. On the other hand, the proposed PVRC damping of 5% [17] and the damping values of 7.5% proposed by Hadjan [18], are too high. The latter values were obtained by extrapolation from fairly low level experiments (stresses usually less than one half of yield [18]), and do not appear to be substantiated by the SHAM test results in which the yield limit for the piping materials was substantially exceeded.

The newly proposed German KTA standard [19] with a uniform damping of 4% appears to be quite realistic on the basis of the SHAM test results. For a given seismic spectrum the application of this damping value will not necessarily always yield conservative values for specific pipe stresses. However, there are sufficient additional conservatisms embedded both in the definition of the design spectrum and even more so in the stress allowables (as again evidenced by the SHAM results) to assure that safe designs will result.

4.4 Comparison of Computational and Experimental Results

The different pipe support configurations in the SHAM tests were all designed for a given loading spectrum using typical design analysis procedures. A detailed comparison of calculational results with the measured data indicates [13, 20] that typical design analysis procedures (time-history analysis, response spectrum methods) are not necessarily conservative, even when superposition of the responses in different excitation directions (3D-Excitation) was used. Real conservatisms are only introduced through spectrum broadening or the selection of proper damping values. Most importantly it was found that the design analysis, at least in this application, underpredicted the maximum dynamic support forces.

The purpose of most of the post-test calculations was to verify how well the piping response could be represented by linear modeling using realistic damping values and the actual excitation loads. In order to provide a certain variability in modeling and calculational approaches, three different German institutions were involved in the post-test analyses. In all their modeling Rayleigh damping is used as was also the case for the KWU pretest calculations [20]. Figure 22 gives a statistical evaluation obtained by comparing the maximum values of the four linear German

predictions, including the KWU pretest analysis (BKWU), with the corresponding measured values (KWU configuration, 100% SSE test). The mean values, standard deviations, and smallest/largest values for acceleration, strut forces and bending stresses are given. Values larger than 1 indicate calculational overestimates and values smaller than 1 are underestimates. In the statistical evaluation the results at all measurement locations were equally weighted, regardless of the absolute value.

In general, the accelerations and support forces are underpredicted and the mean values of the calculational results differ little from each other, with the exception of model CKWU for the accelerations and CMPA for the strut forces. The mean values for the stresses are all close to unity, i.e., in the mean the calculations essentially provide a good estimate of the maximum stresses.

Similar linear computations were performed by ANL [21] for both the KWU and NRC configuration. As seen in Fig. 22, the statistical evaluation of the results is not very different from that of the German studies. Again support forces and accelerations are underpredicted and the variability in the results is quite large. The best estimate is obtained for the pipe stresses. The large discrepancies relative to the measurements, for the accelerations and support forces, are related to higher frequency components in the measurements that result from the nonlinearities in the actual system. It is gratifying to note that pipe stresses, which govern the design, are at least in the mean, relatively well estimated by the calculations.

To account for the inherent nonlinearities of some of the supports (energy absorbers, seismic slops, snubbers), nonlinear modeling was used to estimate their response [20]. In the mean the results are somewhat closer to the measurements than those of the linear models, in particular, for the forces in the nonlinear supports. However, the insignificant improvement in predicting the forces in the remaining supports, the accelerations and the stresses, does not justify the large calculational effort required for the nonlinear time-history analyses.

Extensive nonlinear material response in the 800% SSE test with the KWU configuration was limited to the two most highly stressed pipe regions. This made it possible to estimate the local nonlinear effects using a simplified approach in which the nonlinear contributions to global behavior of the affected regions are derived from static calculations and added to the linear response [20, 22]. Extending the method to time history analysis and using parameter variation computations, it was possible, with this approach and reasonable computational effort, to define the essential differences between linear and nonlinear structural responses.

Fully nonlinear simulations of the 800% SSE test with the KWU support configuration were carried out by ANL using the NONPIPE computer code [23]. The elastic-plastic behavior in this case is modeled by assuming moment-curvature and torque-twist relationships to be trilinear and by an approximate treatment of strain hardening based on this trilinearity. There is again significant variability in the quality of the predictions. The results are statistically evaluated by comparing maximum values of the prediction to measurements for accelerations, strains, and support forces. As seen in Fig. 23, the mean values of the nonlinear predictions are, in general, better than those for the low level tests using linear analysis. While support forces are still underpredicted, the results are closer to the measurement. The best predictions are obtained for the strains. Some of the outliers in the latter are due to the fact that the calculations predict strain ratcheting at some locations. This phenomenon did not occur in the test because the material had been strain-hardened in preceding experiments.

4.5 Seismic Margins Evaluation

Because of their reasonable prototypicality in support design, piping layout and seismic excitation, the SHAM experiments provided an opportunity to demonstrate that piping systems

designed to current practice have large margins against failure and to quantify the excess capacity of pipe components and dynamic supports. Such an evaluation was undertaken [24] using both the system design information and the experimental measurements for the KWU and NRC configurations.

Different design approaches, standards and philosophies were used in the two system designs, resulting in some discrepancies in support strength and allowable stress values. To account for this, the design results were normalized to a common basis (Level C allowables) and margins were adjusted by overdesign factors [24]. Seismic margins were estimated for both the piping itself and the dynamic supports. These were calculated in two ways. On one hand design load level was used as a basis and on the other hand component capacity was used. Both of these estimates give deterministic excess capacities and do not represent seismic margins in the probabilistic sense.

Based on loading level alone, it was determined that the margin against pipe failure is at least 8 (KWU configuration). However, using the yield strain as an indication of nominal capacity, it was found that the excess capacity for the pipe material is at least 4. Similarly, for the struts, the margin against failure based on load level alone appears to be at least 8, since no struts failed even at 800% SEE. For the snubbers, the same margin is about 3 because some malfunctions occurred at that level. Taking into account overdesign and comparing the actual forces experienced by a particular support with its capacity, the lowest margin for snubbers is found to be about 2, and for struts, on the order of 6. Finally, making allowances again for overdesign, the SHAM tests show that the margin for the overall piping system is at least 4. This clearly demonstrates again the ruggedness of piping systems when subjected to the seismic loading.

5. Discussions and Conclusions

The high level vibrational/seismic experiments at the HDR have provided much useful information and insight concerning the behavior of reactor systems, piping, and components. Thus, in the SHAG experiments the reactor building was tested to incipient failure, as indicated both by measurement and probabilistic structural analysis, demonstrating that even structures not designed for earthquake loading have considerable capacity to resist such loads. The data show that as loads are transmitted from the building to equipment/piping considerable response amplification (up to 20 times in the SHAG tests) may be expected. Also nonlinear effects, such as impacts, may shift the response spectra to significantly higher frequencies than those contained in the excitation proper. The soil-structure interaction phenomena at the SHAG load levels (approximately equivalent to SSE loads) were inherently nonlinear as indicated by strong rocking mode frequency reduction and simultaneous increases in damping. Hence, in any computational modeling of soil-structure interaction response it is essential to include the nonlinear effects, such as the reduction in soil stiffness and shear modules with increasing deformations.

The SHAG experiments also demonstrated that piping systems with well designed compliant dynamic support configurations perform as well as those with stiff support configurations. It was also found that snubber replacement devices (energy absorbers and seismic stops) perform as well as snubbers in limiting pipe stresses. These findings were further amplified in the SHAM test series where six different support configurations were subjected to seismic loads exceeding design levels manyfold. In the latter tests it was also found that there is no correlation between the number of supports and pipe stresses as long as the support system is properly designed for the given seismic input spectrum.

The SHAM test again established that piping is very rugged in resisting seismic loads and that inspite of significant local pipe plastification and multiple support failures, there is no danger of pipe failure during the limited number of high loading cycles occurring in a typical earthquake. Similarly rigid struts were found to be very strong; none of them failed in the tests inspite of the

fact that some of them experienced six-fold overloads relative to their nominal capacities. Failures and malfunctions did occur in snubbers, some at loads less than three times their capacities. However, the failures of individual supports did not necessarily result in load increases at other supports and/or pipe stress increases. The overall margin or excess capacity for the piping system was found to be at least four.

A detailed and careful evaluation of pipe damping up to load levels of 400% SSE resulted in an overall system damping of approximately 4%. This indicates that piping damping values used in current codes and standards are conservative. On the other hand some of the proposed pipe damping values that are based on extrapolation from lower level tests appear to be too high.

Finally, extensive comparisons between measurements and both linear and nonlinear calculations showed that considerable scatter can be expected in the prediction of pipe response. Further calculational procedures, whether they be design or best estimate calculations, are not necessarily conservative in predicting peak responses. In particular, peak support forces may be significantly underpredicted. In general, the best predictions are for pipe stresses which govern the piping design and the inherent conservatisms built into the design process assure that piping systems are ruggedly designed and in no danger of failing under seismic loads.

References

1. L. Malcher and H. Steinhilber, "A Review of 15 Years Full-Scale Seismic Testing at the HDR," Trans. 11th Intl. Conf. on Structural Mechanics in Reactor Technology, Vol. K1, paper No. K15/1, pp. 397–408, Tokyo, Japan, 18–23 Aug. 1991.

2. L. Malcher and C. A. Kot, "HDR Phase II Vibrational Experiments," Proc. U. S. NRC 14th Water Reactor Safety Information Meeting (27–31 Oct. 1986), NUREG/CP-0082, Vol. 3, pp. 295–312, Febr. 1987.

3. C. A. Kot, L. Malcher and H. Steinhilber, "Vibrational Experiments at the HDR: SHAG Results and Planning for SHAM," Proc. U.S. NRC 15th Water Reactor Safety Information Meeting (26–29 Oct. 1987), NUREG/CP-0091, Vol. 3, pp. 251–277, Febr. 1988.

4. F. Stangenberg and R. Zinn, "Structural Safety of HDR Reactor Building During Large Scale Vibration Tests," Trans. 8th Intl. Conf. on Structural Mechanics in Reactor Technology, Vol. K(b), paper No. K20/11, pp. 473–478, Brussels, Belgium, 19–23 Aug. 1985.

5. H. Werkle and G. Waas, "Computed Versus Measured Response of HDR Reactor Building in Large Scale Shaking Tests," Trans. 9th Intl. Conf. on Structural Mechanics in Reactor Technology, Vol. K1, paper No. K9/3, pp. 479–487, Lausanne, Switzerland, 17–21 Aug. 1987.

6. P. Jehlicka, L. Malcher, H. Steinhilber and B. Brendel, "Earthquake Investigations at the HDR-Shaker Experiments at Intermediate and High Excitation Level" (In German), Quicklook Report V63, Technical Report PHDR 13–80, July 1980.

7. B. Weber and J. P. Wolf, "Earthquake Investigations of the Reactor Building, Nonlinear Soil–Structure Interaction," (In German), Elektrowatt Ingenieurunternehmung AG, Zürich, Working Report PHDR No. 4.290/85, Aug. 1985.

8. L. Malcher and H. Steinhilber (editors), "Structural Dynamics Investigations at the HDR, Earthquake Experiments up to the Load Bearing Capacity of the Reactor Building," (In German), Evaluation Report: SHAG, Technical Report PHDR 90-89, March 1990.

9. H. Steinhilber, G. Flade and D. Schrammel, "Approach and Status of the Evaluation of the Earthquake Experiments with the Large Building Shaker," (In German), 11th Status Report of the HDR Safety Program, Contribution No. 10, PHDR Working Report 05.37/89, 9 Dec. 1987.

10. D. K. Vaughan, R. Mak, and T. Piland, "Analysis of the HDR Containment Structure Subjected to High Level Shaker Loading," Weidlinger Associates, Final Report for ANL Contract No. 5152401, R 8663 DV, March 1987.

11. G. I. Schueller, H. J. Pradlwarter and P. Jehlicka, "Failure Probability of the HDR-Containment under Shaker Loading," Trans. 10th Intl. Conf. on Structural Mechanics in Reactor Technology, Vol. M, paper M06/2, pp. 149-154, Anaheim, CA, 14-18 Aug. 1989.

12. B. J. Hsieh, C. A. Kot and M. G. Srinivasan, "Vibration Testing and Analysis of a Multiply Supported Piping System," Trans. 9th Intl. Conf. on Structural Mechanics in Reactor Technology, Vol. K2, pp. 969-974, Lausanne, Switzerland, 17-21 Aug. 1987.

13. C. A. Kot, M. G. Srinivasan, B. J. Hsieh, L. Malcher, D. Schrammel, H. Steinhilber and J. F. Costello, "SHAM: High-Level Seismic Tests of Piping at the HDR," Nuclear Engineering and Design, Vol. 118, pp. 305-318, 1990.

14. L. Malcher, H. Steinhilber and D. Schrammel, "Design Report-HDR Test Group SHAM T41," (In German), PHDR Working Report 4.338/88, March 1988.

15. P. Wenzel, L. Löhr and R. Grimm, "Test Protocol - HDR Test Group SHAM T41, Volume I: Overall Test Sequence," (In German), PHDR-Working Report 4.345/88, 20 April to 27 May, 1988.

16. H. Steinhilber, L. Malcher and D. Schrammel, "Seismic Margins Tests of a Piping System at the HDR Facility," Trans. 10th Intl. Conf. on Structural Mechanics in Reactor Technology, Vol. K2, pp. 757-762, Anaheim, CA, 14-18 Aug. 1989.

17. Pressure Vessel Research Committee (PVRC), "Damping Values-Piping Systems, Technical Position and Justification," 1987

18. A. H. Hadjian and H. T. Tang, "Piping System Damping Evaluations," Proc. Second Symposium on Current Issues Related to Nuclear Power Plant Structures, Equipment and Piping, EPRI NP-6437-D, Session 10, pp. 43-65, May 1989.

19. KTA 2201.4 (Proposed new German Standard), "Design of Nuclear Power Plants Against Seismic Influences, Part 4: Requirements for Procedures for the Verification of Earthquake Safety of Mechanical and Electrotechnical Components," Version 6/89.

20. D. Schrammel and H. Steinhilber, "Structural Dynamic Investigations at the HDR, High Level Earthquake Experiment of a Piping System with Different Support Configurations," (In German), Technical Report PHDR 96-90, Sept. 1990.

21. M. G. Srinivasan, C. A. Kot and B. J. Hsieh, "Response of HDR–VKL Piping System to Seismic Test Excitations – Comparison of Analytical Predictions and Test Measurements," Trans. 10th Intl. Conf. on Structural Mechanics in Reactor Technology, Vol. K2, pp. 751–756, Anaheim, CA, 14–18 Aug. 1989.

22. J. D. Wömer, D. Schrammel and G. König, "Time–History Estimation by Using the Ultimate Load Method," Trans. 11th Intl. Conf. on Structural Mechanics in Reactor Technology, Vol. K2, paper K32/7, pp. 469–473, Tokyo, Japan, 18–23 Aug. 1991.

23. M. G. Srinivasan, C. A. Kot and M. Mojtahed, "Analytical Simulation of Nonlinear Response to Seismic Test Excitations of HDR–VKL Piping System," Trans. 11th Intl. Conf. on Structural Mechanics in Reactor Technology, Vol. K2, paper K32/6, pp. 463–468, Tokyo, Japan, 18–23 Aug. 1991.

24. C. A. Kot, M. G. Srinivasan and B. J. Hsieh, "Evaluation of Seismic Margins for an In–Plant Piping System," Trans. 11th Intl. Conf. on Structural Mechanics in Reactor Technology, Vol. K2, paper K19/5, pp. 25–30, Tokyo, Japan, 18–23 Aug. 1991.

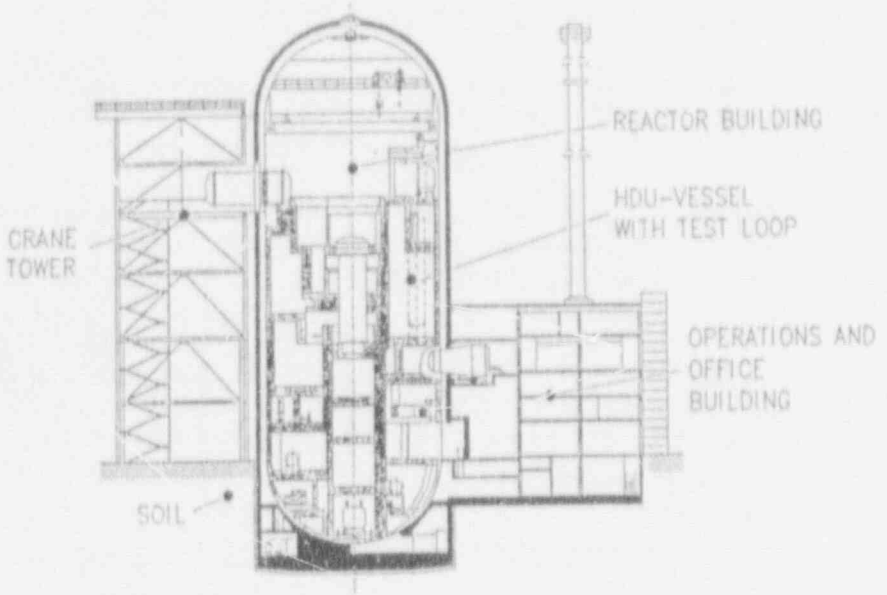

Fig. 1. HDR Reactor Building and Adjacent Structures.

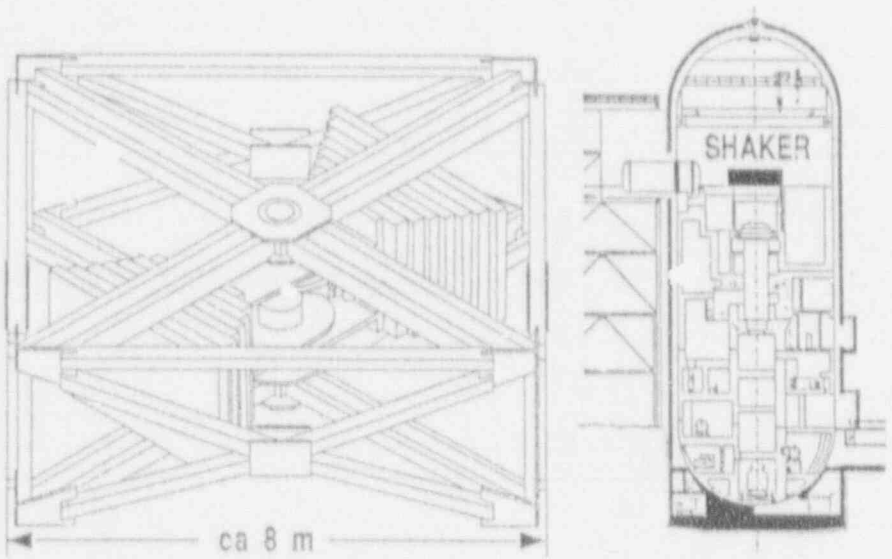

Fig. 2. Coast-Down Shaker Used in SHAG Experiements.

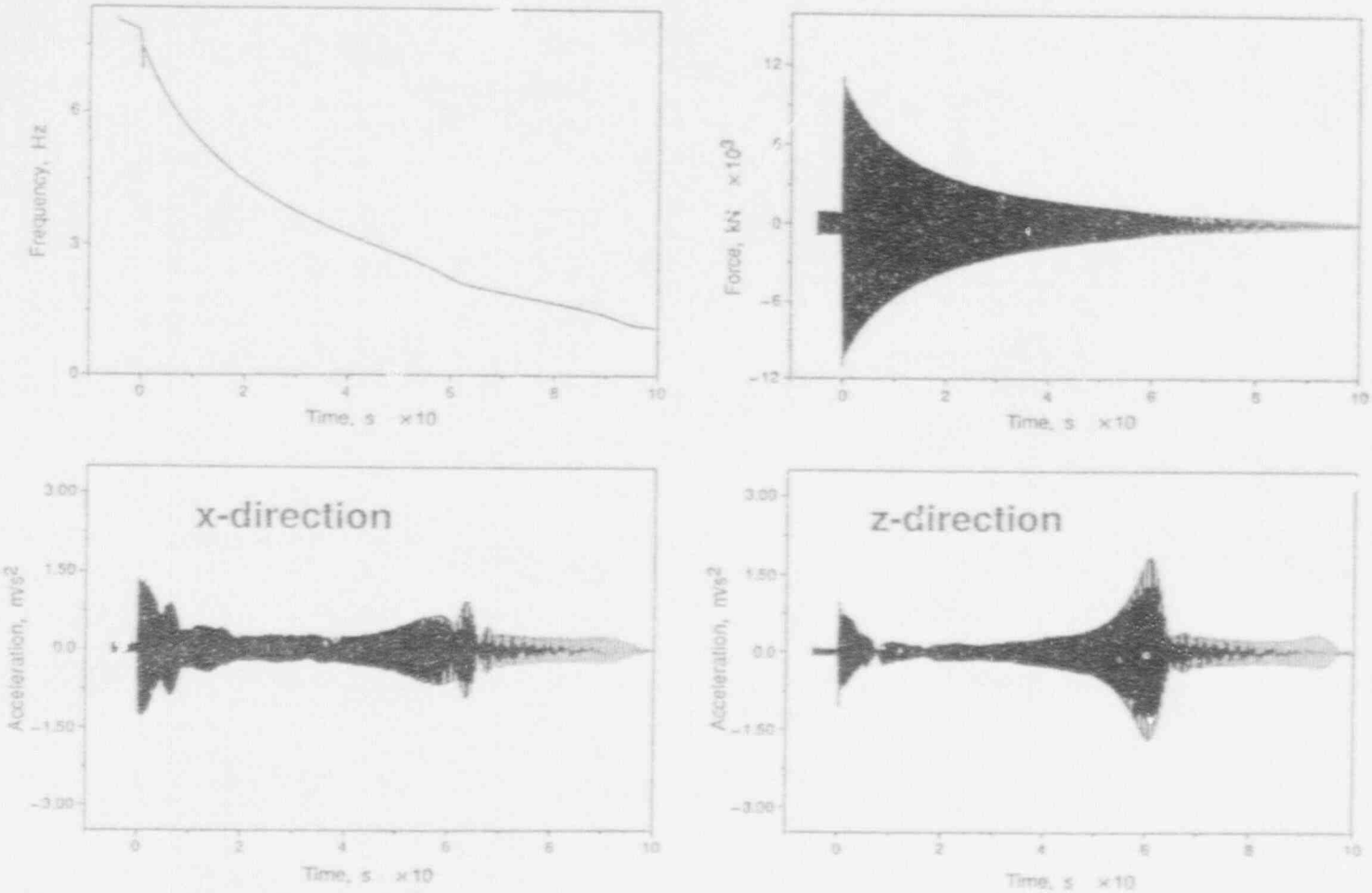

Fig. 3. SHAG Shaker Frequency, Force, and Horizontal Accelerations at Top of HDR Concrete Containment. (8-Hz Run, 4700-kgm Eccentricity.)

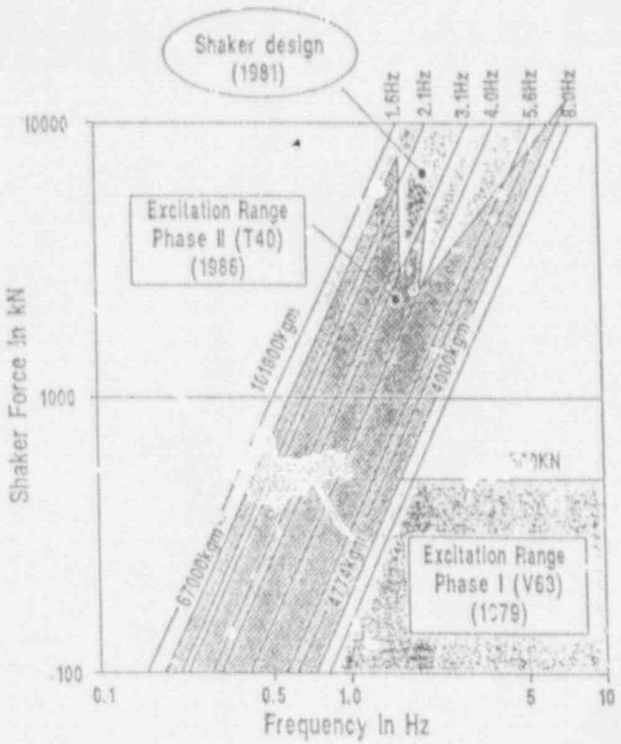

Fig. 4. Range of Excitation Load in SHAG Experiments.

		T40.13 Rocking	T40.37 Bending	Friauler E. quake	El Centro E. quake
Acceleration	(m/sec²)	1.42	1.22	1.05	0.65
Operating floor +30m	%	135	116	100	80
Displacement	(cm)	3.5	1.9	1.2	1.2
Operating floor +30m	%	292	148	100	100
Moment	(MNm)	391	335	183	173
Inner structure	%	214	183	100	95
Moment	(MNm)	400	485	101	107
Outer structure	%	396	480	100	106

Test parameter T40.13: Eccentricity 67000kgm, Starting frequency 1.6Hz
T40.37: Eccentricity 27800kgm, Starting frequency 2.1Hz

Fig. 5. Comparisons of Building Responses, SHAG Test Measurement Versus Computed for Earthquake.

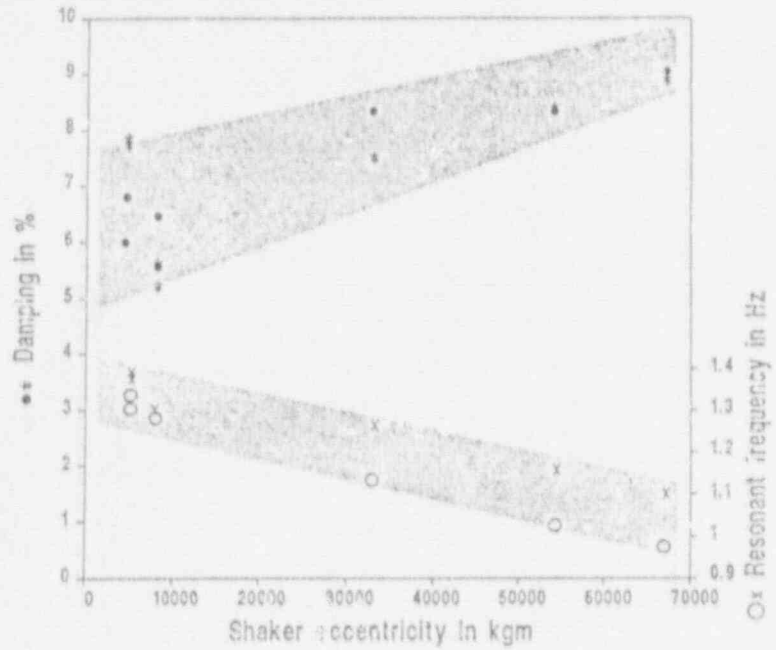

Fig. 6. Change in Rocking Mode Frequency and Damping with Shaker Load.

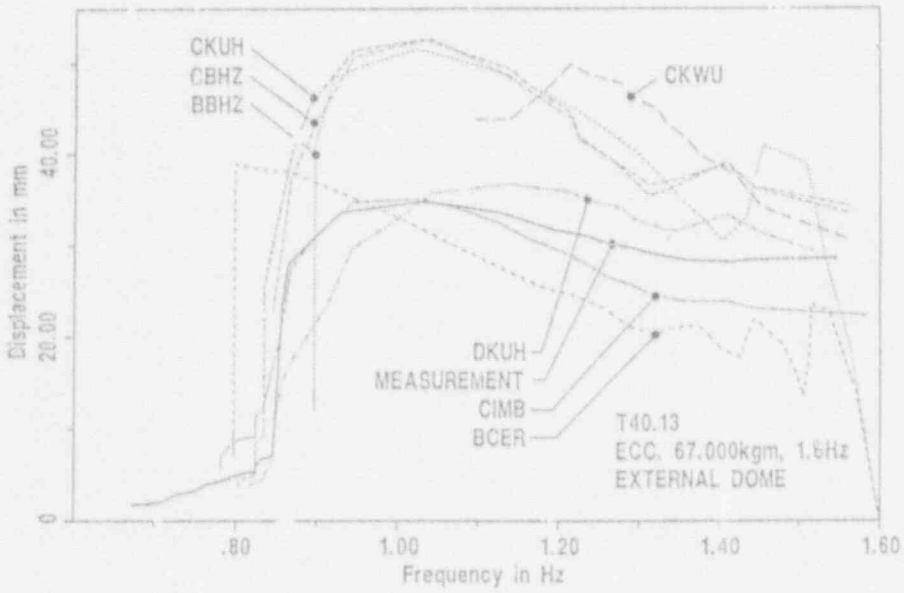

Fig. 7. Comparison of Calculated and Experimental Displacements in SHAG Test.

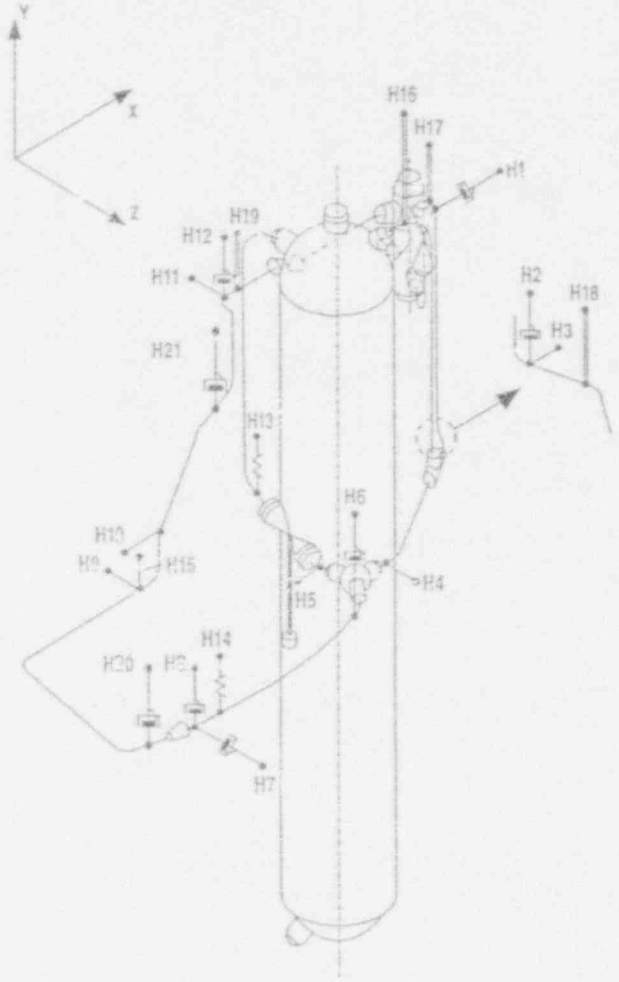

Fig. 8. Schematic of VKL Piping and Support Location in SHAG Tests.

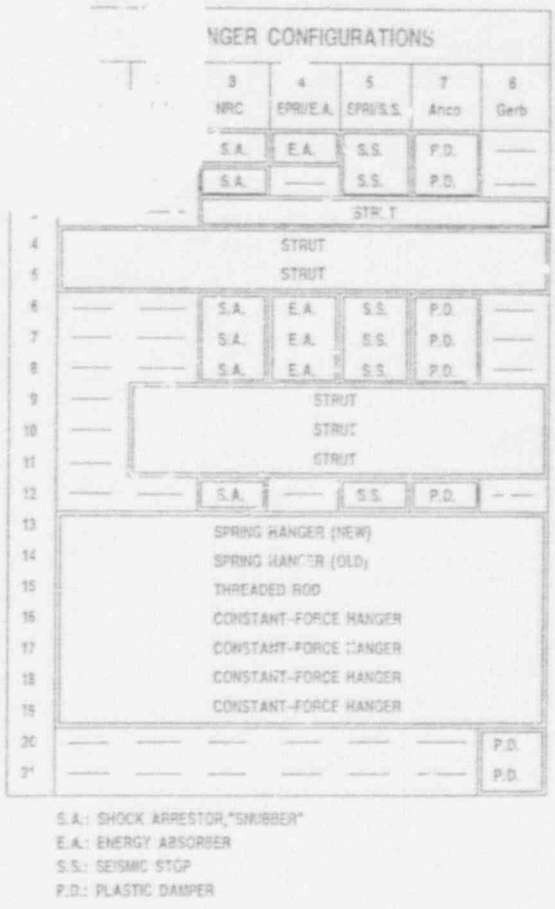

Fig. 9. Hanger Configurations Used in in SHAG Tests.

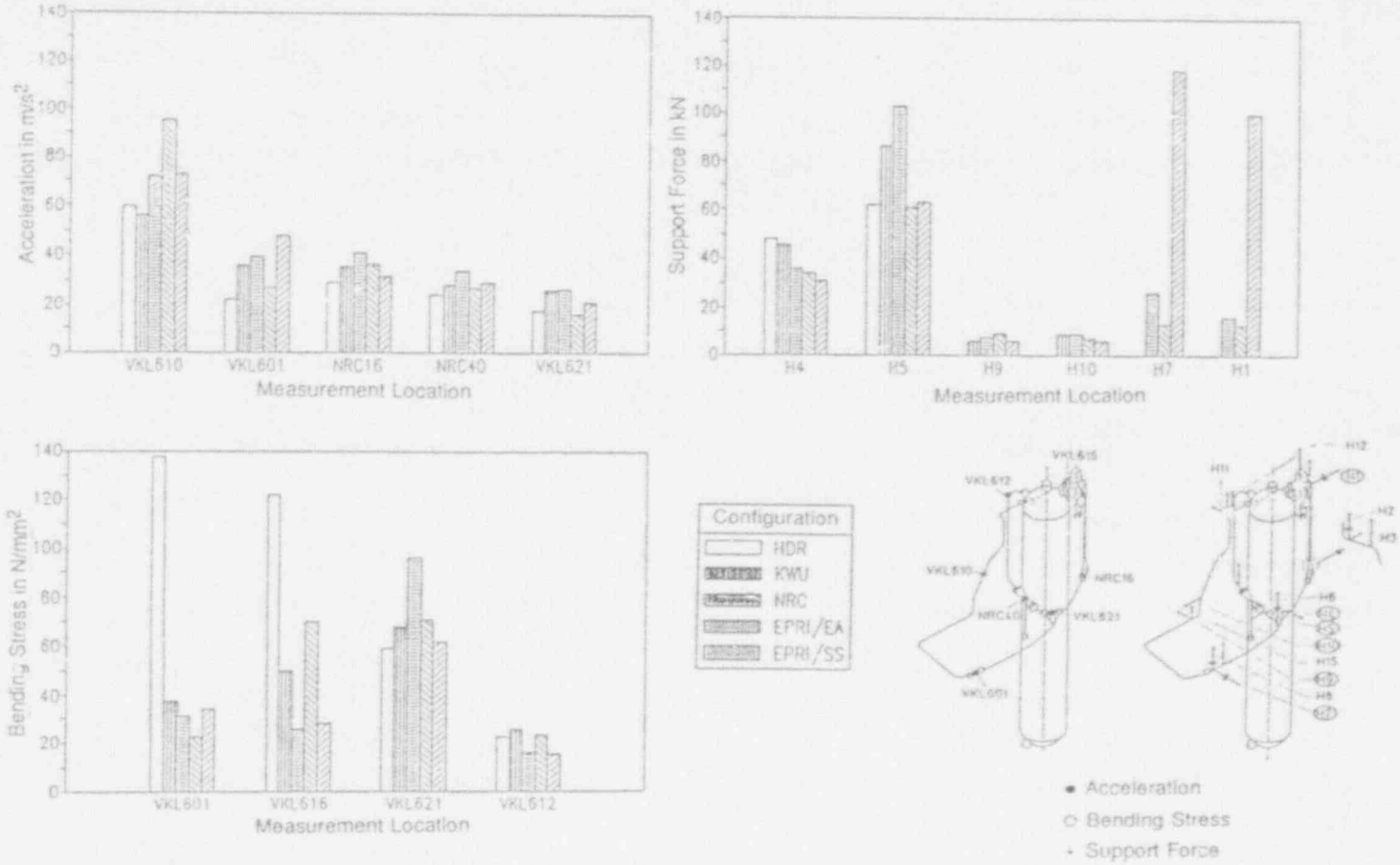

Fig. 10. Comparisons of Normalized VKL Piping Responses for the Different Support Configurations in SHAG.

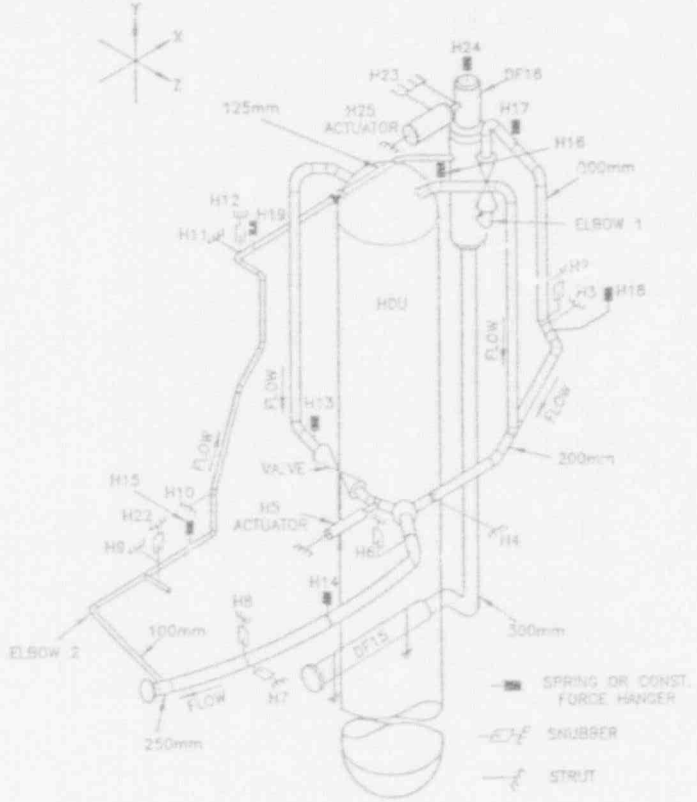

Fig. 11. VKL Piping for SHAM Experiments NRC Support Configuration.

	DYNAMIC SUPPORT CONFIGURATIONS					
Hanger No.	1 HDR	2 KWU	3 NRC	4 EPRI/EA	5 EPRI/SS	6 CEGB
2	—	—	Snubber PSA1	—	Seismic stop	—
3	—	—	Strut Size B			—
4	Strut Size 20					
6	—	—	Snubber PSA 1/2	—	Seismic stop	—
7	—	—	Snubber A/D 150	Energy Absorber	Seismic stop	Strut RS-15
8	—	—	Snubber A/D 70	Energy Absorber	Seismic stop	Strut RS-7
9	—	Strut Size B	Strut Size A			Strut RS-7
10	—	Strut Size B	Strut Size A			—
11	—	Strut Size B	Strut Size A			—
12	—	—	Snubber A/D 40	—	Seismic stop	Strut RS-15
22	—	—	Snubber PSA 1/4	Energy Absorber	Seismic stop	—
23	Two Struts 2 x Size 20					

Fig. 12. Dynamic Support Configurations for SHAM Tests.

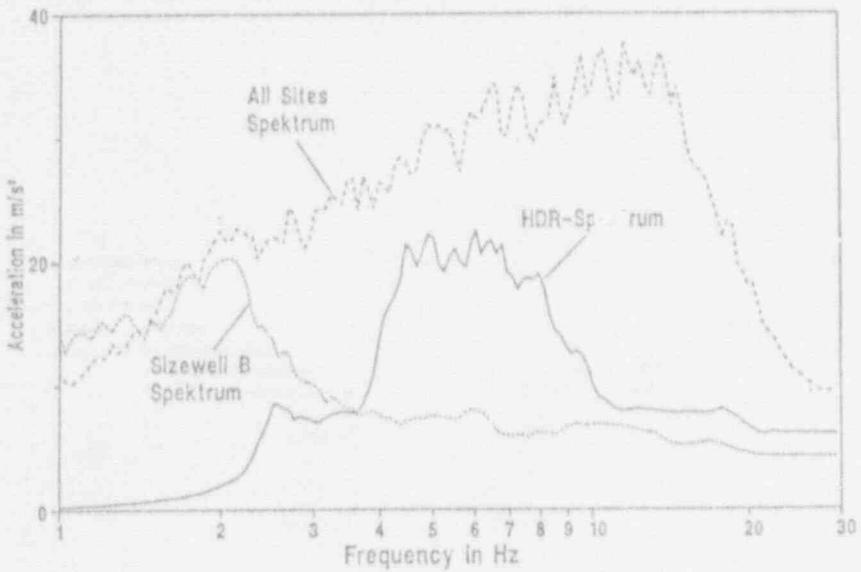

Fig. 13. Response Spectra for the 100% SSE Earthquake Excitation (4% Damping).

Type and Location of Exitation		Hanger Configuration							
		HDR	KWU	NRC	EPRI/ EA	EPRI/ SS	CEGB	CEGB mod.	NRC mod.
		1	2	3	4	5	6	7	8
Random	DF 16	■	■	■	■	■	■		
	H-5	■	■	■	■	■	■		
Earthquake HDR – Spectrum	100 %	■	■	■ ■ ■	■	■ ■ ■	■ ■		
	200 %	■	■	■		■			■
	300 %		■	■ ■	■	■			
	400 %		■		■				
	600 %		■						■
	800 %		■						■
Sizewell B Spectrum	100 %						■	■	
	300 %						■		
All Sites Spectrum	50 %						■		
	200 %						■		
Sine Burst	10 mm						■		
	20 mm						■		
	30 mm						■		
	45 mm						■		
	60 mm						■		

Fig. 14. SHAM Test Matrix.

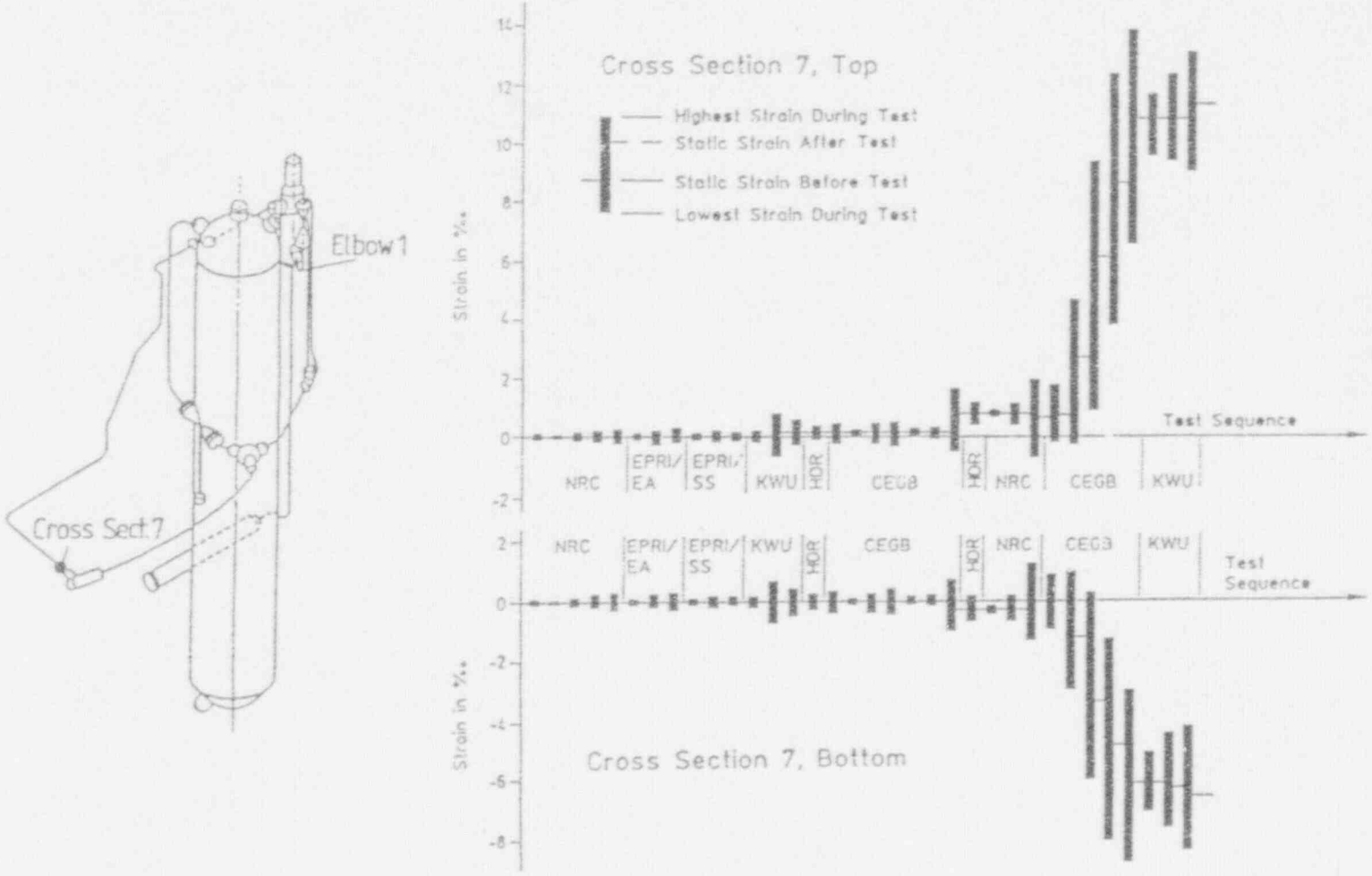

Fig. 15. Range of Strain Amplitudes and Accumulation of Permanent Strains at Cross Section 7.

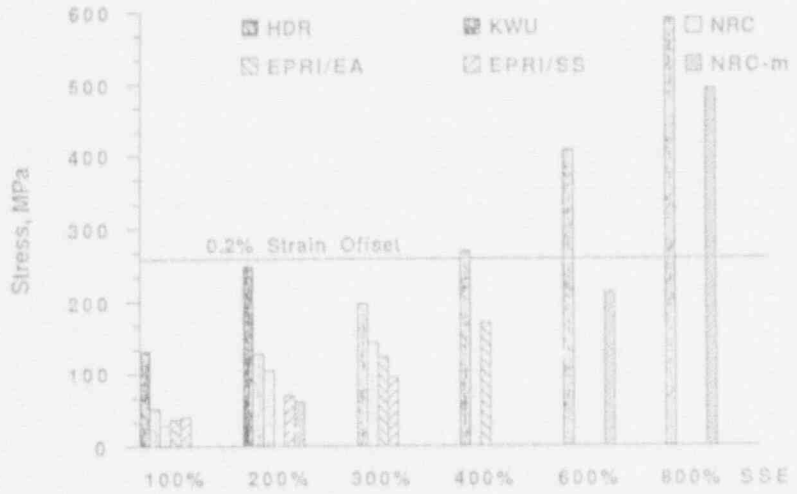

Fig. 16. Maximum Bending Stresses at Tee - 100 mm Pipe (Cross Section 7 in Fig. 15).

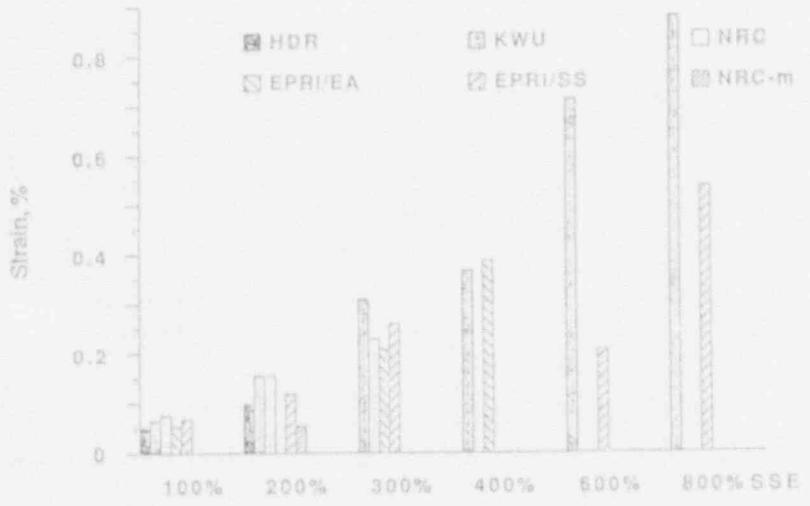

Fig. 17. Maximum Strains at Elbow 1 - 200 mm Pipe (Elbow 1 in Fig. 15).

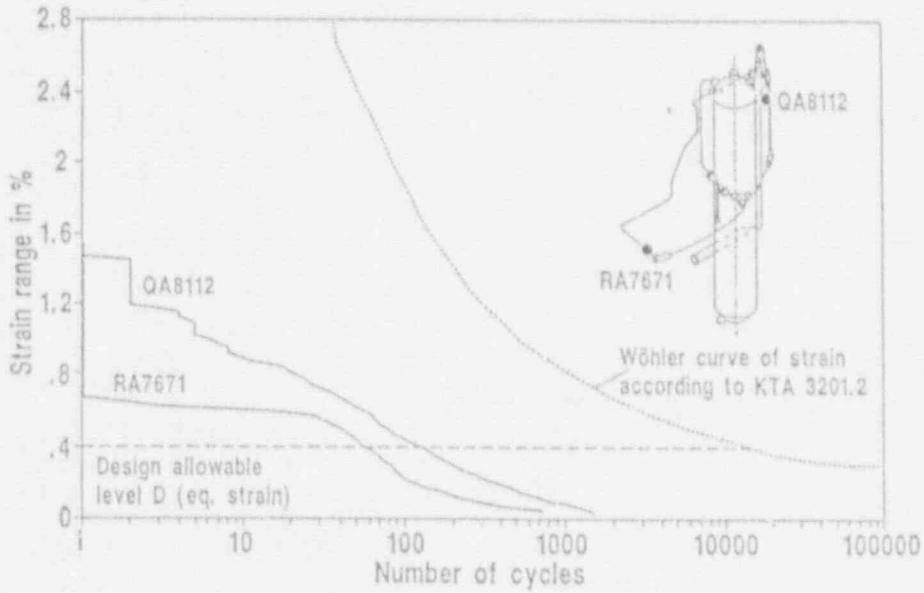

Fig. 18. Frequency Distribution of Measured Strain Amplitude Ranges Compared to Allowables: Level D Design and Fatigue Cycles.

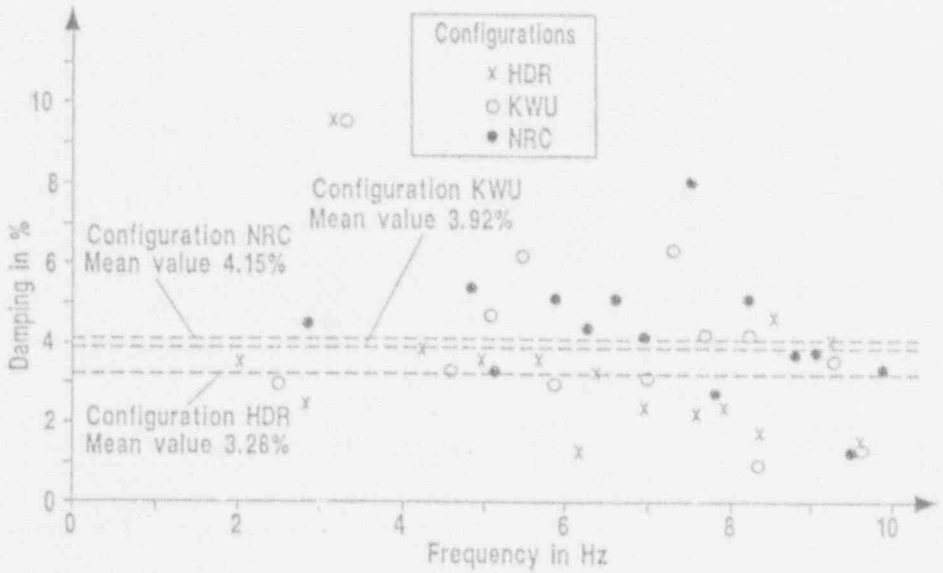

Fig. 19. VKL Piping - Modal Damping and Mean Values for Different Support Configurations (Random Tests).

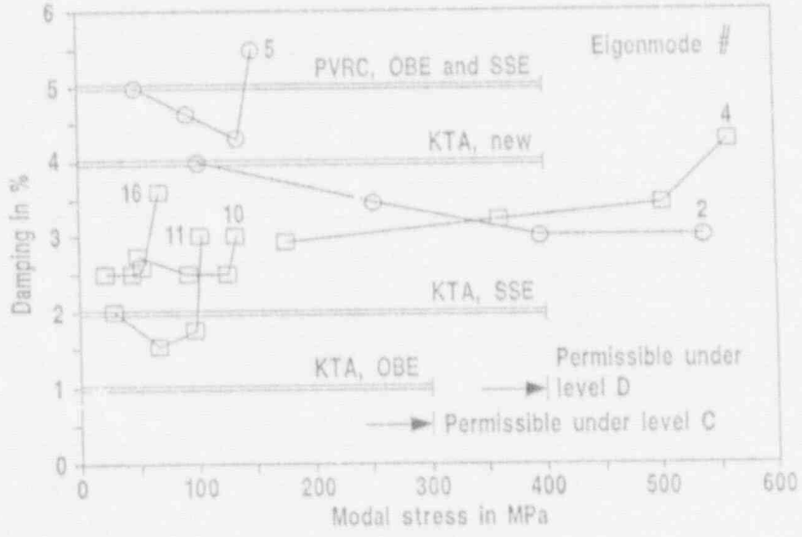

Fig. 20. Dependence of Modal Damping on Load Compared to Standard Damping Values.

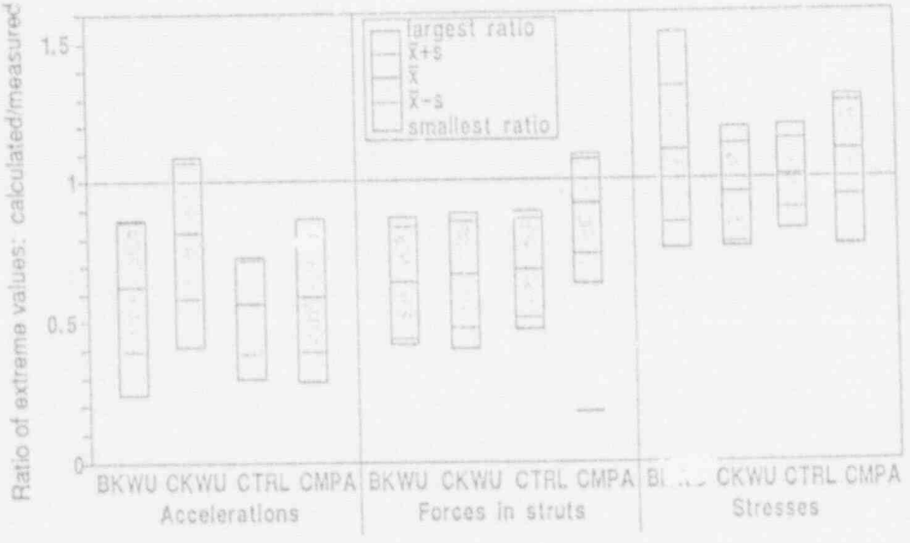

Fig. 21. Statistical Comparison of Linear German Calculations with Measurements for the 100%-SSE Test of the KWU Configuration.

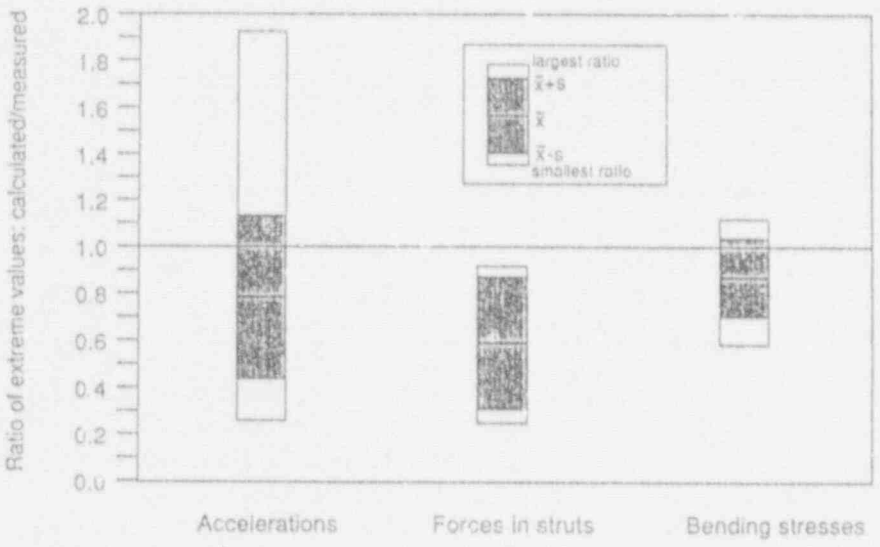

Fig. 22. Statistical Comparison of Linear (SMACS) Post-test ANL Calculations with Measurements for the 100%-SSE Test of the KWU Configuration.

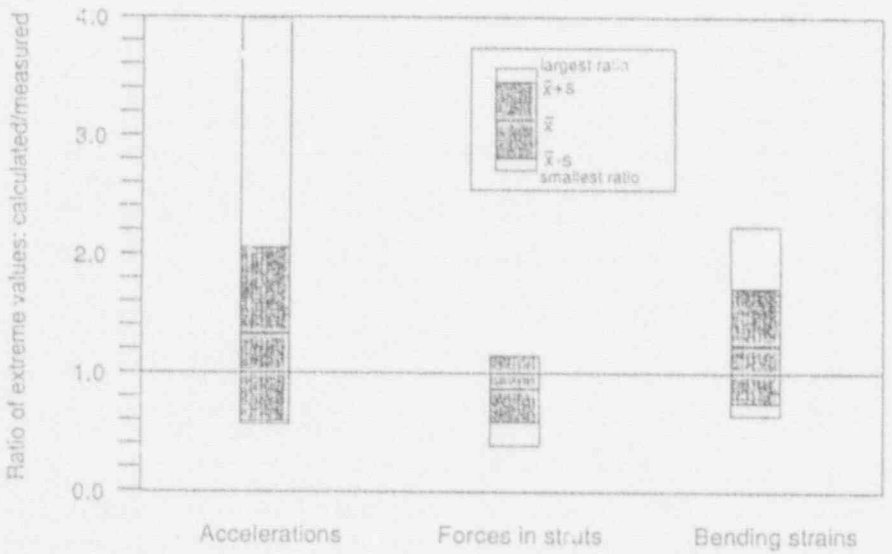

Fig. 23. Statistical Comparison of Nonlinear (NONPIPE) Post-test ANL Calculations with Measurements for the 800%-SSE Test of the KWU Configuration.

PROGRESS IN RESEARCH ON AGING OF STRUCTURES*

D. J. Naus and C. B. Oland
Engineering Technology Division
Oak Ridge National Laboratory (ORNL)
Oak Ridge, TN 37831-8056

B. Ellingwood and Y. Mori
The Johns Hopkins University
Baltimore, MD 21218

E. G. Arndt
U. S. Nuclear Regulatory Commission (NRC)
Washington, D. C. 20555

ABSTRACT

The Structural Aging (SAG) Program is conducted for the Nuclear Regulatory Commission. The program has the overall objective of preparing an expandable handbook or report which will provide the NRC with potential structural safety issues and acceptance criteria for use in nuclear power plant evaluations for continued service. Initial focus of the program is on concrete and concrete-related materials which comprise the safety-related (Category I) structures in light-water reactor facilities. The program consists of a management task and three technical tasks: materials property data base, structural component assessment/repair technology, and quantitative methodology for continued service determinations. Objectives, background information, and accomplishments under each of these tasks are presented.

*Research sponsored by the Office of Nuclear Regulatory Research, U.S. Nuclear Regulatory Commission under interagency Agreement 1886-8084-5B with the U.S. Department of Energy under Contract DE-AC05-840R21400 with Martin Marietta Energy Systems, Inc.

1. INTRODUCTION

History tells us that concrete is a durable material. However, a number of factors can compromise its performance: (1) faulty design, (2) use of unsuitable materials, (3) improper workmanship, (4) exposure to aggressive environments, (5) excessive structural loads, (6) accident conditions, and (7) a combination of the above. Furthermore, aging of nuclear power plant concrete structures occurs with the passage of time and has the potential, if its effects are not controlled, to increase the risk to public health and safety. Many factors complicate the contribution of aging effects to the residual life of the various safety-related concrete structures in a plant. Uncertainties arise due to the following: (1) differences in design codes and standards for components of different vintage; (2) lack of past measurements and records; (3) limitations in the applicability of time-dependent models for quantifying the contribution of aging to overall structure, system, or component failure; and (4) inadequacy of detection, inspection, surveillance, and maintenance methods or programs.[1]

2. BACKGROUND

Within the nuclear power industry, the aging of plant structures, systems, and components has become the subject of significant research in the last few years.[2-4] This interest is prompted by the need to quantify the effects of aging in terms of potential loss of component integrity or function and to support current or future condition assessments of critical components. Since certain concrete structures (Category I) play a vital role in the safe operation of nuclear power plants,[5-8] guidelines and criteria for use in evaluating the remaining structural margins (residual life) of each structure are needed.

3. CATEGORY I CONCRETE STRUCTURES

3.1 Design Considerations

Category I structures are those essential to the function of the safety-class systems and components, as well as those whose failure could lead to loss of function of safety-class systems and components housed, supported, or protected. In addition, these structures may serve as barriers to the release of radioactive material and/or as biological shields. The basic laws that regulate the design (and construction) of nuclear power plants are contained in Part 50 of Title 10 of the *Code of Federal Regulations* (10 CFR 50)[9], which is clarified by Regulatory Guides, Standard Review Plans, NUREG reports, etc. The "General Design Criteria" of Appendix A to 10 CFR 50 require that structures, systems, and components important to safety shall be designed,

fabricated, erected, and tested to quality standards commensurate with the importance of the safety functions to be performed. "General Design Criteria 2" require that the structures important to safety be designed to withstand the effects of natural phenomena (e.g., earthquakes, tsunamis, hurricanes, floods, seiches, and tornados) without loss of capability to perform their safety function. "General Design Criteria 4" require that structures important to safety be able to accommodate the effects of and to be compatible with the environmental conditions associated with normal operation, maintenance, testing, and postulated accidents, including loss-of-coolant accidents. Furthermore, these structures must be appropriately protected against dynamic effects including the effects of missiles, pipe whip, and flooding that may result from equipment failures and from events and conditions outside the nuclear power plant.

Design and construction requirements for Category I concrete structures of early light-water reactor (LWR) designs were specified in American Concrete Institute (ACI) Standard 318 "Building Code Requirements for Reinforced Concrete," (Ref. 10) as supplemented by regulatory guides and by the NRC Standard Review Plan.[11] Current design and construction requirements for concrete structures which perform safety-related functions at nuclear power plants are contained in ACI 349.[12] The procedures and requirements in this document are endorsed by *U.S. Nuclear Regulatory Guide 1.142*[13] as providing an adequate basis for complying with *General Design Criteria for Nuclear Plants* (Appendix A to 10 CFR 50) for structures other than reactor vessels and containments. Section III, Division 2 of the American Society of Mechanical Engineers Boiler and Pressure Vessel Code (ASME Code), first published in 1975, contains rules for the design and construction of concrete containments.[14]

3.2 Description of Category I Concrete Structures

A myriad of concrete structures are contained as a vital part of an LWR facility to provide support, foundation, shielding, and containment functions. The names and configurations of these structures vary somewhat from plant to plant depending on the nuclear steam supply system vendor, architect-engineer firm and owner preference. Primary containment construction types utilized in the U.S. include: steel (PWR ice condensor, PWR large dry, BWR pre-MK, BWR MK I, BWR MKII, and BWR MK III), reinforced concrete (PWR ice condensor, PWR large dry, PWR subatmospheric, BWR MK I, BWR MKII, and BWR MK III), and post-tensioned concrete (PWR large dry and BWR MKII). More detailed descriptions of the primary containments and other safety-related concrete structures are provided in Refs. [7, 8, 15, and 16].

3.3 Potential Degradation Factors

The longevity, or long-term performance, of the Category I concrete structures is primarily a function of the durability or propensity of these structures to withstand potential degradation effects. Over the life of a nuclear power plant, changes in the properties of the structure's constituent materials will in all likelihood occur as a result of aging and environmental stressor effects. These changes in properties, however, may not be detrimental to the point that the structure has deteriorated and is unable to meet its functional and performance requirements.

Concrete in many structures, however, can suffer undesirable degrees of change with time because of improper specifications, a violation of specification, or environmental stressor or aging effects. Primary mechanisms (factors) which can produce premature deterioration of concrete structures include those that impact either the concrete or steel reinforcing materials. Degradation of concrete can be caused by adverse performance of either its cement paste matrix or aggregate materials under chemical or physical attack. Chemical attack may occur in several forms: efflorescence or leaching, sulfate attack, attack by bases and acids, salt crystallization, and alkali-aggregate reactions. Physical attack mechanisms for concrete include: freeze/thaw cycling, thermal exposure/thermal cycling, irradiation, abrasion/erosion/cavitation, and fatigue or vibration. Degradation of mild steel reinforcing materials can occur as a result of corrosion, irradiation, elevated temperature, or fatigue effects. Prestressing materials are susceptible to the same degradation mechanisms as the mild steel reinforcement, plus loss of prestressing force due primarily to tendon relaxation and concrete creep/shrinkage. A more detailed discussion of the degradation mechanisms is provided in Refs. [8, 15, and 16].

4. STRUCTURAL AGING PROGRAM

Results of a study[15] conducted under the NRC Nuclear Plant Aging Research Program[17] were used to help formulate the Structural Aging (SAG) Program which was initiated in mid-1988. The SAG Program has the overall objective of preparing a handbook or report which will provide NRC license reviewers and licensees with the following: (1) identification and evaluation of the structural degradation processes; (2) issues to be addressed under nuclear power plant (NPP) continued service reviews, as well as criteria, and their bases, for resolution of these issues; (3) identification and evaluation of relevant inservice inspection or structural assessment programs in use, or needed; and (4) quantitative methodologies for assessing current, or predicting future, structural safety margins. The results of this study will provide an improved basis for the NRC staff to evaluate requests to continue operation beyond the nominal 40-year design life of a NPP.

The SAG Program consists of a management task (Task S.1) and three technical tasks: materials property data base (Task S.2), structural component assessment/repair technology (Task S.3), and quantitative methodology for continued service determinations (Task S.4). The tasks interface with each other and are augmented by documentation and technology transfer activities. The following sections provide a brief objective statement, background discussion, and summary of accomplishments for each of these tasks.

4.1 Task S.1 - Program Management

4.1.1 Objective

The overall objective of the program management task is to effectively manage the technical tasks undertaken to address priority structural safety issues related to nuclear power plant continued service applications. Management duties include planning, integrating, monitoring, reporting, and technology transfer. A key part of the management function is the integration of the technical objectives and the efforts of various program participants.

4.1.2 Background

The SAG Program is administratively carried out through the Engineering Technology Division of ORNL. A key part of the management function is the integration of the technical objectives and the efforts of the various program participants. Program developments are transferred to the technical community through progress and topical reports, program review meetings, information meetings, open-literature papers, and technical committee participation.

4.1.3 Summary of Accomplishments

Program Planning and Resource Allocation Subtask. Under this subtask, two five-year plans (Ref. 18 is the most recent and final) were prepared and eleven subcontracts have been administered: Construction Technology Laboratories (2); Johns Hopkins University; Multiple Dynamics Corporation; National Institute of Standards and Technology (2); EQE Engineering; Jack R. Benjamin and Associates; Taywood Engineering, Ltd.; Wiss, Janney, Elstner Associates, Inc.; and Sargent & Lundy Engineers. Certain of these subcontract activities will be discussed later in this document under the appropriate program task.

Program Monitoring and Control Subtask. Program monitoring and control activities have included: preparation of annual technical progress reports (Ref. 19 is the most recent), presentation of papers at the Water Reactor

Safety Information Meetings,[16,20-22] and several briefings to NRC personnel.

Documentation and Technology Transfer Subtask. Documentation and technology transfer actions have included the preparation of 26 technical reports and papers, technical presentations at 15 meetings, and participation in 11 technical committees.[19] Technology exchange has continued at both the international and domestic levels with contacts at more than 80 international and 70 domestic research organizations.

4.2 Task S.2 - Materials Property Data Base

4.2.1 Objective

The objective of the materials property data base task is to develop a computer-based structural materials property data base which will contain information on the time variation of material properties under the influence of pertinent environmental stressors and aging factors. The data base will have use in the prediction of potential long-term deterioration of critical structural components in NPPs and in establishing limits on hostile environmental exposure for these structures. The results also will have application in helping to establish maintenance or remedial measures programs that will assist in prolonging component service life and improving the probability of the component surviving an extreme event such as a LOCA.

4.2.2 Background

One of the findings in Ref. 15 was that materials property data for concrete over an extended time period are limited. This is especially true for concretes which have been subjected to aging factors or environmental stressors characteristic of those that could occur in a NPP. Another limitation on materials property data availability is that in order for the data to be considered as being of "high quality," detailed information such as constituent composition, mixture proportions, curing conditions, environmental exposure, etc., are required. Unfortunately, for most structures that have been in service for the period of interest, 30 to 100 years, this information and the time variation of the properties of the construction materials are not available.

4.2.3 Summary of Accomplishments

Structural Materials Information Center (SMIC) Formulation/ Implementation Subtask. A vital component of the SAG Program is the development of the SMIC. The SMIC will consist of two formats: the data base will be available in an expandable, hard-copy handbook version (*Structural Materials Handbook*) and in an electronic version (*Structural Materials Electronic Data Base*) for use on

an IBM-compatible personal computer.[23] The handbook will serve as the information source upon which the electronic data base is built. Initially, information related to concrete, metallic reinforcements, prestressing steels, and structural steels will be incorporated into the data base. As the data base is developed, other structural materials will be added.

Structural Materials Handbook

The *Structural Materials Handbook* is an expandable, hard-copy reference document that contains complete sets of data and information for each material in SMIC. The handbook consists of four volumes that are provided in loose-leaf binders for ease of revision and updating. Volume 1 presents design and analysis information useful for structural assessments and safety margins evaluations, for example, design values for mechanical, thermal, physical, and other properties presented as tables, graphs, and mathematical equations. Volume 2 provides test results and data used to develop the design values in Volume 1. Volume 3 presents material data sheets which provide general information, as well as material composition and constituent material properties, for each material system contained in the handbook. Volume 4 contains appendices describing the handbook organization, as well as updating and revision procedures.

Initially, Volumes 1, 2, and 3 of the handbook each will contain four chapters of materials property data and information, with the chapters consistent between volumes. Each material in the data base is assigned a unique seven-character material code[23] which is used in both the handbook and electronic data base to organize materials with common characteristics. This code consists of a chapter index, a group index, a class index, and an identifier. The chapter index is used to represent the various material systems in the data base. The group index is used to arrange materials in each chapter into subsets of materials having distinguishing qualities such as common compositional traits. The class index is used to organize groups of materials with common compositional traits into subsets having a similar compositional makeup or chemistry. The identifier is used to differentiate structural materials having the same chapter, group, and class indices according to a specific concrete mix, ASTM standard specification for metallic reinforcement, etc.

A wide variety of information and materials property data is collected and assembled for each material system included in the data base, for example, general description, composition, mechanical property data, etc. In setting up the data base, each material property has been identified by a unique four-digit property code[23] selected from an established set of material property categories, e.g., general information, constituent material and plastic concrete properties, mechanical properties, etc.

Associated with each entry of data (numerical results of tests) or values (results of evaluation of data) into the data base is an assessment of the quality of the entries presented in the form of a letter grade. Although the criteria for assessing the quality of data and values are somewhat subjective, five quality levels have been developed. These levels, presented in order of descending quality, include recommended, selected, typical, provisional, and interim. Eleven criteria are utilized in the evaluation of the quality of data and values.[23]

Structural Materials Electronic Data Base

The *Structural Materials Electronic Data Base* is an electronically accessible version of the *Structural Materials Handbook*. It has been developed on an IBM-compatible personal computer using a data base management system. To ensure that the handbook and electronic data base are compatible, each material included in the electronic data base is identified by the same common name and material code that has been used to represent the material in the handbook. Due to software limitations, the electronic data base is not as comprehensive as the handbook, but it does provide an efficient means for searching the various data base files to locate materials with similar characteristics or properties.

The electronic data base management system includes two software programs: MatDB[24] and EnPlot.[25] MatDB is a menu-driven software program that employs window overlays to access data searching and editing features. It is capable of maintaining, searching, and displaying textual, tabular, and graphical information and data contained in electronic data base files. EnPlot is a software program that incorporates pop-up menus for creating and editing engineering graphs. It includes curve-fitting and scale-conversion features for preparing engineering graphs and utility features for generating output files. The graphs generated with EnPlot can be entered directly into the MatDB data base files. These graphs are compatible with Microsoft Word, the word processing software used to prepare the handbook. Both MatDB and EnPlot operate on an IBM PC, PC/XT, PC/AT, or compatible computer. System requirements include 640 K of memory, hard disk, graphics card, monitor, and DOS 3.0 or later.

Data Collection Subtask. In parallel with the efforts to develop SMIC, numerous activities are being conducted relative to development of materials property data for input into SMIC. Potential sources of information include cognizant foreign research establishments in Europe, North America, and Asia; domestic research establishments such as government facilities, universities, and consulting/engineering firms; and obtaining and testing of aged material samples from prototypical nuclear power plants or civil works structures. To date, data bases have been prepared for 37 material systems: 34 concretes, one metallic reinforcement, one prestressing tendon and one structural steel.

Material Behavior Modeling Subtask. Prediction or explanation of the complex inter-relationships that occur between concrete's constituents and between concrete and its environment requires the development of mathematical models based on scientific and engineering principles. Such models play a vital role in the development of reliability-based life prediction methodologies for concrete structures in nuclear power plants.

Activities under this subtask are being conducted at the National Institute of Standards and Technology (Gaithersburg, Maryland) and address evaluation of: (1) models which possibly could be used for predicting the remaining service life of concrete exposed to major environmental stressors and aging factors, and (2) accelerated aging techniques and tests which either provide data for service life models or which themselves can be used to predict the remaining service life of existing structures. Possible significant degradation processes which were identified for concrete structures in nuclear power plant facilities included corrosion of steel reinforcement, sulfate attack, alkali-aggregate reactions, frost attack, leaching, radiation, salt crystallization, and microbiological attack. Models identified for these processes were evaluated. Methods used for prediction of service lives of construction materials have included estimates based on experience, deductions from performance of similar materials, accelerated testing, applications of reliability and stochastic concepts, and mathematical modeling based on the chemistry and physics of degradation processes. A draft report has been prepared presenting results of this study.[26]

4.3 Task S.3 - Structural Component Assessment/Repair Technology

4.3.1 Objective

The overall objectives of this task are to (1) develop a systematic methodology which can be used to make a quantitative assessment of the presence, magnitude, and significance of any environmental stressors or aging factors which could impact the durability of safety-related concrete components in NPPs and (2) provide recommended inservice inspection or sampling procedures which can be utilized to develop the data required both for evaluating the current structural condition as well as trending the performance of these components for use in continued service assessments. Associated activities in meeting the objectives of this task include the identification and evaluation of techniques for mitigation of any environmental stressors or aging factors which may act on critical concrete components, and an assessment of techniques for repair, replacement, or retrofitting of concrete components which have experienced an unacceptable degree of deterioration.

4.3.2 Background

Evaluation of Concrete Material Systems. Since the ability of a concrete component to meet its functional and performance requirements over an extended period of time is dependent on the durability of its constituents, techniques for the detection of concrete component degradation should address evaluation of the concrete, mild steel reinforcing, prestressing system, and anchorage embedments.

Concrete cracking, voids, and delaminations can be detected by visual inspections, nondestructive testing (ultrasonic and stress wave, acoustic impact, radiography, penetrating radar, thermal mapping), and core examination. In-situ concrete strength determinations are through either direct (core tests) or indirect techniques (surface hardness, rebound, penetration, pullout resistance, break-off resistance, and ultrasonic pulse velocity). The primary distress to which mild steel reinforcement could be subjected is corrosive attack. Techniques for corrosion monitoring and inspection of steel in concrete include visual, mechanical and ultrasonic tests, core sampling in conjunction with chemical and physical tests, potential and thermal mapping, and rate of corrosion probes. The present basis for conducting tendon inspections is presented in NRC Regulatory Guide (RG) 1.35, "Inservice Inspections of Ungrouted Tendons in Prestressed Concrete Containments (Rev. 3)" and companion RG 1.35.1, "Determining Prestressing Forces for Inspection of Prestressed Concrete Containments." Failure of a concrete embedment will generally occur as a result of either improper installation or deterioration of the concrete within which it is embedded. A combination of visual examinations and mechanical tests is used to evaluate the general condition of an embedment.

More detailed information on many of the above techniques can be obtained from Ref. 27. Quantitative interpretation of the results obtained from many of the nondestructive evaluation (NDE) methods can be difficult, however, due to the absence of correlation curves to relate in-situ strength to NDE parameters. Also, many of the methods only make surface determinations of concrete properties which can be quite different from internal properties, particularly where a component may be several meters thick. In addition, none of the techniques provide rate effect data which can be used for continued service considerations.

Inservice Inspection of NPPs. Inservice inspection requirements are imposed on nuclear plants through documents such as the following: 10 CFR 50, NRC Regulatory Guides, Plant Technical Specifications, Inspection and Enforcement Bulletins, NRC letters, and Section XI of ASME *Boiler and Pressure Vessel Code*.[28] However, because each nuclear plant has its unique construction permit issue and operating license issue dates, each plant could potentially have a different set of minimum inservice inspection requirements. Therefore,

to simplify continued service evaluations, it would be advantageous to have a standardized inservice inspection program that could not only be used to identify but also to quantify any deteriorating influences. Limited information on criteria, inspection, and testing requirements for development of such a procedure are available in the form of documents published by the American Concrete Institute.[29-32] Additional information is provided in Refs. 33-35. However, the application of requirements presented in these documents to nuclear safety-related concrete structures requires evaluation.

Remedial Measures. Objectives of remedial work are to restore the component's structural integrity, arrest the mechanism producing distress, and ensure, as far as possible, that the cause of distress will not reoccur. Basic components of a program to meet these objectives include diagnosis (damage evaluation), prognosis (can repair be made and is it economical), scheduling (priority assignments), method selection (depends on nature of distress, adaptability of proposed method, environment, and costs), preparation (function of extent and type of distress), and application.[36]

Typical types of distress that can occur in LWR concrete structures and necessitate repair actions include cracking, spalling or delamination, nonvisible voids, and fracturing or shattering. Although a wide variety of materials are available for the repair or maintenance of concrete exhibiting distress, they generally include one or more of the following materials: epoxy resins, shotcrete, preplaced aggregate concrete, epoxy ceramic foams, replacement mortar or concrete, wedge anchors and additional reinforcement, and miscellaneous sealant materials.[37] Selection of the technique for repair of a concrete structure depends to a large degree on the size, depth, and area of repair required. Existing elements can also become inadequate due to either a change in performance requirements or occurrence of an overload condition. Under these conditions retrofitting may be required to reestablish serviceability. Retrofitting can be accomplished by either strengthening of existing elements, replacement, addition of new force-resisting elements, a combination of element strengthening and addition, or use of supplemental connecting devices.[37] Criteria for application of the repair techniques require development.

4.3.3 Summary of Accomplishments

LWR Critical Concrete Component Classification Subtask. Under a subcontract with Multiple Dynamics Corporation (Southfield, Michigan), a report has been prepared which presents an aging assessment methodology for concrete structures in nuclear power plants.[38] Pertinent components of the methodology include a concrete component classification system, a degradation factor significance assessment technique, and a structural subelement and cumulative ranking system.

Typical safety-related concrete structures in LWR facilities are identified, described, and their design and construction requirements and primary materials of construction designated. The relative importance of the structure's subelements, safety significance of each Category I structure, and influences of environmental exposure are presented in terms of numerical rating systems. The importance of a subelement to a specific structure is related to its impact on the ability of the structure to meet its functional and performance requirements. The rating system established for structural subelement importance is based on a 1 to 10 scale, with 10 being highest. The safety significance of the subelement is assessed based on the importance of the safety function the subelement may be (or is) required to perform, as well as the number of safety functions it must meet. Each subelement is ranked on a scale of 0 to 10, with 10 being highest, using ranking criteria that have been established. Since environmental effects are highly influential on the service life of concrete structures, an environmental exposure classification procedure was also developed. A rating system was established to incorporate environmental exposure conditions and includes seven categories, ranging from most severe (subterranean) to mildest (controlled interior). The resulting environmental rating system is based on a 1 to 10 scale, with 10 being most aggressive.

Potential degradation or aging factors which could affect the performance of the Category I concrete structures during their lifetime were previously identified (Section 3.3). The significance of a particular degradation factor is evaluated for a particular structure/subelement in terms of (1) its effect on overall structural integrity, (2) environmental conditions present, and (3) materials of construction. Because of the variability in likelihood of occurrence of degradation to concrete structures in U.S. LWR plants due to design differences, material utilization, geographical location, etc., the grading system for degradation factors is provided in terms of a possible range of values. Pertinent degradation factor grading values are selected from the ranges of possible values, based on site-specific characteristics. The resulting degradation factor grading values for the individually evaluated subelement (between 1 and 10) are then combined into a single degradation factor significance value by summing the degradation factor grading values and dividing by the number of degradation factors, for instance,

$$DFS = \left(\sum_{i=1}^{n} DFG_i\right) / n, \qquad (1)$$

where

DFS = degradation factor significance value, rounded to nearest integer,

DFG = degradation factor grading value, and

n = number of degradation factors, up to a total of three.

Determination of the relative ranks of the Category I structures and their subelements is based on the weighted contributions of: (1) structural importance of subelements, (2) safety significance, (3) environmental exposure, and (4) degradation factor significance. A subelement rank within each Category I structure is determined as follows:

$$SR = w_1(I) + w_2(SS) + w_3(DEG), \quad (2)$$

where

SR = subelement rank,
I = subelement importance,
SS = safety significance
DEG = (EE + DFS)/2, rounded to nearest integer,
EE = environmental exposure,
DFS = degradation factor significance [Eq. (1)], and
w_1, w_2, w_3 = weighting factors.

Use of weighting factors (1 to 10, with 10 highest) permits certain components of Eq. (2) to be emphasized. Since the degradation factor significance was considered to be heavily influenced by the environmental exposure, these two criteria have been combined, averaged, and rounded to the nearest whole integer. The cumulative rank for each Category I concrete structure is determined as follows:

$$CR = \sum_{i=1}^{N} SR_i / N, \quad (3)$$

where

CR = cumulative rank,
SR = subelement rank, and
N = number of subelements for the particular primary structure.

Application of Eq. (3) ensures that the cumulative rank of a Category I concrete structure is based on aging importance rather than total number of subelements.

NDE/Sampling Inspection Technology Subtask. The major emphasis of work under this subtask has been related to activities conducted at the Construction Technology Laboratories, Inc. (Skokie, Illinois), to review and assess inservice inspection techniques and methodologies for application to concrete structures in nuclear power plants. Both direct and indirect methods used to detect degradation of concrete materials have been reviewed. Direct techniques generally involve a visual inspection of the structure, removal/testing/analysis of material, or a combination. Periodic visual examinations of exposed concrete provide a rapid and effective means for identifying and defining areas of distress, for example, cracking, spalling, and volume change. In areas exhibiting extensive deterioration, or when

quantitative results are desired, core samples can be removed for strength testing and petrographic examination. The indirect techniques measure some property of concrete from which an estimate of concrete strength, elastic behavior, or extent of degradation can be made through correlations that have been developed. Several potential nondestructive techniques for evaluating concrete materials and structures include (1) audio, (2) electric, (3) impulse radar, (4) infrared thermography, (5) magnetic, (6) microscopic refraction, (7) modal analysis, (8) nuclear, (9) radiography, (10) rebound hammer, (11) ultrasonic, and (12) pulse echo. In addition to core sampling, potential destructive testing techniques that can be used to evaluate concrete materials include (1) air permeability, (2) break-off, (3) chemical, (4) probe penetration, and (5) pull out. A description of each of these test methods, as well as their capabilities and limitations, has been compiled and a report prepared.[39]

Remedial/Preventative Measures Considerations Subtask. Two subcontracts have been implemented under this subtask. The first subcontract has been placed with Taywood Engineering, Ltd. (TEL), (London, England) and the second with Wiss, Janney, Elstner Associates (WJE) (Northbrook, Illinois). Basic activities conducted under each of these subcontracts are related to a review of repair procedures for concrete material/structural systems, establishment of criteria for their utilization, and evaluation of their effectiveness. Whenever possible, actual applications of repair procedures to nuclear power plant concrete structures are to be factored into the assessment. Any potential impacts of a repair on the inspection procedures are to be addressed as well as techniques which can be used to mitigate the effects of environmental stressors or aging factors. Recommended preventative measure procedures which can be used to effectively offset, counteract, or minimize any minor deterioration effects to prevent them from becoming significant will be established. The subcontract with TEL is addressing repair practices from the European perspective and the WJE subcontract from the U.S. perspective. Both of these subcontracts will be completed during FY 1992.

4.4 Task S.4 - Quantitative Methodology For Continued Service Determinations

4.4.1 Objective

The overall objective of this task is to develop reliability-based procedures that can be used for performing condition assessments and making life predictions of critical concrete structures in nuclear power plants.

4.4.2 Background

Once it has been established that a component has been subjected to environmental stressors or aging factors that have resulted in deteriorating influences, the effects of these influences must be examined and related to a

condition or structural reliability assessment, especially where the component is being considered for a continuation of its service past its initial licensing period. In order to continue the operation of NPPs, evidence should be provided that the critical safety-related concrete structures in these facilities in their current condition are able to withstand potential future design events (over the continued service period) with a level of reliability adequate to meet requirements for protecting public health and safety.

A methodology for conducting such an assessment presently does not exist;[15,18] however, structural reliability techniques have advanced to the point where it should be possible to make a quantitative evaluation of the durability (residual life) of a concrete structure based on a knowledge of the condition of the structure when it was built, its service history, its present condition, and projected use during a time interval past its initial licensing period.[40,41] Such techniques would provide guidance to utilities and regulators alike regarding the technical data to be submitted in support of an application for continued service, current structural condition, and the need, if any, for future inspections or regular maintenance as a condition for granting a license for continued operation.

4.4.3 Summary of Accomplishments

A reliability-based methodology for assessing the current condition and future structural performance of concrete structures subjected to aging, particularly from environmentally aggressive stressors, is being developed by researchers at the Johns Hopkins University (Baltimore, Maryland). The methodology takes into account the stochastic nature of past and future loads due to operating conditions and the environment, randomness in strength and in degradation processes. The methodology is summarized below. More detailed information is contained in Refs. 22 and 42.

Component Aging and Structural Resistance. A large volume of statistical data has been gathered in research over the past decade to develop improved bases for structural design of common reinforced concrete structures[43] and concrete structures in nuclear power plants.[44] The strength statistics presented in Ref. 44 are based on the assumptions that (1) the rate at which load is applied to the component is relatively slow, (2) variabilities in material properties and dimensions correspond to levels of on-site quality control that are typical of those found at a nuclear plant construction site, and (3) long-term strength changes in the concrete or steel due to maturity of concrete, environmental stressors, and possible corrosion of reinforcement are ignored. Time-dependent effects on in-situ strength were ignored in developing probability-based limit state design procedures for concrete structures (for example, Ref. 45). However, such effects must be considered in assessing the effects of aging and possible structural deterioration and in performing condition assessments of existing concrete structures in nuclear plants.

Environmental stressors may attack the integrity of the concrete and/or steel reinforcement in concert with or independent of operating environmental or accidental loads.[46-48] For concrete strength, the most significant factors are freeze-thaw cycling, sulfate attack, alkali-aggregate reactions within the concrete, and temperature and irradiation effects. For deformed bar reinforcement, the possibility of corrosion is the most important, followed by elevated temperature and irradiation effects; for prestressing tendons, detensioning due to tendon relaxation, anchorage failure, or creep in the concrete must be considered in addition to the factors that affect deformed bars. Conceptually, a time-dependent degradation function, g(t), defining the fraction of initial strength remaining at time t, can be associated with each of these environmental stressors.[42] Moreover, g(t) may not be monotonic because of the presence of several mechanisms, some of which may degrade concrete strength while others may cause the strength to increase. Due to uncertainty in the degradation mechanisms and the lack of experimental data, the functions g(t) ultimately should be treated as stochastic rather than as deterministic.

Stochastic Load Models. Events giving rise to significant structural loads occur randomly in time and are random in their intensity. If the load intensity varies negligibly or slowly during the interval in which it occurs, its effect on the structure is essentially static. For reliability analysis purposes, then, the load intensity can be treated as constant during an event. When viewed on a timescale of 40 years, the duration of design-basis events generally is very short, and thus such events occupy only a small fraction of the total life of a component. With these assumptions, a structural load history can be modeled as a sequence of randomly occurring pulses with random intensity, S_j, and duration, τ, as illustrated in Fig. 1. It is assumed that the event duration is sufficiently short that any change to the state of the structure occurs only during the application of the load (for instance, cumulative damage during a load event does not occur). Many of the operating, environmental, and accidental loads that act on nuclear power plant structures can be modeled by such processes.[49]

The load process shown in Fig. 1 must be described statistically in order to be useful in performing time-dependent reliability analyses. Based on the above description of design events, the occurrence in time of a particular event (for example, accidental pressurization) may be described by a Poisson point process. With the Poisson model, the probability that N(t) load events occur within the interval (0,t) is

$$P[N(t) = n] = \frac{(\lambda t)^n \cdot \exp(-\lambda t)}{n!}; n = 0,1,2,... \qquad (4)$$

in which $P[\cdot]$ = probability of event in brackets and λ = mean rate of occurrence of the events. The sequence S_j, $j = 1,2,\ldots,n$, are assumed to be identically distributed and statistically independent random variables described by distribution function $F_S(x)$. This simple stochastic load model allows the temporal variation in the load to be described by the mean rate of occurrence, the event duration, τ, and the distribution function of the intensity of the structural action, S, arising from the event. These statistical descriptors are illustrated in Fig. 1.

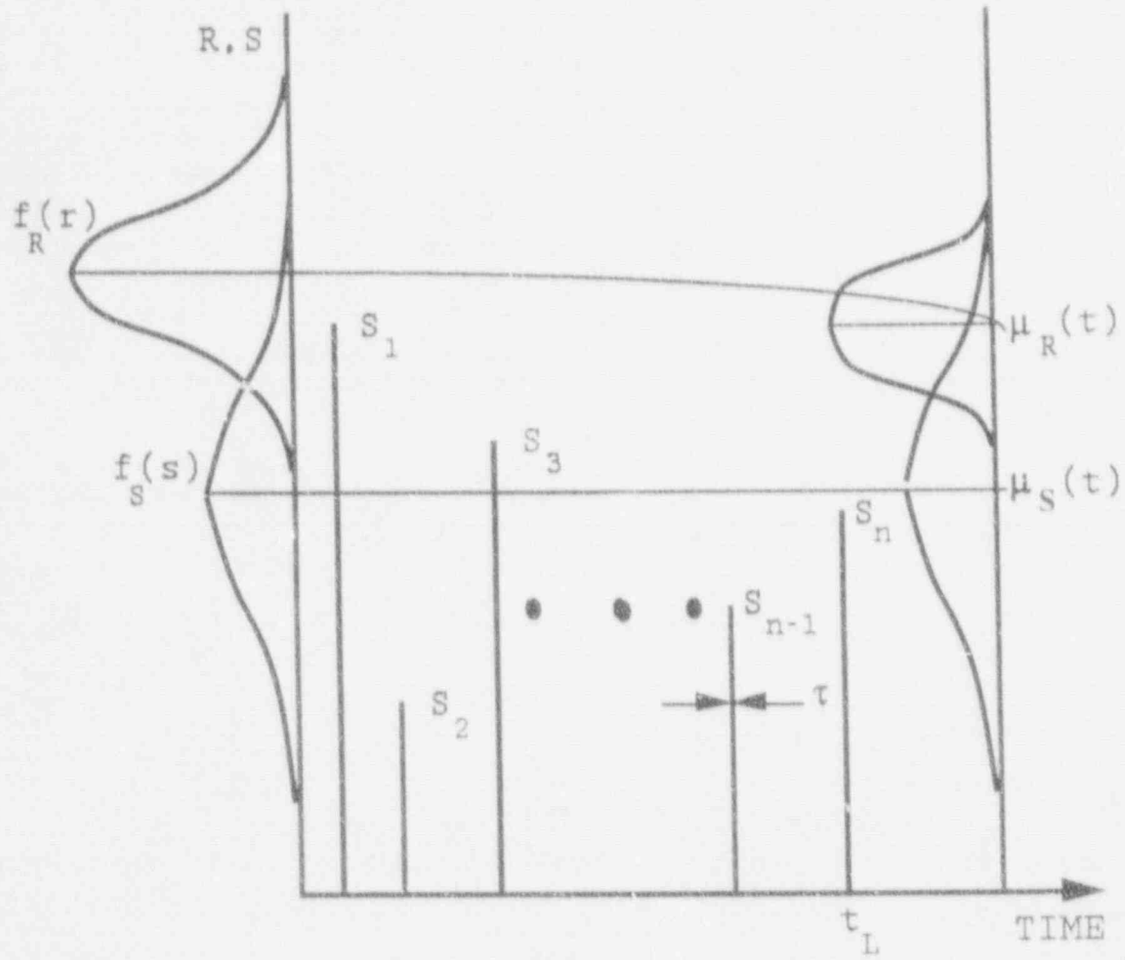

Fig. 1. Schematic presentation of load process and degradation resistance.

Time-Dependent Reliability Analysis for A Single Component. When structural safety under a single load is in question, the structural reliability, as measured by the probability of survival, L, is represented by[50,51]

$$L = P[R > S] = \int_0^{\infty} F_s(r) f_R(r) dr \qquad (5)$$

in which $F_S(x)$ is the probability distribution function of the structural action due to the applied load, S, and $f_R(r)$ is the probability density function of the resistance of the structure, R, expressed in units that are dimensionally consistent with S. Structural loads and strength vary in time, making structural reliability time-dependent.[52] Reference 22 presents an illustration of the basic concepts of time-dependent reliability analysis for a structural component subjected to a sequence of discrete stochastic load events such as shown in Fig. 1. Also presented in Ref. 22 is an illustration of the effect of degradation in component strength on the reliability function when several simple parametric representations of time-dependent load and strength have been utilized.

System Reliability. A structure is a system composed of members such as beams, columns, slabs, and walls. A system can be modeled by a combination of two fundamental subsystems: series systems and parallel systems.[50] A series system fails if any of its components fail, while a strictly parallel system fails only if all its components fail. Because structural redundancy is modeled by a parallel system, the reliability of a structure modeled as a series system of components provides a lower bound estimate of the actual system reliability.

If F_i denotes the event that the i^{th} component fails within time interval $(0,t_L)$, the reliability function of a series system, $L_s(t_L)$, can be expressed by

$$L_s(t_L) = 1 - P[F_1 \cup F_2 \cup \ldots \cup F_m] = P[\bar{F}_1 \cap \bar{F}_2 \cap \ldots \cap \bar{F}_m] \quad (6)$$

in which $\bar{F}_i$ is the complement of event Fi and m is the number of the components. The sensitivity of the reliability function to the number of components and the stochastic dependence between their strengths is illustrated in Ref. 22.

Preliminary Conclusions and Research Needs. As noted on Refs. 22 and 42, the reliability is sensitive to choice of initial component strength and strength degradation models, including time variation, the mean occurrence rate of load events, and coefficient of variation of load intensity. Less sensitivity was shown to degradation rates below a threshold and to dependence in component strengths within a system. Appropriate degradation characteristics and load process statistics must be identified to utilize the above methodology, especially in realistic condition assessments.

Periodic in-service inspection provides additional statistical data on the condition of a structure. These data can be used to update structural characteristics using Bayesian theory.[53] The revised reliability function evaluated with an updated resistance model would facilitate an improved assessment of condition and future performance. In general, the accuracy of estimation of structural characteristics should increase with the additional data. In the absence of in-service inspection, the confidence interval on the reliability function increases with time because of uncertainty in the deterioration models. Thus, shorter intervals between inspections and more comprehensive inspections will lead to narrower confidence intervals on the reliability function. Maintenance may delay the initiation of deterioration and/or improve the resistance of a deteriorated structure and accordingly, increase the reliability function. As with inspection, more frequent and comprehensive maintenance will lead to higher reliability.

Since inspection and maintenance are costly, there are tradeoffs between extent and accuracy of inspection, required level of reliability, and cost. Time dependent reliability analysis can provide a tool to determine strategies of inspection and maintenance that are necessary to maintain reliability at an acceptable level. The methodology to determine the inspection/maintenance strategies will be developed in a subsequent phase of the SAG Program.

5. APPLICATION OF RESULTS

When completed, the results of this program will provide an improved basis for the NRC staff to evaluate requests for continued operation beyond the nominal 40-year design life of a nuclear power plant. More specifically, potential regulatory applications of this research include: (1) improved predictions of long-term material and structural performance and available safety margins at future times, (2) establishment of limits on exposure to environmental stressors, (3) reduction in total reliance by licensing on inspection and surveillance through development of a methodology which will enable the integrity of structures to be assessed (either pre- or post-accident), and (4) improvements in damage inspection methodology through potential incorporation of results into national standards which could be referenced by standard review plans.

6. REFERENCES

1. "Regulatory Options for Nuclear Power Plant License Renewal," NUREG-1317, Division of Reactor and Plant Systems, Office of Nuclear Regulatory Research, U.S. Nuclear Regulatory Commission, Washington, D.C., June 1988.

2. "LWR Plant Life Extension," EPRI NP-5002, Electric Power Research Institute, Palo Alto, CA, January 1987.

3. "*BWR Pilot Plant Life Extension Study at the Monticello Plant*, EPRI NP-5181M, Electric Power Research Institute, Palo Alto, CA, May 1987.

4. PWR Pilot Plant Life Extension Study at Surry Unit 1: Phase 1," EPRI NP-5289P, Electric Power Research Institute, Palo Alto, CA, July 1987.

5. D. J. Naus, "Appendix B, Concrete Material Systems in Nuclear Safety-Related Structures - A Review of Factors Related to their Durability, Degradation Detection and Evaluation, and Remedial Measures for Areas of Distress," in *The Longevity of Nuclear Power Plant Systems*, by I. Spiewak and R. S. Livingston, EPRI NP-4208, Electric Power Research Institute, Palo Alto, CA, August 1985.

6. "Pressurized Water Reactor Containment Structures License Renewal Industry Report," Nuclear Management and Resources Council (NUMARC), Washington, D.C., August 16, 1989 (draft).

7. C. J. Hookham, "Life Assessment Procedures for Major LWR Components - Concrete Containments," NUREG/CR-5314, Idaho National Engineering Research Laboratory, Idaho Falls, April 1990 (draft).

8. "Class 1 Structures License Renewal Industry Report," NUMARC 90-06, Nuclear Management and Resources Council, Washington, D.C., June 1990 (draft).

9. 10 CFR Part 50, *Domestic Licensing of Production and Utilization Facilities.*

10. "Building Code Requirements for Reinforced Concrete," Am. Concr. Inst., Detroit, Mich., *ACI Standard* 318, 1989.

11. "Concrete Containment," Section 3.8.1, *Regulatory Standard Review Plan*, U.S. Atomic Energy Commission, Washington, D.C., June 1975.

12. "Code Requirements for Nuclear Safety-Related Concrete Structures," Am. Concr. Inst., Detroit, Mich., *ACI Standard* 349, 1976.

13. "Safety-Related Concrete Structures for Nuclear Power Plants (Other than Reactor Vessels and Containments) (For Comment Issue)," *Regulatory Guide 1.142*, Office of Standards Development, U.S. Nuclear Regulatory Commission, Washington, D.C., April 1978.

14. "Code for Concrete Reactor Vessels and Containments," Am. Concr. Inst., Detroit, Mich., *ACI Standard* 359 (or American Society of Mechanical Engineers Boiler and Pressure Vessel Code, Sect. III, Div. 2, New York), July 1989.

15. D. J. Naus, "Concrete Component Aging and Its Significance Relative to Life Extension of Nuclear Power Plants," NUREG/CR-4652 (ORNL/TM-10059), Martin Marietta Energy Systems, Inc., Oak Ridge Natl. Lab., Oak Ridge, TN, September 1986.

16. D. J. Naus, C. B. Oland, and E. G. Arndt, "Management of the Aging of Critical Safety-Related Concrete Structures in Light-Water Reactor Plants," *Proceedings of United States Nuclear Regulatory Commission Eighteenth Water Reactor Safety Information Meeting* held at Holiday Inn - Crowne Plaza, Rockville, Maryland, NUREG/CP-0114, Vol. 1, p. 527 - 552, April 1991.

17. B. M. Morris, and J. P. Vora, *Nuclear Plant Aging Research (NPAR) Program Plan*, NUREG-1144 (Rev. 1), Division of Engineering Technology, Office of Nuclear Regulatory Research, U.S. Nuclear Regulatory Commission, Washington, D.C., July 1985.

18. D. J. Naus, C. B. Oland, M. F. Marchbanks, and E. G. Arndt, *Structural Aging (SAG) Program Five-Year Plan: FY 1989 - 1993*, ORNL/NRC/LTR-89/15, Martin Marietta Energy Systems, Inc., Oak Ridge National Laboratory, Oak Ridge, Tenn., December 1989.

19. D. J. Naus and C. B. Oland, *Structural Aging Program Technical Progress Report for Period October 1, 19[illegible], to December 31, 1990*, ORNL/NRC/LTR-91/2, Martin Marietta Energy Systems, Inc., Oak Ridge Natl. Lab., Oak Ridge, Tenn., March 1991.

20. D. J. Naus, M. F. Marchbanks and E. G. Arndt, "Evaluation of Aged Concrete Structures for Continued Service in Nuclear Power Plants," *Proc. of United States Nuclear Regulatory Commission Sixteenth Water Reactor Safety Information Meeting* held at National Institute of Standards and Technology, Gaithersburg, Maryland, NUREG/CP-0097, Vol. 3, *Structural and Seismic Engineering*, March 1989.

21. C. B. Oland and D. J. Naus, "Development of the Structural Materials Information Center," *Proceedings of United States Nuclear Regulatory Commission Eighteenth Water Reactor Safety Information Meeting* held at Holiday Inn - Crowne Plaza, Rockville, Maryland, NUREG/CP-0114, Vol. 1, p. 579 - 596, April 1991.

22. B. Ellingwood and Y. Mori, "Probabilistic Methods for Condition Assessment and Life Prediction of Concrete Structures in Nuclear Power Plants," *Proceedings of United States Nuclear Regulatory Commission Eighteenth Water Reactor Safety Information Meeting* held at Holiday Inn - Crowne Plaza, Rockville, Maryland, NUREG/CP-0114, Vol. 1, p. 553 - 577, April 1991.

23. C. B. Oland and D. J. Naus, *Structural Materials Information Center for Presentation of the Time Variation of Material Properties*, ORNL/NRC/LTR-90/22, Martin Marietta Energy Systems, Inc., Oak Ridge Natl. Lab., Oak Ridge, Tenn., November 1990.

24. *Mat.DB*, Version 1.0, ASM International, ASM/Center for Materials Data, Materials Park, Ohio, 1990.

25. *EnPlot*, Version 2.0, ASM International, ASM/Center for Materials Data, Materials Park, Ohio, 1989.

26. J. R. Clifton, "Predicting the Remaining Life of In-Service Concrete," NISTIR XXXX, National Institute of Standards and Technology, U.S. Department of Commerce, Gaithersburg, Maryland, 1991 (draft).

27. *In Situ/Nondestructive Testing of Concrete*, V. M. Malhotra (Ed.), Publication SP-82, American Concrete Institute, Detroit, Mich., 1984.

28. "Rules for Inservice Inspection of Nuclear Power Plant Components," American Society of Mechanical Engineers Boiler and Pressure Vessel Code, Sect. XI, New York, 1983.

29. ACI Committee 201, "Guide for Making a Condition Survey of Concrete In-Service," *Proc. J. Am. Concr. Inst.* **655**(11), 905-18, November 1968.

30. ACI Committee 437, "Strength Evaluation of Existing Concrete Buildings," *J. Am. Concr. Inst.* **64**(11), 705-10, November 1967.

31. ACI Committee 207, "Practices for Evaluation of Concrete in Existing Massive Structures for Service Conditions," *Concr. Int.* **1**(3), 47-61, 1979.

32. ACI Committee 311, "Guide for Concrete Inspection," *Concr. Int.* 2(10), 81-85, October 1980.

33. B. Bresler, *Essential Steps in Adaptation of Old Buildings*, Workshop on Earthquake-Resistant Reinforced Concrete Building Construction, University of California, Berkeley, July 11-15, 1977.

34. D. Kaminetzky, *Verification of Structural Adequacy*, Workshop on Earthquake-Resistant Reinforced Concrete Building Construction, University of California, Berkeley, July 11-15, 1977.

35. T. L. Rewerts, "Safety Requirements and the Evaluation of Existing Concrete Buildings," *Concr. Int.* 7(4), 50-55, April 1985.

36. J. J. Waddell, "Basic Steps of a Concrete Repair Program," *Concr. Int.* 2(9), 30-33, September 1980.

37. J. Warner, *Methods for Repairing and Retrofitting (Strengthening) Existing Buildings*, Workshop on Earthquake-Resistant Reinforced Concrete Building Construction, University of California, Berkeley, July 11-15, 1977.

38. C. J. Hookham, *Structural Aging Assessment Methodology for Concrete Structures in Nuclear Power Plants*, ORNL/NRC/LTR-90/17 (Subcontract Report 11X-SD343V from Multiple Dynamics Corp., Southfield, Mich.), Martin Marietta Energy Systems, Inc., Oak Ridge Natl. Lab., Oak Ridge, TN., March 1991.

39. T. M. Refai and A. K. Lim, *Inservice Inspection and Structural Integrity Assessment Methods for Nuclear Power Plant Concrete Structures*, ORNL/NRC/LTR-90/29 (Subcontract Report 17X-SE611V from Construction Technology Laboratories, Inc., Skokie, Ill.), Martin Marietta Energy Systems, Inc., Oak Ridge Natl. Lab., Oak Ridge, Tn., September 1991.

40. J. T. P. Yao et al., "Stochastic Fatigue, Fracture and Damage Analysis," *J. Str. Safety* 3(4), 231-267, 1986.

41. A. J. M. Siemes, A. C. W. M. Vrouwenvelder, and A. Van den Beukel, "Durability of Buildings: A Reliability Analysis," *Heron* 30(3), 1985.

42. B. Ellingwood and Y. Mori, "Probabilistic Methods for Life Prediction of Concrete Structures in Nuclear Power Plants," Session D03(M)-Probabilistic Assessment of Component Life, *Proc. 11th International Conference on Structural Mechanics in Reactor Technology*, Tokyo, Japan, August 18-23, 1991.

43. J. G. MacGregor, J. G. Mirza, and B. Ellingwood, "Statistical Analysis of Resistance of Reinforced and Prestressed Concrete Members," Am. Concr. Inst., Detroit, Mich., *J. ACI* 80(3), May-June 1983.

44. B. Ellingwood and H. Hwang, "Probabilistic Descriptions of Resistance of Safety-Related Structures in Nuclear Plants," *Nucl. Eng. Des.* 88(2), 1985.

45. H. Hwang et al., "Probability-Based Design Criteria for Nuclear Plant Structures," Am. Soc. Civil Eng., New York, N.Y., *J. Str. Eng.*, **113**(5), 1987.

46. K. Tuutti, *Corrosion of Steel in Concrete*, Swedish Cement and Concrete Research Institute, CBI 4:82, Stockholm, 1982.

47. "Prediction of Service Life of Building Materials and Components," CIB W80/RILEM 71-SPL, *Materials and Structures* **115**, Paris, 1987.

48. J. R. Clifton and L. I. Knab, *Service Life of Concrete*, NUREG/CR-5466, U.S. Nuclear Regulatory Commission, Washington, D.C., November 1989.

49. B. Ellingwood, *Probability Based Safety Checking of Nuclear Plant Structures*, NUREG/CR-3628, U.S. Nuclear Regulatory Commission, Washington, DC, 1983.

50. P. Thoft-Christensen and M. J. Baker, *Structural Reliability Theory and Its Application*, Springer-Verlag, New York, N.Y., 1982.

51. R. E. Melchers, *Structural Reliability: Analysis and Prediction*, Ellis Harwood Ltd., West Sussex, England, 1987.

52. H. Kameda and T. Koike, "Reliability Analysis of Deteriorating Structures." *Reliability Approach in Structural Engineering*, Maruzen Co., Tokyo, Japan, 1975.

53. W. B. Hall, "Reliability of Service-Proven Structure," *Journal of Structural Engineering* **114**(3), pp. 608-623, March 1988.

TESTS IN THE ATLE LOOP ON THE PIUS DESIGN

Ulf Bredolt, Dusan Babala, John Kemppainen
ABB Atom AB
S-721 63 Västerås, Sweden
+46 (0)21-107000

ABSTRACT

This paper describes experimental demonstration of the self-protective features of PIUS in a large scale test loop in ABB Atom engineering laboratories. The loop employs real time simulation of core power as a function of coolant conditions in an electrically heated fuel assembly model.

System responses to various severe transients were studied. Comparisons were made with predictions of the RIGEL code, which has been developed specifically for study of PIUS type reactors. The selected results presented in this paper are based on previous papers, see reference [1] and [2].

A comparison between test results and calculated results was made for main state variables such as pressure, temperatures, concentrations, heat fluxes and mass flow rates.

The tests have demonstrated the self-protective thermal-hydraulics of Pressurized Water Reactor primary systems designed according to the PIUS principle and verified the capability of the RIGEL code to predict their behaviour during severe accidents and in normal operation transients.

1 INTRODUCTION

By basing the reactor design on the PIUS (Process Inherent Ultimate Safety) principle, avoidance of severe accidents can be made as a built-in characteristic of the primary system, independent of engineered safety systems and virtually immune to human error or mischief, see reference [3]. This makes it possible both to satisfy stringent safety requirements and to substantially simplify the plant design.

Employing the PIUS principle, ABB Atom has introduced pressurized water reactor concepts: the SECURE reactor for low temperature heat generation, e.g. district heating, and the PIUS reactor for

electric power generation. SECURE operates at a pressure of 2.0 MPa with a 190°C core exit temperature, while these values for PIUS are 9.0 MPa and 290°C, respectively.

The thermal-hydraulic function and the transient response of PIUS during accidents have been tested at the ABB Atom laboratories in an electrically heated mock-up, ATLE, of a SECURE reactor. Computer simulations of the transients have been made before each test run in order to predict the thermal-hydraulic behaviour of the test loop in advance. After the tests were carried out, new computations were made in order to ensure that initial conditions and disturbances, boundary conditions, were identical to the measured one.

The simulation of transients has been made by the RIGEL code [4] which is a computer program developed by ABB Atom for dynamic analysis of PIUS/SECURE reactors. This program is an important tool in the design work on these reactors, due to its relative simplicity. For the simulations a nodal model of the ATLE loop was made comprising the primary system, the pool and the intermediate cooling loops.

A comparisons between some of the test results and calculations as well as a discussion of these comparisons are presented in this paper. The aim of these comparisons is to verify the RIGEL code's ability to predict the dynamic behaviour of the PIUS/SECURE reactor in normal operation and during severe accidents. The comparisons are made mainly for the primary state variables in each transient with different initial disturbances.

2 THE ATLE TEST LOOP

A scale model of a SECURE reactor, the ATLE loop was built in ABB Atom's engineering laboratory to verify the computational methods and to demonstrate the self-protective thermal-hydraulics of the PIUS/SECURE type reactors.

The volume scale of the loop is 1:308 of a real SECURE reactor, there are 308 fuel assemblies in a 400 MWth SECURE core. The height of the test loop is the same as in the full scale design to ensure similarity in the driving buoyancy force during a transient. The test loop and the reactor operate with identical temperatures and system pressure. Figure 2.1 shows the outline of the loop.

2.1 Thermal-hydraulic design

The loop consists of the main reactor parts: reactor pool, primary system, pressurizer, heat exchangers.

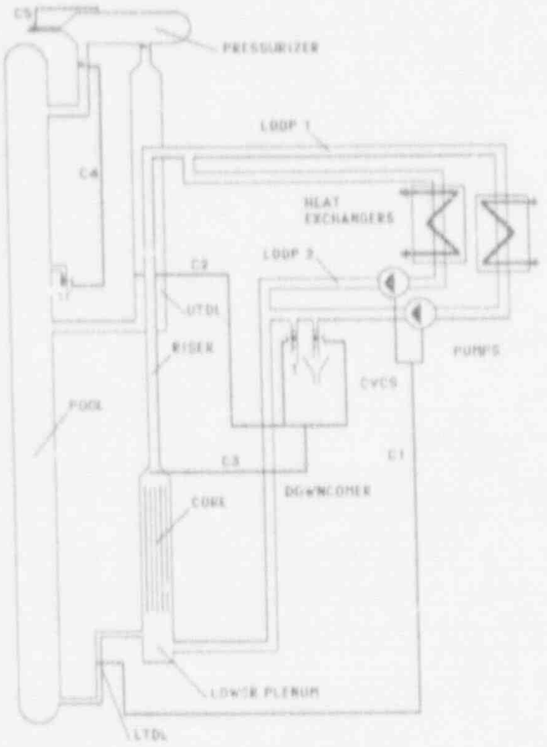

FIGURE 2.1 Outline of the ATLE test loop

The water flows upward through the riser from the simulated nuclear core. The Upper Thermal Density Lock.(UTDL) connects the riser to the pool via a pipe filled with pool water in the upper part of the riser.

The free water surface of the primary system is in contact with steam in the pressurizer. The pressurizer volume is connected to the pool both directly and via UTDL. The steam supply to the pressurizer is generated in an electrically heated boiler.

From the upper end of the riser, the water is divided into two parallel paths and flows through two heat exchangers and two circulation pumps.

The two flow paths merge in the downcomer downstream of the pumps. The water flows downwards to the lower plenum just below the inlet orifice to the rod bundle. The lower plenum is connected to the pool via the Lower Thermal Density Lock (LTDL). Further details on the test loop can be found in reference [1] and [2].

The pool and the primary system water contain boron, in the form of boric acid, in the PIUS/SECURE reactors. In the test loop, the content of boric acid is simulated by means of an easily measurable indicator substance, such as a strong electrolyte, sodium sulfate. The electrical conductivity of the fluid, compensated for the temperature dependence, serves as a measure of the boron concentration.

2.2 Simulated nuclear core

The "core" in the test loop is a full scale 8x8 electrically heated rod assembly with uniform heat generation.The supply of DC current from a static converter to the rod bundle is controlled by a point reactor kinetics model running in real time on an ABB MASTER process computer to simulate the nuclear behaviour of the

core. The point kinetic model simulates neutron kinetics and heat conduction in the fuel. The inlet and outlet temperatures, conductivities and voids from the core are used as input data for the model. The mean fuel temperature is calculated in the model. Reactivity feedback from changes in the moderator temperature, fuel temperature, "boron" concentration and void, if any, is considered. Figure 2.2.1 shows schematically the "simulated nuclear core" in the test loop.

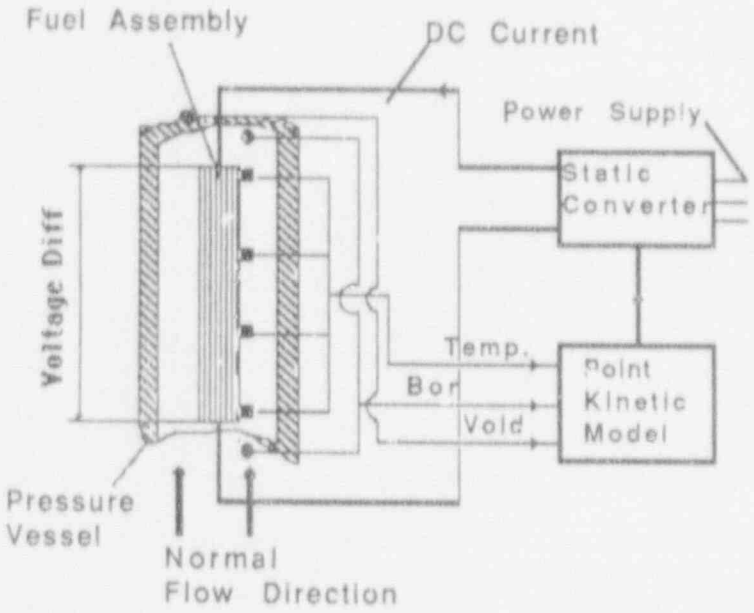

The concentration of the sodium sulfate had to be kept very low, however, to minimize water conductivity becasuse the potential difference between the heated element and the pressure vessel led to a production of oxygen-hydrogen gas mixture.

FIGURE 2.2.1 Core model

2.3 Control system design

The ATLE loop includes control systems in the same way as in an actual SECURE reactor, see figure 2.1.

The hot/cold water level in the LTDL is controlled in the loop C1. The level is primarily a function of the density difference between pool and riser and the pressure drop in riser and core, depending on the pump speed. The hot/cold interface level is determined from the measured average temperature along the density lock. The calculated water level is compared with a set point value for the hot/cold water level. The difference is processed in a PI controller. The output signal is used in a static frequency converter which controls the feed frequency of the power supply to the pump.

The hot/cold water level in the UTDL is controlled in loop C2. The hot/cold level is primarily a function of the mass inventory in the primary system. The position of the hot/cold interface is determined from the measured average temperature along the density lock. The calculated position is compared with a set point value. The difference is processed in a PI controller. The output signal controls a control valve for discharge water, low water level, otherwise the reactivity control system injects water to the primary system without changing its conductivity.

The water level in the pressurizer, pool side, is controlled in loop C4. The water level is primarily a function of the pool mass inventory. Actual water level is determined by dp-measuring. The calculated level is compared to a set point value. An on/off controller controls a discharge valve in the pool. The valve is closed if actual water level is below set point value.

The pressure is controlled in the loop C5. The measured pressure in the pressurizer is compared to a predetermined set point value. The difference is processed in a PI controller. The output signal controls the electric power to the boiler.

The "reactor" is controlled in the loop C3. The "reactor power" is primarily a function of the water conductivity and the water temperature. The reactivity control system consists of a core outlet temperature measurement device, one clean water pump and one "conductivity water pump". The measured core outlet temperature is compared to a set point value. The difference is processed in a specially designed P controller. The output signal from the controller controls both the clean water pump and the "conductivity water pump". The conductivity of the injected water to the primary system is predetermined function of the core outlet temperature. A decrease in core outlet temperature causes an injection of water with less conductivity than at nominal power to increase the reactor power.

It should be emphasized that all control devices are designed to aid in operation of the system, not to ensure its safety, which is totally independent of such devices.

2.4 Instrumentation

The test loop is equipped with several thermometers, mass flow meters, dp-cells, absolute pressure meters and conductivity meters. More than 200 measuring points are available for recording. The maximum sampling frequency is 10 Hz which is rapid enough even for fast transients.

3 THE RIGEL CODE

The design of a new reactor system as PIUS/SECURE, required an assessment of a large number of alternatives in the initial phase of development. A special computer program, RIGEL, has been developed for that purpose [4]. Initially, the emphasis in the RIGEL program was on the speed of computation without an undue sacrifice in accuracy, and on the flexibility to accommodate design changes. As the optimal PIUS design crystallized the emphasis in RIGEL gradually shifted to more sophisticated modelling. As illustrated in this paper, the present level of modelling allows us to predict the behaviour of the physical system with good confidence.

As input to RIGEL, the hydraulic network is divided into a number of fluid volumes interconnected by fluid junctions. In booth types of nodes, thermal equilibrium between phases is assumed. The basic variables integrated in a fluid cell are the pressure, specific enthalpy and boron content, In fluid junctions, one integrates mass flow, energy flow and boron flow, except for those nodes which have a boron delay model. Steam velocity is assumed to be a linear function of the water velocity. In parts of the network where no heat transfer occurs and where the fluid is known to be in single phase, one can opt for a special modelling of non-dissipative propagation of temperature and boron fronts [2].

Heat transfer is modelled by heat capacity cells and heat flow junctions, where the energy and energy flow, respectively, are integrated in time. A number of different correlations for heat transfer and also a lookup table for critical heat flux calculations can be selected, reference [6]. Thermodynamic functions of water/steam are read from tables generated from analytical expressions.

Special node models are provided for the pressurizer where thermal unequilibrium is taken into account and the density locks, where the fluid phases, or fluids at different temperatures, are stratified. Further, separate models are provided for pumps and controllers. The neutron kinetics is represented by a point reactor model.

A semi-implicit numerical integration scheme is used, employing linearization about the old time values by the Jacobian matrix of the system of equations.

4 MODELLING OF THE ATLE LOOP

The model of the primary system contains the reactor core, the riser, the pressurizer, the recirculation loops with the pumps and heat exchangers and finally the downcomer and the inlet plenum, Figure 4.1.

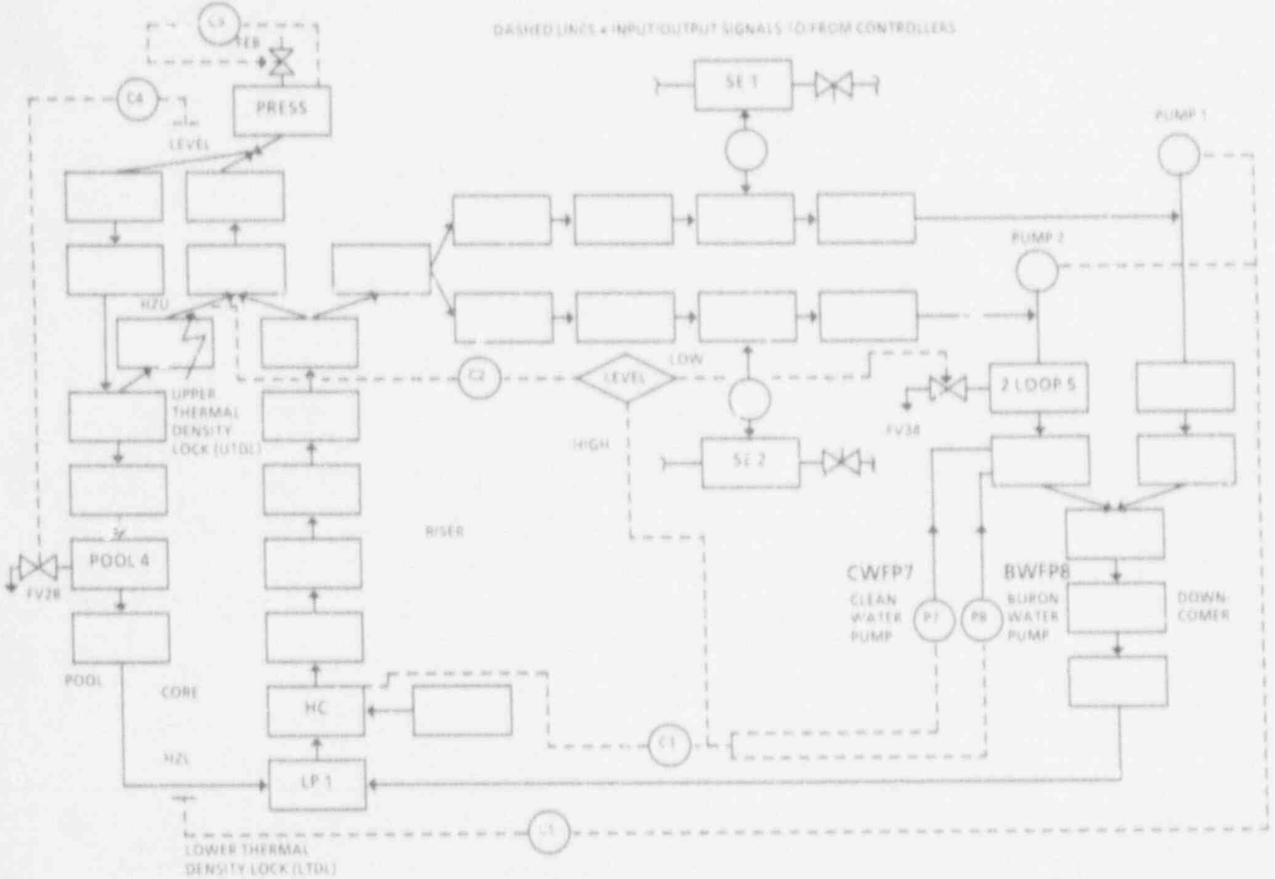

FIGURE 4.1 Nodalization of the ATLE loop for RIGEL

A point reactor model is used to simulate the neutron kinetics in the core. Reactivity effects of fuel and coolant temperatures, void and boron concentration, i.e. conductivity, are taken into account. The reactor core is divided into four hydraulic nodes and four fuel cells, not shown in figure 4.1.

The pool, i.e. the pressure vessel which contains the highly conductive cold water, is divided into a number of fluid cells interconnected by fluid junctions. The primary system is connected to the pool through the two thermal density locks and via the pressurizer. The recirculation pumps and the pump motors are modelled as two hydraulic nodes connected by heat flow junctions to the heat transfer wall. The heat transfer coefficients are flow dependent.

The secondary system, i.e. the intermediate cooling loops are modelled as flow paths to each secondary side of the two heat exchangers in the primary system.

The model of the control system covers the control of the hot/cold water interface level in the two thermal density locks, loop C1 and C2, the water level in the pressurizer, loop C4, the pressure control in the pressurizer, loop C5, and the reactivity control system, loop C3.

5. COMPARISON OF ATLE TESTS AND RIGEL POST CALCULATIONS

The test results from the transients performed in the ATLE loop have been compared to computer simulations by the RIGEL program. Representative transients have been selected in order to examine the capability of the RIGEL code to predict different events in the dynamic behaviour of the loop both during normal operation and accidents.

The starting steady state conditions in individual tests were used as input to the computer simulations. The calculated steady state solution for the model was exposed to identical disturbances as in the ATLE loop.

The results from the test and from the simulation were plotted together on the same diagram for the final analysis and comparison. The broken lines in each plot indicate the test results, while the solid lines show computed values.

One of the variables of interest is the mass flow rate through the lower density lock. It is important to predict correctly how fast the lock is penetrated after a disturbance. Other interesting variables are "boron concentration" in the core and the outlet water temperature from the core. We have investigated the ability of the code to predict the interaction between different control systems, during normal operation transients.

The first two tests, load following and power grid disturbance, demonstrate normal operation of a SECURE/PIUS plant under different conditions. The third test was used to verify the improved method to track boron front propagation before simulating transients where boron front phenomena take place. The remaining three tests, pump trip, loss of heat exchanger and uncontrolled boron dilution, illustrate the response of the reactor to severe disturbances that would require intervention by safety systems in conventional PWR's.

5.1 Power Control

A comparison between the test results and the predicted behaviour of the power control has been made in a load following transient. The aim of this comparison is to check the RIGLE code capability to simulate the behaviour of the reactor with activated control system during a normal load change in the district heating system.

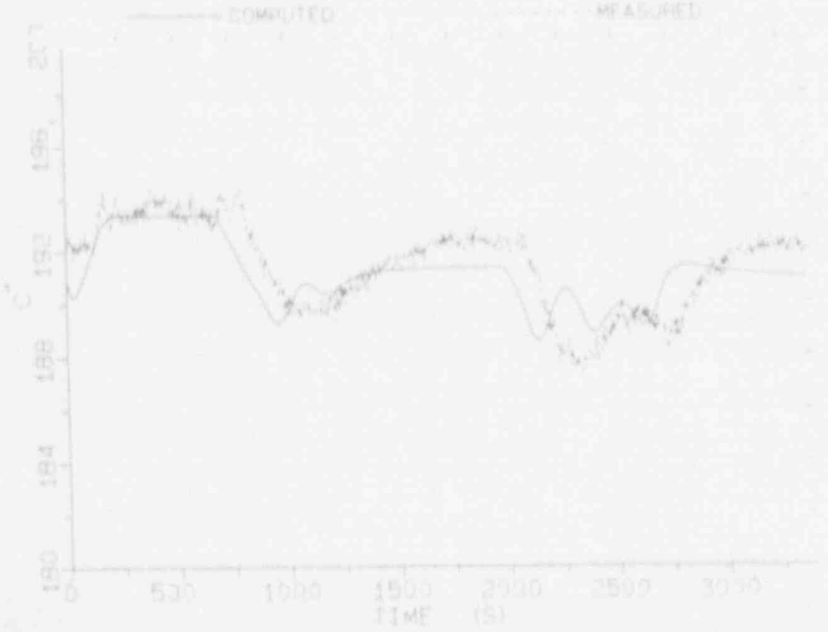

FIGURE 5.1.1 Water temperature at the outlet during load following

The transient starts when the demand for heat from the district heating system decreases. The decrease in heat output from the primary system causes the outlet temperature from the core to rise above 190°C. This temperature rise activates the reactivity control system.

Figure 5.1.1 shows the measured outlet temperature from the core and the one predicted by the RIGEL code. The agreement between calculated and measured temperatures is good, but some delay in the measured temperature profile is observed. The measured slopes of the temperature profiles during the heat load decrease/increase agree very well with the computed ones.

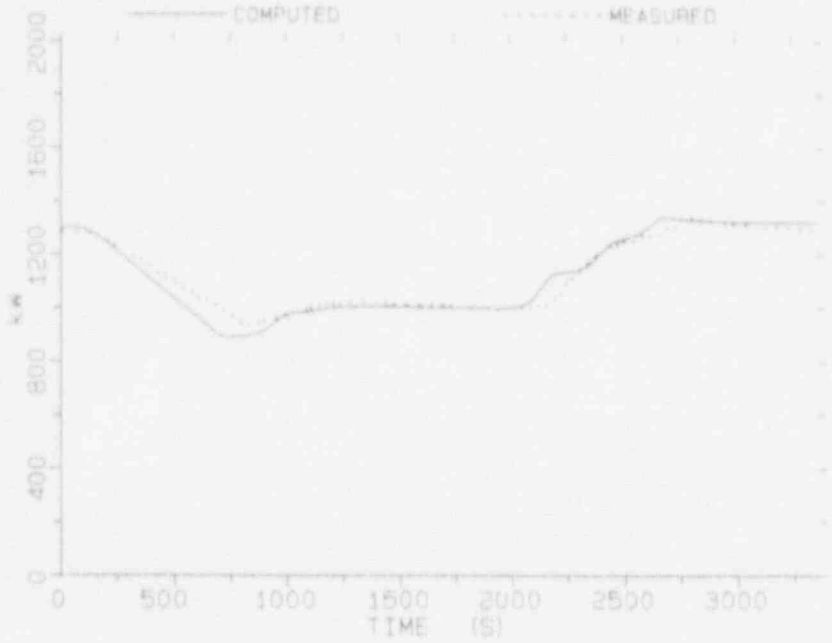

FIGURE 5.1.2 Reactor power during load following

Figure 5.1.2 shows the measured power transferred to the coolant, i.e. the power to the electrically heated rod bundle, and the predicted power to the coolant. The overall agreement between predicted and measured power to coolant is very good during the entire transient.

A comparison of the slope for the two curves shows good agreement, i.e. the dynamic behaviour of the ATLE loop is very well simulated by the model of the ATLE loop in the RIGEL code during the entire transient.

The "boron concentration", i.e. the conductivity in the test loop is compared to the predicted conductivity at two locations in the loop, namely at the inlet to the core and at the outlet from the core.

Figure 5.1.3 shows the measured and predicted outlet conductivity. The agreement between measured and predicted conductivity is very good. The agreement in conductivity level and the agreement in the slope of the measured and predicted curves show that the reactivity control system and the dynamic behaviour of the test loop is very well simulated by the RIGEL code during the entire transient.

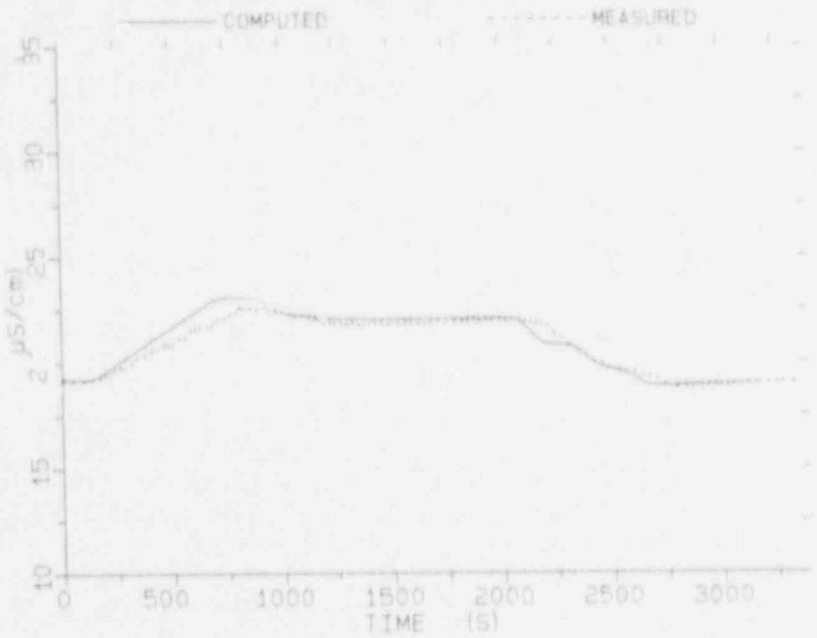

FIGURE 5.1.3 Electrical conductivity of water at the core outlet during load following

5.2 Grid voltage disturbance

The PIUS/SECURE reactor under normal operation should tolerate smaller disturbances in the grid power supply without unnecessary and time consuming shutdowns. A typical grid disturbance that a power plant in Scandinavia is required to withstand without disconnection from the grid, is a total loss of voltage lasting 0.25 s followed by a full recovery in 0.5 s. The temporary loss of power effects the recirculation pumps, with the ensuring disturbance in the hot/cold interface in LTDL. The response is strongly damped and the interface level swings only once above and once below its steady state value. The LTDL is designed to accommodate the anticipated changes in the interface level, without being penetrated by the pool water. We have selected the duration of the loss of power to be 2.1 s - sufficiently long for a small amount of borated water to enter the primary loop. All controls were active. The excess boron was subsequently automatically diluted by the reactivity control system. The full-power operation of the reactor remained undisturbed.

Figure 5.2.1 shows the total mass flow and the flow trough LTDL during the disturbance. The computed response of the system to the disturbance is faster and smaller than the measured one, probably due to insufficient detail in modelling the built-in control systems in the frequency converter of the power supply to the recirculation pumps. The overall agreement with the measured response is good.

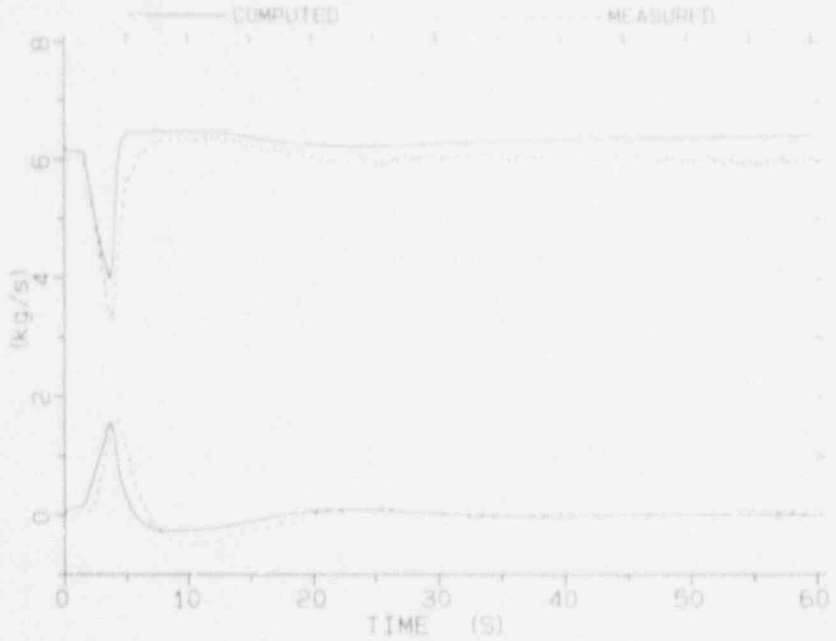

FIGURE 5.2.1 Response of water flows to a power grid disturbance

5.3 Boron front propagation

The transient starts with an injection of highly conductive water to the loop upstream the downcomer. The shape of the conductivity water pulse is similar to a square pulse with a duration of about 25 seconds. In the test, the dispersion process is dominated by turbulent diffusion with a very small amount of pure mixing in branches.

5.3.1 Improved transport model

The comparison between test and computation shows a good overall agreement. Figure 5.3.1.1 shows the conductivity in the inlet plenum to the core.

We can note that the transport time for the conductivity pulse to the first conductivity meters is almost equal in test and calculation.

Comparison of the first rise in conductivity shows good similarity, which implies an identical exposition of the disturbance in the computation. However, we can observe a small phase error, approximately 20 degrees after one recirculation time. This phase error is accumulated during the transient which causes a total

phase error to be greater than one period at the end of the transient.

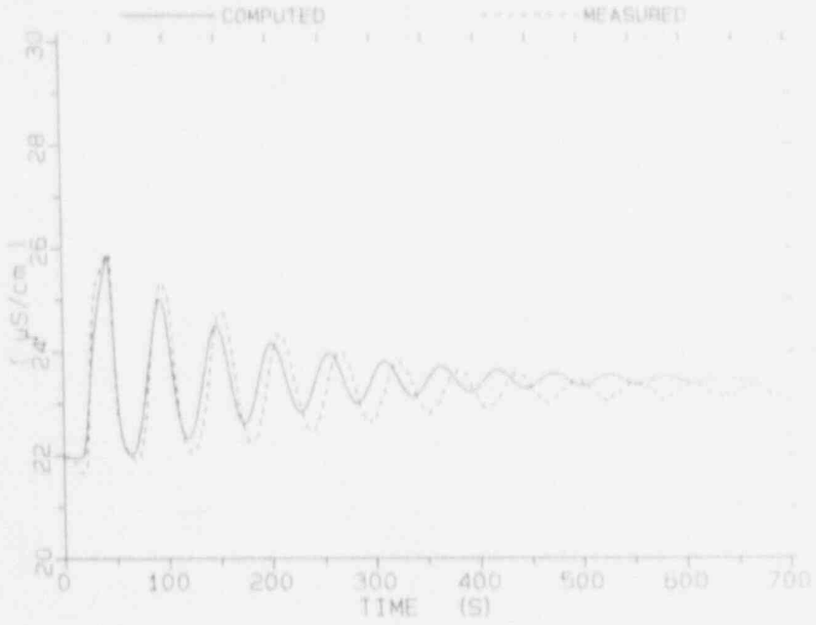

FIGURE 5.3.1.1 Electrical conductivity versus time, improved transport model

There are uncertainties in the measurement of mass flow rate and in the volume of the primary system, these two uncertainties can explain the accumulated phase error.

Finally the decay ratios for the test is 0.8 and for the computation is 0.75 and the conductivity at the end of the transient differs less than a few percent. In reference [2] a number of boron front propagation test are compared to the RIGEL code, all of them shows good agreement test versus simulation.

5.3.2 Standard transport model

As an illustration we have made an identical simulation of the transient with use of standard techniques to compute boron transport. Figure 5.3.2.1 shows a comparison between test and the standard method to track boron front propagation.

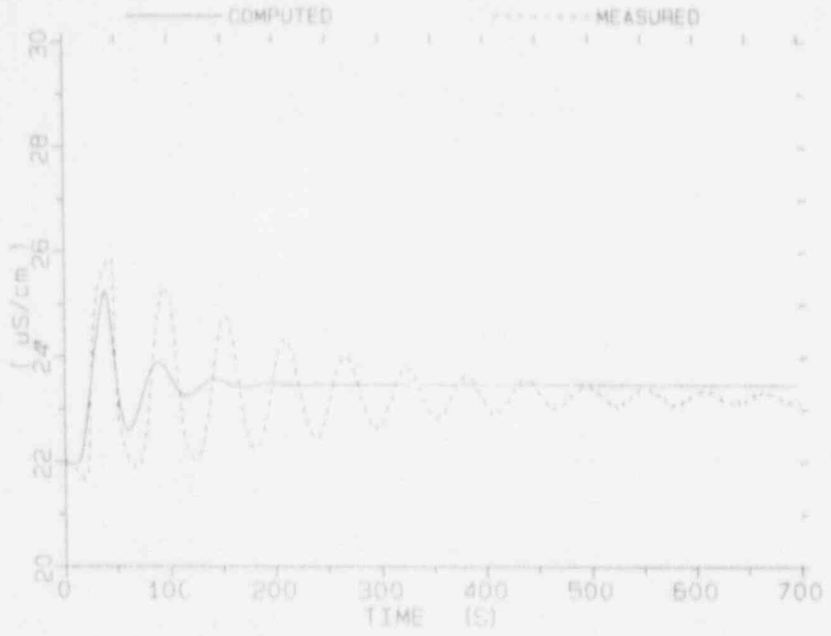

FIGURE 5.3.2.1 Electrical conductivity versus time, standard transport model

5.4 Recirculation pump trip

The recirculation pump trip involves a rapid transfer from power operation to reactor shut down and natural circulation with borated pool water. The predictions of mass flow through the lower thermal density lock and the conductivity in the core have been studied in the most detail.

The transient starts when the power to the recirculation pumps is shut off. When the pump revolution rate decreases, an inflow of highly conductive water through the lower thermal density lock starts, due to the disturbance in the pressure balance between the riser and the pool.

Figure 5.4.1 shows the mass flow rate through the lower thermal density lock. The overall agreement between calculated and measured flow rate is good. However, after the peak in flow through the density lock occurs, we can observe a faster decay of the predicted flow.

This discrepancy is probably caused by neglecting the pressure vessel heat capacity, thick walled pressure vessel, in the computer model. In the model without any energy stored in the pressure vessel walls, the temperature in the riser will decrease faster.

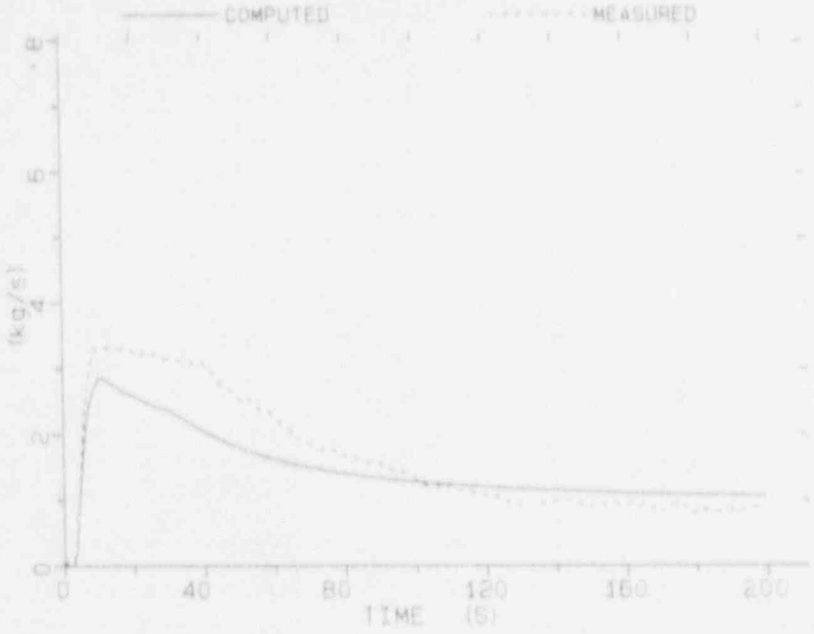

FIGURE 5.4.1 Water flow through LTDL following a pump trip

The mass flow rate through the lower thermal density lock is presently only a function of the temperature distribution in the riser. Therefore, the mass flow decays faster in the simulation than in the test.

When the recirculation flow decreases due to the pump trip, the core outlet temperature increases very rapidly. Figure 5.4.2 shows the outlet water temperature from the core. The discrepancy between predicted and measured temperature is small.

The conductivity in the "core" starts to rise when the lower thermal density lock is broken. Figure 5.4.3 shows the increase of conductivity in the lower plenum. The agreement between simulations and test data is very good.

A comparison between measured power to coolant and predicted power shows a good agreement. However, the predicted power decays somewhat faster than the measured power after about 30 seconds, see figure 5.4.4.

FIGURE 5.4.2 Water temperature at the core outlet following a pump trip

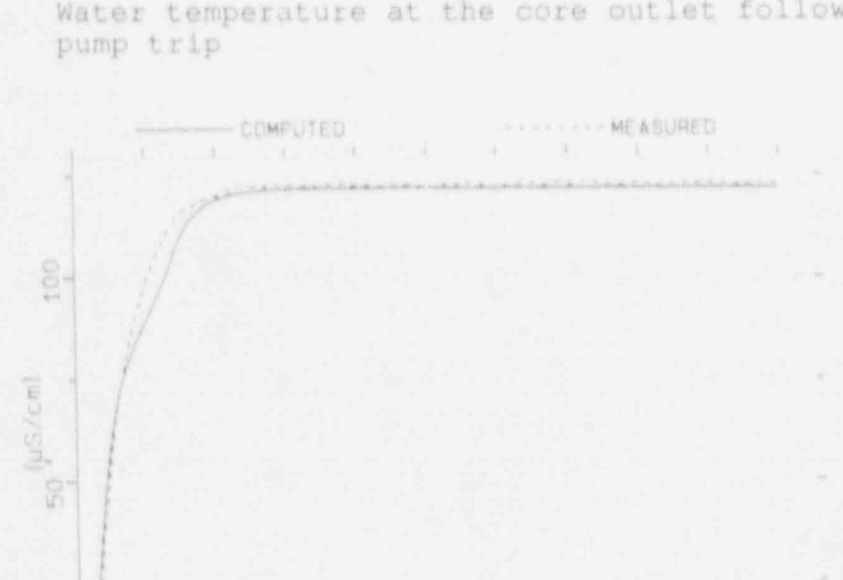

FIGJRE 5.4.3 Electrical conductivity of water at the core inlet following a pump trip

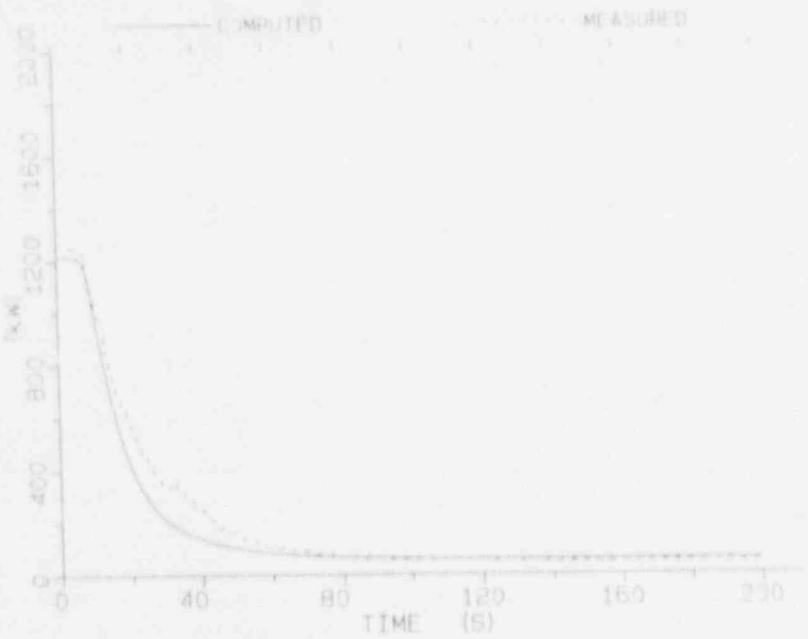

FIGURE 5.4.4 Reactor power following a pump trip

5.5 Partial loss of heat sink

A loss of heat sink involves a fast decrease in the power load due to an event like isolation of a steam generator, PIUS, or a pump trip in an intermediate cooling loop, SECURE.

The transient starts when the power supply to one of the intermediate cooling loop pumps is shut off. The heat extracted from the primary loop decreases rapidly and a hot water front starts propagating along the downcomer.

When the hot water reaches the core region figure 5.5.1, the pressure balance between the hot riser and the cold pool is affected. The LTDL is penetrated and the borated pool water starts flowing into the loop figure 5.5.2.

The inflow of borated water is intermittent, until the pump controller, C1 restores a stable hot/cold interface in the LTDL. The system response is oscillatory, with damped oscillations of a period equal to the recirculation time figure 5.5.3.

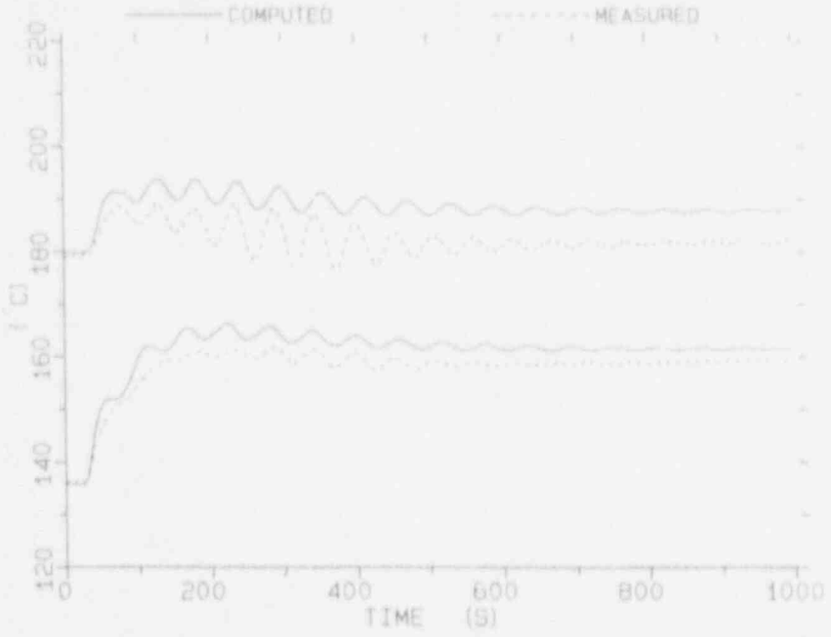

FIGURE 5.5.1 Water temperature in the reactor core after a partial loss of heat sink

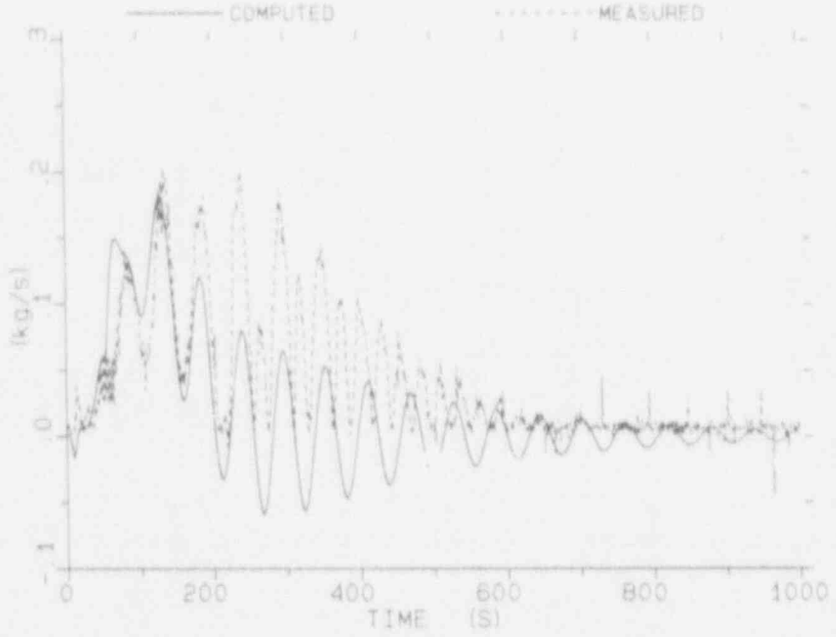

FIGURE 5.5.2 Water flow through LTDL following a partial loss of heat sink.
The flow meter shows absolute value of the flow.

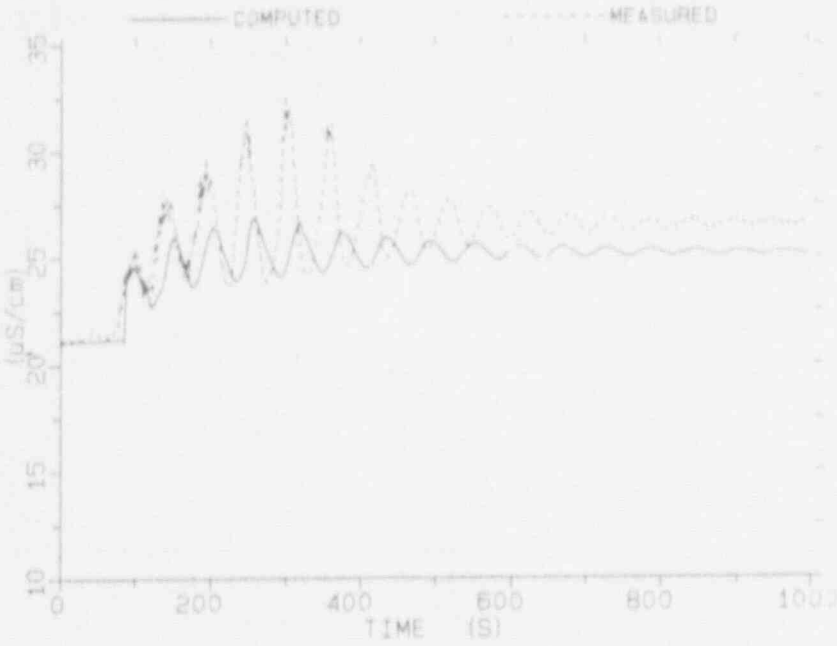

FIGURE 5.5.3 Electrical conductivity of water at the core inlet after a partial loss of heat sink

The amplitudes of oscillations are very sensitive to the exact mechanism of dissipation of the circulating boron and temperature fronts.

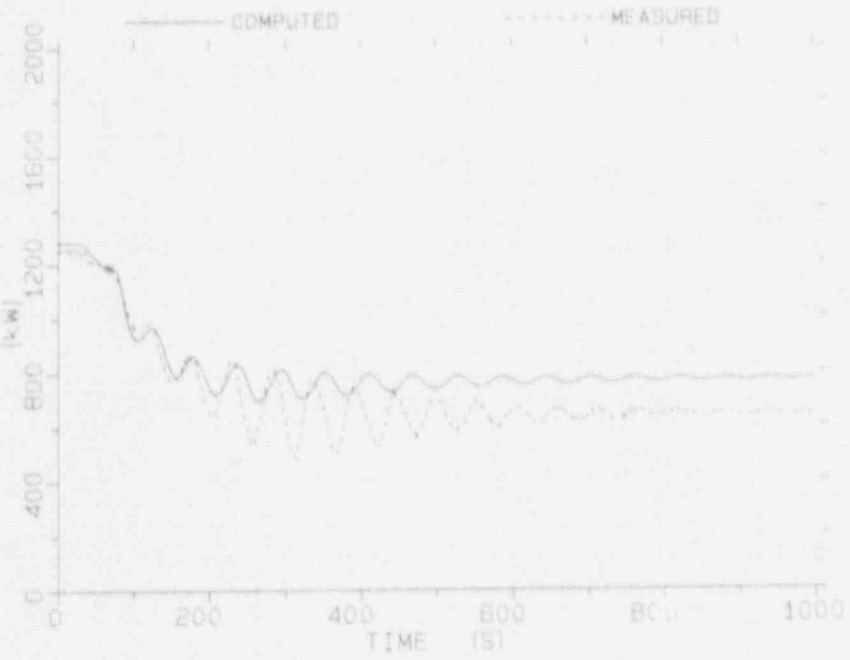

FIGURE 5.5.4 Reactor power after a partial loss of heat sink

After the oscillations die out, the system reaches a new steady state at a lower power. Since only two controllers are active, C1 and C5, the final state depends only on the total amount of boron that entered the primary loop. In the absence of feedback, the disagreement between measured and computed final states depends on the accumulated error in the integrated water flow through LTDL. Considering the complicated flow regime in LTDL during oscillations, the error in the computed final state is not excessively large.

A total loss of heat sink, i.e. a loss of power supply to both cooling loop pumps, leads to a strong ingress of borated water into the primary loop, shutting the reactor down.

5.6 Uncontrolled boron dilution

We have studied the response from the primary system to an uncontrolled injection of clean water. The reactivity system, C3 was switched off and the by-pass valves in the intermediate loops were closed during the entire transient.

The total amount of clean water injected to the primary system is limited to the size of clean water storage vessels for the plant. The disturbance corresponds to an unmonitored control-rod withdrawal accident in a conventional PWR.

Points of special interest are the conductivity in the core, the power level and the intermittent flow through the lower thermal density lock, LTDL.

The behaviour of the transient can be divided into three phases, namely:

- The dilution phase. During the dilution phase boron on the primary system is diluted and the reactor power increases. In the test this phase lasts up to 300 seconds.

- The boration phase. During this phase boration of the primary system takes place, due to an intermittent inflow of highly "borated" water from the pool through the LTDL. In the test it occurs between 300 - 1500 seconds.

- The recovery phase. The boron concentration in the primary system is stabilized and a new steady state is reached. The recovery phase starts when the available clean water storage has been used. This phase is not described in this paper.

5.6.1 The dilution phase, 0 - 300 seconds

The transient starts when the clean water pump starts up to its maximum possible flow rate. This cold water injection to the primary system causes a temporary decrease of the core inlet and outlet temperatures.

The hot/cold interface level in LTDL will be lowered due to the disturbance in the pressure balance between the riser and the pool. The LTDL control system C1 suppresses the recirculation pump revolution rate to compensate for the new temperature distribution in the riser.

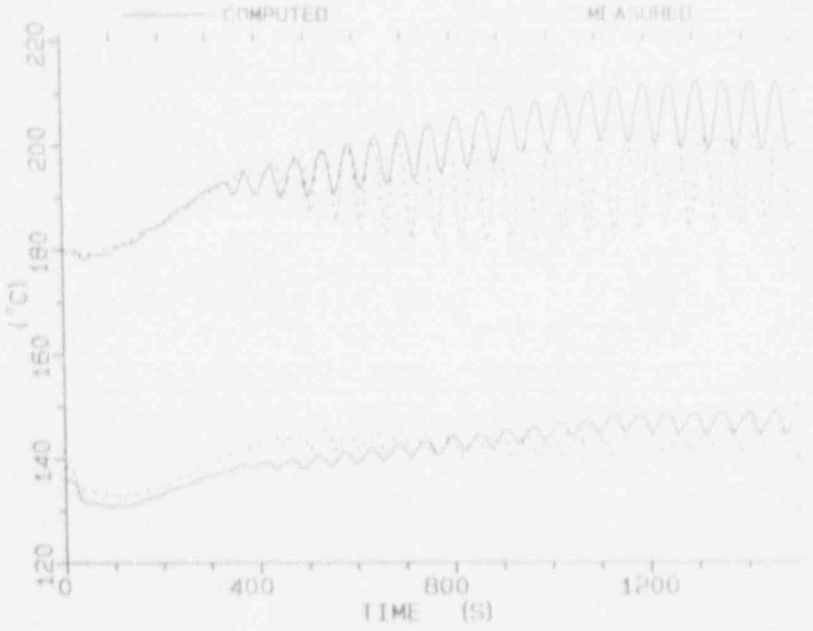

FIGURE 5.6.1.1 Water temperature in the reactor core during an uncontrolled boron dilution

Figure 5.6.1.1 shows the core inlet and outlet water temperatures.The small discrepancy for the core inlet temperature is constant, due to an initialization error of the core inlet temperature during the steady state calculation of the loop.

The boron concentration in the primary system decreases during this phase. Figure 5.6.1.2 shows the core outlet water conductivity. At the beginning of transient the dilution takes place stepwise. The lenght of the step is equal to the recirculation time of one loop. After about four recirculation times the sharp concentration front has diffused mainly due to turbulent mixing in the primary system.

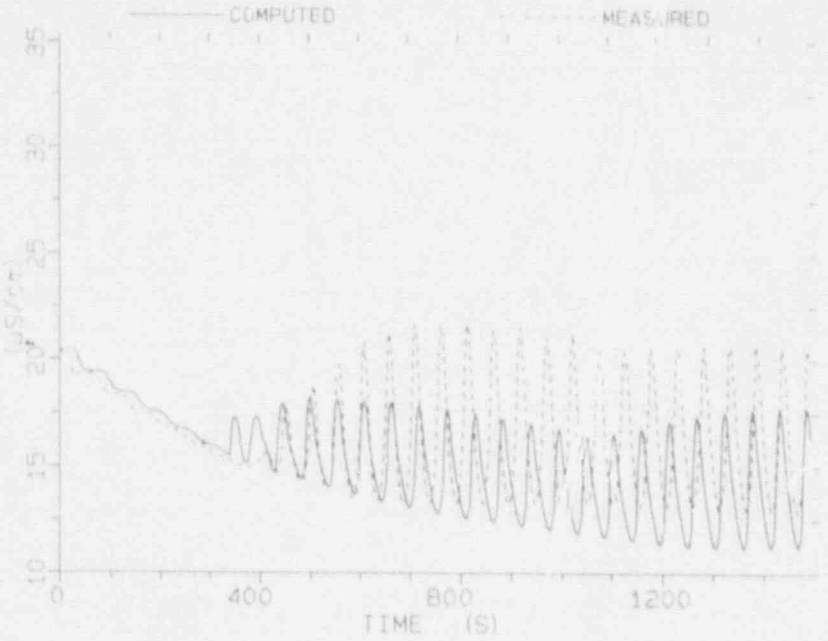

FIGURE 5.6.1.2 Electrical conductivity of water at the core inlet during an uncontrolled boron dilution

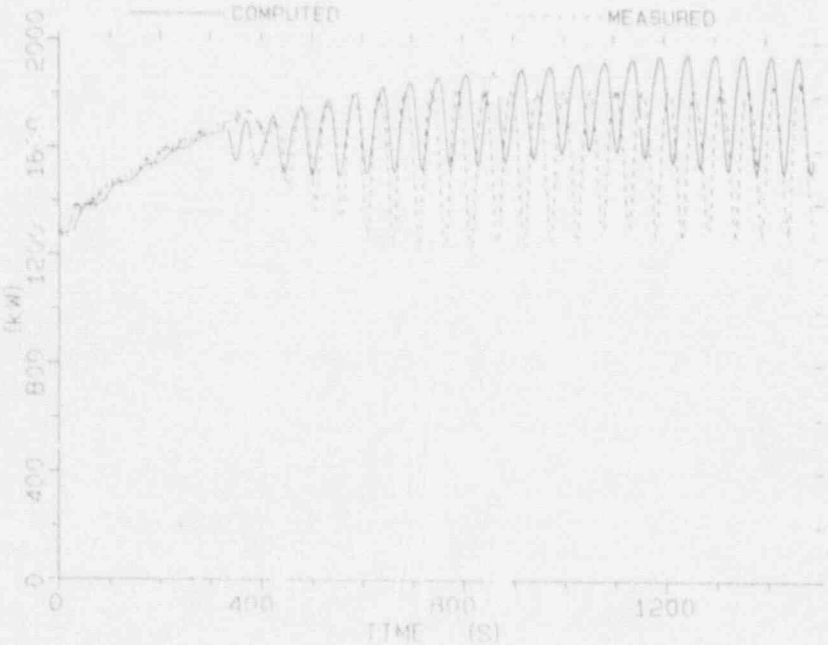

FIGURE 5.6.1.3 Reactor power during an uncontrolled boron dilution.

A comparison between test results and calculated ones shows an excellent agreement both in magnitude and in attenuation of the boron wave due to the turbulent diffusion.

The reactor power increases in response to the boron dilution and, to a smaller degree, to the variation of the inlet water temperature. The power to coolant is shown in figure 5.6.1.3.

The total reactor power increase is mainly limited by the allowed pump revolution rate increase. A comparison of power to coolant, shows also a very good agreement.

The flow through the LTDL is almost zero during this phase of the transient, see figure 5.6.1.4.

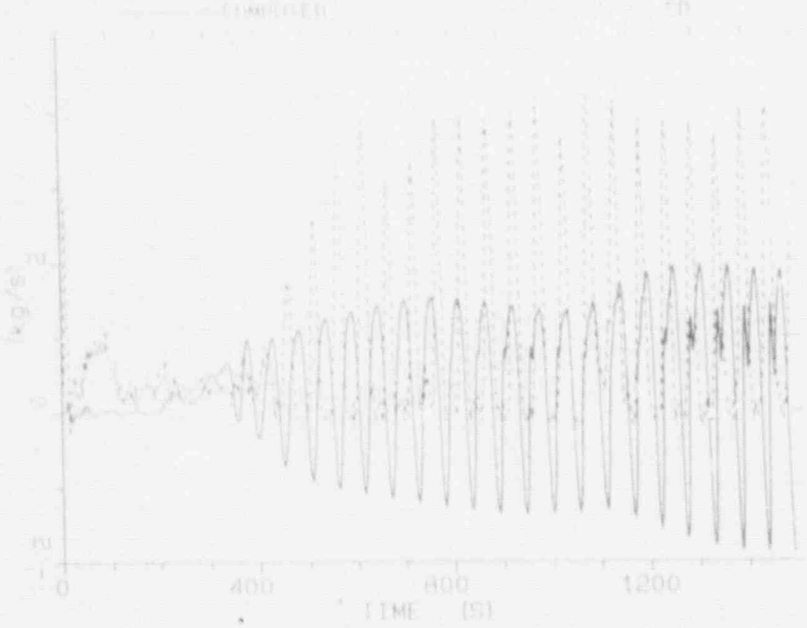

FIGURE 5.6.1.4 Water flow through LTDL during uncontrolled boron dilution.
The flow meter shows the absolute value of the flow.

5.6.2 The boration phase, 300 - 1500 seconds

When the pump recirculation rate has reached the upper limit of the control range, further increase of the temperature in the riser causes the hot/cold interface in the LTDL to move upwards.

At about 350 seconds the LTDL is penetrated and an inflow of cold highly conductive water starts. The inflow is intermittent with the period equal to the recirculation time for the loop. The con-

ductivity rises, see figure 5.6.1.2, each time an inflow from the LTDL occurs. The inflow of water stops whenever the temperature in the riser falls due to the fast power decrease, caused by the highly conductive water reaching the core.

The conductivity of the core inlet water continues to decrease to a lower overall level than before the inflow of highly conductive water from the pool. The decrease in the mean conductivity is caused in part by the fact that the plug of highly borated water injected through LTDL is shorter than the recirculation path of the loop.

The minimum conductivity of clean water pockets finally levels off due to the turbulent diffusion from the plugs of highly conductive water. An equilibrium state is now reached between the injection of clean water and the inflow of highly conductive water through the LTDL. At this time, the reactor power has reached its maximum value and a new state of the loop is reached with an almost constant power amplitude oscillation. Figure 5.6.1.3 shows the power to coolant.

A comparison of test results with the calculated behaviour of the transient shows an overall good agreement for this phase too. However, there are some discrepancies. In figure 5.6.1.3 the oscillation of the power to coolant is shown. The predicted power amplitude is lower because the prediction of the amplitude of the "boron oscillation" is lower.

Figure 5.6.1.4 shows the mass flow rate through the LTDL. The underestimation of the amplitude of the mass flow causes an inadequate boration of the primary system which has feedback to the mass flow through the LTDL. Otherwise there is a good agreement between measured and calculate data.

The conductivity in the primary system is shown in figure 5.6.1.2. Comparison of test results with the calculated ones shows a good overall agreement, both in amplitude and damping. A small discrepancy is observed in the prediction of the conductivity in the clean water pocket. This error is caused by the underestimation of the flow through the LTDL.

6. DISCUSSION

We have compared the results of simulations made by the RIGEL code against the results from a number of tests in the ATLE loop. These comparisons include the transient behaviour during small and large disturbances, i.e normal power control and boron dilution.

The comparisons show a good agreement both in magnitude and time of various physical events. A discrepancy is observed in the core coolant outlet temperature caused by an unsuitable location of the thermocouple probe in the ATLE loop and due to limitations in the RIGEL code to predict the propagation of temperature fronts. The computed results differ less than ten percent from the measured ones, even though the nodalization of the ATLE loop is relatively coarse. The average node volume in the primary loop is about four percent of the total volume of the primary system.

From the results, in part presented above, we conclude that the RIGEL code is a suitable computational tool for simulating the dynamics of the ATLE loop. The simulations give reasonably accurate information about the response of variables like temperature, flows and concentration of boron following operational disturbances in the system.

Thus the test results constitute a confirmation of the predicted self-protective thermal-hydraulics of a PIUS type primary reactor system.

REFERENCES

1 D. Babala, U. Bredolt, J. Kemppainen, A Study of the dynamics of Secure reactors: Comparison of experiments and computations. Nuclear Engineering and Design,122 (1990) pp 387-399.

2 U. Bredolt PIUS-Verification of primary system boron transport phenomena by comparison of experimental results with simulations using the RIGEL code. ANS Winter Meeting 1990, Washington DC.

3 K. Hannerz, The PIUS PWR, Energia Nucleare (Rome) 4 (1987), no 2, pp 10-21.

4 D. Babala, A fast semi-implict integration method for thermo-hydraulic networks. Trans. Am. Soc., 47, 295-7 (1984).

5 D. C. Groeneveld, S. C. Cheng and T. Doan, 1986 AECL-UO Critical Heat Flux Lookup Table, Heat Transfer Engineering vol. 7 nos. 1-2 1986

EXPLOITING DIGITAL SYSTEMS TECHNOLOGY TO IMPROVE NUCLEAR SAFETY

R.A. Olmstead, N.M. Ichiyen, J. Pauksens
Atomic Energy of Canada Limited, AECL CANDU

ABSTRACT

Nuclear plant designers in the 1990's have exceptional opportunities to exploit rapidly evolving computer and information system technology to make significant improvements in public safety. The Canadian experience with digital systems indicates that these improvements will be realized in two areas.

1. Reliability, functionality, and simplicity in the design of Safety Protection Systems and Engineered Safety Features Systems (ESFS).
2. Improved performance and fewer errors from the operations staff. Benefits achieved by automation, superior information management, and simplified maintenance.

1. INTRODUCTION

This paper describes some of the safety benefits that have been realized from digital systems technology applied to the reactor designs in the Canadian nuclear program. The biggest challenge was to establish and licence an adequate methodology to be used to ensure sufficient quality for "safety critical" software. The area with the greatest potential for improvements to plant safety is the man/machine interface.

2. MAN/MACHINE INTERFACE

The man/machine interface represents an exceptional opportunity for industrial plant designers to realize significant gains through cost avoidance, operational reliability and safety. This opportunity exists because of rapid technological development in computers and electronics, coupled with significant progress in the behavioural sciences that greatly increases our knowledge of the cognitive strengths and weaknesses of human beings.

Significant event data from operating nuclear plants in many countries consistently indicates that the root cause of events leading to equipment or safety barrier impairment results from operator/maintenance human error in 40–60% of the cases. The contribution of human error to the accidents at Three Mile Island and Chernobyl further underscores the need for design features that accommodate human cognitive strengths and weaknesses. Equally important, the significant events attributed to human errors represent a large cost iceberg in operating power stations.

In CANDU stations, as in most complex industrial plants, the man/machine interface design has progressed through three generations.

- First Generation control rooms consisted entirely of fixed, discrete components (handswitches, indicator lights, strip chart, recorder, annunciator windows, etc.) Human factors input was based on intuitive common sense factors which varied considerably from one designer to another.

- Second Generation control rooms incorporated video display units and keyboards in the control panels. Computer information processing and display are utilized. There is systematic application of human factors through ergonomic and anthropometric standards and cookbooks. The human factors are applied mainly to the physical layout of the control panels and the physical manipulation performed by the operators.

- Third Generation control rooms exploit the dramatic performance/cost improvements in computer, electronic display and communication technologies of the 1980's. Further applications of human factors address the cognitive aspects of operator performance.

At AECL, second generation control rooms were installed on CANDU stations designed in the mid 70s and early 80s. Third generation features will be incorporated in the CANDU 3 station design and future CANDU stations.

There have been significant improvements in the man/machine interface in CANDU stations over the past three decades. The continuing rapid technological developments in computers and electronics, coupled with an increasing understanding and application of human factors principles is leading to further enhancements. This paper outlines progress achieved in earlier stations and highlights the features of the CANDU 3rd generation control room.

2.1 SECOND GENERATION MAN/MACHINE INTERFACES

The control centre in the four operating CANDU 6, single unit stations represent a typical second generation man/machine interface. Some of the features are described below:

The Dark Panel Concept

Human factors research and experience in the aircraft industry has made this concept standard practice in the cockpit. In the CANDU 6 control room, a light always signals a situation that requires operator action – an annunciator, handswitch discrepancy, a computer program that has failed, etc.

The Fifteen Minute Rule

There is sufficient automation to ensure that no operator action is required in the first fifteen minutes of the worst case dual failure event, analyzed as part of the safety analysis for the plant. Consequently, CANDU operators have, as a minimum, fifteen minutes to perform diagnostics and planning before taking direct action but for single event cases at least 10 hours is available.

Automation

The use of computers in process and safety systems has, in many cases freed the operator from tedious, distracting, stressful tasks to allow him to concentrate on more strategic matters. For example, the boiler feedwater transient after a reactor trip requires no operator attention. Automation warm-up and cool down of the primary and secondary process systems is another example.

Human Engineered Testing

In the later second generation units, some periodic testing has been automated to reduce human errors that are often associated with tedious, boring, repetitive tasks. When manual tests are required, the design ensures that the tests are "non-intrusive". This ensures that maintenance staff do not modify or contact the internals of the plant equipment to carry out the tests.

Reduced Panel Congestion

This was accomplished in three ways:

1. Reducing the number of annunciator windows by limiting their use to major alarms and group alarms.
2. Use of CRTs to present displays that integrate information from different systems and equipment.
3. Automation of tasks previously accomplished by operator manipulation of control panel devices.

Good Anthropometrics

Making reference to the appropriate design "cook books", the size, shape, slope, illumination level, and many other parameters of the physical interface were optimized to accommodate the physical characteristics of the operator.

Good Control Panel Layout

The design incorporates logical grouping and clear delineation of panel switches and indicators. Panel mimics are utilized with hand switches located to represent the location and status of the controlled device as it relates to the mimic. The design incorporates standard shapes, position codes, colour codes, and a systemic and consistently applied method for labelling panel components. The alarm annunciation system classifies, sorts and allows conditional suppression of unnecessary alarm messages.

2.2 THIRD GENERATION MAN/MACHINE INTERFACES

Future CANDU stations will include a third generation man/machine interface. The principles underlying many of the design requirements are based on theories established by the discipline of Cognitive Science that seeks to integrate engineering and psychology to describe the behaviour of humans as components in an information processing system. In particular, the work of Rasmussen (13), Weiner (14) and Woods (3) has had a significant impact.

The superordinate goals for the design of CANDU third generation control rooms are the following:

1. Operational Design Objectives

   Change the design process so that high level operational objectives drive the detailed design of the cognitive and physical man/machine interface.

2. Elevate the Role of the Operator

   Apply additional automation selectively in order to remove tedious, distracting activities and provide the operator with tools to function on the level of a situation manager who plans, organizes activities and solves problems.

3. Context Sensitive Information

   Package and present information, to suit the context of particular situation, so that the operator can quickly absorb the relevant data.

4. Keep the Operator in Touch with the Plant

   Provide information and activity that will keep the operator alert and in touch with the plant.

5. Flexible Control Room

   Provide the operating utility with a control room that uses a minimum number of standardized components in a flexible interface that can be tailored to suit a different operating philosophies and methodologies.

The Nature of Man

For the third generation man/machine interface, the designer must be aware of certain unique characteristics of men that set them apart from machines. Figures 2 and 3, for example, list some intuitively derived strengths and weaknesses of men and machines in performing plant control functions.

Exploiting Human Creativity

Some of the features of the third generation control room are designed to facilitate man's unique ability to synthesize volumes of information and make good decisions, even when the data is incomplete or inconsistent. This is the key to ensuring an adequate response to the unanticipated or obscure case events that are a fact of life in complex industrial facilities.

A Fresh Perspective

Regardless of the quality of the man/machine interface design, the public perceives human variability to be such that any task given to man has a relatively high probability of being performed in error. This perception tends to suggest that there are higher probability failure modes than those identified in the random equipment failures covered in the probabilistic safety analyses.

The familiar concepts of redundancy and diversity will be applied so that a second human is available to confirm the safety critical actions of the operator. The most difficult requirement is to ensure that the redundant human is also sufficiently "diverse". This means his knowledge, training and recent activities should be sufficiently different to ensure that he does not make the same cognitive error as the first man and become part of a common mode human error. In CANDU stations, separation of perspective is achieved through the roles and activities assigned to the shift supervisor and the first operator respectively.

Providing Time for Operators to Think and Plan

In the CANDU 3 design, no operator actions are required for the first 8 hours after any design-basis initiating events, provided safety systems operate as designed. Simple design changes can extend this to 36 hours or more. Even for event sequences where mitigating systems are assumed to fail, the operator is not called on to act in less than 15 minutes. The role of the operator is changing form first-line response to one of verifying the plant's own automatic response.

Rationalizing Conflicting Objectives

The Chernobyl and the Three Mile Island incidents were partly the result of conflicting operational objectives. Procedures in these plants did not adequately resolve the potential for inappropriate action. For example, at Three Mile Island, the objective to cool the fuel conflicted with the objective to maintain two phases in the pressurizer. For the third generation MMI, man/machine interface detailed procedures and the detailed interface design will be systematically derived from a complete set of high level operational objectives. If implicit objectives are present, they must be made procedurally explicit.

The Information Interface

the "human" interfaces with the plant mainly through information while the direct manipulative interface, by comparison, is trivial. The interface is not man to machine but to information about a machine. (See Reference 6).

Information will be available to the operator in the context of his specific objectives in a particular situation. This means that, instead of organizing information in association with systems, areas of the plant or equipment, the operator will have access to information and control facilities focused on functions such as maintenance of fluid or energy balance, achievement of poison override or execution of an emergency operating procedures.

Automation

For third generation control rooms, automation will seek to transfer the low level, distracting and stressful procedural tasks from the man to the machine. Both manipulative and cognitive tasks of this type will be automated. For example, the normal equipment sequencing required to valve in the shutdown cooling system will be performed by the machine. This will allow the man more freedom to perform at the level of a planner or situation manager. When complex manual sequences are automated, a few manual operations will be retained in order to keep the operator aware of and involved with the process.

Flexibility

In the past, the control room design left the operating station staff with insufficient scope to apply their experience to determine the form of information presentation or the define operating methodologies. Third generation control rooms will utilize standard keyboard/CRT based operating consoles for interaction and banks of CRTs for information displays. The utility will have more capability to influence operational procedures and make changes over the life of the plant.

Changing the Design Process

For the advanced CANDU control room, the design process is a significant departure from previous practice. The traditional approach was to break the information interface down by plant system or equipment. Each system designer then specified the alarms, displays and control interactions they believed were adequate in that narrow context. the station technical unit was then given the job of creating operating and emergency procedures based on the design as given. In the new approach, after the basic plant operational requirements are

established, draft procedures will be produced. Then, a mixed team of designers and operating staff will define an information/interface system design that will be baed on the real objectives, tasks and activities of the operators.

Context Sensitive Information

The traditional large area of panels containing complex configurations of handswitches, recorders, meters and indicator lights will be eliminated. The control room will be compact module containing a few sit-down computer consoles that will provide information to the operator that has been processed to reflect the context of his specific objectives and tasks in each particular situation. Figure 5 illustrates these features. The detailed operating procedures are written at the beginning of the design and form the basis for the information system design.

"Blackboard Displays"

The control room environment will be dominated by several large dynamic colour graphic mural mimics. One will depict the major equipment and system status of the entire plant. Another will provide an easily interpretable picture of critical plant parameters and how they are changing or interacting. These displays are the "blackboards" upon which information is presented to everyone in the control centre without censoring because of limitations in the size of regular CRTs. Current plant status at the most detailed level will be available on both the "blackboards" and console CRTs. Traditional annunciation windows will be replaced by indicators on the blackboards and pattern displays on the CRTs.

Computer Assisted Procedures

Computer assisted procedures will minimize the need for paper procedure books. The operators will use CRT screens that present integrated text, graphics and check lists, possibly supported by a computer synthesized voice. The displays will guide them in a systematic and rapid execution of the procedure. A particularly valuable aspect of the procedure presentation is an Event Confirmation Field which, at each stage of an event specific procedure, indicates to the operator if plant conditions are confirming the correct event diagnosis. Some of the procedures will be "context sensitive" in that the computer will edit and simplify them based on its knowledge of the actual state of the plant (e.g. it will not display an instruction to turn on a pump that is already on).

Decision Support Facility

In advanced, third generation control rooms a knowledge based decision support system utilizing several online expert systems will provide the operator with information and, when appropriate, a "what if" query facility to help him anticipate and plan for future action. Associated with this facility are knowledge based event diagnostics that will help locate root cause events. The output is in the form of recommendations with the rationale for each recommendation provided on request.

Already available is a system to inform the operator which channel to fuel next and another to indicate the exact channel containing a defective fuel bundle.

Pattern Recognition

Cognitive science recognized that humans are particularly effective in learning to associate significant meaning from shapes and patterns. Control room displays will seek to exploit this factor by presenting alarm configurations and plan parameter deviations in the form of interpretable patterns.

Critical Safety Parameters

Critical safety parameters, a short list of "vital signs" relating to the public safety defence barriers, will be prominently displayed in graphical pattern form permanently on a dedicated CRT screen or blackboard displays.

Voice Annunciation

Voice annunciation will be utilized in a few selected situations where redirecting the operators' attention is imperative. For example, voice will be used to announce the at the entry conditions for an Emergency Operating Procedure have been realized.

Equipment Configuration and Status Display

Plant Equipment Status Schematics on the control room CRT will be operated directly from the plant Computer Aided Design and Drafting data base. The state of devices such as locally operated valves will be semi-automatically updated on the CRT displays from bar code readers connected into data highways by the plant operating personnel.

Operation Information

The basis for an Operation Information System will be provided. This capability will electronically integrate and automate many of the tedious, labour intensive activities associated with operating a nuclear station. For example, maintenance records, work control, man-rem statistics, equipment status, event logging and reporting and work scheduling. The result will be a significant reduction in operating costs and operator stress levels and perhaps operations staff. This facility will be developed by the operating utility associated with the plant.

Computer Annunciation Alarm Overload

With approximately 6000 measured and calculated variables for a single nuclear unit, there are operational circumstances when so many alarms can arrive that an overload situation develops. Such alarm overloads can impose severe demands upon the operator and have significant implications in terms of training, the structure of procedures and safety.

To some extent, the problem is a consequence of the availability of better instruments and tools to handle direct and derived data. Computerized techniques have contributed to the problem; they will also be part of the solutions. It is easy to present a very large volume of alarm data spanning many different fault scenarios with various degrees of importance and credibility. The challenge is to package the messages that are relevant in a particular situation and time and to articulate the alarm information in such a way that it directs the operator's attention to the remedial task at hand. Notice that we are not proposing to suppress information but rather to package and prioritize it in ways that make sense in a particular situation.

Recognition of the above problems has stimulated development of solutions. These include the following:

- The use of a high level, easy to use, programming language so that the station staff will be able to introduce the results of real operating experience.
- Improved alarm categorisation strategies, including:

a. Plant State (e.g. reactor shutdown or at power, heat transport system pressurized hot or pressurized cold, class IV power available or not).

b. Action Time (e.g. Operator action within one hour, maintenance action within 8 hours, longer term maintenance action.

c. Response Category (i.e. plant diagnostic message, equipment status message, maintenance message, software and hardware error messages).

- Increased use of interpretable shapes and patterns for presentation of alarms and deviation displays.
- Nuisance alarm suppression.
- Selected voice annunciation.

Standardization

Although there may be several design and architect engineers performing the detailed design, the layout, architecture, ergonomics and control philosophies of the entire control room will be universally consistent.

Access to Control Room Data

Because all plant data is available on high speed data highway, simple interfacing will provide controlled access to all control room information for use in the plant management computer system or on terminals on or off the site.

Cost

The elimination of fixed panels, utilization of standard operator consoles, the application of computers to operational configuration control and the reduction in trunk cabling will yield significant cost benefits.

Conclusion

Third generation CANDU control room brings together the principles of cognitive science, new technology and lessons learned by CANDU operators. In this control room, the operator will work with tools that were crafted to serve his objectives and work on his tasks. Most important, he will function on a level that exploits his unique ability to innovate and form strategies to deal with unanticipated obscure case events.

This design approach should result in improved operator reliability while, at the same time, reducing costs.

2.3 REDUCED COMPLEXITY THROUGH DISTRIBUTED COMPUTER CONTROL

The AECL CANDU 3 station will achieve a significant reduction in the number and diversity of control and instrumentation hardware components. Implementation of all plant controls in a distributed system is central to this objective.

Scope of Application

Data acquisition and process control functions for most of the non-safety systems are performed by an advanced distributed digital control system. Completely separate control equipment is used for the separate backup safety systems and their support systems. The scope of the Distributed Control System includes the conventional balance of plant process systems, as well as the nuclear steam plant systems.

The DCS control functions include low-level control and interlocking functions for individual process devices such as pumps and valves, as well as high-level control and co-ordination functions for groups of devices and systems. Examples of the high-level group control functions are reactor regulation, heat transport system pressure and inventory control, and steam generator level control. The scope of the DCS control functions includes manual and automatic control modes.

Concept

The DCS consists of a number signal scanning and processing stations linked by high performance data highways. Process instrumentation and control devices are connected to stations assigned to specific plant areas and functions, in order to reduce the amount and complexity of plant cabling and wiring.

The overall configuration is based on the same concepts that have been successfully applied to the current generation of CANDU plants; i.e. the system is divided into three separate channels to match the channelization of redundant sensors and process devices. Within each channel, redundancy, self-checking, and automatic switchover concepts are used to provide a fault tolerant system.

Watch-dog times are used to ensure that safety related output signals are reset to a safe state if they are not cyclically updated with valid data.

Benefits

The functions performed by the DCS are implemented in current CANDU plants by a dual digital computer control system (DCC), in combination with a relay logic system and a number of analog control loops using electronic controllers, current alarm units, and other analog devices. All of these systems and devices are connected to process instrumentation devices, and to each other, via multiconductor trunk cables and about 80,000 cross connection wires in a large central control distribution frame.

The DCS concept makes a significant contribution to the reduction of project cost and schedule. The plant construction and commissioning schedule is reduced by at least 2 months, due to the reduction in site cabling and wiring. The design costs are reduced due to the use of a functional process control language and computer aided design methods. Equipment cost, design cost and maintenance cost are all reduced by increased use of up-to-date standardized equipment.

Improved reliability is obtained by the elimination of a large number of wiring connections, and by the use of continuous comprehensive self-checking, and more comprehensive redundancy and channelization.

2.4 DIGITAL PROTECTION SYSTEMS

Introduction:

The approach in Canada to digital systems in protection systems is a combination of the techniques from successful use of computers for control, world trends in software engineering, and the overall principles of safety system design, such as simplicity, and defence-in-depth.

Historically, CANDU was among the first reactors to include computers in safety systems with the PDCs (Programmable Digital Comparators) used in the CANDU 600 reactors (early 1980s). PDCs were used to implement the trip decision logic for the process trip parameters (see Figure 1).

The operating statistics indicate a significant contribution to plant safety. The three CANDU 600 stations (Wolsong 1, Gentilly 2, and Pt. Lepreau) have a total of 288 PDC-years of operating history without a single unsafe failure reported. All PDC failures have been safe failures which can be contrasted with the experience with the conventional portions of the system where about 1/4 of the failures are potentially unsafe, i.e. temporarily diminish the redundancy of protection, until corrected. This is due largely to the design that employs features such as self-checks, "continuous" testing, hardware watch-dog timers, etc. which convert detected unsafe faults into safe failures (i.e. trip the channel). From the production reliability viewpoint, there have been no spurious reactor trips attributed to PDC related failures.

This experience has confirmed our original reasons for using computers, that they enhance safety availability (convert unsafe failures into safe ones), and also improve production reliability.

This concept evolved further in the Darlington fully computerised shutdown systems (see Figure 1). Here the functionality has increased to include not only the safety trip decision logic but also channelized displays to the Operator and automated testing and monitoring functions as well. It is important to note that while the overall functionality has been increased, the safety critical portions have been localized (to the channelized trip computers only) and the trip functions kept as simple as possible. This is a key component of the "Canadian" approach.

Regulatory Issues:

In the course of design evolution, a number of issues have arisen, mainly with respect to software. The main issues are:

a. no agreed upon, measurable definition of acceptability exists for the engineering of safety critical software.

b. no widely accepted and adopted practices for the specification, design verification and testing of safety critical software exists.

c. it is not possible to quantify the achieved reliability of the software component of a safety system.

d. it is not possible to quantify the benefits of using diverse software.

e. it is not possible to exhaustively test software in all of its possible modes; thus it is unclear what constitutes a sufficient degree of testing.

Because of these issues, obtaining a license from the regulatory authority, the Atomic Energy Control Board (AECB), for the Darlington shutdown system trip computers was difficult. Several additional design and verification processes were backfitted after the original software development process was completed. The key additional processes were:

a. preparation of a mathematically precise software requirements specification.

b. formal verification of the code against the requirements specification.

c. statistically valid, trajectory based random testing to demonstrate that the software reliability was consistent with the system reliability requirement.

d. hazard analysis of the code to identify failure modes that may lead to an unsafe event.

The application of many of the techniques used represented their first use in a nuclear safety critical application. Many valuable lessons were learned about the merits and applicability of the techniques.

To avoid similar difficulties in the future, to document some of the lessons learned, and to document how to apply the techniques rationally during the software development process as opposed to after- the-fact, Ontario Hydro and AECL formulated a strategy for the development of a set of standards, procedures and guidelines for software engineering. The set of standards, procedures and guidelines will address the requirements for all levels of criticality.

To date, a high level standard for the software engineering of safety critical software, the highest criticality level, has been produced. This standard defines the software engineering process, the outputs from the process and the requirements to be met by each output. The requirements are expressed in methodology independent terms so that various techniques for software engineering may be used to meet the requirements of the standard. This allows the standard to be used to assess the acceptability of various proposed techniques and allows for techniques to evolve without requiring changes to the standard.

Current Work:

The software engineering development efforts in both Ontario Hydro and AECL are co-coordinated through a committee called OASES (Ontario Hydro/AECL Software Engineering and Standards). Through OASES, a program has been established to determine the detailed methodologies to be used for all phases of the software development cycle. Detailed (methodology specific) procedures and tools to support the methodologies will be produced for safety critical software by the end of the calendar year.

Review of the standards and methods by the AECB is being sought during their development to increase the probability of their acceptance.

Standard for Software Engineering of Safety Critical Software:

The fundamental principles which were the basis of the requirements in the high level standard for safety critical software are described below. These principles were the basis of the requirements within the standard

A planned and systematic Software Engineering Process must be followed over the entire lifecycle of the software. Both the original development and any revisions must be treated as an integral, continuous and interactive process. Any changes must be verified to the same degree of rigour as the original development.

In order for software to be "engineered" it must be developed according to a planned and systematic process that has been designed to produce software of the required quality. In order to maintain the quality, all revisions made to the software until its retirement should also be performed according to a planned and systematic process.

Documentation must be prepared to clearly describe the required behaviour of the software using mathematical functions written in a notation which has a well defined syntax and semantics.

Mathematical functions provide a mechanism for completely, precisely and unambiguously specifying the required behaviour of the software.

By having the behaviour of the outputs specified by mathematical functions the following advantages are achieved:

i. the requirements will be more complete since input domain coverage can be checked to determine if the required behaviour of the outputs has been specified for the complete, valid range of each input and for all combinations of inputs that affect each output.

ii. the requirements can be uniquely interpreted since the notation has a well defined syntax and semantics.

iii. the mathematical representation facilities the use of mathematical verification techniques that allow the design to be transformed into a mathematical function form for direct comparison with the requirements.

The outputs from each development process must be reviewed to verify that they comply with the requirements specified in the inputs to that process. In particular, those outputs written using mathematical functions must be systematically verified against the inputs using mathematical verification techniques.

Stepwise refinement is an important concept not only because it allows the developer to tackle several more manageable problems instead of one large one, but also because it allows the verifier to more effectively perform review. It is very difficult to review software listings to determine if they represent a solution to the right problem. It is much more manageable to first verify that the requirements are correct, then verify that the design description correctly satisfies the software requirements, and then, finally, verify that the code satisfies the design description.

Mathematical verification provides and effective mechanism for demonstrating conformance to specifications. Mathematical verification is most effective when it is integrated into the design process.

The structure of the software must be based on "Information Hiding" concepts. Information hiding is a software design technique in which the interface to each software module is designed to reveal as little as possible about the module's inner workings. It was developed by Dr. D.L. Parnas in 1972 and is described in reference [3]. In this way, if it is necessary to change the functions internal to one module, the resulting propagation of changes to other modules is minimized. This results in modules that are loosely coupled or independent of each other as much as possible.

Loosely coupled modules are easier to review since the reviewer can focus on the module under review instead of the dependencies between several modules. Also, loosely coupled modules mean less interaction between various software developers which results in higher productivity.

Both systematic and random testing must be performed to ensure adequate test coverage.

Testing is the process of executing a program with the intent of finding errors. Errors may consist of non-conformance with the requirements specification or the design description, or incorrect object code produced by the compiler or assembler. It is impractical to exhaustively test the software because the number of test cases to provide every input combination (exhaustive input testing) or to cause every path through the software to be executed (exhaustive path testing) is too large. The question is therefore "What set of tests, less than exhaustive tests, constitutes an adequate set of tests?".

Adequate test coverage must be accomplished through a combination of systematic white-box and black-box test cases along with randomly generated test cases. The design of the black-box and white-box test cases should be such that a predefined coverage is accomplished that should uncover many of the most common errors. The purpose of the random test cases is to improve the effectiveness of the test cases by compensating for false assumptions and biases of the tester.

Reliability of the safety critical software must be demonstrated using statistically valid, trajectory-based, random testing.

As discussed above, it is not practical to exhaustively test software. As a result the software will be placed in service with the knowledge that it may encounter a combination of input conditions never tested for and for which the software may fail to meet its requirements. As far as possible this degree of uncertainty must be quantified so that it can be shown to be consistent with the reliability requirements of the overall system.

It si possible to use random testing as a means of determining the probability that software product will encounter an input sequence that will lead to errors. From this it is possible to determine the number of random test cases required to demonstrate a specific reliability value. [2]

Configuration management must be maintained throughout the entire life of the software to ensure up-to-date and consistent software and documentation.

The objective of Configuration management is to identify the configuration so a software system at discrete points in time for the purposes of systematically controlling changes to the configuration and maintaining the integrity and traceability of the configuration over the entire lifecycle of the software. Configuration management of the outputs of the processes must be maintained to ensure that the correct version of each output is being used at any point in time.

The objective is also to control all changes made to the software. Software engineering is iterative in nature since changes to requirements, design, code, and verification procedures occur at many points during the process.

Ongoing training must be undertaken to ensure that personnel have the skills required to perform their jobs.

Since software engineering is a relatively new field, there is not yet a definition of the minimum set of skills that a software engineer must possess. This problem is also complicated by the fact that software is being introduced in areas where personnel are not familiar with the specialist techniques required to develop safety critical software.

Therefore it is necessary that the skills required to perform the various software engineering process be identified and compared with the skills of the individuals performing the processes.

Verification of the software must be carried out throughout its entire life. All changes to an output must be verified in the same way as the original output.

Between the time software is first released for use and its final retirement it undergos changes to correct detected errors and to respond to modifications and enhancement in requirements. To ensure that the software does not degrade over time, the level of verification must be maintained. The verification of changes must therefore be performed in the same manner and to the same degree of rigour as changes would be verified during initial development.

Independence of design and verification personnel must be maintained to help ensure an unbiased verification process.

The effectiveness of the verification process is greatly enhanced when personnel other than the designers perform the verification. Independence of the verifiers provides a perspective to the verification that is not biased by the design of the software but is strictly based on the available documentation.

Analyses must be performed to identify and evaluate safety hazards associated with the computer system with the aim of either eliminating them or assisting in the reduction of any associated risks to an acceptable level.

To provide adequate confidence that the safety critical software will operate in a safe manner at all times an analysis must be performed whose purpose is to identify any failure modes that may lead to an unsafe action, and then either eliminate them or, where possible, ensure that the failure mode can be detected and the system put into a safe state.

The high level standard captures the essence of the Canadian approach to use of software in safety systems. The fundamental principles which were the basis of the requirements in the high level standard for safety critical software are described below.

Summary:

The Canadian approach to digital systems in safety systems represents an incorporation of our experience in control computers and world trends in software engineering with our overall principles of safety system design, such as simplicity, and defence-in-depth. Feedback from the world community indicates that we are at the forefront of efforts in this area.

3. REFERENCES

1. Atomic Energy of Canada Limited/Ontario Hydro, "Standard for Software Engineering of Safety Critical Software".
2. Parnas, D.L., "On the Criteria to be Used in Decomposing Systems into Modules", Communications of the ACM, Vol 15, No. 12, December 1972, pp. 1053-1058.
3. Roth, E.M., Woods, D.D., "Aiding Human Performance 1: Cognitive Analysis". Le Travial humain, tone 51 No. 1/1988.
4. Hurst, R & L (Editors). "Pilot Error – the Human Factors". Jason Aronson, New York, 1982.
5. Wagner, E.L., Nagel, D.C. (Editors) "Human Factors in Aviation". Academic Press Incorporated, 1988.
6. Lipsett, J.J., Olmstead, R.A., Stevens, J.E.S. "Balancing the Roles of Humans and Machines in Power Plant Control". AECL-9959, Atomic Energy of Canada Limited, Chalk River, Ontario, 1989.
7. Swaton, E., Neoyan, V., Lederman, L., Human Factors in the Operations of Nuclear Power Plants by Nuclear Power and Safety. Date Unknown.
8. Sheridan, T.B., Vamos, T. Aida, S. "Adapting Automation to Man, Culture and Society", Automacia, Volume 19, #6 pp 605-612, 1983.
9. Adams, J.A., Issues in Human Reliability. Human Factors, 1982, 24 (1), 1-10.
10. Dunn, J T., Finlay, R.B., Olmstead, R.A., Advanced CANDU Reactors, AECL-9817, Atomic Energy of Canada Limited, Chalk River, Ontario, December 1988.
11. Olmstead, R.A., Fenton, E.F. "The Advanced CANDU Single Unit Control Room", Atomic Energy of Canada Limited and E.F. Fenton, Ontario Hydro. Presented at the Conference on Advances in Nuclear Technology, Madrid, Spain, April 1989.
12. Woods, D.D., Roth, E.M., Aiding Human Performance 11: From Cognitive Analysis to Support Systems, Le Travail humain, tone 51, #2/1988.
13. Wiener, E., "Cockpit Automation: In Need of a Philosophy" Presented at the Aerospace Technology Conference & Exposition, Long Beach, Calif. October 14-17, 1985.
14. Rasmussen, J. "Information Processing and Human-machine Interaction – An Approach to Cognitive Engineering". Elsivier Science Publishers, New York, 1986.
15. Wiener, E., "Fallible Humans and Vulnerable Systems: Lessons Learned from Aviation" NATO ASI Series, Vol. F322.

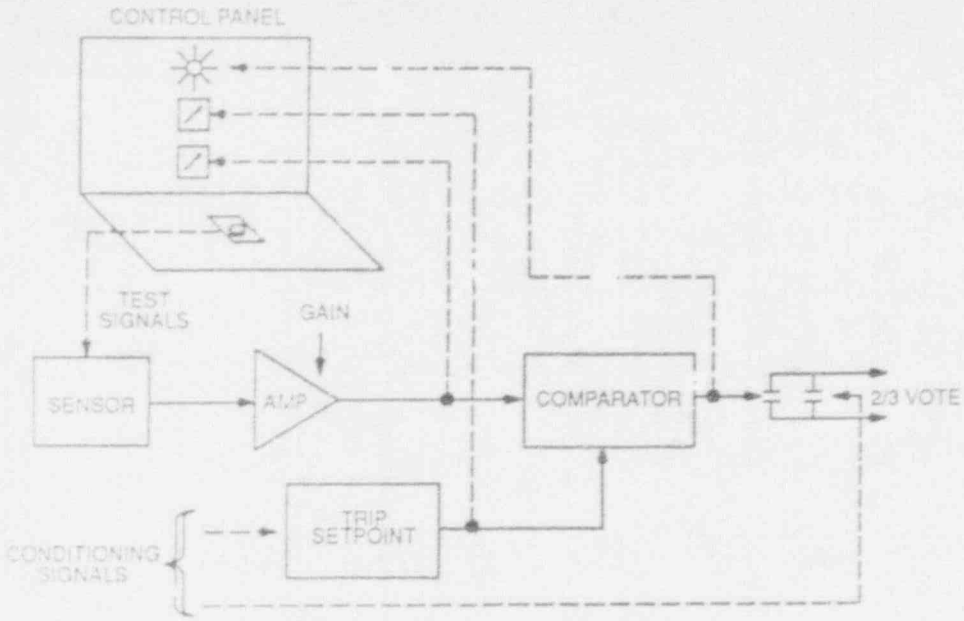

Traditional shutdown system design

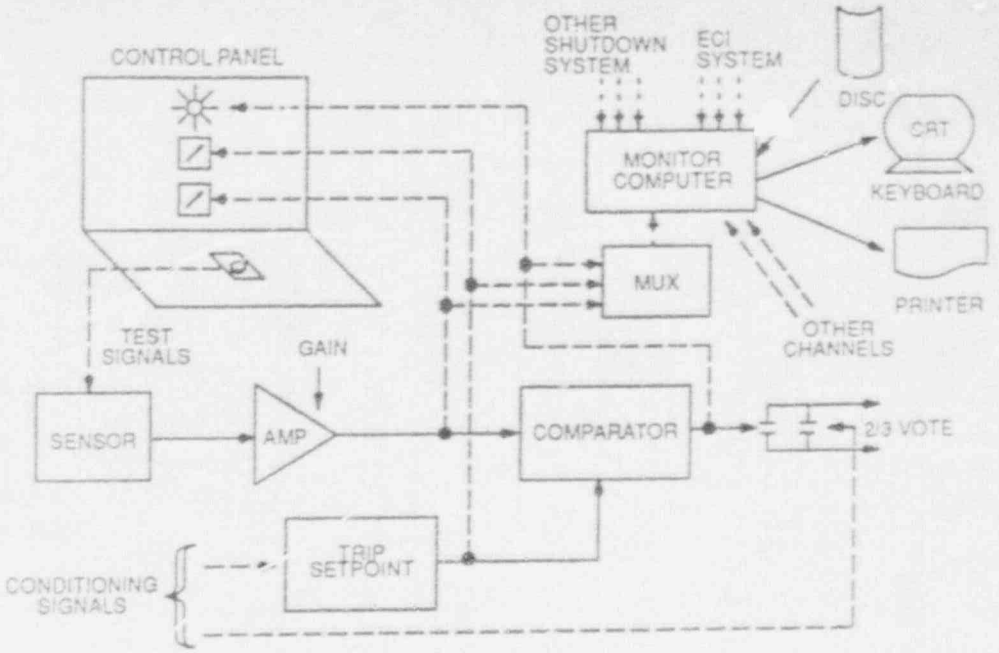

Traditional shutdown system design plus monitoring computer (Bruce)

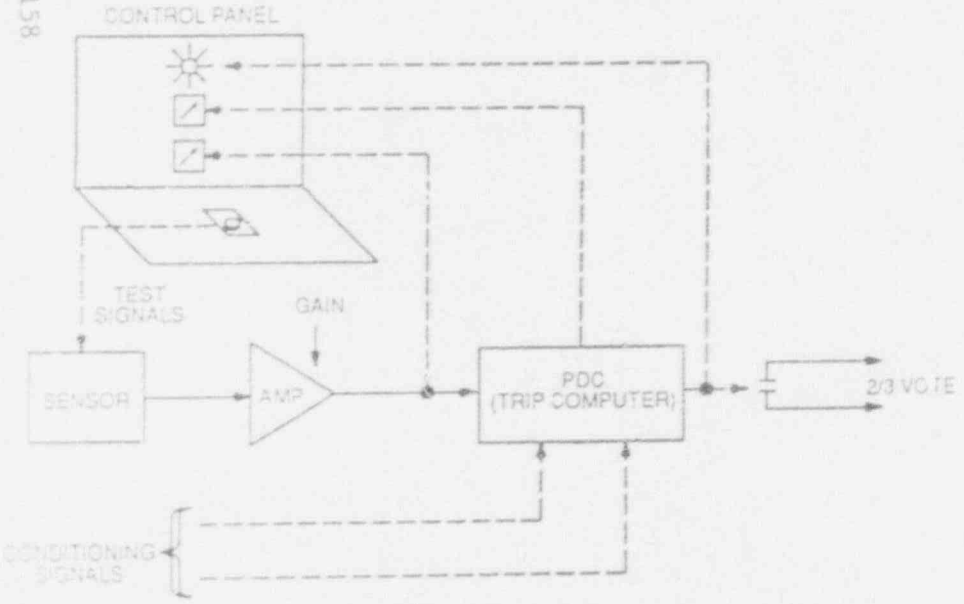

Trip computer (600 MW design)

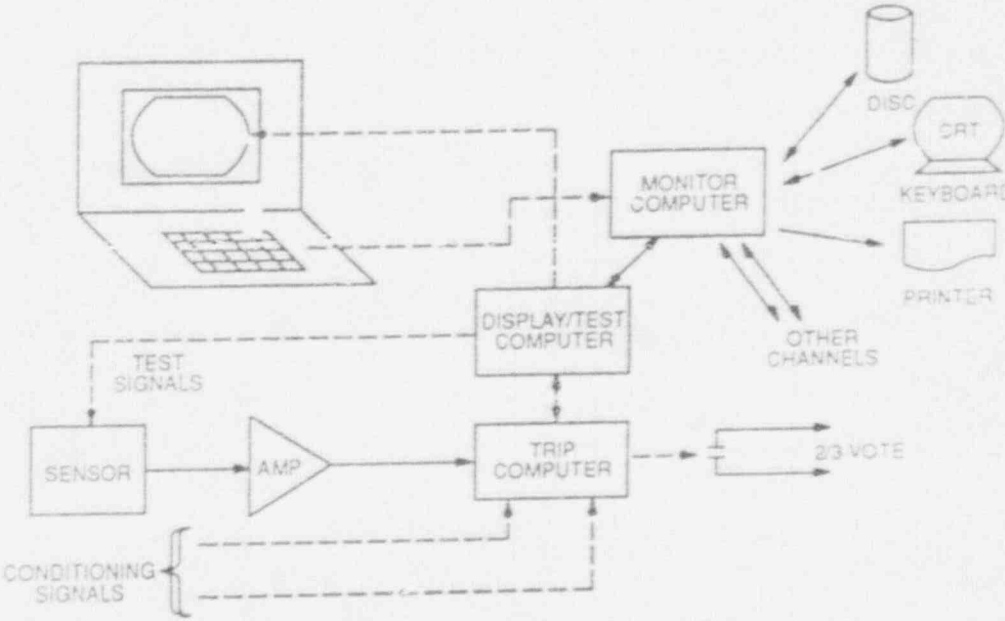

Fully computerized shutdown system
(Darlington SDS–1, SDS–2)

FIGURE 1 THE EVOLUTION OF COMPUTER APPLICATION IN CANDU SHUTDOWN SYSTEMS

MAN

+ CREATIVE
+ USE OF JUDGEMENT, EXPERIENCE, HEURISTICS
+ MAKES DECISIONS OUT OF INCOMPLETE DATA
+ CAN SYNTHESIZE SUPERORDINATE OBJECTIVES

- FORGETS
- GETS OVERLOADED
- TUNNEL VISION
- SUBJECT TO FATIGUE AND EMOTIONAL INTERFERENCE
- LOGIC AND REASONING FAULTS OCCUR

Figure 2

MACHINE

+ REPEATABLE RESULTS

+ PREDICTABLE CAPACITY

+ NOT SUBJECT TO FATIGUE OR EMOTION

+ CAN SIMULATE LEARNING AND JUDGEMENT

+ CAN PERFORM COMPLEX COMPUTATION AND LOGIC

- NEEDS COMPLETE SET OF INPUTS TO FUNCTION

- LIMITED ABILITY TO LEARN

- SUBJECT TO DESIGN ERROR

- REQUIRES MAINTENANCE

- SOMETIMES FAILS CATASTROPHICALLY

Figure 3

ANALYSIS OF POSTULATED EVENTS FOR THE REVISED ALMR/PRISM DESIGN*

G. C. Slovik and G. J. Van Tuyle
Brookhaven National Laboratory

ABSTRACT

The Nuclear Regulatory Commission (NRC) is continuing a pre-application review of the 471 MWt, Liquid Metal Reactor, PRISM by General Electric, with Brookhaven National Laboratory providing technical support. The revised design has been evaluated, using the SSC code, for an unscrammed loss of heat sink (ULOHS), an unscrammed loss of flow (ULOF) with and without the Gas Expansio Modules (GEMs), and a 40¢ unscrammed transient overpower (UTOP) event. The feedback effects for U-27Pu-10Zr metal fuel were modeled in SSC. The ULOHS accident was determined to be a benign event for the design, with the reactor power transitioning down to a decay heat level within 500s. The power during the postulated ULOF events, with the GEMs functioning, transitioned to decay heat levels without fuel damage, and included a 300K margin to sodium saturation. The case without the GEMs nad only a 160K margin to sodium saturation and higher fuel temperatures. In addition, the clad was predicted to quickly pass through the eutectic phase (between fuel and clad), and some clad wastage would result. The 40¢ UTOP was predicted to raise the power to 1.8 rated, which later stabilized near 1.2 times full power. SSC predicted some localized fuel melting for the event, but the significance of this localized damage has not yet been determined. If necessary, the vendor has options to reduce the maximum reactivity insertion below 40¢.

1. INTRODUCTION

The Nuclear Regulatory Commission (NRC), with technical support provided by the Brookhaven National Laboratory (BNL), is continuing a pre-application review of the 471 MWt PRISM advanced reactor design. The evaluation of the initial design has already been released (Ref. 1) with the supporting technical analyses performed by BNL (Ref. 2). Among the findings of the report was the determination that there were apparent vulnerabilities in the passive shutdown response to certain improbable, unscrammed, events. In particular, events which involved a rapid flow reduction without scram were of concern since the sodium margin to sodium boiling was not large enough to account for all the uncertainties. Since boiling of the sodium could introduce positive reactivity and trigger a power excursion, any potential for sodium boiling is a cause for concern.

In response to the initial findings by the NRC (Ref. 1), General Electric (G.E.) revised the PRISM design (Ref. 3). In several cases, the changes were made to directly address the NRC concerns. Other changes were dictated by the U.S. Department of Energy (DOE) as design improvements or revisions to enhance the economics of the plant. As the result of these changes, nearly all of the

---

*This work was performed under the auspices of the U.S. Nuclear Regulatory Commission.

BNL analyses were repeated to factor in the new components and the revised operating conditions. Key findings with respect to the postulated unscrammed cases are summarized in this paper.

2. THE ALMR DESIGN

The ALMR plant, as presently proposed by G.E., consists of three identical power blocks of 465 MWe, for a total plant electrical rating of 1395 MWe (Table 1 and Figure 1). Each power block is comprised of three reactor modules with individual thermal ratings of 471 MWt. Each module has its own steam generator which is combined in each power block to feed a single turbine generator. The reactor module (Figure 2) is about 19 meters (62 feet) high and about 6 meters (20 feet) in diameter, and is placed in a silo (i.e., below grade).

Under normal operating conditions, four EM pumps draw sodium from the cold pool and drive it through eight pipes to the core inlet plenum. The sodium is heated as it passes upward through the fuel assemblies (hexagonal cans containing wire wrapped pins) and into the hot pool above the core region. The heat is transferred to the intermediate loop sodium by the intermediate heat exchanger (IHX), as the primary sodium passes from the hot pool to the cold pool.

The core design is illustrated in Figure 3. A "limited free bow" constraint system is utilized to assure an outward bow in the active core region of the assemblies as long as the peak temperatures are in the core center and decrease radially. The bowing is only one of several reactivity feedbacks that are significant. The other feedbacks are Doppler, sodium density, fuel expansion, core radial expansion (via grid plate and above core load pads), the control rod drive line expansion, and the Gas Expansion Modules (GEMs). Most of these feedbacks are negative for off nominal conditions, since increasing the power and core average temperature causes the core criticality to decrease. This characteristic gives the core power the tendency to transition to a lower level at an elevated temperature (unless the sodium boils). Predictive calculations are performed to determine the rate, direction, and magnitude of the reactivity feedback components during postulated transients. Linkage between the reactor modules is only through the turbine systems, and is further reduced by the use of a saturated steam cycle. As a result, one can generally decouple the reactor modules, particularly for the shorter unscrammed events.

Table 1. ALMR Plant Design Data

Reactors Modules Per Power Block:		Three
Number of Power Blocks:		One/Two/Three
Electrical Output:		465/930/1395 MWe
Reactor Power:		471 MWt
Turbine Throttle Conditions:		7.58 MPa (Saturated)
Primary Sodium	Inlet:	610K
	Outlet:	758K
Secondary Sodium	Inlet:	555K
	Outlet:	716K
Peak Fuel Pin Linear Power:		305 W/cm
Peak Fuel Burnup:		135 MWd/kg
Refueling Interval:		18 months

3. PRISM SHUTDOWN AND HEAT REMOVAL

The PRISM reactor shutdown system utilizes six control rods, with each control rod capable of shutting the reactor down. Extensive diversity in the system, i.e., each rod has its own electrical system, independent drive motors,

and a gravity drop alternative, greatly reduces the likelihood of this system failing entirely.

In the center of the core is a hollow assembly beneath a container holding B_4C balls. Dropping the balls is another independent means of terminating power. G.E. calls this system the "Ultimate Shutdown System" (USS). However this is a comparatively slow system, which requires a minute or two to respond.

When the passive-shutdown response is triggered, it can reduce the reactor power in response to most postulated unscrammed events. However, criticality of the system must be terminated as soon as possible to remove the risk of uncertainties. The potential for positive reactivity insertions through sodium boiling, or fuel relocation, dictates that this class of events be evaluated. Calculations provided the timing at which events progress and gave insight into the inherent response of the system during unscrammed events.

If there is failure to remove enough heat from the primary system, the sodium will expand, and the hot pool sodium will eventually (a few hours) spill over the reactor vessel liner. This will establish an alternate flow path and will increase the heat being rejected off the reactor vessel surface to the atmosphere (Figure 2). Once this has occurred, the Reactor Vessel Auxiliary Cooling System (RVACS) becomes fully functional and removes the decay heat load efficiently enough to prevent damage to the reactor vessel and other key components. Even without the spill-over, including normal operating conditions, there is substantial parasitic heat removal by conductance through the vessel liner, vessel, and containment vessel.

In the PRISM design, the use of sodium coolant and the relatively small reactor power facilitates this type of passive decay heat removal. Both the normal cooling and auxiliary cooling system (ACS is a natural circulation air jacket around the steam generator) can work well under natural circulation conditions. However, G.E. prefers to emphasize the RVACS performance rather than the reliability of the normal plant cooling systems. It is very difficult to completely fail this system even if partial blockages of atmospheric air are postulated. Even if all three heat removal systems fail completely, it would be at least twelve hours before significant core damage would result, because of the large thermal mass of the system.

4. U-10Zr-27PU FUEL

The current metal fuel composition proposed for PRISM is U-10Zr-27Pu. The initial data indicates that the burnup response of the ternary metal fuel is more complex than that for the original U-Zr metal fuel, showing axial expansion early in the burnup cycle, as well as fuel component migration. In theory, the behavior of the three component ternary fuel should be more complex than binary fuel, and it should require some time to characterize fully. Argonne National Laboratory (ANL) will be obtaining more data on the ternary fuel within the next year and hopes to address some of the questions that have resulted from the data obtained from the first few pins. The radial migration of the uranium and zirconium components during burnup is very substantial and causes large changes in local fuel thermal conductivities and significant changes in the fuel solidus and liquidus temperatures. In addition, there may be some radial relocation of the plutonium component, which could change the radial power distribution within the fuel pin. Consequently, some problems with metal fuel have been identified, but judgement will be reserved until more conclusive data has been compiled.

5. PRISM MODELING

The SSC (Ref. 4) and MINET (Ref. 5) codes were used in this analysis for complimentary purposes. SSC was developed at BNL for analyzing LMR transients.

SSC can model core regions in detail, as well as the primary system, the IHX, intermediate loop, steam generator, and the major components of the ternary loop. However, alternate flow patterns that may develop during loss of heat sink events or certain loss of flow can become very complicated, which requires the MINET flexibility for that part of the analysis.

5.1 SSC Model

In Figure 4 a schematic drawing of the PRISM model is shown. The core was represented using 7 channels: fuel (or driver), internal blanket, radial blanket, control assembly, shield assemblies, hot driver, and hot internal blanket. Each channel has 2 axial nodes in the lower shield, 6 axial nodes in the fuel region, and 4 nodes to represent the upper gas plenum.

5.2 Reactivity Feedback Models

Several reactivity feedbacks are important in the passive shutdown response for the metal cores. Because of the smaller Doppler feedback in the metal cores, reactivity feedbacks having little importance in oxide cores are significant in the metal core. The main reactivity feedbacks are as follows:

5.2.1 Doppler Feedback

As the fuel temperature increases, more neutrons are parasitically absorbed in the resonance energy range. For metal fuel, Doppler feedback is smaller than it is for oxide fuel because of the harder neutron energy spectrum, which places fewer neutrons in the resonance energy range. Also, due to high thermal conductivity, metal fuel operating temperatures are much lower than those in oxide fuel cores. This allows the power and temperature defect in a metal core to be small (~$1.20), allowing the criticality of the system to be influenced by other natural feedbacks.

Each of the 6 axial levels in the SSC fuel representation was given equal weight and was referenced to the cold shutdown temperature. The Doppler coefficient is given in the form of:

$$\alpha = T \frac{dk}{dT},$$

which leads to the reactivity equation for the Doppler as:

$$\rho_R^{(t)} = \sum_{i=1}^{3} \sum_{j=1}^{6} \alpha_i \ln\left(\frac{T_{Avi}}{T_{Ref}}\right) - \rho_{Ro}, \qquad (1)$$

k = Multiplication factor
α_i = Node Weighted Doppler Coefficient
T_{AV} = Average Node Fuel Temperature
T_{Ref} = Reference Fuel Temperature on an Absolute Scale (K or R)
j = 6 Axial Levels in the Fuel Channel
i = 3 Different Fuel Channels (i.e., driver, internal blanket, and radial blanket)

ρ_{Ro} = Steady-State Reference Value for Doppler Reactivity

The standard definition of neutronic reactivity is used (i.e., $\rho = \frac{k-1}{k}$.)

By definition, the reactivities are referenced to zero at the steady state conditions, i.e., before the transient begins.

5.2.2 Axial Fuel Expansion

Metal fuel expands axially when it heats up. Axial expansion increases the core height and decreases the effective density of the core material. This increases the probability that a neutron will escape the core, giving a negative reactivity feedback.

All analyses performed using SSC assumed that the fuel is in contact with the HT9 clad. This is the most common state for the equilibrium core since only 25% of the core will be reloaded at each refueling, and the fuel is in an unlocked state, i.e., below 2 a/o burnup, only briefly. Axial expansion is dominated by the clad after lockup since metal fuel is weak (i.e., small Young's Modulus). The fuel elongations in SSC calculations were calculated by using an average strain, weighted with Young's modulus:

$$\epsilon = \frac{\epsilon_f Y_f A_f + \epsilon_c Y_c A_c}{Y_f A_f + Y_c A_c}$$

where

ϵ = strain ($\Delta\ell/\ell$)
Y = Young's Modulus
A = Nominal cross sectional area
c = clad
f = fuel

The PRISM axial fuel expansion feedback evaluation was performed using an equation similar to Eq. (1). The reactivity worth was determined from the difference between the initial fuel length and the elongated length at any given time.

5.2.3 Sodium Density Feedback

Thermal expansion of the sodium is the only significant positive reactivity feedback, except for the long term withdrawal of the control rod drive line with vessel heatup. The thermal expansion results in fewer sodium atoms within and surrounding the core. The dominant effect is the reduction of the collisions between neutrons and sodium atoms, which hardens the neutron energy spectrum and yields a net positive reactivity feedback effect from the increased neutron importance.

The feedback formulation was of the same form as Equation (1), with the reference density at the refueling temperature. Each node was given equal weight within the given category (i.e., driver, internal blanket, and radial blanket).

5.2.4 Control Rod Drive Line and Vessel Thermal Expansion

The magnitude of this feedback is dependent upon the initial position of the control rods on the control rod worth curve. The control rod drive lines, which are in the upper internal structure, expand when they are heated, inserting

the control rods further into the reactor, adding negative reactivity.

The thermal expansion of the reactor vessel ultimately limits the amount of negative reactivity inserted by the control rod drive line. The reactor vessel is cantilevered from the top, and expands down and slowly withdraws the control rods from the core up to the control rod stop positions. The time constant for the reactor vessel is about 700s, while the control rod drive line expansion time constant is around 28s. Thus, the initial response to increased sodium outlet temperatures is a negative feedback, while the long term effect could end up being positive.

Control rod and vessel expansion are calculated in SSC using single node temperatures for the vessel and control rod drive line masses. The total elongated length is calculated by subtracting the vessel expansion from the control rod drive line expansion to determine the net control rod expansion into the core.

5.2.5 Radial Expansion

The radial dimension of the core is determined largely by assembly spacing. This spacing is determined by the grid plate below the core and by two sets of load pads above the core. When the structures heat up and expand it increases the core radius, which reduces the core average density in the radial direction. The effect increases neutron leakage and generates a negative feedback response.

In the SSC calculation, no credit was given for the thermal bowing of the assemblies. It is noted that the bowing effect may reduce the risk associated with several severe accident sequences. However, the total worth of the (limited-free) bowing carries significant uncertainties. Bowing should add negative reactivity to the system. At this time, it doesn't appear that bowing can insert any positive reactivity during any portion of the postulated accidents reviewed to date. Hence, neglecting it is a conservative assumption.

SSC tracks the radial expansion of the core from thermal expansion only. This is accomplished by tracking the structure temperatures at the above core load pads (just above the fueled area) and at the grid plate.

The coefficients supplied for radial expansion were calculated using a uniform increase over the core radius. However, the above core load pad (ACLP) responds to the core exit sodium temperature while the grid plate responds to the core inlet temperature. This causes non-uniform expansions, and the worth of each component must be weighted. From geometrical considerations, the split for PRISM is 65% from ACLP and 35% from grid plate, and this was utilized in both the BNL and GE calculations.

5.2.6 CEM Modeling

The GEM is essentially an empty assembly duct, sealed at the top, open at the bottom and connected to the high pressure in the inlet plenum of the core.

The range of operation of the GEMs tested in FFTF can be seen in Figure 5. A hexagonal cross section duct, with a wall thickness slightly greater than the standard fuel and blanket duct, forms the unit. When the pumps are at full flow, the plenum pressure (minus the static head to the GEM level) compresses the gas in the GEM cavity to the portion of the GEMs above the core. This causes more neutrons to be scattered and deflected back into the core, as compared to when the gas is adjacent to the core. When the flow decreases, the trapped helium expands and drops the sodium level into the core region. As a result, fewer neutrons are scattered back into the core region. The effect increases as the gas expands into the core, until the gas-liquid interface drops below the core. At this point the maximum negative reactivity of 69 cents (i.e., 23 cents each) is imposed. This device offers a passive negative feedback which can protect the power-to-flow ratio during sudden loss of flow events.

In SSC, three equations are solved iteratively until they converge to give the correct sodium level in the GEMs. They are

$$Vt = V_\ell + Vg \tag{2}$$

$$Pg = \rho * h\ell * Pci \tag{3}$$

$$Pg * Vg = Mg * R * T \tag{4}$$

where

Vt	=	total GEM volume	(m**3)
V_ℓ	=	GEM sodium volume	(m**3)
Vg	=	GEM gas volume	(m**3)
Pg	=	GEM gas pressure	(Pa)
Pci	=	Core Inlet Plenum pressure	(Pa)
ρ	=	sodium density	(kg/m**3)
g	=	gravity	(m/s**2)
A	=	GEM area	(m**2)
h_ℓ	=	sodium level in GEM	(m)
Mg	=	Mass of Helium in GEM	(kg)
R	=	helium gas constant	(-)
T	=	GEM gas temperature	(K)

The gas temperature closely follows the GEM shell temperature which is determined by tracking the heat transfer between the neighboring assemblies and the GEM

$$Cp * Mg * dT/dt = Q \tag{5}$$

where Cp = GEM helium specific heat (J/kg*K)
Q = heat from conduction from surrounding fuel assemblies (watts),
t = time (s)

These equations are solved at each time step to determine the sodium level in the core. The worth of the GEMs when the level is equal to, or greater than, the top of the core is zero. When the level reaches bottom of the core, the GEMs are worth -69 cents. Intermediate levels are interpolated.

6. ANALYSIS OF UNSCRAMMED EVENTS

The transient response of the PRISM module to various unscrammed events was evaluated using SSC, and complemented using MINET calculations when necessary. SSC has been benchmarked against both ARIES (G.E.) and SASSYS (ANL) (Ref. 6) over the years, and has consistently generated similar results for similar events. The calculations contained in this section used models that were more conservative than those used by the vendor.

Three unscrammed (beyond design base accidents) events are covered in this section. They are the unscrammed loss of heat sink (ULOHS), loss of flow (ULOF), and the transient overpower (UTOP) event. This set of transients is not all inclusive, but it does demonstrate the passive shutdown response of the current PRISM design.

6.1 Unscrammed ULOHS

This event is initiated by a sudden stoppage of the intermediate loop flow. Physically, this would be equivalent to the intermediate loop sodium being dumped into the system dump tank during a sodium-water reaction event. All heat generated after that event is retained in the reactor module. The reactor scram system is also assumed to fail, while the rest of the system continues to function. The initial operating conditions for PRISM, and the corresponding initial conditions from SSC are shown in Table 2.

Table 2
Table of Initial and Key Operating Parameters

Description	PRISM	SSC
Power (MW_t)	471	471
Cover Gas (kPa)	99.3	99.3
Primary Flow (kg/s)	2513	2507
Primary Sodium Inlet (K)	610.9	610.9
Primary Sodium Outlet (K)	758.1	758.0
Core Height (m)	1.342	1.3462
Peak Fuel Pin ..erage Fuel Pin	1.31	1.31
Fuel Pin OD (	.00668	.00668
Driver Fuel ...s/Assembly	331	331
Intermediate Sodium Flow (kg/s)	2293	2275
Intermediate Sodium IHX Inlet (K)	555.4	557.0
Intermediate Sodium IHX Outlet (K)	716.5	720.0

The system remains at rated power for many seconds. The slow increase of core inlet sodium temperature, due to the large thermal mass in the cold pool, is shown in Figure 6. The figure also indicates that the power begins to transition downward once the core inlet temperatures increase significantly. The core outlet temperature does not pass through the same temperature increment as the inlet because the core power is decreasing.

The increase in the core inlet temperature had a dramatic effect on the neutronic feedbacks as shown in Figures 7 and 8. The total reactivity remained constant (at zero) until the higher temperature sodium entered the core. A negative feedback then resulted from the thermal expansion of the fuel (axial), the core radius, and control rod drive line. Those effects were only slightly countered by the positive sodium density effect. It should be noted that the control rod drive line's negative reactivity worth was reduced after 200 seconds by the thermal expansion of the reactor vessel, which pulls the control rods from the core (Figure 8). The net effect is that the increase in core temperature generated a negative reactivity response, which reduced the power to decay heat levels by 500s.

A representative temperature profile for a peak node in the hot channel is shown in Figure 9. The temperature decrease after 75s is representative of all the mid-core fuel temperatures. Some of the fuel centerline temperatures below the core mid-line increased because of the higher inlet sodium temperatures, but these locations do not contain the limiting fuel temperatures. The ability of the reactor to transition to a lower power level removes the concern of fuel failure for this event. Figure 10 shows the margin to sodium saturation is about 560K.

Thus, the ULOHS event does not present a significant challenge to the PRISM passive shutdown response. The peak fuel temperatures decrease; thus there is no concern for fuel damage for the calculated event. The only issue might be the length of time this transient is allowed to continue and the impact on service limits. A remaining safety issue is the tendency of the vessel to expand and pull the control rods out of the core (to the rod stop position) which reduces the negative worth and can even insert positive reactivity. However, the ultimate shutdown system could be activated to establish shutdown, and would preclude prolonged unscrammed events.

6.2 ULOF Events

The loss of flow event is assumed initiated by a trip and coast down of the EM pumps from full power (Table 2). It is further assumed that the secondary loop continues to operate and the scram signal fails to insert the rods. This event was the most challenging for the previous design, which did not include GEMs. Since GEM reliability is still an issue, we analyzed this event for a ULOF with and without GEMs.

6.2.1 ULOF with GEMs

The trip and coast down of the pumps results in a power reduction almost immediately (Figure 11). Figure 12 shows that the core outlet temperature peaks

at about 50K above operational and drops to below 700K by 300s. Power deceases and reduces the peak fuel temperature (Figure 13). Consequently, no fuel damage would be expected.

The various reactivity feedbacks are shown in Figures 14 through 16. The total reactivity was predicted to quickly drop to -40¢, then slowly back off to -15¢ by 600s. The grid plate and ACLP in Figure 14 are the components of the radial expansion term on Figure 15. The grid plate is in contact with the inlet sodium, which experiences little change in temperature, while the ACLP above the core sees a reduction in core exit temperatures. This causes a contraction and insertion of positive reactivity. The core cool down causes a contraction from the fuel (axial expansion), sodium density (this is a negative effect), and the control drive line. These effects, except for the sodium density, are all positive reactivity feedbacks. The dominant negative feedback is the GEMs, which reduces the power in proportion to the core inlet plenum pressure and overrides the positive reactivity feedback from the thermal contractions. Thus, the overwhelming negative feedback from the GEMs causes the core power to decrease to decay heat levels by 500s. The fact here is that the reactor power level is reduced by the GEMs, rather than a balance established between the thermal expansion (or contraction) feedbacks of the core. Consequently, the GEMs function more like passive control rods, with the reactivity worth dependent on the core inlet pressure for this event. Finally, Figure 17 shows the margin to sodium boiling to be approximately 300K with the GEMs.

6.2.2 ULOF Without GEMs

This event was analyzed identically to the ULOF with GEMs, except for the removal of the GEMs from the modeling. From Figures 11 and 12, it can be seen that the power and core outlet temperature are higher than the previous case. The power level drops to about 10% of the initial power level by 600s, which results in the core outlet temperature being about 100K above the case with GEMs.

The neutronic feedback behavior for the case without GEMs is quite different, as shown in Figures 18 through 20. Without the GEMs, there isn't a large dominant negative feedback. Actually, the increase in temperature in this event generates the transition to a lower power by establishing a new reactivity balance between the thermally activated feedbacks. Heating up the sodium flowing in the core generates a negative feedback from radial expansion (i.e., ACLP), axial expansion, and control rod drive line thermal expansion. The Doppler term is initially negative since the core average temperature of the fuel increases, but as the power declines, the average fuel temperature decreases and turns positive. The increase in the sodium temperatures contributes a positive response. However, the feedbacks all combine to produce a net negative feedback which reduces the core power to 10% by 600s.

The difference between the two cases with and without GEMs can be judged in terms of the peak fuel and sodium temperature. As shown in Figure 21, the peak fuel temperature was predicted to be 1150K which is higher than before, but still lower than the solidus temperature of the fuel, which is 1249K. As shown

in Figure 17, the peak sodium temperature in the core came within 160K of the saturation temperature, which remains a significant margin.

6.2.3 ULOF Conclusion

The SSC predictions indicate PRISM would be able to withstand the ULOF events with and without the GEMs. When available, the GEMs dominate the neutronic feedbacks and bring the power down to decay heat levels within 500s, with a margin to sodium boiling of 300K. The fuel temperatures decrease demonstrates that fuel damage is not a significant risk for this event. For the case without the GEMs, SSC predicted that the thermal expansion feedbacks would be activated and combine to reduce power to 10% rated by 600s. The fuel temperatures for the case without GEMs do not indicate significant damage, but the margin to sodium boiling is reduced to 160K. Without the GEMs, however, there could be a small amount of cladding wastage during this event.

6.3 UTOP

An unprotected transient over power (UTOP) accident results when positive reactivity is inadvertently inserted into the core, leading to increased reactor power. The scram signal is assumed to fail to insert the rods. The limiting case is the accidental withdrawal of all of the control rods. This event is bounded by the excess amount of reactivity in the core. In an oxide core, the temperature and power defect, along with the built in excess reactivity for the burnup swing, can amount to several dollars. This makes the event very severe. In the metal fuel core of PRISM, a small temperature and power defect (~$1.2) and negligible burnup swing (~$0.04), and the excess reactivity to account for a fuel axial growth with exposure, are the only excess reactivities built into the system. The amount of potential reactivity available for the insertion is reduced further by adding control rod stops, which reduce the available reactivity by limiting withdrawal distance. GE's current objective is for the rod stops to prevent the net rod insertion worth available for withdrawal from exceeding 40¢, which includes a 10¢ uncertainty allowance. The reference PRISM UTOP rate is 2¢/s (since it is the maximum control rod withdrawal speed to a total of 40¢).

6.3.1 Component Migration and the UTOP Event

Based on experimental data from EBR-II, it is clear that annular zones develop in the ternary metal fuel pins during burnup. Component migration changes the local thermal conductivity, solidus and liquidus temperatures, which impact the peak fuel temperatures and the margin to fuel melting. In addition, any plutonium migration could redistribute the power within the pin. The SSC calculations here used the most conservative estimation of the thermal conductivity, which included the effect of plutonium and zirconium migration, as well as a redistribution of power in the pellet. These calculations will be re-evaluated and revised as new ternary fuel data becomes available.

Starting from normal operating conditions (Table 2), a reactivity insertion of 2¢/s was continued for 20s, for a total of 40¢. It was further assumed that the scram system failed to insert the control rods, but that the rest of the

system (i.e., IHX, EM Pumps) continued to function. The power increase for this event would be limited in an oxide core by the Doppler effect. However, in PRISM's metal fuel core, the thermal expansion (negative) feedbacks must supplement the (small) Doppler feedback to terminate the power excursion.

The power is predicted to reach 1.8 times the rated level (Figure 19), and then falls back to about 1.2 times the rated power level. The core outlet peaks at about 880K, and drops to 840K after the new power level has been stabilized by the reactivity feedbacks.

The reactivity feedbacks of the system are shown in Figures 23 through 25. The total reactivity increases during the control rod withdrawal process. The components of the radial expansion term, shown in Figure 23, indicate that the ACLPs respond quickly to the increase in exit sodium temperature, while the grid plate reactivity is delayed until hotter sodium enters the core. The reactivity figures indicate that the increased temperatures resulting from the power increase activates the thermal expansion (negative) reactivities. This reverses the power increase and gradually reduces the power to 1.2 times the rated power level. The only positive feedback in the system was due to the decreased sodium density, which contributed less than 10¢ during the event.

The peak fuel temperatures at the hottest location can be seen in Figure 26. The fuel temperatures reaches 1400K, which is far above the solidus temperature for nominal fuel (i.e., ~1275K). Further, if we consider the migration of the zirconium and uranium components, the local solidus temperature could be as low as 1200K. Both the ARIES (GE) and SSC (BNL) calculations predicted some melting. The GE analysis predicted a small fraction of melting for a few seconds while the SSC results, reflecting reduced thermal conductivity due to component migration, predicted a significant fraction of the peak pin to melt. The degree and possible acceptability of local fuel melting during a postulated 40¢ UTOP is an open issue. Certainly G.E. has some options for reducing the size of potential UTOP initiators, e.g., by moving the control rod steps more frequently. However, the performance of the ternary metal fuel is not fully understood at this time, and the fuel developers at ANL are hopeful that further data will support their position regarding the acceptability of the 40¢ UTOP. The margin to sodium boiling (Figure 27) was predicted to be about 340K.

7.0 SUMMARY

The revised PRISM design has been evaluated using SSC for an unscrammed loss of heat sink (ULOHS), an unscrammed loss of flow (ULOF) with and without the Gas Expansion Modules (GEMs) functioning, and a 40¢ unscrammed transient overpower (UTOP) event. The feedback effects for U-27Pu-10Zr fuel were modeled. The ULOHS accident was predicted to be a benign event for the design, with the reactor power transitioning down to a decay heat level within 500s. The power during ULOF events, with the GEMs functioning, decreases to decay heat levels without causing fuel damage and leaving a 300K margin to sodium saturation. The case without the GEMs had a 160K margin to sodium saturation and higher fuel temperatures. The clad was predicted to quickly pass through the eutectic phase

(between fuel and clad), which would waste some clad. The 40¢ UTOP was predicted to raise the power to 1.8 times rated power initially, with the power later decreasing to 1.2 times rated power. SSC predicted some localized fuel melting for the event, but the significance of this localized damage has not yet been determined. If necessary, the vendor has options to reduce the maximum reactivity insertion below 40¢.

REFERENCES

Ref. 1 R. R. LANDRY, T. L. KING, and J. N. WILSON, Draft Preapplication Safety Evaluated Report for Power Reactor Inherently Safe Module Liquid Metal Reactor, Nuclear Regulatory Commission Report, NUREG-1368, September 1989.

Ref. 2 G. J. VAN TUYLE, G. C. SLOVIK, B. C. CHAN, R. J. KENNETT, H. S. CHENG, and P. G. KROEGER, Summary of Advanced LMR Evaluations - PRISM and SAFR, Brookhaven National Laboratory Report, NUREG/CR-5364, BNL-NUREG-52197, October 1989.

Ref. 3 G. L. GYOREY, D. R. PEDERSON, and S. ROSEN, Safety Aspects of the U.S. Advanced Liquid Metal Cooled Reactor Program, Proceedings of the 1990 International Fast Reactor Safety Meeting, Snowbird, Utah, August 12-16, 1990.

Ref. 4 J. G. GUPPY, et al., Super System Code (SSC, Rev. 0) An Advanced Thermohydraulic Simulation Code for Transients in LMRBRs, NUREG/CR-3169, BNL-NUREG-51659, April 1983.

Ref. 5 G. J. VAN TUYLE, T. C. NEPSEE, and J. G. GUPPY, "MINET Code Documentation", NUREG/CR-3668, BNL-NUREG-51742, Brookhaven National Laboratory, February 1984.

Ref. 6 F. E. DUNN, et al, "The SASSYS-1 LMFBR Systems Analysis Code", ANL/RAS 84-14, June 1984.

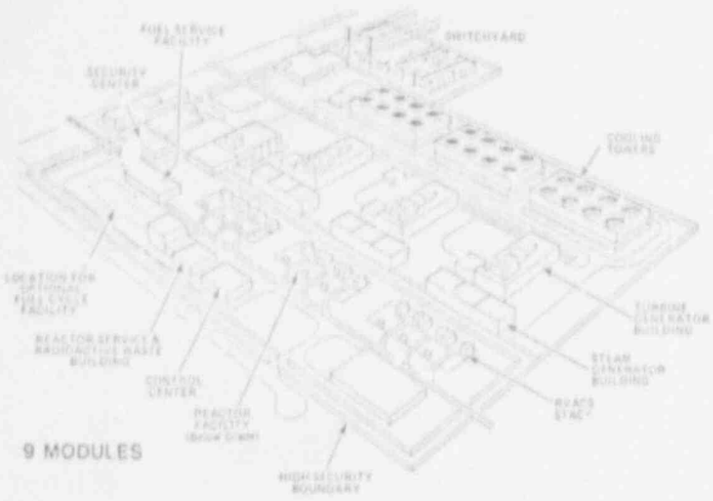

Figure 1. The 1395 MWe ALMR Power Plant With 3 Power Blocks

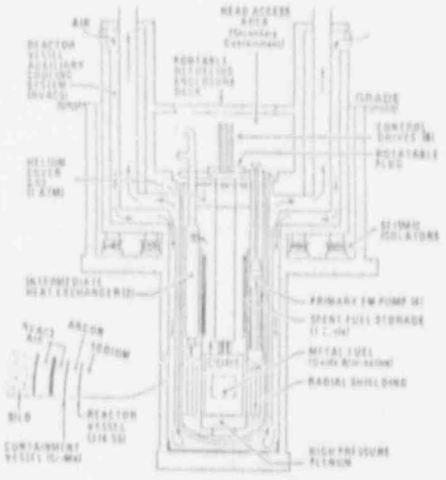

Figure 2. ALMR Reactor Module

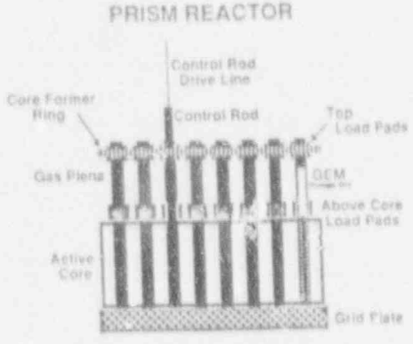

Figure 3. PRISM Core

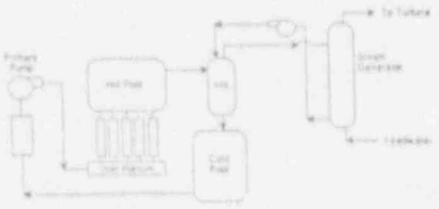

Figure 4. SSC Representation of LMR Systems

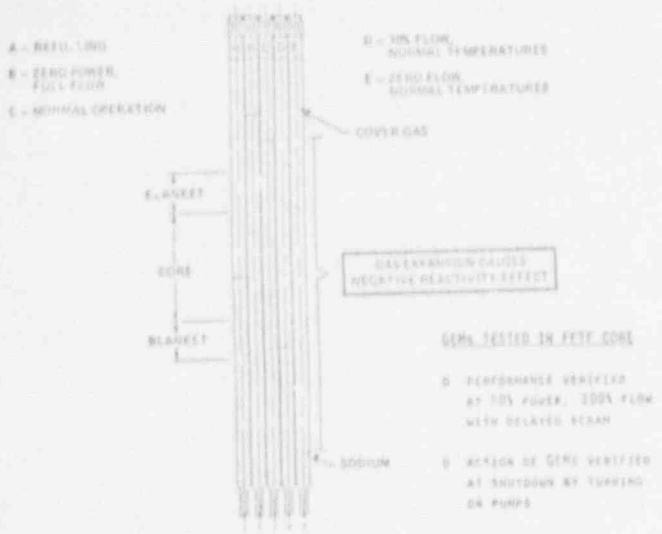

Figure 5. Operation of the Gas Expansion Module (GEM) Tested in FFTF (Which has a Similar Behavior in PRISM)

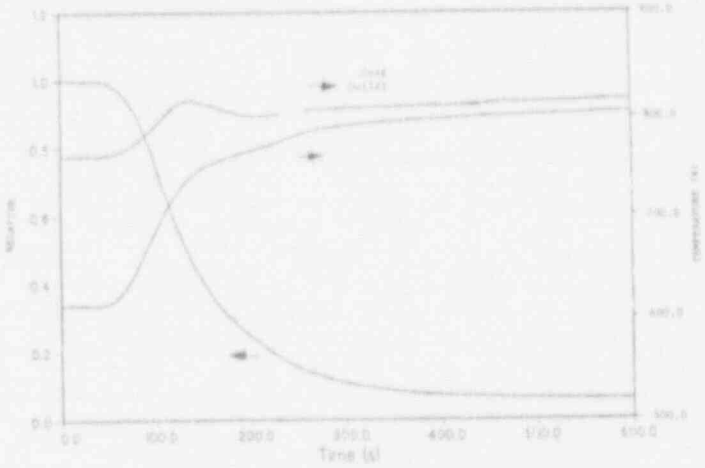

Figure 6. Predicted Core Outlet and Inlet Temperature Along with the Relative Power from SSC for ULOHS

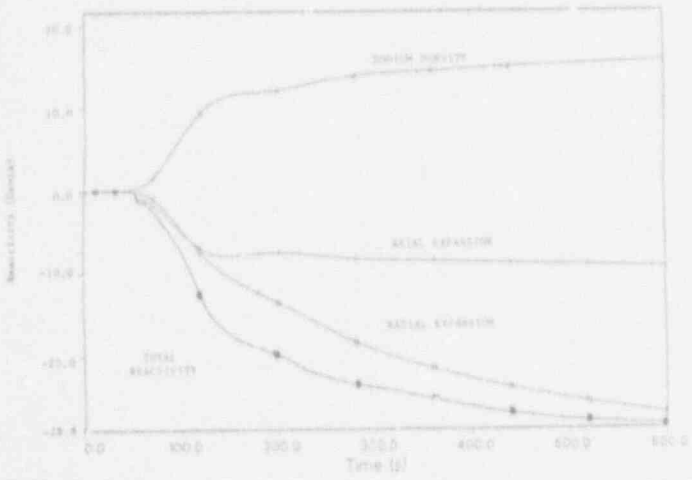

Figure 7. Predicted Neutronic Feedback from SSC for a ULOHS

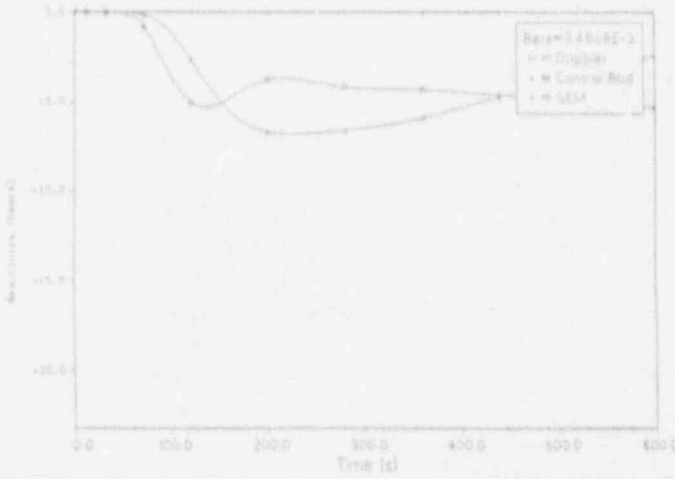

Figure 8. Predicted Doppler, Control Rod Expansion, and GEM Reactivity Feedback from SSC for a ULOHS

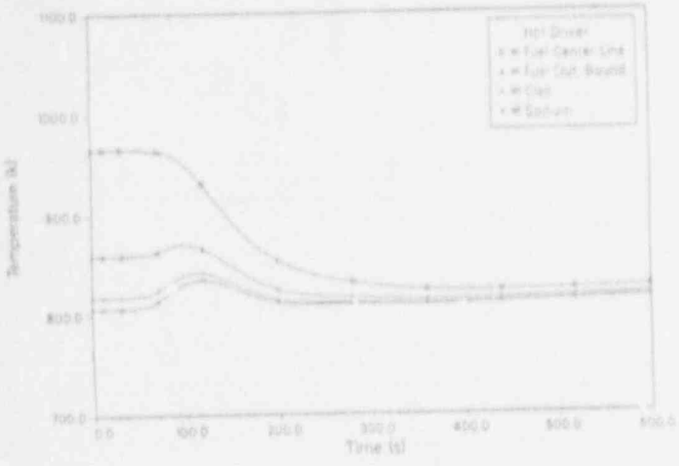

Figure 9. Predicted Fuel Temperature Distribution from SSC for the TOP Node (i.e., 1.346 m - 1.122 m) for a ULOHS

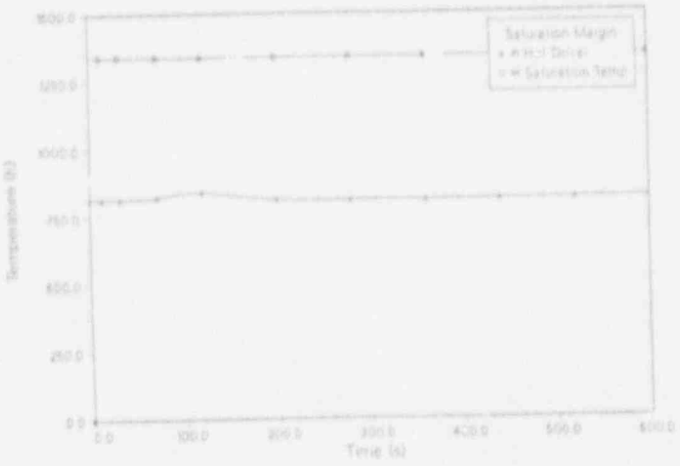

Figure 10. Predicted Margin to sodium Saturation from SSC for a ULOHS

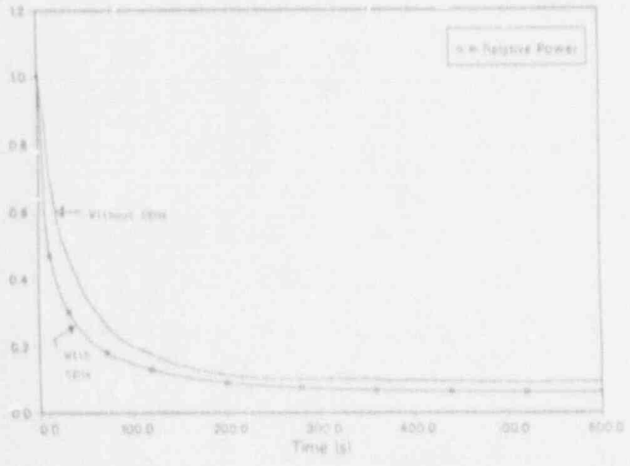

Figure 11. Predicted Relative Power from SSC for a ULOF With and Without GEMs

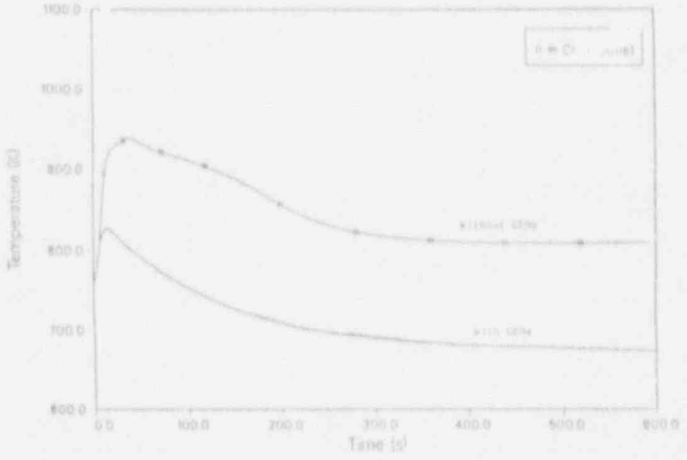

Figure 12. Average Core Outlet Temperature from SSC for a ULOF With and Without GEMS

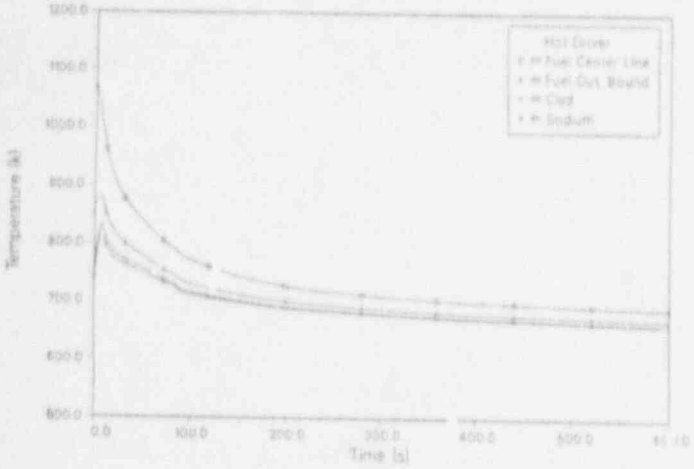

Figure 13. Predicted Fuel Temperature Distribution from SSC for the Third Node from the Top (i.e., 0.897 m - 0.673 m) for a ULOF with GEMs

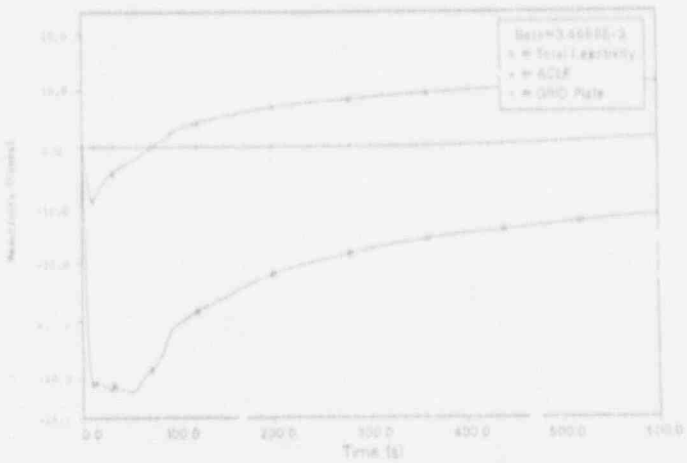

Figure 14. Predicted Total, ACLP, and GRID Plate Reactivity Feedback from SSC for a ULOF with GEMs

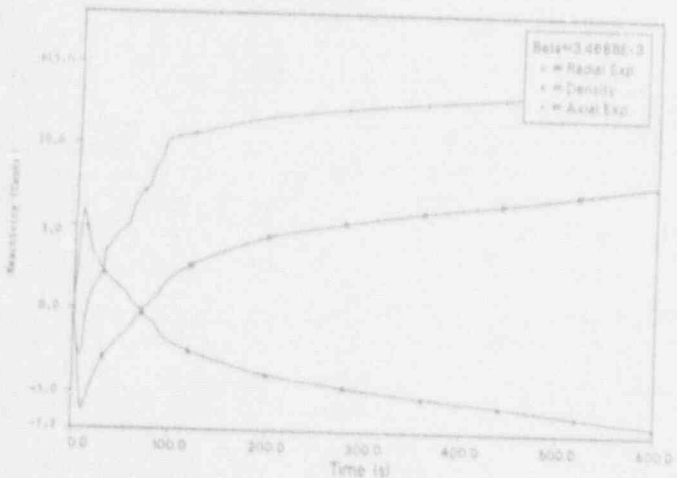

Figure 15. Predicted Radial Expansion, Sodium Density, and Axial Expansion Reactivity Feedback from SSC for a ULOF with GEMs

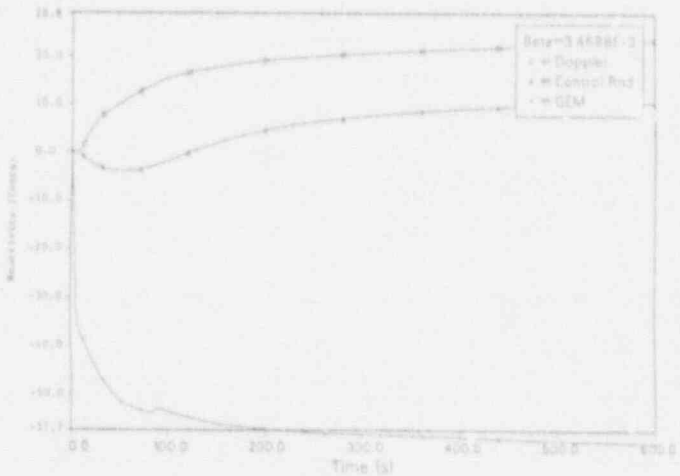

Figure 16. Predicted Doppler, Control Rod Expansion, and GEM Reactivity Feedback from SSC for a ULOF with GEMs

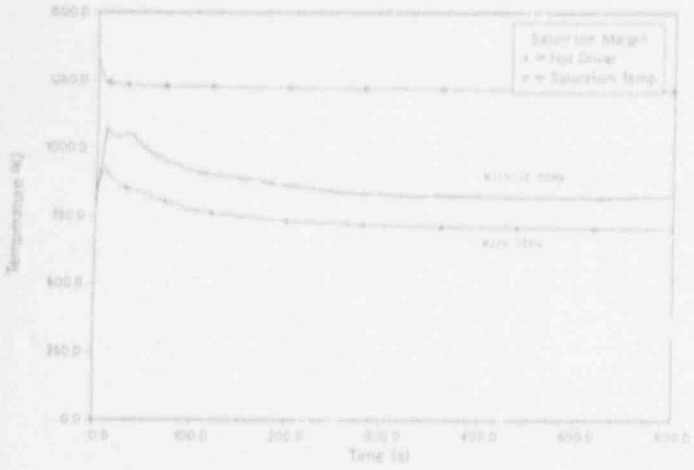

Figure 17. Predicted Margin to Sodium Saturation from SSC for a ULOF With and Without GEMs

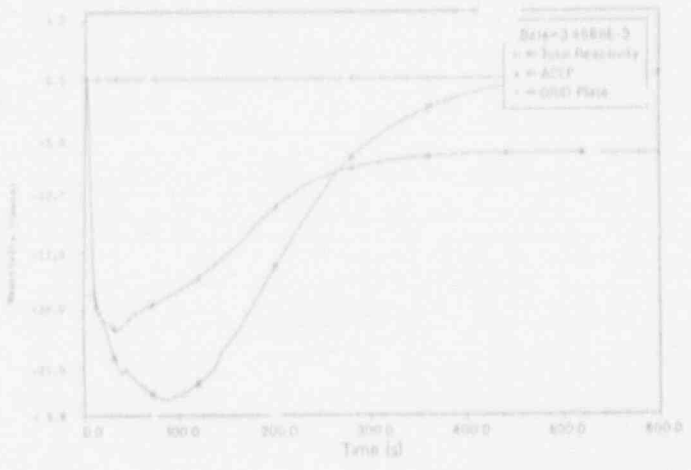

Figure 18. Predicted Total, ACLP, and GRID Plate Reactivity Feedback from SSC for a ULOF Without GEMS

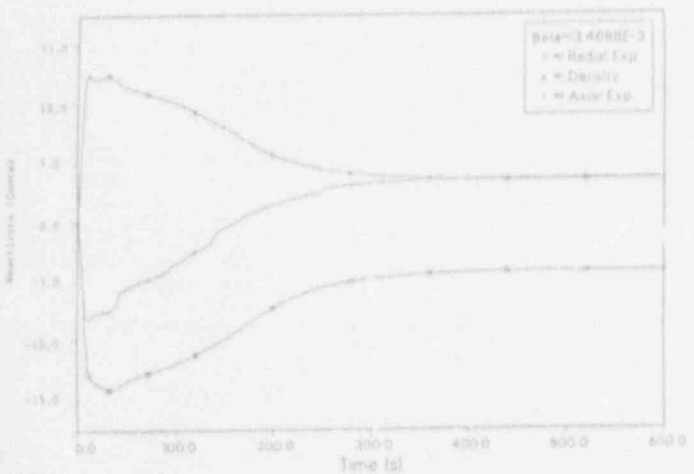

Figure 19. Predicted Radial expansion, Sodium Density, and Axial Expansion Reactivity Feedback from SSC for a ULOF Without GEMs

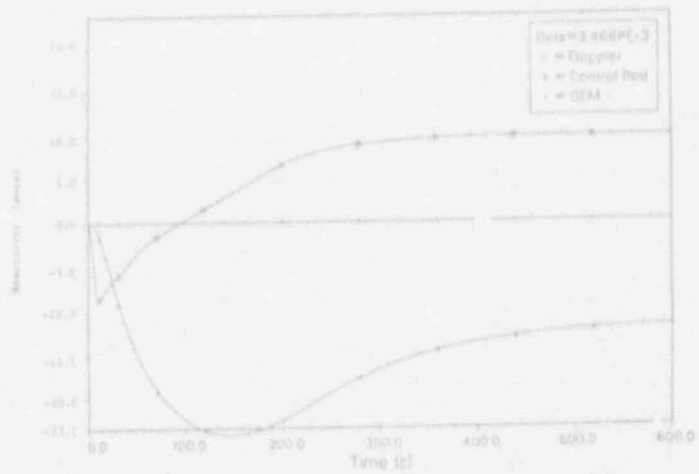

Figure 20. Predicted Doppler, Control Rod Drive Line Expansion, and GEM Reactivity Feedback from SSC for a ULOF Without GEMs

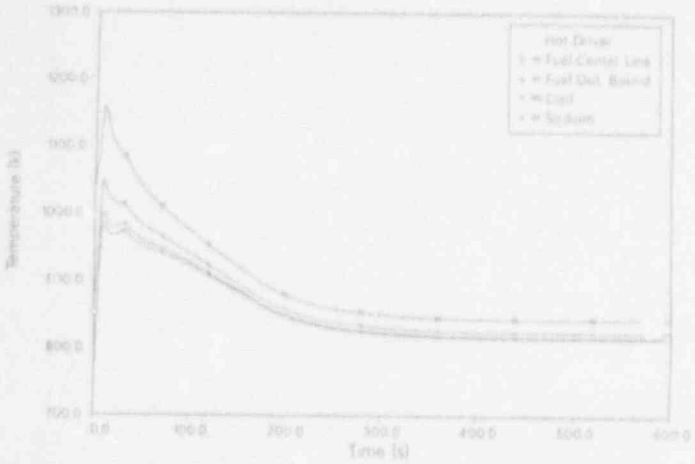

Figure 21. Predicted Fuel Temperature Distribution from SSC for the Second Node from the TOP (i.e., 1.122 m - 0.897 m) for a ULOF Without GEMs

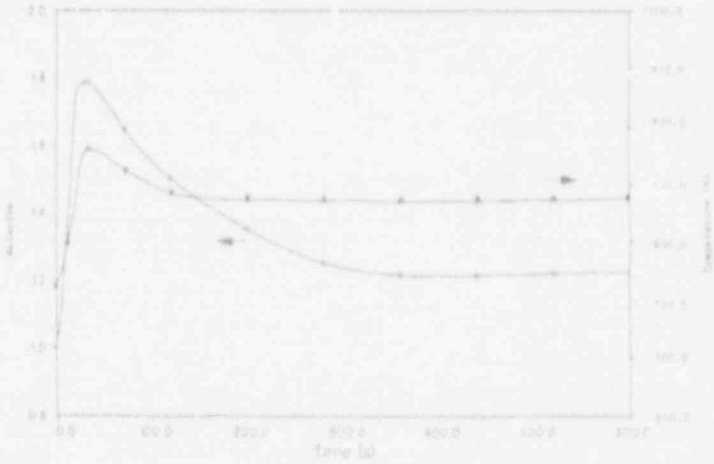

Figure 22. Relative Core Power and Average Core Outlet Temperature Predicted by SSC for PRISM During a 40 Cent UTOP

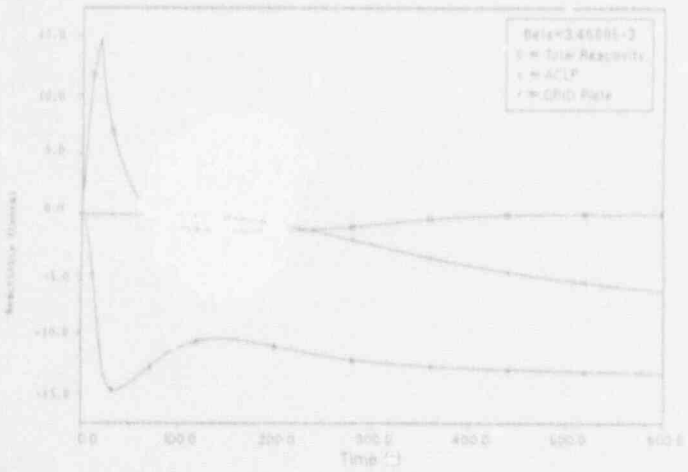

Figure 23. Predicted Total, Above Core Load Pad (ACLP) and Core Support Grid Plate Reactivity Feedback from SSC for a 40 Cent UTOP

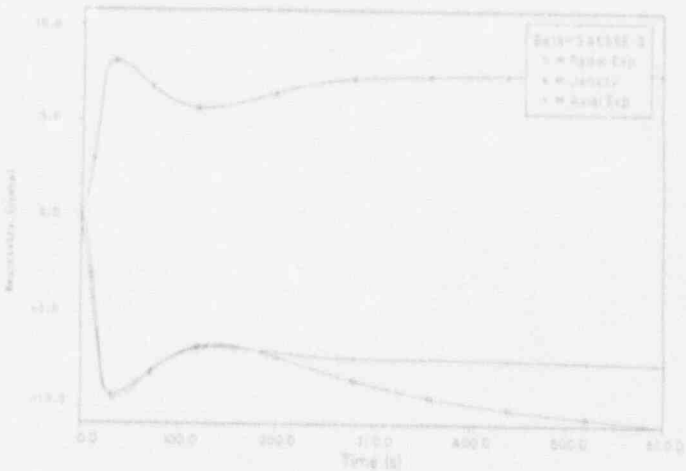

Figure 24. Predicted Radial Expansion, Sodium Density (Density), and Axial Expansion Reactivity Feedback from SSC for a 40 Cent UTOP

Figure 25. Predicted Doppler, Control Rod Expansion, and Gas Expansion Module (GEM) Reactivity Feedback from SSC for a 40 Cent UTOP

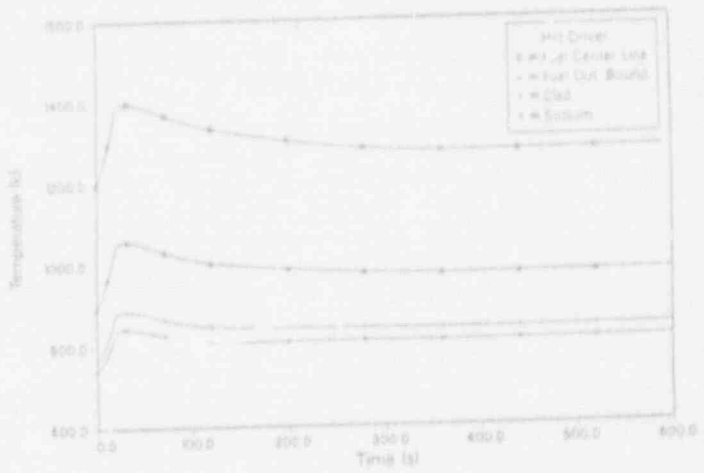

Figure 26. Predicted Fuel Temperature Distribution from SSC for the Third Node from the Top (i.e., 0.897 m - .673 m) During a 40 Cent UTOP

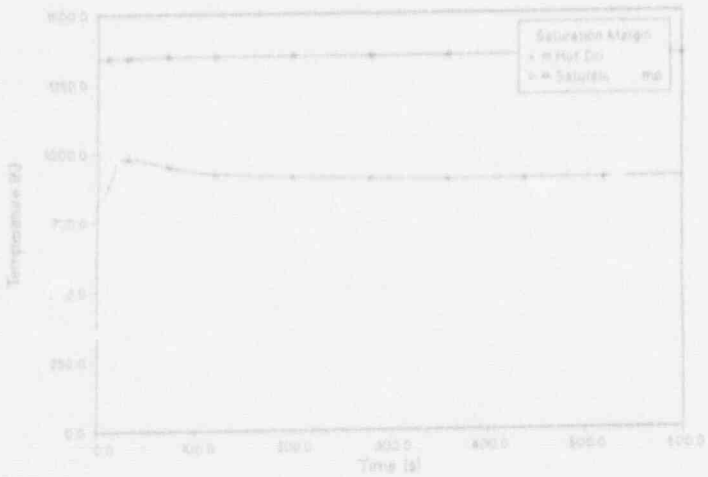

Figure 27. Predicted Sodium Saturation Margin from SSC for the 40 Cent UTOP

Accident Simulation and Consequence Analysis in Support of MHTGR Safety Evaluations

S. J. Ball, R. P Wichner, O. L. Smith, J. C. Conklin
Oak Ridge National Laboratory
Oak Ridge, Tennessee 37831-6010

W. P. Barthold
Barthold Associates, Inc.

ABSTRACT

This paper summarizes research performed at Oak Ridge National Laboratory (ORNL) to assist the Nuclear Regulatory Commission (NRC) in preliminary determinations of licensability of the U. S. Department of Energy (DOE) reference design of a standard modular high-temperature gas-cooled reactor (MHTGR)[1]. The work described includes independent analyses of core heatup and steam ingress accidents, and the reviews and analyses of fuel performance and fission product transport technology.

Reactor Description

The MHTGR consists of four tall cylindrical ceramic core reactor modules each with a thermal power rating of 350 MW and a single once-through steam generator with a superheater to provide high-temperature (538°C, 1000°F) steam (Fig. 1). High-pressure helium is driven downward through the annular core cooling channels by the single motor-driven main circulator. A smaller-capacity circulator/heat exchanger loop, the shutdown cooling system (SCS), is located within the steel reactor vessel. In cases for which neither the main nor the SCS loop is available, afterheat is removed by a passive, safety-grade air-cooled reactor cavity cooling system (RCCS) surrounding the reactor vessel. The RCCS is in operation at all times and does not require operator or automatic actuation in the event of an accident. Instead of a conventional sealed containment building, there is a "tight" reactor building with contamination control. The overall "containment" design is centered on the multiple silicon carbide and pyrolytic carbon coatings on the microscopic fuel kernels, which together with the primary pressure boundary, are considered to be a sufficient containment barrier.

Core Heatup Accident Analyses

The ORNL MORECA code[2] was developed to study core heatup accident scenarios, and thus includes detailed thermohydraulic models for the core, vessel, SCS, and RCCS, with the recent addition of core point kinetics. The steam generator and balance of plant are currently not modeled.

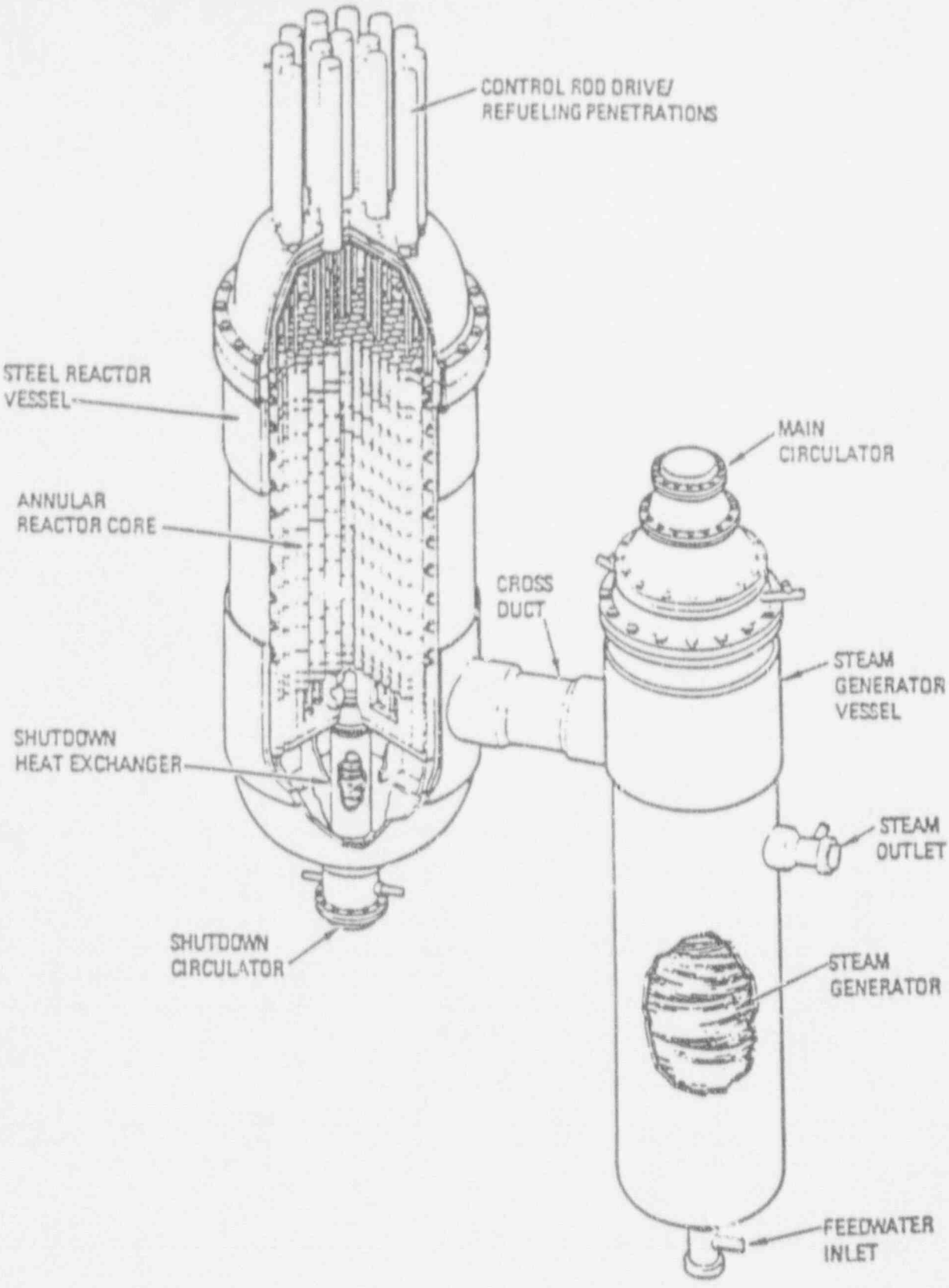

Fig. 1. The 350-MW(t) modular high-temperature gas-cooled reactor module. Source: U.S. Department of Energy, Licensing Plan for the Standard MHTGR, HTGR-85-001, Rev. 3, 1986 (this document is classified as "Applied Technology" and is not in the public domain; requests for this document should be made through the U.S. Department of Energy, Washington, D.C.).

Model Description The 3-D core model uses one node each for the 66 fuel and 139 reflector elements in each of 14 axial regions. The core representation (205 X 14 = 2870 nodes) allows for detailed investigations of azimuthal temperature asymmetries in addition to axial and radial profiles. Variable core thermal properties are computed functions of temperature, orientation, and radiation damage.

The primary coolant flow models cover the full ranges expected in both normal operation and accidents, including pressurized and depressurized (and in between), for forced and natural circulation, upflow and downflow, and for turbulent, laminar, and transition flow regimes. The primary loop pressure calculation considers variable inventory (due to depressurization actions) and loop temperature changes, with a simplified model of the steam generator cavity gas temperatures.

MORECA code capabilities have been expanded to include anticipated transients without scram (ATWS) events. Using the ATWS option, a scram does not to occur, as would be expected, at the time of a loss of forced circulation (LOFC), but instead is assumed to occur at an arbitrary time later (or not at all). The model for fuel (as distinct from moderator) temperature is a rough approximation valid only for slow transients characteristic of LOFCs. The point kinetics approximation for the neutronics is a prompt-jump, single-precursor group model which has been compared, for transients of the appropriate rate and magnitude, against calculations using a model with prompt generation time and six precursor groups. Temperature-reactivity feedback from the 3-D modeling of fuel, moderator, and reflectors utilizes nuclear importance weighting. Models for xenon and samarium poisoning are included.

Workstation Version With the workstation version of MORECA, it is possible for the operator/analyst to have direct on-line involvement with the postulated accident scenarios. Long-term LOFC accidents are simulated both with and without total or partial depressurization of the primary coolant. Wide varieties of LOFC accidents are studied interactively, including long-term core heatup scenarios for which active cooling systems are either unavailable or available only intermittently in degraded states.

The workstation display screen (Fig. 2) presents a summary status of the simulation for the RCCS, vessel, core, and SCS. Along the bottom of the screen are the "buttons" (accessed by a mouse) allowing operator intervention, including control of the simulation speed, control of the SCS operating parameters, allowance for "degrading" the effectiveness of the RCCS, and control of total or partial depressurization transients. The maximum vessel and core temperatures are displayed at elevations corresponding to their location in the core. This display feature is expected to be useful for review and confirmation studies of the safety system design, operator emergency procedures, operator training procedures, and post-accident monitoring systems. Because computations are fast (up to 2100 times faster than real time on a Sun SPARC station-2 for non-ATWS transients), sensitivity studies can be run readily.

Analysis Results The analyses show fuel temperatures closely approaching or slightly exceeding the nominal failure onset limit (1600°C) or for some ATWS cases and for some of those in which the RCCS is assumed to fail catastrophically. For certain LOFC scenarios, predicted maximum vessel temperatures exceed slightly the extended ASME pressure vessel code's upper temperature limits. All of the transients are characterized by very slow heatups due to the small power densities and large heat capacities associated with the core materials. In reference case calculations of the depressurized LOFC, maximum fuel temperatures are reached in 4-5 days. Pressurized LOFC maximum fuel temperatures are typically lower, with the peaks occurring after 3-4 days.

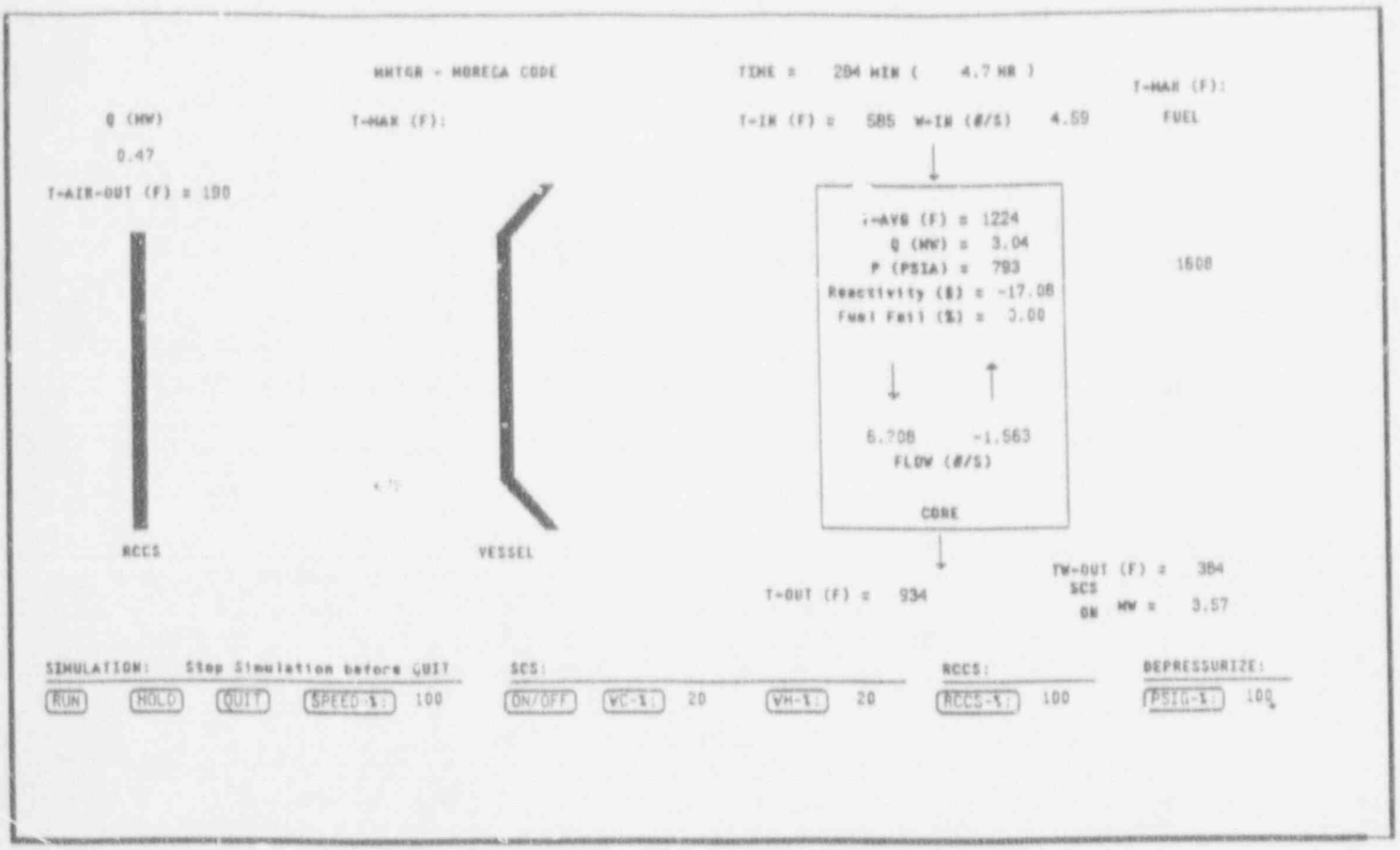

Fig. 2. MORECA Interactive workstation version accident scenario display screen.

For an LOFC event accompanied by an ATWS and with no operator action, recriticallity following xenon poisoning decay may occur after about 40 hours. Depending on the scenario, with no corrective actions taken, some fuel damage would be predicted after 3-4 days. Several of the operator interaction scenarios were found to be of particular interest. For example, it was found that in certain later stages of ATWS-LOFCs, operator use of a degraded SCS for core cooldown could actually cause significant increases in maximum fuel temperature. This is due to the fact that the additional core cooling, which causes an increase in reactivity (and power), does not cool the hotter parts of the core in proportion to the power increase.

Reactivity Consequences and Fission Product Release Resulting from Accidental Moisture Ingress into the MHTGR Core

Preliminary safety analyses of MHTGRs have identified the accidental admission of secondary-side steam (and/or water) into the primary circuit as a potentially serious event. Problems arise from (1) the resulting positive reactivity insertion, and (2) the hydrolytic enhancement of fission product release from flawed coated fuel particles. This section describes the development and application of two preliminary mathematical simulations which treat the neutronics, thermohydraulics, and certain physical chemistry processes believed to be important in such accidents. A neutronics, thermohydraulics and control system submodel of the primary system permits moisture ingress to be coupled with reactivity and control feedback effects, and a physical chemistry submodel characterizes processes contributing to the release of fission gases into the primary system.

The purpose of this research is to perform scoping studies of postulated accident scenarios, and to determine the relative importance of design features, mitigating actions, model assumptions, and parameter values to the severity of the predicted results. Insights gained from these studies provide guidance on regulatory technology development needs.

Thermohydraulics Submodel The thermohydraulics moisture ingress submodel treats processes which are inherently very complex and for which comprehensive models and data are not available. Hence engineering judgments were made in developing the submodel such that reasonably-well-known processes were modeled from first principles, while other less-tractable phenomena were treated parametrically. For example, sensitivity analyses were used to determine the importance of parameters treating steam injection into and subsequent transport around the primary system, which is complicated by such factors as condensation on surfaces at temperatures below saturation. Factors affecting the entrainment and redistribution of condensate, the unrated and uncertain ability of the circulator to pump steam, the damaging effects of steam or a steam-water mixture on the safety relief valves, and the heat transfer coefficient of the helium-steam mixture were also studied parametrically. The resulting submodel is a fast and efficient analytical tool that avoids the long setup and running times characteristic of conventional broad-spectrum hydraulics codes. A fully implicit finite difference scheme is used to solve the model equations, which circumvents the common stiffness problem of coupled neutronics and thermodynamics systems.

The thermohydraulics submodel was run to reproduce two transients from an independent analytical model reported in the literature[3]. In the first of these the power level was ramped back to approximately 20% in one minute by reducing feedwater flow, with the reactor tracking. In the second test the helium flow rate was reduced to 50% and then restored to full flow over a period of three minutes. The results of both of these transients compare well with their counterparts in the literature.

Applications of the model to date treat main-steam ingress via steam generator tube ruptures with normal controls either operating or failed, and with primary safety relief valves operating or failed open.

Sensitivity studies investigating ranges of possible operational actions included events with reactor and/or feedwater pump trips, variations in steam generator isolation and dump times, and tube breaks occurring in different parts of the steam generator. Initial studies suggest that even for catastrophic postulated breaks (five steam generator tubes), ingress rates and steam accumulation in the primary system is relatively slow, requiring typically 10 minutes to reach maximum vapor densities of approximately 1 lb/ft^3 (Fig. 3). This result is encouraging in that there appears to be time for appropriate operator actions such as trips and isolation of the steam generator in case automatic trips fail. In previous scoping studies, displacement of the helium in the primary system was not accounted for, leading to fast steam density buildups and subsequently to very large power excursions. Here the excursions were found to be comparatively mild, typically with a maximum power increase of less than 50% (without scram). Steam ingress rates and magnitudes are dominated by major system features such as break size in comparison with safety relief valve capacity and reliability.

Physical Chemistry Submodel In the physical chemistry submodel, the time-delay of steam and fission product diffusion through the core structural graphite is treated in one-dimensional spatial resolution (Fig. 4). This representation is based on the standard equivalent cylindrical cell for the MHTGR geometry. The cell is approximately 1.4 cm in diameter with a central fuel zone surrounded by a graphite annulus and then an outer coolant annulus. Steam density in the coolant channel is a time-dependent boundary condition (eventually to be provided by the thermohydraulics submodel). Transport of steam through graphite is modeled by considering adsorption of steam on pore surfaces and oxidation of the graphite.

Multi-component diffusion theory treats the interactive effects of helium, hydrogen, carbon monoxide, steam and fission product gases. Upon reaching fuel compacts, the steam causes hydrolytic reactions with exposed fuel kernels. Production, decay and transport of krypton and xenon isotopes are simulated, as well as the production, sorption, and decay of iodine to xenon. Released gaseous fission products are transported through the graphite web to the coolant channels by back-diffusion, and then may escape through safety relief valves if primary system overpressure has occurred. It is recognized that important processes involving non-gaseous fission products are yet to be characterized and added to the model.

Initial validation activities for the physical chemistry submodel include comparison of calculated gas diffusion coefficients with selected data. While no multicomponent data have been found for MHTGR gas mixtures of interest, good agreement between model and experiment in some special cases lend credibility to the multicomponent formulation.

Applications of the physical chemistry submodel include analysis of the sensitivity of fission gas release to three key parameters in the model: (a) steam adsorption in the graphite, (b) magnitude of fuel hydrolysis, and (c) the diffusion coefficients. Results to date indicate fission gas release rates to the coolant channel to be very sensitive to the level of hydrolysis and comparatively insensitive to steam adsorption on graphite and the diffusion coefficients.

Fuel Reliability Study

A review of MHTGR fuel is currently in progress, motivated principally by the recommendation of the DOE designers to substitute a tight reactor building for the conventional, sealed containment

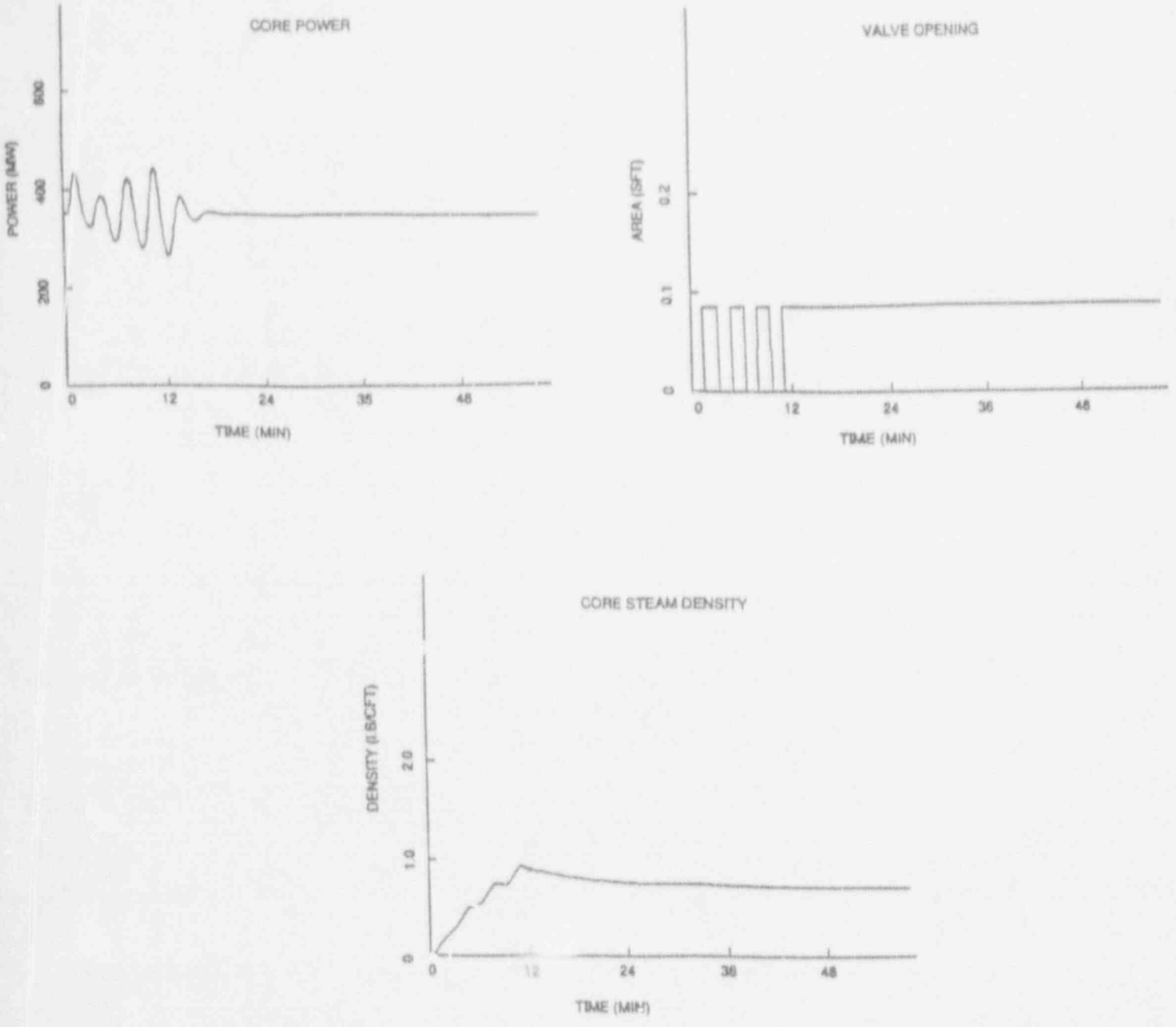

Fig. 3. Steam ingress with normal controls operating but all safety actions defeated plus relief valves fail open

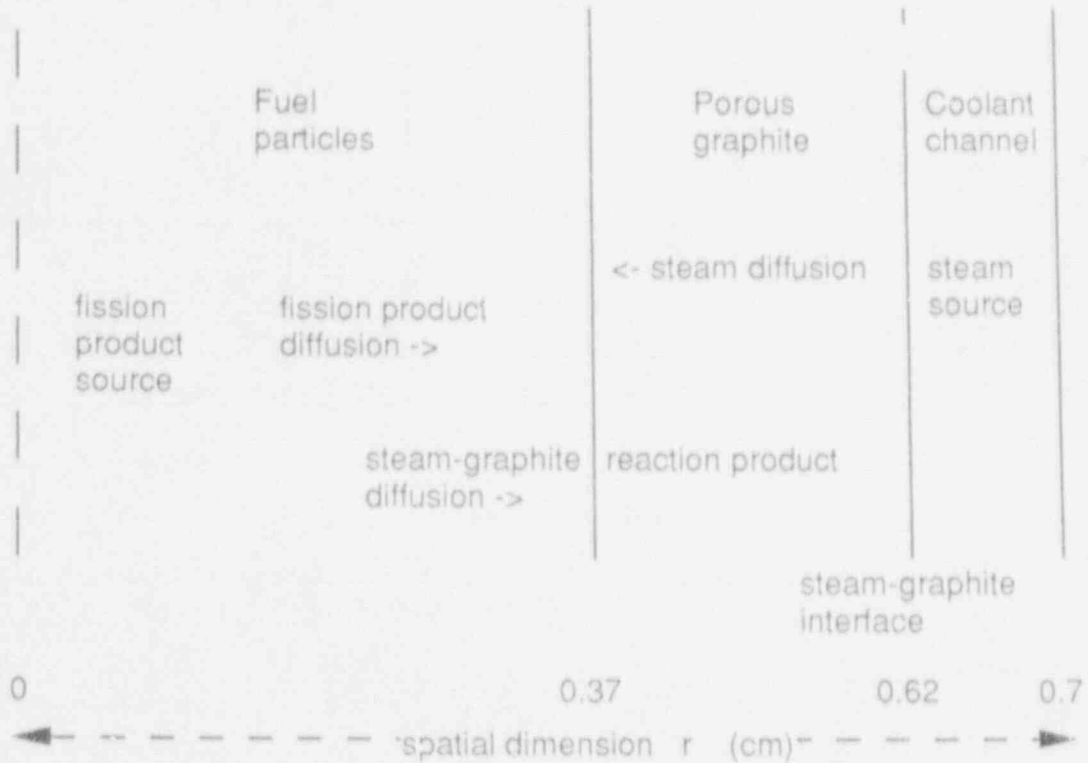

Fig. 4. Equivalent cell used for modeling fission product release to coolant. (Width of coolant zone not drawn to scale.)

vessel. Conventional LWR designs rely primarily on the fuel cladding, pressure vessel, plus the sealed containment building as barriers to fission product release. The MHTGR approach capitalizes on the strength and integrity of the ceramic fuel coatings as the primary barrier with the primary system steel vessels as the secondary barriers. In the process, one traditional containment barrier is replaced, so there is added dependence on the fission product barriers within the fuel particles.

Fuel "reliability" is here defined as behavior in accord with model predictions in both normal service and under accident conditions. When applied to accident consequence estimates, the current behavioral models indicate that reactor safety goals can be met without the sealed containment. Moreover, the preliminary safety assessment in the draft Safety Evaluation Report (SER)[1] states that neither DOE or NRC contractors have identified accidents that would require the additional barrier of a sealed vessel. Also, extensive in-pile fuel tests, as well as both U.S. and foreign reactor operation experience, using fuel similar to the current selection, have all been used to support this assessment.

Nevertheless, several considerations encourage a conservative or cautious approach on the part of the NRC. It is noted that the current fuel design is relatively new, and while enhanced future performance is promised, no extensive testing record exists at this time. The existing fuel behavior models are based on older designs, principally the high quality fuel produced in Germany for the AVR and THTR HTGRs. In addition, a prototype fabrication facility for the selected fuel design does not currently exist. Bench scale facilities were used to fabricate the fuel for the limited testing conducted thus far.

The "Weak Fuel" Concept Therefore, as an expression of caution, the NRC has adopted a concept termed "weak fuel" to explore the effect of miscalculation regarding the degree of fuel integrity. The "weak fuel" concept is a penalty placed on consequence estimates in which a poorer fuel response is assumed than is predicted by the behavioral models. The concept is currently being applied, on an interim basis, to MHTGR concepts which do not employ a sealed containment vessel.

MHTGR Fuel Reliability Fuel reliability depends on (a) proper fuel design to satisfy performance specifications, (b) fabrication and process control techniques which accurately produce the design, (c) well constructed QA and QC procedures and, (d) behavior of the product in service that is in accord with expectations. Hence, evaluation of fuel reliability must cover these areas.

Fuel Fabrication Lab-scale MHTGR-quality coated fuel particle fabrication has been demonstrated overseas. The German company HOBEG has fabricated MHTGR-quality fuel particles that were irradiated followed by heatup tests and this fuel performed as expected. However, at this time, (1) no U.S.-made MHTGR-quality UCO fuel has been fabricated in more than capsule test quantities and (2) this fuel has not been irradiated under prototypical conditions. The performance of MHTGR fuel is inferred from earlier U.S.-made UC_2 fuel and German-made, mostly UO_2 fuel.

The fabrication process for coated particle fuel is highly complex. Temperature, pressure, gas composition and flow rates, coating rates and raw product compositions have an impact on the fuel product attributes and need to be tightly controlled in the fabrication process. The process parameters affect the geometry of the fuel particle, the density of its components, and attributes like microporosity, isotropy/anisotropy and SiC phase composition.

The coated particle is a highly complex fission product containment system, consisting of multiple interacting coating layers whose properties change under irradiation. How simultaneous changes within the specifications in, for example, coating thickness affect fuel performance in the reactor under normal operating and accident conditions is only inferred from models developed for different

fuel types operating under different conditions. There is no universal fuel model but models developed so far are design-specific, and how the fuel designs perform depend also on specifications, fabrication, quality assurance and control.

The fuel compact fabrication process introduces the possibility for coating failures. While the protective pyrocarbon (Ppyc) layers are intended to provide protection in the compact fabrication process against excessive loads that could crack coating layers, the relationship between coating failure and the need for a Ppyc layer has not been clearly established.

QA/QC Methods While many quality assurance and quality control (QA/QC) methods have been developed and used in the past, there are questions about the reliability of the quality control of the burn-leach process, which is used to determine the integrity of the very important SiC coating layer.

Most of the currently available quality control techniques are destructive methods. Because the initial fuel defect fraction is to be in the 10^{-5} range, large samples sizes in the 10^{5} range need to be analyzed for proof of the low defect fraction. In this regard it is very important to emphasize that even a perfect QA/QC program can only ensure as-manufactured fuel quality, but it cannot ensure that the fuel is also reliable.

While different sample sizes have been proposed for the sampling of different attributes, no relationship between sample size, attribute and impact on performance has been documented, i.e., the current QA/QC plan does not explicitly prioritize quality control activities. Such a prioritization needs to be based on the relative (and quantifiable) importance of particular measurements with respect to achievement of the fuel design requirements.

At this time it is also not known how uncertainties in quality control techniques have to be accounted for in quality assurance. Furthermore, it seems necessary for fuel QA/QC to distinguish between an evolving fabrication technology and a mature fabrication technology. For a first of a kind reactor, different constraints have to be applied than for the n-th reactor.

The proposed QC methods test the measurable properties of the fuel, such as thickness and uniformity of the coatings. However, none tests the functional requirements for the fuel particles and compacts, i.e., the overall radionuclide retention capability of the complex multi-layer particle design and fuel compact.

Conditions for Reducing the "Weak Fuel" Burden Because of these risks/uncertainties, the imposition of a weak particle penalty seems to be justified, based the current state of the art in fuel and fission product technology. As the technology basis is broadened with the understanding of fuel performance and fission product transport, the weak fuel penalty can be lessened.

The following conditions are judged to be conducive to the reduction and possible elimination of the "weak fuel" penalty for MHTGRs with no sealed containment:

1. the existence of a mature MHTGR fuel fabrication industry with an established record for producing fuel which performs to expectations in reactor service;

2. a good comprehension of fuel failure mechanisms to provide an unambiguous interpretation of capsule test data;

3. a good understanding of fission product transport; and

4. a successful testing/demonstration program of sufficient scope on the selected fuel design, produced using prototypical methods.

Fission Product Plateout and Liftoff Evaluation

A review has been conducted regarding the technical status of "plateout" and "liftoff" modeling as it relates to a dry depressurization event of an MHTGR primary system.[4] These terms are in quotation marks to signify that they represent a number of chemical and physical processes which follow different rules of behavior. Moreover, the behavioral rules differ significantly between fission product elements due to major differences in chemical affinities and physical properties. This study covered the plateout and liftoff characteristics of the fission product elements iodine, cesium, strontium and silver. Iodine is treated in a relatively complete fashion. The unique features of plateout and liftoff behavior of the other three elements are qualitatively summarized.

Deposition Mechanisms The various possible modes of deposition in the primary system were evaluated. Because of the relative simplicity of iodine chemistry under these conditions, the principal inventory locations of iodine can be cited with a good degree of certainty. These are (a) circulating as a gas, (b) chemisorbed on circulating dust, (c) chemisorbed on metal surfaces (d) chemisorbed on the extensive graphite surface which forms the open, connected porosity, (e) chemisorbed on plated dust. A test calculation indicates that by far the principal deposition mode of iodine is as chemisorbed material on steel alloys.

Because of the relatively complex chemistry of cesium, its principal plateout modes (and hence also its response to depressurization conditions) require careful evaluation. The principal characteristic of cesium is its tendency for reacting with many oxides to form stable compounds of the form Cs_xMO_y (where M is any metal). For example, cesium chromate is readily formed, either in dust or in the adherent oxide coating on steel alloys. The liftoff characteristics of these two modes are vastly different. In addition, there is indication of cesium diffusion into oxide coatings on steel, which further enhances the opportunity for a permanent, immobile repository for cesium. An additional feature of cesium is its relatively high sorptivity in graphite. Therefore, the cooler graphite regions may be a significant inventory location for cesium.

The principal deposition (hence liftoff) features of strontium relate to its high oxygen affinity. Strontium will form the refractory oxide even under the expected strong reducing conditions. Because of the high melting point and extremely low vapor pressure of the oxide, SrO will very likely permanently deposit where it forms, on dust or on structure and perhaps even within graphite. The liftoff behavior of strontium depends heavily on determining where the oxide forms. In addition, similar to cesium, graphite has a significant sorptivity for strontium.

Since silver is essentially chemically inert under primary system conditions, its deposition and liftoff behavior depend on the effects of its physical properties. Silver's low vapor pressure and high melting point (1234 K) signify that it will freeze permanently upon any opportune surface. It is very likely that silver condensed or fixed surfaces will not lift off. If the vapor pressure of silver in higher temperature areas is sufficient, thermal transport will gradually move condensed deposits to low temperature regions where it would collect as a distinct phase. In addition, Peach Bottom HTGR data indicate that there is some association of silver with dust.

Chemical Environment The chemical environment in the primary system is dominated by the presence of graphite, which imposes reducing conditions throughout, and is modified by unpredictable

ingress rates of oxidants from various sources, e.g., minute leaks from the steam generator, graphite outgassing, and maintenance operations. The oxidants react with graphite to form mainly CO and H_2, which exist in equilibrium with the oxidants CO_2 and H_2O, the ratio being indicative of the oxygen potential of the system.

Information on reactor dust characterization and dust plateout modeling was reviewed. Reactor dust data are available from the Peach Bottom HTGR and the AVR pebble bed reactor, the latter currently only in preliminary form. The Peach Bottom HTGR surveillance data are by far the most complete dust data set for a non-pebble bed HTGR. The AVR dust data indicate that a significantly greater mass of dust is produced in pebble bed reactors due to a much higher degree of graphite attrition.

Materials found in the Peach Bottom samples were (a) graphite particles from fuel and fuel surfaces, however frequently containing materials other than expected and occasionally containing of carbides, (c) carbon filamentary material from surfaces evidently growing from metallic surfaces, (d) debris from maintenance or core replacement activities, (e) much other, unidentified material usually containing silica. Generally, the dust samples contained significant cesium activity, especially at end of life conditions. Some iodine, strontium and silver were also observed associated with dust.

Dust Plateout and Liftoff Modeling. The status of dust plateout modeling was reviewed and applied to conditions in the MHTGR heat exchanger. Although some weaknesses exist, dust plateout modeling is in a fairly advanced state compared with dust liftoff estimation. The weaknesses lie with predictions relating to crossflow exterior to tightly packed tubes, which is the typical steam generator condition. Application of available plateout models to such a flow configuration is highly uncertain. An additional uncertainty relates to predicting plateout of large particles (i.e., > 1 μm) where the net deposition rate is affected by a fractional bounce-off.

In general, dust liftoff models fall into two categories which may be termed either "force ratio" or "turbulent burst" models. "Force ratio" models postulate that liftoff occurs when drag or lift forces exceed the force of attraction. "Turbulent burst" models postulate that liftoff results from the penetration of the laminar sublayer by bursts of turbulence from the turbulent zone. The framework for a liftoff model may be developed from either postulate; however, most recent developments are based on the "turbulent burst" concept. Physical reality appears to favor the turbulent burst mechanism for particle liftoff. An important implication of the "turbulent burst" approach is that the liftoff process occurs continuously, even at steady state (i.e., at shear ratios of unity) at which time deposition and liftoff rates are in equilibrium. Thus, during depressurization, some liftoff is predicted for shear ratios of unity and below.

Iodine Plateout and Liftoff Estimate. A sample calculation of iodine plateout and liftoff attempts to integrate the numerous influential factors. The motivation is to place these factors in a proper perspective. The estimation assumes iodine to exist in five forms: circulating as gas, sorbed on circulating dust, and chemisorbed on steel, graphite and on plated dust in the steam generator. Simple models are used to estimate the total iodine inventory in the primary system, its distribution among the five forms, the amount chemically desorbed due to depressurization and, the amount removed with the liftoff of dust.

Some conclusions resulting from the sample calculation for iodine liftoff are the following: (a) The dust liftoff effect is predicted to be quite small, the primary reason being that only a small and brief increase in shear ratio is predicted in the tubing. The evident reason is that the tubing region is

protected from high shears by the large flow resistance afforded by the circulator, which is situated between the break (i.e., the open relief valve) and the tubing. If true, the depressurization flow is such that the steam generator tubing region is at least partially a dead zone. Regardless of which liftoff model is used in such case, only extremely small du. liftoffs would be predicted from the steam generator. (b) A second reason for the small effect of d. liftoff is that only ~3% of the iodine inventory is predicted to be associated with plated dust. The bases for this estimate are the observed circulating dust levels in the Peach Bottom HTGR, and an approximate factor of 100 lower iodine sorptivity for "dust" relative to steel. (c) A possibly surprising result is that chemical desorption from graphite and from plated dust is about as significant as from steel, despite significantly lower inventories. The reason is that weak chemisorbers like graphite, which capture only about 2% of the primary system iodine despite its enormous surface, therefore also more readily desorb iodine under depressurization conditions for the same reason. The net result is a predicted 0.005% iodine release from the primary system due to a base case dry depressurization. The estimate would increase by including higher shear zones, e.g., the core, in addition to the steam generator.

Conclusions

The LOFC heatup accident analyses and sensitivity studies have shown that the current MHTGR design appears not to be susceptible to significant fuel failure from postulated LOFC accidents, even from those of very low probability. Several days would elapse before worst-case ATWS-LOFC combination events lead to the initiation of fuel failures. Initial steam ingress accident scenario analyses indicate much milder consequences than those previously seen in bounding calculations. The ORNL results generally corresponded well with independent calculations by DOE contractors and by Brookhaven National Laboratory. Considering the fact that these are calculations of some of the most serious types of accidents that can be reasonably postulated, the fact that there is such good general agreement is strong evidence that the analyses are relatively straightforward and therefore credible. The one major area of concern was with possible vessel overheating, and that would not be considered an immediate safety concern unless RCCS or partial RCCS failures occurred.

A study of fuel reliability, with principal emphasis on the "weak fuel" issue, noted the interrelated importance of many steps in the production of the fuel. How fabrication process parameters and uncertainties in QC methods affect fuel reliability is not yet well defined. The tolerance for error must be extremely low, considering that without a sealed containment building, fuel particle barrier integrity must provide a major containment function. Recommended steps for reducing the "weak fuel" penalty were outlined.

A review of the mechanisms for plateout and liftoff of fission products in "dry depressurization" accidents concluded that a sufficient technical basis for modeling these phenomena does not currently exist. The behavior of iodine, cesium, strontium, and silver was studied. The more significant conclusions are: the iodine-131 released from the primary system would probably be quite small, in the order of a few millicuries; releases due to dust transport would also be quite small due to the fact that shear forces in "worst case" depressurizations barely exceed normal sheer forces; and that chemical reactions and radioactive decay tend to work in favor of reducing releases.

References

1. P. M. Williams, et al., Draft Preapplication Safety Evaluation Report for the Modular High-Temperature Gas-Cooled Reactor, NUREG-1338, U.S. Nuclear Regulatory Commission, 1989.

2. S. J. Ball, MORECA: A Computer Code for Simulating Modular High-Temperature Gas-Cooled Reactor Core Heatup Accidents, NUREG/CR-5712, (ORNL/TM-11823), November, 1991.

3. C. M. Woodworth, et al., The Approach to Multimodule Control of the MHTGR, presented at IAEA Technical Committee Meeting on Design Requirements, Operation, & Maintenance of Gas-Cooled Reactors, San Diego, Sept. 21-23, 1988, GP 88-66, NG/ICE, Stone & Webster Engineering Corp., Boston, 1988.

4. R. P. Wichner, Fission Product Plateout and Liftoff in the MHTGR: A Review, NUREG/CR-5647, (ORNL/TM-11685), April, 1991.

Initial Performance Assessment of the Westinghouse AP600 Containment Design and Related Safety Issues*

J.L. Tills
Jack Tills and Associates, Inc.

K.E. Washington and V.F. Nicolette
Sandia National Laboratories

Abstract

The CONTAIN code is currently being used to predict containment thermal hydraulic conditions during design basis and severe accidents for advanced light water reactor (ALWR) designs such as the Westinghouse AP600. In the AP600 design, a passive containment cooling system (PCCS) is used for reducing long-term overpressure during accidents. CONTAIN models for heat and mass transfer within the AP600 containment and outer air cooling channel are verified by comparing recent CONTAIN calculations to integral test data obtained by Westinghouse in their PCCS Integral Test Facility. The comparison includes tests in which the outer containment wall is both dry and wet, that is, the wet tests involve an evaporative water film that enhances heat transfer as will be the case for AP600. The appropriateness of the heat and mass transfer analogy methodology used in the CONTAIN code is demonstrated. Code model limitations are discussed along with model development plans and applications for AP600.

1. Introduction

Containment designs are being developed for conceptual advanced light water reactors (ALWR's) that incorporate passive cooling and decay heat removal features for protection against long term containment overpressure in accident situations. The passive nature of these containment systems poses technical challenges to containment analysis codes for predicting containment response in both design basis and beyond design basis events. Such challenges include natural draft flow in the channel outside the containment shell, behavior of an evaporative flowing water film on the containment shell, stratification of gases within the containment, internal containment condensate film behavior not adequately represented by existing correlations, and numerical challenges arising out of the need to efficiently perform long-term containment response calculations.

The CONTAIN code[1] is the principal code in the regulatory complex for performing such predictions. This code has been developed for the analysis of existing light water reactor containments, with emphasis on performing best-estimate predictions under severe accident conditions. For existing plants and severe

* This work was supported by the U.S. Nuclear Regulatory Commission and performed at Sandia National Laboratories, which is operated by the U.S. Department of Energy under contract number DE-AC04-76DP00789.

accident conditions, the CONTAIN code has been extensively tested and validated. Some examples of the demonstrated capabilities of CONTAIN can be found in References [2-8]. A relatively complete summary of other CONTAIN code validations can be found in Reference 9. However, this demonstrated capability of CONTAIN for existing designs does not directly translate into the same capability for the challenges posed by the passive advanced reactor containment designs described above. It is therefore appropriate that the CONTAIN code be assessed for its ability to meet the challenges posed by these new designs.

Preliminary steps taken to perform this assessment and model correlation improvements resulting from this assessment are the topics of this paper. In particular, this paper focuses on the assessment of the CONTAIN code for use in analyzing the Westinghouse AP600 containment design. (The CONTAIN code version is 1.12, with developmental updates to implement a crude evaporative film model and to correct a known error in the structure heat transfer model.[10]) The methodology used to date has been the analysis of the Westinghouse Passive Containment Cooling System (PCCS) experiment[11] performed to assess the performance of the passive heat removal feature of the AP600. Future work on CONTAIN assessment will include other advanced passive designs, such as the GE SBWR containment; however, this paper is limited to the AP600 features.

In the next section, pertinent heat and mass transfer models used in the CONTAIN code are briefly described. Each model is later referred to in the sections dealing with calculational results. Section 3 provides a description of the Westinghouse Integral Test Facility, and selected tests conducted to assess the performance of a simulated PCCS heat removal channel. The results of a comparison between the integral test data presented in Section 3 and CONTAIN calculations are discussed in Sections 4 and 5. A summary of the integral test calculations is included in section 6 along with a brief discussion on the significance of this study and plans for future CONTAIN applications for AP600 containment analyses.

2. Heat and Mass Transfer Models

The emphasis in this paper is on the heat and mass transfer modeling of the Westinghouse Integral Tests which demonstrate energy transfer mechanisms important to the AP600 PCCS. Three models required in the analysis of these experiments are (1) duct convective heat transfer, (2) wall condensation and evaporation mass transfer, and (3) structure-to-structure thermal radiation energy transfer. Each of these energy and mass transport mechanisms is modeled in the CONTAIN code as described in this section. Specifically, the total heat flux to a wall surface q (J/m^2-s) consists of four components representing convective heat transport (q_c), the heat transported by the mass flux (q_m), radiative transport (q_r), and sensible heat carried by aerosol water deposited on the surface (q_a). Since aerosol deposition is not occurring in the integral tests, this model is not discussed here, but is considered in section 5 in relation to a modification of the CONTAIN code to allow treating a structure flooded by an external water source. The total heat flux for structures is the sum of these components,

$$q = q_c + q_m + q_r + q_a \qquad (2.1)$$

In the analysis of the Integral Tests, the correlations that quantify each component are investigated and verified, with the exception noted for the aerosol water deposition model. In the following discussions each component is briefly reviewed; further detail on each model can be found in Reference 12.

2.1 Convective heat transfer model

The convective heat transfer is calculated using the relation

$$q_c = h_c (T_{bulk} - T_f) \tag{2.2}$$

where T_f is either the water film surface temperature or the dry wall surface temperature.

The heat transfer coefficient h_c for convective heat transfer is related to the Nusselt number Nu by

$$h_c = \frac{Nu\ k}{L} \tag{2.3}$$

Here, k is the thermal conductivity of the gas-vapor mixture and L is the characteristic length of the wall. Several standard correlations are available in CONTAIN for determining Nu in either forced or natural fully developed convection regimes. For laminar natural convection,

$$Nu = 0.27 (GrPr)^{1/4} \tag{2.4}$$

For turbulent natural convection,

$$Nu = 0.14 (GrPr)^{1/3} \tag{2.5}$$

For forced convection,

$$Nu = 0.037 (Re^{4/5} Pr^{1/3}) \tag{2.6}$$

In these equations, Gr is the Grashof number, and Re is the Reynolds number. In the code, the larger of the natural or forced convection Nusselt numbers is always used in modeling the heat transfer.

The forced convection Nusselt number for a structure requires an estimation of the velocity of the gas mixture parallel to the structure surface. This velocity can either be specified by the code user, or calculated from flow path velocities that lead into or out of the cell where the structure resides. In the case where the velocity v is calculated by the code, the velocity across a structure is defined as the average of the inlet and outlet velocity for a cell:

$$v = (v_{in} + v_{out})/2 \tag{2.7}$$

The expression for v_{in} is

$$v_{in} = \sum_{\substack{Incoming \\ flows}} C_{in,fp} |W_{fp}|\ RT_{in} / (M_g A_{hd} P_c) \tag{2.8}$$

where $C_{in,fp}$ is a coefficient, which can be specified for each flow path and each structure, W_{fp} is the mass flow rate in the flow path, A_{hd} is a hydraulic area, which can be specified for each structure, R is the gas constant, M_u is the upstream cell molecular weight, P_c is the pressure of the downstream cell, and T_{in} is the inlet temperature of the incoming gas. The outlet velocity v_{out} is determined by

$$v_{out} = \sum_{\substack{outgoing \\ flows}} C_{out,fp}|W_{fp}|/(A_{hd}\rho_c) \qquad (2.9)$$

where ρ_c is the density of the gas mixture in the cell and $C_{out,fp}$ is a coefficient which can be specified for each flow path and each structure. (In the case where the cell is a duct, the cell velocity is approximately modeled by using the duct hydraulic area for A_{hd}, with $C_{in,fp}$ and $C_{out,fp} = 1.$)

2.2 Condensation and Evaporation Model

The second component of the total heat flux, accounting for the heat transported by the mass flux, is given by

$$q_m = J[H_v(T_{bulk}) - H_l(T_l)] \quad \textit{for condensation;} \qquad (2.10)$$

and,

$$q_m = J\,[H_v(T_l) - H_l(T_l)] \quad \textit{for evaporation;} \qquad (2.11)$$

where H_v is the vapor specific enthalpy and H_l is the liquid specific enthalpy. The vapor mass flux J in Equations (2.10) and (2.11) is given by

$$J = K_g M(P_{vb} - P_{vl}) \qquad (2.12)$$

In Equation (2.12), M is the vapor molecular weight, P_{vb} is the partial pressure of the vapor in the bulk atmosphere (at the bulk temperature, T_{bulk}), P_{vl} is the saturation pressure at the film surface temperature, T_l,

and

$$K_g = \frac{Sh\ P\ D_v}{R\ \bar{T}\ P_{nn}\ L} \qquad (2.13)$$

where

P = cell pressure,
D_v = mass diffusivity of vapor in the noncondensible gas,
R = gas constant,
$\bar{T}$ = the average of T_{bulk} and T_{wall},
L = characteristic length,

and

$$P_{nm} = \frac{P_{vb} - P_{vw}}{\ln\left[\frac{(P - P_{vb})}{(P - P_{vw})}\right]} \tag{2.14}$$

where P_{vw} is the saturation pressure at the interior or exterior wall temperature.

The Sherwood number Sh itself is determined by using an analogy between heat transfer and mass transfer.

$$Sh = Nu(Sc/Pr)^{1/3} \tag{2.15}$$

In this expression, Sc is the Schmidt number for the bulk gas-vapor mixture. The Nusselt number Nu is defined by Equations (2.4), (2.5), or (2.6).

2.3 Thermal Radiation Model

The third component of the total heat flux q_t is the radiation heat flux from the gas mixture and the direct flux from other surfaces that enclose the gas mixture. The net radiation flux $q_{r,i}$ to the i-th surface with area A_i is the difference between the incoming radiation flux density Ξ_i and the outgoing radiation flux density, or radiosity, Ψ_i.

$$q_{r,i} = \Xi_i - \Psi_i \tag{2.16}$$

Since the outgoing flux is the sum of the reflected flux and the blackbody flux multiplied by the emissivity ϵ_i of the surface, the following equation, obtained from Kirchhoff's law, is used to determine the net radiation flux:

$$q_{r,i} = \frac{\epsilon_i}{(1-\epsilon_i)} (\Psi_i - B_i) \tag{2.17}$$

where

$B_i = \sigma T_i^4$ = blackbody flux emitted from the surface,
σ = Stefan-Boltzmann constant, and
T_i = surface temperature.

The radiosities are determined by solving the following system of simultaneous equations

$$\Psi_i - (1 - \epsilon_i) \sum_{j=1}^{N} F_{ij}[1 - \epsilon_{mji}]\Psi_j$$

$$= \epsilon_i B_i + (1 - \epsilon_i) \sum_{j=1}^{N} F_{ij} \epsilon_{gij} B_g \qquad (2.18)$$

where

N = number of surfaces,
F_{ij} = view factor from surface i to surface j,
B_g = σT_g^4 = Planck blackbody flux for the gas, at temperature T_g, and
ϵ_{gij} = emissivity of the gas, which is a function of the beam length to the receiving surface.

The dry surface emissivities, view factors, and characteristic beam lengths between surfaces are provided by the code user. Whenever a water film is present on the surface, the emissivity for that surface is automatically equated to the emissivity of water, which is set to 0.94. Since the surface and gas temperatures are known, a network of equations for the radiative heat transfer among the surfaces can be constructed, and the resulting linear systems of equations is solved to give the net radiative heat flux to each surface. These equations are solved with a standard linear equation solver.

3. Description of Integral Tests

The main purpose of the Westinghouse PCCS Integral Tests was to investigate and demonstrate water film behavior, mass transfer (evaporation), and convective heat transfer on the external surface of a steel tank initially filled with one atmosphere of nitrogen and heated on the inside with dry steam. The tests provided heat transfer data at near prototypic conditions for inside containment heat transfer by condensing steam, and external heat transfer by conduction, convection, radiation, and water evaporation. The test facility shown in Figure 3.1 consists of a 7.3 meter tall, 0.91 meter diameter, steel tank surrounded by a cooling air annulus constructed to simulate the Westinghouse PCCS. The steel tank is pressurized with steam over a range of anticipated design basis pressures (1.6 to 3.7 bars) and cooled externally by air and external water flowing down along the vessel outer wall.

The flow of air up through the annulus is driven by a fan located above the steel tank; therefore, flow in the annulus is forced flow as opposed to the natural draft flow conditions that will be present in the AP600 PCCS annulus. The forced air flowrates in the annulus however have been matched to the estimated bulk natural draft flowrates that are expected in the PCCS annulus during long term pressurization scenarios (2 - 5 m/s).

The test matrix for the PCCS simulation test contains 36 separate tests. In each test, data is obtained for near steady-state conditions. Data, presented in Reference 11, is given in the form of average vessel heat flux verses internal tank pressure; therefore, the experimental measurements as given are integral test results.

The location of injected steam into the tank is varied. The majority of the tests were run with a uniform axial steam injection to simulate a well-mixed steam environment within the tank. In other tests the steam injection location was varied from a bottom inlet to a high inlet location. The tests analyzed in this report are restricted to the uniform injection tests. In Figure 3.1 the axial distribution pipe for distributing the steam is shown. There are holes drilled in the pipe, which is surrounded by an outer sheath with offset holes of

larger diameter. The outer sheath serves as a baffle to help prevent steam jets from impacting directly on the pressure vessel walls. The total area of the outer sheath holes is approximately 1.2 m^2.

The first series of tests are the so called "dry" tests in which there was no water flooding of the outer vessel wall. These tests, #1 through #4, are described in Table 3.1. For the "wet" tests in which a water film covered the vessel outer surface, four tests are selected as representative, and these tests are defined in Table 3.2. For each selected wet test, the water film completely covers the outer vessel wall such that there are no dry-out regions.

4. Integral Test Facility (Dry) Modeling Results

The dry tests are used to verify the correlations for single phase heat transfer in a simulated PCCS duct under forced flow conditions. The tests are also useful for quantifying wall condensation on the inside of the pressure vessel wall for steam/gas mixture conditions that are prototypical of AP600 containment interior atmospheric conditions. Shown in Figure 4.1 is the CONTAIN nodalization model of the facility. Cell number 1 represents the interior of the pressure vessel (containment), cell 2 approximates the plenum region where air flows into the outer annulus (PCCS duct), and cell 3 is the outer annulus (duct). A fourth cell, not shown, represents the outside environment. A cross-section of the facility showing the vessel wall and duct wall heat transfer components, discussed above, is presented in Figure 4.2.

A common correlating equation for single-phase fully developed convective heat transfer in long noncircular ducts is the Dittus-Boelter equation

$$Nu = 0.023 Re^{4/5} Pr^{1/3} \tag{4.1}$$

where the characteristic length of the duct is the hydraulic diameter, D_h. For the circular-tube annuli such as the Integral Test duct, the hydraulic diameter is

$$D_h = 4 \frac{cross\text{-}section\ area\ for\ flow}{wetted\ perimeter} = D_2 - D_1 \tag{4.2}$$

where D_2 is the outer diameter of the annular channel, and D_1 is the inner diameter of the channel. The hydraulic diameter of the test facility air duct is 0.76 meters.

Equation (2.6) is a Nusselt number correlation for forced flow parallel to a flat plate with characteristic length, L. Combining Equation (2.3) and (2.6), a slightly more general correlation for the duct Nusselt number can be written as

$$Nu = C Re^{4/5} Pr^{1/3} \tag{4.3}$$

where

$$C = \frac{0.037}{\gamma^{0.2}} \tag{4.4}$$

and

$$\gamma = \frac{D_h^*}{D_h} \tag{4.5}$$

which is the ratio of an adjusted hydraulic diameter D_h^* to the actual hydraulic diameter of the duct. The *heat transfer coefficient* h_c, determined by the Dittus-Boelter correlation, can therefore be effectively formulated from the flat plate correlation given in Equation (2.6) by substituting D_h^* for L. For this case $C = 0.023$, and D_h^* is determined from Equation (4.5) with D_h set to the facility duct hydraulic diameter.

A review of test facility geometry, showing a duct of length 6.4 meters, together with the range of air flowrates suggests that the velocity and temperature profiles within the duct will not be fully developed during the experiments; therefore, entrance-effects must be considered. A method for accounting for entrance-effects is to include a multiplication factor on the infinite length heat transfer coefficient calculated by the Dittus-Boelter equation. The recasting of the CONTAIN forced flow heat transfer equation in the more general form allows entrance-effects to be included by varying the "adjusted" hydraulic diameter appropriately. In this application the duct air velocity is calculated by the code, using Equation (2.7), with the coefficients $C_{in;fp}$ and $C_{out;fp}$ in Equations (2.8) and (2.9) set equal to one.

Before the results of the CONTAIN calculations are discussed, it is should be noted that the vessel pressure is very sensitive to the interior gas/mixture temperature, Figure 4.3. Vessel pressure is therefore a useful and appropriate parameter to focus on in assessing the integral energy transport from the interior of the vessel to the air duct. Since the experiments are intended to simulate near prototypical accident conditions, agreement between measured and calculated vessel pressure provides verification data for an integral assessment of a containment code, where in the experiment the pressure vessel is the "containment".

To investigate entrance-effects, a series of CONTAIN calculations were completed for test #3 by varying the "adjusted" hydraulic diameters, as discussed above, so that entrance-effects could be accounted for using a correction factor applied to the Dittus-Boelter *infinite* duct length heat transfer coefficient, Figure 4.4. Agreement with the experimental vessel pressure is obtained with a correction in the infinite length heat transfer coefficient, $h/h_\infty = 1.32$. Review of the literature on recommended entrance correction factors gives no conclusive guidance on this experiment since the geometry and experimental conditions are such that the flow in the duct in not fully developed turbulent. In this case, the most reasonable approach is to use the correction for entrance-effects given in Reference 13,

$$h/h_\infty = 1 + \frac{3.0}{L/D_h} \tag{4.6}$$

where h_∞ is the heat transfer coefficient calculated using the Dittus-Boelter equation, L is the duct length (6.4 meters, excluding lower plenum region), and the value 3.0 is selected for a flow region that is developing. Using the above equation with the facility duct geometry, the correction factor for entrance-effects is 1.36. The agreement between the CONTAIN calculations and the

engineering estimate is quite satisfactory. The correction factor of 1.32 is therefore used in subsequent calculations.

In Reference 11 the results of the Integral Tests are presented as plots of vessel average heat removal flux verses measured vessel internal pressure. The heat removal is determined from a heat balance on measured inlet and outlet steam/condensate flow. A comparison of the experimentally determined results for duct performance versus the CONTAIN results are shown in Figure 4.5. The agreement between the pressure calculation and data is within 5%, which is quite good. The slightly lower heat removal rates calculated with CONTAIN are, in part, due to the differences in the measured and calculated condensate drainage temperatures. The measured condensate temperatures, which are lower than the calculated temperatures by a few 10's of degrees K, probably reflect the lower plenum collection pan heat loss, which is not accounted for in the CONTAIN model.

Two sensitivity calculations are also plotted in Figure 4.5. In the first calculation the vessel nitrogen gas is replaced with steam so that the interior condensation occurs without a noncondensible gas present. As shown, the heat transfer without the noncondensibles is significantly higher.

In the analysis of the dry test it became clear that thermal radiation heat transfer between the vessel wall and outer duct wall is required to predict the vessel pressure. This is evident from the other sensitivity case (without thermal radiation) plotted in Figure 4.5. A heat transfer summary of the CONTAIN code results for test #3 is given in Table 4.1. The heat transfer components, Q_g, Q_m, Q_r are tabulated along with surface temperatures and bulk gas temperatures. A similar table for the case without radiation from vessel to outer duct wall is presented in Table 4.2. When thermal radiation between structures is included, approximately 28% of the total vessel energy is transferred from the vessel wall directly to the outer duct wall. The majority of the transferred energy is in turn transported to the air flow by convection. The result is that the temperature of the vessel wall is reduced by about 10 K since the effective heat transfer area for convective heat transfer has been significantly increased by the direct transfer of vessel wall thermal energy to the outer duct wall. The outer duct wall with radiation heat transfer is about 10 K higher than an identical calculation without radiation. (In this test calculation, as well as all others, the emissivity of the dry walls is estimated to be 0.8.)

5.0 Integral Test Facility (Wet) Modeling Results

In comparison to the dry test energy transport model, Figure 5.1, the wet tests are modeled with a water film on the outer vessel wall such that the mass heat flux component from the film to the air is included in the total energy transferred from the vessel wall. The "wet" model is shown in Figure 5.1. The tests are modeled in the CONTAIN code by making a minor code modification to allow the wall flooding rate to be simulated as a pseudo water aerosol deposition rate. The aerosol heat transfer term, referred to in Equation (2.1), given by

$$Q_a = H_1(T_{bulk})\, J_a \qquad (5.1)$$

where J_a is the mass flux of aerosol water being deposited on the surface, which is modified so that

$$Q_a = H_1(T_{film\ source})\, J_{film} \qquad (5.2)$$

In Equation (5.2), the mass flux of water flooding the vessel surface J_{film} is specified by dividing the total water flooding rate (given in Table 3.2) by the total vessel wall surface area (duct plus plenum). This model of a wetted vessel outer wall is one-dimensional; that is, the film thickness does not vary along the length of the vessel. The maximum film thickness is specified by the user to approximate a thickness for gravity draining films on vertical surfaces neglecting film surface to air shear.[14] Water added in excess of the maximum film thickness is drained off the surface at the film temperature. In these calculations, the CONTAIN default maximum film thickness, 0.0005 m, is used. This method of modeling the water film on the vessel outer wall is a reasonable approach provided that the film does not dryout and that the film thermal resistance is relatively small compared to other resistances between the interior vessel gas and duct air, which is the case in these tests. (In most tests, the film resistance is less than 15% of the total resistance. For actual containment conditions where the condensation coefficient in the containment is lower than observed in these tests, as discussed later, the film resistance is considerably less than the total resistance between interior gas mixture and duct air.)

Because film evaporation on the outer vessel wall is such an efficient manner of heat transport, the rate of steam injection into the pressure vessel is almost an order of magnitude higher than in the dry tests at identical vessel pressures. This means that the steam flow conditions within the vessel probably are not the same as that effectively modeled in the dry test according to an assumed natural convection algorithm for flow parallel to a vertical flat plate, Figure 5.2 (a). In the case of the higher injection rates, the steam flow pattern within the vessel changes from one of parallel flow driven by buoyancy forces to a momentum jet directed normal to the vessel wall as indicated in Figure 5.2 (b). In the latter, the "jet" velocity is determined based on the steam injection rate and sheath hole area. To estimate the expected increased condensation rate for this different flow pattern, the heat and mass transfer analogy is used to provide a model.

From the engineering literature,[15] average heat transfer from fluid streams directed normal to a plate can be approximated by

$$Nu = 0.228 Re^{0.731} Pr^{1/3} \tag{5.3}$$

To model the convective as well as condensation conditions within the pressure vessel, a modification of the flat plate Nusselt number correlation, Equation (2.6), is made so that a more general correlation

$$Nu = CRe^{m}Pr^{n} \tag{5.4}$$

can be used to override the default equation, with the user specifying values for C, m, and n for each selected heat transfer surface.

To estimate the coefficient C, a series of CONTAIN calculations are made for increasing values of C, starting with the flat plate coefficient, 0.037. The results of these calculations for test #17 is shown in Figure 5.3 for a case in which m=4/5 and n = 1/3. (Note that with m = 4/5 and n = 1/3, the same method used in section 4, that is, using an "effective characteristic length" for a structure, can be used to approximate flow directed normal to the vessel surface.) The results of the series indicate that a value of C = 0.2 gives good agreement between measured and calculated vessel pressures. The value of the coefficient obtained empirically here is comparable to the coefficient reported

in Equation (5.3); it is noted that $C = 0.2$ corresponds to a slightly higher exponent on Re (0.8 vs. 0.731).

A comparison of the wet integral test data to the CONTAIN calculations for the four wet tests tabulated in Table 3.2 is shown in Figure 5.4. Two CONTAIN calculation series are presented indicating heat removal rates for correlations in which the Nusselt multiplication coefficients is 0.037 (CONTAIN default) and 0.2 (approximate normal flow coefficient as determined above). In both calculational series m = 4/5 and n = 1/3, and the plate characteristic length is the vessel height (uniform injection directed toward the entire vertical vessel wall). The divergence of the flat plate correlation with increasing steam injection rates in clearly evident, indicating that the flow pattern within the vessel along the vessel wall surface is changing. Improved agreement by using the correlation for flow normal to the vessel wall shows that the integral behavior of the experiment can be obtained with CONTAIN using the existing models for mass transfer.

A breakdown of the total heat flux, similar to the dry test case above (same interior vessel pressure), is presented in Table 5.1 for Test #17 (C = 0.2). The energy component values can be compared to the dry test case. In the wet case, the dominant energy transfer component is clearly the evaporation component whereas in the dry case the main component is convective energy transport. Radiation heat transfer in the wet test is about half the dry case (not negligible) which is a reduction of the approximately 40 degree K drop in the outer vessel radiating temperature for the wet case.

In a truly prototypical experiment simulating an accident scenario, the pressure vessel would be scaled to a much larger dimension such that steam momentum jets would not directly impact on the vessel interior wall, at least not the entire wall. In such cases the computational methods normally used in CONTAIN for interior heat and mass transfer to the containment wall would be expected to provide a good approximation of wall heat transfer and condensation, as was the case for the dry tests. However, in the tests described here, the integral behavior of the test could only be approximated by adjustments in the vessel interior heat transfer correlations to approximate a non-typical flow condition.

6. Summary

The analysis of the Westinghouse Integral PCCS tests has been completed using the CONTAIN code, version 1.12 (with modifications noted). Four dry tests and four wet tests have been calculated, and the results compared to the integral test results. In the case of the dry tests, good agreement between data and calculations were obtained only when channel thermal radiation heat transfer and thermal entrance-length effects were taken into account. The importance of structure-to-structure thermal radiation within the PCCS channel is clearly demonstrated in these tests. The capability of the CONTAIN code to accurately calculate energy exchange with the net radiation enclosure model is shown in these tests. Entrance-effects for air flow within the test channel also significant in these tests, and an accounting of this effect is required to predict the integral data. In these calculations, by an appropriate modification of the channel characteristic diameter, entrance-effects were approximated, and good agreement with test data was obtained. Results of the comparison between dry test data and CONTAIN calculations indicate that the current CONTAIN models of heat and mass transfer are appropriate for PCCS modeling without the presence of water film.

In the wet tests a water film covers (no dryout) the vessel wall. This was simulated with CONTAIN by treating the flooding as a pseudo water aerosol

deposition, specified by the user. Evaporation of the water on the vessel wall surface is determined using existing mass transfer models in the code. Mass transfer in the PCCS channel is determined using the heat and mass transfer analogy methodology used in CONTAIN with appropriate correlation adjustments to the heat and mass transfer equations to account for entrance-effects. Agreement between the wet test data and calculations is obtained at the higher vessel pressures by using a heat transfer correlation that approximates the assumed condition of steam flow directed normal to the vessel interior wall surface. The relatively high steam injection rates in the relatively small pressure vessel tends to make the wet integral test somewhat non-typical of anticipated containment wall boundary conditions. Nevertheless, a method similar to the manner for adjusting the heat transfer correlation for entrance-length effects was found to be successful in bringing the test data and calculated results into agreement. This agreement, obtained using correlations found in the heat transfer literature, indicates that the condensation and evaporative modeling methodology within the CONTAIN code are appropriately suited for PCCS modeling application.

Although the success of the CONTAIN code in predicting the Westinghouse Integral PCCS tests is gratifying, and shows the correctness and flexibility of the heat and mass transfer modeling approach, there remain a number of limitations in the current CONTAIN models for treating the actual PCCS in the context of the AP600 geometry and accident conditions. First, the tests considered here have been purposely selected for film coverage that is essentially one-dimensional so that no film thickness tracking would be required. CONTAIN's one-dimensional heat sink models need to be modified to approximate the 2-dimensional film drainage that can lead to partial coverage and possible dryout of surfaces. A more general correlation for heat and mass transfer needs to be implemented to treat wavy film interfaces, non-vertical wall surface orientations, and conditions in which the film may be unstable. Obviously, as shown in these integral tests, the presence of film on the containment outer wall is extremely important to the pressure response of the containment. PCCS models must therefore be developed to predict conditions in which a film may or may not be present. In addition, the models for film evaporation in the CONTAIN code do not account for the possibility of film boiling, which might occur during some accident events. Finally, the verification of the heat transfer correlations in the Westinghouse Integral tests is only strictly applicable for forced convective conditions. Natural drafting in the PCCS channel may require an alternative model for predicting surface heat transfer[16] (and therefore mass transfer). This natural draft model may be considerably more complicated than the forced convective correlations explored in this paper for the Integral PCCS tests, and more difficult to verify since test facilities of very large scale may be required.

The future prospects for accident simulations using CONTAIN appear bright, however, in light of this analysis. Current plans are to continue the ALWR design basis and severe accident calculational efforts with improved models and features, as suggested by these comparison calculations and as discussed above. The models will be applied to an AP600 plant design. The CONTAIN AP600 plant deck is now being constructed using recently obtained Westinghouse specifications. This deck will be used to investigate various DBA long-term pressurization scenarios, rapid pressurization events such as hydrogen burns, and other containment threat issues regarding hydrogen gas distributions.

7. References

1. K. K. Murata et al., "User's Manual for CONTAIN 1.1, A Computer Code for Severe Nuclear Reactor Accident Containment Analysis," NUREG/CR-5026, SAND87-2309, Sandia National Laboratories, Albuquerque, NM, 1989.

2. F. W. Sciacca et al., "Testing of the CONTAIN Code," NUREG/CR-3310, SAND83-1149, Sandia National Laboratories, Albuquerque, NM, 1984.

3. K. E. Washington and D. E. Carroll, "Assessment of Models for Steam Release from Concrete and Implications for Modeling Corium Behavior in Reactor Cavities," SAND88-2329C, Sandia National Laboratories, Albuquerque, NM, 1988.

4. D. C. Williams, K. D. Bergeron, P. E. Rexroth, and J. L. Tills, "Integrated Phenomenological Analysis of Containment Response To Severe Core Damage Accidents," Progress in Nuclear Energy, Vol. 19, 1987.

5. F. Gelbard, J. L. Tills, and K. K. Murata, "CONTAIN Code Calculations for the LA-4 Experiment," The 2nd International Conference on Containment Design and Operation, Vol. 2, October 14-17, 1990.

6. P. N., Smith and G. J. Roberts, "Application of the CONTAIN Code to the Analysis of Large-Scale Aerosol Experiments," CEC/NEA Workshop on Water-Cooled Reactor Aerosol Code Evaluation and Uncertainty Assessment, Brussels, Belgium, September 1987.

7. L. Wolf, and L. Valencia, "Hydrogen Mixing Experiments in the HDR-Facility," 17th Water Reactor Safety Information Meeting, NUREG/CP0105, Vol. 2, October 23-25, 1989.

8. H. Karwat, "ISP-23, Rupture of a Large Diameter Pipe in the HDR Containment," Vol. 1 & 2, CSNI Report No. 160, December 1989.

9. K. E. Washington and R. G. Gido, "CONTAIN Developmental Assessment," FIN A1198, Task 3 Letter Report enclosed in October 22, 1990 letter to Dr. Allen Notafrancesco (U.S. Nuclear Regulatory Commission) from Richard G. Gido (Sandia National Laboratories, Albuquerque, NM).

10. CONTAIN Newsletter, CONTAIN 1.11 and 1.12, No. 7, Sandia National Laboratories, Albuquerque, NM, March 1991.

11. L. E. Conway, "Tests of Heat Transfer and Water Film Evaporation from a Simulated Containment to Demonstrate the AP600 Passive Containment Cooling System," WCAP-12667, Westinghouse Electric Corporation, Pittsburgh, PA, January 1990.

12. K. E. Washington, K. K. Murata, R. G. Gido, "Reference Manual for the CONTAIN 1.1 Code for Containment Severe Accident Analysis," NUREG/CR-5715, SAND91-0835, Sandia National Laboratories, Albuquerque, NM, 1991.

13. L. C. Burmeister, Convective Heat Transfer, Wiley & Sons, New York, NY, pp. 490, 1983.

14. R. B. Bird, W. E. Stewart, and E. N. Lightfoot, Transport Phenomena, 6th Edition, John Wiley and Sons, New York, NY, 1965.

15. F. P. Incropera and D. P. DeWitt, Fundamentals of Heat Transfer, John Wiley & Sons, New York, NY, 1981.

16. F. B. Cheung and D. Y. Sohn, "Numerical Study of Turbulent Natural Convection in an Innovative Air Cooling System," Numerical Heat Transfer, Part A, 16, 1989.

Table 3.1 AP600 PCCS Test Data and Results for Dry Operation[a]

	Test No.			
	1	2	3	4
Nominal Test Conditions:				
Test Vessel Inter. Pressure (Pa-gauge)	6.9e4	1.4e5	2.1e5	2.8e5
Test Vessel Inter. Pressure (Pa)	1.7e5	2.4e5	3.1e5	3.8e5
Annulus Air Velocity (m/s)	2.4	2.4	4.9	4.9
Annulus Air Inlet Temperature (K)	296.8	305.5	302.3	295.2
External Water Film Supply (kg/s)	0.0	0.0	0.0	0.0
Measured Conditions:				
Internal Steam and Condensate:				
Steam Inlet Pressure (Pa)	1.7e5	2.4e5	3.0e5	3.7e5
Steam Inlet Temperature (K)	387.3	398.0	406.7	413.5
Steam/Condensate Flow (kg/s)	5.7e-3	8.2e-3	1.5e-2	1.8e-2
External Air Flow:				
Water Evaporation (kg/s)	0.0	0.0	0.0	0.0
Annulus Air Flow (kg/s)	3.9	3.9	7.9	8.5
Annulus Air Δ T (deg K)[b]	3.4	3.7	4.6	5.0
Heat Balance Summary:				
Internal Steam and Condensate (W/m^2)[c]	734.4	986.6	1780.9	2190.6

[a] Uniform Steam Inlet Arrangement

[b] $\Delta T = T_{outlet} - T_{inlet}$

[c] Based on an effective wall area = 20.25 m^2

Table 3.2 AP600 PCCS Test Data and Results for Wet Operation[a]

	Test No.			
	12	13	17	18
Nominal Test Conditions:				
Test Vessel Inter. Pressure (Pa-gauge)	6.9e4	1.4e5	2.1e5	2.8e5
Test Vessel Inter. Pressure (Pa)	1.7e5	2.4e5	3.1e5	3.8e5
Annulus Air Velocity (m/s)	2.4	2.4	4.9	4.9
Annulus Air Inlet Temperature (K)	327.6	327.6	327.6	327.6
External Water Film Supply (kg/s)	1.9e-1	1.9e-1	3.0e-1	3.0e-1
Measured Conditions:				
Internal Steam and Condensate:				
Steam Inlet Pressure (Pa)	1.7e5	2.4e5	3.1e5	3.8e5
Steam Inlet Temperature (K)	394.3	413.3	420.8	425.0
Steam/Condensate Flow (kg/s)	2.8e-2	7.0e-2	1.3e-1	2.0e-1
External Air Flow:				
Water Evaporation (kg/s)	2.2e-2	6.1e-2	1.2e-1	1.7e-1
Annulus Air Flow (kg/s)	4.1	4.7	8.0	8.1
Annulus Air Δ T (deg K)[b]	-1.2	-1.1	0.3	0.8
Heat Balance Summary:				
Internal Steam and Condensate (W/m^2)[c]	3511.3	8444.2	15517.3	22836.2

[a] Uniform Steam Inlet Arrangement

[b] $\Delta T = T_{outlet} - T_{inlet}$

[c] Based on an effective wall area = 20.25 m^2

Table 4.1 CONTAIN Heat Transfer Summary[a] for Test 3 (w wall radiation)

Surface	T_{gas} (K)	T_i (K)	Q_r (Watts)	Q_c (Watts)	Q_m[b] (Watts)	Q_{net} (Watts)
1	390.4	385.6	770.5	474.4	29862.4	31107.3
2	305.9	383.3	-8817.8	-22124.7	0.0	-30942.5
3	305.9	315.7	8356.3	-5730.7	0.0	2625.6
4	302.29	314.8	0.0	-2625.6	0.0	-2625.6

[a] Summary excludes lower plenum heat transfer out of vessel which is 3017.97 Watts

[b] Condensate runoff = 7079.81 Watts

Table 4.2 CONTAIN Heat Transfer Summary[a] for Test 3 (w/o wall radiation)

Surface	T_{gas} (K)	T_i (K)	Q_r (Watts)	Q_c (Watts)	Q_m[b] (Watts)	Q_{net} (Watts)
1	401.4	398.09	743.35	369.38	30060.0	31173.0
2	306.05	395.73	0.0	-30701.2	0.0	-30701.2
3	306.05	305.17	0.0	603.17	0.0	603.7
4	302.2[a]	304.98	0.0	-605.0	0.0	-605.0

[a] Summary excludes lower plenum heat transfer out of vessel which is 2105.5 Watts

[b] Condensate runoff = 7813.02 Watts

Table 5.1 CONTAIN Heat Transfer Summary[a] for Test 17

Surface	T_{gas} (K)	T_i (K)	Q_r (Watts)	Q_c (Watts)	Q_m[b] (Watts)	Q_{net} (Watts)
1	388.59	380.16	2755	5630	2.64e5	2.67e5
2	328.23	341.3	-4792	-4097	-2.63e5	-2.72e5
3	328.23	326.64	3928	795.3	0.0	4723
4	302.04	325.1	0.0	-4723	0.0	-4723

[a] Summary excludes lower plenum heat transfer out of vessel, which is 3.0425e4 Watts

[b] condensate runoff = 5.888e4 Watts

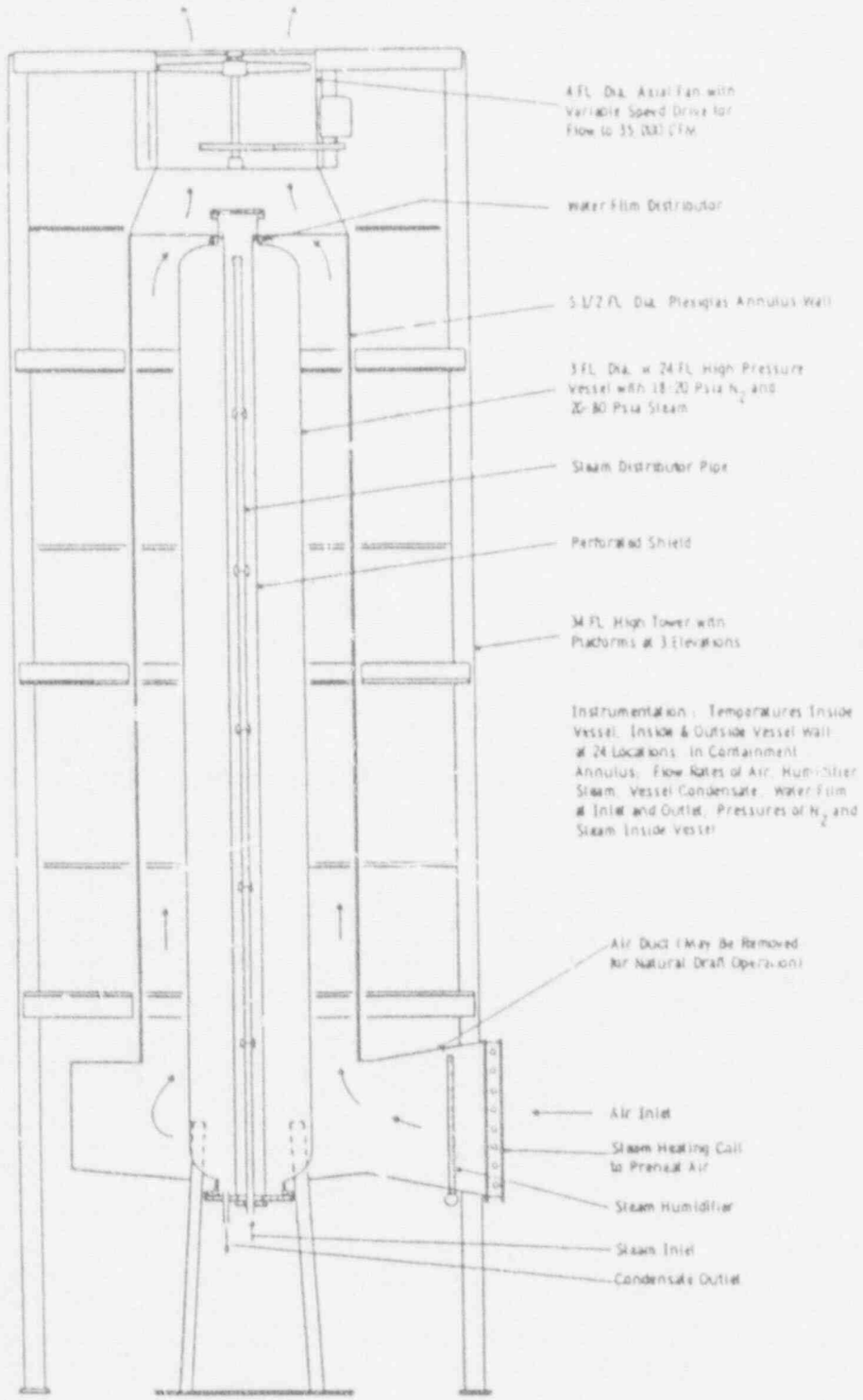

Figure 3.1 AP600 Passive Containment Cooling Integral Test Facility [11]

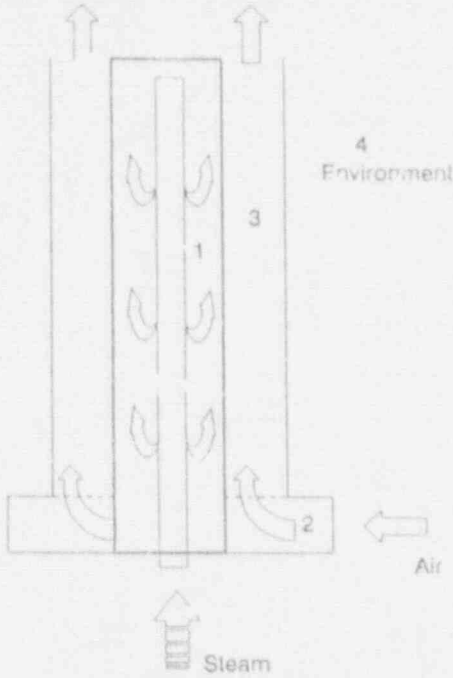

Figure 4.1 CONTAIN nodalization model of the Integral Test Facility where cell #1 is the pressure vessel, cell #2 is the plenum, and cell #3 is the air duct.

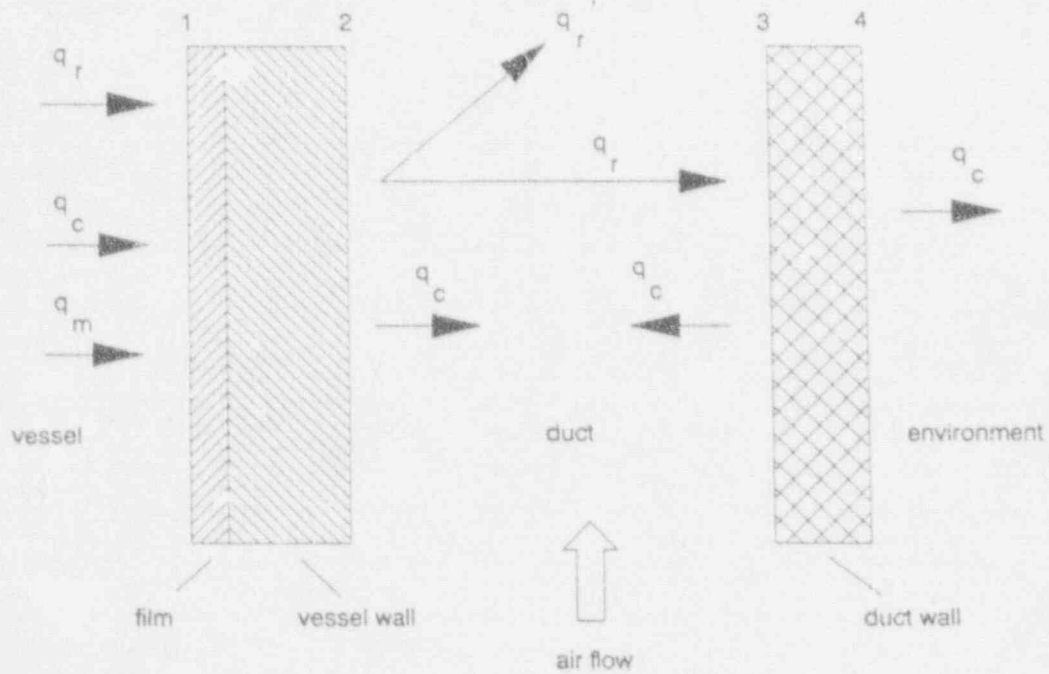

Figure 4.2 Heat and mass transfer phenomena modeled in CONTAIN for the dry outer vessel wall Integral PCCS tests (see Section 2 for terminology).

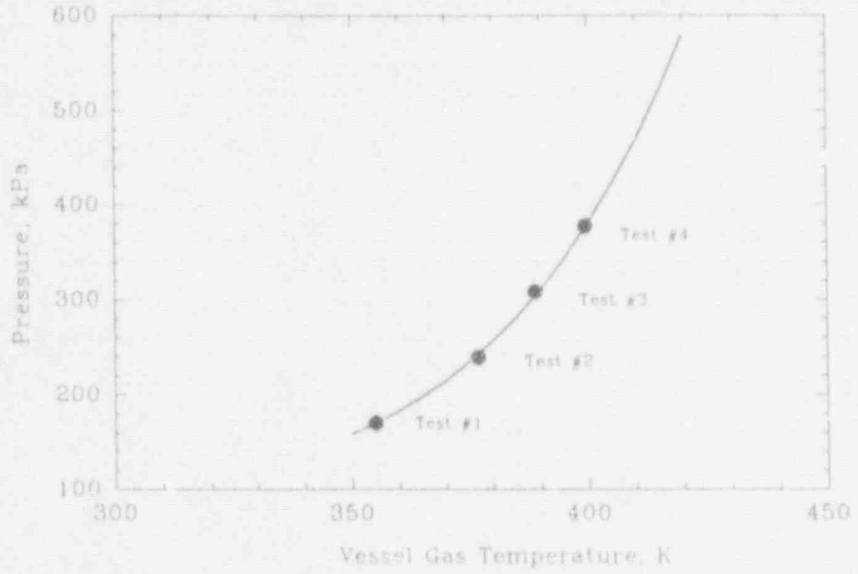

Figure 4.3 Vessel steam/gas mixture pressure versus temperature for saturated steam conditions

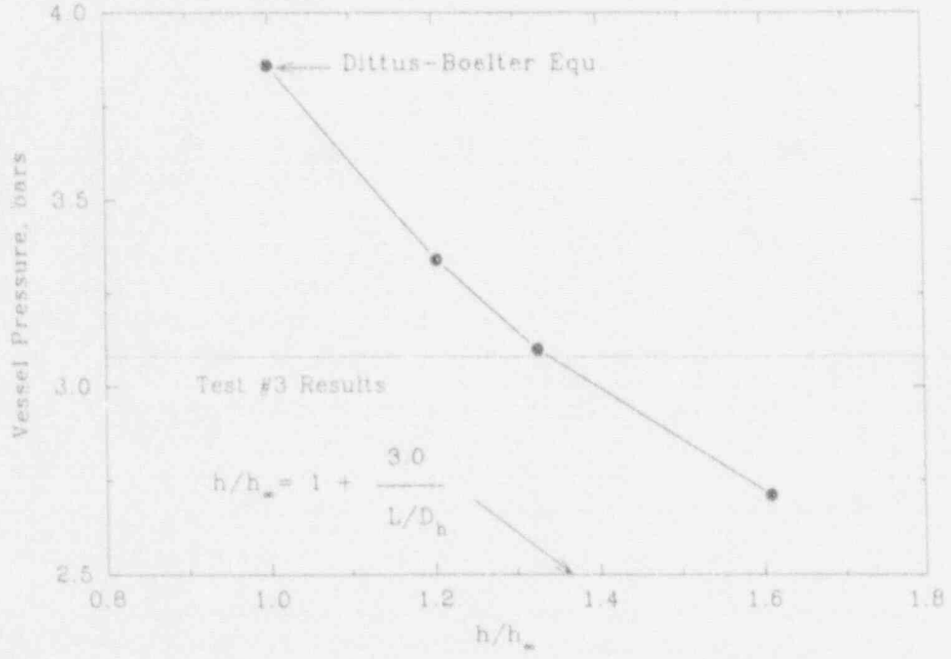

Figure 4.4 Calculated vessel pressures for various entrance length correction factors applied to the Dittus-Boelter equation for duct heat transfer (Test #3)

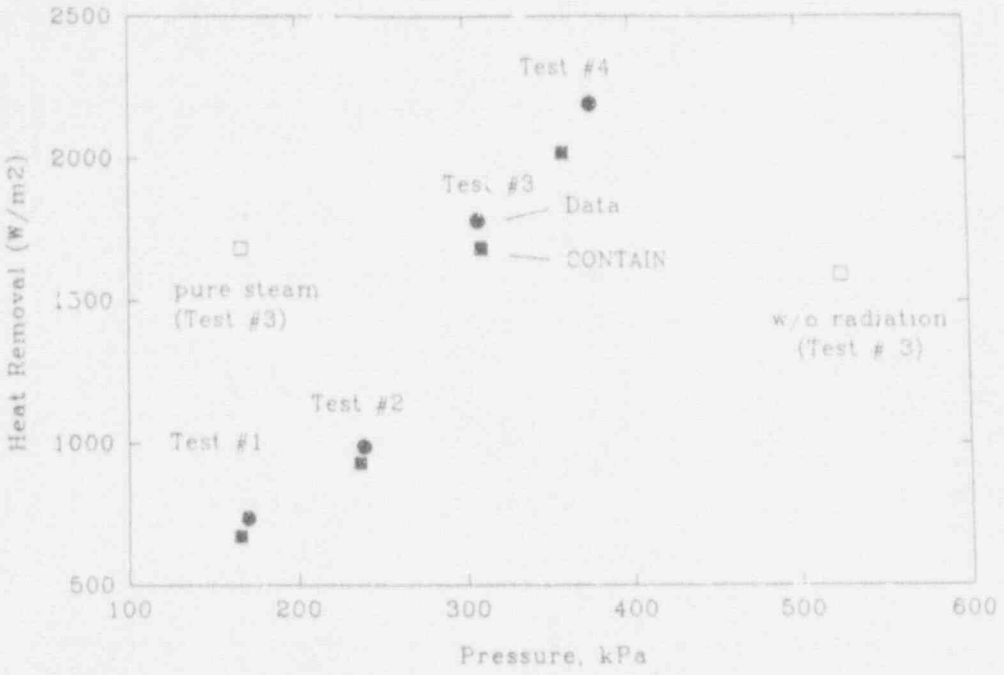

Figure 4.5 Comparison of CONTAIN calculations and Integral Test data for dry tests (open symbols indicate sensitivity studies)

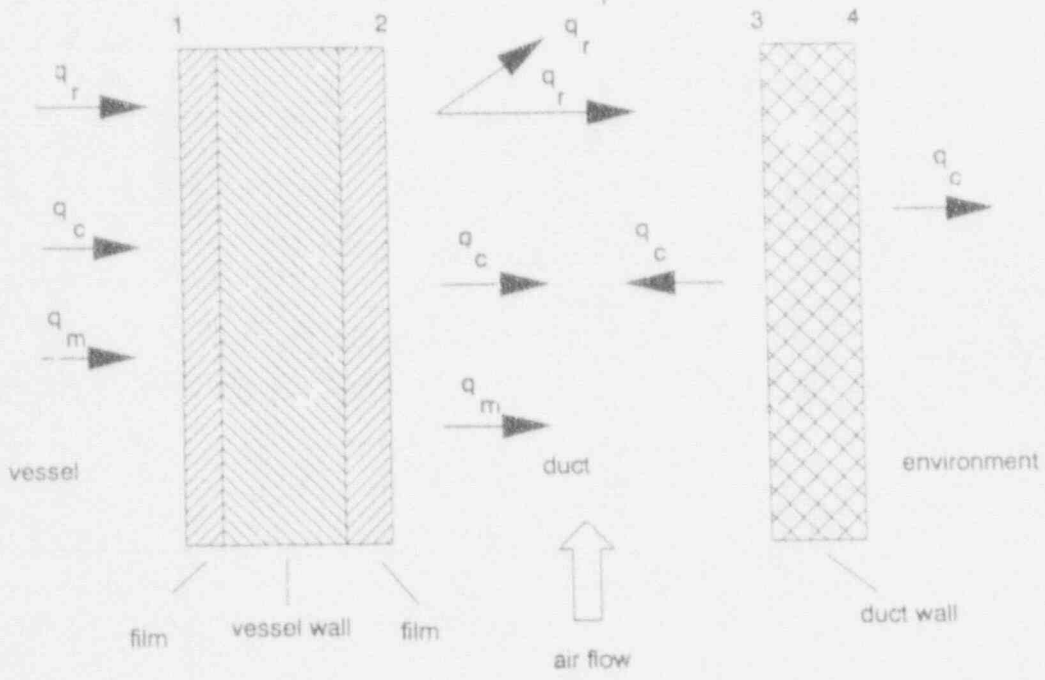

Figure 5.1 Heat and mass transfer phenomena modeled in CONTAIN for the wet outer wall Integral PCCS tests (see Section 2 for terminology)

Figure 5.2 Flow patterns assumed for steam/gas mixture on the inside vessel wall for (a) dry and (b) wet integral tests

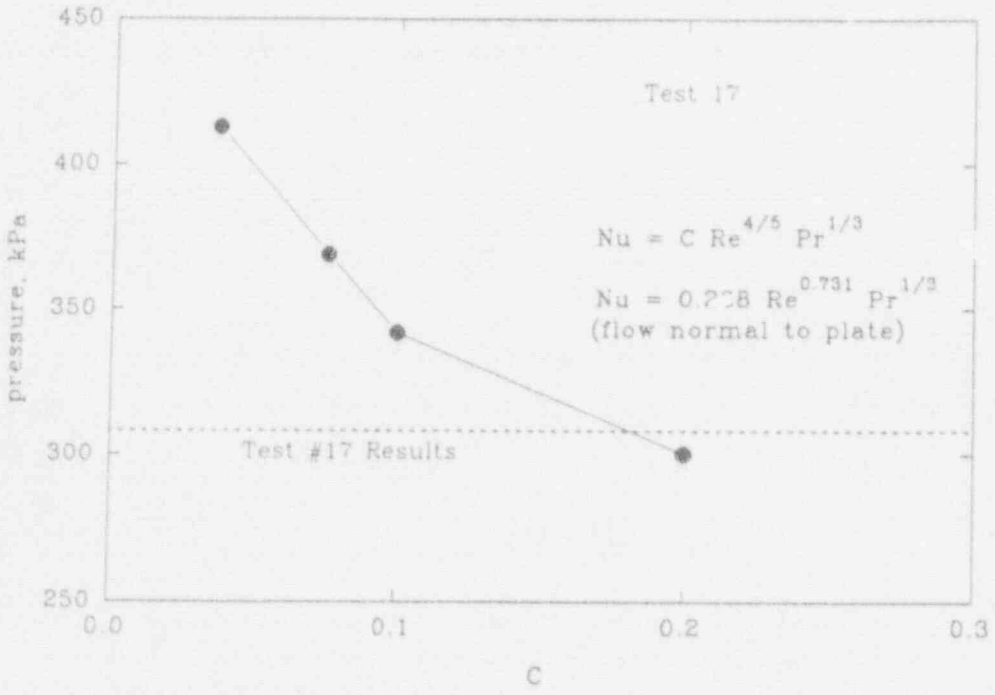

Figure 5.3 Vessel pressure sensitivity to the multiplication coefficient, C, in the Nusselt heat transfer correlation given by Equation (5.4) with m=4/5 and n=1/3.

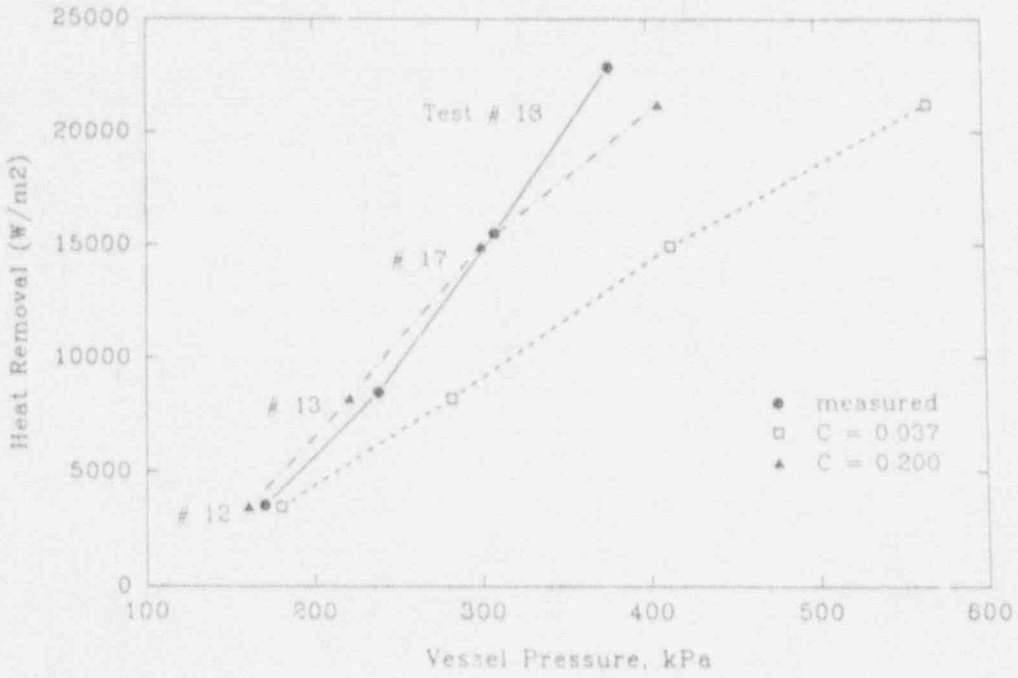

Figure 5.4 Comparison of CONTAIN calculations with two values for the coefficient C (see Figure 5.3) and Integral Test measured data for selected wet tests (uniform steam injection)

1

IMAGE EVALUATION TEST TARGET (MT-3)

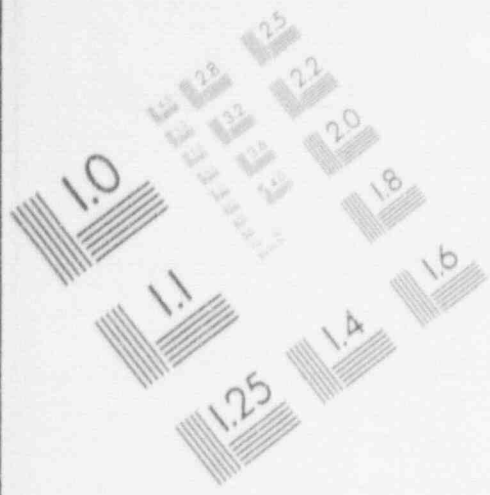

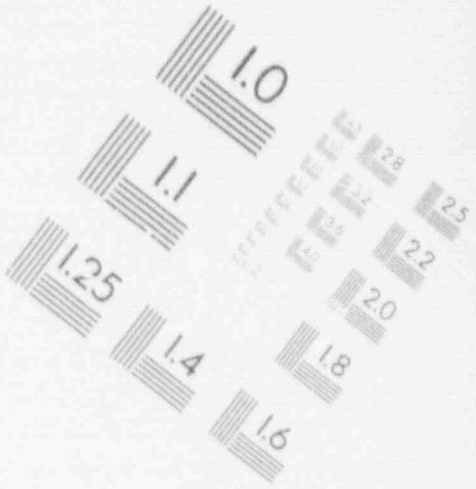

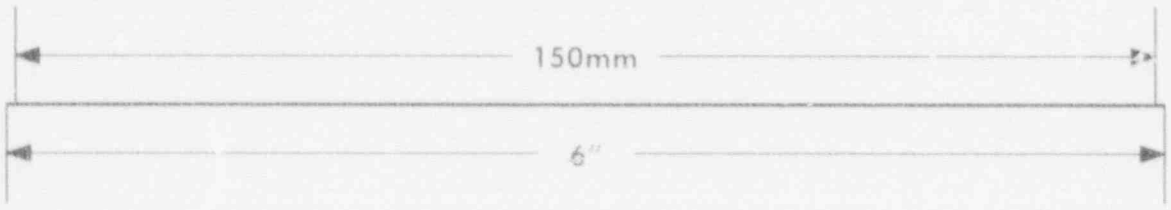

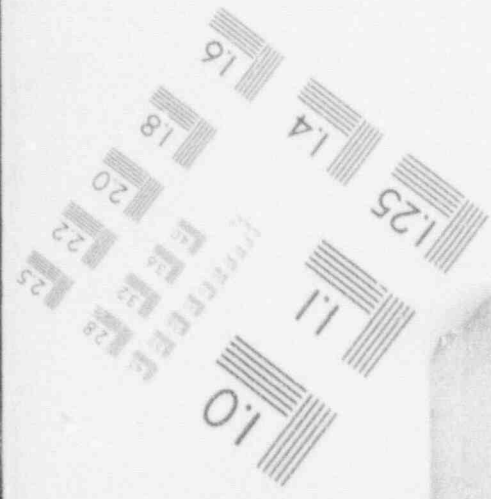

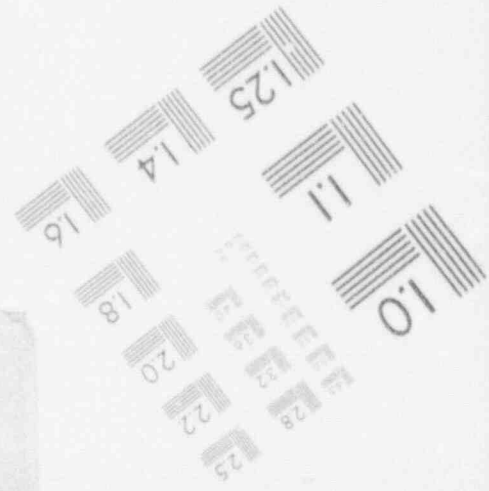

1

IMAGE EVALUATION TEST TARGET (MT-3)

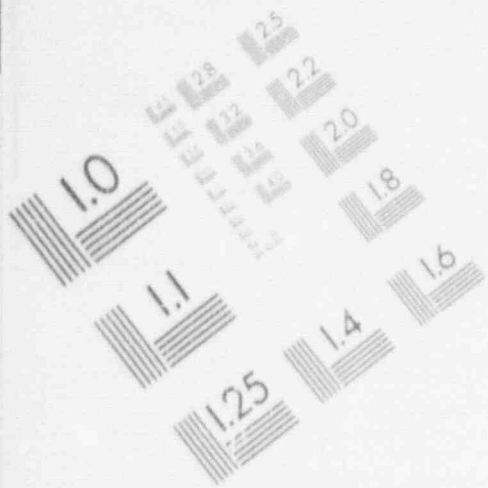

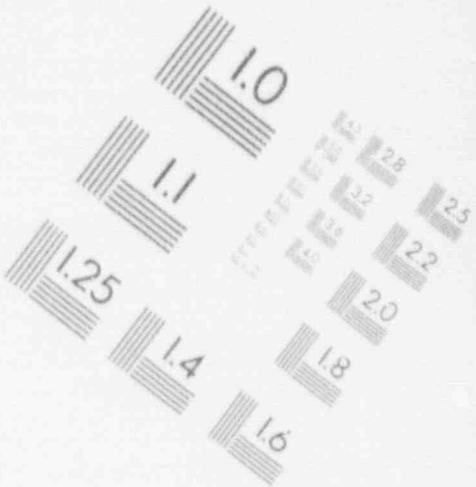

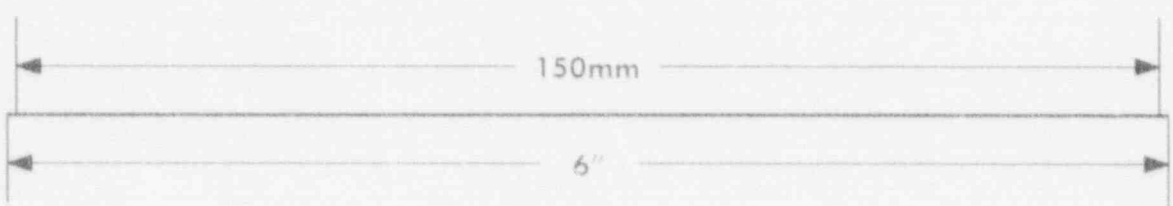

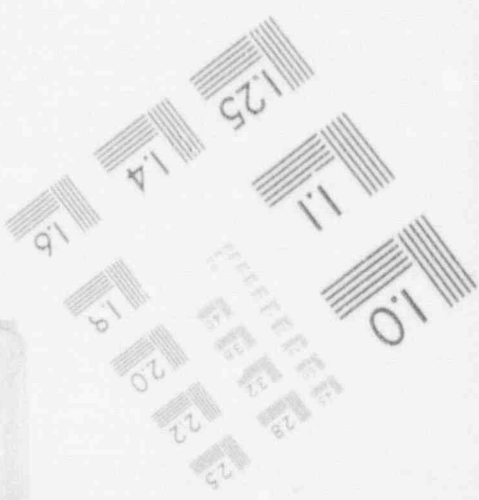

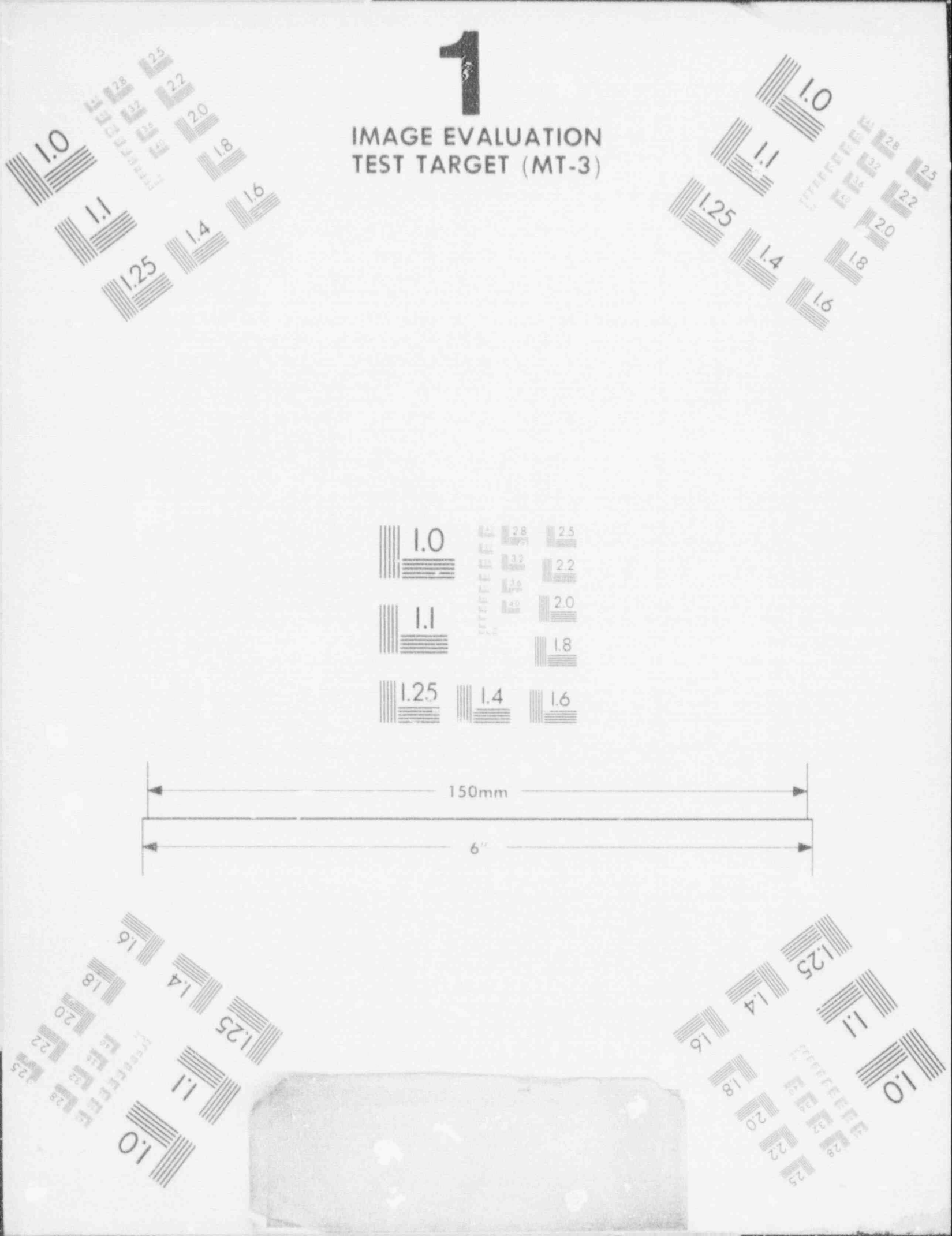
1
IMAGE EVALUATION
TEST TARGET (MT-3)
1.0
1.1
1.25
1.4
1.6
1.8
2.0
2.2
2.5
2.8
3.2
3.6
4.0
150mm
6"

SAND91-1459C

AN APPROACH FOR ASSESSING ALWR PASSIVE SAFETY SYSTEM RELIABILITY[a]

Tania M. Hake

Reactor Systems Safety Analysis Division
Sandia National Laboratories
Albuquerque, New Mexico 87185

ABSTRACT

Many advanced light water reactor designs incorporate passive rather than active safety features for front-line accident response. A method for evaluating the reliability of these passive systems in the context of probabilistic risk assessment has been developed at Sandia National Laboratories. This method addresses both the component (e.g. valve) failure aspect of passive system failure, and uncertainties in system success criteria arising from uncertainties in the system's underlying physical processes. These processes provide the system's driving force; examples are natural circulation and gravity-induced injection. This paper describes the method, and provides some preliminary results of application of the approach to the Westinghouse AP600 design.

INTRODUCTION

A program to develop and implement a method for evaluating passive system reliability in advanced light water reactors (ALWRs) is being conducted at Sandia National Laboratories (SNL). The purpose of this paper is to provide a brief overview of this method and results obtained thus far.

Many of the ALWR concepts proposed for the next generation of nuclear power plants rely on passive rather than active systems to perform safety functions. Despite the reduced redundancy of the passive systems as compared to active systems in current plants, the assertion is made that the overall safety of the plant is enhanced due to the much higher expected reliability of the passive systems. In order to investigate this assertion, a study is being conducted at SNL to evaluate the reliability of ALWR passive safety features in the context of probabilistic risk assessment (PRA).

The term "passive" as used here refers to systems which rely heavily on natural processes such as natural circulation to perform their function, rather than on

[a]This work is supported by the United States Nuclear Regulatory Commission and is performed at Sandia National Laboratories, which is operated for the U.S. Department of Energy under Contract Number DE-AC04-76DP00789.

decidedly "active" components such as pumps. However, many passive safety systems do contain mechanical components, valves in particular, that must change state for the system to operate. Generally these valves will have to change state only once during their mission, and motive power is in the form of stored energy such as compressed air or battery power.

Fast reactor PRA methods are directly applicable for the component failure aspect of passive system modeling. On the other hand, accounting for uncertainty in the natural processes involved in passive system operation requires an alternate approach. This is essentially an uncertainty in the success criteria for the passive systems. Specifically, given proper component functioning (valves open or close as required), a measure is needed of the degree of certainty that the natural process (natural circulation, gravity-induced flow, evaporative cooling, etc.) provides the fluid driving force or heat removal required to avert core damage. This uncertainty derives to some degree from uncertainty in parameters associated with the process of interest, such as heat transfer coefficients or friction factors. Further considerations include initial or "boundary" conditions, such as break location for a loss of coolant initiating event, and thermal-hydraulic modeling uncertainties.

OBJECTIVES/SCOPE

The objective of this study is to compare the reliability of passive safety systems in an ALWR with the reliability of corresponding active safety systems in a current generation reactor. The quantification of passive system reliability is not as straightforward as for active systems, due to the lack of operating experience, and to the greater uncertainty in the governing physical phenomena. Thus, the adequacy of current methods for evaluating system reliability must be assessed, and alternatives proposed if necessary.

For this study, the Westinghouse Advanced Passive 600 MWe reactor (AP600) was chosen as an "example" advanced reactor for analysis, because of the availability of AP600 design information. This study will compare the reliability of AP600 emergency cooling systems with that of corresponding systems in a current generation reactor. The evaluation of passive system reliability will take place in the framework of PRA, so that the final results can be compared in a direct way to measures (e.g. core damage frequency, CDF) of current plant safety.

The comparison between current and advanced reactor designs will be on the functional level, rather than on a system-by-system basis. The reason is that it is not generally possible to identify a single system in the ALWR design which directly corresponds to a single system in a current plant. Rather, a collection of systems in the advanced reactor performs the same function as a usually larger collection of systems in a current plant.

The function of interest for this study is the emergency cooling function, conditional on reactivity control following an accident initiating event. In other words, reactivity control systems will not be analyzed, but will be assumed to be 100% reliable. Analyzing reactivity control in addition to emergency cooling would introduce a great deal of complexity without much added

benefit for demonstrating the methodology. Here, emergency cooling refers not only to those systems required to inject coolant, but also to remove decay heat.

The performance of the emergency cooling function will be evaluated for response, starting from full-power conditions, to a typical set of PRA internal initiating events: transients and loss-of-coolant accidents (LOCAs). This will allow direct comparison to the response of current reactor systems to these initiators. The issue of identifying potentially new initiating events for the AP600 is being addressed in a separate, related NRC-sponsored analysis.

BRIEF AP600 DESIGN DESCRIPTION

This section presents an brief overview of the more pertinent aspects of the AP600 design. A multitude of references in the literature can provide more information regarding the design. The following description and figures are based on references [1], [2], and [3].

The design approach for the AP600, as for other ALWR concepts, involves simplification to improve economics, construction, maintenance, operation, and safety. Passive safety systems are employed which use natural driving forces only, and minimal dependence on support systems. Active non-safety systems perform during normal plant operations, and also provide backup to the passive safety systems in response to accidents.

The 600 MWe PWR incorporates a low power density core, and no bottom-head vessel penetrations. The reactor coolant system contains two hot legs and four cold legs, with two standard Model "F" steam generators (SGs), four canned-motor reactor coolant pumps (RCPs), and a 1300-cubic-foot pressurizer. The RCPs are mounted integrally to the SGs, which eliminates the pump suction leg piping. Figure 1 provides a depiction of the reactor coolant system (RCS).

Passive decay heat removal for response to transient initiators (after failure of normal, active systems) is provided by the passive residual heat removal (PRHR) system. Figure 2 is a simplified schematic of the system, which incorporates three heat exchangers housed in a large tank, the in-containment refueling water storage tank (IRWST). Natural circulation drives the fluid from the surge line of the pressurizer, through the heat exchangers, to the cold-leg side of the steam generator. The heat exchangers are cooled by the fluid in the IRWST, also through a process of natural circulation within the tank.

Passive coolant injection following loss of coolant accidents is provided by a redundant arrangement of high- and low-pressure injection systems. These systems feed into the reactor vessel via two safety injection, or direct vessel injection (DVI), lines. Figure 3 provides a depiction of the passive safety injection systems. The high pressure passive injection systems are the core makeup tanks (CMTs) and the accumulators (ACCs). The two CMTs are capable of injecting by gravity at any reactor pressure, because of pressure-equalization lines from the RCS cold legs to the top of the CMTs. Two accumulators, similar to current PWR accumulators, are maintained with a nitrogen overpressure of approximately 700 psi. One CMT and one accumulator feed each DVI line.

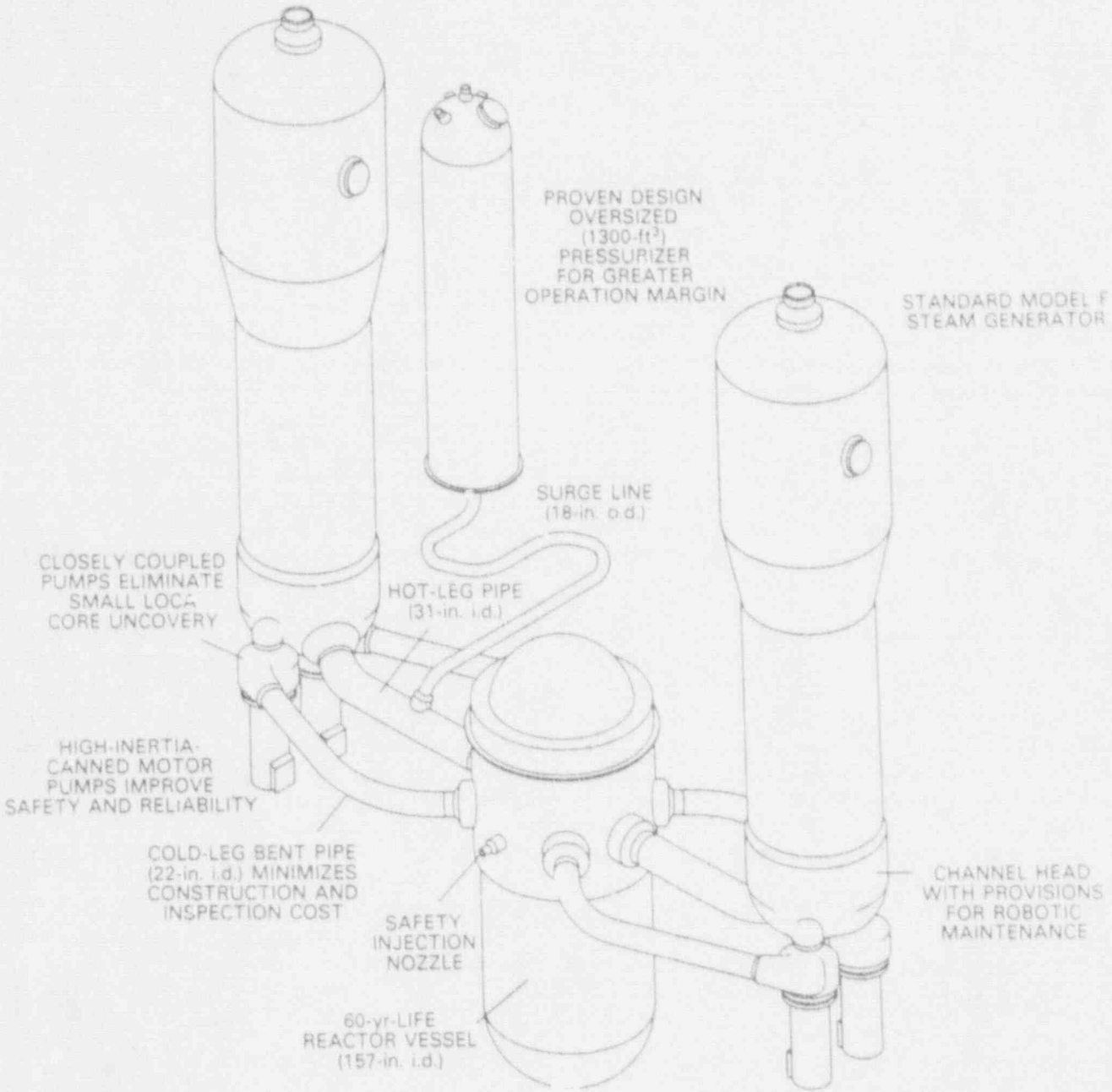

Figure 1. AP600 Reactor Coolant Loop. [1]

Figure 2. Passive Residual Heat Removal System Simplified Schematic. [3]

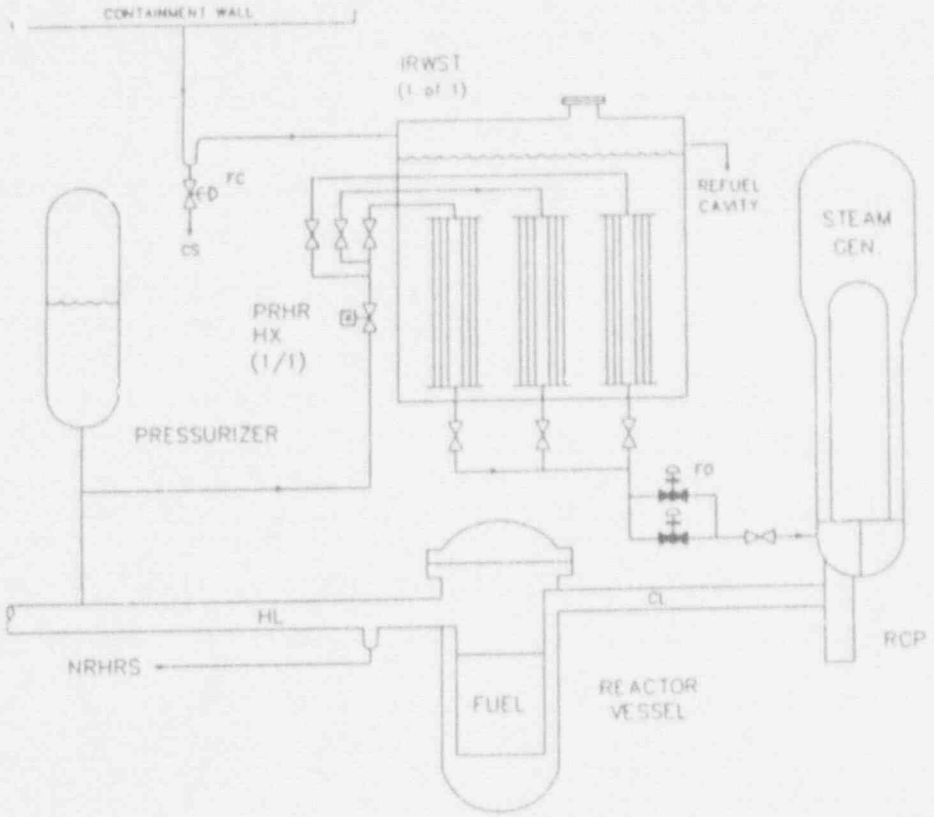

Figure 3. Passive Safety Injection Systems Simplified Schematic. [3]

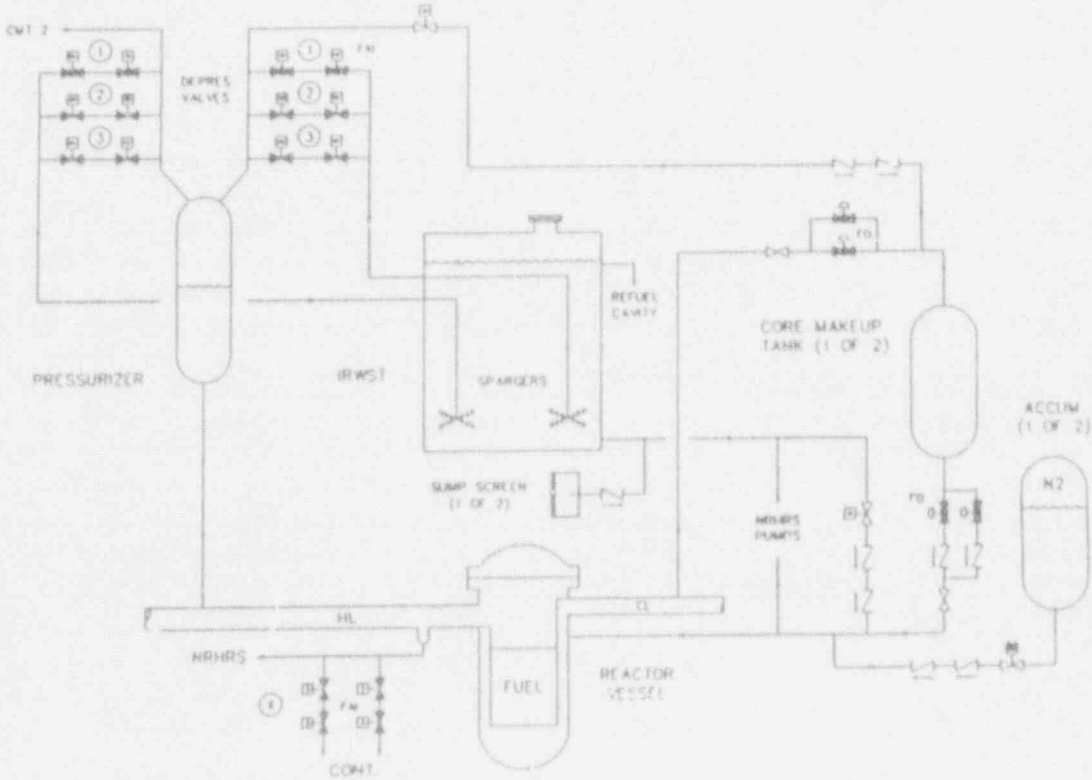

A four-stage automatic depressurization system (ADS) is employed to allow the use of low-pressure passive injection systems, or "feed and bleed" cooling following an accident initiator. For low pressure, longer term coolant injection, the ADS actuates to reduce RCS pressure to near-containment atmospheric. Then the IRWST can inject via gravity-induced flow through two redundant lines, one to each DVI line.

The passive containment cooling system, shown in Figure 4, provides heat removal to the ultimate heat sink during use of the passive core cooling systems, and controls containment pressure. The containment is cooled by natural convection of air, as shown in Figure 4, and assisted by evaporative cooling of fluid sprayed onto the exterior surface of the steel containment vessel.

APPROACH

This section describes a method developed to meet the objective for this study of comparing the emergency cooling functional reliability for the AP600 to that for a current generation reactor. The specific steps to be performed are outlined below. Existing methods and screening techniques are proposed where possible to efficiently attack the problem. The method which has been developed should be generally applicable to any advanced reactor concept's passive features, although this has not been investigated in depth.

Three phases form the approach to this study of passive system reliability: (1) methodology development and component failure quantification, (2) natural process assessment methodology demonstration, and (3) passive system reliability method implementation. The method developed in phase 1 involves splitting the problem into two parts: (1a) the aspects that current PRA techniques can address (component failure quantification), and (1b) aspects for which a new technique is needed (natural process assessment). The natural process assessment portion involves an interim demonstration phase, where the method is applied to a small portion of the problem to verify its merit and identify any problems (phase 2). Upon successful completion of the phase 2 demonstration, phase 3 will involve full method implementation for the AP600 emergency cooling function.

At this time, phase 1 is essentially complete, and work has begun on phase 2. A draft NUREG/CR documenting the results of phase 1 is currently being distributed for comment at NRC. A brief discussion of the results of the phase 1 quantification follows this section describing the program approach.

In developing the methodology, the goal was to maximize use of existing PRA technology, in this case NUREG-1150 [4] methods. Further, a literature survey formed the starting point for the methodology development task, to identify any potentially useful methods which have been proposed or applied for analyzing advanced reactors. From this survey it was apparent that nearly all past studies of passive reactor designs quantitatively consider only the component failure aspect of passive system failure. One study, however, quantitatively examined uncertainties in inherent shutdown processes for an advanced liquid metal reactor by propagating uncertainties through an analysis code [5]. The method developed for this study incorporates an analogous approach.

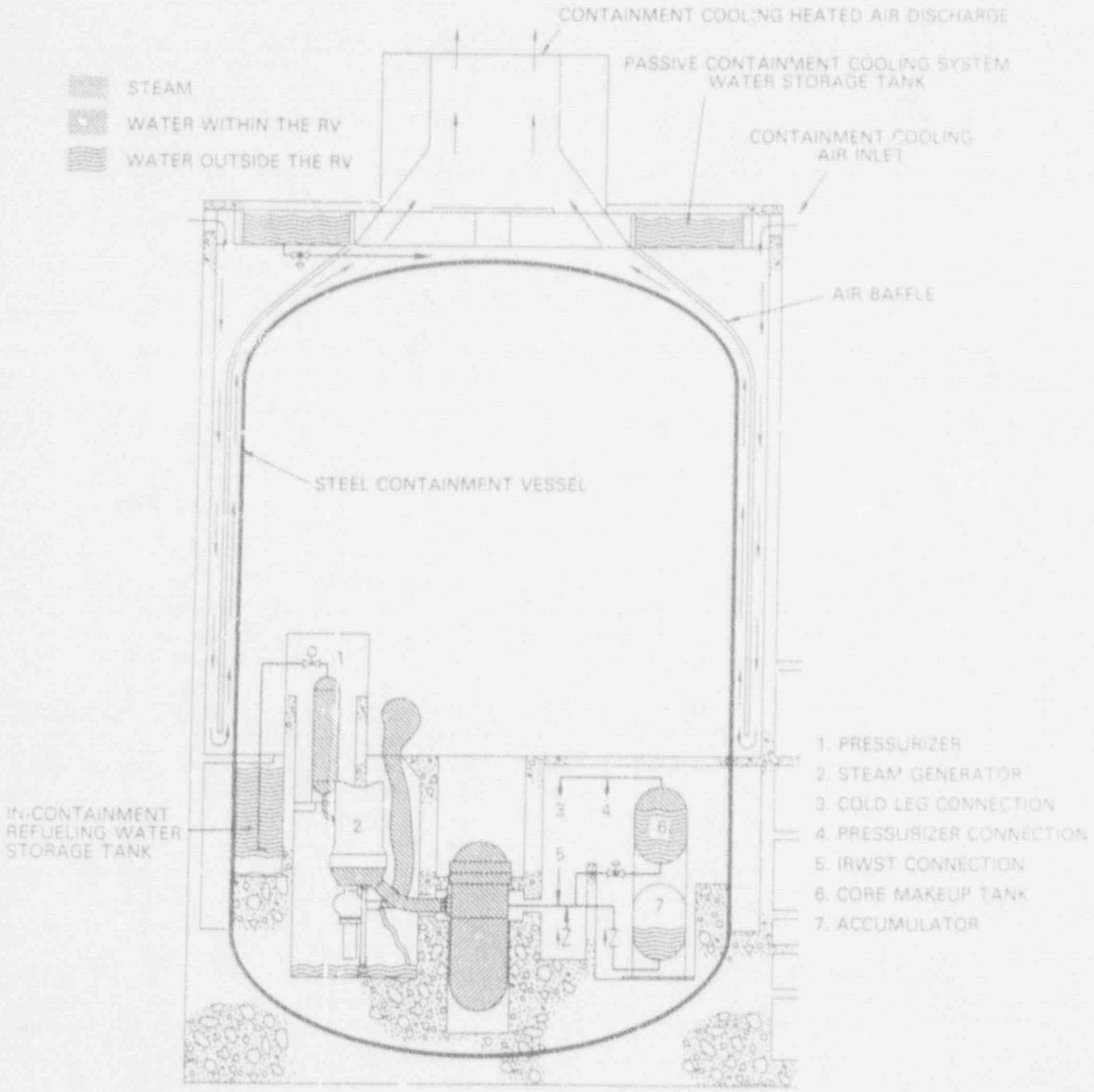

Figure 4. Passive Safety Injection During LOCA Initiation. [1]

As indicated in Figure 5, the methodology developed for this program can be grouped into five steps:

(1) System-level qualitative analysis to identify systems with potentially important natural process uncertainties,
(2) In-depth sequence-level component failure quantification using NUREG-1150 Level 1 methods,
(3) Sensitivity calculations to evaluate importance of success criteria uncertainties,
(4) Assessment of contribution to mean core damage frequency from uncertainties associated with the natural processes involved, and
(5) Combination of results from the sequence-level component failure analysis and natural process assessment.

The remainder of this section presents a more detailed discussion of each of these steps.

STEP 1: System-level qualitative analysis

The purpose of the system-level qualitative evaluation is to gain a better understanding of the passive systems to be analyzed, and the natural processes upon which they rely for their driving force. In addition, we seek a rough prioritization of passive systems, based in large part on the expected importance of process uncertainties to system failure. This amounts to a preliminary screening of systems for which detailed natural process assessment (Step 4 of the method) will be applied. This prioritization is necessary because of the resource-intensive nature of natural process assessment.

The system-level evaluation begins with investigating the components, such as valves or tanks, which must operate within each passive system. A high-level screening fault tree model of the component failures is constructed, to provide a rough quantitative measure of system failure probability based on component failures only. Next one examines the types of passive systems to be analyzed, and identifies the natural processes on which they depend for their operation. These processes may include alternative motive fluid forces, such as gravity or gas-pressure, or heat transfer processes, such as natural convection or radiative cooling.

A screening comparison is then made between the contribution to mean system failure probability from failure of its components, and the expected importance of natural process uncertainties. In other words, if the components which must function for a passive system to operate have a high failure probability, then any uncertainty in their natural processes will likely be less important to overall system failure. For this preliminary evaluation, the level of natural process uncertainty importance is determined primarily using engineering judgment; thermal-hydraulic models are not constructed until Step 4. The engineering judgment can be based on such considerations as current-generation plant information, vendor analyses and tests, and rough system performance calculations. For example, the uncertainty in a flow loss coefficient in the downstream piping of a gravity flow system may be more or less important, depending on the level of design margin in the head of the fluid. The result

Figure 5. Simplified overview of ALWR passive system reliability evaluation method

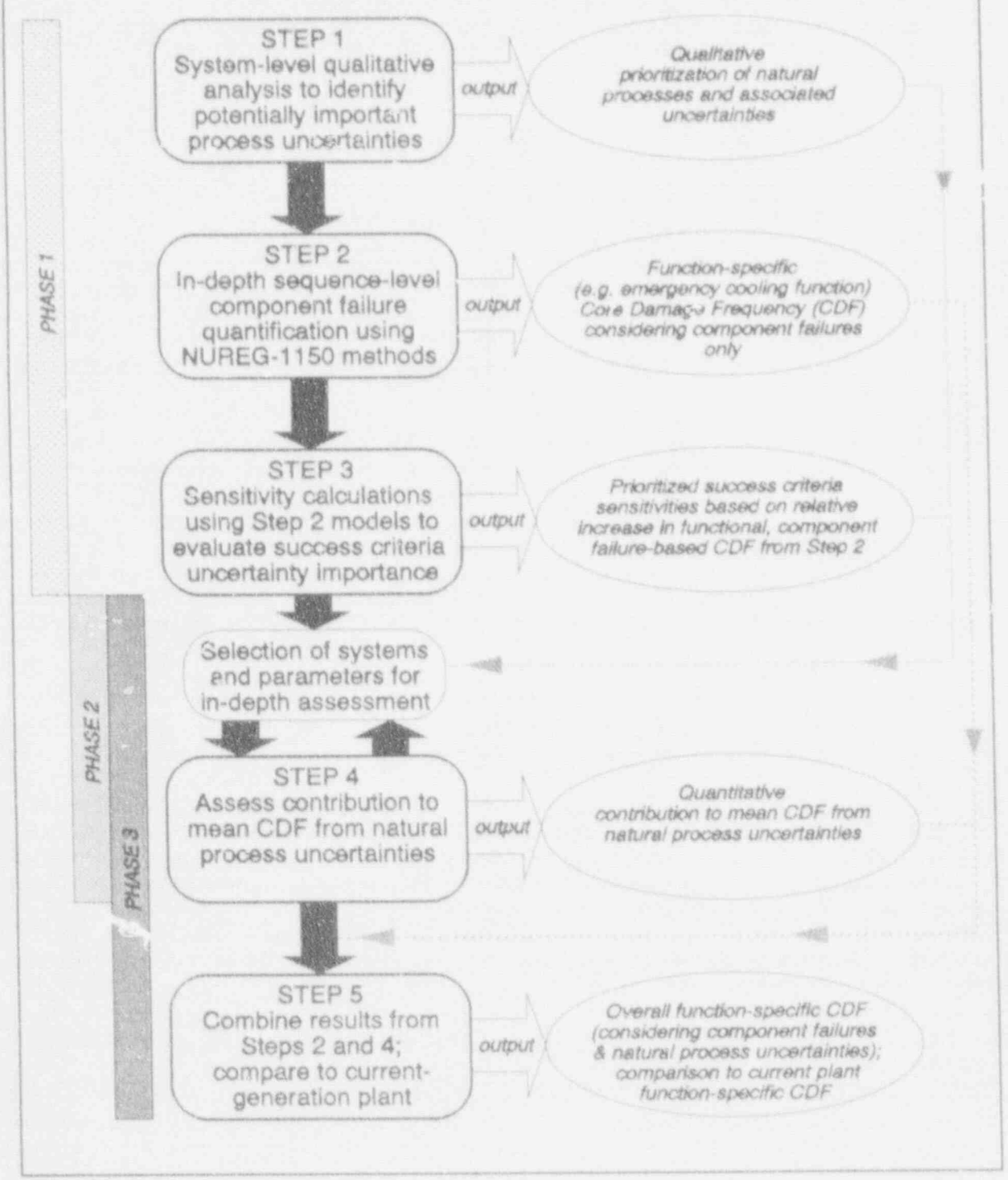

of this system-level analysis is a coarse prioritization of passive systems based on natural process importance.

STEP 2: Sequence-level component failure quantification

The next step of phase 1 involves in-depth analysis of component failures. NUREG-1150 PRA methods [4,6] are used here. Four distinct tasks are involved:

(1) Event tree development
(2) Fault tree model development
(3) Data, common cause, and human reliability analyses
(4) Quantification of core damage frequency for base case

Event trees delineate the systems which can be used to fulfill a specific function (emergency cooling for this analysis) in response to an accident initiator. For the AP600 this includes credit not only for passive safety systems but also active non-safety systems. Fault tree models are constructed to represent component failures for the systems of interest, including any support system requirements. In the event and fault tree development, a "base-case" set of success criteria is assumed, based for example on preliminary vendor analyses.

Failure data from past PRAs and existing databases are applied to the component failure basic events. Current plant data are generally applicable due to similarities of components included in advanced reactor designs and in current operating units (particularly true for the AP600). There are some exceptions which result from differences in areas such as component usage or system safety classification (i.e. safety versus non-safety grade). Here, the current data can be supplemented with such items as vendor test data, the EPRI ALWR Requirements Document goals for component reliability [7], and expert opinion.

The data analysis task includes a common cause analysis as well as pre- and post-initiator human reliability analyses (HRA). For the HRA, numerous assumptions are generally necessary for an advanced design, because of lack of operating procedures and knowledge of specific plant operator practices.

Once fault and event tree models have been built and the database developed, a "base-case" quantification of functional core damage frequency is performed. For the AP600, this step results in an emergency cooling function CDF based on Westinghouse-specified success criteria. This forms a baseline for later comparison in Step 3. In addition, the models and results of this task will be combined with the results from Step 4 (natural process assessment). The result will be an overall measure of passive cooling system reliability, considering both component failures and natural process uncertainties.

STEP 3: Sensitivity calculations to evaluate success criteria importance

A primary focus of this study is uncertainty in the natural processes governing passive system operation. This translates, as mentioned previously, to uncertainty in the success criteria for the various systems used in accident response. One can examine cases where the components of a passive system have

functioned according to "base-case" system success criteria, e.g., the proper combination of valves have changed state. If inadequate flow or heat removal is realized due to uncertainties in the natural processes involved in the system's operation, then a more restrictive set of success criteria applies.

Say, for example, that in a natural circulation, passive heat removal system, two of three heat exchangers are necessary according to base-case success criteria. However, a greater-than-expected flow loss coefficient may apply due to corrosive processes or other uncertainties in the natural circulation loop. The flow in the loop may then be inadequate to remove core heat. Perhaps three of three heat exchangers are required in this case to generate a great enough temperature differential and provide a greater fluid driving force.

To investigate the importance of potentially more restrictive success criteria, which may apply due to natural process uncertainties, the fault and event tree models from Step 2 are modified to reflect the more limiting criteria. The point-estimate CDF is then requantified for each case to examine the change relative to the base-case CDF. For this study, three different types of sensitivity calculations are investigated:

(1) within-system success criteria sensitivities
(e.g., requiring two-of-two instead of one-of-two trains of a passive system);
(2) cross-system success criteria sensitivities
(e.g., postulating that after success of one passive system, which leads directly to aversion of core damage for the base case, another system is postulated to be required); and
(3) passive system risk increase importance
(here, the passive system is assumed to fail, even if the system components function properly according to system success criteria).

The first and second groups deal with the effect of degraded passive system performance. That is, the system operates at a level of effectiveness not adequate to prevent core damage alone, and requires either an additional train of the same system, or another system operating in concert, to avert core damage. The third group addresses cases where the passive system components function according to base-case success criteria, but the natural processes are completely ineffective. The passive system is therefore failed, and the "backup" systems which can be used following system failure are added as branch points in the event tree. In other words, the system's failure path in the event tree is followed. These sensitivity calculations should consider correlations among systems, i.e., whether failure of one passive system due to natural process inadequacies implies failure of other passive systems possibly dependent upon the same natural process.

The results of these sensitivity analyses will provide guidance as to which passive systems are more important to core damage frequency, given different levels of degraded performance due to natural process uncertainties. A quantitative prioritization can be constructed based on largest increase in CDF relative to the base case. This will aid in selection of passive systems and associated natural processes for analysis in Step 4, natural process assessment.

STEP 4: Natural process assessment

As mentioned previously, the second phase of the program will examine the feasibility of the natural process assessment methodology. This methodology will be applied to only a few accident sequences in phase 2, to demonstrate the method. Such a demonstration is needed because the approach for natural process assessment is resource-intensive. Upon successful demonstration, a comprehensive implementation of the methodology will be completed in phase 3. This section briefly describes the natural process assessment method.

In order to incorporate natural process uncertainties in the quantification of passive system reliability, selected accident sequences involving passive system operation are analyzed using thermal-hydraulic models. Only sequences which indicate successful component functioning for the passive system(s) of interest will be analyzed. That is, we are interested only in situations where the natural process uncertainties may negatively impact overall core damage frequency. Here, although the mechanical components have operated correctly to meet the assumed system success criteria, uncertainties in parameters such as heat transfer coefficients or as-built dimensions of components may result in inadequate flow or heat removal by the passive system(s). A more restrictive set of success criteria applies, with a particular degree of certainty.

The sequences to be analyzed are selected based on the results of Steps 1 and 3: qualitative information on the expected importance of the natural process to passive system operation, and quantitative results of the component failure sensitivity calculations. The sequence-level approach to the analysis is necessary because evaluation on the system level, i.e. one passive system at a time, would not consider the influence of other passive and active systems which operate (or fail) in the sequence. Thus, each sequence potentially represents a unique set of conditions affecting the outcome of the thermal-hydraulic analyses, although some binning of similar sequences is possible.

First, thermal-hydraulic models of the ALWR are built. Sensitivity calculations are performed using the thermal-hydraulic code to determine the most important code input parameters, such as heat transfer or flow-loss coefficients. Next, expert elicitation is performed using the NUREG-1150 structured approach, to obtain distributions on values for the important input parameters. Latin Hypercube Samples are constructed from the distributions on the input parameters in order to build multiple input decks for the thermal-hydraulic code. The multiple code calculations are performed for a given sequence and the results analyzed to determine the contribution of the natural process uncertainties to overall sequence outcome. Output distributions are generated, and the results are finalized with input from the expert panel. In this final step, the experts will also be asked to provide measures of modeling uncertainties.

For phase 2 of this study (method demonstration), the above steps will be performed for a few sequences involving operation of AP600 passive systems associated with core cooling only, as opposed to including containment heat removal. The AP600's core and containment cooling systems are to a great extent coupled, and complete evaluation of the core cooling systems will require consideration of the containment systems. However, modeling of these coupled

processes will be a great deal more involved than modeling just the primary system. This comprehensive modeling is unnecessary for demonstration of the method. Such a complete analysis is to be performed in phase 3, the implementation phase, of the program.

STEP 5: Calculation of overall CDF and comparison to current plant

In this step, completed after the phase 3 implementation of Step 4, the results of Steps 2 and 4 are combined to provide an overall measure of the reliability of systems serving the emergency cooling function. The product of Step 5 is a complete distribution of the emergency cooling functional failure probability, considering component failures and natural process uncertainties in both core and containment heat removal processes. The result can be compared with the similar quantities for the current-generation reactor design. The current plant quantities can be extracted from an existing PRA of the current-generation plant.

For this study, Surry Unit 1 will be used as an "example" current plant for comparison. Surry is similar to the AP600 in that it is a Westinghouse pressurized water reactor. Further, a detailed PRA exists for Surry, since it was analyzed as part of the NUREG-1150 analyses [8].

RESULTS OF PHASE 1

To date, phase 1 of this program is complete. This section presents some preliminary calculational results of phase 1. A NUREG/CR draft documenting phase 1 in detail is currently being circulated at NRC for comment; the final report will be issued within two months after receipt of NRC comments.

Step 1 of the method, the qualitative system-level analysis, provided a coarse prioritization of passive systems in terms of expected importance of their natural process uncertainties. The systems found to be more important, and thus deserving of further analysis in the natural process assessment (Step 4), were those associated with natural circulation cooling in the primary and containment. This includes the PRHR system, and the internal containment recirculation involved in long-term IRWST injection.

The first result of the sequence-level quantification effort (Step 2 of the method) was a base case value for the CDF, considering only the emergency cooling function (i.e. conditional on successful reactivity control). Only internal initiators were included in the analysis. Westinghouse-specified success criteria were used to form the "base case". AP600 design changes through July 1991 were considered in the analysis. The results reported here should be viewed with caution, however, since the design is in a state of flux, and assumptions had to be made in cases where design detail was unavailable.

An additional assumption in the analysis involved assigning current plant check valve data (failure probability and uncertainty range) to the check valves in the gravity flow systems which operate under low pressure differentials. This assumption was based on a cursory analysis and expert guidance. Further, the testability of components was not considered in great detail.

The base case quantification, considering internally generated transients and LOCAs, resulted in an estimated mean CDF for the *emergency cooling function only* of 3.9E-6/yr. The 5th and 95th percentile values were 6E-7 and 1.1E-5/yr, respectively. This compares with a previously reported Westinghouse value for overall CDF of 1.2E-6/yr from a preliminary analysis (1989) [3], which was based on an earlier version of the AP600 design. The dominant initiator was predicted to be a small LOCA (69%), with the most dominant failures involving operator failure to properly align non-safety backup systems after failure of front-line passive systems.

This core damage frequency does not include natural process uncertainties. Step 3 of the method involves performing sensitivity calculations for varying success criteria assumptions. These calculations were performed to determine those systems that would have the greatest impact on the core damage frequency if the natural process failed to provide adequate driving force for the system, and the system success criteria were incorrect. These results provide input for selection of systems and processes for analysis in phases 2 and 3 of the study, where uncertainties in the natural processes are quantified.

As described above under the Step 3 methodology discussion, three cases of success criteria sensitivities were examined. Case 1 examined within-system success criteria variations, e.g. requiring two-of-two instead of one-of-two trains of a system. Case 2 looked at cross-system success criteria sensitivities, where more systems were postulated to be necessary than specified by the base case success criteria. The importance of each passive system was investigated in Case 3, by postulating that the passive system is totally ineffective.

Figures 6 through 8 provide the results for each case of the sensitivity studies, in terms of relative increase over the base-case results. As can be seen from Figure 6, the IRWST in the injection mode causes the greatest relative increase versus any other single system. CMTs and ACCs are important only when combined (more restrictive system success criteria for both systems). Figure 7 provides the results for Case 2 and combined Cases 1 and 2. Here, PRHR is shown to be important. The CMT/ACC combined case result is driven by incorporating the Case 1 CMT/ACC result. Finally, Figure 8 presents the Case 3 results. From this table, PRHR, IRWST, and CMT are the more important, although there is not a great distinction among any of the systems. They all involve an increase of about two orders of magnitude over the base-case CDF.

Based on these sensitivity studies, those systems determined to be most important are PRHR, CMT injection, and IRWST injection. These systems involve natural circulation in the primary (PRHR) and within containment (long-term IRWST injection), and gravity injection to the primary (CMT and IRWST injection). As discussed in the previous section, the method for explicitly addressing the natural process uncertainties in these key systems will be demonstrated in phase 2.

Figure 6. Case 1 Success Criteria Sensitivity Results

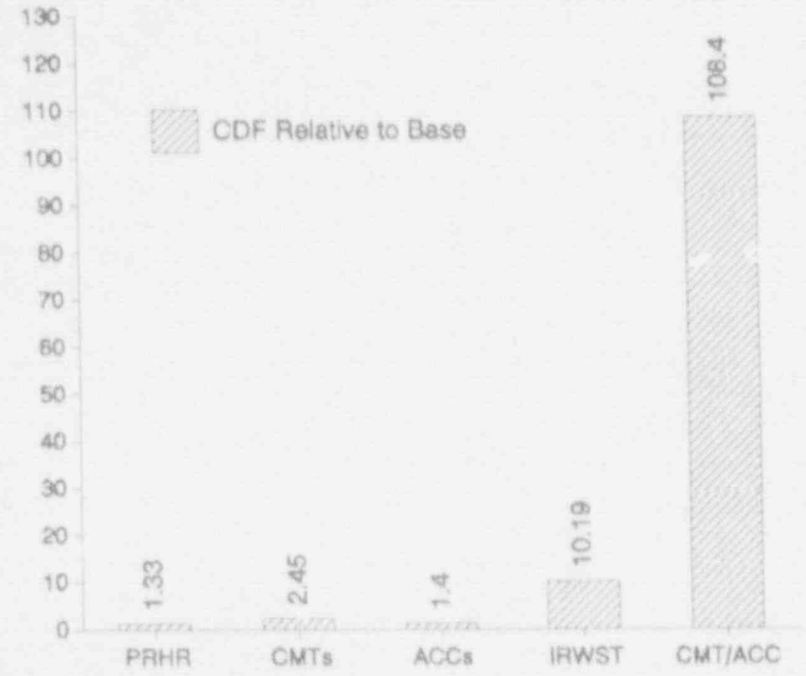

SUMMARY

A methodology has been developed to evaluate ALWR passive system reliability in the context of PRA. The method considers the component failure aspect of passive system failure, and quantitatively addresses uncertainties in the natural processes upon which these systems rely for their driving force. The Westinghouse AP600 serves as the example ALWR for demonstration of the method. The first phase of the program is complete, yielding an estimate for emergency cooling function core damage frequency (component failures only) for the AP600.

Sensitivity calculations were performed to determine the importance of various success criteria uncertainties, which arise from uncertainties in the natural processes. From these calculations, and other qualitative evaluations of the passive systems, those systems involving natural circulation in the primary system and within containment, and gravity injection to the primary system, appear most important.

The method for explicitly addressing the natural process uncertainties in these key systems will be demonstrated and implemented in phases 2 and 3 of the program. Thermal-hydraulic calculations will be incorporated into a formal expert judgment process to address uncertainties in selected natural processes and success criteria.

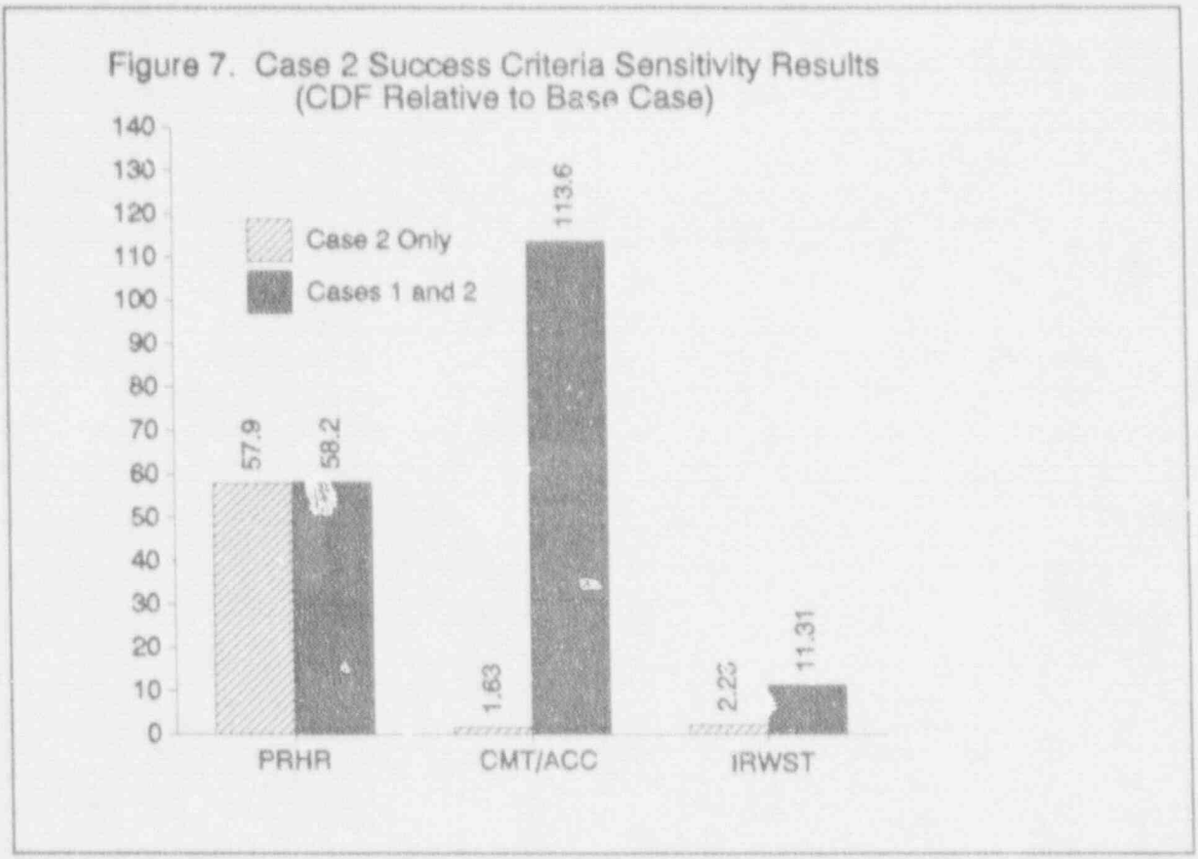

REFERENCES

[1] H. J. Bruschi and R. P. Vijuk, "Safety: Evolving Technologies for Tomorrow's Power Reactors," Nuclear Technology, Vol. 91, July 1990.

[2] R. M. Kemper and C. M. Vertes, "Loss-of-Coolant Accident Performance of the Westinghouse 600-MW(electric) Advanced Pressurized Water Reactor," Nuclear Technology, Vol. 91, July 1990.

[3] "AP600 Plant Description," Westinghouse Electric Corporation presentation to the Advisory Committee on Reactor Safeguards, June 6, 1991.

[4] "Severe Accident Risks. An Assessment for Five U.S. Nuclear Power Plants," NUREG-1150 Vols. 1 and 2, Final Summary Report, U.S. Nuclear Regulatory Commission, December 1990.

[5] C. J. Mueller and D. C. Wade, "Probabilistic Evaluation of Successful Inherent Shutdown in Unprotected Accidents in Innovative Liquid-Metal Reactors," Nuclear Technology, Vol. 91, August 1990.

Figure 8. Case 3 Success Criteria Sensitivity Results

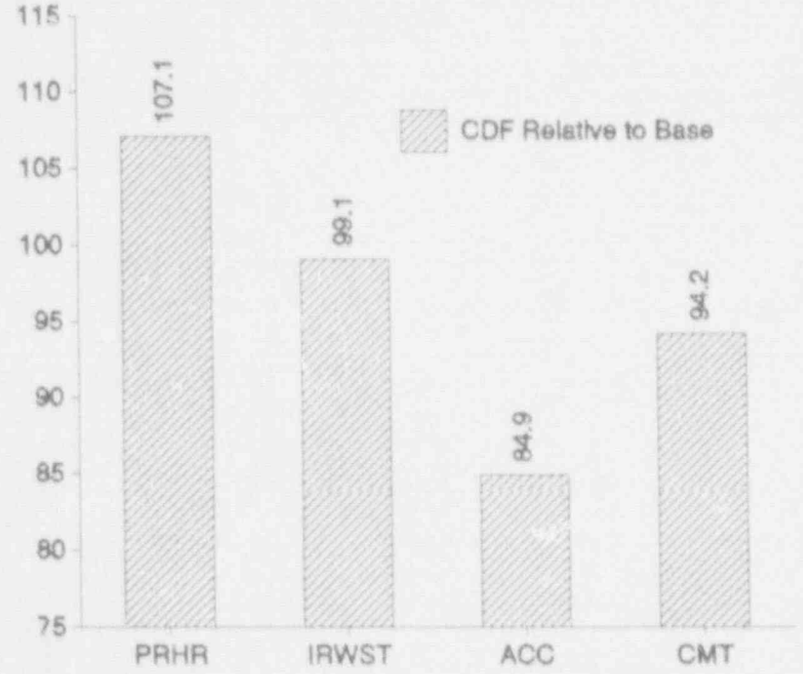

[6] D. M. Ericson, ed., "Analysis of Core Damage Frequency: Internal Events Methodology," NUREG/CR-4550, SAND86-2084, Vol. 1, Rev. 1, Sandia National Laboratories, Albuquerque, NM, January 1990.

[7] EPRI Advanced Light Water Reactor Requirements Document, Appendix A of Volume 2, Chapter 1, Feb 1990.

[8] R. C. Bertucio and J. A. Julius, "Analysis of Core Damage Frequency: Surry, Unit 1 Internal Events," NUREG/CR-4550, SAND86-2084, Vol. 3, Rev. 1, Sandia National Laboratories, Albuquerque, NM, April 1990.

Expanding the Modeling Capabilities of the Cognitive Environment Simulation

Emilie M. Roth
Westinghouse Science & Technology Center

Harry E. Pople, Jr.
Seer Systems

Randall J. Mumaw
Westinghouse Science & Technology Center

Abstract

We have been developing an artificial intelligence (AI) computer simulation called Cognitive Environment Simulation (CES). CES simulates the cognitive activities involved in responding to a NPP accident situation. It is intended to provide an analytic tool for predicting likely human responses, and the kinds of errors that can plausibly arise under different accident conditions to support human reliability analysis (HRA). Recently CES was extended to handle a class of interfacing loss of coolant accidents (ISLOCAs). This paper summarizes the results of these exercises and describes follow-on work currently underway.

Introduction

The U. S. Nuclear Regulatory Commission has been conducting a research program to develop more effective tools to model the cognitive activities that underlie intention formation during NPP emergencies. Under this program an artificial intelligence (AI) computer simulation called Cognitive Environment Simulation (CES) has been developed (cf. NUREG/CR-4862; NUREG/CR-5213). CES simulates the cognitive activities involved in responding to a NPP accident situation. It is intended to provide an analytic tool for predicting likely human responses, and the kinds of errors that can plausibly arise under different accident conditions to support human reliability analysis (HRA). Recently CES was extended to handle a class of interfacing loss of coolant accidents (ISLOCAs). This paper summarizes the results of these exercises and describes follow-on work currently underway. A full description of the results of the ISLOCA exercises are provided in NUREG/CR-5593.

Cognitive Environment Simulation

CES is an artificial intelligence (AI) system that simulates the cognitive activities involved in emergency response under dynamic conditions. CES monitors and tracks changes in process state, identifies abnormal and unexpected process behaviors, builds and revises a situation assessment (what influences are currently acting on the monitored process), formulates hypotheses to account for unexplained process behavior, and formulates intentions to act based on its situation assessment.

CES is built on top of an AI problem-solving system called EAGOL[1] that was developed especially for performing diagnostic reasoning in dynamic, data rich situations. It has been developed based on detailed studies of cognitive activities in a variety of applications, including internal medicine diagnosis (Gadd and Pople, 1990), emergency operations in nuclear power plants (Woods and Roth, 1986), NASA shuttle operations, critical care medicine, and intelligence analysis.

In the sections that follow we begin by providing a description of the critical features of dynamic NPP emergency situations that distinguish them from other types of applications and pose challenges to cognitive modeling. We then provide a description of CES and how it handles dynamic emergency situations. This is followed by a NPP case study that illustrates how a cognitive simulation such as CES can be used to help illucidate the cognitive demands imposed by NPP emergency situations.

Dynamic Emergency Situations

Emergency response in dynamic situations such as NPP emergencies has a different character from the classic paradigm of troubleshooting a static device that has been removed from service. In dynamic applications there is some underlying process (an engineered or physiological process which will be referred to as the monitored process) whose state changes over time. Failures disturb the monitored process and diagnosis goes on in parallel with responses to maintain process integrity. These situations frequently involve time pressure, multiple interacting goals, severe consequences of failure, and multiple interleaved tasks.

In dynamic process applications, incidents extend, develop and change over time. A failure disturbs the monitored process and triggers influences that produce a time dependent set of disturbances. This cascade of disturbances unfolds over time due to the development of the failure itself (e.g. a leak growing into a break) and due to functional and physical interconnections within the monitored process (Woods, 1988). These situations are further complicated by the possibility of multiple failures each producing a temporally evolving set of disturbances which can interact.

An additional complicating characteristic of NPP emergency situations is that during the course of the event both manual and automatic system actions will be taken to cope with the initiating disturbance that themselves affect the monitored process. The effect of these actions on the process further complicate the diagnostic task. The current and future state of the monitored process is a combined function of control influences and the influences produced by the failures in the monitored process (Woods, Pople and Roth, 1990). Thus there is a need to maintain and constantly update the set of normal and abnormal influences impinging on a process at any given point in time in order to account for plant behavior and untangle the effects due to the underlying failure from the effects due to subsequent control actions.

CES as a Cognitive Simulation of Emergency Response in Dynamic Applications

The Cognitive Environment Simulation is one specific example of a cognitive simulation designed to handle some of the demands of dynamic emergency response situations (cf. Elkind, Card, Hochberg & Huey, 1990; Amendola, Bersin, Cacciabue, and Mancini,1987). CES contains specific symbolic processing mechanisms designed to:

---

[1]EAGOL is a proprietary product of Seer Systems

- build and maintain a coherent situation assessment in a changing environment where multiple influences are at work including failures and operator and automatic system activities,
- discriminate expected from unexpected events based on qualitative reasoning about influences thought to be acting on the monitored process,
- engage in diagnostic search to evaluate possible hypotheses that would explain unexpected findings given that multiple influences are acting on the monitored process,
- generate intentions to take action to respond to diagnosed failures and/or re-establish safety goals.

There are three major information processing activities that underlie CES behavior (See Figure 1). These include:

- a *monitoring* process that monitors plant parameters (data channels) and identifies anomalous plant behavior;
- a *diagnostic search* process that attempts to search for a hypothesis that could account for unexplained plant behavior;
- a *corrective response* generator that identifies actions that should be taken in response to abnormal plant state. These actions are selected from pre-stored responses based on emergency procedures.

The information processing activities are carried out by a set of software "agents" each with a distinct responsibility and communication protocol. One kind of software agent is activated when the data changes on an input channel. This type of agent uses information about the set of influences thought to be active currently, and knowledge about influence relationships (an increasing flow will result in an increase tank level) to determine if the change is expected or unexpected given the current situation assessment. Qualitative reasoning techniques are employed to generate expectations about process behavior based on the set of known influences (Forbus, 1988). For example, increasing tank level is expected if an influence has been posted that there is a source of flow into the tank.

If the current set of known influences cannot account for the observed process behavior (an anomaly), an unknown influence is postulated and another software agent is invoked to identify the unknown influence. For example, an unexpected change direction or rate of change invokes an agent that uses knowledge of influence relationships to create a list of hypotheses -- influences that could account for the unexpected behavior. It then engages in knowledge-driven search to evaluate each hypothesis against other data about the state of the monitored process.

During an evolving incident, CES creates many software agents. To integrate the evaluations across the multiple agents, CES creates a special software agent that is responsible for coming up with a coherent explanation for all of the unexplained findings. These two layers in the architecture are needed to enable the AI system to separate and track the multiple factors affecting process behavior (automatic system responses, manual responses, and influences created by one or more failures), especially as they evolve dynamically. Does a new anomaly represent disturbance

propagation from the original failure, a sensor failure, or the effects of another breakdown? Control influences inserted to mitigate the consequences of disturbances change the pattern of findings, and expected control influences may fail to materialize due to execution error or additional breakdowns. The multiple layers of analysis allow the system to track multiple influences that may be affecting process state and to investigate different ways to put the pieces together to form a coherent overall assessment (Woods et al., 1987).

Exercising CES On NPP Incidents

Applying CES to NPP emergency situations requires building a knowledge base that contains information about NPP functions, failures, goals and control actions (the influence relationships needed for the qualitative reasoning mechanisms in the program). The CES knowledge base includes information on plant parameters available to be monitored, and their normal operating limits; the inter-relationships among plant physical processes; goals for safe plant operation; abnormalities (e.g., power failures; breaks) and the effect they have on plant processes; and what actions can be taken to correct abnormalities. As such it provides a mechanism for modeling the kind of knowledge of NPP that an operator would be presumed to have based on training, procedures, and experience.

As described above, the inference engine within CES provides reasoning mechanisms that enable CES to monitor changing plant parameters, to formulate and revise situation assessments, and to generate intentions to act. While the particular reasoning mechanisms utilized by CES do not mimic in detail the cognitive processes of human operators (e.g., short term memory; detailed monitoring or diagnostic strategies), it performs the major cognitive activities that are required to successfully assess and respond to a NPP emergency event (i.e., the cognitive tasks that human operators would necessarily have to perform to successfully handle the event). By performing the major cognitive activities required to handle a NPP emergency event, it provides a tool for assessing the cognitive challenges imposed by different accident sequences (e.g.,what evidence needs to be examined, what knowledge needs to be accessed, what alternative hypotheses arise that need to be discriminated, what safety goals need to be considered in managing the accident), and potential opportunity for error.

The CES modeling strategy to date has focussed on developing knowledge and reasoning capabilities that enable CES to successfully handle the NPP case of interest and close variants. The premise is that the knowledge and reasoning capabilities that are required for the CES computer simulation to successfully handle the case provide a specification of the knowledge and reasoning demands imposed by the application tasks.

In keeping with the cognitive simulation tradition, the information processing behavior of the simulation provides a concrete basis for comparison with empirical data on operator crew performance. Analysis of similarity and differences in the performance of the computer simulation and that of human practitioners can illuminate the cognitive demands imposed by the NPP incident, the knowledge and reasoning capabilities required for successful performance, and knowledge and information processing limitations of human crews that restrict performance. In this way a computer simulation can serve to illuminate and amplify available data on human performance.

The goal of the simulation exercise is not to produce an exact match between the information processing behavior of the computer simulation and that of the crew. Because of the breadth of information processing activities involved in NPP accident situations, and both pragmatic and theoretical limits on the ability of computer simulations to embody a comprehensive model of

human cognition, a computer simulation is necessarily only a partial embodiment of a larger scope conceptual model of human performance (Newell, 1990). The goals of the simulation enterprise are to learn from juxtaposing the behavior of the simulation and the behavior of human crews. By examining the similarities and differences between simulation behavior and crew behavior it becomes possible to understand the cognitive demands of the situation, the sources of error and potential for expertise.

CES Exercises on an Interfacing System Loss of Coolant Accident

As part of the CES development process CES was recently exercised on two interfacing system loss of coolant accidents (ISLOCAs) Two crews made up of NPP training instructors were observed responding to the ISLOCAs on a high fidelity NPP control room simulator. One crew was observed on each event. At the same time the the instructor crews were run on the incidents, the plant parameter values were recorded from the NPP simulator onto a data file. This data file was used as input to CES[2]. Thus the behavior of CES could be examined on exactly the same events that were used with the human crews.

The results of the exercises illustrate how cognitive simulations such as CES, coupled with small-scale data on human performance, can provide insight into the sources of operator performance problems, and the potential for human error.

The ISLOCA scenarios involved a leak from the high pressure RCS to the low pressure Residual Heat Removal (RHR) System. A simplified diagram of the NPP systems including the RHR system is presented in Figure 2. Specifically two isolation valves that are normally closed were failed open. This led to an increase in pressure in the RHR which resulted in a break approximately three minutes into the event[3]. Two versions of the ISLOCA event were run. In case 1 the break was in the RHR piping and led to reactor coolant fluid falling to the floor of the auxiliary building. In case 2 the break was in a heat exchanger between the RHR and the Component Cooling Water (CCW) System. This resulted in reactor coolant fluid leaking into the CCW system.

On the surface the ISLOCA cases would seem to be straightforward to diagnose. There were clear indications in the control room of overpressurization in the RHR system, and specific procedures for dealing with ISLOCA events. However, when human crews (NPP training instructors) were run in the events using a full-scope simulator, they had difficulty diagnosing the event.

In spite of the availability of what would appear to be a clear leading indicator of a problem in the RHR and the availability of procedural guidance, the instructor crews failed to diagnose the leak from the primary system into the RHR system until late in the event. In the first case the crew did not identify the ISLOCA until 16 minutes in the event. In case 2, while the instructor crew correctly diagnosed and responded to the repercussions of the ISLOCA, they never explicitly pursued the source of the coolant water in the RHR -- that is the ISLOCA. In contrast CES

---

[2]In these incidents 232 plant parameters were used as input to CES. Values for these were input to CES every 10 seconds.

[3] The SNUPPS simulator does not fully model the RHR system. As a result it was necessary to explicitly put a break in the RHR system to simulate the type of break that would be expected from the increase in pressure in the RHR system caused by the ISLOCA. In the first case (break in piping) the break size was approximately 2000 GPM. It started 200 seconds into the event and took 10 seconds to ramp to full size. In the second case (break in CCW heat exchanger), the break size was approximately 180 GPM. It started 180 seconds into the event and ramped to full size in 5 seconds. The size and timing of the breaks were determined by the simulator instructors who served as advisors to the project based on their judgment of plausible consequences of ISLOCAS into the RHR.

diagnosed the ISLOCA as soon as pressure symptoms in the RHR began to appear. It then projected potential future consequences of the ISLOCA and was quick to observe and explain plant symptoms that later appeared that were consistent with its expectations.

Contrasting the performance of CES with the performance of the instructor crews reveals a variety of factors that limited the ability of the instructor crews to follow the same straight path as CES. It reveals several areas where human performance is vulnerable and points to a variety of ways to improve the person-machine system.

The cognitive demands of the incident will be highlighted by tracing the dynamic flow of events. The first symptom is a high pressure alarm in the RHR system which the instructor crews as well as CES noted in both cases. While this alarm suggests a problem in the RHR system, it is rapidly followed by symptoms that suggest a primary system break inside containment. The pattern of findings -- primary system level decreasing, primary system pressure decreasing, indication of radiation within containment are the classic signature of a primary system break into containment. Note that this conclusion while consistent with a salient subset of the anomalies does not account for the RHR symptoms. At the first evidence of primary system disturbance the attentional resources of the instructor crews appear to have been diverted away from the RHR. From that point on, until more severe symptoms of the RHR break occurred, the instructor crews appeared to "forget" about the RHR problem. They neither tried to pursue the source of the RHR pressure buildup, nor tried to anticipate potential consequences of the RHR disturbance. Instead their main attentional focus was on trying to diagnose and attempt to respond to the primary system symptoms.

In contrast CES doggedly pursued the RHR symptoms. The success of CES resulted mainly from three factors: (1) its ability to diagnose the RHR ISLOCA early on -- the instructor crews attended to RHR alarm but then didn't follow up once symptoms in containment arose; (2) its ability to project potential consequences into the future that allowed it to absorb and connect seemingly disparate findings and (3) its ability to notice anomalies as soon as they arose.

The failure of the instructor crews to pursue the RHR symptoms becomes more readily understandable when one considers the dynamics of the event and the operational context. Because of the importance of maintaining primary system integrity, all the attentional resources of the crew appear to have been absorbed by that problem. Further, when radiation alarms inside containment occurred (because the pressurizer relief tank ruptured due to inflow from the RHR relief valve), the emergency operating procedures directed the crew to procedures for responding to primary system break inside containment, thus further diverting the operator's attention away from the RHR problem. In the particular procedures employed in these exercises, there was a specific procedure for diagnosing and responding to ISLOCA events. However, once the crew is directed to the primary break inside containment procedure, there is no provision within the structure of the emergency operating procedures to redirect redirect them to the ISLOCA procedure. In order to get to the correct procedure, the crew must diagnose the situation on their own, recognize that there is a relevant procedure for this condition, and take the initiative to switch to that procedure. Static analyses can easily underestimate the role of dynamic factors in human behavior. A cognitive simulation forces the analyst to think about the temporal evolution of the incident and the temporal aspects of a crew's response.

As the incident progresses additional symptoms appear that point to disturbances in other plant systems. In the first case, when the RHR piping breaks, the reactor coolant water spills into the auxiliary building resulting in an RHR Room Sump Level High alarm and auxiliary building

radiation alarms. In the second case symptoms appear in a third system -- component cooling water (CCW).

At this point the crews as well as CES have another cognitive task -- how to put together two or three subsets of findings: is there one underlying explanation for all of the subsets of findings or are there several factors at work? This task is difficult because, while the source of the problems is in the RHR system, symptoms are manifested in multiple systems that are normally not connected. As a result the crew needs to actively integrate seemingly independent problems to correctly assess the situation.This requires knowledge of the physical connections among the systems and active diagnostic effort that goes beyond the guidance provided in the procedures. In particular, diagnosis requires activating knowledge about the points of interface among the primary system (RCS), the RHR system, and the CCW system in order to put the various subsets of findings together.

Both CES and the crews had to go through this reasoning task. CES, at its current stage of development, is able to carry out the necessary information processing and knowledge activation very quickly. The crews, on the other hand, at first entertained the possibility of separate independent failures. As the severity of the symptoms increased the instructor crews had to actively pull back and attempt to resynthesize the pattern of symptoms. They took advantage of physical schematics of the relevant systems as an external knowledge base and a source of retrieval cues to activate knowledge relevant to the problem at hand and as a visual representation aid to support reasoning through the possible flow paths among the systems. There are a variety of ways that this diagnostic cognitive task can break down and eventually we plan to be able to use CES as a tool to explore the consequences of these.

In spite of the fact that the two crews were made up of training instructors, who are proficient in the plant and the use of the procedures, and who are highly familiar with the range of NPP accidents that are simulated on the plant simulator, the ISLOCAs were not diagnosed until fairly late into the event - substantially after the pressure build up in the RHR led to a break. The crew in case 1 did not attempt to check on the status of the RHR isolation valves until approximately 16 minutes into the event. The crew in the second case did not check on the status of the valves during the time period observed.

The diagnostic process can affect the selection and execution of appropriate recovery actions. Even if operators correctly diagnose the incident, a delay in diagnosis can mean that what was at one time an isolatable leak can no longer be isolated directly, or, in the case of an unisolatable leak, action to conserve RWST coolant water and to perform a plant cooldown may not be taken soon enough. As it happens, in the specific scenarios we ran, the leaks into the RHR were not isolatable. The results suggest that, even in cases where the leaks into the RHR are isolatable, realization of a need to check on the status of the isolation valves may not arise sufficiently soon to prevent a break in the RHR.

Note that the human performance data used in this analysis is limited on a variety of dimensions. First the crews were made up of instructors rather than operators. Perhaps, more importantly, the crews were made up of only two people, which meant that they had fewer attentional resources. Normally an operator crew would include 3 to 5 people. Similarly, there are interpretative limits to the behavior of CES on these incidents. The current working version of CES does not capture the cognitive demands associated with attentional control well, does not include all of the tasks and the associated workload operators must perform, and is more efficient at knowledge retrieval than people observed. Together however the two sets of data provide a converging picture of the cognitive demands and vulnerabilities for human performance in this class of incidents.

One of the clear strengths of CES is that it provides a tool for assessing the extent to which the environment supports the diagnostic task confronted by the problem solver. The process of building CES to successfully handle the accident situation provides insight into the NPP knowledge an operator must have, and the evidence he must attend to and integrate, in order to correctly diagnose and handle the incident of interest. In order for CES to correctly diagnose the failure and subsequent break, it was necessary to encode in CES information about the physical interconnections among various plant systems, and about the disturbances that result from breaks between these systems (i.e., the equivalent of a mental model of the system and their interconnections). It was also necessary to activate reasoning mechanisms that allowed CES to project into the future disturbances that result form the break. This was critical to enable CES to anticipate future disturbances and integrate seemingly independent symptoms into a coherent picture (cf. Klein, 1990 for evidence of the importance of mental simulations for future projections in human diagnosis).

An implication of the CES exercise is that in order for people to correctly diagnose and handle the ISLOCA, they would need to access the same type of knowledge and utilize the same type of logic. Successful diagnosis requires accurate knowledge of the physical interconnections among the systems and potential flow paths among normally separate systems in order to account for the full set of symptoms observed. In Rasmussen's terminology, accurate diagnosis and response in this incident requires knowledge-based behavior (Rasmussen, 1986). Observation of the instructor crews confirm this. The crews used the same knowledge and reasoning to solve the problem, although it took them much longer to access the relevant knowledge and form the necessary connections.

In summary, juxtaposition of the human performance data and the CES performance suggest that successful diagnosis requires:

- Knowledge of the physical interconnections among the relevant systems.
- Active search for a common root cause to account for the seemingly independent symptoms.
- Calling to mind the possibility of an ISLOCA, i.e., a primary system leak to the RHR.
- Knowing that there is a procedure for diagnosing and managing an ISLOCA.
- Actively shifting away from the LOCA procedure to the ISLOCA procedure.

Conclusions From ISLOCA Exercises

The results of the ISLOCA exercises served to clarify the strengths and limitations of the current version of CES. CES was shown to be a powerful tool for analyzing the problem-solving demands of a situation. It can be used to uncover what knowledge an operator must possess, what plant parameters he must monitor, and what evidence integration he must perform to successfully handle the task. It can also provide a lower limit on how quickly a correct diagnosis can be made.

The ISLOCA exercises serve as a model of how a cognitive simulation such as CES can be used to provide practical insight on human reliability issues of concern. CES, as a computer simulation, provides a means of specifying objectively the NPP knowledge and cognitive activities required to

diagnose an incident of concern. As such it provides an objective tool for establishing the generality of a human reliability analysis derived from limited observations of human crews.

A cognitive simulation such as CES provides a way to assess the cognitive demands of the environment. A cognitive simulation can reveal:

- what knowledge an operator must possess to handle the event;
- what evidence must be observed and integrated;
- an absolute lower limit on how quickly a disturbance can be diagnosed (i.e., the time at which all the evidence required to diagnose the disturbance becomes available).
- the kinds of diagnostic confusions and intention errors that can arise.

The current implementation of CES represents a working hypothesis of the set of competencies required to adequately respond to the demands of the problem-solving environment. When contrasted with empirical results of human crew performance it provides a way to disentangle performance limits that are due to inherent demands of the situation from limitations due to particular strategies or processing constraints. In turn the results of the analyses provide the basis for further development of the simulation.

While CES was successful in revealing the knowledge and reasoning required to handle this class of incidents, it did not model the difficulty people had in accessing the relevant knowledge and integrating the evidence. CES was able to detect disturbances sooner, and follow implications of disturbances more thoroughly than the human crew could. This suggests a need to incorporate mechanisms in CES that more accurately simulate human processing limitations.

Current CES Project Activities

The NRC is currently sponsoring a follow-on research project. One goal of this project is to identify and implement additional features in CES to better model human processing limitations. A second goal is to convert CES to run on a more widely available computer to improve its accessibility to potential NRC users.

As part of this effort a peer review committee was convened to evaluate the current status of CES and recommend future directions the project should take. The four member peer review committee included experts in artificial intelligence, cognitive modeling, human reliability assessment and probabilistic risk assessment.

In general the peer review committee was positive about the achievements and contribution of the current version of CES. They also pointed to a need for a number of additional enhancements to improve the ability of CES to capture the cognitive behavior and limitations of operators in NPP emergency situations.

The Peer Review Panel helped define what psychological processing limitations and heuristics would need to be incorporated in a comprehensive model of operator performance. Based on their input a subset of these processing constraints were selected to attempt to incorporate into CES during this phase of the project. The selection was strongly guided by joint consideration of (a) what psychological constraints are most critical for modeling operator behavior in NPP

emergencies and (b) what psychological constraints could be most readily implemented within the EAGOL framework.

Specifically, we are attempting to incorporate mechanisms that will allow CES performance to be more goal-driven. These changes are expected to make the behavior of CES more closely resemble the procedure-constrained behavior of nuclear power plant operators.

We are also attempting to model human diagnostic limitations and biases more closely . One of the characteristics of human diagnostic behavior is that people tend to call to mind and pursue only the most familiar or "high frequency" explanations for a given symptom. Reason (1990) has referred to this as the "frequency-gambling" heuristic. Only when the "high frequency" explanations fail to be confirmed, do people call to mind other, less familiar, potential explanations. As an example, in the ISLOCA event we ran with human crews, an ISLOCA was not initially called to mind as a possible explanation for the pressurizer relief tank and containment symptoms. In contrast to the behavior of people, in the current version of CES, when a plant symptom is detected, all the possible explanations for that symptom that are stored in the CES knowledge-base are retrieved in diagnosing the problem. We intend to explore alternative computational mechanisms for capturing the types of processing limitations and diagnostic heuristics exhibited by people.

As part of this phase of the program we also plan to collect additional data on operator crew performance during simulated emergencies.The objective of the data collection effort is to obtain empirical data on the performance of actual operators in simulated emergencies to be used in developing and testing the new psychological modeling features to be added to CES.

Plans are to replicate some of the events we ran with training instructors using actual operator crews as part of training exercises at a utility training simulator. A utility has already agreed to participate and we expect to collect data in the Fall of 1991. The events to be run were selected because we believe they will be cognitively challenging to operators based on some preliminary empirical data that we obtained using simulator training instructor crews. The operator crew data will allow us to assess how actual operator crews respond to the events. In addition the ability to run the same event on multiple crews will allow us to observe and try to explain variability in performance among crews.

Finally we plan to transport the CES system to an NRC facility to make CES more widely available to potential users within the NRC and their contractors. This change entails two activities: (1) converting CES code to allow it to run on a more widely available computer ; and (2) interfacing CES to an NPP plant simulation that is available to the NRC. CES currently runs on a Symbolics computer (a computer specialized for running AI programs) that is interfaced to a high-fidelity plant simulation located at the Westinghouse Energy Center in Monroeville, PA.

A review was conducted of the types of computers and NPP simulators available to the NRC, and the requirements necessary to run CES. Based on this review it was recommended that a facility for further development and exercise of CES be set up at the NRC Technical Training Center in Chattanooga. It was further recommended that CES be converted to run on a Sun workstation and be interfaced to the SNUPPS training simulator at Chattanooga.[10] Current plans are to implement these recommendations.

---

[10] The specific Sun workstation configuration recommended is a SUN SPARC2 workstation with 24 megabytes of RAM and a hard disk.

Summary and Conclusions

The ISLOCA exercises suggest how a cognitive simulation such as CES can be used to provide practical insight on human reliability issues. A cognitive simulation can provide a tool for assessing the extent to which the environment supports the diagnostic task confronted by the problem-solver. As such, it provides an objective tool for validating and generalizing the results of small-scale simulator observations of operator performance.

The exercise suggests that a cognitive simulation such as CES can provide a way to assess the cognitive demands of the environment. A cognitive simulation can reveal:

- what knowledge must be possessed to handle the event;
- what evidence must be observed and integrated;
- an absolute lower limit on how quickly a disturbance can be diagnosed (i.e., the time at which all the evidence required to diagnose the disturbance becomes available).
- the kinds of diagnostic confusions and intention errors that can arise.

The exercises also served to highlight the importance of considering the dynamics of an event in performing human reliability evaluations. What made the ISLOCA cases examined cognitively challenging was the dynamic pacing of the events. The cognitive demands imposed by the dynamic evolution of the event and consequent potential for error may not be easily revealed in a static walk-through. This argues for the need to include dynamic simulations of critical accident evolutions as part of human reliability studies.

The value of a cognitive simulation is in helping to see the demands imposed by the problem-situation independent of the strategies that people bring to bear. A key element of the analysis is to compare the performance of the cognitive simulation with empirical data on human crew performance. It is the juxtaposition of data on human performance (even if limited in scope) with the performance of the cognitive simulation that allows the inherent demands of the cognitive environment to stand out.

While CES was successful in revealing the knowledge and reasoning required to handle this class of incidents, it did not model the difficulty people had in accessing the relevant knowledge and integrating the evidence. CES was able to detect disturbances sooner, and follow implications of disturbances more thoroughly than the human crew could. This is because CES currently does not model the attention and processing resource limits of people. We are currently attempting to incorporate more psychologically plausible processing limitations into CES.

While there are clear attractions to the cognitive simulation strategy, there are also clear limitations that are important to keep in mind especially because they modulate how one should use the technique. First, given the breadth of human cognitive activities that come into play in complex applications (Woods and Roth, 1986), the evolution of knowledge in the field of cognitive science, and pragmatic factors in large software development projects, it is very difficult to see a cognitive simulation as a finished system. Rather, cognitive simulations are always in a state of evolution. Second, it must be kept in mind that cognitive simulations are instantiations of concepts about

human cognitive activities, not the concepts themselves. As a result, it is better to see cognitive simulation as a tool for modeling rather than as a strong model in itself.

The goals of the simulation enterprise are to learn from juxtaposing the behavior of the simulation and the behavior of human crews. By examining the similarities and contrasts between simulation behavior and crew behavior one can extract information about error, expertise and potential improvements to the person-machine system. At the same time the results of the analyses can serve to guide the continuing evolution of the cognitive simulation to better capture both cognitive task demands and human strategies for meeting those demands. In other words, cognitive simulation can be part of the process of theory based empirical investigation and data based theory building that is the classic model for a scientific growth.

ACKNOWLEDGEMENTS

This research is being supported by the Office of Nuclear Regulatory Research, U. S. Nuclear Regulatory Commission. The authors would like to thank Dr. Thomas G. Ryan, who has served as NRC Project Manager, and Dr. Paul Lewis, who is the current NRC Project Manager, for their guidance and support on this project.

We would also like to acknowledge the contributions of David D. Woods who participated in earlier phases of the CES project.

REFERENCES

Amendola A., Bersin U., Cacciabue P., and Mancini G. 1987, Modeling operators in accident conditions: Advances and perspectives on a cognitive model. *International Journal of Man-Machine Studies*, 27, 599-612.

Elkind J., Card, S. , Hochberg, J. and Huey b. (Eds) 1990, *Human Performance Models for Computer Aided Engineering*. (Academic Press, New York).

Forbus, K. 1988, Qualitative physics, Past, present, and future. In *Exploring Artificial Intelligence*. (Morgan Kaufmann, San Mateo, CA).

Gadd, C. S. and Pople, H. E. 1990, Evidence from internal medicine teaching rounds of the multiple roles of diagnosis in the transmission and testing of medical expertise, in N. Frederiksen and R. Glaser and A. Lesgold and M. G. Shafto (eds) *Diagnostic Monitoring of Skill and Knowledge Acquisition* (Erlbaum, Hillsdale, NJ)

Klein, G. A. 1989, Recognition-primed decisions. In W.B. Rouse, editor, Advances in *Man-Machine Research*, Volume 5. (JAI Press, Greenwich, CT).

Klein, G. A. 1990, Mental simulation and decision-making. *Proceedings of the 5th Mid-Central Ergonomics/Human Factors Conference*. (Dayton, Ohio).

Klein, G. A., Calderwood, R. and D. MacGregor, 1989, Critical decision method for eliciting knowledge. *IEEE Systems, Man, and Cybernetics*, SMC-19, 462-472.

Newell, A. 1990, *Unified Theories of Cognition*. (Harvard University Press, Cambridge, MA)

Rasmussen, J. 1986, *Information Processing and Human-Machine Interaction, An Approach to Cognitive Engineering*. (New York, North-Holland).

Reason, J. 1990 *Human Error*. (Cambridge University Press).

Roth, E. M., Pople, H. E., and Woods, D. D., *Extending the Modeling Capabilities of the Cognitive Environment Simulation, Modeling an ISLOCA Scenario*, NUREG/CR-5593, in preparation.

Woods, D. D. and Roth, E. M. 1986, Models of Cognitive Behavior in Nuclear Power Plant Personnel, U. S. Nuclear Regulatory Commission, Washington D. C. Technical Report NUREG-CR-4532.

Woods, D. D., Roth, E. M. and Pople, H. 1987, *Cognitive Environment Simulation, An Artificial Intelligence System for Human Performance Assessment*. U. S. Nuclear Regulatory Commission, Washington, D. C., (NUREG/CR-4862).

Woods, D. D., Roth, E. M. and Pople, H. 1988, Modeling Human Intention Formation for Human Reliability Assessment . *Reliability Engineering and Systems Safety*, 22, 169-200.

Woods, D. D., Pople, H. E. and Roth, E. M. 1990, *The Cognitive Environment Simulation as a Tool for Modeling Human Performance and Reliability*. U. S. Nuclear Regulatory Commission, Washington, D. C., (NUREG/CR-5213).

List of Figures

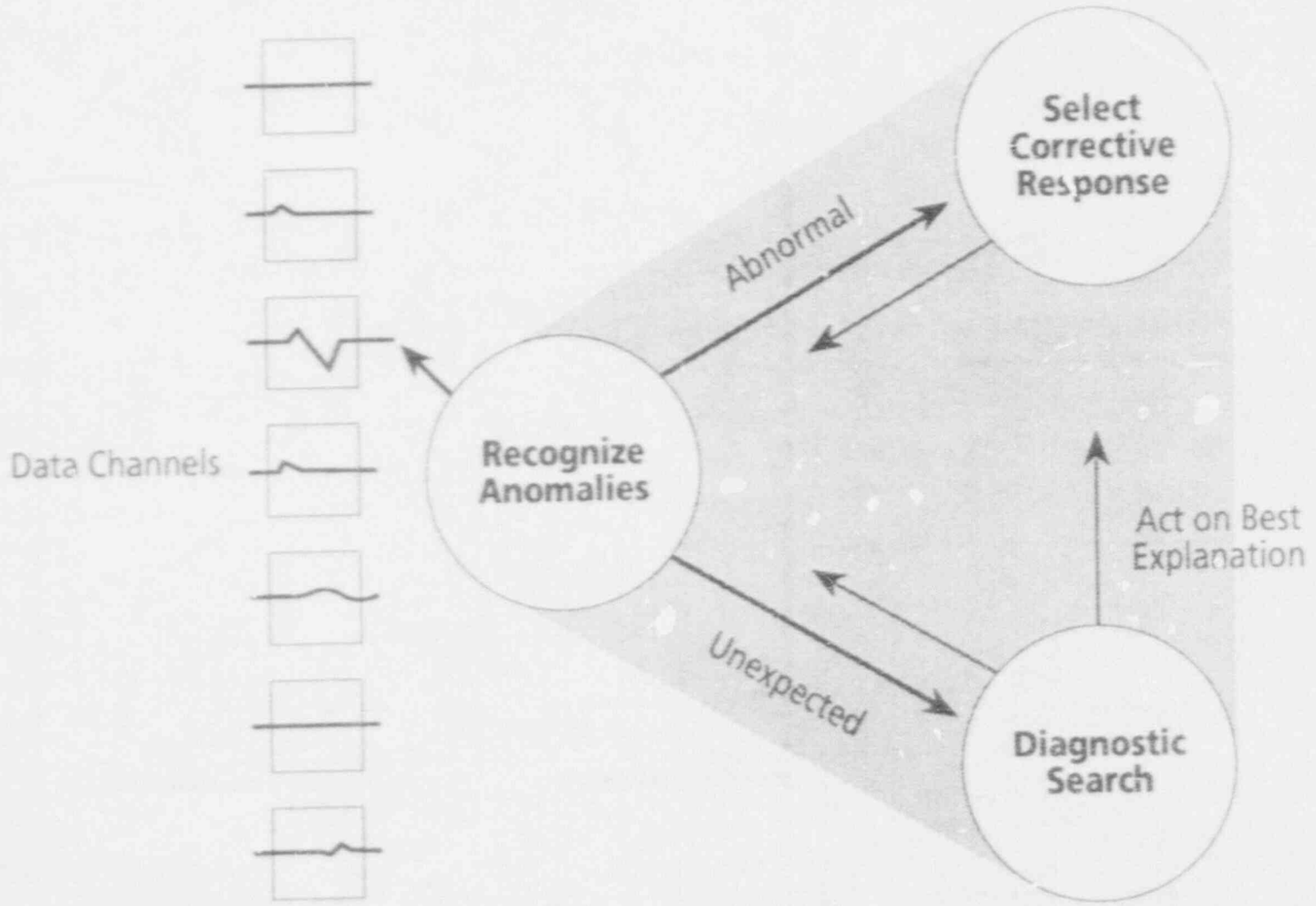
Select
Corrective
Response
Abnormal
Data Channels
Recognize
Anomalies
Act on Best
Explanation
Unexpected
Diagnostic
Search

Figure 3

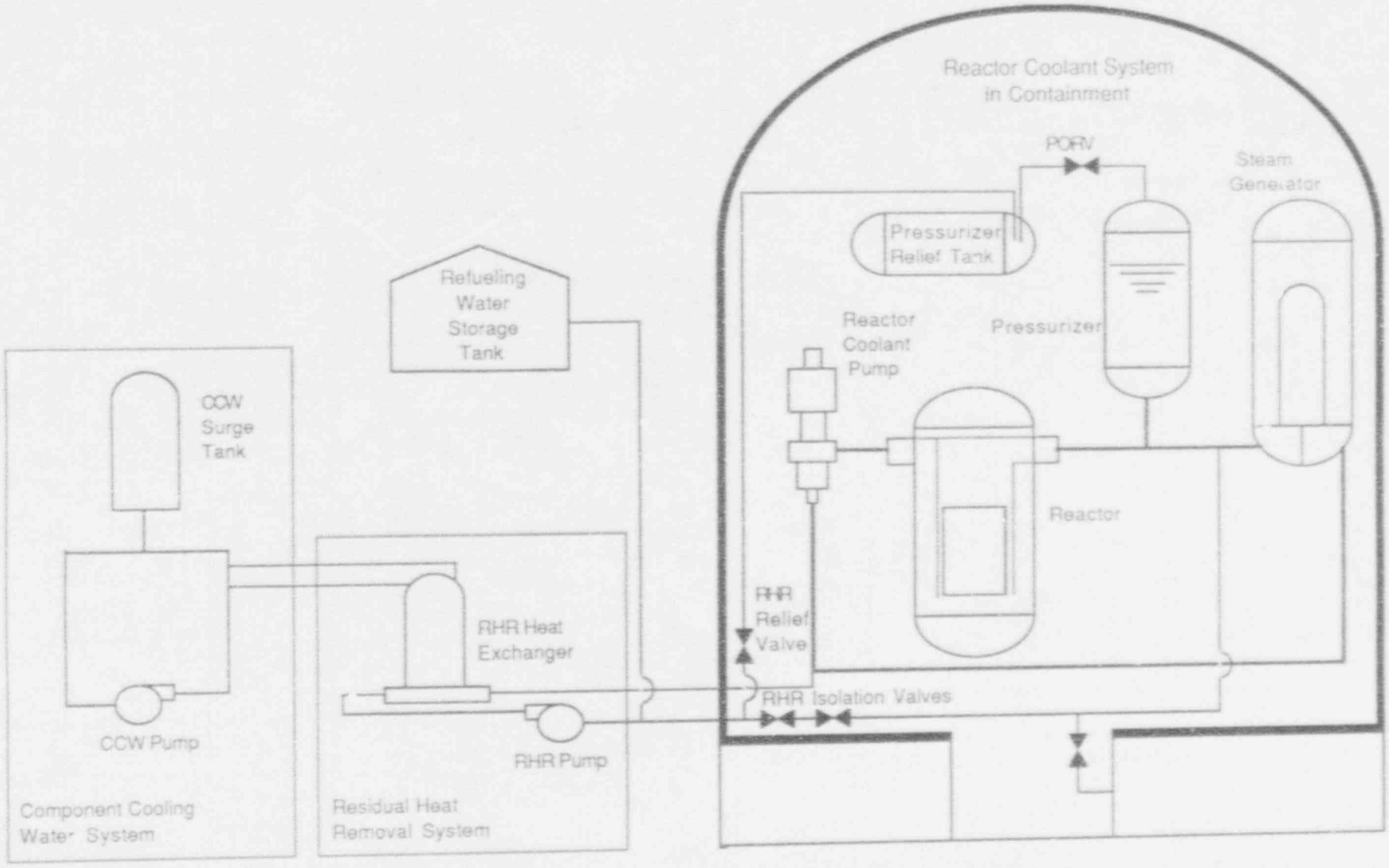
Reactor Coolant System
in Containment
PORV
Steam
Generator
Pressurizer
Relief Tank
Refueling
Water
Storage
Tank
Reactor
Coolant
Pump
Pressurizer
CCW
Surge
Tank
Reactor
RHR
Relief
Valve
RHR Heat
Exchanger
RHR Isolation Valves
CCW Pump
RHR Pump
Component Cooling
Water System
Residual Heat
Removal System

HUMAN PERFORMANCE INVESTIGATION PROCESS (HPIP)

Mark Paradies & Linda Unger, System Improvements, Inc.

BACKGROUND

The nuclear power industry has gone through a transition from a period of plant construction to a period of plant operations. As the industry went through this transition, the U.S. Nuclear Regulatory Commission (NRC) has likewise changed its regulatory emphasis. Today, with nuclear construction and licensing complete, the NRC is focusing on safe operation and maintenance of nuclear plants. This change in focus has caused the NRC's regulatory efforts to be less oriented toward design basis studies and more oriented toward operating experience and the human contribution to plant performance. Therefore, plant performance indicators and operational events now receive special attention.

As increased attention is paid to human performance, its contribution to plant safety becomes more evident. In the NRC Regions, resident inspectors or other regional personnel frequently review human performance when investigating the causes of incidents and when assessing the adequacy of proposed corrective actions to prevent the recurrence of incidents. Certainly if all NRC personnel involved with the review of incidents and human performance could receive weeks of training in incident investigation and human factors, the understanding of the causes of these incidents would increase. This improved understanding could lead to new ways to identify unsafe trends and improve plant safety. However, this much training is a tremendous investment of one of the NRC's scarcest resources - staff time.

Another option is the development of an investigation process to help field personnel perform more insightful incident investigations without extensive training. To be successful, this process would:

- Help investigators more accurately pinpoint the root causes of human performance related incidents, thereby leading to a better understanding of human performance problems.
- Be easily understood by the user and require little initial training (perhaps no more than one day).
- Be easily understood by management.
- Be compatible with database applications for ease of trend analysis.
- Not require significantly more effort by investigators in the field.

Although these requirements are ambitious, they are the goals used in the development of the Human Performance Investigation Process (HPIP), an investigation process being developed through the Human Factors Branch, Office of Nuclear Regulatory Research for use by U. S. Nuclear Regulatory Commission personnel when investigating human performance related incidents at nuclear power plants. This paper describes HPIP's development, the HPIP process and techniques, and the testing of the process currently being performed.

DEVELOPMENT EFFORT

In developing HPIP, a large portion of the effort focused on identifying the NRC's special needs. In individual and group interviews and five major meetings with NRC field and headquarters personnel, 154 people helped assess user needs and provide feedback. Three of these five meetings were held at regional headquarters to provide field personnel the opportunity to shape the process. Some 123 regional personnel, 60 of whom were resident inspectors, participated in these spirited sessions and provided excellent input to the development of the system criteria, the HPIP flow chart, and the investigation techniques.

Much of the remaining effort was spent assessing and developing human performance and root cause analysis techniques to be incorporated into HPIP. This work included conducting a computerized literature review, interviewing human performance and root cause analysis experts, and attending meetings on root cause analysis.

The results of this effort is a process developed to meet the special needs of NRC personnel, especially NRC resident inspectors. HPIP combines current NRC procedures and field practices, expert experience, NRC human performance research, and the best applicable investigation techniques into a procedure with stand-alone investigation modules for use by investigators in the field. The intent of the system is to be intuitive, and easy to learn and use. HPIP is designed to help NRC personnel perform field investigations resulting in a better understanding of human performance problems at nuclear power plants.

Now that the process has gone through the initial development phase, the next step is to pilot test the system in the field and get additional feedback from the eventual users. Therefore, the testing includes trial use by trained field personnel with some assistance by the development team. Feedback from this pilot testing effort and the resulting revisions will assure that the implemented version of HPIP is readily accepted in the field.

When completed, HPIP will represent a step forward in providing NRC personnel, both in the field and at headquarters, with the information needed (that is, the root causes of human performance problems) to better understand the reasons for human performance difficulties. This understanding will be helpful in evaluating the utilities' plans for improving performance and in setting the NRC's research and policy goals in the coming years.

INCIDENT INVESTIGATION PROCESS AND TECHNIQUES

A flow chart of the investigation process was used to integrate the techniques into the investigation process. Figure 1, the HPIP Flow Chart, outlines the basic process (to which there are many variations and simplifications) that NRC

FIGURE 1: NRC HPIP Flow Chart

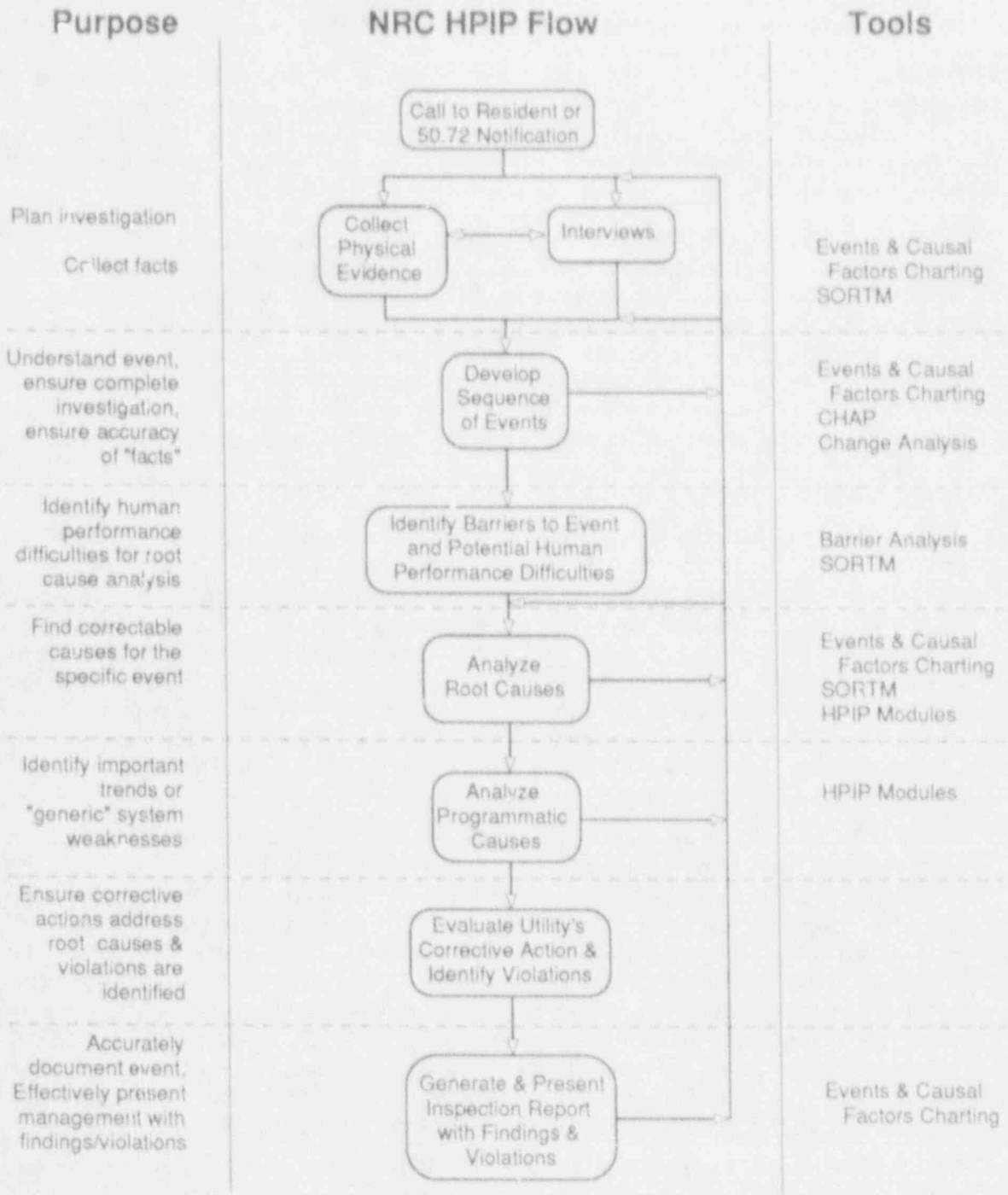

personnel in the field would use to investigate a fairly complicated incident. The flow chart consists of three parts: (1) the NRC HPIP Flow (center column) displays the steps used to investigate an incident; (2) The Purpose (left column) lists the purpose of each major section of the process; (3) The Tools (right column) lists the techniques used to perform each major section of the process.

HPIP uses six techniques to help investigators decide where to spend their investigative effort and to identify the incident's root cause(s). These techniques are described in detail in NUREG/CR-5455, Development of the NRC Human Performance Investigation Process (HPIP) (to be published late in 1991). These techniques are:

- **Events and Causal Factors Charting** - a technique that lays out the flow of an incident in a graphic format so that potential causal factors can be identified for further investigation. The cart includes the sequence of events that led to the incident and the potential reasons (causal factors) for those events. The Events and Causal Factors Chart helps the investigator identify holes or inconsistencies in information about the incident. Using charts during interviews can help focus the discussion on what really happened. The charts also provide good visual displays for describing an incident to management. An example of an Events & Causal Factors Chart is shown in Figure 2.
- **SORTM** - a simple paper-based expert system designed to lead the investigator to those human performance areas most likely to have contributed to human error. SORTM (Figure 3) provides questions similar to those that an expert in human performance would consider during an incident investigation. The answers to SORTM's questions lead the investigator to those human performance areas most likely to have contributed to human error during the incident. SORTM therefore helps the investigator allocate resources (time and people) to those areas where the discovery of problems, and their correction, would decrease the likelihood of the incident's recurrence.
- **HPIP Modules** - individual procedures for investigating common human performance problems. One of these procedures was developed for each of SORTM's six human performance areas: (1) procedures; (2) training; (3) human engineering; (4) supervision; (5) communications; and (6) organizational factors / management systems. Sections in the HPIP Modules: help the investigator decide who should be interviewed and what documentation should be collected; provide the investigator with lists of reference material; and provide the investigator with questions to be asked to find correctable root causes for the incident. Part of a module (a graphic depiction of the potential root causes covered in the Procedures Module and a sample of the Procedures Module questions) is shown in Figures 4 and 5.
- **Barrier Analysis** - a formal method of identifying the events that, if avoided, would have prevented the incident from occurring or would have significantly mitigated its consequences. The following questions should be answered to complete a barrier analysis: (1) What physical boundaries,

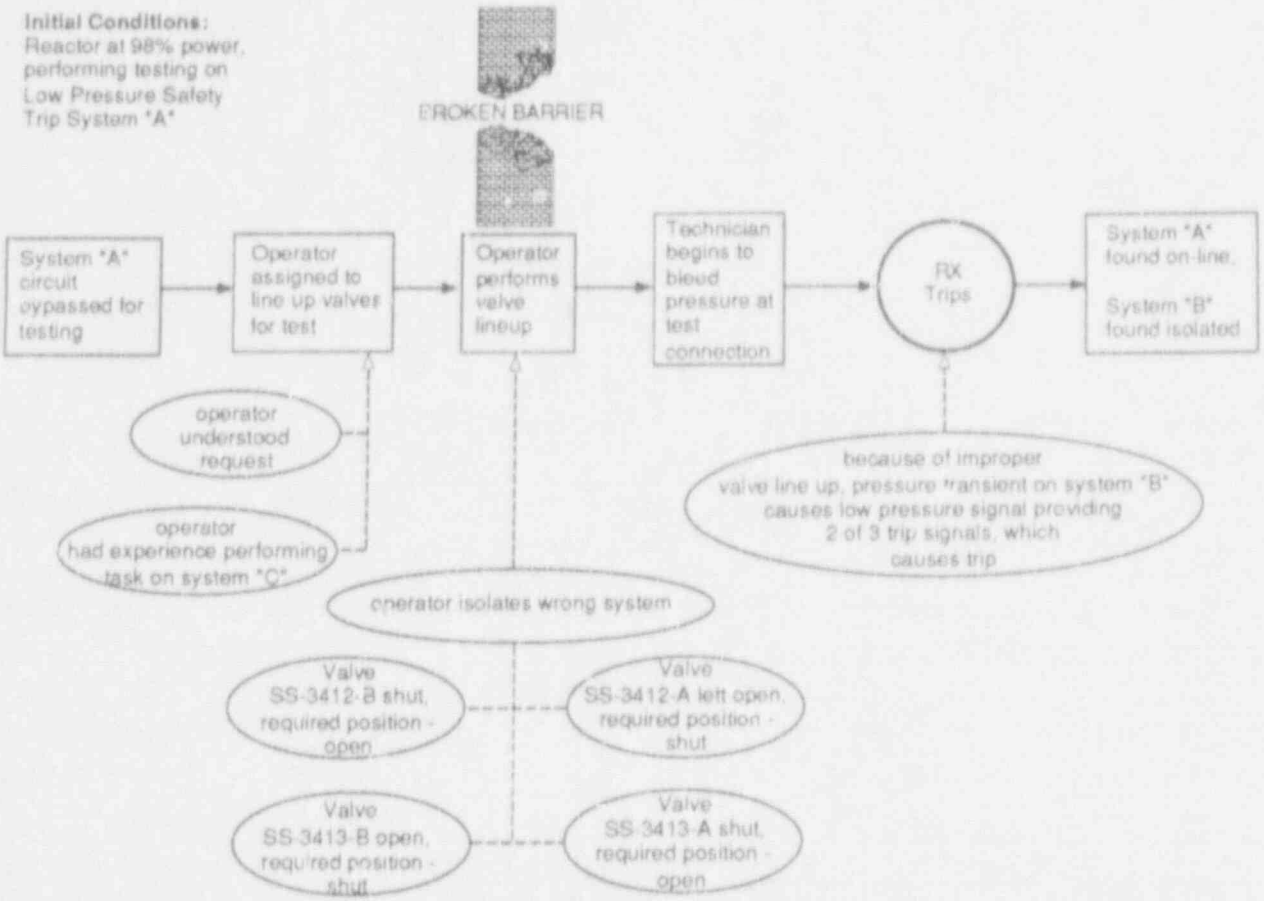

FIGURE 2: Events & Causal Factors Chart with a Broken Barrier

natural occurrences, human actions and administrative controls are in place as barriers to prevent this incident? (2) Where in the sequence of events would these barriers prevent this incident? (3) Which barrier(s) failed and allowed the incident to occur? (4) Which barriers succeeded and kept the incident from becoming an accident? (5) Are there additional physical boundaries, natural occurrences, human actions, and administrative controls that would have prevented this incident if they had been in place? Barriers and broken barriers can be illustrated by displaying them on an Events and Causal Factors Chart. An example of a broken barrier is provided on the Events and Causal Factors Chart in Figure 2.

- **Change Analysis** - a technique to help analyze an incident in a system that had previously been working properly, but that may have been negatively impacted by a change in the system or process. The focus of a Change Analysis is identifying the differences between past cases where the tasks were performed successfully and the current case where an incident occurred. Changes that contributed to the incident may require corrective action. Also the fact that changes were introduced that contributed to the incident may prompt the investigator to review the change control process.

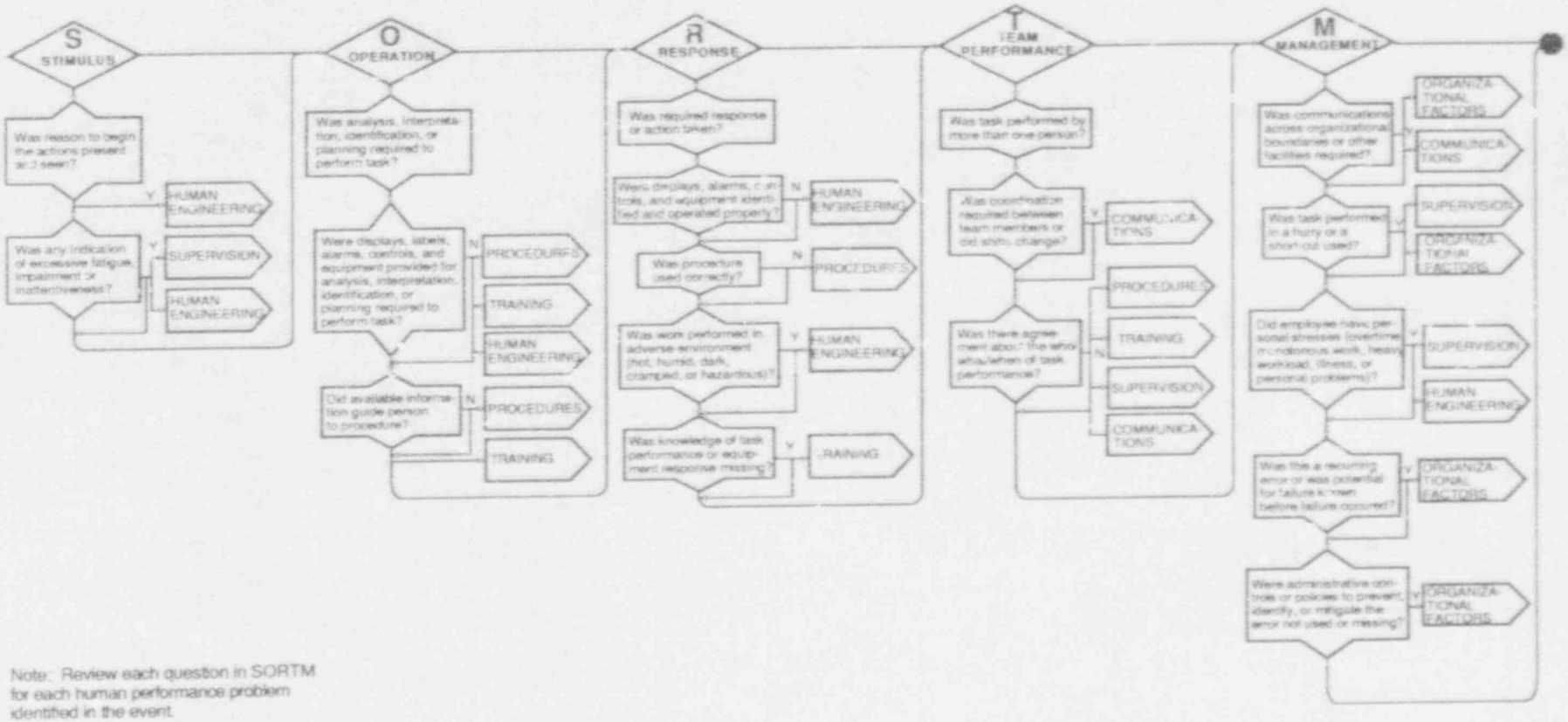

Note: Review each question in SORTM for each human performance problem identified in the event.

FIGURE 3: SORTM - Guide to HPIP Modules

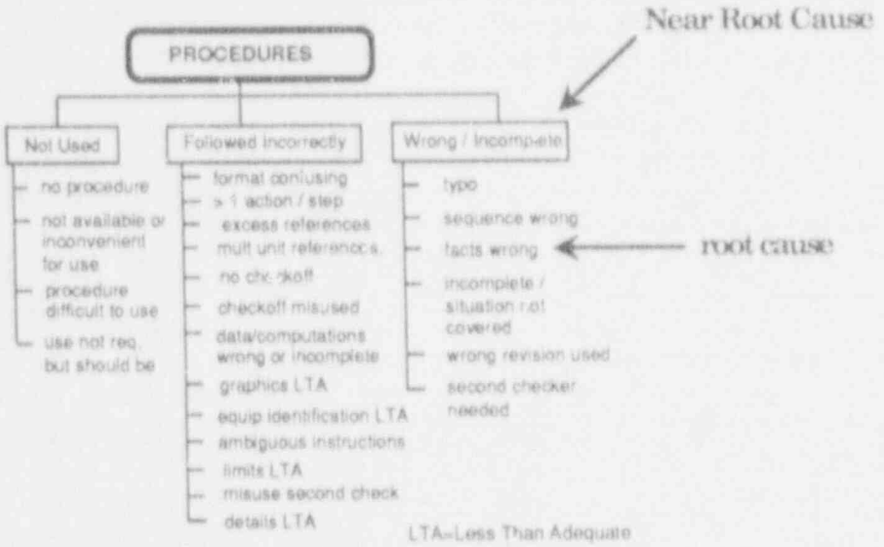

FIGURE 4: Procedures Module Potential Root Causes

PROCEDURE WRONG / INCOMPLETE		
QUESTION	PROBLEM IF	ROOT CAUSE
(22) Was a typographical error in the procedure responsible for the event?	yes	*Wrong / Incomplete -- typo*
(23) Are tasks and action steps sequenced according to technical necessity and physical layout of equipment involved?	no	*Wrong / Incomplete -- sequence wrong*
(24) Are the steps in the procedure factually correct (for example, proper set points, valve numbers, valve positions/settings, etc.)?	no	*Wrong / Incomplete -- facts wrong*
25) Were instructions left out that should have been included, or did the procedure fail to address all situations that reasonably should have been expected to occur during completion of the procedure?	yes	*Wrong / Incomplete -- incomplete / situation not covered*

FIGURE 5: Sample Procedures Module Questions

- **Critical Human Action Profile (CHAP)** - a technique based on task analysis and used to identify the human actions most critical to the failure of interest and to document the requirements that were necessary if these actions were to be performed successfully. CHAP is usually performed in the early stages of an investigation and the information provided is used throughout the investigation. The process of developing a CHAP involves three main steps: (1) Identify and record the human actions to be analyzed. The investigator must use his or her judgment to decide if all the human actions in the incident need to be recorded or just those in a particular part of the investigation that is of interest (perhaps areas where potential causes of the incident are suspected). (2) Decide which human actions, if they had been performed correctly, could have prevented the incident from occurring or could have significantly mitigated its consequences (these human actions are then called Critical Human Actions). (3) Collect and record information about the Critical Human Actions (the Profile) including: Who was to perform the action and with what? When was the action performed and what was the cue to perform the action? Where was the action performed and under what conditions?

Investigators will seldom, if ever, use all of these techniques during a single incident investigation. At a minimum, however, Events and Causal Factors Charting, SORTM, and one or more of the HPIP Modules will be used to identify the root causes of a human performance difficulty.

Once the root causes of an incident have been determined, the investigator needs to consider whether the cause is an isolated occurrence or the result of a programmatic weakness. For example, if a procedure is found to be difficult to use because it is written with more than one action per step (paragraph format), other procedures may have similar weaknesses. This procedures problem may, in turn, be the result of a programmatic problem: poor guidance and no training for the procedure writers. This type of programmatic cause is often uncovered by the review of the plant's operating experience or by reviewing additional procedures for similar problems. If similar problems are detected, the investigator then needs to dig deeper to uncover the reasons for the programmatic problems.

From the NRC's regulatory perspective, the results of an HPIP analysis (the incidents root causes) can then be used to review the utility's corrective actions (Did they address all the root causes?) and identify potential violations of rules and regulations. If the incident has been identified as being similar to past incidents: why weren't the previous corrective actions effective; how are the corrective actions currently proposed different from those proposed in the past; and are additional barriers proposed?

EVALUATION PROCESS

As noted earlier, HPIP is currently being evaluated in the field. This evaluation includes:

- Review of the process by the NRC's Research Program Review Group to evaluate HPIP's readiness for testing and suggest testing criteria.
- Review of the process at a usability workshop during which NRC personnel suggested improvements to HPIP.
- Independent evaluations of two HPIP training courses with recommendations to improve the training's effectiveness.
- Field testing of HPIP by 34 trained investigators.
- Firsthand observation by the development team of HPIP's use in the field.
- Assessment of the improvements in reports generated when using HPIP.
- Independent human factors review of HPIP.

ACKNOWLEDGMENTS

This work was sponsored by the U.S. Nuclear Regulatory Commission (NRC) under contract number NRC-04-90-78. The views, opinions, and/or findings contained in this paper are those of the authors and should not be construed as an official NRC position, policy, or decision.

ORGANIZATIONAL FACTORS INFLUENCING IMPROVEMENTS IN SAFETY

Dr. Alfred Marcus and Dr. Mary L. Nichols
Strategic Management Research Center
University of Minnesota

(With Dr. Jon Olson, Battelle; Dr. Richard Osborn, Wayne State University; and Dr. James Thurber, American University)

ABSTRACT

Research reported here seeks to identify the key organizational factors that influence safety-related performance indicators in nuclear power plants over time. It builds upon organizational factors identified in NUREG/CR-5437, and begins to develop a theory of safety-related performance and performance improvement based on economic and behavioral theories of the firm. Central to the theory are concepts of past performance, problem recognition, resource availability, resource allocation, and business strategies that focus attention. Variables which reflect those concepts are combined in statistical models and tested for their ability to explain scrams, safety system actuations, significant events, safety system failures, radiation exposure, and critical hours. Results show the performance indicators differ with respect to the sets of variables which serve as the best predictors of future performance, and past performance is the most consistent predictor of future performance.

1.0 INTRODUCTION

The Nuclear Regulatory Commission effort to develop leading indicators of safety-related performance in nuclear power plants requires use of longitudinal data and the analysis of relationships over time. In support of that need, this research has developed theory, derived from two prominent streams of literature, concerning expected effects of organizational factors on safety-related performance over time. Longitudinal data are employed to test the theoretical ideas.

The fact that conditions in an industry are continually changing causes some to view historical data and longitudinal analyses with skepticism. However, if leading indicators or historical trends are to provide valid regulatory tools, they must be interpreted within the context of an explanatory theory of relationships that is robust over time. This explanatory theory and not the specific relationships discovered in a single time period are what is important. Longitudinal analyses are required to test the adequacy of the explanatory theory. Thus, this research has sought to develop and test a robust theory to meet the NRC needs. It is this theory that can be most useful to the NRC in

pinpointing factors that have to be examined in more detail for their impact on the performance of nuclear power plants.

In NUREG/CR-5437 conceptualizations of safety from the perspectives of industry, academe, and the NRC are reviewed, and the use of NRC performance indicators for research purposes is supported as follows (NUREG/CR-5437, p.86):

> "In NRC's charter, safety is defined as the requirement to protect the public health, prevent accidents, and in case of accidents to minimize the consequences. Ultimate and final indications of lack of safety would be serious accidents, significant overexposure, and massive releases of radioactivity. So-called penultimate safety measures are concerned with conditions that would dramatically increase the likelihood of direct safety effects--substantial degradation of plant safety systems or excessive challenges to these systems, and exposures or releases that approach or exceed regulatory limits....In October 1986, based on the work done by the Interoffice Task Group (1986), NRC selected a group of safety indicators that had such desirable features as nonsusceptibility to manipulation and comparability between licensees...The logic model NRC used in developing these indicators...is concerned with low frequency of transients, high availability of safety systems, inherent design features, and low potential for cognitive errors."

The indicators the NRC selected for tracking include scrams, safety system actuations, significant events, safety system failures, and radiation exposure. As shown in NUREG/CR-5437, these indicators are the same or consistent with safety-related indicators suggested by INPO and previous academic research. Because of the properties they possess, the extent to which they are supported by theory and practice, and the availability of consistent, longitudinal data, these NRC performance indicators are used in large part in the empirical studies in this research.

2.0 ECONOMIC AND BEHAVIORAL PERSPECTIVES ON NUCLEAR POWER PLANT PERFORMANCE

In NUREG/CR-5437, a framework was proposed which links organization factors and nuclear power plant performance. The framework was developed by surveying and merging perspectives from industry, academe, and the NRC. Preliminary and limited tests of the model showed that it is a promising foundation for studying the role of organization factors in nuclear power plant performance.

The framework (NUREG/CR-5437) portrays, and the limited empirical testing confirmed, that nuclear power plants are complex entities affected by forces both inside and outside plant management's control that develop and exert an influence over time. The organizational factors presented in the framework point toward factors to look at, but they do not in themselves reveal how they may combine to create forces that influence nuclear power plant performance, nor do they tell how the forces work to influence performance. That is the task of theory development in the present research effort.

The goal of developing theory is to provide understanding of how the forces that influence performance work, and through that understanding to gain useful

knowledge which can be applied by regulators, corporate-level utility executive and plant management personnel. Since nuclear power plants are complex systems, insights into how to manipulate single organizational factors may only be partially useful, in the long term, to regulators or managers. Therefore, the aim of this section is to develop a well-grounded theory of how known organizational factors may combine to influence safety performance and safety improvement in nuclear power plants.

Two well-established bodies of theory about firm behavior — economic and behavioral theories of the firm — are drawn upon to create a theory of how organizational factors combine to influence safety-related performance in nuclear power plants. Both economic and behavioral theory of the firm are general theories of organizations. Both have proved extraordinarily useful. However, they were not developed with nuclear power plants in mind. In this section the general theories are drawn upon and applied to nuclear power plants and in some instances to the utility level of analysis.

In economic theory (Panzar and Savage, 1989), safety is determined by:

*the ability of a producer to afford safety since safety is both desirable and costly;

*government regulation to account for a lack of safety incentives because of market defects such as imperfect information and limited liability; and

*firm production decisions such as allocating resources to different categories of fixed and variable costs (e.g. plant investment versus supervision and engineering costs).

The type of technology and the producer's cumulative experience with that technology also have an impact.

The body of theory known as "the behavioral theory of the firm," suggests that additional factors may affect safety including:

*the organization's past routines which reflect its accumulated skills and standard operating procedures; and

*its strategic choices.

Routines have a central place in the behavioral theory of the firm. The largest portion of organizational activity is determined by them (March and Simon, 1958; Cyert and March, 1963; and Nelson and Winter, 1982). Organizations respond habitually to common circumstances according to routines which unfold automatically at an inert level based on well-learned "scripts" (Weick, 1987; Leibenstein, 1976; Langer, 1978). The routines focus the organization's attention and allow it to operate in ways which have been learned from the past to be successful, given the goals. Limits on the ability to process information and solve problems afresh for each problem that arises make it impossible for

organizations to function without them. On the other hand, the routines maintain current behavior, whether it is functional or not, and make change difficult to accomplish (Bromiley and Marcus, 1987). Thus, the organization's strategy choices are important since they channel attention to certain categories of activities within a constellation of competing claims for attention and may divert attention from other activities.

Integrating these two perspectives, the basic premise of a theory of safety-related performance and change in performance at nuclear power plants is that inertia prevails (past performance determines future performance) unless the organization focuses its attention on its problems. The problems must be identified (here the role of the regulatory agency can be important). The organization must have the resources to address its problems (here the concept of being able to afford safety is important); and it must appropriately apply these resources toward resolving its problems (here the resource allocation and the strategic decisions it makes are important). Its experience and the production technology it uses set limits on the improvements it can make (Figure 1. (For a full exposition of the theory, see NUREG/CR-5705, forthcoming.)

The theory which links the concepts in the model to improvement in performance is a theory of organizational learning in which problems are recognized via such means as comparisons with past performance, internal surveillance, SALP score evaluations, and violations. The utility has to have the resources to formulate solutions to the problems, and these resources have to be applied to implement the solutions. The problems are diagnosed based on the utility's capacity to focus attention on its nuclear power operations. If its attention is distracted by other priorities dictated by its business strategies, it is likely to be less successful in its problem-solving abilities.

2.1 Problem Recognition

The behavioral theory suggests that innovations and deviations from routines that upset an organization's equilibrium are relatively rare. The starting point for change is problem recognition. Bhopal, Challenger, TMI, and the Valdez oil spill all were preceded by warnings that something was wrong, but adequate steps were not taken to change the situation.

PROPOSITION 1: The level of safety is affected by the organization's ability to detect problems.

Detection errors arise because the noise to signal ratio is too high. Irrelevant information exists that obscures from attention what may be relevant to safety. Correctly noticing, interpreting, and incorporating stimuli are necessary for effective problem identification. Managers, however, may ignore or overlook undesirable events that have taken place; or they may assume that appropriate events have happened, even if they did not occur. Managers ignore overly discrepant information and fail to recognize information that is highly surprising (Kiesler and Sproull, 1982). Problem solving requires an awareness of problems that have to be solved, but key problems may go unnoticed when managers pay attention to peripheral and unimportant ones.

Figure 1

A Model of Improvement
Combining Economic and Behavioral Elements

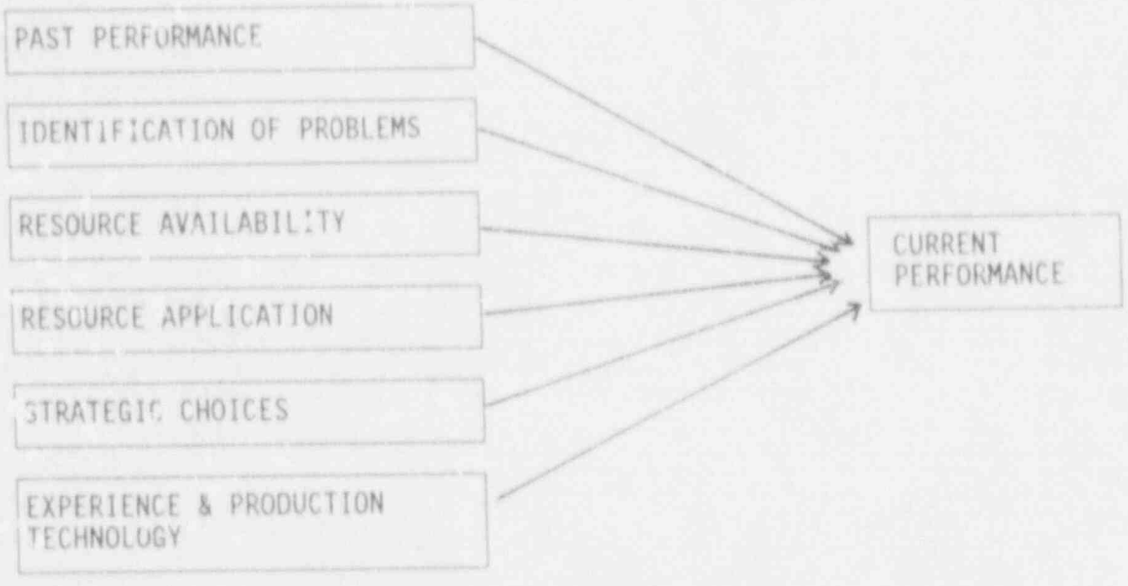

Some organizations are likely to view problem recognition as first steps to improvement, others as an impediment to normal business operations. The more openness there is to problems, the more likely it is that improvement can take place in an even, continuous, and progressive rather than in sudden, traumatic, and destabilizing fashion.

The NRC role in the nuclear industry is to make sure that this process of regular problem recognition occurs. It holds the plants to a philosophy of defense-in-depth, compelling them to adhere to a host of primary, secondary, and tertiary systems to control the reactor and prevent radiation (Osborn and Jackson, 1988). The philosophy of defense-in-depth commits the plants to multiple backups for important technical systems. To minimize the consequences of human error, it means that safety systems are automatically triggered if key equipment malfunctions. The NRC inspects plants to assure that they are complying with this philosophy and it does periodic on-site assessment. For failure to comply, plants can be cited for major and minor violations and deviations which are recorded and become part of their permanent record. The major violations, which occur at infrequent rates, can be major jolts to the system.

2.2 Resource Availability

The organization notices discrepant events signaling danger through internal efforts and those of outside regulators. When it becomes aware that problems exist, it requires resources to do something about them. To solve problems, the utility must have adequate resources to apply to the problem and implement solutions. Both the behavioral and economic perspectives stress the financial costs of safety. Neither accepts the idea that safety can be guaranteed by the intervention of outside regulators alone. The utility has to do something to enhance safety.

PROPOSITION 2: The level of safety is affected by the resources available for safety enhancing activities.

Considerable discretionary resources have to be invested in problem diagnosis and prevention activities. Systems have to be in place for classifying problems, tracking them, and doing causal analysis as to what prior conditions and actions produced the problems. Analysis of consequences is needed to ascertain the importance of problem. These processes are not possible if there is inadequately trained or inexperienced engineering support on-site or at corporate headquarters, if there is a lack of training in root cause or human error analysis, and if there is a lack of data on equipment history.

Discretionary resources may be needed so that engineers have the possibility of becoming senior reactor operators, and so managers and supervisors can gain on-site experience by involvement in job rotation (Olson and Thurber, 1991). These programs are costly. There has to be a high level of support for them. Training with simulators is needed for reacting to and understanding unexpected sequences of events. To support these and other types of problem diagnosis and prevention activities, the utility must have a strong record of prior earnings growth (Osborn and Jackson, 1988). The plant needs resources to

comply with NRC requirements, to acquire new and more sophisticated equipment, to carry out new and sophisticated training, to finance additional engineering support and safety review groups, and to achieve the defense-in-depth safety philosophy NRC requires.

The type of "gold plating" that is necessary is very expensive, and therefore only utilities with high earnings growth should be able to afford it. If they run safe plants then there will be a positive feedback on their earnings: they will not have to purchase power from other utilities if there are fewer safety mishaps and they are not shutdown as much.

2.3 Resource Application

Having the resources is not enough. The resources have to be applied so that specific groups in the utility are aware that there are problems. They have to discover the sources of error and create strategies to correct them. To the extent that utilities commit resources to groups capable of identifying problems and devising solutions, they are likely to be safer.

PROPOSITION 3: The level of safety is affected by resources that have been committed to groups with strong problem solving capabilities.

The two key groups at the power plant are operations and maintenance. Operations units are often heavily staffed with people with nuclear Navy backgrounds, maintenance units with people with craft and trade union (machinists and electricians) backgrounds. A third group is the engineers. Among these three groups there are likely to be differences in education, status, skills, modes of work, and motivation. Resource allocation plays an important role in nuclear power plant safety by distributing resources across these key problem solving groups. Resource allocation influences the distribution of power and the practical reality of how many people of what type are available to problem solve.

2.4 Focusing Attention

The behavioral approach emphasizes that well-defined routines structure a large part of the organization's behavior. Nelson and Winter (1982) place in the category of an organization's rules the strategies it adopts. These strategies focus its attention. They structure both consciously and unconsciously its actions by (March and Olsen, 1976). Since many demands are made on the organization and it cannot pay attention to them all, the organization's strategies transfer demands among possible sets of active, inactive, and unconsidered activities (Cyert and March, 1963).

PROPOSITION 4: The level of safety is affected by the organization's attention-focusing strategies.

2.5 Technological Experience

Economic theory suggests the importance of the relationship between experience and safety. Classic studies in manufacturing show that as production experience grows, learning increases and organizational performance improves. Producer skills rise with the accumulated knowledge about the physical equipment and the materials used in production. Productivity grows continuously with experience because of increasing organizational knowledge about the technology (Dutton et. al., 1984).

Many of the initial studies of learning in manufacturing were carried out in the American aviation industry where unit costs declined rapidly with cumulative output. Greenberg (1969) extended this type of analysis to safety contending that as organizations matured they would have fewer accidents. Prolonged experience with the hardware reveals information about performance and operating characteristics (See Rosenberg, 1982) that in turn should lead to new practices that increase safety.

PROPOSITION 5: The level of safety is affected by production experience with a technology.

2.6 The Past As Determinant of Current Behavior

The behavioral theory of the firm predicts that organizational performance in a particular time period is likely to be influenced by performance in the past time period. As Nelson and Winter (1982; p. 10) state, "the regularities observable in present reality are...the result (of) understandable dynamic processes..produced from known...conditions in the past." Since the conditions of an industry in a prior period bear the seeds of what it is going to do in the next period (p.29), by considering what an organization has done in the past it is possible to sharpen predictions about what it is to do in the future (p. 89).

Furthermore, the rules which establish an organization's predictable behavior cover a vast array of activity. The predictable behavior patterns and routines that guide behavior range from the well-specified technical routines that enable production to take place, to the organization's schedules, plans, and precedents. They also involve the policies the organization has regarding investment, research and development, and marketing.

PROPOSITION 6: The current level of safety is influenced by the organization's past safety performance.

3.0 EMPIRICAL STUDIES OF PERFORMANCE INDICATORS (INCLUDES CRITICAL HOURS)

Drawing on perspectives from economic and behavioral theories of the firm, our combined model stresses the following concepts: past performance, problem recognition, resource availability, resource application, and business strategy. The objective of this section is to test these concepts with a systematic

analysis of the safety and reliability-related performance of nuclear power plants including the improvement and degradation in their performance over time. Five performance indicators as well as critical hours are examined to assess their relationship to the explanatory concepts in the model. Since most of these safety indicators are event count data, a Poisson regression model has been used when appropriate.

Event count models are appropriate for understanding some of the NRC performance indicators. The Poisson distribution is useful in describing the number of events that will occur in a specific time period. The Poisson shows the probability of an event occurring in a given unit of time or the mean or expected number of events per unit. Other examples for which the Poisson provides a good model (McClave and Benson, 1985) are: the number of industrial accidents in a given period of time observed by a plant supervisor; the number of noticeable defects found by quality inspectors; the number of errors per time period that employees make in an industrial plant; and the number of breakdowns of equipment or machinery per period in the plant.

Typically, event count models like these are not normally distributed, and the values of the variables are quite low (as is the case with NRC performance indicators). Research involving event count models suggests that these models typically follow a Poisson distribution.

Poisson models have the advantage of providing a better fit for event count data because a Poisson distribution is constrained to only positive values, unlike a linear model in which variables may take on positive or negative values. And unlike logit models, Poisson models do not limit the positive values to be between zero and one. The NRC performance indicators that have been used are always positive, therefore, using least squares estimation would lead to biased estimates of parameters. Least squares analyses of event counts are inappropriate because they can produce these biased and inconsistent estimates (King, 1988). The method of least squares with its assumption of linearity does not constrain the expected value of the dependent variable to be non-negative and thus can produce implausible predicted values.

Because event count models and Poisson estimation provide a more plausible representation of event data, they have been used to investigate the performance of nuclear power plants for four performance indicators: Scrams, Safety System Actuations, Safety System Failures, and Significant Events. Because radiation exposure and critical hours are measured by the amount per year, an event count model is not appropriate. Therefore, analysis of these dependent variables was conducted with ordinary least squares.

This section develops appropriate statistical models for the four safety-related performance indicators which use discrete non-negative integers that measure the number of times an event occurs in a fixed time, as well as traditional least squares regression models for the two indicators which are continuous variables. In this case, data from a period of two years, 1987 through 1988, have been used as the dependent variable.

3.1 Dependent Variables

The dependent variables in these analyses consist of the five NRC performance indicators and critical hours. A detailed definition of each performance indicator as described in NUREG/CR-5137 is as follows:

Unplanned Automatic Scram

An unplanned automatic scram (scram) occurs as an actuation of the reactor protection system that results in a scram signal at any time when the unit is critical. The scram signal may result from exceeding a set point or may be spurious. Scrams planned as a part of special evolutions or tests and manual scrams are not counted by this indicator. The number of scrams while critical is closely related to unit safety. Since unplanned automatic scrams are initiated to prevent the reactor from exceeding the safety limits and system safety settings, scrams usually indicate that something is wrong that could place the plant in a less safe condition. In addition, due to the fact that every scram challenges the safety systems and accumulates transient age on plant equipment, the absence of scrams is an indicator of good performance.

Safety System Actuation

Safety system actuation (SSA) occurs when a set point for the system is reached or when a spurious/inadvertent signal is generated and major equipment is actuated. The equipment that is considered in the actuation is the emergency core cooling system and AC emergency power. Any unplanned actuation of a safety system indicates a set point or limit established for safety has been reached. The systems have been selected because their actuation is considered to be a direct indication of a significant off-normal plant condition.

Safety System Failure

A safety system failure (SSF) occurs when the system is unable to perform its intended function during the time that the reactor is in an operating mode that would normally require the availability of the safety system. Unavailability is caused by component failure or removal of components from service for corrective or preventive maintenance when the safety system is required to be available. System unavailability is calculated from component unavailable hours, using a model of the selected system. Therefore, it reflects not only the time the complete system is actually unavailable, but also includes a contribution due to partial system unavailability. In PWRs, emergency AC power, the high pressure safety injection system, and the auxiliary feedwater system are monitored. In BWRs, the systems monitored are emergency AC power, high pressure coolant injection or high pressure core spray system, and the reactor core isolation cooling or isolation condenser system.

Significant Events

As defined in NRC's AEOD annual report, 1988, "Significant events are those operational events reported to the NRC that the NRC staff identifies through detailed screening and evaluation as meeting certain selection criteria enumerated in this paragraph. The screening process includes a

daily review and discussion of selected operating reactor events. Significant events normally involve one or more of the following selection criteria: (1) the degradation of important safety equipment; (2) an unexpected plant response to a transient or a major transient itself; (3) a degradation of fuel integrity, primary coolant pressure boundary, or important associated structures; (4) a reactor trip with complications; (5) an unplanned release of radioactivity exceeding plant Technical Specifications (TS) or other regulations; (6) operation outside the limits of TS; and (7) other events that are considered significant."

Collective Radiation Exposure

This is a measure of the average collective radiation exposure to utility employees, contractors and visitors by unit. This indicator is an indirect measure of plant safety since plants with low collective radiation exposure are generally regarded as being well-managed in the control of plant contamination and efficient in the administration of the ALARA (maintaining radiation exposures as low as reasonably achievable) program.

All performance indicators are totals for 1987 and 1988, thus they are represented, respectively, as TSM78, TSA78, TSF78, TSE78, and RAD78.

In addition, a measure of plant efficiency, critical hours, was included in the analysis to compare the results from the safety variables with efficiency. Critical hours (CRT) is the number of hours operating during a given year. In this analysis, the total critical hours for 1987 and 1988 were used.

3.2 Independent Variables

The independent variables used in these analyses are specified below:
Past Performance: For each model where past performance is used in an equation to explain improvement or degradation, it is represented as follows:

in models in which TSM78 is the dependent variable, one of the independent variables is TSM56 (scrams in 1985-86);

in models in which TSA78 is the dependent variable, one of the independent variables is TSA56 (safety system actuations in 1985-86);

in models in which TSE78 is the dependent variable, one of the independent variables is TSE56 (significant events in 1985-86);

in models in which TSF78 is the dependent variable, one of the independent variables is TSF56 (safety system failures in 1985-86);

in models in which RAD78 is the dependent variable, one of the independent variables is RAD56 (radiation in 1985-86);

in model in which CRT78 is the dependent variable, one of the independent variables is CRT56 (critical hours in 1985-86).

Problem Identificatio. For all models, NRC problem identification is represented by:

number of major violations in 1985 (NOMAJV85); and

1985 SALP scores (SALP).

The SALP scores (Systematic Assessment of Licensee Performance) are NRC evaluations of licensee performance in 1985, which are the sum of the total of operations, maintenance, surveillance and quality program scores, (each with a value of from 1 to 3, where 1 is excellent, and 3 is poor).

Resource Availability: Utility financial performance is represented in different models by:

return on assets in 1985 (ROA85)

debt to equity ratio in 1985 (DE85);

return on investors capital in 1985 and 1986 (ROI);

and operating efficiency in 1985 and 1986 (OPEFF), which is the earnings before taxes as a percentage of total assets

Resource Application: Utility application of resources is represented by:

a fixed cost component, 1985-86 plant costs per megawatt capacity (PLANT2); and

two variable cost components --

1985-86 operations supervision and engineering expenses per megawatt capacity (SEOP) and

1985-86 maintenance supervision and engineering expenses per megawatt capacity (SEMT); or

RSEOP, the ratio of operations supervision and engineering spending over total supervision and engineering (including maintenance) in 1985 and 1986 (RSEOP).

The final variable measures the amount of total supervision and engineering spending dedicated to operations. The higher the ratio for RSEOP, the greater emphasis management is placing on operations supervision and engineering as opposed to maintenance. This variable simplifies the analysis as it captures in a single dimension both SEOP and SEMT. It therefore permits a more careful assessment of the trade-off between spending on these two items.

Plant Experience: For all the models, plant experience is represented by:

historic production as of 1985 (E2X).

Historic production is defined as reactor age x its size in megawatts x its historic capacity factor as of 1985.

Technology: For all models, a control variable is introduced for:

type of reactor (TYPE).

A dummy variable is used with 0 representing pressurized water reactor and 1 representing boiling water reactor.

Business Strategies: Utility business strategies are represented in different models as follows:

Focus Diversification = Equity in Earnings of Subsidiary Companies/Net Generation Revenues 1984-86 (DIVER);

Focus Transmission & Distribution = Transmission and Distribution Plant Costs/Nuclear Power Plant Costs 1984-86 (TD);

Focus Alternative Power Generation = Other Generation/Total Generation 1984-86 (OTHER); and

Focus Power Production = Dollars from sales for Resale/Net Generation Revenues 1984-86 (PROD).

In some models a focus on the continued construction of generating capacity replaces the focus on production.

Focus On Continued Construction = Electric Construction Work in Progress 1984-86 (ecwp).

For all of the independent variables, lagged values have been used. A correlation analysis of concurrent years of the independent and dependent variables reveals weak contemporaneous effects. However, our explanatory models assume a time-lag. For an independent variable to affect a dependent variable, it must occur prior to the occurrence of the dependent variable. If independent and dependent variables are concurrent, it is not possible to know which set of variables causes the other. Lagged values therefore are presented here.

3.3 Plant Population

The analysis was conducted on 58 of the 100 privately-owned U.S. nuclear power plants. Due to the theory being tested, only privately owned plants where financial data on the parent utility is available can be used. The number of plants was reduced due to missing data. If a plant was missing data for any of the dependent or independent variables in the model, standard convention was followed and the plant was dropped from the analysis. Closer study of the distribution of the plants shows that it is quite representative with most plants coming from the northeast, southeast and the midwest, where most plants actually are located. There are fewer plants from the west and south as would be expected. There are 38 plants with pressurized water reactors and 20 plants with boiling water reactors, which is also similar to the actual distribution.

Nuclear Power Plants included in the study

NRC Region		Reactor type	Plant Name
North East	1	BWR	OYSTER CREEK
North East	1	BWR	NINE MILE PT. 1
North East	0	PWR	INDIAN POINT 2
North East	0	PWR	SALEM 1
North East	1	BWR	PEACH BOTTOM 2
North East	1	BWR	PEACH BOTTOM 3
North East	0	PWR	THREE MILE IS. 1
North East	1	BWR	PILGRIM
North East	0	PWR	SALEM 2
North East	1	BWR	SUSQUEHANNA 1
North East	1	BWR	SUSQUEHANNA 2
South East	0	PWR	TURKEY POINT 3
South East	0	PWR	TURKEY POINT 4
South East	0	PWR	ROBINSON 2
South East	0	PWR	OCONEE 1
South East	0	PWR	OCONEE 2
South East	0	PWR	SURRY 1
South East	0	PWR	SURRY 2
South East	0	PWR	OCONEE 3
South East	1	BWR	HATCH 1
South East	1	BWR	BRUNSWICK 2
South East	1	BWR	BRUNSWICK 1
South East	0	PWR	ST. LUCIE 1
South East	0	PWR	NORTH ANNA 1
South East	0	PWR	NORTH ANNA 2

South East	2	0	PWR	FARLEY 1
South East	2	0	PWR	FARLEY 2
South East	2	1	BWR	HATCH 2
South East	2	0	PWR	MCGUIRE 1
South East	2	0	PWR	MCGUIRE 2
South East	2	0	PWR	ST. LUCIE 2
South East	2	0	PWR	SUMMER
Midwest	3	1	BWR	BIG ROCK POINT
Midwest	3	1	BWR	DRESDEN 2
Midwest	3	1	BWR	DRESDEN 3
Midwest	3	1	BWR	QUAD CITIES 1
Midwest	3	0	PWR	PALISADES
Midwest	3	1	BWR	MONTICELLO
Midwest	3	1	BWR	QUAD CITIES 2
Midwest	3	0	PWR	PRAIRIE ISLAND 1
Midwest	3	0	PWR	ZION 1
Midwest	3	0	PWR	ZION 2
Midwest	3	0	PWR	KEWAUNEE
Midwest	3	0	PWR	PRAIRIE ISLAND 2
Midwest	3	0	PWR	COOK 1
Midwest	3	0	PWR	COOK 2
Midwest	3	1	BWR	DUANE ARNOLD
Midwest	3	1	BWR	LASALLE 1
Midwest	3	1	BWR	LASALLE 2
Midwest	3	0	PWR	CALLAWAY
South	4	0	PWR	ARKANSAS 1
South	4	0	PWR	ARKANSAS 2
South	4	0	PWR	BYRON 1
South	4	0	PWR	WOLF CREEK
West	5	0	PWR	SAN ONOFRE 1
West	5	0	PWR	DIABLO CANYON 1
West	5	0	PWR	TROJAN
West	5	0	PWR	SAN ONOFRE 2

Region total		Reactor type total
North East = 11	South = 4	PWR = 38
South East = 21	West = 4	BWR = 20
Midwest = 18		

3.4 Results

The results of the analyses are presented in this section. The purpose of the analyses is to test the concepts set forth in the combined theory described in Section 2. Five points should be made at the outset so that the results are somewhat easier to understand:

(1) What is being tested are full statistical models, that is, statistical models containing variables representing each of the different concepts thought to influence the performance indicators and critical hours. The theory states

that variables work together to influence performance, and thus they are tested in combination rather than individually. In testing a full model, the assumption is that an independent variable influences a dependent variable in the presence of, or controlling for, the other independent variables.

(2) The empirical work is an attempt to test the theory and the concepts and not the specific variables. In fact, the analyses are sometimes deliberately run with different variables representing the various concepts in an effort to cross-validate the model and explore the robustness of it.

(3) The models are tested with regard to their ability to explain performance in a given time period, as well as their ability to explain improvement or decline (change) in performance. In tests where explanation of change in performance is sought, this is accomplished by controlling for past performance, so the actual dependent variable becomes the change in performance from one time period to the next.

(4) These are statistical models and therefore, the results when significant indicate that the greater the amount of an independent variable in a time period, the greater the amount of the dependent variable. With the theory, they have explanatory power, but they are not deterministic models in the sense that every time the independent variable exceeds a certain threshold, the dependent variable has to occur. Rather, in aggregate in the entire population, there is a strong tendency for the independent and dependent variables to be related. The best analogy is epidemiology, where the presence of a disease is found to a greater extent in a population, not microbiology, where the presence of a virus, holding everything else constant, always causes the disease.

(5) For the Poisson regressions the overall fit is evaluated using a chi-square test of the significance of the log-likelihood ratio. In all the results presented, the p-values are approximately zero. This implies that the full models (Ha: not all β=0) are significantly better than the null models (Ho: all β=0) for all four safety indicators tested using Poisson regression. This test is similar to a test of the overall fit conducted in linear regression. In ordinary least squares regression, an F-test of the null hypothesis is conducted.

The purpose of the analyses in this section is to construct refined statistical models of the performance indicators and critical hours for purposes of prediction. What is presented represents an attempt to construct the best statistical models possible for each performance indicator using variables derived from the theory. Determination of what appear to be the "best" models to date, given the theory, is based on these criteria: (1) they provide the best fit to the data (or explain the most variance in the data); (2) where alternative variables are available, they employ variables with the most face validity, making them more interpretable; and (3) where possible they employ variables that are less prone to accounting manipulation in financial reports than comparable variables may be.

The results of the analyses are in Tables 1-2. The goal is to develop the best models possible for each of the variables, in light of the current theory and available data. In the discussion, the interpretation will focus on

what explains improvement in performance (i.e. positive change instead of negative change). The interpretation can be readily reversed to explain degradation.

Scram Model:

The fewer scrams a plant has in the past, the fewer it is likely to have in the future; the more production experience it has, the fewer likely scrams it will have. Each of these predictors are significant at $p < .05$. Another theoretical concept which is also related to scrams ($p < .10$) is resource application, represented by plant costs. As the cost of the plant increases, the number of scrams decreases. This indicates that as the nuclear utilities spend more money on building, improving and re-structuring plants, they also lower the number of scrams. The model suggests that a well-built and well-maintained plant has fewer incidents of scrams.

Significant Event Model:

Significant events are negatively associated ($p < .05$) with ROI, return on investors' capital. Therefore, the more profitable the utility is the less likely its plants will experience significant events. Resource availability in the past leads to fewer significant events in the future. The results also indicate resource application can help reduce the number of significant events a plant experiences. The more that supervision and engineering expenses are dedicated to operations (as opposed to maintenance) as measured by the ratio of SEOP and SEMT, the fewer significant events a plant will have ($p < .05$). In addition, past performance has an important influence ($p < .05$) on current performance. Significant events are not influenced by other factors such as the NRC problem identification and utility business strategies.

Safety System Actuation Model:

For safety system actuations, problem identification has some impact on future performance. The number of major violations is negatively related to safety system actuations ($p < .10$), suggesting that violations in the past lead to better performance in the future. It could be interpreted that by issuing citations, the NRC sends a message to the violating plants and, on average, plants address the problem and experience fewer safety system actuations in the future. For this model, past performance on safety system actuations had a significant impact on future performance ($p < .05$). The type of reactor also had a significant impact on safety system actuations ($p < .05$). PWR's experience fewer actuations than BWR's.

Safety System Failure Model:

Safety system failures are influenced by a variety of the concepts in the theoretical model. Both of the NRC problem identification variables are significant here ($p < .05$). This model suggests that as the lagged SALP score improves, the number of safety system failures decreases. Further as the number of past major violations increases the number of safety system failures decreases for the range found in the data.

Table 1 Refined Models of Performance Indicators Using Poisson Regression Estimation (RSEOP)

	Scram		SE		SSA		SSF	
Independent Variable	Est. Coef.	t-Stat	Est. Coef.	t-Stat.	Est. Coef.	t-Stat.	Est. Coef.	t-Stat.
Nomajv85	-0.020	-0.418	-0.059	-0.626	-0.136	-1.672	-0.084	-2.444***
Salp	-0.016	-0.390	5.916	0.856	-0.076	-1.226	0.185	5.043***
ROI	4.988	0.601	-28.069	-2.180**	-6.044	-0.504	-11.992	-1.924*
Opeff	4.627	0.656	15.302	1.436	10.228	1.030	12.765	2.280**
Pleat	-0.833	-1.778*	0.131	0.179	0.123	0.199	-0.088	0.225
Rseop	-0.058	-0.152	-1.313	-2.062**	0.868	1.455	-1.720	-5.791***
Prod	0.839	0.986	1.357	1.021	1.557	1.271	-0.468	-0.687
Td	0.033	0.802	-0.026	-0.409	0.005	0.086	-0.019	-0.504
Diver	10.012	-0.637	5.360	0.209	-6.316	-0.326	-0.505	-0.040
Other	1.970	1.095	3.486	1.281	-1.734	-0.638	2.928	2.144**
E2x	-0.731	-2.071**	0.522	0.771	-0.661	-1.239	0.289	1.101
Type	0.002	0.009	0.180	0.640	0.435	1.968**	0.571	4.490***
Past	0.037	2.604***	0.083	2.172**	0.118	3.070***	0.025	1.792*
Constant	0.723	1.064	1.577	1.478	0.180	0.190	1.367	2.593
N	58		58		58		58	
Log Liklihood & Ratio	174***		50***		80***		1156***	

*p< .10
**p< .05
***p< .01

Table 2 Refined Models of Performance Indicators Using Ordinary Least Squares Estimation

Independent Variable	Dependent Variable: Radiation Exp. (1987-88) Est. Coeff.	t-Stat	Critical Hours. (1987-88) Est. Coeff.	t-Stat
Nomajv85	123.520	4.046***	-335.741	-1.135
Salp	-34.586	-1.312	15.731	0.061
ROI	3267.160	0.713	11334.100	0.216
Opeff	-3176.760	-0.801	-1654.090	-0.037
Plant	-490.506	-1.855*	-2841.200	-1.147
Rseop	-328.318	-1.361	2149.870	0.868
Prod	-276.245	-0.626	2748.420	0.550
Td	21.403	0.803	153.954	0.502
Diver	-12087.000	-1.633	107273.000	1.269
Other	125.087	0.084	3831.940	0.255
E2x	229.919	1.030	-5836.910	-2.705***
Type	160.054	1.301	-1150.540	-1.102
Past	0.510	5.190***	0.626	2.700***
Constant	651.306	1.438	6194.730	1.200
N	49		53	
Adjusted R-squared	0.74		0.25	

*p< .10
**p< .05
***p< .01

There is an influence of the resource availability variables on safety system failures. Both ROI ($p < .10$) and operating efficiency ($p < .05$) were significantly related to safety system failures. For ROI, the more profitable the utility was the fewer safety system failures it had. On the other hand, operating efficiency was positively related to failures. Operating efficiency (Opeff) is the ratio of earnings before taxes to total assets employed. If earnings are high relative to total assets, it may suggest that expenses are being minimized and the benefits of running the assets are being harvested, with less concern for maintaining safety systems in an effective and efficient state. Another interpretation is that some slack in the resources and a willingness to spend them is necessary to be able to improve the plant's performance (see Figure 3.12). When resource availability is measured as ROA and debt no significant relationship with safety system failures are found. The nuclear utility application of resources also plays a significant role in this model. As in the significant events model, higher spending on RSEOP was associated with fewer safety system failures ($p < .05$).

In addition, other power generation, plays an important role in this model ($p < .05$). As the utility focuses on other power generation technologies, it may divert attention from nuclear power generation, thus resulting in higher safety system failures. Finally, past safety system failures ($p < .10$) and the type of power plant ($p < .05$) are present in the model predicting change in future safety system failures. Plants with few past safety system failures tend to stay good while plants with many previous failures tend to show more in the future. For the type of plant, the model suggests that plants with pressurized water reactors have a lower incidence of safety system failures than boiling water reactors.

The refined model for safety system failures shows significant predictors from each of the major theoretical groups of factors (problem identification, resource availability, resource allocation, business strategies). It suggests not that the theory works "better" than for other dependent variables (for all the models are highly significant) but that all the factors in the theory work in combination to allow prediction of safety system failure. The model predicts that plants that will have the fewest safety system failures in the future are pressurized water reactors which had few failures in the past, received good (low) salp scores, had good earnings, expended resources in such a way as to favor supervision engineering operations expenditure versus supervision engineering maintenance expenditures, and do not distract themselves by pursuing "other" alternative forms of energy production.

Radiation Exposure Model:

The results for ordinary least squares analysis of radiation exposure (see Table 2) suggest that problem identification, resource application, and past performance have a strong influence, and resource allocation plays some role as well. For problem identification, the number of major violations was positively related to radiation exposure ($p < .01$). This suggests that plants experiencing few major violations in the past have low radiation exposure in the future, while those having problems in the past continue to experience them later on. However, the model suggests that spending resources in the plant can reduce the amount of exposure in the future. Finally, as with many of the safety indicators, the past

seems to be a strong predictor of radiation exposure ($p < .05$). The model as a whole explains 74 percent of the variance in the radiation variable, indicating a strong fit.

Critical Hours Model:

Critical hours is not explained particularly well by the model, (adjusted $R^2 = .25$). The only important predictors ($p < .05$) in this model were past performance on critical hours and operating experience (Table 2). Plants with high critical hours in the past have high critical hours in the future, and plants that have less experience (i.e. fewer total megawatts generated) have more critical hours.

The overall results of this analysis suggest several key concepts which are important to understanding nuclear power safety. First, problem identification is shown to be important to both safety system failures and radiation exposure. NRC has a particularly important role to play in regard to these performance indicators. Resource availability, too, has an effect on several of the safety-related indicators. As measured by return on investment and operations efficiency, it is significantly related to both safety system failures and significant events. Resource application is an important factor which influences a number of the safety-related indicators. Both plant costs and spending on operations (and not maintenance) as a percent of total supervision and engineering prove useful in explaining safety-related performance. The findings are very strong and stable in the case of safety system failures and significant events. The measures of business strategy, on the whole, have a less stable impact; nonetheless, there is evidence in the models that distractions in various forms negatively affect performance. Alternative power production has a fairly consistent negative relationship to safety system failures and to significant events. The past has a very strong effect on nearly all the performance variables. Overall, the organizational learning model which combines elements from economic and behavioral theory has proven to be a very useful means for examining the effects of various variables on nuclear power plant performance.

3.5 Issues of Multicollinearity

Multicollinearity, (i.e., strong correlations among the independent variables) can pose problems for interpretation of regression results. The main effect of multicollinearity is to increase the variance of the coefficient estimates, therefore making it less likely that significant relationships with the dependent variable will be found. However, even with multicollinearity, the coefficient estimates are unbiased.

The correlations among the independent variables are shown in Table 3. The only particularly high correlation is the .70 correlation between ROI and operating expenditures. The effect of this correlation may lead us to conclude that resource availability has less impact than it in fact does (i.e., we are more likely to accept the null hypothesis). In order to examine the extent of the problem, the full model was re-run first dropping the operating efficiency variable, then excluding the ROI variable. The results of this analysis do not change the substantive conclusions of the model. Therefore, although some

Table 3 Correlations Among the Independent Variables

	Nomajv85		Salp	ROI	Opeff	Plant	Rseop	Prod	Td	Diver	Other	E2x
Nomajv85		1.00										
Salp	.40	1.00										
ROI	.09	-.02	1.00									
Opeff	.11	-.23	.70	1.00								
Plant	.09	-.24	-.19	-.14	1.00							
Rseop	.21	.14	.04	-.19	-.12	1.00						
Prod	-.06	.21	.11	-.15	-.22	-.01	1.00					
Td	-.15	-.11	-.26	-.01	.02	-.12	-.04	1.00				
Diver	-.10	-.19	.32	.15	-.26	.09	.07	-.27	1.00			
Other	.01	-.09	-.31	-.19	-.07	.19	-.17	.03	-.06	1.00		
E2x	-.29	-.09	.23	.19	-.29	.17	.05	-.13	.27	.06	1.0	

N=52

multicollinearity is evident in these models, it appears to have little substantive importance.

4.0 CONCLUSIONS

Results of the quantitative analyses reported in this paper can be summarized in the following conclusions:

1. Central concepts in the theory of safety in nuclear power plants, which have roots in the economic and behavioral theories of a firm, are effective in predicting safety-related performance in plants. Furthermore, the patterns of results can be logically interpreted in light of the proposed theory. While the central concepts of the theory, taken together, are not necessary to predict each performance indicator, they combine in different ways across indicators such that:

*Past performance on a given performance indicator generally predicts future performance.

*Improvement is most likely to occur when NRC problem identification plays a role, resources are available, the resources are allocated to a set of problem solving activities, and utility attention is not diverted by the pursuit of business strategies unrelated to nuclear production.

2. Different performance indicators have different sets of explanatory concepts which predict them. Some are only predicted by their past performance, while others have fuller sets of predictors which explain improvements in operations. It is the sets of concepts (or "profiles") which are predictive and explanatory, and not the individual variables. The individual variables are representative of the broader concepts. The statistical analyses are viewed as validation of the broader model, not the individual measures.

3. The theory shows that plant performance is influenced by utility-level factors in addition to plant-level factors. Valid plant profiles must include such utility-level variables as financial condition, allocation of resources, and business-level strategies.

4. The sets of predictive concepts which comprise the "profiles," taken together, are robust and could serve to provide leading information about future plant performance on selected performance indicators. Such leading information can be used as further input to the decision making process, though it is not expected to yield a single indicator that could be regulated directly. The promise is in using the theory as a whole to track and interpret patterns in the measures of the central concepts.

If striking oscillations take place in the patterns then the theory suggests that further investigation by NRC may be called for. For instance, aberrations in utility profitability, debt, and operating efficiency might call for NRC investigations about their impact on nuclear performance. So too, changes in resource allocation to the categories of expenses classified as supervision and engineering for operations versus maintenance might require NRC

assessment of impacts. If a utility decides to deemphasize nuclear operations by focussing on other business or power generation strategies, this should alert NRC. A combination of many changes at once means a likely impact on nuclear power plant performance. NRC should question utility and plant staff about the ramifications of these changes.

5. Organizational factors that are measurable exert an influence over time on safety-related performance. The factors require a lag time to show influence, but once they do, inertial forces may cause the influence to persist over time. Further research is needed to investigate this. Plants may get drawn into beneficent or vicious cycles from which they do not readily depart. When they do depart, for better or worse, it is due to changes in organizational factors described in the derived models in Section 3.

6. Improvement in safety-related performance can be obtained through management attention to processes of organizational learning and the context in which such learning processes occur.

REFERENCES

Bromiley, P., and A. Marcus. "Deadlines, Routines, and Change," Policy Sciences, 20(2):85-103.

Cyert, R., and J. March. A Behavioral Theory of the Firm. Englewood Cliffs, NJ: Prentice-Hall, 1963.

Dutton, J., A. Thomas, and J. Butler. "The History of Progress Functions as a Managerial Technology," Business History Review, pp. 204-233.

Greenberg, L. "The Application of Accident-Experience. Learning Curves to the Study of Occupational Accidents in the American Petroleum Industry," New York:New York University Dissertation, 1996.

Kiesler, S., and L. Sproull. "Managerial Response to Changing Environments: Perspectives on Problem Sensing from Social Cognition," Administrative Science Quarterly. Vol. 27, 1982, pp 548-570.

King, Gary. "Statistical Models for Political Science Event Courts. Bias in Conventional procedures and Evidence for the Exponential Poisson Regression Model," American Journal of Political Science, 32(3), August 1988, pp. 838-63.

Langer, E., "Rethinking the Role of Thought in Social Interactions," in J.H. Harvey, W.J. Ickes and R.F. Kidd (eds), New Directions in Attribution Theory, Vol. 2, Hillsdale, NJ:Erlbaum, 1978.

Leibenstein, H. Beyond Economic Man: A New Foundation for Microeconomics. Cambridge, MA: Harvard University Press.

McClave, J., and P. Benson. Statistics for Business and Economics. San Francisco:Ellen Publishing Company, 1985.

March, J., and J. Olsen. Ambiguity and Choice in Organizations. Bergen, Norway: Universitetsforlaget, 1976.

March, J., and H. Simon. Organizations. New York:Wiley, 1958.

Nelson, R., and S. Winter. An Evolutionary Theory of Economic Chance. Cambridge, MA: Belknap Press of Harvard University Press, 1982.

Olson, J., and J. Thurber. "Learning in Nuclear Power Plants." Preliminary Draft, March 1991.

Osborn, R.N., and D.H. Jackson. "Leaders, Riverboat Gamblers, or Purposeful Unintended Consequences in the Management of Complex Dangerous Technologies," Academy of Management Journal, 20(4), 1988, pp. 924-947.

Weick, K.E. "Organizational Culture as a Source of High Reliability," California Management Review, 30(2), 1987, pp. 112-127.

INCLUDING TEST ERRORS IN EVALUATING SURVEILLANCE TEST INTERVALS*

I.S. Kim, S. Martorell,** W.E. Vesely,† and P.K. Samanta

Engineering Technology Division
Department of Nuclear Energy
Brookhaven National Laboratory
Upton, New York 11973, U.S.A.

**Universidad Politecnica of Valencia, Spain
†Science Applications International Corporation, U.S.A.

ABSTRACT

Technical Specifications require surveillance testing to assure that the standby systems important to safety will start and perform their intended functions in the event of plant abnormality. However, as evidenced by operating experience, the surveillance tests may adversely impact safety because of their undesirable side effects, such as initiation of plant transients during testing or wearing-out of safety systems due to testing.

This paper first defines the concerns, i.e., the potential adverse effects of surveillance testing, from a risk perspective. Then, we present a methodology to evaluate the risk impact of those adverse effects, focusing on two important kinds of adverse impacts of surveillance testing: (1) risk impact of test-caused trips and (2) risk impact of test-caused equipment wear. The quantitative risk methodology is demonstrated with several surveillance tests conducted at boiling water reactors, such as the tests of the main steam isolation valves, the turbine overspeed protection system, and the emergency diesel generators. We present the results of the risk-effectiveness evaluation of surveillance test intervals, which compares the adverse risk impact with the beneficial risk impact of testing from potential failure detection, along with insights from sensitivity studies.

1. BACKGROUND AND INTRODUCTION

Surveillance tests are required in nuclear power plants to detect failures in standby equipment as a means of assuring their availability in case of an accident. However, operating experience suggests that the tests may have adverse impact on safety,[1-3] that may be caused by test errors, e.g., human errors of omission or commission, including the potential for common-cause failures. This potential for adverse impact on safety is aggravated by the "overwhelming" amount of testing[1-3] presently required by Technical Specifications.

To address the problem of surveillance testing, i.e., the adverse effect on safety exacerbated by the significant amount of testing, the U.S. Nuclear Regulatory Commission (NRC) performed a series of studies. NUREG-1024[2] made recommendations to enhance the safety impact of surveillance requirements. NUREG-1366[3] implemented the recommendations by "qualitatively" examining all Technical Specifications surveillance requirements to identify those that should be improved. Four different types of adverse effects of testing were used in the NUREG-1366 study as screening criteria:

---

*Work performed under the auspices of the U.S. Nuclear Regulatory Commission.

(a) leading to a plant transient, (b) unnecessary wear to equipment, (c) unnecessary radiation exposure to plant personnel, and (d) unnecessary burden on plant personnel.

This paper summarizes the work[4] performed for the NRC by Brookhaven National Laboratory to help enhance the safety impact of surveillance testing. We first define the adverse effects of surveillance testing from a risk perspective, and then present a methodology to "quantify" the adverse risk impact, i.e., the penalty or increase in risk caused by the test. The quantitative methodology focuses on two important adverse effects, i.e., transients and equipment degradations. These adverse effects generate significant safety concerns because of: (1) plant abnormality which may challenge safety systems and plant operators and (2) equipment wear-out which increases the unavailability of the safety system or function, and thereby, reduces the plant's accident mitigating capability.

The risk impact of test-caused plant transients was evaluated by recognizing that the transients, which cause or require a reactor scram, are initiating events as typically called in probabilistic risk assessments (PRAs). The risk impact of equipment degradations was assessed using a test-caused component degradation model which was developed in this study from considerations of the stresses on equipment and degradation mechanisms induced by testing and aging.

The methods for evaluating the adverse effects of testing were applied to several surveillance tests at boiling water reactors, such as those on the main steam isolation valves, the turbine overspeed protection system, and the emergency diesel generators. The risk associated with these tests was assessed using a PRA conducted in the NUREG-1150 study.[5] Risk-effectiveness was evaluated by comparing the risk impact of plant transients and equipment degradations from these tests to the beneficial risk impact of testing resulting from the detection of failures. Sensitivity studies were also carried out on risk impact versus test interval.

Section 2 of this paper defines the adverse effects of testing from a risk perspective. Sections 3 and 4 present the methodology to evaluate the risk impacts of testing associated with transients and equipment degradations, along with the results of the risk-effectiveness evaluation and sensitivity studies. Section 5 gives our conclusions.

2. RISKS ASSOCIATED WITH A TEST

Surveillance testing may have two different types of risk impact on the plant: a beneficial impact, i.e., the reduction in risk, and an adverse impact, i.e., the increase in risk. The beneficial risk contribution results from the detection of failures which occur between tests. This risk contribution "detected" by a test here will be called R_D. The adverse risk contribution results from degradations or failures that are due to or related to the test, and from the component unavailability during or as a result of the test. This contribution "caused" by a test will be called R_C.

The test-detected risk contribution, R_D, resulting from the detection of failures can be quantified in the framework of a PRA, as demonstrated in reference 6. The test-caused contribution, R_C, may have several different kinds of contributions. Table 1 lists the different risk contributions which can be associated with a test, along with the root causes of the risk.

From Table 1, the test-caused risk can be expressed in a general form as

$$R_C = R_{trip} + R_{wear} + R_{state} + R_{down} \qquad (1)$$

where, for any specific test, some contributions may be irrelevant or insignificant compared to the others. When a test program or procedure is evaluated for its risk-effectiveness by conducting tests on a number

Table 1. Test-Caused Risk Contributions and Their Root Causes

Identifier	Risk Contribution from Test	Root Causes of the Risk
R_{trip}	Risk from trips	Human error, equipment failure, procedure inadequacy.
R_{wear}	Risk from equipment wear	Inherent characteristics of the test, procedure inadequacy, human error
R_{state}	Risk from misconfigurations or errors in component restoration	Human error, procedure inadequacy.
R_{down}	Risk associated with downtime in carrying out the test	Unavailability of the component during the test. Affected by the test override capability.

of individual components, then the contributions for each test plus the contributions from any test interactions need to be considered.

In addition to those effects defined in Table 1, two other adverse effects may be sometimes encountered: radiation exposure to plant personnel and unnecessary burden of work on plant personnel. These adverse effects differ from those in the table in that: (1) the radiation exposure to plant personnel is not amenable to a risk analysis based on the core-damage frequency as a risk measure, and (2) the unnecessary burden of work on plant personnel in general is not subject to a risk analysis. Although excluded from the quantitative risk analysis, these adverse effects can be considered qualitatively along with the results of quantitative risk analysis for the evaluation of surveillance requirements.

Among the various root causes of the risk delineated in Table 1, human errors of component restoration following tests are the root cause which previous studies[7,8] concentrated on to address adverse effects of testing. In terms of the risk contributions in the table, the studies focused on R_{state} that is most likely to be caused by human errors, with some consideration of R_{down}.

The risk also can be evaluated for a specific root-cause, such as human errors (or more specifically, errors of omission or commission). For instance, presume that human errors during a test may cause a transient and also may cause the components not to be restored to the normal status. The risk contribution due to potential human errors during the test can then be estimated by first evaluating the contributions of the risk from trips, R_{trip}, and from component restoration error, R_{state}, due to only human errors, and then adding the contributions.

In evaluating the risk-effectiveness of a test (or group of tests), the test-detected contribution, R_D, can either be compared to specific test-caused contributions or to all relevant contributions constituting R_C. When R_C is assessed by considering all significant contributions, we can define the risk-effectiveness of a test as follows: a test is risk-effective if $R_D > R_C$, otherwise it is risk-ineffective. If only specific contributions are considered, then the evaluation of the risk-effectiveness of the test is considered with regard to the specific test-caused contributors. For example, if test-caused risk contributions due to trips, R_{trip}, are only considered and we assess that $R_D > R_{trip}$, then we can say that the test is risk-effective with regard to test-caused trips. When more test-caused contributions are considered, then broader conclusions can be reached.

3. RISK IMPACT OF TEST-CAUSED TRANSIENTS

The operating history of nuclear power plants suggests that a surveillance test conducted at power may cause a transient that will lead to or require a reactor trip. The risk impact of such transients depends on the various responses of the plant safety systems, and also on plant operators. Typically, in PRAs the various plant or operator responses that may affect the plant risk are taken into account using event trees to delineate the progressions of accident sequences and system fault trees to identify the failure modes and their effects on the system unavailabilities. Hence, the risk contribution from test-caused transients to the plant risk can be evaluated within the framework of a PRA model.

The risk impact of a test-caused transient, R_{trip}, can be evaluated through that of the PRA initiating event group associated with the transient:

$$R_{trip} = \phi \, R_{IE\text{-}j} \tag{2}$$

where $R_{IE\text{-}j}$ denotes the risk impact of the j-th initiating event group which is assumed to be associated with the test-caused transient, and ϕ is the proportion by which the frequency of the PRA initiating event group is attributable to these transients. The proportion, ϕ, can be estimated by analyzing plant operating data:

$$\phi = \frac{N_{test}}{N_{IE\text{-}j}} \tag{3}$$

where,

N_{test} = the number of test-caused transient events, and
$N_{IE\text{-}j}$ = the number of transient events belonging to the initiating event group associated with the test-caused transient.

To obtain ϕ, the test-caused transients must be associated with the relevant initiating event groups. For this purpose, the EPRI (Electric Power Research Institute) transient categories[9] that were originally developed to analyze the historical transient events in a study of anticipated transients without scram (ATWS) can be used. Such use will facilitate and improve the accuracy of the data analysis, because the extent of detail on the test-caused transients and the PRA initiating event groups is usually quite different. The ATWS study defined 37 transient categories for BWRs based on the different characteristics of a variety of transient events that had occurred or might occur in the plants.

For sensitivity studies (in terms of risk impact versus test interval that will be discussed later), we first get the following equation for the probability, p_{trip}, that a transient will occur during or as a result of a test:[4]

$$p_{trip} = I_j \, T \, \phi \tag{4}$$

where T and I_j denote the test interval and the frequency of the j-th initiating event group used in the PRA model, respectively. Substituting an expression for ϕ from Equation (4) into Equation (2) we have:

$$R_{trip} = \frac{P_{trip}}{I_j \, T} \, R_{IE-j} \qquad (5)$$

These formulas discussed above were used in the framework of a NUREG-1150 PRA for a BWR to evaluate the risk impact and effectiveness of the following tests: a) a quarterly test of the main steam isolation valve (MSIV) operability and b) a weekly test of the turbine overspeed protection system (TOPS).

Table 2 shows the BWR transient categories that were identified as being associated with the tests, based on the test characteristics and the effects of the test-caused transients on the plant. For example, a TOPS test may cause the turbine control valve to fail closed, resulting in high steam pressure in the main steam system, and consequently, in a turbine trip. Hence, the transient due to the TOPS test can be classified into Category 3, "Turbine trip," and Category 13, "Turbine bypass or control valves cause increased pressure (closed)."

Table 2. Association of Transient Categories Relevant to Test-Caused Transients with PRA Initiating Event Groups

Test	Transient Category	Description	PRA Initiating Event Group
MSIV	6	Inadvertent closure of one MSIV	T2
	7	Partial MSIV closure	T2
TOPS	3	Turbine trip	T3A
	13	Turbine bypass or control valves cause increased pressure (closed)	T3A

The transient categories were then associated with the initiating event groups modeled in the plant-specific PRA, based on the characteristics of the categories and the groups. The plant-specific PRA initiating event groups which were identified to be associated with the transient categories are listed in Table 2. Categories 3 and 13 of the TOPS test are associated with initiating event group T3A, i.e., transients with the power conversion system initially available except those due to an inadvertent open relief valve in the primary system and those involving loss of feedwater. Categories 6 and 7 of the MSIV operability test are associated with initiating event group T2 which incorporates transients with the power conversion system unavailable.

The results of the core-damage frequency impact of test-caused transients, R_{trip}, and the probability that a transient will occur during or as a result of a test, p_{trip}, are the following:

a) For quarterly MSIV test:

R_{trip} = 1.8E-7 per reactor year
p_{trip} = 6.7E-2 per test

b) For weekly TOPS test:

R_{trip} = 3.7E-8 per reactor year
p_{trip} = 1.7E-3 per test

Comparing the results for the two different tests, we see that, for these test intervals, the risk contribution from test-caused transients and the probability of a transient occurring during a test for the MSIV test is greater than those for the TOPS test by a factor of 5 and 4, respectively.

We can also examine whether the test is risk-effective with respect to test-caused transients by comparing the value of R_D to that of R_{trip}. The quarterly MSIV test is risk-effective, because the R_D is 5.2E-7 per year which is larger than the R_{trip}; the risk-effective margin is 3.4E-7 per year. The risk-effectiveness of the TOPS test could not be evaluated based on the NUREG-1150 PRA, because the turbine control valves are not modeled in the PRA. Hence, for the TOPS test, only the quantitative values of R_{trip} and p_{trip} can be taken into account in the evaluation of the test, unless the value of R_D is obtained by modifying the PRA model.

Figure 1 shows the result of the sensitivity study of MSIV operability testing for three different kinds of core-damage frequency impacts to the variation of the test interval, T: (1) the test-caused core-damage frequency contribution due to transients, R_{trip}, (2) the test-detected core-damage frequency contribution, R_D, and (3) the total core-damage frequency impact of the test, R_T, which is simply the sum of R_{trip} and R_D. R_{trip} decreases as T is increased, because less transients are expected as the test is conducted less frequently. However, R_D increases with the increasing test interval, because the test is more likely to detect a failure.

The risk-effectiveness of the test on test-caused transients also can be seen by comparing the test-detected risk contribution to the test-caused risk contribution due to transients. In the region where T > 54 days, R_D is larger than R_{trip}, and therefore, the test is risk-effective. In the other region where T ≤ 54 days, the test is risk-ineffective.

An important conclusion relevant to the redefinition of a standard test interval is that the interval for MSIV operability testing, i.e., 91 days, can be extended without undue increase in the risk impact. For example, if the test interval is extended to 150 days, R_D increases because the test is more likely to detect failures, while R_{trip} decreases because less testing during a given time period will result in less transients. However, as shown by a dotted curve in Figure 1, the total risk impact of the test, R_T, only marginally increases when T is changed from 91 days to 150 days. (R_T increases from 6.99E-7 per year to 9.64E-7 per year.)

In this study, we used the LER data base for 30 BWRs for 1985, assuming that the operability of MSIVs is tested quarterly at all the plants. However, the data analysis indicated that some plants test the operability of MSIVs more frequently; e.g., the operators of a nuclear plant were performing a biweekly surveillance when the test failure occurred in the plant. If we assume that the minimum test interval of 54 days is also applicable to this plant, we can say that the biweekly test is risk-ineffective with regard to test-caused transients, because the interval is shorter than 54 days. Even if we consider other types of adverse risk impacts and they are not negligible compared to R_{trip}, the test will be risk-ineffective.

Sensitivity analyses, such as that shown in Figure 1, can be very useful in defining test intervals. However, they should be carefully interpreted. In Figure 1, the sensitivity curves of R_{trip} and R_T to the variation of T are based on the assumption that the probability, p_{trip}, of a transient occurring during testing is constant. However, the value of p_{trip} may change (tend to increase), especially when the test

is conducted far less frequently than it used to be, because the operators are more likely to make errors. Therefore, when considering an extension of test interval based on the sensitivity analyses, one should not prolong the test interval too much, e.g., by more than a factor of two. The extension of the test interval mainly depends on the likelihood that p_{trip} will vary following the change of the test frequency.

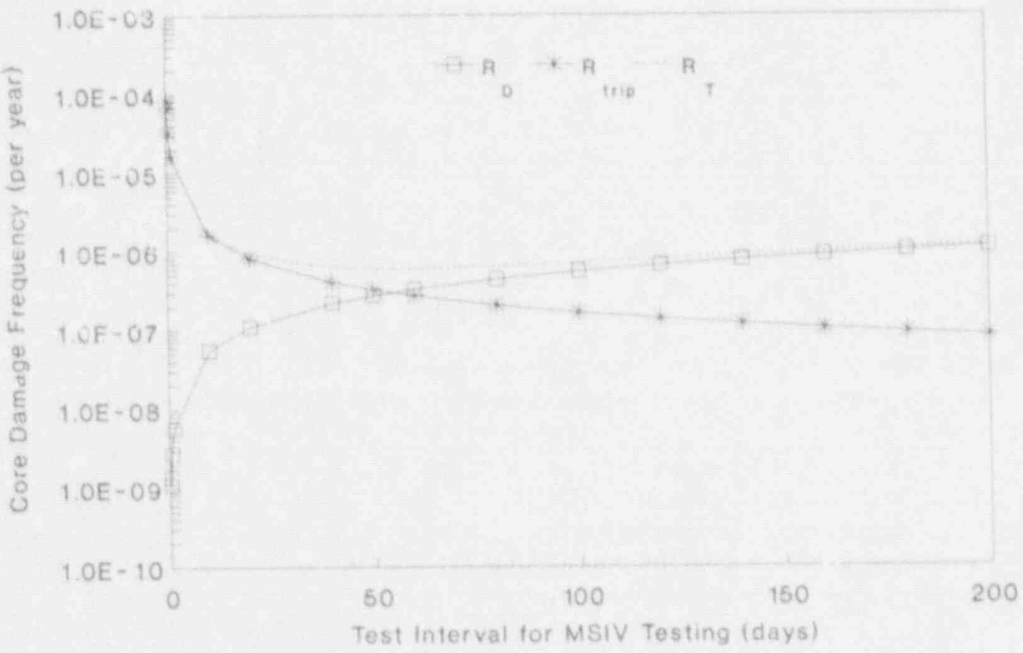

Figure 1. Sensitivity of the core-damage frequency impact to the test interval for the main steam insolation valve testing (R_D = test-detected risk impact; R_{trip} = test-caused risk impact due to transients; R_T = total risk impact of the test)

4. RISK IMPACT OF TEST-CAUSED DEGRADATIONS

The safety-significant components of nuclear power plants, such as a diesel generator or an auxiliary feedwater pump, are tested so often--generally monthly and sometimes more often--that the tests may lead to progressive wear-out of the equipment due to the accumulation of the test-caused degradation effects. Furthermore, as time passes the component will also show aging effects, such as corrosion or erosion. The accumulating test-caused degradation and aging effects will increase the unavailability of the component, and thereby, the unavailability of the associated safety system and function. This increase will, in turn, reduce the plant's accident mitigating capability.

The degradation from testing and aging effects are induced by two kinds of stresses, i.e., demand and standby stresses. Demand stress acts on equipment only when the equipment is asked to function or is operating. Standby stress acts while it is in the standby state. For standby components which are periodically tested, generally the combination of both stresses causes the equipment to degrade, and ultimately, to fail.

Based on the concept of stress on equipment and the characteristics of the degradation mechanisms caused by testing and aging, we can formulate the following test-caused component degradation model:

$$q(n,t) = \rho(n) + \int_{nT}^{nT+t} \lambda(n,t')\,dt' \qquad \text{for } t \in [0,T] \tag{6}$$

$$\rho(n) = \rho_0 + \rho_0 p_1 n \tag{7}$$

$$\lambda(n,t) = \lambda_0 + \lambda_0 p_2 n + \alpha u \qquad \text{for } u \in [0,nT+t] \tag{8}$$

where,

n = number of tests performed on the equipment
t = time elapsed since the last test
$\rho(n)$ = failure probability for demand caused failures
$\lambda(n,t)$ = standby failure rate (per unit time) for failures occurring between tests
T = test interval
nT + t = time since the last renewal point
ρ_0 = residual demand-failure probability
p_1 = test degradation factor associated with demand failures
p_2 = test degradation factor for standby time-related failures
α = aging factor associated with pure aging

Equations (6) to (8) represent a model which has been linearized from the original, non-linear test-caused degradation model.[4] This linear model can be used for most purposes and is used in this paper.

In Equation (6) the unavailability, q(n,t), and the standby failure rate, $\lambda(n,t)$, are represented as a function of n and t. The reason for this functional notation is that the standby failure rate is assumed to be affected by not only the standby time, but also by test-caused degradation. Therefore, component unavailability becomes a function of the number of tests performed on the component since the last renewal point, as well as the time elapsed since the last renewal. However, the demand failure probability is represented in Equation (6) as a function of only the number of tests, n, i.e., it is assumed that the demand-failure probability depends only on how many tests have been conducted on the component.

The expressions for the two basic degradation parameters, $\rho(n)$ and $\lambda(n,t)$, are formulated in Equations (7) and (8) in terms of their variables n and t. In Equation (8) the time-dependent aging mechanism on the standby failure rate is represented by a Weibull distribution.

The test-caused component degradation model, Equations (6) to (8), provides a means to estimate the time-dependent component unavailability and its resultant risk impact as a function of the number of tests on the component and the time elapsed since the last overhaul time.

Let

$\bar{R}_{C,n}$ = the average increase in core-damage frequency or test-caused risk contribution resulting from test-caused degradations of n tests on the equipment

We can evaluate $\bar{R}_{C,n}$ using the following formula:

$$\bar{R}_{C,n} = \text{the average risk level between } [t_0, t_0 + T] - \text{the average risk level between } [0,T]$$

$$= \Delta\bar{q}_n \, [R_1 - R_0]$$

$$= (p_1\rho_0 n + \frac{1}{2} p_2\lambda_0 Tn)[R_1 - R_0] \qquad (9)$$

where $\Delta\bar{q}_n$ denotes the average increase in component unavailability that results from n tests, and only the test-caused degradation effect is taken into account without considering the aging effect, i.e., $\alpha = 0$.

Based on these formulas, we can establish the following criterion on the number of tests for risk-effectiveness with regard to test-caused degradation:

$$n < \frac{\frac{1}{2}\lambda_0 T}{\rho_0 p_1 + \frac{1}{2}\lambda_0 p_2 T} : \quad \text{n-th test risk-effective with regard to test-caused degradation} \qquad (10)$$

For the n-th test to be risk-effective with regard to test-caused degradation, the number of tests performed on the component since the last overhaul should satisfy the above criterion. When the number of tests on the component is less than the value of the right-hand side in the criterion, then the contribution to core-damage frequency caused by the test will be less than the contribution to core-damage frequency detected by the test, and vice versa.

The test-caused component degradation model not only incorporates aging effects, but separately takes into account test-caused degradation. However, the degradation model and the formulas for evaluating the risk impact associated with such degradations are based on the following assumptions that may shed light on some limitations in the use of the approaches:

(1) Test-caused component degradations affect demand failure probability, and also standby failure rate; i.e., the component will be more vulnerable to both demand and standby time-related failures as more tests are performed on the component.

(2) The standby time-related failure rate increases because of test-caused degradation effects, as well as aging effects. However, aging does not affect the probability that the component will fail upon demand, i.e., the demand-failure probability.

(3) The time-dependent aging mechanism on the standby failure rate can be represented by a Weibull distribution.

(4) The demand degradation or failure mechanism is not affected by time. In other words, the demand failure probability depends on only the number of tests performed on the equipment, but not on the idle or dormant time.

Using the test-caused degradation model we have discussed, a sensitivity study was performed on the risk impact of test-caused equipment degradations versus test interval. The risk impact was evaluated in the framework of a NUREG-1150 PRA model. We chose the emergency diesel generator as the sample component, because of the concern about test-caused degradations on this component and the availability of the necessary reliability data to estimate the degradation parameters of the model. However, the method presented here can also be applied to any other component.

The values of the degradation parameters, such as p_1 and p_2, were estimated for diesel generators under the following assumption:

> When the number of tests is large, the average increase in component unavailability which is evaluated by the test-caused component degradation model is the same as that estimated by the aging model.[19]

Figures 2 and 3 show the results of the sensitivity study for monthly and quarterly testing of the diesel generators, respectively. They show the sensitivity of three different kinds of core-damage frequency impacts to the variation in the number of tests: (1) the test-detected core-damage frequency contribution, $\bar{R}_D$, (2) the test-caused core-damage frequency contribution due to equipment wear, $\bar{R}_{C,n}$, and (3) the total core-damage frequency impact of the test, $\bar{R}_{T,n}$.

For monthly testing, the component degradation model indicates that the test is risk-effective until 61 tests have been performed, i.e., approximately 5 years after the last overhaul. For quarterly testing, the model indicates that the test is risk-effective until 111 tests have been performed, i.e., about 28 years after the last renewal time. However, when the test is no longer risk-effective, the total risk impact for quarterly testing is greater than that for monthly testing by approximately a factor of 3.

The numerical results from this analysis should be interpreted cautiously, because the values of the degradation parameters, which are component-specific, were estimated using the results from reliability studies of a number of different diesel generators. For more meaningful results, the model should be used with the degradation parameters for the specific diesel generator whose risk-effectiveness is to be evaluated.

5. CONCLUSIONS

The safety significance and risk-effectiveness of surveillance test requirements can be evaluated by explicitly considering the adverse effects of testing, based on the concepts and methods discussed in this paper. The results of quantitative risk evaluation can be used in the decision-making process to establish the safety significance of the surveillance testing and to screen surveillance requirements. These results should be used in conjunction with qualitative evaluations from engineering considerations and operating experience, such as qualitative evaluations of radiation exposure to plant personnel from the tests and test-caused operator burden.

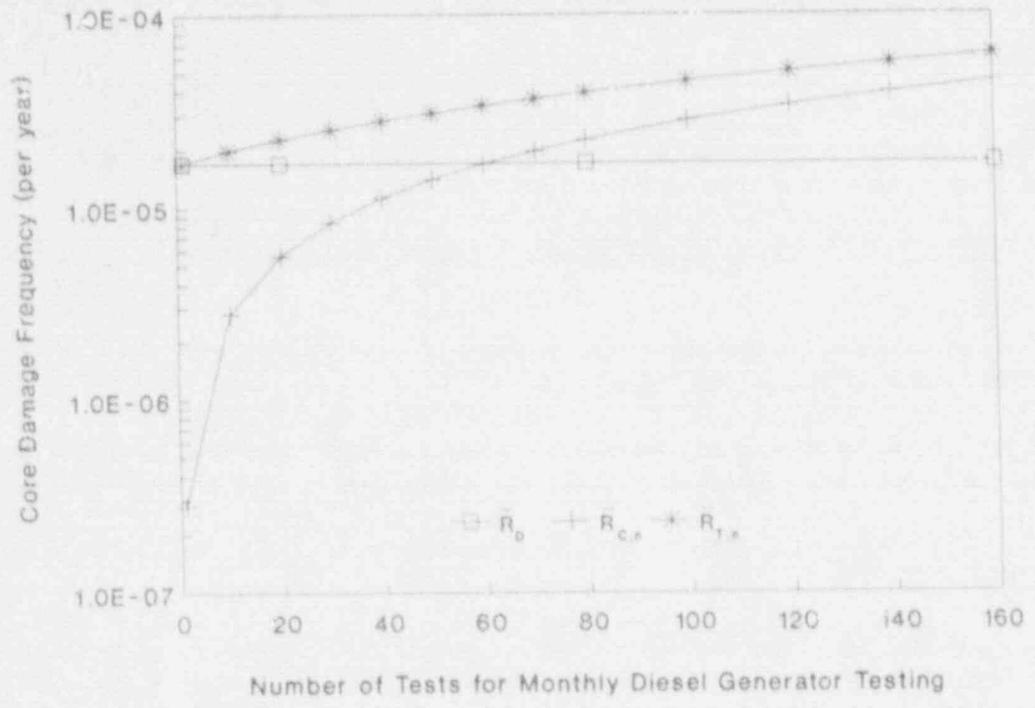

Figure 2. Evaluation of risk-effectiveness for monthly diesel generator testing ($\bar{R}_D$ = test-detected risk impact; $\bar{R}_{C,n}$ = test-caused risk impact due to equipment wear; $\bar{R}_{T,n}$ = total risk impact of the test)

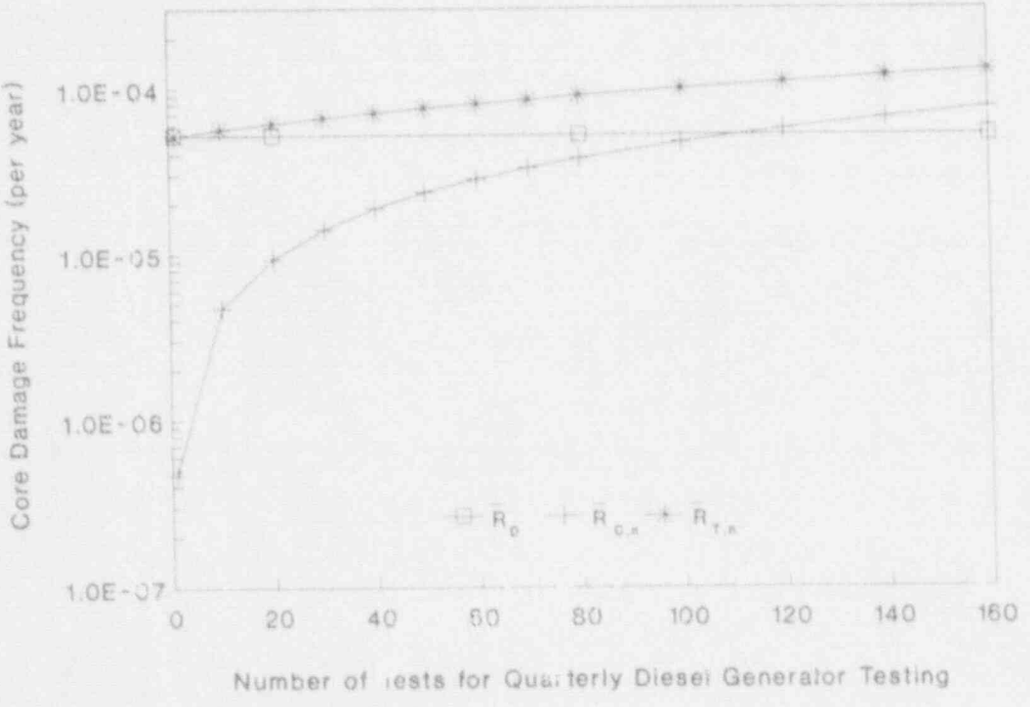

Figure 3. Evaluation of risk-effectiveness for quarterly diesel generator testing ($\bar{R}_D$ = test-detected risk impact; $\bar{R}_{C,n}$ = test-caused risk impact due to equipment wear; $\bar{R}_{T,n}$ = total risk impact of the test)

REFERENCES

1. U.S. Nuclear Regulatory Commission (NRC), "A Survey by Senior NRC Management to Obtain Viewpoints on the Safety Impact of Regulatory Activities from Representative Utilities Operating and Constructing Nuclear Power Plant," NUREG-0839, August 1981.

2. U.S. NRC, "Technical Specifications -- Enhancing the Safety Impact," NUREG-1024, November 1983.

3. R. Lobel and T.R. Tjader, "Improvements to Technical Specifications Surveillance Requirements," NUREG-1366, August 1990.

4. I.S. Kim, S. Martorell, W.E. Vesely, and P.K. Samanta, "Quantitative Evaluation of Surveillance Test Intervals Including Test-Caused Risks," NUREG/CR-5775, BNL-NUREG-52296, in press.

5. U.S. NRC, "Severe Accident Risks: An Assessment for Five U.S. Nuclear Power Plants," NUREG-1150, Vols. 1-2, Final Report, December 1990.

6. P.K. Samanta, S.M. Wong, and J. Carbonaro, "Evaluation of Risks Associated with AOT and STI Requirements at the ANO-1 Nuclear Power Plant", NUREG/CR-5200, BNL-NUREG-52024, August 1988.

7. G.E. Apostolakis and P.P. Bansal, "Effect of Human Error on the Availability of Periodically Inspected Redundant Systems," IEEE Transactions on Reliability, Vol. R-26, No. 3, August 1977.

8. T.P. McWilliams and H.F. Martz, "Human Error Considerations in Determining the Optimum Test Interval for Periodically Inspected Standby," IEEE Transactions on Reliability, Vol. R-29, No. 4, October 1980.

9. A.S. McClymont and B.W. Poehlman, "ATWS: A Reappraisal, Part 3: Frequency of Anticipated Transients," EPRI NP-2230, January 1982.

10. W.E. Vesely, R.E. Kurth, and S.M. Scalzo, "Evaluation of Core Melt Frequency Effects due to Component Aging and Maintenance", NUREG/CR-5510, June 1990.

A PERFORMANCE INDICATOR OF THE EFFECTIVENESS OF HUMAN-MACHINE INTERFACES FOR NUCLEAR POWER PLANTS: PRELIMINARY RESULTS

Neville Moray, John Lee & Kim J.Vicente
Department of Mechanical and Industrial Engineering
University of Illinois at Urbana-Champaign

Barclay G. Jones, Rick Brock & Toufik Djemil
Department of Nuclear Engineering
University of Illinois at Urbana-Champaign

Jens Rasmussen
Risø National Laboratory
Denmark

NRC CONTRACT NO. NRC-04-09-094
NRC B&R NO./FIN NO.: 0601922030 / B56970

Contract Monitor L.Beltracchi

Abstract

In this paper we report the results of experiments to assess the value of memory tests for measuring the quality of displays and the level of expertise of operators.

Three kinds of display, and observers with three levels of expertise were included in the experiments. The displays were computer generated versions of traditional analog meters, traditional analog meters supplemented by a dynamic graphic representing the relation between temperature and pressure in some subsystems, and a dynamic graphic representing the underlying thermodynamics of power generation using the Rankine cycle. The levels of expertise were represented by undergraduates with one or two semesters of thermodynamics ("novices"), graduate students studying thermodynamics and nuclear engineering, and professional nuclear power plant operators ("experts").

Each group watched a set of transients presented on the displays, using data generated by a high fidelity NPP training simulator, and were then asked three kinds of questions. The first measured their ability to recall the exact values of system state variables. The second measured their ability to recall what qualitative states the system had entered during the transient. The third measured their ability to diagnose the nature of the transient.

The results of the experiments are reported in relation to the possible use of memory tests to evaluate both displays, the level of expertise of operators, and the interaction of the quality of displays with the level of expertise of operators.

Introduction

High hazard systems such as nuclear power plants pose special problems for the identification of performance indicators, since performance during particular, unforeseen and rare events is as important as performance during design base scenarios. Performance in such rare events, punctuating long periods of familiar normal operation, depends on a shift from a rule-based mode of operation to knowledge-based situation analysis. The hypothesis to be tested by the present set of experiments has been that a test of the match between a display format and the mental model required for rare events would be preferable to direct performance measurements in simulated tasks, because separate simulation of "rare events" negates their nature as incidents embedded in a long stream of familiar events. Since testing on well practised incidents does not demand knowledge-based reasoning but rather pattern recognition of specific display configurations, we have looked for a more general or generic test of underlying knowledge, and have tried to find a way to tap the extent of that knowledge independent of its having been acquired during training with specific scenarios.

This paper reports the preliminary results of a project which was described at the 1990 WRSM by Moray, Vicente, Jones and Rasmussen (1990). The purpose of the research is to investigate the potential of memory recall tests as indirect performance indicators to assess the level of expertise of operators and the effectiveness of different kinds of displays, both conventional and proposed, to support the cognitive tasks of operators diagnosing the state of nuclear power plants. The theoretical basis for the proposed tests lies in observations that highly skilled experts appear to be able to recall and reconstruct the state of complex systems far better than do novices, but that this advantage is only found when the data are presented to them in patterns which are meaningful in the context of their expertise and reflect the semantics of the domain. The syntax and semantics of the displays should reflect the structure of the underlying processes. Examples of such relations between expertise and displays can be found in the work of Beveridge and Parkins (1987), Gick and Holyoak (1983), Vicente (1988), and particularly in the classical work of deGroot (1965). Those studies suggest that experts will be able to recall system state variable values more accurately than will novices, and that this will depend on the kind of display observed. If we can establish that this is indeed the case, then memory tests can be used as indirect performance indicators for the quality both of displays and expertise in NPP operations.

Method

Realistic NPP data for nine different transients were presented to three groups of observers using three types of displays. The data were obtained from a full scale NPP training simulator and showed the values taken by 35 variables during transients lasting approximately 5 minutes each. The transients were chosen after discussions with the contract monitor and the training staff at a NPP utility. Three groups of 42 observers each were obtained, one of undergraduate mechanical engineers who had had one or two semesters of thermodynamics courses, one of graduate students in thermodynamics or nuclear engineering, and one of professional NPP operators. Each observer viewed the nine transients in a different order.

Each of these groups were divided into three subgroups of 14 observers. One subgroup monitored a dynamic computer graphic display representing 35 analog meters, one for each variable, representing a "single-sensor-single-instrument" (SSSI) display. The second subgroup monitored a similar display modified to include a temperature-pressure dynamic graphical plot, (the PT display, see USNRC, 1988). The third viewed a dynamic graphical display which represented the Rankine Cycle of the system, (the Rankine display, see Beltracchi, 1987).

At the end of the transient the display was blanked out and the observers were asked to recall properties of the system state variables, to state whether there had been any abnormal behavior of the system during the run, and to diagnose the nature of the transient. Each of the three groups was divided into two further subgroups of 7 observers. The first was asked to recall

the exact value of the 35 state variables, to state whether there had been anything abnormal, and then, if so, to diagnose the nature of the transient. They indicated their memory of the state variable values by pointing with a mouse to each of 35 scales on the screen to indicate the value they remembered for each variable. This group will be called the "Quantitative Recall" group. The second group was asked a set of qualitative questions about the system, such as "Did the primary coolant remain sub-cooled for the duration of the trial", and then asked to say whether anything abnormal had happened, and if so to diagnose the nature of the transient. This group will be called the "Qualitative Recall" group.

The final subgroups were composed of seven observers in each group, each of whom saw nine transients. The formal statistical design was thus a repeated measures design over transients, and a between subjects design by display type and recall type.

Results

The recall and diagnosis scores were submitted to appropriate Analysis of Variance, c^2 tests, and Newman-Keuls tests. Only a summary of the results can be presented here, and we will concentrate on those main effects which were statistically significant.

The purpose of the study was to determine whether recall tests are a sensitive measure of the quality of the displays and the level of expertise of the observers. We use the success in diagnosing the nature of the transient as a base against which to measure the effectiveness of the recall scores. If the recall measures are sensitive as a measure of performance, we should find differences in the recall scores when there are differences in the quality of diagnosis behavior, and where there are no differences in diagnosis we should find no differences in recall scores. The diagnosis and recall scores must covary if the recall measures are to be an acceptable performance indicator. The logic of this analysis is shown in Figure 1.

Difference in Recall Scores	Difference in Diagnosis Scores: +	Difference in Diagnosis Scores: =	Difference in Diagnosis Scores: -
+	D(a) > D(b) 1 R(a) > R(b)	D(a) = D(b) 2 R(a) > R(b)	D(a) < D(b) 3 R(a) > R(b)
=	D(a) > D(b) 4 R(a) = R(b)	D(a) = D(b) 5 R(a) = R(b)	D(a) < D(b) 6 R(a) = R(b)
-	D(a) > D(b) 7 R(a) < R(b)	D(a) = D(b) 8 R(a) < R(b)	D(a) < D(b) 9 R(a) < R(b)

Figure 1. Rationale for analysis of recall and diagnosis scores

Figure 1 shows how recall and diagnosis scores can be related for two conditions which we will call (a) and (b). In cell 1, Diagnosis under condition (a) is better than Diagnosis under condition (b), and Recall under condition (a) is better than Recall under condition (b). In cell 3, Diagnosis under condition (a) is worse than Diagnosis under condition (b), but the relation between recall scores is the same as in cell 1. Each cell represents some combination of diagnostic and recall behavior. If the diagnosis and recall data both fall in cells 1,5 and 9, then the recall tests are a sensitive measure of diagnostic ability. If the data fall in cells 3, 5, and 7, that would still be consistent with the recall scores being a sensitive measure, but in a counterintuitive sense, since poor recall would be correlated with better diagnosis, and one would be hesitant in accepting the memory tests as sensitive measures without considerable further explanation of the effect. If the recall data fall in cells 4, 5 and 6 this shows that the measure is insensitive, and unsuitable as a diagnostic performance indicator. If diagnosis data fall in cells 1, 4, (or 3, 6, 9), this shows that condition (a) provides better support for diagnosis than does condition (b) (or vice versa).

We can identify conditions (a) and (b) with any independent variables. For example, we might make condition (a) the use of NPP operators as observers, and condition (b) the use of undergraduates. In that case we would be testing to see whether the recall scores could differentiate levels of observer expertise due to training, as measured by differences in their ability to diagnose transients. As another example, we could identify condition (a) with the Rankine cycle display, and condition (b) with the analog (SSSI) display, and we would then be testing for the sensitivity of the recall scores in relation to differences in quality of diagnosis as a function of type of display. In analyzing data from experiments, we therefore need both to determine what differences in the data are statistically significant, and also to look at the patterns of the relations between diagnosis and recall for pairwise comparisons of the independent variables.

The main results of our experiments are shown in Figures 2 and 3 and in Table 1, which show the scores for recall and diagnosis as a function of display type and expertise, and the main statistically significant effects. Scores on both left and right ordinates of the figures are plotted so that poorer performance is upwards.

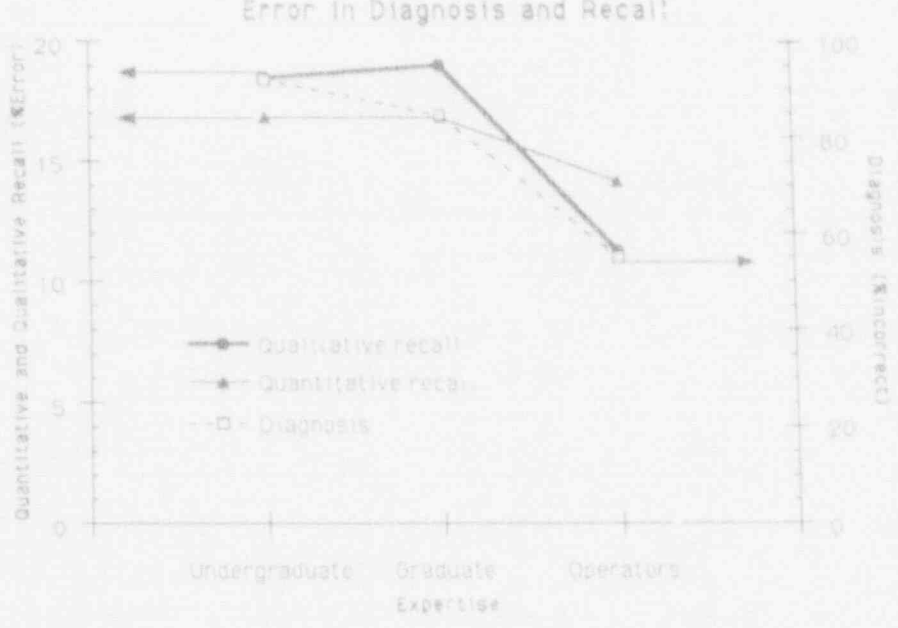

Figure 2. Recall and Diagnosis as a function of levels of expertise.

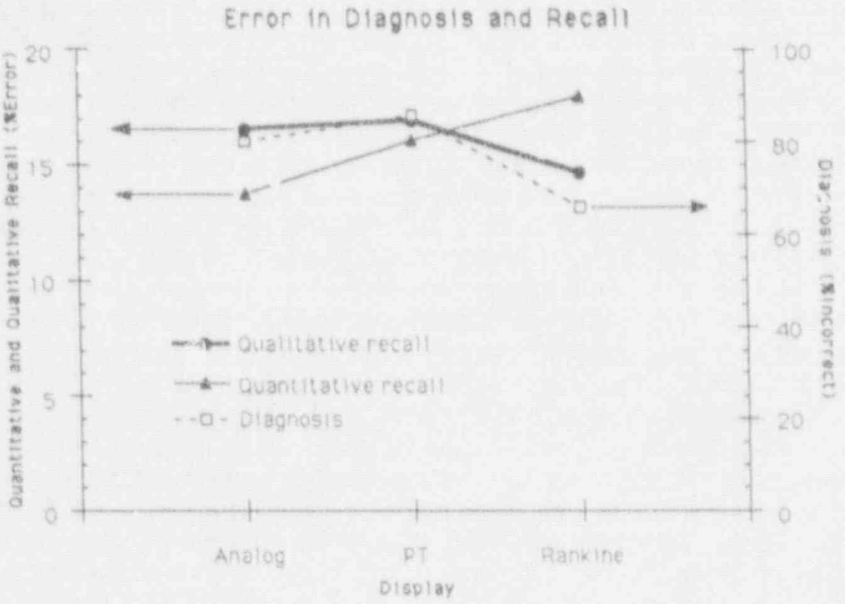

Figure 3. Recall and Diagnosis is a function of type of display.

	Effects	Contrasts	F ratio	p
Quantitative (Values)	Expertise		(2,57) 4.73	0.013
		Grad-Undergrad	N-K diff=3.9	N.S
	Display		(2,57) 10.20	0.000
		PT-Analog	N-K diff=4.1	N.S.
	Learning		(8,456) 16.59	0.000
Qualitative (States)	Expertise		(2,57) 18.63	0.000
		Grad-Undergrad	N-K diff=6.3	N.S.
	Display		(2,57) 1.36	0.264
	Learning		(8,456) 5.35	0.000
	Effects	Contrasts	Pearson's χ^2	p
Diagnosis	Expertise		(2) 165.2	0.000
		Undergrad-Grad	(1) 10.08	0.001
	Display		(2) 48.43	0.000
		PT-Analog	(1) 3.41	0.065
	Learning		(8) 18.78	0.016

Table 1. Summary of statistical analyses of the data shown in Figures 2 and 3.

The results show that recall scores are not in general reliable ways to predict diagnostic performance, and hence cannot be regarded as satisfactory performance indicators. Figure 2 and Table 1 show that there is a decrease in the number of incorrect diagnoses from undergraduates to graduates to NPP operators. This difference is highly significant statistically. The difference between either of the student groups and the NPP operators is very large, approximately 25%, indicating the efficacy of the NPP training program. There is, on the other hand, no difference in the quantitative recall scores between the undergraduates and graduate students, and a small but significant reduction in quantitative recall from the students to the NPP operators. There is no difference in the recall of qualitative information between the student groups, but there is a very large and highly significant reduction in the recall of qualitative information between the student groups and the NPP operators. These results suggest qualitative recall is more sensitive to changes in expertise and that operators' expertise consists in thinking about transients in terms of system state, rather than in terms of the value of state variables. The relative insensitivity to changes in expertise of quantitative recall suggests that this measure is not a good measure of expertise.

Figure 3 and Table 1 show the relation of recall to diagnosis as a function of display type. Figure 3 shows a dissociation between several measures. There is a significant difference in diagnosis as a function of display type, with the PT and analog displays being significantly poorer in supporting diagnosis, and the Rankine cycle significantly and substantially better. Quantitative recall scores on the other hand are best for the Analog (SSSI) display, worse for the PT display and the Rankine display. Recall of qualitative state information shows no significant difference between the displays, although there is some (nonsignificant) improvement with the Rankine display.

Discussion

The pattern of results shows that the reconstruction of the state of the display by the recall of the quantitative values of the state variables, which we thought of as an analog of deGroot's recall technique, is unreliable as a performance indicator. There are significant improvements in the recall of quantitative information in situations where the diagnostic ability declines (cell 7 in Figure 1). There is a better coupling between diagnosis and the recall of qualitative state information, which is not surprising. The recall of qualitative state information is in a sense the precursor of labelling the state of the whole system qualitatively as being in a particular transient state, and hence would be expected to be related to diagnosis. On the other hand, answering questions about the qualitative states through which the system passed during the transient is not, strictly speaking a "deGroot" reconstruction memory method.

The fact that qualitative recall correlates better than quantitative recall with correct diagnosis is probably related to the work of Carswell and Wickens (1987) on integrated and separable displays. It has been found in several experiments that displays which support global judgements are poor at supporting judgements about individual variables, and those which support judgements about individual variables are poor at supporting integrated judgements. The data suggest that analog (SSSI) displays are "separable" displays in this sense, best supporting knowledge of individual values of state variables, while the Rankine display is a good integrated display which supports global integrated knowledge and diagnosis.

Overall, our conclusions from this preliminary analysis of our data is that a recall test in which the observers are asked to reconstruct from memory the values of state variables is not a reliable and sensitive indicator of performance, where good performance is identified with correct diagnosis of transients. On the other hand, memory for qualitative state changes, where what is remembered is not the particular values of variables, but whether or not subsystems entered abnormal states, may be a considerably better test. The latter reflects improved expertise of trained NPP operators compared with students who are knowledgeable about thermodynamics but not

The results show that recall scores are not in general reliable ways to predict diagnostic performance, and hence cannot be regarded as satisfactory performance indicators. Figure 2 and Table 1 show that there is a decrease in the number of incorrect diagnoses from undergraduates to graduates to NPP operators. This difference is highly significant statistically. The difference between either of the student groups and the NPP operators is very large, approximately 25%, indicating the efficacy of the NPP training program. There is, on the other hand, no difference in the quantitative recall scores between the undergraduates and graduate students, and a small but significant reduction in quantitative recall from the students to the NPP operators. There is no difference in the recall of qualitative information between the student groups, but there is a very large and highly significant reduction in the recall of qualitative information between the student groups and the NPP operators. These results suggest qualitative recall is more sensitive to changes in expertise and that operators' expertise consists in thinking about transients in terms of system state, rather than in terms of the value of state variables. The relative insensitivity to changes in expertise of quantitative recall suggests that this measure is not a good measure of expertise.

Figure 3 and Table 1 show the relation of recall to diagnosis as a function of display type. Figure 3 shows a dissociation between several measures. There is a significant difference in diagnosis as a function of display type, with the PT and analog displays being significantly poorer in supporting diagnosis, and the Rankine cycle significantly and substantially better. Quantitative recall scores on the other hand are best for the Analog (SSSI) display, worse for the PT display and the Rankine display. Recall of qualitative state information shows no significant difference between the displays, although there is some (nonsignificant) improvement with the Rankine display.

Discussion

The pattern of results shows that the reconstruction of the state of the display by the recall of the quantitative values of the state variables, which we thought of as an analog of deGroot's recall technique, is unreliable as a performance indicator. There are significant improvements in the recall of quantitative information in situations where the diagnostic ability declines (cell 7 in Figure 1). There is a better coupling between diagnosis and the recall of qualitative state information, which is not surprising. The recall of qualitative state information is in a sense the precursor of labelling the state of the whole system qualitatively as being in a particular transient state, and hence would be expected to be related to diagnosis. On the other hand, answering questions about the qualitative states through which the system passed during the transient is not, strictly speaking a "deGroot" reconstruction memory method.

The fact that qualitative recall correlates better than quantitative recall with correct diagnosis is probably related to the work of Carswell and Wickens (1987) on integrated and separable displays. It has been found in several experiments that displays which support global judgements are poor at supporting judgements about individual variables, and those which support judgements about individual variables are poor at supporting integrated judgements. The data suggest that analog (SSSI) displays are "separable" displays in this sense, best supporting knowledge of individual values of state variables, while the Rankine display is a good integrated display which supports global integrated knowledge and diagnosis.

Overall, our conclusions from this preliminary analysis of our data is that a recall test in which the observers are asked to reconstruct from memory the values of state variables is not a reliable and sensitive indicator of performance, where good performance is identified with correct diagnosis of transients. On the other hand, memory for qualitative state changes, where what is remembered is not the particular values of variables, but whether or not subsystems entered abnormal states, may be a considerably better test. The latter reflects improved expertise of trained NPP operators compared with students who are knowledgeable about thermodynamics but not

about NPP operation, but fails statistically to differentiate the ability of the Rankine display to support state diagnosis better than do SSSI displays or PT displays.

More detailed results will be available in the final report of this contract.

The results of the experiments show that our initial hopes that recall tests would provide a simple and cost effective performance indicators have not been fulfilled. The simplest conclusion is that a direct test of diagnostic ability is the best test, but we believe that such a conclusion misses an important point. Simulator scenarios consist of incidents which are overlearned by the operators, so that they overlearn cue-action patterns to specific incidents. But what is required is a test which will tap their general functional understanding independent of a particular incident, since what we really need to know is how well a display-operator combination will support diagnosis and fault management in a completely unforeseen circumstance where knowledge-based reasoning rather than rule-based reasoning will be required. In this work we had hoped to find a kind of task different from diagnosis, but which tapped the same knowledge which is reflected in diagnosis. This we have failed to do. An alternative, at least for the evaluation of displays, may be to use a different set of people than operators, perhaps designers or builders of NPP systems, who understand the systems but are not trained in overlearned scenarios. The solution of this problem remains to be found, but it is clearly desirable to have a measure of the effectiveness of the coupling of operator expertise to display design which is independent of diagnosis and is more cost effective than the use of full scale simulation.

Acknowledgements

We wish to acknowledge gratefully the outstanding cooperation we received from the staff of the Commonwealth Edison Braidwood Nuclear Power Plant, both in the provision of data for simulating the transients, and in the provision of volunteer NPP operators to take part in our research.

References

Beltracchi, L. 1987. A direct manipulation interface for water-based rankine cycle heat engines. IEEE Transactions on Systems, Man, and Cybernetics, *SMC-17*, 478-487.

Beveridge, M., & Parkins, E. 1987. Visual representation in analogical problem solving. de Groot, A.D. 1965. *Thought and choice in chess*. The Hague: Mouton.

Carswell, C.M. & Wickens, C.D. 1987. Information integration and the object display: an interaction of task demands and display superiority. *Ergonomics, 30*, 511-528.

Gick, M.L., & Holyoak, K.J. 1983. Schema induction and analogical transfer. Cognitive Psychology, *15*, 1-28.

Moray, N. , Jones, B.G., Vicente, K.J., & Rasmussen, J. 1990. *A performance indicator of the effectiveness of human-machine interfaces for nuclear power plants*. Proceedings of the 18th Water Reactor Safety Information Meeting. Maryland.

USNRC 1988. *Safety evaluation report related to the restart of Rancho Seco Nuclear Generating Station, Unit 1, following the event of December 26, 1985*. (NUREG-1286, Supplement No. 1). Washington, DC. USNRC.

Vicente, K.J. 1988. Adapting the memory recall paradigm to evaluate interfaces. Acta Psychologica, *69*, 249-278.

Verification and Validation of Expert Systems

Lance A. Miller, Elizabeth Groundwater, and Steven Mirsky

Science Applications International Corporation
1710 Goodridge Drive, McLean, VA 22102

ABSTRACT

The U. S. Nuclear Regulatory Commission (NRC), and the Electric Power Research Institute (EPRI), have contracted with Science Applications International Corporation (SAIC) to develop guidelines for the verification and validation (V&V) of expert systems for use in the nuclear power industry. This paper reports first on the overall goals and tasks of this ongoing multi-year contract. The results of two completed task surveys are presented: (1) a survey of V&V techniques developed for conventional software and an assessment of their applicability to expert systems; and (2) a survey of activities and techniques actually used for the V&V of expert system, including automated tools. The paper concludes with discussion of likely directions for the remaining work.

1. Overview of Contract Effort

The title of the contract is "Develop and Document Guidelines for Verifying and Validating Expert Systems." An important motivation for the contract is to increase the acceptance of expert systems within the nuclear industry by demonstrating an acceptable methodology for performing V&V which leads to enhanced quality assurance of this type of software. The resulting guidelines are to be consistent with the key standards and regulations concerning the V&V of conventional software systems, shown in Table 1.1.

The scope of the to-be-developed guidelines is quite broad. They are to cover the full life-cycle of developing expert systems, from requirements determination and analysis, through design, implementation, integration and maintenance -- as illustrated by Figure 1.1 taken from NSAC/39. The guidelines are also to cover a variety of different types of expert systems which we tentatively anticipate as being classified into three different levels. Level 1 concerns **safety-related** applications, so-called "safety-critical software." Such applications will involve real-time, data-driven expert systems. Level 2 concerns **important-to-safety** applications, such as SPDS and similar systems. These systems also will likely be real-time and embedded. Level 3 covers stand-alone or advisory systems which do not relate to safety directly.

Throughout this effort, two expert systems will be used as specific testbeds for the V&V procedures examined and developed. One, the Emergency Operating Procedure Tracking System (EOPTS) has been installed and is operational at the Kuosheng nuclear power plant in Taiwan. The purpose of this system is to advise the operator on the correct emergency operating procedures to be applied during events. The second system, the Reactor Safety Assessment System (RSAS) is installed at the NRC Emergency Operations Center. Its development was funded by NRC. Its purpose is to track and advise NRC on the status of key plant systems during an event.

A total of 10 tasks are to be performed, in a carefully formulated sequence to insure that the final guidelines are based on a comprehensive analysis and development of the most effective procedures. These tasks are shown in Figure 1.2. The first two tasks are to survey conventional and expert system V&V techniques. These tasks are completed and are reported on in detail in the next two sections. Task 3 is to assess the applicability of conventional V&V techniques to two selected nuclear expert systems in particular; clearly this task relies on the results of Task 1. Task 4 is somewhat parallel to Task 3 in that it is to assess the merits of the expert system V&V techniques discovered in Task 2 and to synthesize or develop the best combination of techniques for applying to expert systems. Before executing Task 4, we will execute a task whose focus is to develop a method to certify the knowledge bases of expert systems; this is identified as Task 6. The fifth task is to apply the composite approach developed in Task 4 to the two selected expert systems. Task 7 is to evaluate the strengths and weaknesses of the various methods developed and considered in Tasks 3, 4, and 6, and to recommend the best set of procedures for the three levels of expert systems. Task 8 addresses the problem of how realistic scenarios are to be generated for validating systems using the recommended approaches. Finally, Tasks 9 and 10 are to prepare professional

Table 1.1: Key Standards and Regulations Related to V&V of Conventional Software Systems

Key Documents	SPDS	NSAC/39	Verification and Validation for Safety Parameter Display Systems, December 1981
	QA, Design and Analysis Codes	NUREG-0653	Report on Nuclear Industry Quality Assurance Procedures for Safety Analysis Computer Code Development and Use, August 1980
	QA	NUREG/CR-4640	PNL-5784, Handbook of Software Quality Assurance Techniques Applicable to the Nuclear Industry, August 1987
	Class 1E Real Time Systems	ANSI/IEEE ANS-7-4.3.2-1982	Application Criteria for Programmable Digital Computer Systems of Nuclear Power Generating Stations, July 6, 1982
		Reg. Guide 1.152	(Task IC 127-5) Criteria for Programmable Digital Computer System Software in Safety-Related System of Nuclear Power Plants, November 1985
	V&V	ANSI/IEEE Std 1012-1986	Software Verification and Validation Plans, 14 November 1986
		EPRI NP-5236	Approaches to the Verification and Validation of Expert Systems for Nuclear Power Plants (1987)
		EPRI NP-5978	Verification and Validation of Expert Systems for Nuclear Power Plant Applications

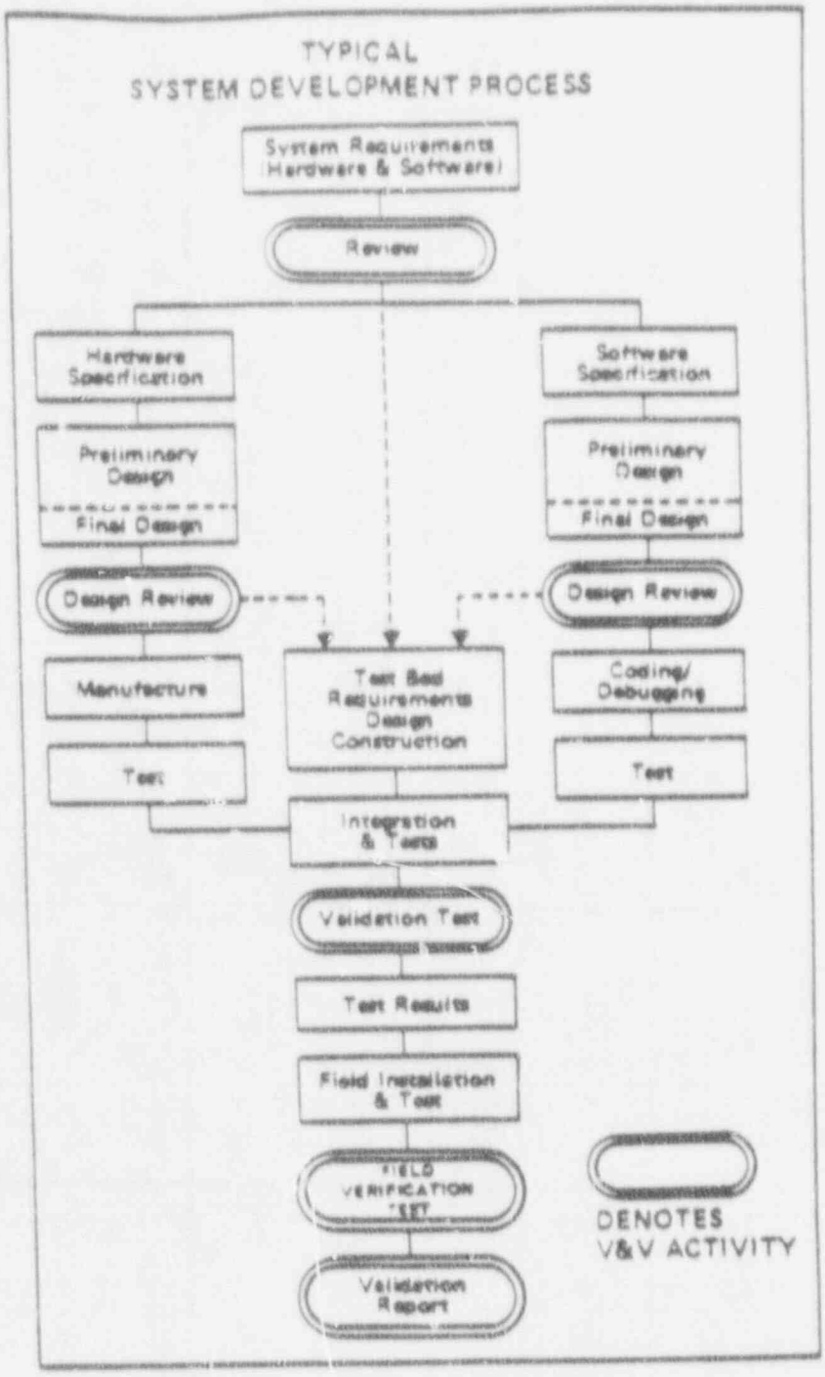

FIGURE 1.1. Relationship of V&V Activities to Generic Project Activities, from NSAC-39 (1981)

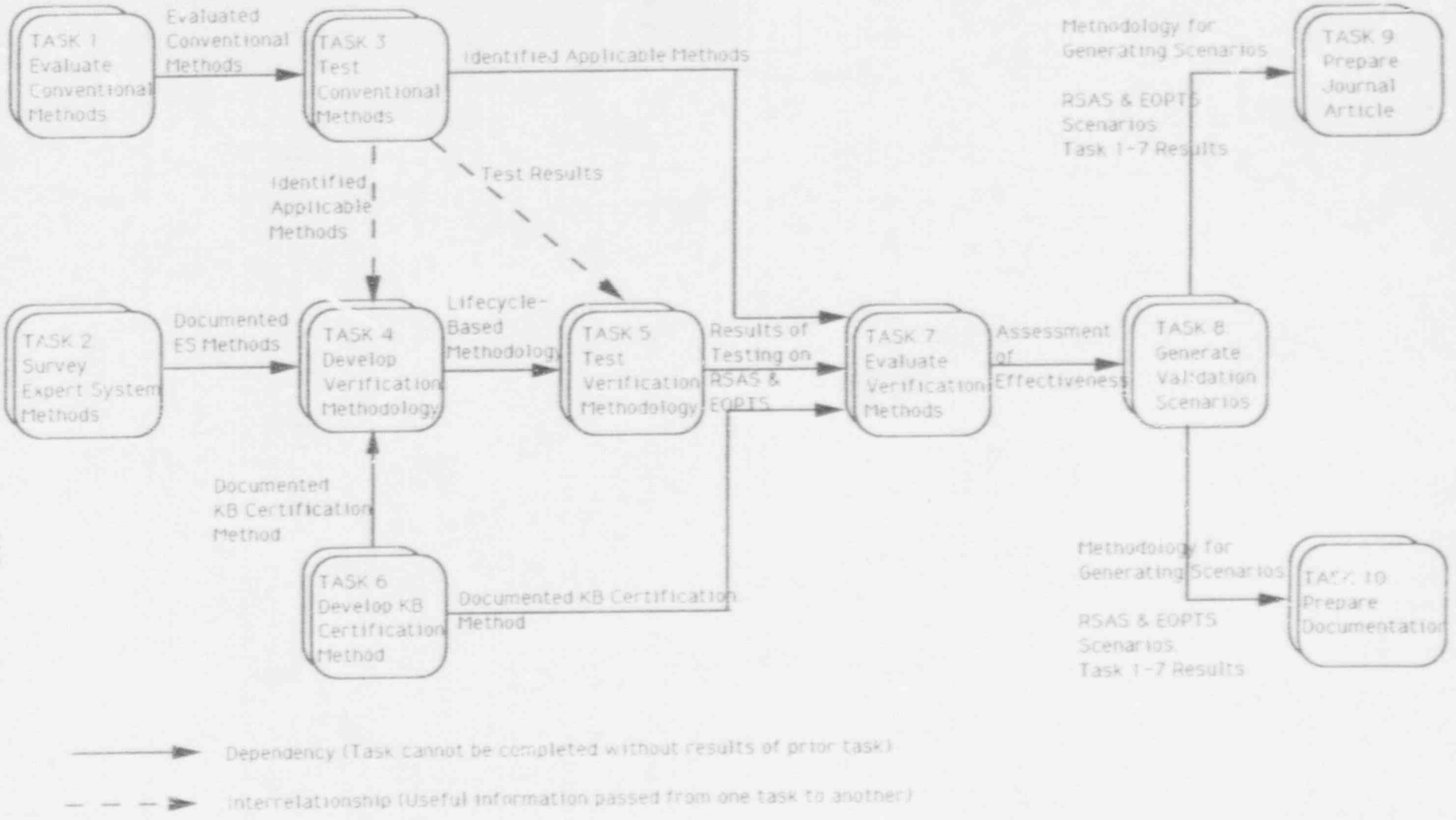

Figure 1.2: TASK DEPENDENCIES AND INTERRELATIONSHIPS

publications of the total effort and to document the results, particularly the guidelines in an easy-to-use form.

At the present time, Task 3 is well under way. The delivery of the final guidelines is scheduled for mid-1993. However, in the interests of involving outside participation to insure the comprehensiveness and validity of the intermediate tasks, we intend to make a strong effort to report on the results of each of the tasks as they are completed, in meetings such as this one and in other appropriate conferences.

2. Task 1: Review of Conventional V&V Methods

In this task we distinguished V&V from the related project management activities of **configuration management** and **quality control**. We adopted the definitions of V&V from the IEEE Standard 729-1983 as being closest to the most widely accepted understanding:

> **Verification** is the process of determining whether or not the products of a given phase of the software development cycle fulfill the requirements established during the previous phase.
>
> **Validation** is the process of evaluating software at the end of the software development process to ensure compliance with the initial software requirements.

The nature of the verification process depends on the adopted developmental life-cycle. NSAC/39 was used for Tasks 1 and 2 (Figure 1.1) as being representative, which includes four major types of verification: requirements verification, design verification, implementation verification and field verification. The major validation activity occurs after integration, and is **system validation**.

Our very extensive review of conventional V&V methods logically could have categorized these with respect to the above verification and validation stages. However, based on the relative paucity of techniques associated with the early stages, we folded methods concerned with requirements or design verification into one category. On the other hand, the high number of techniques for testing implemented systems led us to partition these into two sub-categories: those that involve active execution of the expert system software, **Dynamic Testing** methods, and those that involve inactive inspections, **Static Testing** methods. We show these three categories, along with the major sub-classes we defined, in Figure 2.1. Overall, we identified over 100 specific techniques. Ten major methods were found for the Requirements/Design class, with the remainder roughly split between the two remaining classes.

We described each of the techniques and then evaluated their relative efficacy -- taking into account their ability to discover defects, the difficulty in understanding them, the difficulty in generating test cases or procedures, and

Figure 2.1: Classes OF V&V Techniques Which Have Been Applied to Conventional Systems

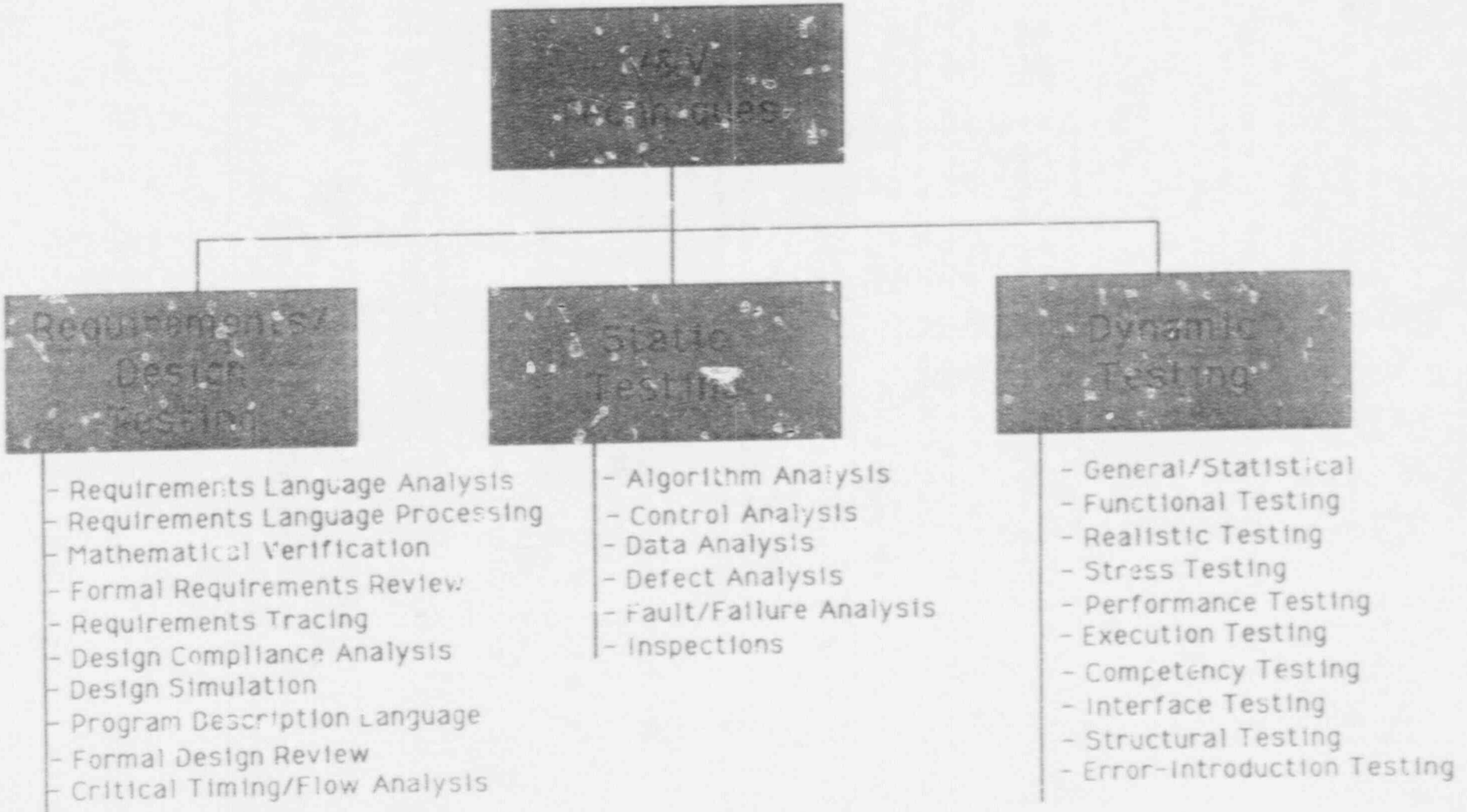

the difficulty in evaluating the results. Early discovery of problems using the Requirements/Design methods can reduce cost and delays and increase quality. The employment of the two simplest of these techniques, formal reviews and requirements decomposition and tracing, would be very effective in revealing a significant portion of problems in the early stages.

Concerning the testing techniques, we similarly emphasize the value of the static methods of inspection techniques and reviews to insure traceability and functional accuracy. Of the dynamic testing methods, the most effective are **structural testing** (to achieve a reasonable but not complete exercising of program paths and branches), **functional testing** (to test the required functionality), certain aspects of **randomized testing** (more and more shown to be effective in identifying elusive problems), and **stress testing** (to assess the system's performance under extreme conditions). **Rregression testing** (using the same test-suite after each major system modification should be mandatory for each sub-system integration or for incremental development approaches.

Having reviewed the conventional approaches we then addressed the question of the applicability of these to expert systems. In doing so, it was useful to characterize the heterogenous nature of the components of expert systems. As shown in Figure 2.2, the four major components of **inference engine**, **knowledge base**, **interfaces**, and **shell utilities** differ in terms of reusability, typical programming language, commercial availability, and complexity. The four expert system components similarly differ in three additional attributes, as shown in Figure 2.3: whether or not they typically involve a procedural programming language, whether the functionality is narrow and relatively constant across applications, and whether the potential defects of a component are relatively well-defined and also amenable to formal theorem-proving methods of detection.

The way the four expert system components are rated on the above three attributes determines how conventional methods can be applied to them, and we identified three potential strategies:

> 1. **For expert system components written in, or largely involving, a procedural language, use the most effective conventional V&V techniques.**

According to this strategy (see the first column in Figure 2.3) the lowest of the conventional V&V techniques should be applied to the **inference engine**, **interfaces**, and **shell utilities** components.

> 2. **For expert system components judged to have very narrow and constant functionality across applications, develop a rigorous** <u>certification</u> **procedure for each.**

Figure 2.2. Components and General Features of Knowledge-Based Systems

Components	FEATURES			
	Reusability[1]	Typical[2] Program Lang	Commercial[1] Availability	Complexity[1]
INFERENCE ENGINE	H	A, C, F, (Lp)	H	M
Pattern Matcher	H		H	M
Conflict Set Handler	H		H	M
Basic Proof Procedures[3]	H		H	M
Extended Proof Procedures[4]	M		L	H
Proof Management[5]	M		M	M-H
KNOWLEDGE BASE	L	Lp, P	L	M
C Rules	L	Lp,P	L	L-M
H Frames	L	Lp,P	L	M-H
O Objects	M	S,C++	M	M-H
I Facts	L	Lp,P	L	L
C External DBs	M	n.a.	L	M
E In-line Procedures[6]	L	C,Pa	L	M
S				
INTERFACES	M-H	A,C	M	M
User Interface	M	A,C,Lp	H	H
DBMS	H	SQL	H	H
Data Channels	M	A,C	M	M-H
Communication (ports/networks/channels)	H	A,C	M	M-H
Other Applications	M	A,C,Lp	M	M
SHELL UTILITIES	H	A,C	M	M
Environment Accesses[7]	H	A,C,Lp	M	M
Knowledge Acquisition	H	Lp,C	M	M
Functional Libraries	M	C,Lp	M	M-H
Other Utilities	H	C,Lp	M	M

[1] H=High, M=Medium, L=Low
[2] A=Assembler, C=C Language, F=Fortran, Lp=LISP, P=Prolog, Pa=Pascal, S=Smalltalk
[3] Forward and Backward Chaining
[4] Opportunistic, fuzzy-probabilistic-reasoning or constraint-directed reasoning, truth maintenance
[5] Of goal tree, constraints, "truths", breath/depth of search
[6] Including Demons and Functions
[7] To operating system, programming environments, etc

Figure 2.3. Components and Typical Testing-Related Features of Knowledge-Based Systems, with Testing Recommendations

	FEATURES[1]		
Components	Typically Written in or Involving Procedural Code	Very Narrow and Fixed Function	Potential Defects, Well-Characterized and Amendable to Formal Theorem-proving Detection Methods
INFERENCE ENGINE	Y	Y	S
Pattern Matcher	Y	Y	Y
Conflict-Set Handler	Y	Y	Y
Proof Procedure	Y	Y	S
Proof Management	Y	S	S
KNOWLEDGE BASE	N	N	Y
C Rules	N	N	Y
H Frames	N	N	S
O Objects	M	N	N
I Facts	N	N	Y
C External DB	M	N	S
E In-line Demons,	Y	N	N
S Procedures, Functions			
INTERFACES	Y	N	N
User Interface	Y	N	S
DBMS	Y	N	S
Data Channels	Y	N	N
Communication Ports/ Networks/Channels)	Y	S	S
Other Applications	M	N	N
SHELL UTILITIES	Y	N	N
Environment Accesses	Y	Y	S
Knowledge Acquisition	Y	N	N
Functional Libraries	Y	N	N
Other Utilities	Y	N	N

[1] Explanation of table entries: Y=Yes, N=No, S=Somewhat, M=Mixed procedural and non-procedural code

The values in column 2 of Figure 2.3 show that the inference engine is the single candidate for this strategy, and the responsibility for V&V of the inference engine should be largely that of the vendor, or possibly, independent evaluation groups.

> 3. For expert system components whose defects are well-characterized and amenable to formal testing, develop specialized methodologies and automated tools to "prove" the presence of these defects in the components.

The knowledge base is the component singled out by this strategy, and, indeed, there has been considerable effort to develop special (i.e. non-conventional) techniques to accomplish this type of testing (as reviewed in the following section).

We concluded the Task 1 survey with the observation that, according to the values in Figure 2.3, there are some expert system sub-components which remain unaddressed by the above three strategies -- namely the frames, objects, and external DBs of the knowledge base, and the non-specific other types of interfaces. For these elements, specialized non-conventional techniques need to be discovered or developed.

3. Task 2: Survey and Document Techniques for Expert System V&V

The purpose of Task 2 was to survey and document techniques for expert system V&V. The survey used the results of Task 1 to determine which of the conventional techniques are being applied to expert systems, and what new techniques have been developed solely for expert system V&V. The survey effort included 1) an extensive telephone interviewing campaign to over 130 points of contact (see Figure 3.1), 2) site visits to nine institutions conducting research in or applying expert system V&V (see Table 3.1), and 3) collection of an extensive library of well over 300 bibliographic references. The survey encompassed work done both within the nuclear power industry and in other industries as well. Contacts included corporations, universities, government agencies, and utilities. Within the last 4-5 years, there has been an explosive growth of interest and work in the field. It has now reached a level of maturity where expert system V&V techniques are being implemented in automated tools and being applied to operational expert system development and maintenance efforts.

As can be seen in Figure 3.2, many of the classes of V&V techniques identified in the Task 1 report as being applied to conventional software systems are also being researched for, or applied to, expert systems. This is particularly true in the areas of Static Testing (tests performed directly on the code itself) and Dynamic Testing (tests performed by running the code and evaluating the results).

Figure 3.1: Task 2 Telephone Interviews

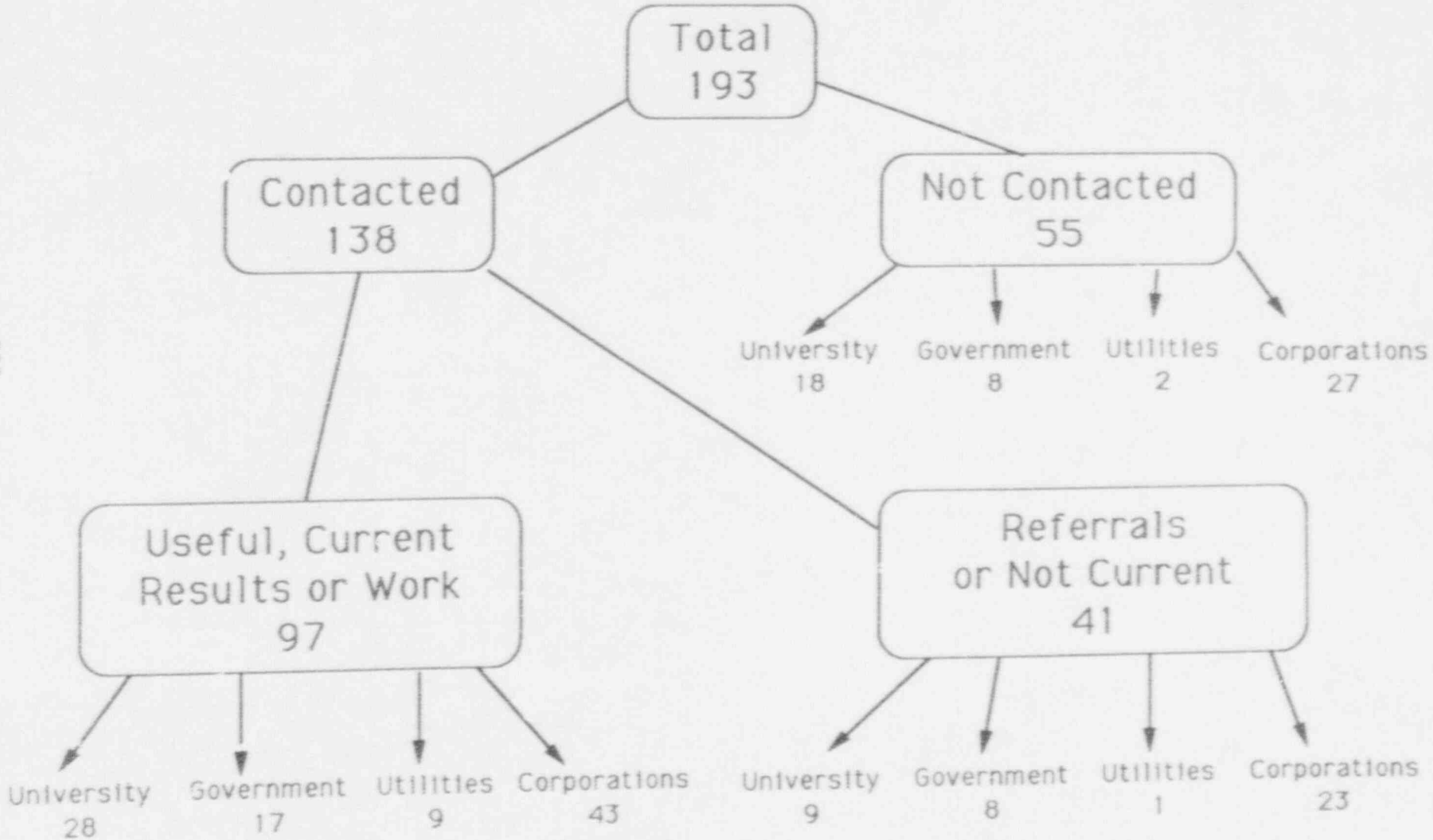

TABLE 3.1. Expert System Verification and Validation Survey Task Actual Site Visits

Washington, D.C. Area	Institute for Defense Analyses (IDA) Decision Sciences Consortium (DSC) U.S. Naval Academy
San Francisco Bay Area	Lockheed Corporation Stanford Research Institute (SRI)
Northeastern U.S.	Digital Equipment Corporation (DEC), Marlboro, MA Worcester Polytechnic Institute (WPI) AT&T Bell Laboratories, Warren, NY
Houston, Texas	NASA Johnson Space Center International Business Machines (IBM)

Figure 3.2: Classes OF V&V Techniques Which Have Been Applied to Conventional Systems

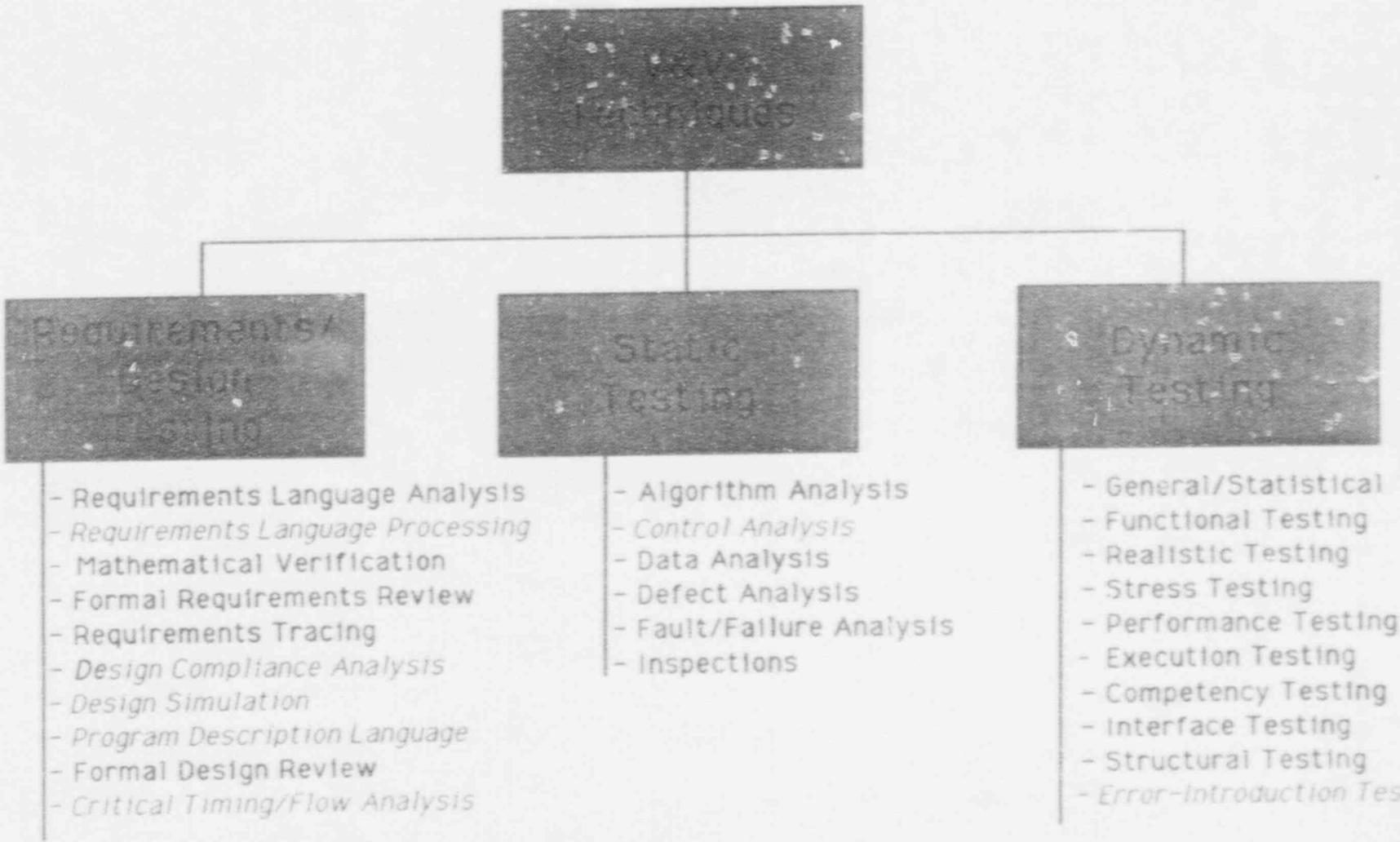

Legend: Bold: Techniques have been used for Expert Systems

Italic - No evidence that techniques have been used for Expert Systems

Very few formal techniques are applied during the **Requirements and Design** phases of expert systems development (only 5 out of 10 possible methods) and then only infrequently. This is primarily because the activities performed during these phases for expert systems are usually informal themselves. Requirements and Design documents for expert systems are often not written at all, or written after-the-fact, and thus cannot be used as a basis for V&V activities. When they are written, usually no more is done with them than to review them and, possibly, trace requirements to design elements. We consider this to be a serious general deficiency in expert systems development. We anticipate we will strongly recommend serious emphasis on early up-front planning in our eventual guidelines.

Fifteen of 46 possible **Static Testing** techniques were researched for or applied to expert systems (including four new ones). Most of the work in Static Testing of expert systems has focused on the development of automated tools to performed sophisticated syntactic checking of rule bases. Many of the sophisticated versions of these tools are approaching commercial software grade, and should be available for sale within a few years if industry interest warrants it. The primary job left to be done is to generalize the tools to handle the rule formats of the most popular expert system shells. The types of errors that may be found by such checkers include redundant or subsumed (one rule's conditions are a subset of another's) rules, rule cycles (there is a path from a rule back to itself), unreachable or dead-end rules, inconsistent rules, and incompleteness (e.g., not all possible input values are covered). Some of the rule base checkers will perform semantic checks of the rule base using meta-constraints defined by the programmer, and others will perform checking on the fly during knowledge acquisition and/or refinement of the rule base. Tools that perform syntactic checking of object-oriented or frame-based knowledge bases are still in infancy and will require more research before commercialization is likely.

Semantic checking is the next logical tier of capabilities to add to current syntactic checking tools. Some teams have already begun adding this capability to their tools. One major issue must be resolved before semantic checking become commercially viable. The vendors of the popular expert system shells have to add capabilities for the meta-rules or constraints to be expressed within their format, versus being a separate component (usually in a different rule format) useable only by the automated knowledge base checking tool. Then, generalization and commercialization of the semantic checking tools may begin in earnest.

There has been little activity in the Static Testing subclass of Fault and Failure Analysis. Only Fault-tree (Event-tree) Analysis and Heuristic Testing have been applied to some extent. Some of these techniques may not have been considered because they are usually associated with software that directly affects safety systems and most expert system software, especially in the nuclear industry has not yet been involved with these systems. We see this to be a fertile area for future research.

Other work in Static Testing has included conducting various kinds of inspections (e.g. structured walk-throughs and expert panel reviews), performing dependency analyses of the output values on the inputs, and attempts at applying

program proving techniques. We agree with an observation made on one of our site visits (John Rushby, SRI) that inspections and analyses to insure that a system fails safely are among the most important.

In **Dynamic Testing**, there is a wide range of activities: 38 of 55 techniques have been researched or applied to expert systems. The state-of-the-art in the operational expert system world is still Ad-hoc Testing, or defining test cases at whim, with no systematic guidance. Newer work has focused on more systematic methods for specifying test case sets, such as Structural Testing--attempting to cover all rules or rule paths in the expert system, Random Testing--attempting to cover a representative sample of the possible inputs, and Performance Testing to assure timing, memory, and other constraints are met. Some operational expert systems, such as those developed for safety-related functions (e.g. NASA space shuttle diagnostics), do undergo various forms of Realistic Testing using scenario files, simulators, or actual field conditions.

There are still very few tools to support Dynamic Testing of knowledge bases and there is a strong need for research in this area. The primary issue is to determine how, when, and where automated tools could help. Two areas that have been proposed are: 1) suggesting structured or random test cases by examining the knowledge base structure and 2) managing, running, and scoring the results of large regression test suites. There is certainly room for creative research to discover other areas of Dynamic Testing where automated tools could help.

The state-of-the-art in expert system verification and validation testing techniques directly reflects the immaturity of expert system technology when compared to conventional software and the large chasm between new expert system development interest and resources allocated to expert system V&V. The current practice of not developing requirements and design documentation coupled with a concomitant deficiency in the involvement of V&V during the early stages of the software development process has resulted in the emphasis on expert system V&V being directed towards Dynamic Testing and away from Requirements and Design Testing. Most of the scientists and engineers involved in the development and V&V of expert systems do <u>not</u> have strong backgrounds in conventional software V&V where V&V activities are ingrained as an integral component of the entire software lifecycle. This is reflected in the dearth of Requirements and Design Testing techniques for expert systems and further substantiates the reliance on Dynamic Testing for expert systems. In summary, although there are some notable exceptions in the areas of Requirements and Design Testing and Static Testing techniques, the bulk of current expert system verification and validation activities occur only after the system is implemented.

The last aspect of our study was to determine if there was a need for the development of new techniques in some general domain or subarea of expert system V&V. Upon analysis of the V&V techniques being applied to expert systems, we have found that there is sufficient coverage across all the components of expert systems and across all error types (static versus dynamic, anomalies versus invalidities) as can be seen in Figure 3.3. The challenge is in selecting the appropriate combination of techniques to use for performing V&V on a particular expert system that is both effective and cost efficient.

Figure 3.3. Comprehensive Expert System V&V Matrix

TESTING TARGET	TYPE OF TESTING: Static	TYPE OF TESTING: Dynamic
Anomalies	• Syntactic Defect Analysis (many automated tools exist) • Dependency Analysis (automated tools exist)	• Structural Testing (automated tools exist) • Stress/Performance Testing • Execution Testing • Intelligent Compilation (automated tools exist)
Invalidities	• Semantic Defect Analysis (automated tools exist) • Program Proving • Fault, Failure Analysis	• Random Testing (automated tools exist) • Functional Testing • Realistic Testing • Competency Testing
Both	• Inspections	• Interface Testing • Error Introduction Testing

4. Conclusions

We make 4 general conclusions about the V&V of expert systems based on our findings so far:

1. Very little V&V is performed for expert systems; usually neither a requirements document nor a design document is produced or maintained.

2. Most of the conventional V&V techniques could be applied to expert systems; some conventional techniques have been used, and we know of four new non-conventional methods developed for expert systems.

3. Software practices associated with expert system development, in general, are immature with respect to conventional software development practices.

4. The deficiency of early up-front planning and verification is of particular concern.

5. Future Directions

Although we are just now beginning, in Task 3, to consider applying various V&V techniques to expert systems, we nonetheless have a number of growing convictions about what features may be contained in the ultimate guidelines. We provide these here for discussion purposes, in the form of a series of expectations:

- Whatever life-cycle is adopted, adequate V&V will require the production and maintenance of one essential and one near-essential document: a requirements document and a design document.

- We expect that some form of iterative or cyclic developmental approach will be recommended, as well as the concept of moderate incremental builds followed by extensive testing (particularly for level 1 systems).

- Effective methods which are applicable early in the life-cycle will be strongly urged.

- The use of CASE tools, especially for front-end specification analysis and high-level design, will be strongly recommended because of their error-controlling and quality-inducing characteristics.

- Static-testing methods will be emphasized over dynamic ones, especially those which can be automated; these methods will have an optimum order of application, and all should be applied (with detected-errors corrected) before dynamic-testing.

o All levels of expert systems will require some minimum of V&V techniques, probably including reviews and inspections, requirements tracing, and various kinds of dynamic testing. However, for Level 1 expert systems, we would expect much more emphasis on formal "proving" methods, particularly for the knowledge-base component.

A Model For Calculation of RCS Pressure During Reflux Boiling Under Reduced Inventory Conditions and Its Assessment Against PKL Data

D. E. Palmrose[1]
Idaho National Engineering Laboratory
EG&G Idaho Inc.
PO Box 1625
Idaho Falls, ID 83415-2404

R. M. Mandl[2]
Siemens AG-UB KWU E43
Postfach 3220
8520 Erlangen
Fed. Rep. of Germany

ABSTRACT

There has been recent interest in the United States concerning the loss of residual heat removal system (RHRS) under reduced coolant inventory conditions for pressurized water reactors. This issue is also of interest in the Federal Republic of Germany and an experiment was performed in the integral PKL-III experimental facility at Siemens-KWU to supply applicable data. Recently, an NRC-sponsored effort has been undertaken at the Idaho National Engineering Laboratory to identify and analyze the important thermal-hydraulic phenomena in pressurized water reactors following the long term loss-of-RHRS during reduced inventory operation. The thermal-hydraulic response of a closed reactor coolant system during such a transient is investigated in this report. Some of the specific processes investigated include: reflux condensation in the steam generators, the corresponding pressure increase in the reactor coolant system, and void fraction distributions on the primary side of the system. Mathematical models of these and other physical processes were developed and assessed against the experimental data from the PKL III Experiment B4.5.

NOMENCLATURE

A_{fc}	= flow area of the core
C_o	= distribution coefficient
ΔT	= primary and secondary side temperature difference
D	= diameter
G_i	= Grashof number
g	= acceleration due to gravity
h_{fg}	= latent heat of vaporization
$\overline{h_p}$	= average heat transfer coefficient on primary side
$\overline{h_s}$	= average heat transfer coefficient on secondary side
j_g	= superficial vapor velocity

[1]Work supported by the U.S. Nuclear Regulatory Commission, Office of Nuclear Regulatory Research, under DOE Contract No. DE-AC07-76ID01570.

[2]Work supported by the Federal Ministry of Research and Technology, Federal Republic of Germany.

j_f = superficial liquid velocity
k = thermal conductivity
L_c = condensing length
m_a = mass of air/nitrogen
N_{act} = number of active steam generators
N_{Dams} = number of steam generators with a pair of nozzle dams installed
N_L = number of primary loops
N_T = number of steam generator tubes per steam generator
Nu = Nusselt number
p = pressure
p_{Total} = total RCS pressure
Pr = Prandtl number
Q = power or heat transfer rate
Q_o = initial decay heat level
Q_o^* = nondimensional power
R = universal gas constant
Re_T = saturated liquid Reynolds number
T = temperature
t = thickness
V = volume
V_{gj} = vapor drift velocity

Greek symbols

α = void fraction
δ = liquid film thickness
γ = ratio of vapor and liquid in two-phase nonannular flow
ρ = density
μ = viscosity

Subscripts

f = liquid
fs = saturated liquid
g = vapor
gs = saturated vapor
iSG = steam generator inside
LSgas = noncondensable gas in the loop seal
NC = noncondensable gas
OP = steam generator outlet plenum
OTS = steam generator outlet tube sheet
oSG = steam generator outside
sat = saturation
sec = secondary side
Tubes = steam generator U-tubes
UP = upper plenum
w = U-tube wall
wp = primary side of the U-tube wall
ws = secondary side of the U-tube wall

INTRODUCTION

A study conducted at the INEL identified various natural circulation cooling modes that might be utilized in the removal of decay heat following loss of the residual heat removal system (RHRS) during maintenance or refueling shutdown of U.S. pressurized water reactors (PWRs).[1] The study also identified the important thermal-hydraulic phenomena that could occur during such an event. One of the modes identified that required further investigation is reflux cooling, initiated during reduced inventory conditions with the upper regions of the reactor coolant system (RCS) filled with nitrogen or air. Of particular concern was the RCS pressure that would be reached in establishing stable refluxing. If this pressure approached approximately 4.4 bar (50 psig), it might be sufficient to cause failure of temporary closures, such as nozzle dams and pressures as low as about 2.7 bar (25 psig) could threaten thimble tube seals.

An analytical model has been developed that makes some assumptions concerning the process leading to and during reflux condensation.[2] Some of the assumptions are derived from the scenario itself on how the noncondensable gases are transported during the process of establishing steam generator heat removal. Others come from the physical processes occurring in the vessel, coolant system, and steam generators. Each are discussed in more detail in the next section followed by a brief description of the development of the model. The model is validated using the natural circulation results from Semiscale Test NC-6. The PKL III Experiment B4.5 was selected to assess the model against a full simulation of a loss-of-RHRS under reduced inventory conditions. The PKL III facility is a scaled-down (1:145) model of a 1300 MW_e 4-loop PWR operated by Siemens AG-UB KWU at Erlangen, FRG. A full description of the experiment and its results are given in this paper.

LOSS-OF-RHRS

Scenario Description

The operating condition and configuration of the system assumed at the time of loss-of-RHRS is reduced inventory operation with all RCS openings secured (i.e., primary coolant system closed from the containment). One or more of the steam generators is in wet layup and nozzle dams may or may not be in place, but at least one steam generator remains operational (i.e. in wet layup with no nozzle dams installed). Air or nitrogen (noncondensable gas) fills all RCS space above the coolant level. Such a configuration can exist shortly after shutdown before refueling operations begin (within two or more days), or after refueling has been completed and preparations are underway to start-up.

In the event of a loss-of-RHRS, core decay heat causes a rise in reactor coolant temperature until boiling begins. During this first phase, it is assumed that buoyancy-driven natural circulation causes all of the water above the bottom of the core to heat to the boiling point. A second phase begins after the core coolant begins to boil, during which the resulting steam expands into the primary coolant system and eventually reaches the steam generators. The interaction between the noncondensable gas and the steam is highly complex and is driven by buoyancy, diffusion, and entrainment processes. The end effect is for the noncondensable gas to be swept from the reactor vessel and other RCS locations into the steam generator U-tubes. This can be likened to the compression of the noncondensable gas by a piston from a large initial volume into a small final volume. Thus, this phase might be referred to as the air compression phase.

In the third phase, condensation of steam inside the steam generator tubes occurs, with the condensate draining back into the hot legs in the case of U-tube steam generators or cold legs for once-through steam generators, and eventually to the reactor vessel. One or more steam generators may be available to condense the steam. The transfer of heat into the secondary coolant causes its temperature to gradually increase, and therefore the primary vapor temperature and pressure also increase with time.

The fourth and final phase begins when the secondary coolant starts to boil. Here, it is assumed that a secondary vent path can be established to relieve the steam. A pseudo-steady condition then prevails in which the primary pressure remains stable, as long as sufficient secondary coolant exists to cover the condensing length of the tubes. Eventually, if the secondary coolant is not replenished, it will boil off. However, for most cases examined in this study, it is assumed that the steam generator tubes remained covered.

Physical Phenomena

There are several important physical phenomena that must be accounted for to perform an analysis of reflux cooling . The first is the heating of the water and metal mass in the reactor vessel and hot legs. Since the main concern is the final RCS pressure reached, the metal mass heat up is considered to have already been completed. Therefore, all of the decay heat goes to boiling the water in the vessel. The steam thus generated will eventually make its way to the steam generators. If the core decay heat level is high enough, and/or the initial water level is elevated above mid-loop, a two-phase mixture is produced, with the steam voids causing a swelling of the coolant volume. If the swelling is great enough, a two-phase mixture could enter the steam generator tubes. Also associated with high decay heat, the potential for a countercurrent flow limitation in the U-tube steam generators exists which could flood the upper sections of the U-tubes with the condensate. On the secondary side of the steam generators, two possibilities exist, namely boiling or natural convection. Finally, the movement of noncondensable gases that fills the RCS above the water level is subject to some uncertainty. It is presumed that most of the gas will be swept out of the reactor vessel as the steam and/or steam-water mixture expands within the vessel. Some proportion of the gas may enter the pressurizer, which is already filled with noncondensable gas. The remainder will be compressed into the steam generator tubes and downstream spaces (i.e., steam generator outlet plenum and cold legs), until sufficient steam generator tube surface area to condense the steam is created.

MODEL DEVELOPMENT

Piston Model

A simplified, steady-state model was developed to calculate the state of the primary coolant system for a long duration loss-of-RHRS (long enough for boiling in the core to occur). It is well established that a balanced, pseudo-steady heat transfer condition can be reached after the loss-of-RHRS if certain plant conditions exist.[3,4] In this section, the models and associated assumptions used to calculate the conditions of the primary system are presented.

The principal assumption of the so-called Piston Model is that the noncondensable gas from almost every section of the RCS is transported into a noncondensing section (a "passive" region) of the steam generator(s) by the boiling of water in the core. This movement, or transport, of the noncondensable gas into a reduced volume by the steam is similar to the effect of a piston

compressing a gas in a cylinder. Only two basic principles, with a few simple assumptions, are needed to determine the system conditions that will be reached. These principles are the Gibbs-Dalton Law of Partial Pressure and an energy balance across the steam generator tubes. The assumptions used by the model are:

1. The noncondensable gas is compressed by the steam into the steam generator tubes and other non-liquid filled portions of the RCS.

2. An active steam generator is defined as one in a wet-layup condition allowing it to be a heat sink for the loss-of-RHRS analysis. An inactive steam generator is one with the secondary side dry (filled with air or nitrogen).

3. Noncondensable gas is compressed into any inactive steam generator which is not isolated by nozzle dams. The volume that the noncondensable gas occupies in the inactive steam generator(s) is the same volume as the noncondensable gas occupies in the active steam generator(s).

4. The temperature of the steam above the core, in the hot legs, and entering the steam generator equals the saturation temperature corresponding to the primary pressure.

5. Condensation of the vapor entering the steam generator tubes begins at the top of the tube sheet and extends a distance through the tube bundle referred to as the condensing length.

6. In the noncondensing region of the steam generator, steam and noncondensable gas are mixed together and have the same temperature as the secondary side of the steam generator.

7. The steam generator tubes all behave identically.

8. No credit is taken for heat transferred to the structure of the primary coolant system.

Application of the Gibbs-Dalton Law of Partial Pressures to the passive section of the steam generator gives:

$$P_{Total} = P_{sat}(T_{sec}) + P_{NC} \qquad (1)$$

where P_{NC} is determined from the Ideal Gas Law:

$$P_{NC} = \frac{m_a R T_{sec}}{V_{NC}} \qquad (2)$$

Now, the volume of the passive section, V_{NC}, can be calculated from the relationship:

$$V_{NC} = (N_L - N_{Dams})\left[V_{OTS} + V_{OP} + V_{LSgas} + \frac{V_{Tubes}\left[L_{Tubes} - L_c\right]}{L_{Tubes}}\right] \qquad (3)$$

where L_c is the only unknown. By combining Equations (1) through (3), one forms an equation for the pressure necessary to compress the noncondensable gas into the steam generator:

$$p_{Total} = p_{sat}(T_{sec}) + \frac{m_a R T_{sec}}{(N_L - N_{Dams})\left[V_{OTS} + V_{OP} + V_{LSgas} + V_{Tubes}\left(1 - \frac{L_c}{L_{Tubes}}\right)\right]} \quad (4)$$

The heat transfer across the steam generator tubes can be expressed in each of three separate sections: primary, tube wall, and secondary. Thus,

$$Q_o \equiv Q_p = Q_w = Q_s \quad (5)$$

where,

$$Q_p = \bar{h}_p \pi D_{iSG} L_c N_T N_{act} (T_{sat} - T_{wp}) \quad (6)$$

$$Q_w = \frac{k_w 2\pi L_c N_T N_{act}}{\ln(D_{oSG}/D_{iSG})} (T_{wp} - T_{ws}) \quad (7)$$

$$Q_s = \bar{h}_s \pi D_{oSG} L_c N_T N_{act} (T_{ws} - T_{sec}) \quad (8)$$

These equations can be combined and rearranged to yield an equation with only T_{sat} and L_c as unknowns:

$$T_{sat} = T_{sec} + \frac{Q_o}{2\pi L_c N_T N_{act}}\left[\frac{2}{\bar{h}_p D_{iSG}} + \frac{\ln(D_{oSG}/D_{iSG})}{k_w} + \frac{2}{\bar{h}_s D_{oSG}}\right] \quad (9)$$

This gives two equations (Equations (4) and (9)) and two unknowns (T_{sat} and L_c). A mathematical expression can be found for relating saturation temperature to saturation pressure (e.g., the Antoine equation or a similar correlation). This pair of equations and unknowns is then solved by readily available numerical solution schemes. The Newton-Raphson method was selected because of its relative ease of use.

Heat Transfer Coefficient Correlations

In Equation (9), the only variables that are not given by a property table or set equal to a constant are the primary and secondary heat transfer coefficients. Thus, correlations for these two variables must be developed for the particular flow regimes occurring in and outside the steam generator tubes. On the primary side, two types of heat transfer processes may occur: falling film condensation (annular two-phase flow) when only the vapor phase (and possibly noncondensable gas) enters, and condensation of a non-annular two–phase mixture when the froth level, due to mixture–level swelling, enters the steam generator. On the secondary side, heat transfer coefficient correlations for natural convection under both non–boiling and boiling conditions are needed. The heat transfer coefficient correlations used in the present analyses are given in the following subsections.

Primary Heat Transfer Coefficient

The heat transfer coefficient for condensation of a pure vapor onto the inner surface of a steam generator tube is obtained from classical Nusselt analysis.[5] The local heat transfer coefficient from this analysis is obtained as a function of the total condensate length, L_c, giving

$$\overline{h}_p = 0.943\left[\frac{\rho_{fs}(\rho_{fs}-\rho_{gs})gh_{fg}k_{fs}^3}{L_c 4\mu_{fs}(T_{sat}-T_{wp})}\right]^{1/4} \tag{10}$$

The average heat transfer coefficient on the primary side is therefore a function of the condensing length, L_c, which is one of the unknowns in Equations (4) and (9).

If a froth level enters the U-tubes, then a nonannular two-phase heat transfer coefficient must be calculated. From Reference 6, the following equation is used to determine the heat transfer coefficient:

$$\overline{h}_p = h_{2\phi}\gamma + h_{1\phi}(1-\gamma) \tag{11}$$

where $h_{2\phi}$ is determined from Equation (10), $h_{1\phi}$ is calculated using the Dittus-Boelter correlation[7] for forced convection inside tubes which yields:

$$h_{1\phi} = 0.023\frac{k_f}{D_{iSG}}\,Re_f^{0.8}\,Pr^{0.3} \tag{12}$$

and γ is calculated from the relationship:

$$\gamma = \frac{\alpha_{UP}}{\left(1-\frac{2\delta}{D_{iSG}}\right)} \tag{13}$$

Secondary Side Heat Transfer Coefficient

The heat transfer on the secondary side of the steam generator can be either single-phase natural convection or boiling two-phase heat transfer. On the steam generator secondary side, a natural convection heat transfer coefficient is obtained from the Nusselt number given by[8]

$$\overline{Nu} = 0.0210\,(GrPr)^{0.40} \tag{14}$$

or by rearranging in terms of the secondary heat transfer coefficient

$$\overline{h_s} = 0.0210\frac{k_f}{L_c}[GrPr]^{0.40} \tag{15}$$

For boiling conditions on the secondary side, the energy transfer is given by the Thom correlation[5] for fully developed subcooled boiling of water. The Thom correlation, in terms of the secondary side heat transfer coefficient, becomes

$$\overline{h_s} = \frac{\Delta T}{[22.65\ e^{-P_{sec}/87}]^2} \tag{16}$$

where P_{sec} is the secondary side pressure in bars.

Level Swell due to Boiling in the Core

Once boiling begins in the core, steam bubbles will rise into the upper plenum. Since the resulting two-phase mixture occupies more volume than the liquid alone, the water level in the reactor vessel will swell upward and enter the hot leg volume. Under these conditions, a two-phase mixture will flow into the hot leg once the upper plenum and upper head becomes saturated with steam. Due to the low fluid velocity, the flow becomes stratified in the hot legs. Once the fluid flow begins to turn upward into the steam generator inlet plenum, a two-phase froth may form due to the countercurrent flow of condensed water moving down and steam upward. This resulting froth may continue into the steam generator U-tubes. The increase in water level in the heated section of the RCS (the core, reactor vessel above the core, hot legs, and the inlet side of the steam generators) must be in hydrostatic balance with the water level of the unheated section of the RCS (downcomer, cold legs, loop seals, and outlet side of the steam generators). The final result of the froth level entering the steam generator U-tubes is that the water level in the loop seal piping rises into the steam generator outlet plenum.

If the froth mixture enters the steam generator U-tubes, the simplified Nusselt film condensation model for heat transfer is inappropriate and the two-phase heat transfer coefficient of Equation (11) must be used. To properly use Equation (11) the void fraction must be determined. Since the loss-of-RHRS involves stagnant water in the core, the drift flux model can be used to estimate the void fraction in the reactor vessel.

The drift flux model uses continuity equations to describe the distribution of the liquid and vapor phases in a two-phase mixture. The void fraction from the drift flux model is[5]

$$\alpha_g = \frac{j_g}{C_o(j_g + j_f) + V_{gj}} \tag{17}$$

where C_o is the distribution coefficient and V_{gj} is the vapor drift velocity. Correlations are available for C_o and V_{gj}, and they are functions of the flow channel geometry and the two-phase flow regime. The average void fraction is obtained by integrating the local fraction over the heated length of the fuel rods in the core; integration gives

$$\overline{\alpha}_{core} = \frac{1}{C_o}\left[1 - \frac{1}{Q_o^*}\ln(1+Q_o^*)\right] \tag{18}$$

where Q_o^* is

$$Q_o^* = \frac{C_o Q_o}{V_{gj} \rho_g h_{fg} A_{fc}} \qquad (19)$$

The vapor drift velocity, V_{gj}, is obtained from correlations of experimental data appropriate to the flow–channel geometry, two–phase flow regime, and operating conditions. The situation of interest is the case of boiling in a stagnant pool of liquid. Kataoka and Ishii[9] have summarized the application of the drift flux model of two–phase flow to these situations. For the pressure range of interest in analyses of the loss-of-RHRS incidents (0.1 to 0.4 MPa), these correlations give a drift velocity of about 0.2 m/s (0.6 ft/s).

The distribution coefficient C_o, is given as a function of pressure by[5]

$$\overline{C_o} = 1.2 - 0.2\left(\frac{\rho_{gs}}{\rho_{fs}}\right)^{0.5} \qquad (20)$$

which gives a value of about 1.2 for the conditions of the loss-of-RHRS incident. With V_{gj} and C_o from Equation (20), the average core void fraction of Equation (18) can be evaluated. The voids generated in the core move upward by buoyancy into the core outlet and upper plenum. The void fraction in these regions can be evaluated by use of Equation (17) with appropriate values of V_{gj} and C_o.

Code Package Description

The appropriate equations from the previous sections were written into a FORTRAN 77 computer program to solve for the RCS pressure and temperature, and the condensing length (L_c) in the steam generator tubes. The program is broken into approximately 29 subroutines with each one performing a specific task. A computational flow chart and more detail of the code package is given in Appendix D of Reference 2. Code compiling, debugging, and running were performed on a Macintosh IIci using Absoft's MacFortran/020™ software package in conjunction with the file editor QUED/M™ by Paragon Concepts.

Two different methods exist to input the data needed for the calculations: either by reading two files or interactively on the terminal. The two input files are a control input file and a plant data file. Three types of output files are produced by the code. One is an output file with values of the major variables only, such as iteration temperature and pressure. A diagnostic file is produced which prints virtually all variables that are calculated or used in any subroutine to aid in any type of code or run debugging. The last output file is one containing variable values produced in the iteration loop to evaluate the performance of the Newton-Raphson numerical method.

VALIDATION OF THE PISTON MODEL

The distribution of the noncondensable gases in the steam generator tubes is the crucial assumption in the Piston Model. Reference 10 reports experimental results showing where the noncondensable gases go once they enter the steam generator tubes and an analytical calculation to compare with these experimental results. It was determined, for the case when only steam enters the steam generator tubes, that three regions were established in an inverted U-tube (an "active" zone, a very short transition zone, and a "passive" zone) along the length of the U-tube. The active

zone contains only condensing water vapor at the temperature corresponding to the primary side saturation pressure. The passive zone contained a mixture of water vapor and noncondensable gases with no condensation occurring and a temperature equal to the secondary side temperature. The experiment also showed that the mixture of the steam-noncondensable gas in this passive zone is given by Dalton's Law so that the secondary temperature determines the partial pressure of the water vapor.

To truly validate the model, scaled system experiments needed to be found that examined the specific natural circulation regimes of concern. Various closed system U-tube and thermosyphon experiments were examined and discarded due to a lack of information needed to accurately model or evaluate results with the Piston Model. The Semiscale natural circulation experiment NC-6 was identified to have all of the necessary system information and experimental results.[11]

Semiscale Natural Circulation Test NC-6

A series of natural circulation experiments were conducted in the Semiscale Mod-2A test facility to help verify codes that analyze the reactor system response to small break LOCAs. In one of these tests, NC-6, the test facility was placed in a reflux condensation mode under reduced-coolant conditions. Then a series of nitrogen gas injections into the steam generator inlet plenum were performed to determine its effect on the condensation phenomena. This test was conducted at an operating system pressure of approximately 900 psia and at a decay heat level expected after a reactor scram. Reference 11 was used to provide an analytical method as a simple verification of the experiment results.

The Piston Model (using the Nusselt laminar film model) was applied to the conditions present during the NC-6 test run. The results from the model and the test runs are presented in Table 1. It is apparent that the Piston Model predicts the results from NC-6 reasonably well but tends to overpredict the pressure. This is consistent with the observation that the Nusselt laminar film condensing model will underpredict the average heat transfer coefficient, leading to a larger condensing length and greater degree of noncondensable gas compression.

Test NC-6 was useful for partial validation of the Piston Model. However, the injection of set amounts of nitrogen does not give a complete picture of the full scenario that would occur in a PWR following the loss-of-RHRS. Fortunately, the Federal Republic of Germany's PKL III facility performed a comprehensive experiment to study the loss-of-RHRS for the shutdown conditions that normally exist during mid-loop operation.[12]

Table 1 Semiscale Analysis and Experimental Results

N_2 - % of System Volume	Predicted Pressure (MPa)	Experimental Pressure (MPa)	Error (%)
0.86	6.4	6.1	5.1
2.98	6.9	6.5	6.5
5.00	7.4	7.1	4.4
6.34	7.7	7.7	0.6

PKL III EXPERIMENT B4.5

PKL is a 4-loop integral test facility simulating a 1300 MWe PWR (Figure 1). All elevations are preserved, power and volume are scaled down at 1:145. A more detailed description of the test facility can be found in Reference 12.

Test Objectives

The main objective of PKL III Experiment B.4.5 was to determine the thermal-hydraulic response of a PWR following a RHRS failure under cold shutdown conditions. Of special interest were:

1. The pressure and temperature increase necessary to reach steady-state conditions under which the decay heat can be transferred to the secondary of one operating steam generator.

2. Steam nitrogen mixing and the underlying mechanisms.

3. Heat transfer in the operating and isolated steam generators.

Initial System Conditions

A failure of the complete RHRS is postulated to occur approximately 30 hours after shutdown with the plant in a steady-state, the decay heat level being 0.7% (0.175 MW), core exit temperature 50°C (122°F) and primary pressure 1.0 bar (14.7 psia). The reactor pressure vessel head is still in place but the reactor coolant system has been partially drained - the loops are 1/2-filled with water and the rest, including the steam generators, with nitrogen (Figure 2).

All steam generators secondaries are depressurized to 1.0 bar (14.7 psia); one of them (SG1) is filled with water at a nominal level of 12.2 m (40 ft) and at 20°C (68°F). The remaining three steam generators (SG2, SG3, and SG4) are air-filled and isolated throughout the experiment.

Experimental Procedure

Secondary Pressure:

The pressure on the secondary of SG1 was kept below or at 2 bar (29.4 psia) by opening the turbine by-pass valve, and the auxiliary feedwater system was used to maintain the liquid level at its nominal value.

Decay Power:

For technical reasons the experiment was carried out in the evening. After one hour into the experiment the pressure had barely reached the value of 2 bar (29.4 psia). The decision was then made to increase the decay power to 1% and thus speed up the experiment in order to avoid work scheduling problems. After reaching a steady-state some 4 hours into the test, the power was lowered back to 0.7% and a steady-state at this power level was established.

SIEMENS

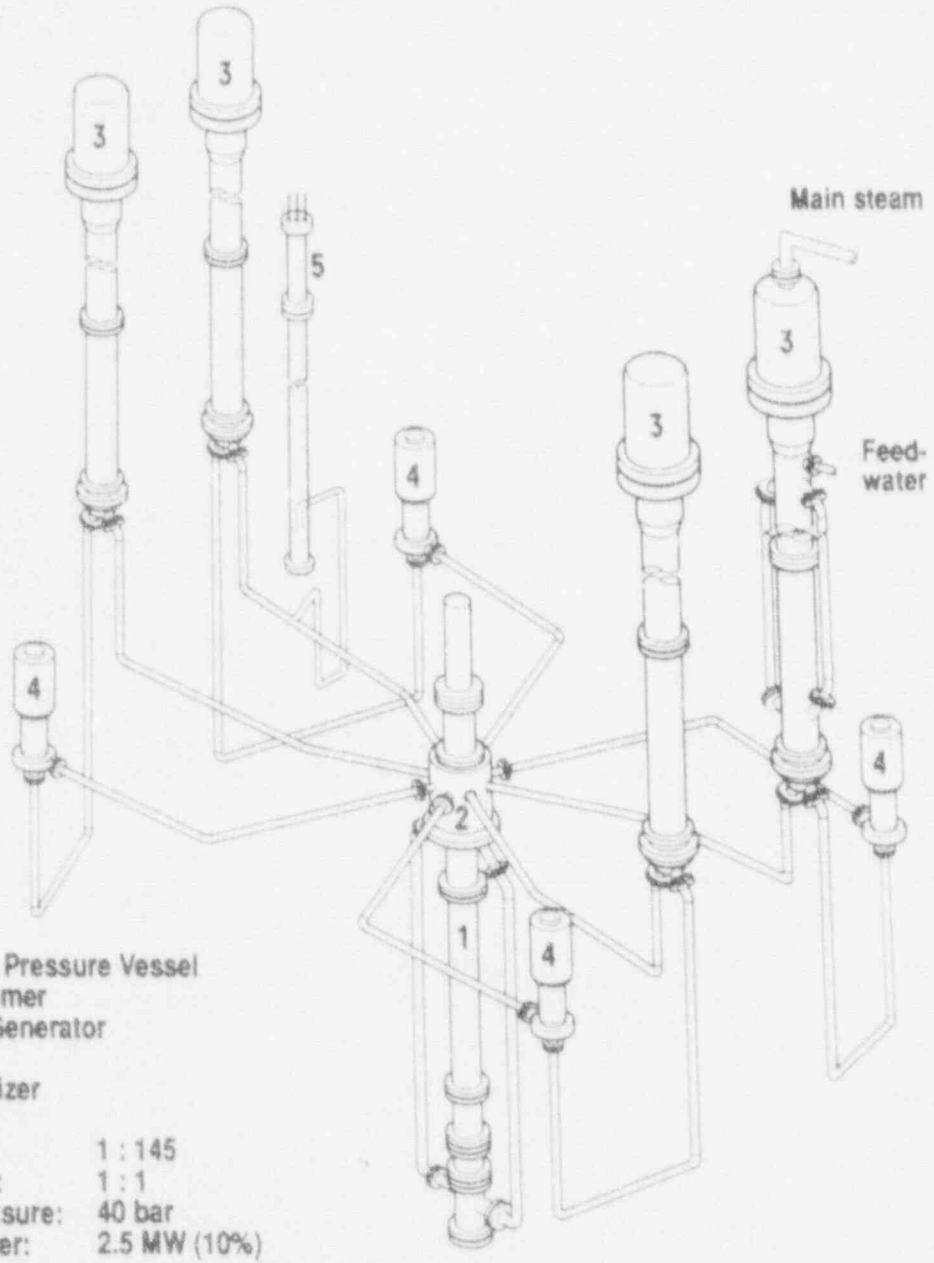

1 Reactor Pressure Vessel
2 Downcomer
3 Steam Generator
4 Pump
5 Pressurizer

Volume:	1 : 145
Elevation:	1 : 1
Max. Pressure:	40 bar
Max. Power:	2.5 MW (10%)

PKL III Test Facility Primary Side

87 PWR 022 e
KWU
E 312
a

Fig. 1

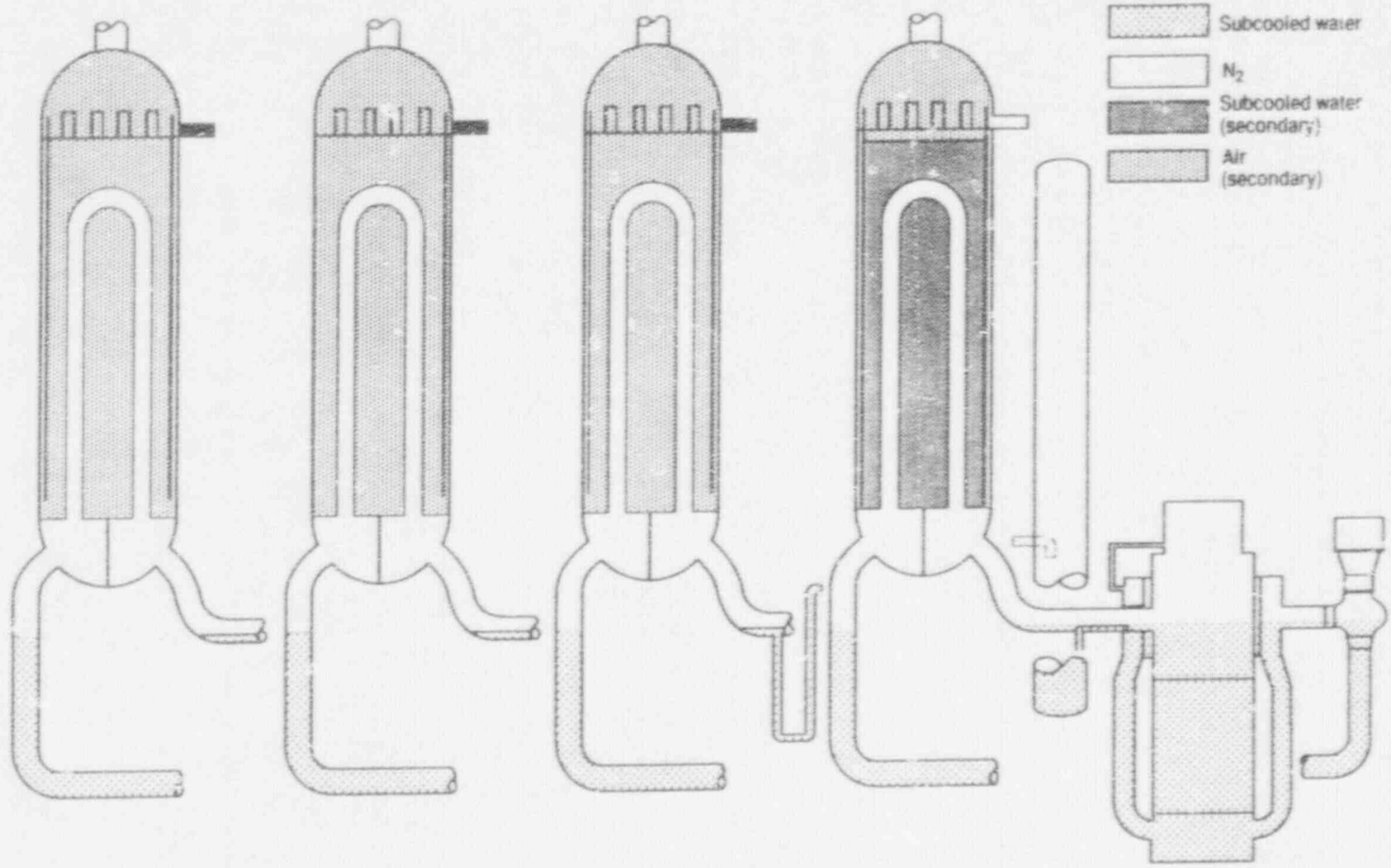

Fig. 2: PKL III B 4.5 : Failure of RHRS Test (t = 0s, p_p = 1.0 bar)

90 PWR 059 e
KWU
E 312
b

Results

After the failure of the RHRS, saturation temperature was reached in the core within 20 minutes (Figure 3). Steam production led to formation of a two-phase mixture which reached into the inlet plena of all four steam generators. The upper head, upper plenum, hot legs and water in the above components acted as heat sinks for a further 20 minutes before they reached saturation temperature. Thereafter, steam penetrated simultaneously into SG1, SG3, and SG4, and shortly afterwards into SG2. At this transient stage they all acted as heat sinks. The water-filled secondary of SG1 offered a greater potential for condensation; it drew more steam than SG2, SG3, and SG4. Due to the low steam density at near atmospheric pressure the steam velocity at the steam generator tubesheet was high enough to cause liquid holdup inside the tubes (Figure 4).

Efficient steam-nitrogen mixing took place in the isolated steam generators as evidenced by the tube temperatures rising with core exit temperature. Figure 5 shows the temperature history of SG3, which is representative of all isolated steam generators. The temperature of the U-tube inlet side is close to the primary saturation temperature, indicating a low proportion of noncondensable gas. The lower U-tube exit temperature indicates a higher concentration of noncondensable gas (Figure 5).

With the secondary side of the operating SG1 being kept constant at a saturation pressure of 2 bar (29.4 psia) and decay power at 1.0%, a steady-state on the primary was reached at a pressure of 6.6 bar (96 psia), some four hours after the RHRS failure (Figure 3). The secondaries of the isolated steam generators (i.e. stagnant air and metal mass) approach asymptotically the temperature level of about 150°C (302°F) and their contribution as heat sinks becomes negligible.

After lowering the decay power back to its original value of 0.7%, a new steady-state was reached at a pressure of 5.8 bar (84 psia). These steady-state conditions could be held for any length of time. They depend only on the availability of the auxiliary feedwater supply.

Important Phenomena

Formation of Swell Level

During heat up, just before the first steam bubbles are formed in the core, the water level rises due to the decrease in water density, and completely fills the hot legs. The formation of steam in the core leads to further redistribution of water from the core and upper plenum into the hot legs, elevating the two phase mixture into the steam generator inlet plenum. At 40 minutes into the transient at a pressure of 1.4 bar (21 psia) the primary inventory ceases to act as a heat sink. At this point the steam begins to enter the steam generator tubes. When at least one steam generator secondary is available for cooling, there is a smooth transition from one form of heat sink (primary inventory and structures) to another; namely the steam generator secondary.

Mass Distribution under Steady-State Conditions

Table 2 shows the difference in mass distribution within the primary system between RHRS operation at 1 bar (14.7 psia), and the reflux condensing mode of operation at 6.6 bar with one steam generator acting as a heat sink. The results show a mass reduction in the reactor vessel of 13% due to steam formation in the core, and a mass increase in the pressurizer (8%), steam generator U-tubes (4%), and hot leg 1 (4%). Despite the reduction of inventory in the core, the redistribution is such that there is never any danger of core dryout.

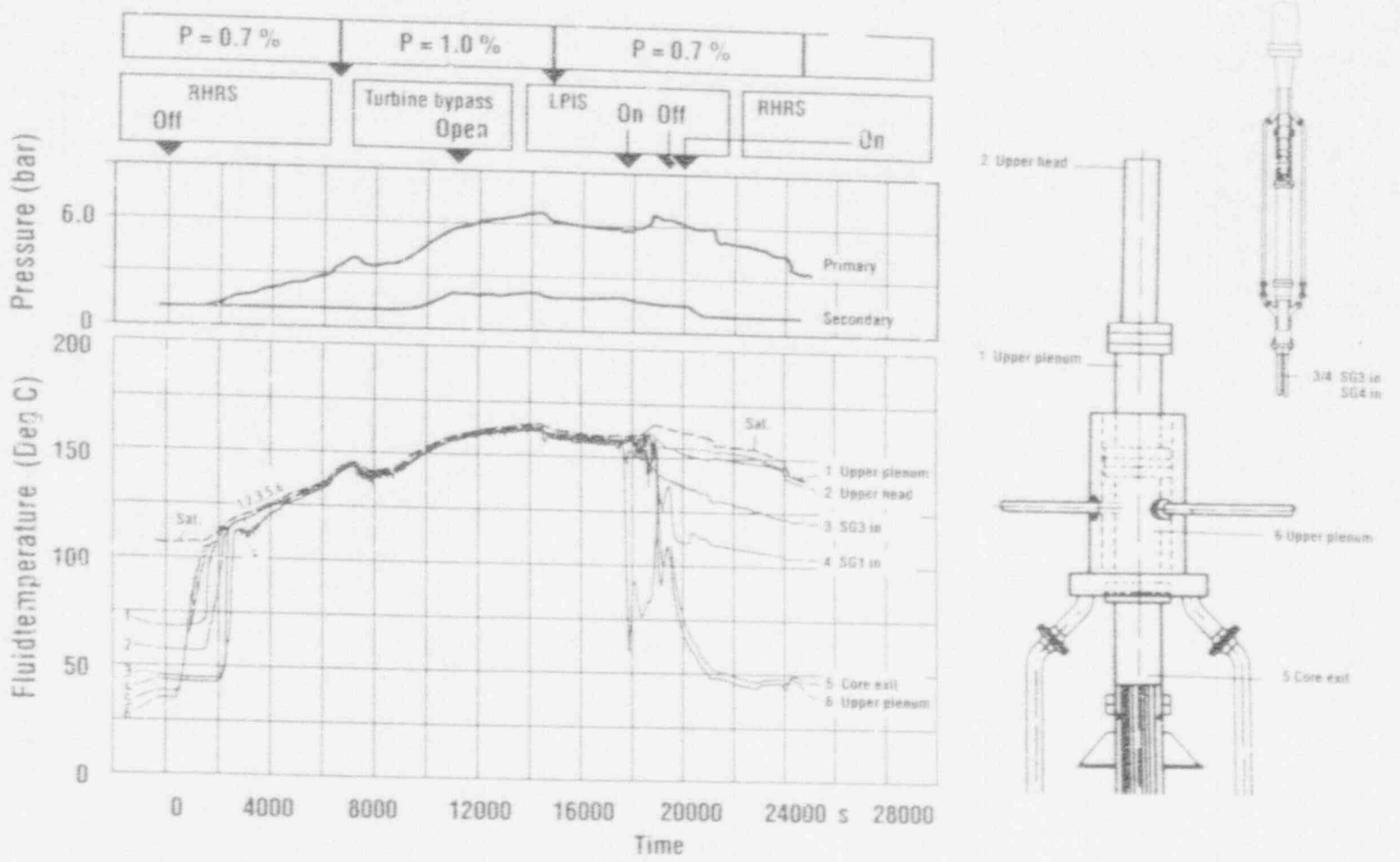

Fig. 3: PKL III B 4.5 : Temperature and Pressure in RPV

91 PWR249 e
KWU
E 312

SIEMENS

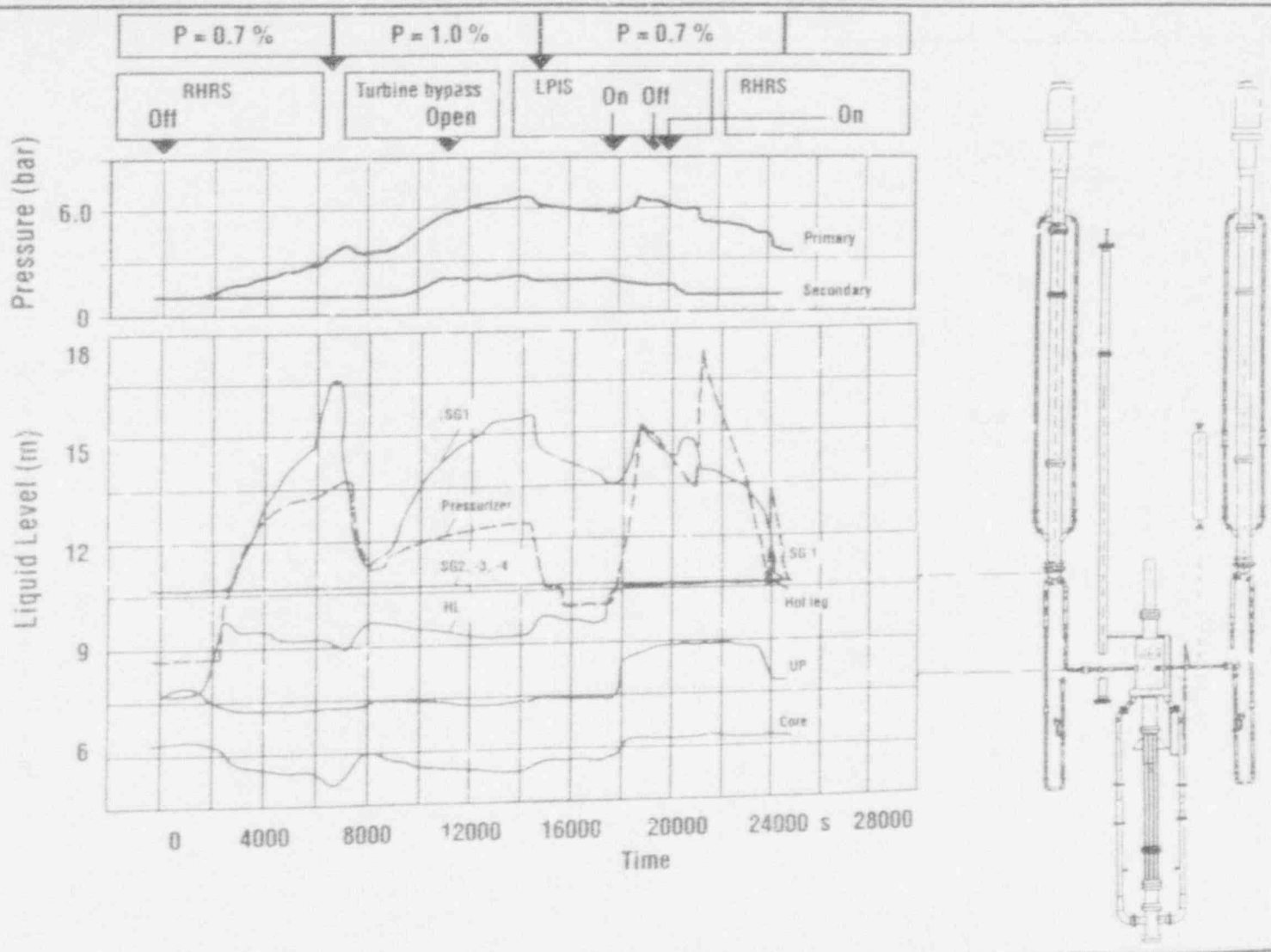

91 PWR 254 e
KWU
E 312

Fig. 4: PKL III B 4.5 : Liquid Level and Pressure

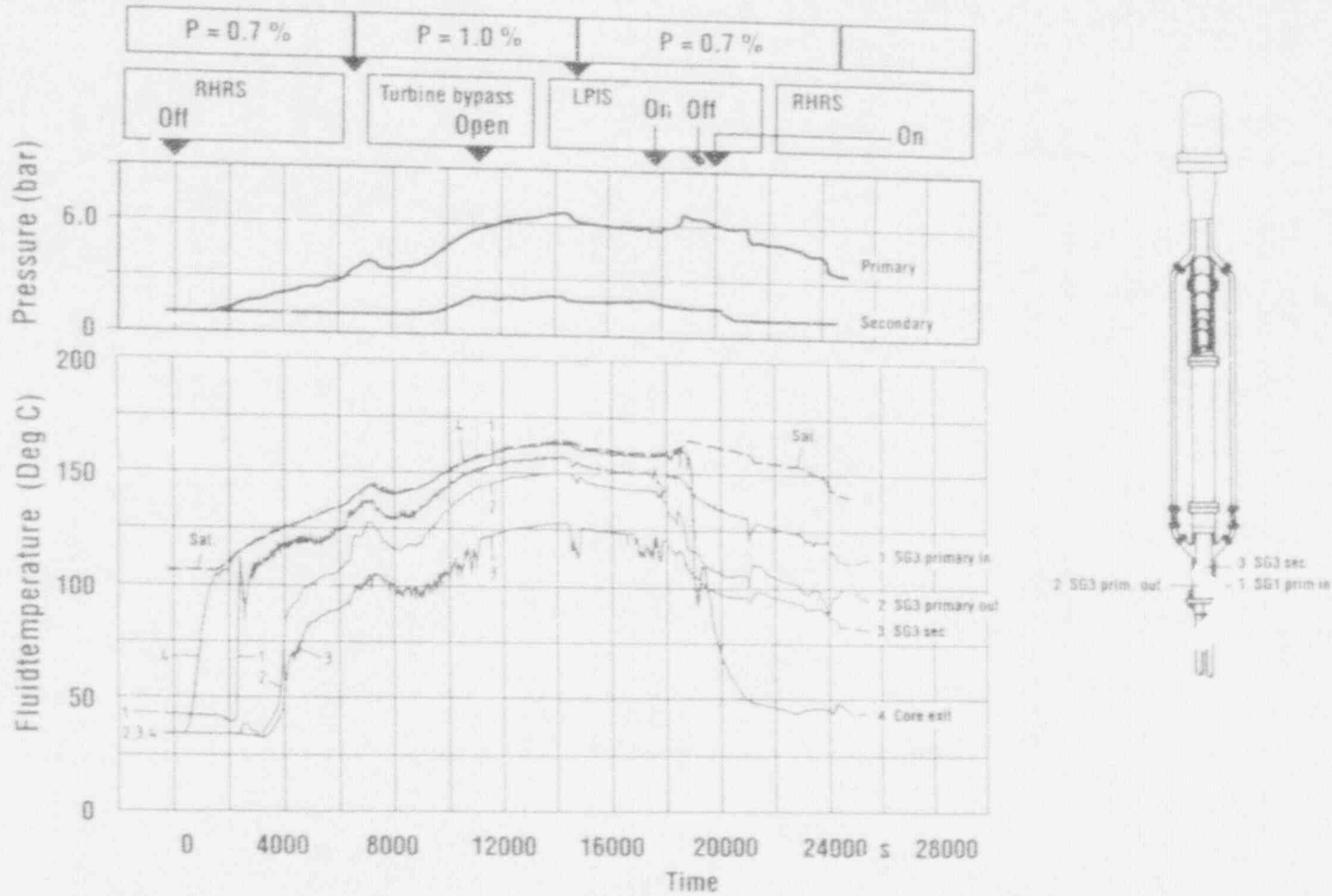

Fig. 5: PKL III B 4.5 : Pressure and Temperature (Fluid) in Isolated SGs

91 PWR 250 e
KWU
E 312

Table 2 Mass Distribution under Steady-State Conditions

	RHRS Operation (%)	Reflux Condenser (%)	Difference (%)
Reactor Vessel excl. Downcomer	45	37	-8
Downcomer	25	20	-5
Hot Leg 1 incl. SG inlet plenum	1	4	+3
Pressurizer incl. Surge Line	6	14	+8
SG U-tubes	0	4	+4
Rest of RCS	23	21	-2

Steam-Nitrogen Mixing

While the level swell was forming in the upper plenum, the steam bubbles rose above the two-phase mixture into the space above the hot legs. Against expectations, excellent nitrogen-steam mixing was observed in the upper plenum as well as in the upper head. The steam penetrated through the upper head bypass into the top of the downcomer and the cold legs as far as the pump housing. These observations, as well as results from other experiments involving nitrogen[13], suggest that apart from buoyancy and entrainment, diffusion plays a significant role in the mixing process. The steam propagation along its path (as shown by temperature measurements) appeared to be independent of direction; either rising (into the upper plenum) or dropping (into the top of downcomer), the steam penetration velocity was about 20 mm/min (3.9 ft/hr). From these results the conclusion was drawn that diffusion dominated the mixing process.

Steam Generator U-tube Performance

The two phase mixture in the steam generator inlet plenum extended into the U-tubes (Figures 6 and 7). Due to condensation, the void fraction steadily decreased along the tube length until there was not any steam left (in equilibrium approximately 0.7 m (2.3 ft)). At these relatively low pressures and low steam densities, the steam velocity at the U-tube inlet was j_g = 4 m/s (13.1 ft/s), which under the given conditions lies above the flooding limit, i.e. before steady conditions were reached, not all the condensate returned to the hot leg. This led to accumulation of condensate in the U-tubes which cuts off the nitrogen-steam mixture above it from the upflowing steam below.

As the pressure in the primary increased, the nitrogen-steam mixture was compressed, creating a temperature difference between the primary and secondary and some of the steam condenses. To replace the volume of the condensed steam (i.e. to preserve pressure equilibrium), condensate was drawn up into the U-tubes. Under equilibrium conditions at 1% power, the pressure of the nitrogen-steam mixture in the U-tubes is 0.5 bar (7.2 psi) lower than the pressure in the steam generator inlet plenum. To preserve equilibrium, a water column of approximately 4 m (13.1 ft) forms in the U-tubes above the condensing length and is "not allowed" to fall down.

The 4 m (13.1 ft) long, stable, subcooled water column supported above the two phase flow region was unexpected. The bottom twenty or so centimeters were at saturation temperature, and

SIEMENS

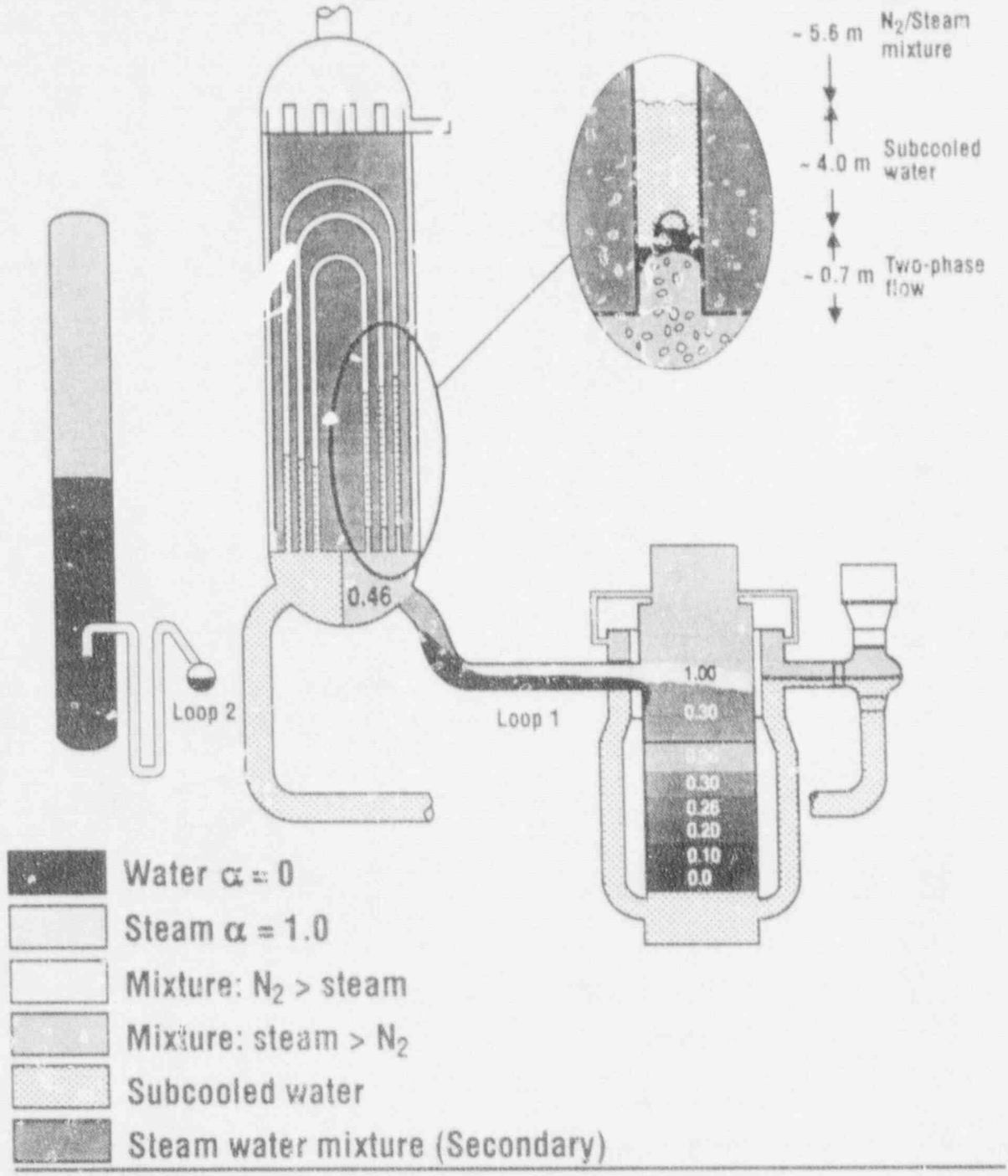

Fig. 6: PKL III 4.5 Coolant and Void Distribution at Steady State for 1% Decay Heat Level (t = 14000 s, p = 6.6 bar)

91 PWR 182
KWU
E 312

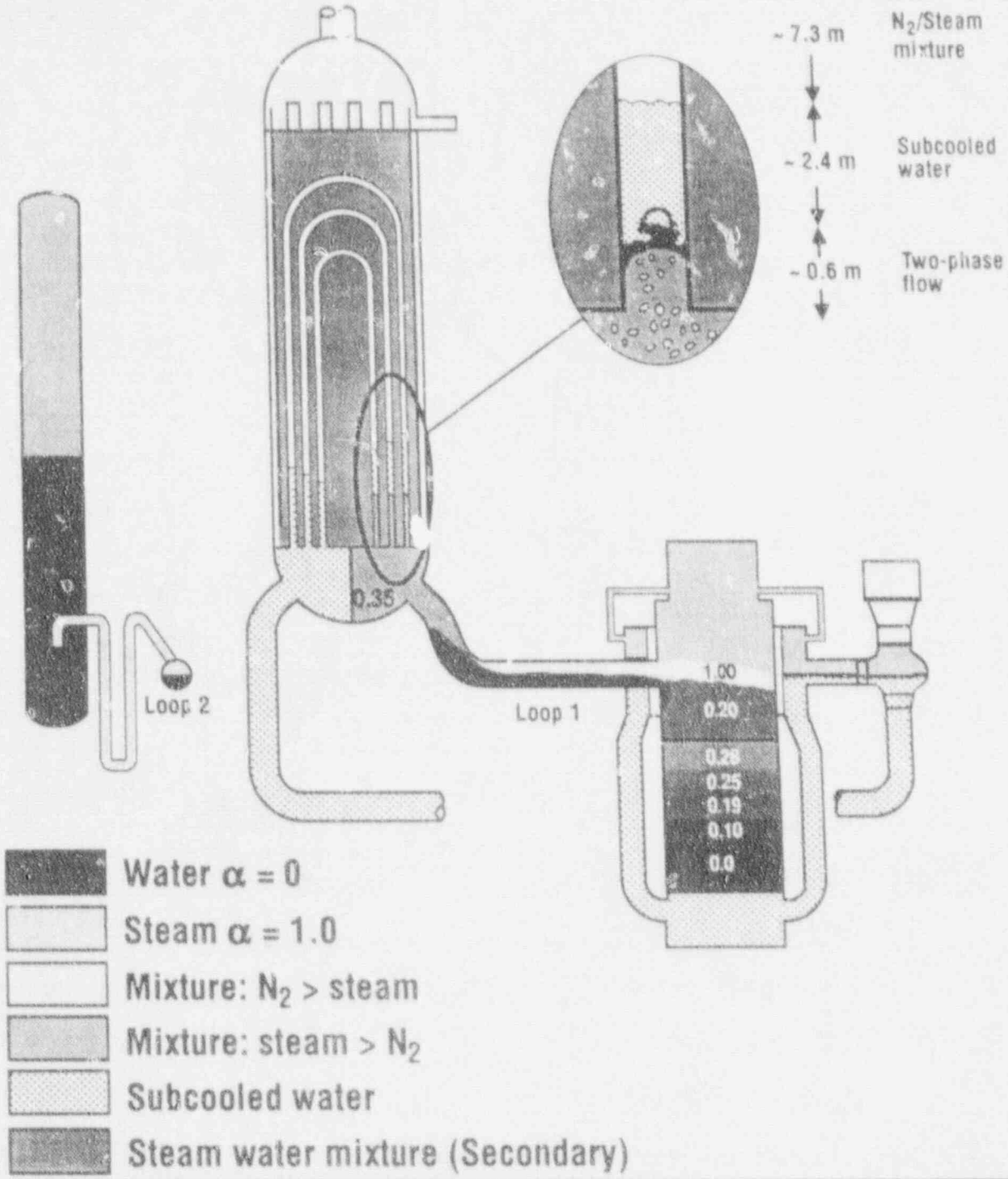

Fig. 7: PKL III 4.5 Coolant and Void Distribution at Steady State for 0.7% Decay Heat Level (t = 17000 s, p = 5.8 bar)

91 PWR 213 e
KWU
E 312

there was a kind of mini-natural circulation within the water column (Figure 6): the warm water rose, was replaced by colder water from above and in turn cooled down to the secondary temperature. The water column was stable but not completely stationary. It oscillated with an amplitude of 0.3 m (0.98 ft) and a period of 50 seconds. The water column's natural tendency to move downwards was counteracted by two effects. The first effect is due to the creation of a drop in pressure of the noncondensable gas/vapor (or the passive section) volume due to expansion following the column's downward movement. The second, of lesser importance, is from the upward momentum of the two-phase mixture entering the U-tubes to support the water column from below. These two effects balance out the gravitational force to keep the water column stationary.

MODEL CALCULATIONS FOR THE PKL III EXPERIMENT B4.5

Using the information presented in the previous section, the necessary input conditions for Experiment B4.5 were developed for the Piston Model code. It should be noted from the measurements in the upper head, that the temperature is slightly below the saturation temperature, indicating the presence of a small amount of nitrogen gas in the upper head. This is different from the assumption in the Piston Model that all noncondensable gas is swept out of the reactor vessel. With all things being equal, this result will tend to make the Piston Model overpredict the RCS pressure due to having more noncondensable gas in the steam generator U-tubes than is really swept into the U-tubes.

Since a hydrostatic head balance must exist between the hot and cold legs, the increase in hot leg level due to the two-phase mixture has a corresponding level increase in the loop seal piping (Figures 6 and 7). The experimental results showed that a water slug formed on top of the condensing length for both power levels (4 m (13.1 ft) at 1% power and 2.5 m (8 ft) at 0.7% power), and that this water slug stays at the temperature of the secondary side. Also, the water level in the loop seal piping rises to the bottom of the steam generator outlet plenum. Both of these effects reduce the available volume which the nitrogen can occupy in the passive section of the steam generator, thus raising the steady-state RCS pressure.

The formation of the two-phase mixture (or froth) is an important effect with respect to the steady-state system conditions. If the Piston Model, as was verified by the Semiscale test, is used on this PKL experiment, the steady-state pressure is calculated to be significantly lower than the measured pressure (4.3 bar (62 psia) vs. 6.6 bar (96 psia) at 1% power (0.25 MW) and 4.1 bar (61 psia) vs. 5.8 bar (84 psia) at 0.7% power (0.175 MW)). This is not unexpected, since the laminar film condensation model is no longer applicable when a two-phase mixture enters the steam generator tubes. Clearly, the void and volume growth in the core as a result of boiling affects the final system conditions and needs to be taken into account in the model when such conditions occur.

The level swell model as applied to the PKL III Experiment B4.5 at 1% power indicates that a froth level reaches the steam generators. When the two-phase nonannular heat transfer coefficient is used and compared to the analysis with the Nusselt heat transfer coefficient, the primary heat transfer coefficient decreases from 5329 to 3062 W/m^2-K (939 to 539 $Btu/hr\text{-}ft^2\text{-}°F$). However, the calculated RCS pressure, based on a change of heat transfer coefficient due to a two phase mixture, increases only slightly from 4.3 to 4.8 bar (62 to 70 psia) for the 1% decay level. The new 0.7% decay level results only improves slightly (less than 0.5 bar). The results improve but clearly not well enough to predict the conditions that occur during the experiment.

As a sensitivity study, the single-phase heat transfer correlation (Dittus-Boelter) was used in the Piston Model and the PKL experiment analysis was repeated. The Dittus-Boelter correlation yields a primary heat transfer coefficient of about 250 W/m^2-K (44 Btu/hr-ft^2-°F). The new results overpredict the RCS pressure by 0.9 bar (13 psia) (7.5 bar (109 psia) vs 6.6 bar (96 psia)) for the 1% decay level and by 0.8 bar (6.6 bar (96 psia) vs 5.8 bar (84 psia)) for the 0.7% decay level.

From the experimental data for the 1% power level, the water slug height is approximately 4 m (13.1 ft), the condensing length is 0.7 m (2.3 ft), and the water level height on the steam generator U-tube outlet side is 3 m (9.8 ft). By taking into account the additional pressure needed to maintain a water slug above the condensing region, the reduction of the passive volume in the steam generator U-tubes due to the level swell, and using a heat transfer coefficient based on the 0.7 m (2.3 ft) condensing length (about 13,000 W/m^2-K), the Piston Model calculates the RCS pressure of 6.3 bar (91 psia) at the 1% power level. The 0.7% power level has the following results: the water slug length is 2.5 m (8 ft), the condensing length is 0.6 m (2 ft), and the reduction of the passive volume length is 2 m (6.5 ft). The Piston Model calculation for the 0.7% conditions is 5.6 bar (82 psia) vs. the experiment's 5.8 bar (84 psia). Therefore, it becomes clear that how well one determines the level swell due to boiling and the hydrostatic balance will determine the accuracy of the Piston Model.

CONCLUSIONS

The PKL experiment shows that complex thermal-hydraulic phenomena are exhibited during a loss-of-RHRS under reduced inventory conditions at high levels of decay heat. The data from the experiment clearly show that the effect of level swell on both sides of the active steam generator can be substantial on the final RCS pressure. While the analytical model does not directly calculate an RCS pressure observed in the experiment, greater accuracy is possible with an accurate level swell determination. As a minimum, one can determine an upper limit of the RCS pressure that could result from a loss-of-RHRS by making conservative assumptions.

Another important, though not unexpected, result is that the condition of the steam generator secondary side govern the steady-state RCS pressure. This can be seen in the primary pressure and the secondary pressure over the duration of the experiment. The model also predicts this result. Therefore, the lowest possible RCS pressure will occur if the steam generator secondary temperature can be kept as low as possible with either an adequate makeup water supply or venting path.

REFERENCES

1. P. R. McHugh and R. D. Hentzen, Natural Circulation Cooling in U. S. Pressurized Water Reactors, NUREG/CR-5769, To be published at a future date.

2. S. A. Naff, G. W. Johnsen, D. E. Palmrose, E. D. Hughes, and C. M. Kullberg, Draft Report: Thermal-Hydraulic Processes During Reduced Inventory Operation with Loss of Residual Heat Removal, SAN-20-91, Dtd July 31, 1991.

3. J. L. Crew, et al., Loss of Residual Heat Removal System, Diablo Canyon, Unit 2, April 10, 1987 (Augmented Inspection Team Report April 15-21, 29, and 1 May 87), Nuclear Regulatory Commission, NUREG-1269, June 1987.

4. Staff Report, Loss of Vital AC Power and the Residual Heat Removal System During Mid-Loop Operations at Vogtle Unit 1 on March 20, 1990, NUREG-1410, June 1990.

5. J. G. Collier, Convective Boiling and Condensation, McGraw Hill Book Company, New York, 1972.

6. C. L. Tien, S. L. Chen, and P. F. Peterson, Condensation Inside Tubes, EPRI-NP- 5700, January 1988.

7. J. R. Welty, C. E. Wicks, and R. E. Wilson, Fundamentals of Momentum, Heat, and Mass Transfer 2nd Edition, John Wiley & Sons, New York, 1976.

8. V. S. Arpaci and P. S. Larsen, Convection Heat Transfer, Prentice–Hall, Inc., Englewood Cliffs, New Jersey, 1984.

9. I. Kataoka and M. Ishii, Prediction of Pool Void Fraction by New Drift Flux Correlation, ANL–86–29, 1986.

10. D. Hein, R. Rippel, and P. Weiss, "The Distribution of Gas in a U-Tube Heat Exchanger and Its Influence on the Condensation Process", International Heat Transfer Conference, Munich, Germany, September 1982.

11. G. Loomis and K. Soda, Results of the Semiscale MOD-2A Natural Circulation, NUREG/CR-2335, EGG-2200, September 1982.

12. R. M. Mandl, K. J. Umminger, and J. v.d. Logt, "Failure of PWR-RHRS Under Cold Shutdown Conditions Experimental Results from the PKL Test Facility," 18th Water Reactor Safety Research Information Meeting, Rockville, Maryland, October 22-24, 1990.

13. K. J. Umminger and R. M. Mandl, "Thermal-Hydraulic Response of a PWR to Nitrogen Entering the Primary: Experimental Investigation in a 4-Loop Test Facility (PKL)," To be presented at the 5th Int'l Topical Meeting on Nuclear Reactor Thermal-Hydraulics, Salt Lake City, Utah, September 21-24, 1992.

Effects of Hydrogen Generation on Severe Accident Natural Circulation

J. E. O'Brien
Idaho National Engineering Laboratory
EG&G Idaho, Inc.

ABSTRACT

During certain pressurized water reactor (PWR) severe accident scenarios, natural circulation can play an important role in determining the failure location and time-to-failure of reactor coolant system (RCS) components. At the time in the transient when fuel cladding temperatures reach about 1800 K, hydrogen generation due to the steam/zirconium reaction becomes significant. Effects of this hydrogen production on natural circulation flow and heat transfer have been considered in this report. Possible flow disruption due to hydrogen stratification in the reactor vessel and/or hydrogen-induced steam generator blockage were both considered. Long-term hydrogen stratification in the reactor vessel appears to be unlikely due to turbulent mixing associated with high Rayleigh number in-vessel natural convection. Mixing times scales were found to be short (a few minutes), even when a fully stratified starting condition was assumed. This finding was consistent with experimental results obtained by Westinghouse with a 1/7-scale PWR RCS model.

If mixing of steam and hydrogen is rapid and no condensation occurs, analysis of the accident progression can be performed by simply accounting for the properties of the gas mixture as the composition changes. This is essentially what is done by RELAP5 since gas mixtures are treated as homogeneous. Therefore, recognizing the inherent limitations of a one-dimensional representation of a multidimensional phenomenon, RELAP5 should provide reasonable estimates of natural circulation heat transfer effects with a steam/hydrogen mixture. If operator actions take place during an accident such that water is reintroduced on the secondary side of a steam generator, condensation would begin, possibly resulting in a sudden enrichment of the gas mixture hydrogen content in the steam generator tubing. This situation could potentially lead to a serious disruption in the natural circulation flow pattern due to U-tube flow blockage.

NOMENCLATURE

c_p	constant pressure specific heat, J/kg K
c_v	constant volume specific heat, J/kg K
g	gravitational acceleration, m/s^2
h	heat transfer coefficient, W/m^2 K
L	characteristic length, m
M	molecular weight, kg/kmol
n	natural convection exponent, eqn. (12), dimensionless
q"	heat flux, W/m^2
Ra	Rayleigh number (defined in eqn. (1)), dimensionless
Ri	Richardson number (eqn. (5)), dimensionless
t	time, s
T	temperature, K
ΔT	temperature difference, K
u_e	entrainment velocity, m/s
u_*	convective velocity (eqn. (4))
V	flow velocity, m/s
x	mole fraction, dimensionless
α	thermal diffusivity, m^2/s
β	volumetric thermal expansion coefficient, K^{-1}
δ_b	height of mixed layer, m
ϕ	gas mixture property parameter, eqn. (6), dimensionless
μ	absolute viscosity, N s/m^2
ν	kinematic viscosity, m^2/s
ρ	fluid density, kg/m^3
ρ_b	density within mixed layer, kg/m^3
$\Delta\rho$	density difference, kg/m^3

INTRODUCTION AND BACKGROUND

During certain postulated severe accident scenarios, for example, loss of both onsite and offsite AC power and early failure of the steam-driven auxiliary feedwater pump (TMLB'), a high pressure boil-off of reactor coolant system (RCS) water occurs, causing the core and upper regions of the reactor vessel to be filled with steam. During the later stages the presence of water in the pump loop seals generally precludes the establishment of full-loop natural circulation through the hot leg, steam generator, cold leg and core. However, both in-vessel and ex-vessel multi-dimensional natural circulation flows can still occur. Due to the radial power distribution in the core, fuel temperatures are higher in the center than at the core periphery. Consequently, a natural circulation flow of steam can become established through the core with down-flow near the periphery and up-flow in the center. In addition, heat sinks in the upper plenum allow for the formation of a vigorous natural circulation flow in the upper portion of the reactor vessel. In Westinghouse and Combustion Engineering plants, hot leg counter-current flow can also become established due to the presence of heat sinks in the hot leg piping and the steam generator. In this flow loop, hot steam exits the reactor vessel through the top half of the hot leg piping and is returned through the lower half. Some of this fluid enters the steam generator tubes where natural circulation flow may also become established, despite significant fluid mixing in the steam generator inlet plenum. An additional complication occurs at the point in the transient when core temperatures become high enough (~1500 K) that the zircaloy cladding begins to chemically react with the steam, producing hydrogen gas and exothermic heating. Generation of hydrogen gas in the RCS has the potential to modify or stop the natural circulation flows due to stratification effects. In addition, the presence of hydrogen affects natural circulation heat transfer rates.

The net result of the natural circulation flows is to transport thermal energy from the reactor core to other structures and to reduce the rate of fuel temperature increase in the core. Ultimately, a passive failure of ex-vessel piping could occur due to creep rupture or even melting, thereby depressurizing the RCS prior to the time of a lower head failure. The possibility of a high-pressure ejection of molten core materials and the resultant direct containment heating would therefore be reduced (but the potential for an in-vessel steam explosion may be increased). The specific location of the ex-vessel failure is critical since initial failure of the steam generator tubes would provide a direct path (through the steam line relief valves) for fission product release outside of containment. The most favorable failure location is therefore the surge line or the hot leg.

A research program has been initiated to evaluate vessel and hot leg natural circulation behavior to aid in predicting the likelihood of passive ex-vessel RCS failure prior to lower head failure and to identify the most likely failure location. One aspect of this project is to evaluate the effect of hydrogen production on natural circulation flow and heat transfer in the RCS. Concerns have been raised that hydrogen stratification could isolate certain regions from natural circulation flows and thus have a significant impact on the timing and location of RCS failure. This type of flow disruption, if present, cannot be modeled using a one-dimensional system code such as RELAP5. Even in the absence of stratification, with a homogeneous mixture of steam and hydrogen circulating in the RCS, natural circulation flow rates and heat transfer will be affected by the presence of hydrogen. This paper will also address quantification and code modeling of these fully mixed binary gas effects.

The objective of the analysis presented in this paper is to assess the effects of hydrogen generation on severe accident natural circulation flow and heat transfer rates. This assessment includes an attempt to quantify the likelihood that in-vessel hydrogen stratification will persist for any significant time period during a severe accident transient. Characteristic turbulent mixing times will be estimated and compared to appropriate transient time scales. Enhancement of natural convec-

tion heat transfer rates due to hydrogen enrichment will be considered. Finally, the implications of operator-induced sudden condensation in the steam generator after significant hydrogen addition will be considered.

HYDROGEN EFFECTS ON NATURAL CIRCULATION

Stratification and Mixing. The possibility for hydrogen stratification in the reactor vessel will be examined first. During hydrogen production via the steam-zirconium oxidation reaction, hot streaks of hydrogen-rich gas will be transported upward by buoyancy forces. A hydrogen-enriched atmosphere could therefore be created (at least temporarily) in the reactor vessel upper plenum. Thermally driven in-vessel natural convection will also be occurring due to buoyant forces associated with temperature differences between the core and reactor vessel internal structures. This natural convection will tend to homogenize the gas mixture inside the vessel by turbulent mixing. The strength of the natural convection flow and associated turbulent mixing is governed by the magnitude of the characteristic Rayleigh number for this enclosure as given by:

$$Ra = \frac{g\beta\Delta TL^3}{\nu\alpha} \qquad (1)$$

Using steam properties at 700 °C and 15 MPa (fluid conditions characteristic of the early stages of core heatup [1]) and choosing a characteristic temperature difference, ΔT, of 400 K (typical value based on results of analysis presented in reference [1] and TMI-2 lead screw data [2]) and a characteristic length scale of 3.4 m (typical reactor vessel diameter), a characteristic Rayleigh number of $1.2 \times 10^{}$ is predicted. Since transition to turbulence occurs at a Rayleigh number around 10^9, vigorous turbulent natural convection is expected at the predicted vessel characteristic Rayleigh number. Chemical energy release from the exothermic steam/zirconium oxidation reaction would be expected to further augment natural convection and mixing during the very time period when hydrogen production is occurring.

The order of magnitude of typical in-vessel flow velocities can be estimated using

$$V = \sqrt{gz\Delta T/T} \qquad (2)$$

where z is the fluid acceleration height. The upper plenum height is about 3 m. Assuming that buoyant acceleration is effective over one third of the upper plenum height, and that $\Delta T/T \sim .4$, a velocity of about 2 m/s is obtained. Recognizing that there will be significant dissipation of flow kinetic energy associated with fluid impingement on the upper plenum support plate and recirculation, a reasonable average velocity magnitude for the upper plenum flow may be 0.5-1 m/s, which is consistent with the results of [1].

A method for estimating turbulent mixing times in initially stratified media is provided in reference [3]. The fluid is characterized by initial stable solutal stratification and is assumed to be uniformly heated from below, as shown in Fig. 1. In this case, a homogeneous mixed layer whose height increases with time forms above the heated surface. A correlation for entrainment (or mixing front) velocity, which quantifies the growth rate of the mixed layer for such systems, is given by

$$\frac{u_e}{u_*} = 0.2\,Ri^{-1} \qquad (3)$$

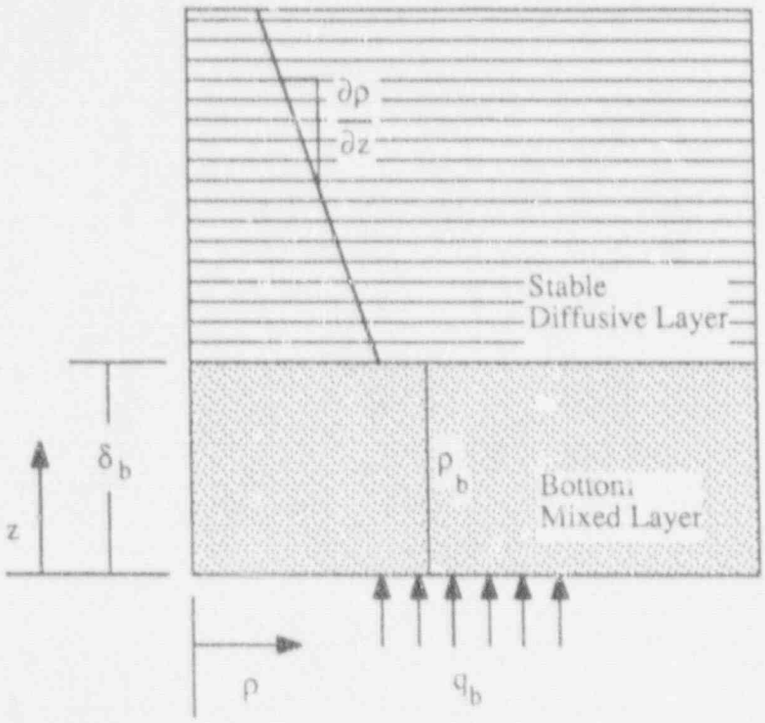

Figure 1. Schematic of penetrative mixing situation.

where

$$u_* = \left[\frac{g \beta_T q_b \delta_b}{\rho_b c_{v,b}} \right]^{1/3} \tag{4}$$

and the Richardson number, Ri, is given by

$$Ri = \frac{g \Delta\rho \ \delta_b}{\rho_o u_*^2} \tag{5}$$

The range of applicability for the correlation of eqn. (3) is approximately $1 < Ri < 10^4$. The density, ρ_b, is the density of the mixed layer, which changes with time according to

$$\rho_b = \frac{1}{\delta_b} \int_0^{\delta_b} \rho_i(z) \, dz \tag{6}$$

in which

$$\rho_i(z) = \rho(z=0) + z\left(\frac{\partial \rho}{\partial z}\right)_i \tag{7}$$

The density difference across the interface, $\Delta\rho$, is therefore given by

$$\Delta\rho(\delta_b) = \frac{1}{\delta_b}\int_0^{\delta_b} \rho_i(z)\, dz - \rho_i(z=\delta_b) \tag{8}$$

Assuming a linear initial density variation,

$$\Delta\rho = \frac{\delta_b}{2}\left(\frac{\partial \rho}{\partial z}\right)_i \tag{9}$$

Now, substituting eqns. (4) and (5) into eqn. (3) and using eqn. (9) for $\Delta\rho$, the mixing front velocity is given by

$$u_e = \frac{d\delta_b}{dt} = \frac{(2)(0.2)\,\beta_{T,b}\,q_b}{\delta_b\left(\frac{\partial \rho}{\partial z}\right)_i c_{v,b}} \tag{10}$$

Integrating to obtain δ_b as a function of time and solving for the mixing time, treating the other mixed layer properties as constant yields

$$t_{mix} = \frac{\delta_b^2\left(\frac{\partial \rho}{\partial z}\right)_i c_{v,b}}{0.8\,\beta_{T,b}\,q_b} \tag{11}$$

which indicates that the mixed layer height increases with the square root of time. In reality, the mixed layer specific heat is also dependent on δ_b. Under the assumption of an initial linear density profile, this dependency is relatively weak and was treated by evaluating the gas mixture specific heat for the mixed layer at an intermediate hydrogen mole fraction of 0.25 (the maximum hydrogen mole fraction for the mixed layer is 0.5).

A mixing time of 99 seconds has been estimated using eqn. (11) for the upper plenum of a PWR, again using steam and hydrogen properties at 700° C and 15 MPa. According to the SCDAP/RELAP5 simulation [1], the time period for significant hydrogen generation lasts about 10 min. Consequently, based on the conservative mixing time estimates provided above, complete hydrogen/steam mixing should occur in a much shorter time period than is required to

generate the bulk of the hydrogen. A modeling treatment of the overall transient in which fully mixed conditions are assumed to prevail at each time step is therefore reasonable. This fully mixed model is adopted in SCDAP/RELAP5.

Characteristic convective velocities, u_*, within the mixed layer can also be estimated using eqn. (4). For the full-scale PWR conditions of 700° C and 15 MPa, values of 0.73 and 1.2 m/s are obtained at mixing heights of 1 and 3 meters, respectively. These values are completely consistent with the order-of-magnitude calculation of eqn. (2) and with the results of [1].

The issue of hydrogen stratification effects on severe accident PWR natural circulation was also addressed during a series of experiments performed at the Westinghouse Research and Development Center [4, 5]. A 1/7-scale model of a Westinghouse PWR was constructed in order to observe natural circulation flow patterns and heat transfer. The apparatus was operated under both transient and steady-state conditions using high-pressure SF_6 [4] as the working fluid in order to achieve approximate similitude. In order to examine the effects of possible hydrogen stratification on natural circulation flows and heat transfer, helium was slowly introduced into the model reactor vessel prior to any heating, forming a fully stratified static region in the upper head. This fully stratified starting condition was thought to represent a worst case in terms of stratification effects. Heating was initiated and transient start-up of natural circulation flow patterns was observed, primarily by means of thermocouple readings in various locations. No gas sampling was performed during the high-pressure tests. Temperature readings indicated no stratification-induced delay in heating of the top upper plenum fluid. Furthermore, fluid temperature readings recorded at the core exit and at the steam generator end of the hot leg also indicated no stratification-induced heating delays. In fact, no significant stratification effects were observed. The authors conclude that in-vessel fluid mixing is rapid and is dominated by turbulence.

Hydrogen production effects were also simulated in the earlier low-pressure (atmospheric) Westinghouse 1/7-scale experiments using air-helium and SF_6-helium [5]. In these low-pressure experiments, measurements included both thermocouple readings and gas sampling, which was carried out at various locations and times in order to provide a direct indication of the degree of fluid mixing. Helium injection and SF_6 withdrawal were carried out differently for the low pressure tests than for the high pressure tests. For the low pressure tests, helium was introduced continuously (and SF_6 withdrawn) near the middle of the core for a period of forty seconds during steady-flow natural circulation. Gas sampling began at the end of the forty second gas introduction period. Gas concentration measurements for the SF_6 tests indicated complete fluid mixing after about 5 minutes in the top of the upper plenum. Gas concentrations in the upper head were observed to acquire their final steady-state fully mixed values virtually instantaneously, however, which is unexpected since the upper head is more isolated from the core than is the upper plenum.

Predictions of mixing times were obtained for the experimental conditions of both the high-pressure [4] and the low-pressure Westinghouse [5] 1/7-scale natural circulation tests using eqn. (12). Results of these calculations are summarized in Table 1, along with the results of a calculation for a full-scale plant at 7 MPa, 700° C.

The predicted convective velocity, u_*, for the Westinghouse low-pressure tests is consistent with results of laser-doppler anemometry measurements obtained in the upper plenum of the 1/7-scale facility [5]. Richardson numbers of Table 1 are all within the range of applicability cited earlier. Mixing time for the Westinghouse low-pressure test is predicted to be 137 seconds, which is lower than the 5 minute value indicated from the gas sampling measurements. Experimental conditions did not correspond exactly to the initially fully stratified condition of the correlation,

however, so this level of disagreement is not surprising. Mixing time for the Westinghouse high-pressure experiments was predicted to be 52 seconds, which is about one twentieth of the overall transient time studied. There were no direct gas sampling measurements obtained during the high-pressure tests, however, so no direct comparison can be made. As mentioned previously, no significant stratification-induced thermal effects were observed during the high-pressure tests.

It should be noted that the predicted mixing times for the 1/7-scale experiments, despite their similarity to the prototypical values, represent a relatively high fraction of the total characteristic transient time for the 1-7 scale model because the time scale for the model is much shorter than for the prototype [6]. Therefore, for similar predicted mixing times, stratification effects would be expected to be more pronounced in the model.

In fact, some significant stratification-induced effects were noted for the nonprototypical (the primary flow similitude parameter used by Westinghouse [6], $g\rho^2\beta q''L^2/c_p\mu^3$, was more than four orders of magnitude too low with atmospheric SF_6) Westinghouse low-pressure tests [5]. About 1 minute after the end of helium injection, a temperature inversion was observed in the hot leg with cold light gas overlying warm heavy gas. This situation was due to the fact that the fluid entering the top of the hot leg from the reactor vessel was helium-enriched. Hot leg temperatures remained steady for about the next ten minutes, apparently indicating a complete flow stoppage during that period. This flow stoppage may have been due to blockage of the inverted U-tube steam generator flow by helium-enriched fluid. In any case, clearly the observed stratification effects were much more severe for the low-pressure experiments than for the near-prototypical high pressure experiments. The severity of the effects was probably due to the longer mixing time (see Table 1) required for the weaker, less turbulent flow conditions of the low pressure experiments, allowing transport of a significantly helium-enriched fluid stream to the steam generator tubes where blockage ensued. The method of helium introduction into the experimental apparatus may have also played a role.

The effect of system pressure on mixing time is indicated by the last row in Table 1. The reduction in predicted mixing time is primarily due to the reduction in density difference between the

Table 1. Summary of mixing time calculation results.

	u_* (m/s)	Ri	t_{mix} (seconds)
full-scale plant, P = 15 MPa	1.22	16	116
Westinghouse 1/7-scale, low-pressure	.315	39	137
Westinghouse 1/7-scale, high-pressure	.431	21	52
full-scale plant, P = 7 MPa	1.51	8.8	51

two gases as the pressure is decreased.

The short mixing times of Table 1 and the results of the high-pressure Westinghouse experiments indicate that hydrogen stratification should not cause any significant disruption of severe-accident natural circulation flows in the reactor vessel.

Several studies have also been performed on hydrogen stratification and mixing in containment atmospheres [6-10]. The consensus of these studies is that turbulent mixing dominates inside containments as well and that hydrogen stratification will persist for time periods only on the order of tens of minutes [6], even with the relatively weak natural convection and much larger volume of a containment compared to a reactor vessel.

Concerns about in-vessel stratification effects on severe accident natural circulation were heightened by observations obtained from metallurgical examination of lead screws from TMI-2 [2]. These observations revealed that an inverted temperature profile existed (at least in the lead-screws) during the accident in the upper region of the reactor vessel, with the lowest temperatures occurring at the top of the vessel. Additional evidence based on oxidation rates indicates that a hydrogen-enriched atmosphere was present in the upper reactor vessel [2]. Solutal stratification of a relatively low-temperature hydrogen/steam mixture has been suggested as a possible explanation for these observations. Expected TMI-2 in-vessel mixing times are so short, however, that hydrogen stratification should not have persisted for any significant time period. Leakage flow of cool gas from the upper head downward along the lead screws has been suggested as an alternative explanation for the inverted temperature observations [11].

Gas Mixture Effects. If the assumption is made that complete mixing of steam and hydrogen has been achieved in the RCS and that no condensation is occurring, the analysis reduces to one in which the properties of the gas mixture must be used in place of pure steam properties to predict natural circulation (other gas components such as volatile fission products may also be present). Natural convection heat transfer rates for hydrogen/steam are higher than for steam alone. Enhancement is due primarily to the significantly higher thermal conductivity of hydrogen. For a given geometry and temperature difference, the magnitude of the enhancement can be approximated by [12]:

$$\bar{h} \sim (c_p \cdot \rho^2/\mu)^n \cdot k^{1-n} \tag{12}$$

where n is the exponent in the relationship

$$\overline{Nu} \sim Ra^n \tag{13}$$

and the properties are evaluated for the gas mixture. Typical values for n are in the range 0.2 - 0.3. Methods for determination of gas mixture properties are given in [13]. For mixtures of ideal gases, thermodynamic properties (expressed on a molar basis) are simply mole-fraction weighted averages of the constituent properties. Transport properties, on the other hand, are not. In particular, viscosity of gas mixtures is determined from the Sutherland formula

$$\mu_g = \sum_{i=1}^{N} \frac{x_i \mu_i}{\sum_{j=1}^{N} x_j \Phi_{ij}} \tag{14}$$

where

$$\phi_{ij} = \frac{1}{\sqrt{8}}\left(1 + \frac{M_j}{M_i}\right)^{-1/2}\left[1 + \left(\frac{\mu_i}{\mu_j}\right)^{1/2}\left(\frac{M_j}{M_i}\right)^{1/4}\right]^2 \qquad (15)$$

A similar formula is used for thermal conductivity. As an example of the fully mixed steam/hydrogen effect on natural convection, properties of steam/hydrogen mixtures at 700°C and 15 MPa required for use in eqn. (12) are plotted in Fig. 1 as a function of hydrogen mole fraction. In addition, the heat transfer enhancement for natural convection with a steam/hydrogen mixture as predicted by eqn. (12) is shown in Fig. 2. It is interesting to note that the maximum heat transfer enhancement occurs with a high mole fraction of hydrogen, but not with pure hydrogen.Equations (14) and (15) are incorporated into RELAP5 [14], which treats steam/noncondensible mixtures as being in complete thermal and mechanical equilibrium (i.e., fully mixed) [15]. Hydrogen properties are also available in the code. Heat addition associated with the exothermic steam/zirconium oxidation reaction is also modeled. Therefore, recognizing the inherent limitations of a one-dimensional representation of a multi-dimensional phenomenon, RELAP5, as it was applied in reference [1], should provide reasonable estimates of natural circulation heat transfer effects with a steam/hydrogen mixture.

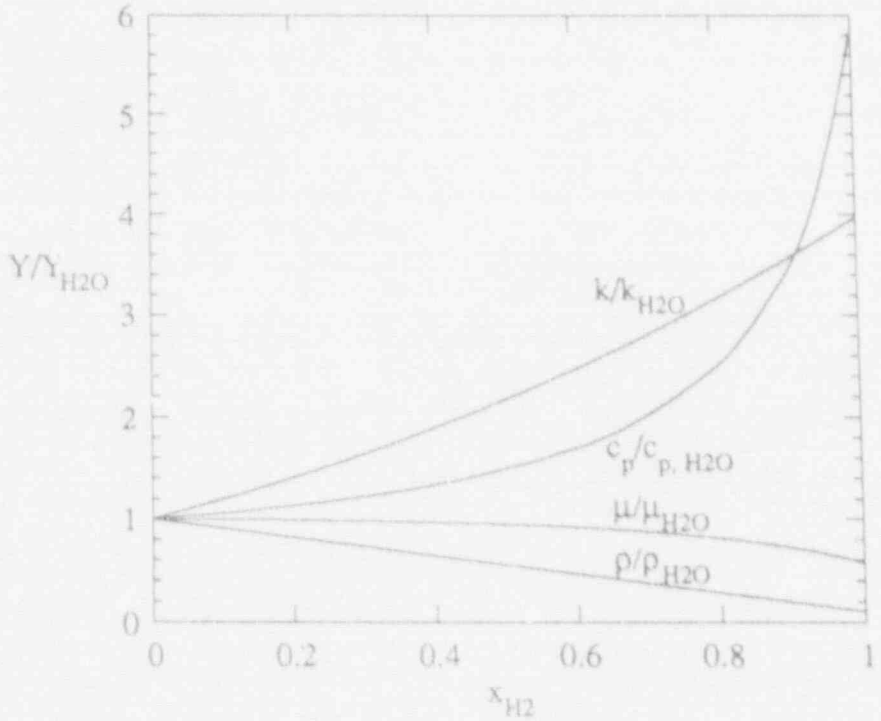

Figure 2. Gas mixture property variations for increasing hydrogen mole fraction.

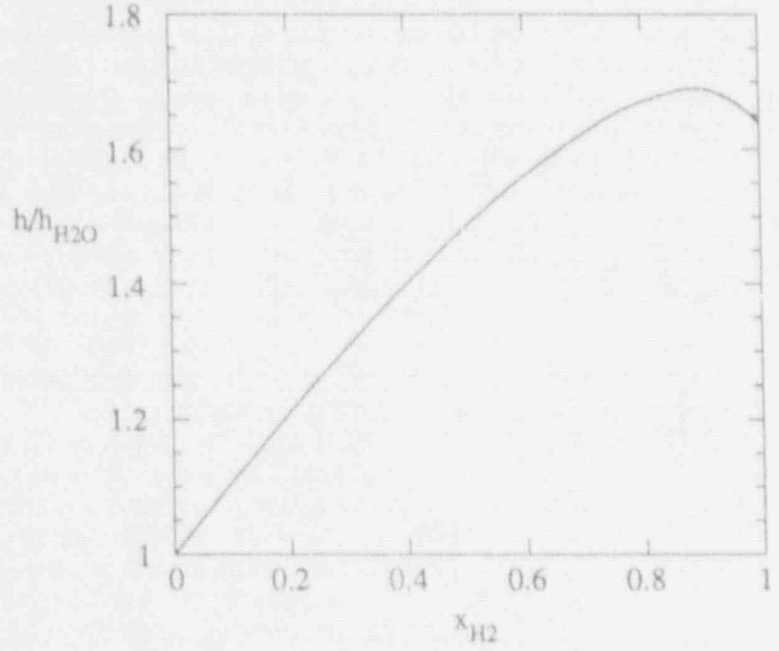

Figure 3. Natural convection heat transfer enhancement due to increasing hydrogen mole fraction.

Condensation. As mentioned previously, condensation in the steam generator would not be expected after boil-off of the secondary side during a TMLB'. However, if operator actions take place such that water is reintroduced on the secondary side of a steam generator (as occurred during TMI-2), condensation would begin inside the steam generator tubing. If the fluid inside consists of a steam/hydrogen mixture, sudden enrichment of the hydrogen content will occur. This situation could potentially lead to a serious disruption in the natural circulation flow pattern, especially for the inverted U-tube steam generator design. In particular, U-tube flow blockage could occur as the concentration of light noncondensible hydrogen gas increases inside the tubing. Buoyancy will tend to stabilize the hydrogen in the inverted U-tubes, preventing further natural circulation through the tubes.

An operator-induced transient involving introduction of water to the secondary side of the steam generator could have a significant impact on the time-to-failure of specific RCS components during an accident scenario, especially if hydrogen is present on the primary side at the time of the transient. System response to this type of transient should also be amenable to RELAP5 modeling, possibly requiring inclusion of a steam generator flow blockage model such as the one used in MAAP [16]. RELAP5 does have the capability to handle condensation in the presence of noncondensibles.

SUMMARY AND CONCLUSIONS

Natural circulation can play an important role during certain PWR severe accidents in determining the failure location and time-to-failure of RCS components. At the time in the transient when fuel cladding temperatures reach about 1500 K, hydrogen generation due to the steam/zirconium reaction becomes significant. Effects of this hydrogen production on natural circulation flow and heat transfer have been considered in this report. Long-term hydrogen stratification in the reactor vessel appears to be unlikely due to turbulent mixing associated with high Rayleigh number in-vessel natural convection. Estimated mixing times were found to be short, compared to overall transient time periods, even when a fully stratified starting condition was assumed. This finding was consistent with experimental results obtained at Westinghouse with a 1/7-scale PWR RCS model.

If mixing of steam and hydrogen is assumed to be rapid and no condensation can occur, analysis of the accident progression can be performed by accounting for the properties of the gas mixture as the composition changes. The gas property changes that occur as a result of hydrogen production include increased thermal conductivity and specific heat, and decreased viscosity and density. The net effect on natural circulation heat transfer is a significant augmentation. The fully mixed gas model is utilized in RELAP5. Therefore, with its inherent limitations in mind, RELAP5 should provide reasonable estimates of natural circulation effects, system temperatures, failure location, and component time-to-failure with a steam/hydrogen mixture. If operator actions take place during an accident such that water is reintroduced on the secondary side of a steam generator, condensation would begin, possibly resulting in a sudden enrichment of the gas-mixture hydrogen content in the steam generator tubing. This situation could potentially lead to a serious disruption in the natural circulation flow pattern due to U-tube flow blockage, possibly delaying or even precluding hot leg or surge line failure.

References

1. Bayless, P. D., "Analyses of Natural Circulation During a Surry Station Blackout Using SCDAP/RELAP5," NUREG/CR-5214.

2. Vinjamuri, K., Akers, D. W., and Hobbins, R. R., "Examination of H8 and B8 Leadscrews from Three Mile Island Unit 2 (TMI-2)," GEND-INF-052, 1985.

3. Bergman, T. L., Incropera, F. P., and Viskanta, R., "Correlation of Mixed Layer Growth in a Double-Diffusive, Salt-Stratified System Heated from Below," *Journal of Heat Transfer*, Vol 108, pp. 206-211, 1986.

4. Stewart, W. A., Pieczynski, A. T., and Srinivas, V., "Experiments on Natural Circulation in a Pressurized Water Reactor Model with High Pressure SF_6," preliminary draft, 1990.

5. Stewart, W. A., Pieczynski, A. T., and Srinivas, V., "Experiments on Natural Circulation in a Pressurized Water Reactor Model for Degraded Core Accidents," EPRI Project No. RP2177-5, Final Report, 1988.

6. Camp, A. L. et al., "Light Water Reactor Hydrogen Manual," NUREG/CR-2726, Sandia National Laboratory, 1983.

7. Langer, G. et al, "Experimental Investigation of the Hydrogen Distribution in the Containment of a Light Water Reactor Following a Coolant Loss Accident," Battelle Institute e. V. Frankfurt, NRC Translation 801, 1980.

8. Willcutt, G. J. E. Jr., and Gido, R. G., "Mixing of Radiolytic Hydrogen Generated Within a Containment Compartment Following a LOCA," NUREG/CR-0304, August, 1978.

9. Trent, D. S., "Mixing of Buoyant Combustibles Gases in BWR Containment Systems," Battelle-Northwest Laboratories report BNWL-B-298, August, 1973.

10. van de Vate, J. F., and Plomp, A., "Atmospheric Stability Inside Containments with a Heated Layer of Liquid on the Floor," *Nuclear Science and Engineering*, Vol. 56, pp. 196-200, 1975.

11. Motley, F., ANS Conference Proceedings, San Francisco, November 1989.

12. Petri, J. G. and Bergman, T. L., "Augmentation of Natural Convection Heat Transfer Using Binary Gas Coolants," *Int. J. Heat Mass Transfer*, Vol. 33, No. 7, pp. 1441-1449, 1980.

13. Reid, R. C., Prausnitz, J. M., and Sherwood, T. K., *The Properties of Gases and Liquids*, third edition, McGraw-Hill, New York, 1977.

14. Lin, J. C., "Heat Transfer with Noncondensible Gas," EG&G Report No. SWR-NSMD-83-205, January, 1983.

15. Carlson, K. E., et al., "RELAP5/MOD3 Code Manual," NUREG/CR-5535, June 1990.

16. Kenton, M. A., Henry, R. E., Sharon, A., and Epstein, M., "Simulation of the TMI-2 Accident Using the MAAP Modular Accident Analysis Program, Version 2.0," EPRI NP-4292, Final Report, Research Project 2392-15, January, 1986.

SCALING ISSUES FOR A THERMAL-HYDRAULIC INTEGRAL TEST FACILITY

Timothy J. Boucher, Idaho National Engineering Laboratory
Marino diMarzo, University of Maryland at College Park
Louis M. Shotkin, U.S. Nuclear Regulatory Commission

Abstract

The USNRC is considering how to best obtain integral system test data for the new reactors with passive safety systems, AP600 and SBWR. This paper discusses scaling issues that must be considered in designing such a thermal-hydraulic integral test facility. Topics covered include experimental requirements for such a facility, a critical review of available scaling methodologies, experience from past testing programs which may aid the design of a new facility, enumeration of minimum dimensions for an integral test facility and application of these concepts to the design of a low pressure test facility.

1. General Scaling Considerations

As part of the design certification process for the new AP600[1,2] and SBWR[2] reactors, the NRC is evaluating the vendor testing programs, both separate effects and integral tests, to determine if any additional data would be desirable. Since new reactor systems differ most significantly from current reactors in that their safety systems are gravity-driven rather than pumped, particular attention is being focussed on integral testing of the interactions of these new passive safety systems under accident conditions. Both of these new designs also rely on automatic depressurization systems to promote the gravity-driven cooling of the core. These new systems must be adequately modeled in the thermal-hydraulic codes used to simulate their performance and sensitivity. Although many concepts in this paper are general, when specific examples are required, the focus will be on the AP600 design. This paper contains information from a recent study performed at INEL[3].

It is recognized that a complete thermal-hydraulic testing program for a new reactor design must include both integral system tests and separate component tests. The test facilities must have adequate instrumentation so that the data will be of sufficient scope and quality for assessing thermal-hydraulic computer codes. The separate effects tests study the response of individual components, often at near to full-scale, to imposed thermal-hydraulic boundary and initial conditions. The integral effects tests identify and quantify system phenomena, sensitivities and interactions. Ideally, the entire length of advanced reactor transients would be simulated in a single, appropriately scaled integral test facility. However, it is feasible to investigate different portions of the transients in integral facilities at more than one scale. For example, a full-height full-pressure facility could investigate the high pressure interactions of fluid flow and heat transfer that may occur before the IRWST injection begins. A separate reduced -height reduced-pressure facility could be used to study the low-pressure system interactions during the latter part of the depressurization. However, if different portions of a given transient are obtained from two differently scaled facilities, the feasibility of establishing appropriate initial conditions for the low pressure integral facility must be investigated early in the planning process to assure that the integrated results are valid for code assessment purposes.

A scaled integral test facility should be designed to satisfy a number of criteria. Preservation of thermal-hydraulic phenomena expected in the full-scale plant is considered to be of major importance. The scaling rationale used in the design of an integral test facility for a new reactor, such as the AP600, must attempt to emphasize and preserve the phenomena thought to be of first-order importance in the prototype system. The experimental facility must also be carefully designed to represent all components that are relevant to the safety research needs. It should be capable of simulating the response to these events as expected during real time accident progression, i.e., including operator actions and non-safety grade systems. Distortions to processes (particularly flow regime transitions, mass and energy transfer) and to time scales should be minimal since even small distortions may lead to different events in the progression of these transients. Additionally, although thermal-hydraulic computer codes are the primary means whereby scaled facility results are extrapolated to full scale, the scaled integral facility design should minimize activities necessary to draw inferences to the plant domain. The key is to identify facility concepts which satisfy the largest portion of phenomenological data needs and provide results which are best suited for drawing inferences to the plant domain.

2. Experimental Requirements for Integral Testing

Considerable experimental data has been obtained over the past 25 years on the thermal-hydraulic behavior of reactors of current design. The first step in defining experimental requirements for a new design is to identify the design differences for which sufficient data was not previously obtained.

For the AP600 design, traditional pumped systems are used for accident prevention and for the first level of defense should an accident occur. The major design difference involves the safety systems which come into action once an upset condition occurs. These new safety systems are gravity-driven, replacing current

pumped injection systems. For example, a passive residual heat removal (PRHR) system bypasses the steam generator replacing the current pumped auxiliary feedwater system in the steam generator secondary. Gravity-driven core make-up tanks (CMT) replace the pumped high pressure safety injection system. The piping used to supply the pressure difference to drive this flow from the CMTs is also a new aspect of the AP600 design. The safety injection goes into the downcomer, rather than the cold-leg as on current designs. An automatic depressurization system (ADS) has been added, which activates on water level in the CMT. No such counterpart exists in operating PWRs, although operating BWRs have an ADS. Gravity flow from a large in-containment refueling water storage tank (IRWST) replaces the pumped low-pressure safety injection. Major design changes have also been made to the containment, and its coupling to the primary system has been made more direct. For example, steam is condensed on the containment walls and flows back into the IRWST, or into the cavity surrounding the reactor vessel. Thus the containment as a long-term heat sink replaces the auxiliary feedwater system and the containment spray. The containment as a passive source of water for the primary replaces the pumped low-pressure safety injection.

An evaluation[4] was conducted to identify AP600 first-order importance phenomena and code assessment data needs. The evaluation showed that the largest uncertainties and unknowns in safety system performance are for late stage accident events when the system will be operating at low pressure in a natural circulation mode and primary inventory lost through the break or ADS will be replenished by water from the IRWST and/or containment sump. The makeup rate under these conditions will be dependent on pressure balances in the system, small hydrostatic heads, and complex interactions between system components. Phenomena and processes that will be prevalent during this time frame include:

- small gravity-driven flows and two-phase pressure losses;
- single and two-phase natural circulation in the primary loops and possibly in the various loops formed by the pressure equalization piping;
- condensation heat transfer in the containment and primary system;
- counter-current flow (including flooding);
- core heat transfer (especially vapor generation);

The most significant new process during the high pressure phase of AP600 transients is the CMT gravity draining which is strongly affected by the overall system response and particularly by CMT and pressure balancing line condensation phenomena. The above phenomena represent the first-order importance phenomena for the AP600. Hence, these high and low pressure phenomena, combined with their controlling phenomena, form the basis upon which the scaling analyses should be conducted. That is, the integral test facility should ideally be sized to preserve these high and low pressure phenomena.

At least three scenarios must be considered at high pressure: the small-break loss-of-coolant accident; the steam-generator tube rupture; and the steam-line break. For these events, the passive systems may be required to function while

the system is at relatively high pressure. For the steam-line break, will over cooling and pressure reduction activate the ADS? How does the control system handle this event?

One must consider what uncertainties there may be in using existing thermal-hydraulic computer codes to predict the safety behavior of these new designs.

First, are there any unique new phenomena connected with operation of these systems? No, but the range of conditions and system configuration differences have not been extensively studied in previous testing programs. The new passive safety systems operate at low driving heads and their performance may be sensitive to small pressure fluctuations and to interactions with new system components.

Second, what are the current uncertainties in existing thermal-hydraulic codes regarding their ability to predict the behavior of these new systems? The two main areas of uncertainty are: system interactions in new geometric arrangement of piping and components, and flows under low pressure gradients at low pressure in the specific geometry of the AP600 design.

In particular, there is concern on the adequacy of the modeling for several specific processes. These include:

- Thermal stratification within the CMT, affecting condensation rate.
- Level tracking in the IRWST, affecting PRHR heat transfer.
- Level tracking in the reactor cavity to determine long-term inventory replacement in the vessel.
- Condensation, with or without non-condensibles, on the containment wall and in the CMT's, and entrainment in the venting lines.
- Boron transport, under ATWS conditions.
- Choked and unchoked flow at low pressure (4th stage ADS).
- ECC injection into the downcomer.

3. Scaling Methodologies

Numerous engineering studies[5-10] have been conducted to define and examine thermal-hydraulic facility scaling and design requirements for conditions similar to those stated above. Scaling laws appropriate for modeling thermal-hydraulic systems are developed from the conservation equations (i.e., the continuity, momentum, and energy equations). The basic techniques[6,9,10] involve first developing geometric, kinematic, dynamic, and energetic similarity parameters (dimensionless groups such as the Richardson number, Friction number, Froude number, length and area scales, etc.) by either: defining scale factors for geometric and kinematic parameters which allow transformation of the equations of motion from the model domain to the reference (plant) domain and requiring that the model equations be equal to the reference equations; or, using reference scales for non-dimensionalizing the equations of motion and appropriate boundary

conditions. Thermal-hydraulic scaling laws for natural circulation have been developed by Ishii et al.[9,10] Basically, Ishii scaling involves the use of one-dimensional, area averaged forms of the conservation equations to develop single-phase flow similarity parameters and perturbation techniques in conjunction with the drift flux model to develop two-phase flow similarity parameters. Similarity laws are developed by requiring that the similarity parameters be equal in two different scale size systems. After certain assumptions and simplifications, it can be shown that two variables must be specified for a natural circulation system. While there are different options available for selecting these variables, typically the length and area (or diameter) ratios are specified. While it appears that the length and diameter scales can be selected independently, independent selection is true only to the extent that hydraulic resistance (friction number) and horizontal flow regime transition scaling requirements allow. With selection of certain free parameters such as length and diameter ratio, parameter ratios (scaling laws) can be developed.[6]

The scaling relationships discussed above provide a strong basis for scaling to preserve local phenomena. However, they are not sufficient to assure the correct global system behavior. To attempt to assure the latter, all relevant system components must be included in the test facility design and each must be properly scaled. For example, scaling condensation effects in a cold leg does not by itself account for the effect on cold leg flow of condensation occurring in a steam generator. The final stage in a scaling analysis is to ascertain the relative degree of preservation of phenomena interactions (synergistic effects) for each of the scaled facility concepts by performing identical transient calculations with a thermal-hydraulic computer code for each of the proposed scaled facilities and the full scale reactor.

Examination of the laws[6] indicate that several different selections for the length and flow area scales appear to be possible. Past integral test facilities, such as Semiscale[11], MIST[12], and FIST[13], have been based on time preservation scaling. These types of "volume scaled", full height, full pressure, water facilities provided the major share of code validation data and proved to be the most successful and commonly applied type of scaling for integral hydraulics facilities to date. Other integral test facilities, such as UMCP[14] and SRI[15] have been based on reduced height scaling. These reduced height, reduced pressure, water facilities provided valuable confirmatory information. Both concepts are subsets of the general Ishii scaling[9,10] described above. For natural circulation, under the assumption of similar working fluid properties between the model and the prototype, these scaling principles can be illustrated by two simple relations:

$$(1) \qquad \tau = \lambda^{1/2}$$

$$(2) \qquad \sigma\tau = 1$$

where τ is the time scale ratio, λ is the length scale ratio, and σ is the power-to-volume ratio. The scale ratio is defined as test model divided by full-scale prototype. For time preservation scaling, $\tau = 1$. This leads to $\lambda = 1$ and $\sigma = 1$. That is, the test facility must be full height and the power-to-volume ratio is preserved. For a test facility with reduced height scaling, $\lambda < 1$, the time scale is reduced ($\tau < 1$) and the power-to-volume ratio is increased relative to the full-scale prototype ($\sigma > 1$).

The historic preference for volume scaled systems stems from the experiment requirements (the desire for real time simulation, need to simulate full steady-state operating power, etc.) and the somewhat simplified design features (reduced power requirements, full size heating elements, etc.) that can be employed relative to a reduced height system. However, because of their atypically large length-to-diameter ratios they tend to be more one-dimensional in nature. Furthermore, because of the full scale lengths in volume scaled systems, it is often necessary to increase flow area (distorting the fluid volume distribution and velocity) beyond that required by the scaling laws in order to avoid excessive frictional pressure drops in the components.

Reduced height systems are generally more conducive to the preservation of multi-dimensional effects and single-phase wall friction by virtue of maintaining length-to-diameter ratios closer to those in the reference system. However, power densities become impractical when the height is reduced significantly.

Low pressure water has been used as a working fluid for thermal-hydraulic experiments (for example, UMCP and SRI). The scaling of low pressure water to high pressure water is not straight forward, but can be scaled on the basis of the initial pressure ratio of the model to the plant. For system scaling, the property groups of interest are given in Reference 6. The initial model pressure must be selected to provide the most constant property ratios over the plant pressure range of interest since the low pressure water property ratios vary considerably with pressure.

4. Lessons Learned from Previous Integral Testing Programs

The INEL evaluation[3] included a review of lessons learned from past and present integral facilities (LOFT[16], Semiscale[11], MIST[12], FIST[13], UMCP[14], SRI[15], ROSA-IV[17], BETHSY[18], LOBI[19], and SPES[20]), which represent a variety of scale sizes and scaling methodologies. As with any scaled facility, each exhibited certain inherent distortions which somewhat reduced the utility of the data ("cons"). They also exhibited certain characteristics which enhanced the utility of the data ("pros"). In addition certain features of the design and scale of these facilities are better suited for code assessment type of information than others. The pros and cons of the utilization of these past and present facilities provide guidance for improvements which would enhance the utility of data obtained in any proposed integral test facility.

Review of the documentation from the various facilities produced a consistent set of identified limitations which can be summarized as follows. Virtually every facility had to address concerns related to distortions due to atypical system heat loss, system leakage, wall frictional pressure drop, metal mass, and geometric effects. Although distortions associated with geometric effects are somewhat facility design specific, for all of these items the following generalization is valid. The potential effects of distortions associated with these items increase as the facility size is decreased. Thus, for example, while heat loss was only a minor concern for larger facilities such as LOFT and ROSA-IV, it was more critical for the other, smaller facilities. Therefore, any new integral facility should be made as large as technical and cost constraints will allow. The design should utilize sufficient insulation and/or automatically controlled heat tracing to minimize heat loss distortions. The design should also

attempt to minimize system leakage (allowable leakage is probably on the order of 5% of the smallest anticipated break flow). Finally, consideration should be given to new techniques for insulating the walls (such as ceramic spray coating) of certain components (such as the downcomer or CMT) to minimize metal to fluid energy transfer distortions.

Geometric distortions tended to be specific to the facility design. However, the review of the various facility geometric distortions showed that the following aspects of geometric considerations are valid for any facility design. Careful consideration should be given to the design of the facility to minimize geometric distortions as follows:

- The facility design should not mix full and reduced height components and all components should be placed at the appropriate relative elevation.

- An internal downcomer design is preferable but if an external downcomer is required consideration should be given to an annular type of design with appropriate connection to the vessel lower plenum.

- Particular attention should also be paid to the design of numerous components such as the core bypass, electrical heater rods (and their thermocouples), pumps and check valve simulators.

- All of the prototype loops should be simulated and should use active components.

- Provide capability for isolating components or loops for separate effects type of experiments.

- Base instrumentation on measurement requirements which should be an integral part of the facility design, not an add on.

The UMCP facility was the first NRC-sponsored integral test facility to be based on reduced height reduced pressure (RHRP) scaling[21]. Previous integral test facilities were based on full-height full-pressure (FHFP) scaling. When this facility was designed, it was based on the following set of modest, but realistically achievable "scaling goals":

A. The model must reproduce the key phenomena of the prototype.
B. They are reproduced in the same sequence.
C. Their quantitative characteristics are approximated.

Detailed principles that were found most important in the UMCP facility design can be summarized as follows:

o Care must be exercised to ensure that all flow geometry discontinuities occur at an equivalent relative volume for both the model and the prototype. It is inevitable that in scaled facilities, distortions in some aspects of the flow geometry occur. Preservation

of the relative liquid inventory at which flow geometry discontinuities are encountered should be given a high priority.

- The preservation of local and global inventory is the key of meaningful scaling for SBLOCA. Careful use of energy conservation will dictate most of the scaling rules for the initial and boundary conditions.

- The $\Delta P/P$ ratio (where ΔP is the elevation and friction caused pressure differences) for model and prototype should be comparable. This will ensure that phenomena driven by state changes during fluid transit (flashing-condensation) have a comparable influence. For slowly evolving, SB-LOCA-type transients, elevation changes are the main ΔP component. Reduced pressure facilities therefore should also include height reductions.

- For SB-LOCA scenarios the operating pressure should be high enough to decouple the system from the ambient pressure (i.e., the break must be choked).

- Flow geometry dimensions should not be decreased to the extent that different flow regime transitions become possible. The most obvious transition in this category is the slug-to-bubbly flow transition in vertical flow. This requires that vertical channels have minimum diameters exceeding ~ 7-9cm.

- In general, flow resistances are of secondary importance. That is so because loop wide velocities are usually low. However, for some flow modes substantial local fluid velocities can be present. They will usually occur at flow geometry discontinuities (e.g., in the region where the cold-leg and downcomer merge). In such regions, care should be exercised to match flow resistances.

The main scaling lesson learned in the UMCP program can be summarized as follows. In the UMCP program a general approach to the scaling rationale was sought because it was felt that scaling invariants derived from the local conservation equations (as in Reference 6) are not an adequate representation of the whole system. The use of local conservation equations is fundamental to guide the selection of scaling laws (or scaling invariants), but cannot be used as the only generators of such scaling invariants. In particular, for SBLOCA transients the energy transport capability at various liquid inventories in the primary system turned out to be the major issue. In the UMCP experiments the global inventory emerged as a strong invariant capable of capturing most of the system phenomenology since the geometrical discontinuities (i.e., hot leg upper lip connection into the vessel upper plenum, etc.) played a fundamental role in determining the system behavior. Local inventory in each component also played a key role. However, the local component inventory turned out to be consistently linked to the global inventory. This discovery led to the definition of a new chronological scale based on system liquid inventory.

By focussing on a particular portion of a SBLOCA it was found that the energy transport had to be scaled between the full and reduced pressure transients. This

was achieved by using the energy conservation statements applied to the portion of the system in thermodynamic equilibrium (i.e., vessel upper plenum, hot legs, steam generators upper portion, cold legs horizontal portion, etc.). For example, for B&W plant interruption-resumption mode simulations, an approach was identified by selecting as invariant the repressurization rate of the system with respect to the new chronological scale under complete interruption of natural circulation.

5. Minimum Requirements for a Scaled Integral Facility.

An important criteria that should be factored into all scaled facility design analyses is the desire to maintain model dimensions large enough to preclude effects due to size that would not be expected in the full-scale system. For example, if surface tension forces are not expected to prevail at reactor scale then the minimum dimension of the limiting component in the model system should also be large enough that surface tension forces do not dominate.

The concept of a minimum dimension can be established from flooding considerations. Bankoff and Lee[22] present results which show that gas flooding velocities and the zero liquid penetration critical Kutateladze number are independent of the dimensionless diameter, (defined as $D^* = [gd^2\Delta\rho/s]^{1/2}$, where d is the diameter, $\Delta\rho$ the density difference, s the surface tension and g the acceleration of gravity) for dimensionless diameters greater than approximately 32-40. These results suggest that as long as the dimensionless diameter is greater than approximately 32-40, the geometry can be considered large enough to minimize surface tension influences.

Phenomena such as flow regimes and condensation in the CMT pressure balancing and safety injection lines will affect CMT, accumulator, IRWST and containment sump injection and overall system response. Since these lines are relatively small diameter, their scaling must be considered carefully. The results[3] show that the full scale cold leg pressure equalization and safety injection lines (which are the same size) can be considered "big" with respect to surface tension effects. However, any significant reduction in their diameter (anything less than a diameter scaling ratio of about 7/8) may produce line sizes which are "small" with respect to surface tension effects. Also, the full scale pressurizer pressure equalization line can be considered "small" with respect to surface tension effects. Hence, the scaling of the pressure equalization and safety injection lines must be addressed separately via analysis and/or separate effects experiments to determine the optimum scaled geometry for preservation of flooding, flow regime and condensation heat transfer phenomena as well as frictional pressure drop effects.

Flooding in the pressurizer surge line will affect the pressurizer, ADS and overall system response. The results[3] show that the criteria of maintaining the dimensionless diameter greater than approximately 32-40 for the pressurizer surge line is only satisfied for diameter scaling ratios greater than about 1/5 for full pressure and 1/4 for reduced pressure. However, evaluation of ADS valve choked flow conditions for saturated steam flow shows that the pressurizer surge line will be flooded during ADS operations until the fourth stage ADS (connected to the hot leg) is actuated (usually at pressures less than 50 to 100 psia). Hence, flooding in the surge line is anticipated for pressures ranging from 2250 down to about 50 psia. Since smaller pipe sizes will preserve this flooding phenomena,

the surge line need not be considered the limiting component. Considerations for minimum dimensions were therefore limited to the hot and cold leg pipes.

Both full pressure and reduced pressure results[3] show that the criteria for maintaining the dimensionless diameters greater than approximately 32-40 for the hot and cold leg pipe sizes is only satisfied for diameter scaling ratios greater than about 1/7 to 1/6.

A further consideration on sizing relates to the selection of the length scale for a reduced height concept. One manner in which this selection can be accomplished is to iteratively examine various combinations of the length and area scales with respect to preservation of the friction numbers (both single and two-phase) in the model, relative to the reference. While consideration for the frictional characteristics may not have a direct influence on the minimum length of the scaled system, the desired resistance characteristics will factor into the ultimate size selection. Friction and orifice number requirements should also be consistent with horizontal flow regime transition criteria that suggest the horizontal sections be scaled with $L/(d)^{0.5}$ as discussed in Reference 16. Using this criteria and a diameter ratio of 1/6.24 results in a length ratio of 1/2.5 for a reduced-height reduced-pressure (RHRP) concept.

An additional consideration relates to the selection of the reduced pressure ratio for a RHRP facility. The selection of the maximum operating pressure of a reduced pressure facility should be based on the conflicting desires to reduce cost but maintain the highest reasonable operating pressure which provides the most constant property ratios over the plant pressure range of interest. Inclusion of such considerations in the study performed by Condie et al.[6] yielded an operating pressure of about 430 psia.

Core power requirements must also be considered for both the FHFP and RHRP scaled systems. Based on past experience and economic considerations, the maximum core power which one could reasonably expect to provide for an electrical core is in the range of 5 to 10 MW. Considering the associated scaled facility characteristics for a full power limit of say, 7.5 MW results in an area ratio of 1/240 for the FHFP system and 1/36 for the RHRP facility. The FHFP area ratio is below the minimum value recommended for the facility and is therefore unacceptable based upon minimum dimension considerations. Power requirements at 5% decay heat are very reasonable (about 2.3 MW for FHFP and 0.3 MW for RHRP). However, if full power simulation is required (for ATWS and some other operational transients), restrictions on system pressure ratio will be required for the full height facility. For example, to simulate full power conditions with a core power of 9.75 MW, the full height system would have to be operated at a pressure of 400 psia. Such simulations represent additional support facility requirements to insure adequate core power supply, heater rod, and pump/pump power capabilities. However, this is quite attractive since it would result in a combined FHFP/FHRP facility which could address full power, full pressure, decay heat level and small gravity head passive safety injection system response concerns with only one set of support equipment. The RHRP facility could be used to simulate full power (about 6.6 MW) operations provided adequate support facilities are available, and power density and volumetric energy generation requirements are not prohibitive.

6. Evaluation of Scaling Concepts for Integral Test Facilities

No scaled facility is free of distortions. However, the results of evaluations performed[3,6] and experience with past integral experimental programs indicate that an FHFP type facility will produce the least distortions and provide the most technical benefits of the various options available for a scaled integral facility.

The results of the analyses using local scaling laws based on conservation equations indicate that the FHFP approach gives minimal scaling distortions, compared to other scaling approaches, for all anticipated local thermal-hydraulic phenomena of importance. It was noted that the FHFP concept is particularly attractive for simulating core heat transfer. For the most part, the FHFP concept provides an ideal simulation of the various heat transfer modes in the core and steam generators. In addition, the FHFP concept provides ideal simulation of condensation phenomena, near ideal simulation of counter-current flow effects (including flooding), and a good simulation of natural circulation and pressure drop.

The UMCP facility, scaled to RHRP concepts, showed that for the SBLOCA transient useful test results could be obtained if proper care is taken in formulating scaled initial and boundary conditions, and if the results are scaled to appropriate variables, such as normalized primary system mass inventory. A recent doctoral thesis by Moskal[24] cited concerns for the RHRP concept in simulating leak flow and natural circulation. Hence, the range of conditions which may be simulated in a RHRP facility for a single transient may be restricted due to constraints placed on boundary or initial conditions.

Comparison between the FHFP and RHRP approaches shows that the latter approach produces results that have greater distortion, require more analysis to produce correct interpretations, and, unless proper attention is paid to scaling key phenomena, may not show the presence of crucial events (e.g., CHF and rewet) at all.

For testing of the AP600 design, the integral testing could be divided into two parts, one to investigate the high-pressure interactions up to the initiation of IRWST injection in a FHFP facility, and the second to investigate the long-term cooling in a low pressure facility. In the latter case the test facility pressure may correspond exactly to the pressure in the full-scale reactor system. The low pressure concept is discussed in more detail in the next section.

7. Application to a Low-Pressure Test Facility

The scaling rationale used for the design of the low pressure integral facility should be documented and justified. It is highly recommended that Ishii scaling criteria be utilized since this is a widely accepted and proven method of scaling. Water should be used as the working fluid. This will simplify the scaling analysis and promote use of the data generated for code assessment.

The operating pressure for a low pressure facility should be carefully considered. Since the majority of the first-order importance phenomena occur during the late stage of the accident when the system pressure is at or below 100 psia, low pressure simulations would provide the lions share of the required information. Additionally, if appropriately designed, a low pressure facility could be operated as a reduced pressure facility for simulating the high pressure aspects of AP600 transients, provided adequate support facilities were available. Whatever option is chosen, it should be clearly stated and justified.

Development of initial and boundary conditions should also be factored into the consideration of the scaling options. The scaling of boundary conditions for a reduced pressure facility is not nearly as straightforward as for a full or low pressure facility. Two examples of this are critical flow, and ECC mixing and condensation phenomena. Critical flow scaling in a reduced pressure facility requires different break areas for single-phase and two-phase conditions. Preservation of ECC mixing and condensation phenomena requires varying ECC fluid temperature as a function of system pressure in a reduced pressure facility. Thus, the range of conditions which may be simulated in a reduced pressure facility for a single transient may be restricted due to constraints placed on boundary or initial conditions.

The test facility diameter scale should be selected to ensure that phenomena expected in the full scale system are also expected in the low pressure system and that any distortions expected in the low pressure system are tolerable. In other words, the extent of the distortion in the low-pressure facility behavior should not be so great as to dominate the behavior of the facility and hence affect the utility of the data. It has been observed that under two-phase flow conditions certain phenomena are observed in small pipes which do not occur in large pipes. For example, plug flow occurs readily in pipes smaller than about 1-1/2 to 2 inches in diameter while Taylor bubble stability analysis and experimental observations show that it does not occur in larger pipes. Experience with the Semiscale integral test facility[11] has shown that the use of 1-1/2 inch Schedule 160 piping (inner diameter = 1.338 inches) for simulating a single loop of a Westinghouse four loop PWR provided adequate representation of a substantial portion of key SBLOCA phenomena.[5,6] However, as discussed in Section 5, preservation of surface tension effects leads to a minimum diameter scaling ratio of 1/6 to 1/7 for the cold leg. These results suggest that the use of similar dimensions for simulating AP600 components in a low pressure integral facility might be prudent.

Careful consideration should also be given to the downcomer area scaling when determining an appropriate scaling ratio. Difficulties in appropriately simulating the downcomer annular geometry have been a concern for most experimental programs. The Semiscale program[11] utilized a single-pipe external downcomer with an annular inlet region in an attempt to overcome distortions predicted for an annular downcomer with an appropriately scaled gap dimension. The LOBI program[19] included the capability of simulating different annular gap dimensions in the facility design in an attempt to reduce potential distortions. Insight into appropriate selection of scaling ratios for simulating the downcomer annular gap may be gained from consideration of flooding behavior. Whatever diameter scaling ratio is chosen, it should be clearly stated and justified.

The length scale for a low pressure facility should be carefully considered. Full height scaling preserves the elevation differences between components, which is an important consideration for the present circumstances where system response will be sensitive to hydrostatic heads (some as small as two feet). Use of full height scaling principles simplifies the design of the core and steam generator components in that the individual components can be of plant typical length and diameter and only the number of components must be scaled. Also, as discussed above, the full height option provides the least distortions to the largest number of key local phenomena.

The attraction of reduced height scaling lies in the potential to reduce frictional pressure drop distortions, distortions associated with metal and fluid interactions, heat loss, support facility requirements, and material costs. However, these must be weighted against concerns for greater distortions to key phenomena such as flooding, condensation heat transfer, core heat transfer, and natural circulation. The scaled time in a reduced height system will be reduced with respect to the time in the full-scale system. Careful analysis will be required to assure that crucial events will be preserved and will occur in the right order. Also, significant interpretation and analysis of reduced height facility results will be required to determine applicability to anticipated full scale plant response. Considerations of selection of a length scale ratio for a reduced height system should include the following. In their investigations of reduced height scaling, Condie et al.[6] discovered that distortions to slip ratios (and therefore related phenomena such as void distributions, two-phase friction losses, flow regimes and heat transfer) were significant for length ratios less than about 3/8. Also, the selection of a length ratio should include considerations of frictional pressure drop (single and two-phase). Frictional pressure drop considerations must include two-phase pressure drop investigations since the velocity in a reduced height system is decreased by the square root of the length ratio and hence the mass flux is reduced, distorting two-phase friction multipliers. Consideration should also be given to horizontal flow regime transition criteria that suggest the horizontal sections be scaled with $L/(d)^{0.5}$ as discussed in Reference 23. Finally, the potential impact of height reductions on hydrostatic heads and their measurability should be evaluated, as well as the provision of adequate piping lengths to allow installation of instrumentation.

The discussions provided above give some general guidance and suggestions for considerations pertinent to the selection of a diameter and length scale for a low pressure integral test facility. Regardless of the selection, it should be analyzed in depth and all potential distortions, (particularly to key phenomena such as flooding, condensation heat transfer, core heat transfer, frictional pressure drops, and natural circulation) should be identified and their potential impact on overall system response evaluated. Additionally, some indication should be given of the analytical requirements for extrapolating results to the full scale plant domain.

Both loops of an AP600 plant should be simulated in a low pressure integral facility. Within each loop, both cold legs and both pumps should also be simulated. Based on the experience of previous experimental programs this is necessary to provide the most appropriate system interactions data for the AP600 simulations being considered.

In a scaled facility the reduction in pipe size results in piping external surface area to fluid volume ratios which are larger than the prototype.[6] Hence, the system heat loss is larger than that scaled from the full-scale reactor. Furthermore, the smaller the facility scale, the greater the distortion in system heat loss becomes. This is particularly a concern for slower transients such as those anticipated for AP600 simulations where the integrated effect of atypically large system heat loss would be most detrimental. Reduced height systems appear to offer an advantage by virtue of reduced time scale and reduced external surface area. Heat loss compensation must be carefully considered since external heaters and/or core power augmentation can produce atypical phenomena and/or drive system response during late stage accident conditions when the system response is sensitive to small energy balances.

The reduction in system fluid volume in a scaled facility enhances the effects of mass lost from the system via system leakage. System leakage rates greater than those scaled from the prototypes produce distortions in system mass inventories and energy balances. The smaller the facility scale, the greater the potential distortion due to system leakage. Here again, this is particularly a concern for slower transients such as those anticipated for AP600 simulations where the integrated effect of atypically large system mass loss due to leakage would be most detrimental.

The size reduction in a scaled facility produces distortions in wall friction losses (single and/or two-phase losses). Thus, for small scale facilities the pipe sizes are typically increased to values somewhat larger than scaled and the piping horizontal lengths are typically reduced from the scaled values to reduce potential distortions. This is more of a problem for full height than reduced height facilities. However, when considering reduced height options, the effect of reduced velocity on mass flux and therefore two-phase friction multipliers must be factored into the analysis.

Reduction in pipe size results in atypically large metal mass-to-fluid volume and metal inner surface area-to-fluid volume ratios for the system. Thus, metal stored energy and metal to fluid energy transfer rates are atypically large in a scaled facility, with smaller facilities exhibiting greater distortions. This is a particular concern for situations where atypically large vapor generation or condensation rates can result from atypically large metal to fluid energy transfer. Such distortions could result in atypical counter-current flow and/or flooding in a component (e.g., downcomer), or atypical system interactions during late stage AP600 simulations where the system is sensitive to small energy, pressure and mass balances. Reduced height systems appear to offer an advantage by reducing metal mass and metal inner surface area. However, reduction in height also produces smaller gravity heads and, for a given diameter scale, reduced fluid volume. Hence, the potential gains of reduced metal mass and reduced metal inner surface area must be weighed against effects of reduced fluid volume and reduced gravity heads. Thus for a low pressure integral facility, metal mass distortions, methods of compensation, and potential impacts must be addressed. Consideration may even be given to new methods of preserving metal to fluid interactions such as insulating walls via spray coating of ceramic materials to minimize metal to fluid energy transfer distortions.

Additional concerns for scaled integral facilities lie in the area of simulation of specific components. Regardless of the choices made for facility scaling parameters, they should be analyzed to determine all potential distortions and their potential impact on the overall system response. In addition, one must consider areas of potential concern with regard to component simulations. A thorough analysis of low pressure facility scaling will in all likelihood cover more numerous considerations than highlighted here. However, the following items should be considered as a minimum.

In the loop components, the Reynolds number will not be maintained due to the diameter effect. Also, the wall friction will not be maintained due to the increased aspect ratio (length to diameter ratio) effect. Hence, consideration must be given to the loop scaling so that single and two-phase friction and orifice number requirements are met. Attempts should also be made to keep geometric parameter selections (length and diameter ratios) consistent with horizontal flow regime transition criteria.

Attempts should be made to insure that entrainment/deentrainment and liquid carryover into the hot legs from the vessel and core in the low-pressure system are sufficiently representative of that expected in the reference system. Thus, considerations of length scale selection should include analysis of this phenomena. Full height scaling in the vessel should preserve this ideally while reduced height scaling may distort this phenomena. Attention should also be given to the vessel internal structures and their impact on this phenomena.

During ADS discharge from the pressurizer, the pressurizer may act as a phase separator or it may be flooded. Also, the pressurizer surge line is expected to be flooded for most of the transient due to ADS operations. Analysis needs to be done to determine the relative degree of preservation of this phenomena for the low-pressure facility over a variety of operating conditions.

The pressure equalization and safety injection lines must contain valves to simulate valves in the AP600 design. These valves and the associated line resistances must meet friction and orifice number requirements. Condensation, flow regime transitions, counter current flow and flooding may occur in these lines. Since these lines are relatively small in diameter and reasonably long in the AP600 design, it may not be possible to maintain strict scaling criteria. These cases will have to be evaluated on a case-by-case basis to minimize distortions.

Critical and inertial flow will occur in the ADS lines and in the break system. When the flow is choked, the most important requirement is that the choke plane be area scaled to provide the representative scaled flow rate. When the flow is not choked, inertial flow dominates, line losses are important, and the design must attempt to preserve friction and orifice number requirements in the discharge lines. The effect of the sparger system and the IRWST fluid on the performance of the first three stages of the ADS system should be simulated. Provisions should be made for simulating breaks in numerous locations, including the cold leg, pressure balancing and safety injection lines, and steam generator tubes.

The IRWST is a large reservoir that provides water storage and a condensation sink. Similarly, the containment sump provides water storage. Elevations must

be maintained to preserve the Froude number and hence the driving heads for primary injection.

The effects of containment pressure and condensation on the system response must be provided for. A containment simulator must be provided to simulate these phenomena. The control of this simulator should be based on the results of containment separate effects tests.

Instrumentation for a low pressure test facility should be part of the design and not an add on. The basis for the selection of instrumentation should be formed on the measurements required to satisfy objectives for the facility. The measurements should be of sufficient quality and quantity to allow for identification and analysis of system phenomena, sensitivities and interactions and satisfy code assessment needs.

Any proposal for a low pressure integral facility must also include a detailed analysis of the feasibility and requirements for determining and establishing appropriate initial conditions.

8. SUMMARY RECOMMENDATIONS

Although it is ideally possible to consider a single integral facility to test the complete length of advanced reactor transients, it is also practical to apportion the testing between two facilities of different scales. Thus, for the AP600 design, integral thermal-hydraulic testing can be separated into two scales: 1) full-pressure full-height testing before and during ADS operation, and 2) low-pressure reduced-height testing during the latter stages of ADS operation and after completion of ADS functions. In following this approach one must carefully consider how to properly link the test results for code assessment purposes.

For local phenorena Ishii scaling is recommended. Water should be used as the working fluid. Component diameter and spacing should be maintained full size in the core and steam generators if detailed information on energy addition and removal is desired. Preservation of surface tension effects leads to a minimum diameter scaling ratio of 1/6 to 1/7 for the cold leg. This leads to a length (height) ratio of about 1/2.5. Smaller diameters would have to be justified. Special consideration must be given to scaling the pressure balancing lines and the pressurizer surge-line, which may not directly meet the surface tension size criterion. It is recommended that the test facility pressure correspond exactly to the full-scale pressure. However, if pressure scaling is used to extend the low pressure results to higher pressure, it should be justified based on Ishii's scaling relations. Once the size and pressure are determined, the power requirement should be found from Ishii's scaling relations. Initial and boundary conditions for each test scenario should be planned, especially low-pressure facility.

References

1. S. N. Tower, et al., "Passive and Simplified System Features for the Advanced Westinghouse 600 MWe PWR, " Nuclear Engineering and Design, Volume 109, 1988, pages 147 to 154.

2. M. W. Golay and N. E. Todreas, "Advanced Light-Water Reactors," Scientific American, April 1990, pages 82 to 89.

3. S. M. Modro ltr. to Dr. L. M. Shotkin, USNRC, "Transmittal of Draft AP600 Integral Facility Evaluation Report," June 13, 1991.

4. S. M. Modro ltr. to Dr. G. S. Rhee, USNRC, "AP600 Experimental Data Base Task," April 30, 1991.

5. T. K. Larson, et al., "Scaling Criteria and an Assessment of Semiscale Mod-3 Scaling for Small Break Loss-of-Coolant Transients," EG&G Idaho, Inc., EGG-SEMI-5121, March 1980.

6. K. G. Condie, et al., "Evaluation of Integral Continuing Experimental Capability (CEC) Concepts for Light Water Reactor Research - PWR Scaling Concepts," EG&G Idaho, Inc., NUREG/CR-4824, EGG-2494, February 1987.

7. T. K. Larson, "An Investigation of Integral Facility Scaling and Data Relation Methods (Integral System Test Program)," EG&G Idaho, Inc., NUREG/CR-4531, February 1986.

8. T. J. Boucher, et al., "Scaling Analysis for a Savannah River Reactor Scaled Model Integral System," EG&G Idaho, Inc., EGG-EAST-9382, November 1990.

9. M. Ishii and I. Kataoka, "Similarity Analysis and Scaling Criteria for LWR's under Single-Phase and Two-Phase Natural Circulation," Argonne National Laboratory, NUREG/CR-3267, ANL-83-32, March 1983.

10. M. Ishii and G. Kocamustafaogullari, "Scaling Criteria for Two-Phase Flow Natural and Forced Convection Loop and Their Application to Conceptual 2 X 4 Simulation Loop Design," Argonne National Laboratory, NUREG/CR-3420, ANL-83-61, May 1983.

11. G. G. Loomis, "Summary of the Semiscale Program (1966-1986)," EG&G Idaho, Inc., NUREG/CR-4945, EGG-2509, July 1987.

12. "Multi-loop Integral System Test (MIST) Facility Description," Babcock and Wilcox Company Document RDD:84:4091-01-01:01, October 1983.

13. A. G. Stephens, "BWR Full Integral Simulation (FIST) Program Facility Description Report," General Electric Company, December 198 UREG/CR-2576, EPRI NP-2314, GEAP-22054.

14. D. W. Sallet, et al., "Final Design Report for the UMCP 2 X 4 B&W Simulation Loop," The University of Maryland, College Park, August 10, 1984.

15. R. L. Kiang and J. P. Sursock, "The EPRI Facility at SRI: Description and Connection with IST Program," IST Program Coordinating Meeting No. 2, Bethesda, Maryland, April 3-4, 1985.

16. C. L. Nalezny, "Summary of the Nuclear Regulatory Commission's LOFT Program Research Finding," EG&G Idaho, Inc., NUREG/CR-3005, EGG-2231, April 1985.

17. The ROSA-IV Group, "ROSA-IV Large Scale Test Facility (LSTF) System Description," JAERI-M 84-237, January 1985.

18. "BETHSY General Description," SETh/LES/90/97, April 1991.

19. E. Ohlmer, et al., "The LOBI-MOD2 Integral System Test Facility," Proceedings of the Specialists Meeting on SBLOCA Analyses in LWRs, Vol. 1, pp. 455-469, Pisa, Italy, June 1985.

20. G. Cattadori and M. Rigamonti, "SPES: PWR Reactor Test Facility - Volume 1, Facility Description and Instrumentation," ENEA, ETDE-IT-89-41, 1987.

21. M. diMarzo, K. Alemas, Y. Y. Hsu, "On the Scaling of Pressure for Integral Test Facilities," Nuclear Engineering and Design, Vol. 125, pp. 137-146.

22. S. G. Bankoff and S. C. Lee, "A Critical Review of the Flooding Literature," Northwestern University, NUREG/CR-3060, February 1983.

23. N. Zuber, "Problems in Modeling of Small Break LOCA," NUREG/CR-0724, October 1980.

24. T. E. Moskal, "Examination of Scaling Criteria for Nuclear Reactor Thermal-Hydraulic Test Facilities," Phd Thesis, Carnegie-Mellon University, 1987.

SMALL BREAK LOCA RELAP5/MOD3 UNCERTAINTY QUANTIFICATION: Bias and Uncertainty Evaluation for Important Phenomena

by

Marcos G. Ortiz, L. Scott Hanan, Judith Vogl
Idaho National Engineering Laboratory
EG&G Idaho Inc.
Idaho Falls, IDAHO 83415-2404

INTRODUCTION

The Nuclear Regulatory Commission (USNRC) revised the Emergency Core Cooling System (ECCS) licensing rule to allow the use of Best Estimate (BE) computer codes, provided the uncertainty of the calculations are quantified and used in the licensing and regulation process. The NRC developed a generic methodology called Code Scaling, Applicability and Uncertainty (CSAU) to evaluate BE code uncertainties. The CSAU methodology was demonstrated with a specific application to a Pressurized Water Reactor (PWR) experiencing a postulated Large Break Loss-of-Coolant Accident (LBLOCA) [1,2]. The current work is part of an effort to adapt and demonstrate the CSAU methodology to a Small Break (SB) LOCA in a PWR of B&W design using RELAP5/MOD3 as the simulation tool [3,4]. The subject of this paper is the Assessment and Ranging of Parameters (Element 2 of the CSAU methodology, Fig. 1), which determines the contribution to uncertainty of specific models in the code. In particular, we show the methodology used to assess the uncertainty of the specific models investigated.

The specific models were chosen based on the Phenomena Identification and Ranking Table (PIRT, step 3 of the CSAU methodology) that was defined, earlier in the program, by two independent panels of experts [3]. The PIRT lists the phenomena believed to most strongly affect the transient scenario, as determined by their impact on a prescribed safety criterion. For the SBLOCA in a B&W plant, the selected criterion was the minimum liquid level in the reactor vessel.

Eight phenomena from this PIRT, regarded as highly important in determining the critical outcome (primary safety criterion) of the simulation, were chosen for performing sensitivity calculations. In this paper, we have selected four phenomena of the highest importance to demonstrate the evaluation of bias and uncertainty; these are the break flow, natural circulation, decay power, and the temperature of the high pressure injection flow (HPI).

Work supported by the U. S. Nuclear Regulatory Commission, Office of Research, Under DOE Contract No. DE-AC07-76ID01570.

IMPORTANT PHENOMENA AND KEY CODE PARAMETERS

The criteria and procedures followed to define the Phenomena Identification and Ranking Table are fully documented elsewhere [3]. For the purpose of this paper it suffices to say that the PIRT was the result of many discussions between recognized experts, experienced analysts, and operators. In any case, the methods demonstrated here can be used for determining the uncertainty of any other models.

The eight phenomena ranked most important in the PIRT are:

(1) break flow,
(2) natural circulation,
(3) decay power,
(4) Reactor Coolant Pump (RCP) performance,
(5) High Pressure Injection flow,
(6) Steam Generator (SG) heat transfer,
(7) phase separation in the candy cane, and
(8) Reactor Vessel Vent Valve (RVVV) performance.

The phenomena, as such, do not appear in the code (i.e. there is no "natural circulation" model). However, there are parameters, models, and even inputs that are used to represent those phenomena. Thus, the next step in our study is to identify the key code parameters or models associated with each phenomenon and, if appropriate, select the ones that contribute the most uncertainty. In our case we can classify the models to be of three different categories: first principles, empirical correlations, and input parameters or tables (some may be combinations of these). Table 1 summarizes the results of this process. For this study, we selected phenomena 1, 2, 3, and 5.

Break flow, the most important of the phenomena, is modelled in the code from first principles [5]. The uncertainty of the break flow representation can be traced to not knowing the exact geometry of the flow at the break and therefore the break discharge coefficients. Natural circulation, the second most important phenomenon, depends greatly on the interactions between the liquid and vapor phases. This interaction is modelled using an empirical correlation [6] to produce an interphase drag coefficient "FI" as a function of void fraction, flow regime, and relative velocities between the phases. The third phenomenon, decay power, is modelled as a user input table into heat structures in the core. Its variability depends on the specific core history and power distribution [7]. The HPI flow, the last phenomenon selected for this study, is reduced in this case to a mere input value, temperature. We decided that since the HPI flow is limited by the operator, below the capacity of the pumps, the real uncertainty is in the temperature at which that flow enters the system. This variable depends on the weather and its variation is bounded by technical specifications between 275 K (35 F) and 316.5 K (110 F). In the course of our study we learned that Reactor Coolant Pump performance, phenomenon number 4 in Table 1, does not participate as much as we had initially

thought and that is why its variability is not included in this paper. The pumps are turned off and coasted down early in the transient, never to be turned on again. Thus, they behave merely as a flow restriction, a user input parameter, throughout the rest of the simulation.

Table 1

List of Important Phenomena During a SBLOCA, their rank, and the model and code parameters that RELAP5/MOD3 uses to represent them

	Phenomena	R5/M3 Model	Key (code) Parameters
1	Break Flow	Junction with assigned location on pipe (top, side, bottom). Parameters: Break Area and Discharge coefficient.	Subcooled discharge coefficient 2-ϕ discharge coefficient
2	Natural Circulation	A complete flow loop made of junctions and volumes with angles of inclination. Interfacial drag and heat transfer, wall-fluid heat transfer, flow regime maps.	2-ϕ : Interphase drag coefficient
3	Decay Power	User Input Into Heat Structures	Input table or function
4	RCP Performance	User Input: homologous curves for head and torque.	RCP torsional friction coefficient
5	HPI Flow	User Input: flow vs pressure curves.	Input Temperature
6	SG Heat Transfer	Heat Structures attached between primary and secondary sides. Interfacial drag and heat transfer, wall-fluid heat transfer, vertical flow regime map.	Coefficients from Heat Transfer correlations (Area)
7	Phase Separation in the Candy Cane	Geometry defined with suitable volumes. Interface drag and heat transfer. Vertical stratified flow model.	2-ϕ : Interphase drag coefficient
8	RVVV Performance	Modeled as a valve whose area is controlled by the pressure difference across of it.	Inertia of the Valve

EVALUATION OF UNCERTAINTY

One way to evaluate the uncertainty associated with each phenomena is to examine how accurately the code represents those phenomena in separate effects tests (SET's). That is the case of the break flow, for which code assessment against suitable test data exists [5]. In the case of empirical correlations, such as the interphase drag or heat transfer correlations, for which specific tests may not available, the uncertainty must be evaluated from the data that gave origin to the corresponding correlation. In the case of input parameters, such as the variability of the decay power curve or the inlet temperature of the HPI flow at the time of the break, where specific data is not available, engineering judgment must be exercised to define boundaries of variability. When forced to this by the lack of information, we chose to err on the conservative side by selecting our variability range generously.

Break Flow

RELAP5/MOD3 has two critical flow models that are used in simulating the break flow: single phase flow and two phase flow. These models, their assumptions, origin, and their implementation are described in detail in the code documentation [5]. Both models are derived analytically from first principles. The bias and uncertainty (accuracy) with which these models contribute are estimated from SET's used in the developmental assessment; specifically Marviken 22 and Marviken 24 tests. The experimental data and the assessment calculations results, corresponding to these SET's, were obtained from the RELAP5/MOD3 code developers to be used in support of this CSAU effort. Therefore, we did not need to repeat the calculations. This is not, however, a repetition of the assessment shown in the code documentation [5], for we processed and manipulated the data further in order to get the bias and uncertainty of the critical flow models in RELAP.

The following diagrams (Fig.1) are schematic descriptions of the break configuration and the Marviken test vessel.

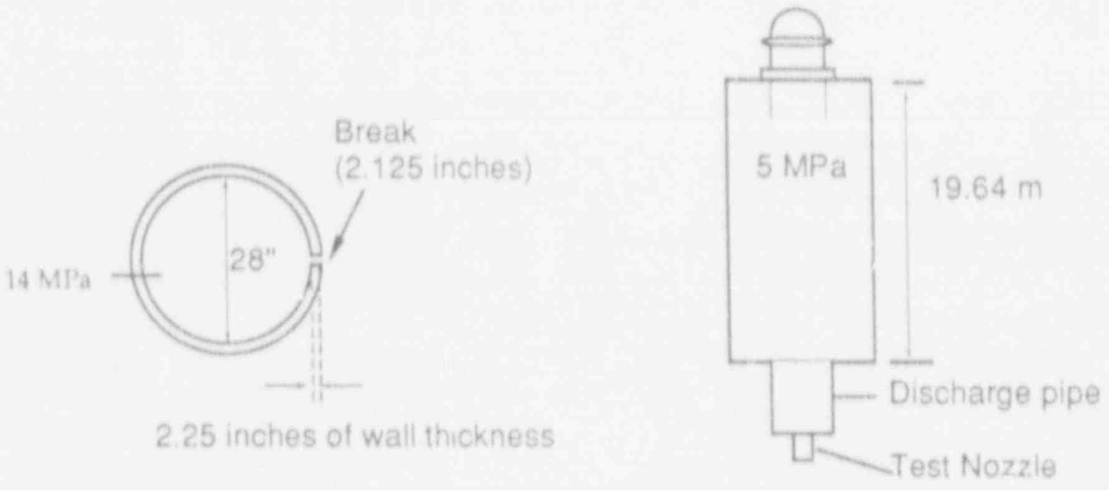

Figure 1. Schematic descriptions of the assumed break configuration in the NPP and the Marviken test configuration.

The most relevant differences between the test configuration and the assumed break geometry are the size of the break openings and the fact that the nozzle in Marviken is aligned with the main flow direction (downward), while the break flow in the NPP is perpendicular to the main flow direction (sideways). The length to nozzle diameter ratio for the tests and for the assumed break compare as follows:

	Marviken 22	NPP	Marviken 24
L/D	1.5	1.06	0.32

Figures 2 through 4 show the comparisons between the test results and the corresponding RELAP5/MOD3 simulations. The usual statement that the code captures the trends and the main events of the transient can be made here based on the obvious comparison (that statement is in fact made in reference [5]). However, to evaluate the uncertainty of the model this is not sufficient. The inadequacy of direct comparisons can be deduced from Figures 2 and 3. These figures imply that RELAP5 underpredicts the flow. In the overall comparison the error seems small. When measured, however, the predicted mass flow is over 60% lower than the test value. Further inspection shows that the simulated pressure decreases faster than the experimental one (Fig. 4) and later tends to remain at a higher level.

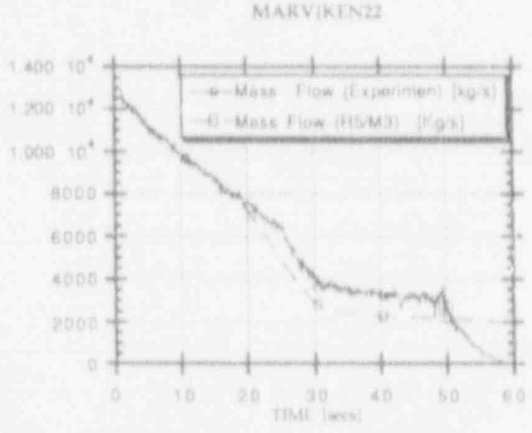

Figure 2. Comparison between simulated and experimental mass flow [kg/s] history for Marviken 22 test.

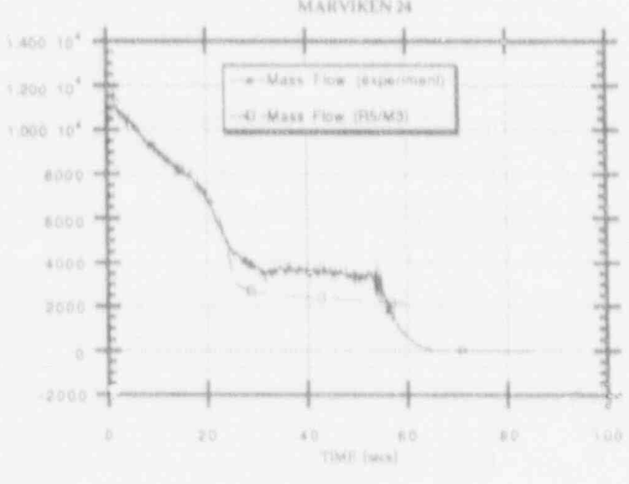

Figure3. Comparison between simulated and experimental Mass Flow [kg/s] history for Marviken 24 test

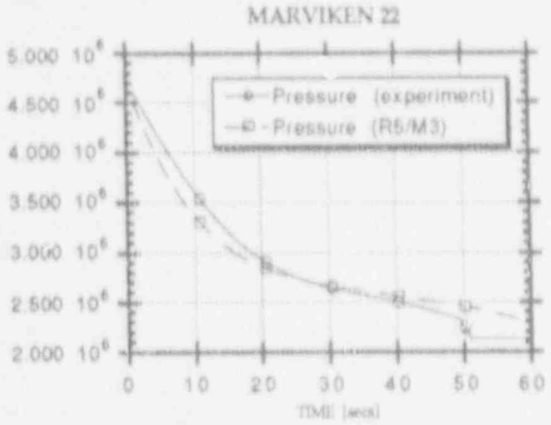

Figure 4. Comparison between simulated and experimental Pressure [Pa] history for Marviken 22 test.

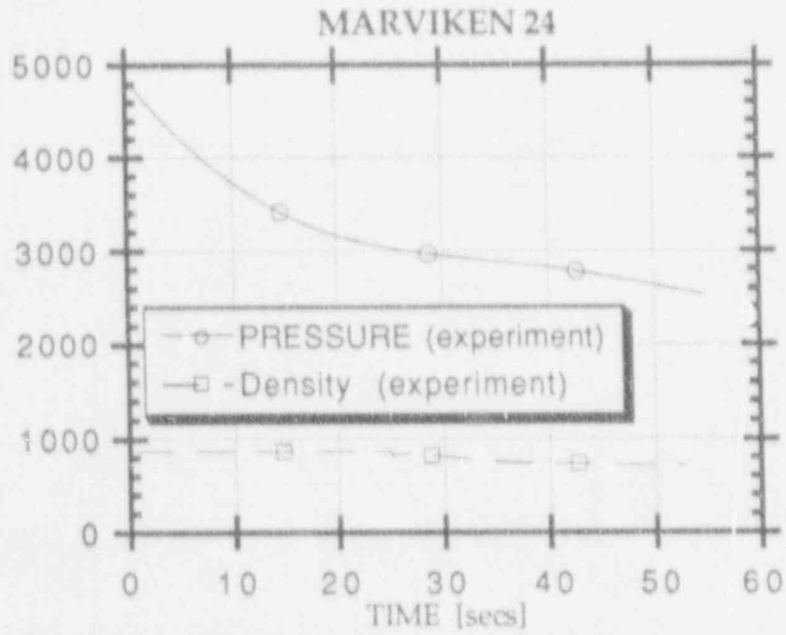

Figure 5. Experimental Pressure [kg/s] and density [kg/m^3] histories for Marviken 24 test.

It would have been preferable to have many more tests. Unfortunately, because of the newness of this code, these were the only relevant assessments available.

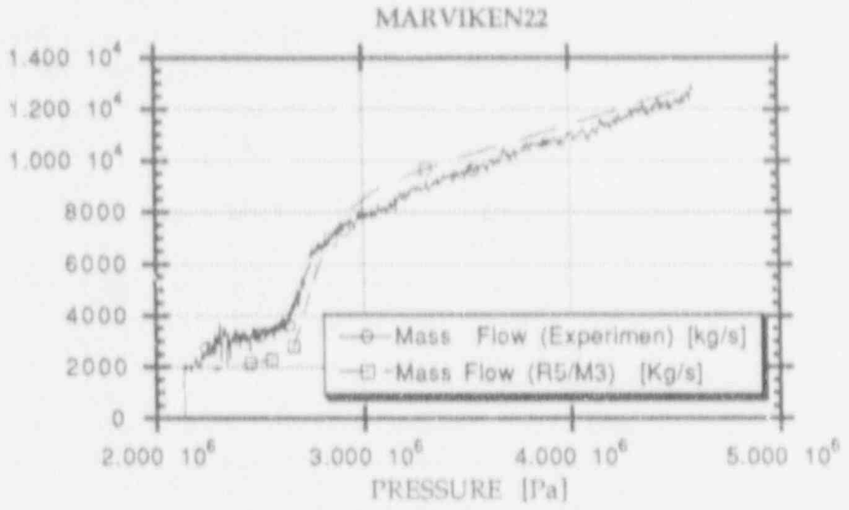

Figure 6. Mass Flow [kg/s] as a function of pressure. Comparison between RELAP5/MOD3 simulation and Marviken 22 test data.

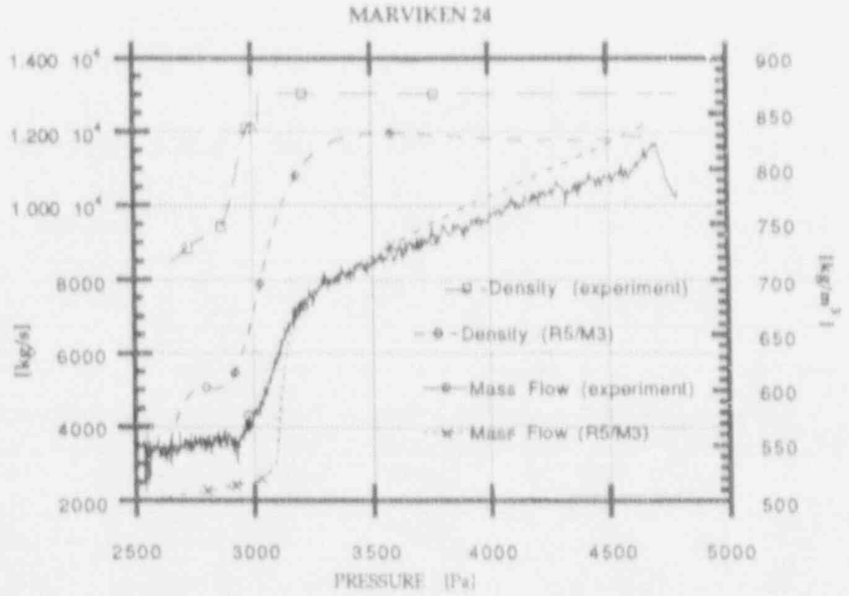

Figure 7. Mass Flow [kg/s] and densiiy [kg/m^3] as functions of pressure. Comparison between RELAP5/MOD3 simulation and Marviken 24 test data.

Thus, in order to quantify the accuracy in a meaningful way, we proceeded to process the available information further. We now make the assumption that the pressure inside the Marviken vessel is the main factor in determining the flow

through the nozzle. The validity of this assumption is suggested by Fig. 5, which shows the measured density throughout the emptying of the vessel indicating much smaller variations than in pressure. Based on this we proceeded to plot the mass flow as a function of pressure for both experiments. Figure 6 illustrates this result and the comparison between simulation and experiment for Marviken 22.

Figures 6 and 7 provide more useful information that Figures 2 and 4 about the accuracy of the code. They clearly show that the code overpredicts single phase break flow and underpredicts two-phase break flow. Furthermore, one can measure the error for each data point and generate a statistical distribution of that error. Noting that there are two distinct flow regimes, we defined and evaluated the error for each regime. The error is defined as follows:

$$\text{Error} = \frac{(\text{Prediction} - \text{Measurement})}{\text{Measurement}}$$

The bias is defined as the average error. Figures 8 and 9 show the observed error for single phase and two-phase break flows respectively. In figure 8 the bias is positive and in figure 9 is negative. Table 2 shows the statistical parameters of the error distribution assuming that it is normal and the adjusted value for the NPP break configuration, according to the interpolation between the corresponding L/D's.

Table 2

Statistical Parameters of the Error Distribution for Marviken 22 and Marviken 24, in single-phase flow and two-phase flow, as well as the corresponding value for the assumed NPP break configuration.

Single-Phase	Marviken 22	Marviken 24	NPP estimate
Calculation bias	0.068	0.107	0.083
Standard Deviation	0.032	0.0586	0.042

Two-Phase	Marviken 22	Marviken 24	NPP estimate
Calculation bias	-0.349	-0.579	-0.435
Standard Deviation	0.048	0.0853	0.062

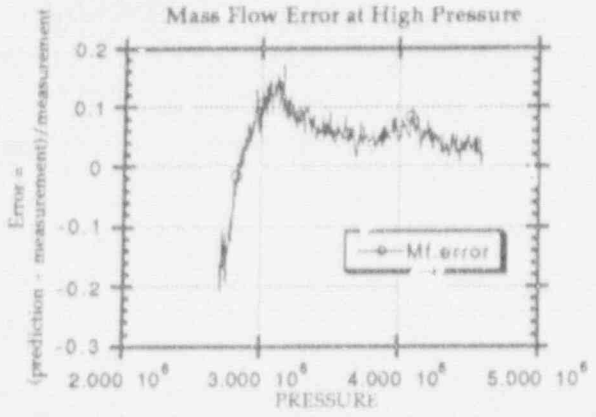

Figure 8. Error vs. pressure for the high-pressure (single-phase) regime of Marviken 22.

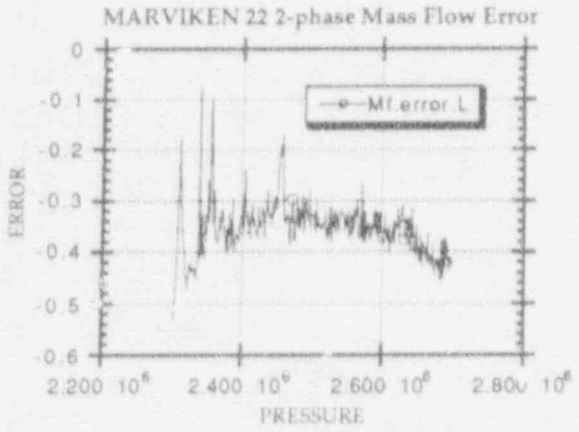

Figure 9. Error vs. pressure for the low-pressure (two-phase) regime of Marviken 22.

Normality Test

To verify our assumption that the error distribution is normal, we performed a normality test, by comparing the observed distribution with the normal distribution [8]. Figures 10 and 11 demonstrate this comparison for the errors in Figures 8 and 9. The "almost linear" character of these comparisons supports the normality assumption made earlier.

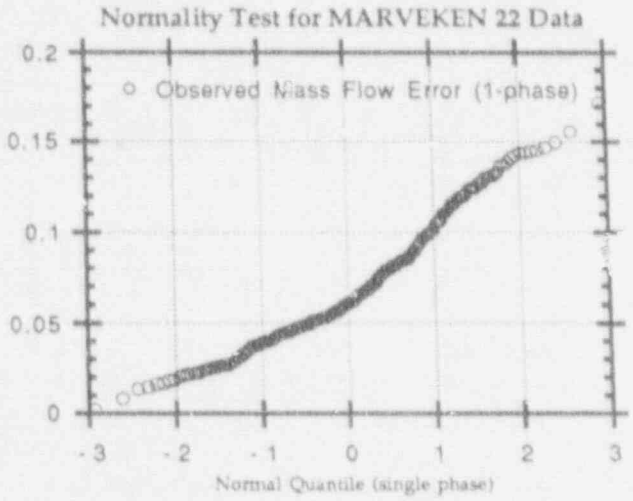

Figure 10. Normality test applied to the data in Figure 8.

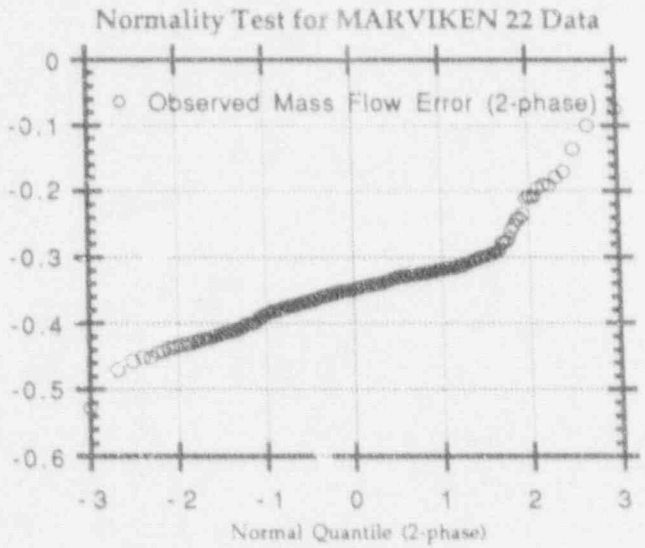

Figure 11. Normality test applied to the data in Figure 9.

In addition to the aforementioned Marviken tests, we also examined LOFT-Wyle TEST WSBO3R (orifice calibration). This test is not full scale like Marviken, and the corresponding L/D=3.33 is much larger than our NPP. However, the pressure is comparable to the scenario and it shows results that are consistent with our previous observations; namely the two-phase flow is 10% to 33% underpredicted.

Interphase Drag

As mentioned earlier, RELAP5/MOD3 evaluates the interface drag in the bubbly/slug regime by means of an empirical correlation [6], which yields parameters that then define an interphase drag coefficient. This interphase drag coefficient appears in the interphase drag term of the momentum equation in difference form as follows [5]:

$$(\rho FI)_j^n (C_1^n v_g^{n+1} - C_0^n v_f^{n+1})_j \qquad (1)$$

The code documentation [5] shows that the interphase drag force term per unit volume and the term FI of the expression above are related:

$$\alpha(1-\alpha)\rho_g\rho_f FI = f_{gf}\,|C_1 v_g - C_0 v_f| \qquad (2)$$

For bubbly and slug flow regimes in vertical flow, which are the flow regimes of interest for natural circulation in an SBLOCA, the drift flux model was adapted. The coefficient f_{gf} is:

$$f_{gf} = \frac{\alpha(1-\alpha)^3(\rho_f - \rho_g)g\sin\phi}{|v_{gj}|v_{gj}} \qquad (3)$$

C_0 and V_{gj} terms are calculated using the Chexal-Lellouche correlation [6]. Minor manipulation of these equations yields the following expression for the term FI:

$$FI = \frac{(1-\alpha)^2(\rho_f-\rho_g)g\sin\phi\,|C_1 v_g - C_0 v_f|}{|v_{gj}|v_{gj}\rho_f\rho_g} \qquad (4)$$

The Chexal-Lellouche correlation [6] is based on a large body of data; specifically thirteen sets of data, totaling several hundreds of points. We combined all of this information to determine the average (bias) and the standard deviation of the data (α vs v_{gj}) which is said to be normal. The result of this calculation gave -0.0003 as the average, and 0.0413 as the standard deviation.

This uncertainty affects the simulation in a less direct way than the break flow uncertainty. It defines the "ignorance" of the code in terms of the right α to use while calculating FI. Equation 4, above, indicates that FI is a function of $(1-\alpha)^2$. If we assume no bias and plot the boundaries of FI for 97.7% of the data (+- 2σ), we obtain the curves shown in Fig. 12. Note that the severe non-linear behavior happens toward the edge of the range of applicability (bubbly or slug flow) and may not be reflected in the actual simulations.

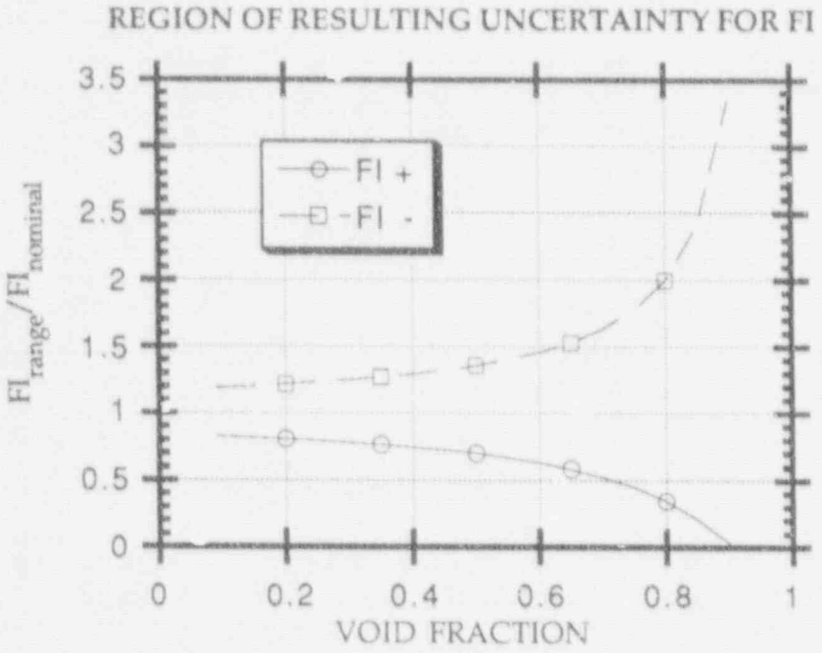

Figure 12. Boundaries (97.7%) of variability of the interphase drag coefficient FI about its nominal calculated value.

Decay Power

The decay power depends on the history of the core at the time of the event and its uncertainty has also a spatial component. It has been suggested, by Tran and Schrock [7], that if we know the core burnup history in some detail, one can estimate the decay power uncertainty more accurately than by only using the ANS standard [9]. We did not have the necessary information to evaluate the uncertainty in fashion suggested by Tran and Schrock [7]; thus we assumed an uncertainty range of 20% (+/- 10% about the nominal), large enough to include the spatial contribution to uncertainty. To implement this, the bounding decay power curves originate at the same power level as the nominal and their values for each time are 10% higher or lower than the corresponding nominal value. The nominal power level drop between time zero and the first step is larger than 10%, which allowed us to implement the variation without an overshoot of power.

HPI Flow

Originally, this phenomena included both flow magnitude and temperature uncertainties [3]. We learned in the process, that in case of an accident that requires HPI the operator will monitor and throttle the flow to no more than a prescribed maximum [10]. Therefore, the magnitude of the HPI flow is no longer as uncertain

as other contributors to uncertainty. Thus, for this study the HPI Flow uncertainty refers to its inlet temperature. This temperature is limited by technical specifications and it is not allowed to go above 316.5 K (110 F), or below 275 K (35 F).

CONCLUSIONS

Despite our limited data base, we are able to establish the accuracy of the code simulation of break flow. The code slightly overpredicts single phase flow and underpredicts the two-phase flow. Exact values depend on the geometry and configuration of the break. The error underpredicting the two-phase flow maybe explained in part by the possibility that superheated liquid may be flowing out the nozzle in the experiment, while the code assumes that the phase change takes place earlier.

We were able to estimate the uncertainty introduced into the calculation by the interphase drag model, based on the large amount of data that was used to build the empirical correlation [6]. We found that the uncertainty is relatively small, although its effect can be large during some states of the flow. We had no available assessments that directly evaluated the accuracy of the code to represent natural circulation. However, the natural circulation study reported by Roth and Schultz [11] concludes that RELAP5/MOD3 is capable of representing this phenomenon reasonably well.

Our evaluation of the decay power uncertainty may be conservative. More information about the core and its history is required to refine our estimates. The HPI flow, on the other hand, is an example of an accurately defined range of user input. The distribution associated with this uncertainty is uniform.

AKCNOWLEDGMENTS

The support and numerous interesting questions that we received from our technical monitor at the USNRC, Harold H. Scott are greatly appreciated. The suggestions, comments, and answers provided by Gary Johnsen throughout this work are also very much appreciated. We would like to thank specially, the RELAP5 developers: Clay Miller, Rich Riemke, Ken Carlson, and Walt Weaver who generously provided us with their calculations and insight whenever we asked.

REFERENCES

[1] R.A. Shaw, S.Z. Rouhani, T.K. Larson, R.A. Dimenna, "Development of a Phenomena Identification and Ranking Table (PIRT) for Thermal- Hydraulic Phenomena During a PWR Large-Break LOCA." NUREG/CR-5074, EGG-2727, October 1988.

[2] Technical Program Group, "Quantifying Reactor Safety Margins." NUREG/CR-5249, EGG-2552, December 1989.

[4] M.G. Ortiz, L.S. Ghan, G.E. Wilson, "Development of a Phenomena Identification and Ranking Table (PIRT) for Thermal-Hydraulic Phenomena During a PWR Small Break LOCA." EGG-EAST-9080, May 1990

[3] M. G. Ortiz and L. S. Ghan, "Code Scaling, Applicability, and Uncertainty Study of RELAP5/MOD3 Applied to a B&W SBLOCA Scenario." NUREG/CR-in preparation. November 1991, Draft.

[5] K.E. Carlson, R.A. Riemke, S.Z. Rouhani, R.W. Shumway, W.L. Weaver, "RELAP5/MOD3 Code Manual." NUREG/CR-5535, EGG-2596, June 1990.

[6] Nuclear Safety Analysis Center of EPRI, "The Chexal-Lellouche Void Fraction Correlation for Generalized Applications." NSAC/139, April 1991.

[7] H. Tran, V.E. Schrock, "Decay Power Evaluation for Licensing Analysis." ANS Transactions vol. 54, pp 246-247, 1987.

[8] L. Sachs, "Applied Statistics: A Handbook of Techniques." Second Edition. Springer Series in Statistics. Springer-Verlag, 1984.

[9] "American National Standard for Decay Power in Light Water Reactors," ANSI/ANS-5.1-1979, American Nuclear Society (1979).

[10] D. G. Newton, "Emergency Operating Procedures Technical Bases Document", Babcock and Wilcox Tecnical Document 74-1152414-00 for the B&W Owners Group. 1985.

[11] P. A. Roth and R. Schultz, "Analysis of Reduced Primary And Secondary Coolant Level Experiments In The Bethsy Facility Using Relap5/MOD3" EG&G-EAST- 9251, July 1991.

UNIVERSAL TREATMENT OF PLUMES AND STRESSES FOR PRESSURIZED THERMAL SHOCK EVALUATIONS

T.G. Theofanous, S. Angelini & H. Yan

Department of Chemical and Nuclear Engineering
University of California, Santa Barbara
Santa Barbara, CA 93106

ABSTRACT

The thermal field in a reactor vessel downcomer and resulting thermal/stress response in the adjacent reactor vessel wall during high-pressure safety injection are examined, especially with regard to departures from one-dimensional behavior. Similarity solutions for the stratification (in the cold leg) that creates the downcomer plumes, and scaling considerations for the thermal conduction and stress fields in the vessel wall are developed to provide generalized criteria for the adequacy of the one-dimensional treatment.

1. INTRODUCTION

Thermally-induced stresses in a reactor pressure vessel (RPV) wall, as a result of high-pressure safety injection (HPI) are an essential component of integrated risk analyses of pressurized thermal shock (PTS) transients (Selby et al. 1985a, Selby et al. 1985b). Limiting cooldowns (i.e., the most severe conditions) arise when this injection occurs under stagnated loop conditions (loss of natural circulation due to voiding in the steam generator tubes) which, in turn, corresponds to a rather narrow range* (in size) of small-break loss-of-coolant accidents (Theofanous et al 1989). For a given system the actual break sizes in this range can be determined from the HPI pump characteristic. This characteristic also ties in the corresponding injection flow rates and system pressures which are the key parameters concerning cooldown and state of stress.

Even though the net loop flow is zero, the cold safety injection causes a recirculating flow pattern that involves (in mixing) all parts of the primary system that can be reached from the point of injection by a sequence of horizontal and *downwards* vertical traverses (Theofanous & Nourbakhsh 1982, Theofanous & Iyer 1987). The recirculation, which is schematically illustrated in Figure 1, has been shown to have a drastic moderating effect on the global cooldown, as well as on the degree of stratification. The global cooldown is referred to the decrease of T_m, the mixed mean temperature, which physically represents the fluid temperature in the lower plenum, and in the downcomer outside the plume regions. The degree of stratification refers to

* In general, larger breaks lead to system depressurization, while for smaller breaks the HPI is sufficient to collapse the steam generator tube voids leading to reestablishment of natural circulation. The former case is clearly of no interest to PTS, while the latter leads to cooldown significantly less severe since both decay heat and the secondary side of the steam generators are now coupled to the thermal response of the downcomer region.

the temperature difference between the hot and cold streams in the cold leg. In practice, the hot stream temperature is close to T_m; thus the degree of stratification reflects also the initial "strength" of cold plume created by the spilling of the cold stream into the downcomer. This flow, and thermal field, structure is the basis of the Regional Mixing Model (RMM), and the associate computer programs, REMIX and NEWMIX, utilized in the NRC Integrated PTS study (Iyer & Theofanous 1991a), and it has been confirmed experimentally (Iyer & Theofanous 1985, Iyer & Theofanous 1991b); a comprehensive comparison with data in experimental simulations ranging from 1/5 to full scale has been compiled recently (Theofanous & Yan 1991).

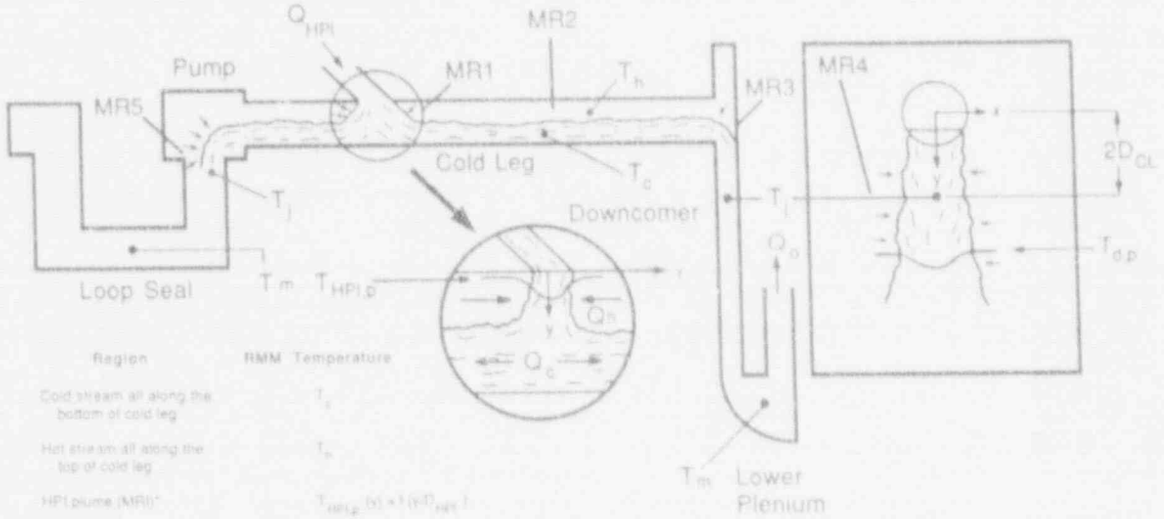

Region	RMM Temperature
Cold stream all along the bottom of cold leg	T_c
Hot stream all along the top of cold leg	T_h
HPI plume (MR1)*	$T_{HPI,p}(0) \times 1/(\dots)$
Pump (MR5)	T_j
Loop Seal	T_m
Downcomer plume at MR3	T_j
Downcomer plume (MR4)**	$T_{d.p}(0,x) = g(x/D_{CL})$
Outside of downcomer plume	T_m
Lower plenum	T_m

* Mixed mean temperature is recalculated using entrainment as a function of x and Ri_{HPI}

** This temperature is the lowest for the given level

Figure 1. Schematic representation of the Regional Mixing Model (RMM).

For the IPTS plants (Calvert Cliffs, H.B. Robinson and Oconnee) the degree of stratification was found to be minimal, and this behavior is expected to be applicable to the vast majority of US-designed plants (Iyer & Theofanous 1991a). Quantitatively, this stratification behavior, along with the predicted cooldown, can be summarized in the form of Figures 2 and 3 (for a Calvert Cliffs example), which provide the boundary conditions for the stress analysis. The significance of T_j in Figure 2 (refer to Figure 1 also) is that it characterizes, in an approximate fashion, the "source" of the planar downcomer plume. Guided by experimental data, this "source" point is taken at 2 cold leg diameters below the cold-leg centerline (Iyer & Theofanous 1991a). Below this point the cold plume decays in the manner shown in Figure 3 (obtained from well-known plume decay laws, i.e., Turner 1973). Above it there is a very complex, three-dimensional, temperature/flow distribution and mixing pattern that although unknown in detail seems to have

been adequatcly characterized as producing an equal volume mixing between the cold stream and the ambient downcomer fluid (this is how T_j is computed). As a rough approximation in REMIX/NEWMIX, the temperature fieid in this region is obtained by linear interpolation between T_c and T_j.

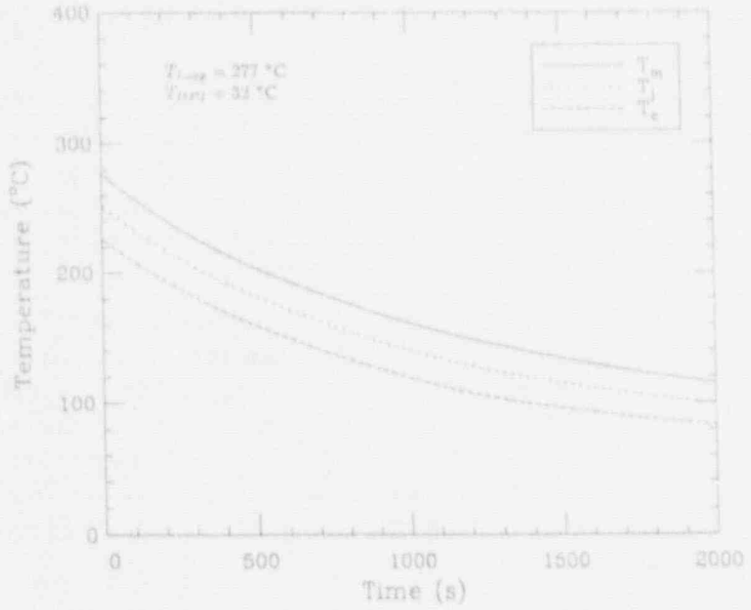

Figure 2. Predicted cooldown transient in Calvert Cliffs for an HPI of 13.5 kg/s in each of the 4 cold legs.

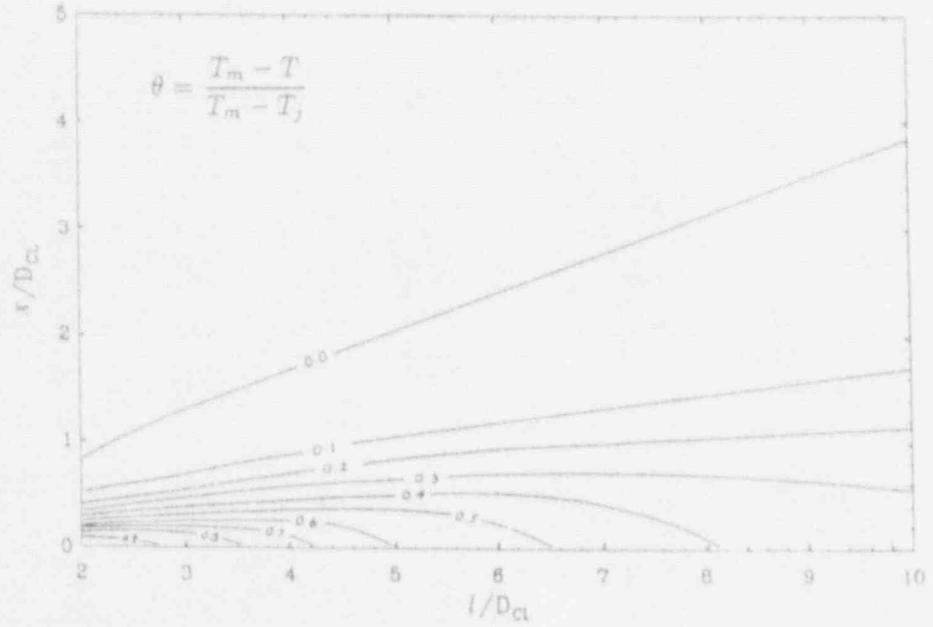

Figure 3. Plume decay (dimensionless) in the downcomer. Actual temperature at any time can be obtained with the help of Figure 2 providing the T_j and T_m values.

In the IPTS, the stress analysis was carried out in a one-dimensional (1D) approximation believed to conservatively bound the stresses everywhere in the RPV wall (Cheverton et al. 1984, Selby et al. 1985). Specifically, the T_J transient was applied, through a heat transfer coefficient, *everywhere* on the inside of the RPV wall, which was taken as a complete cylinder (i.e., without the cold-leg openings). In practice, conduction controls and the procedure is tantamount to imposing (within a few degrees) the T_J transient directly on the inside face of the RPV wall.

A recent publication (Neubrech et al. 1988) strongly questions this procedure and provides analyses which in comparison with data from a full-scale "simulation" imply that the above-described 1D treatment may be highly non-conservative. This, in turn, has created intense concerns about the validity of the IPTS study. The IPTS study, through regulatory guides, has become a sort of prototype for future ones expected to be numerous, in the years to come, as plants age and come up against the specified PTS screening criteria.

The concern is simply illustrated with the help of Figures 4 and 5, reproduced from Geiß (1987) which seems to be the source of the material presented by Neubrech et al. (1988). Exactly the same, non-conservative, trends were shown also for strains. Note that the positions to which Figure 4 refers is 2.6 cold-leg diameters below the cold-leg centerline; that is, the temperature at the plume centerline corresponds closely to T_J and hence the 1D treatment shown should closely correspond to the 1D treatment of the IPTS prescription. At the lower position, Figure 5, the 1D treatment based on the measured local temperature is clearly inadequate; however, it is evidently bounded by the 1D treatment based on T_J.

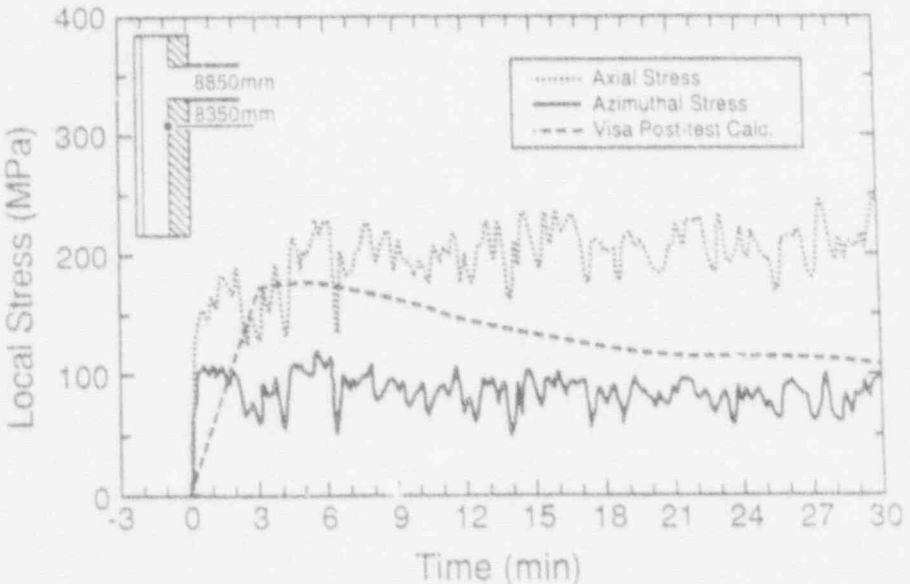

Figure 4. Comparison of calculated stresses in the 1D approximation (VISA) with measured values in HDR test T32.18 (reproduced from Geiß1987). The point shown (measurement) is 2.6 cold-leg diameters below the cold-leg centerline.

This measured, strongly asymmetric, stress field is related to the elongated plume structure and should not have been unexpected. Consider, for example, the thermal stresses in a plane wall assigned a cold, uniform through the wall, elliptical spot. For a temperature difference

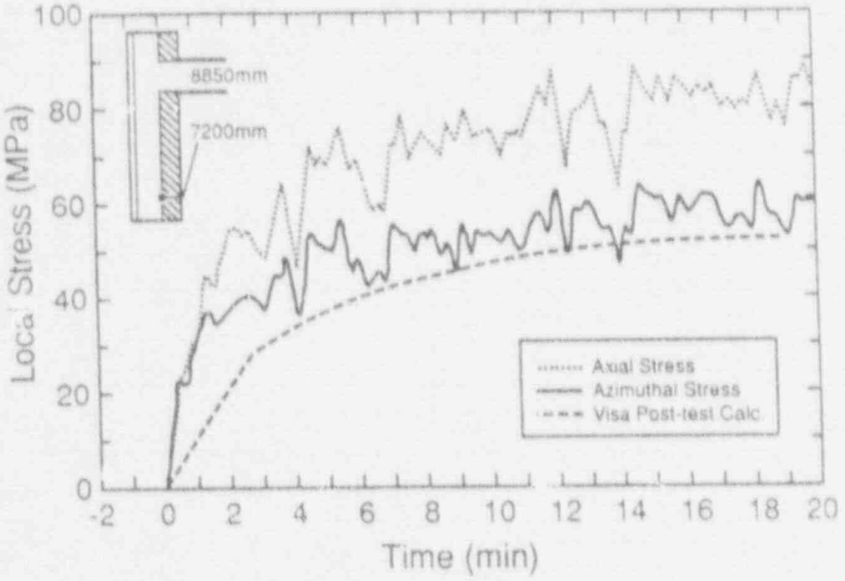

Figure 5. Comparison of calculated stresses in the 1D approximation (VISA) with measured values in HDR test T32.18 (reproduced from Geiß1987). The point shown (measurement) is 7.9 cold-leg diameters below the cold-leg centerline.

of ΔT, and major and minor ellipse semiaxis b and a aligned with the y and x coordinates, respectively, we have

$$\sigma_x = -E\left\{\frac{a}{a+b}\right\}\alpha\Delta T \tag{1}$$

$$\sigma_y = -E\frac{b}{a+b}\alpha\Delta T \tag{2}$$

Thus

$$\frac{\sigma_y}{\sigma_x} = \frac{b}{a} \tag{3}$$

and the stress asymmetry increases with the elongation of the ellipse. On the other hand, the through-the-wall temperature gradient, in this example, would be zero, and so the calculated stress in the 1D approximation would also be zero.

The discrepancy in the above example is clearly an exaggeration; it serves to vividly illustrate, however, that the potential concern is legitimate. What remains to be done is to explore quantitatively the impact of this concern on reactor predictions and to examine under what conditions, if any, the 1D treatment is adequate. The reason for this latter aspect is that in the scope of an IPTS study a very large number of wall stress calculations need to be carried out to properly sample the space of uncertainty in the key parameters, and transients, that have to be considered; as a consequence, a full 3D treatment becomes rather impractical. The purpose of this paper is to provide some results relevant to these goals. We begin, with section 2, by discussing similarity of stratification and associated fluid thermal transients in the downcomer. We demonstrate that the particular HDR test (T32.18) chosen by Geiß (1987) and Neubrech et al. (1988) suffers from gross dissimilarity to US reactor conditions. We find another HDR test, T32.34, to provide a very close simulation; unfortunately, no stress/strain data have been published for it. REMIX

results are found to be in excellent agreement with both of these tests. In section 3 we develop finite element models for 1D and 3D treatments of the RPV and demonstrate that the 3D model accurately depicts the measured stress/strain fields shown in Figures 2 and 3 (for test T32.18). As expected, we find that the 1D treatment, based on T_j as per IPTS study, is non-conservative for a significant fraction of the downcomer area (down to ~7 cold-leg diameters below the cold-leg centerline). By contrast for test T32.34, this area of non-conservative behavior is predicted to shrink down to an axial distance of only 4 cold-leg diameters. The same structural model is applied to the Calvert Cliffs geometry and thermal-hydraulic conditions similar to those of test T32.34. We find that the 1D treatment is even more appropriate than in test T32.34; only an area down to 2 cold-leg diameters is affected (i.e., the axial stress being greater than that computed in the 1D IPTS approximation); that is, the 1D treatment is entirely adequate. Finally, in section 4 we generalize these structural analysis results to four simple, generalized similarity maps that define the regions of potential difficulty with the 1D IPTS prescription. These maps show rather clearly that *all* HDR tests are far from applicable to simulate the thermal stress field in a reactor vessel wall, because they have failed (single loop injection) to represent the global cooldown.

2. THERMAL TRANSIENTS AND SIMILARITY CONSIDERATIONS

A scaled representation of the HDR in comparison to the world PTS facilities is shown in Figure 6. The particular geometric data and those relevant to a large US PWR are shown in Tables 1 and 2, respectively. The complete experimental matrix on thermal mixing (TEMB) is summarized in Table 3. These data represent a cornerstone of the total available data base because they uniquely combine full-scale (prototypic) pressure/temperature conditions in a large reactor-like geometry. In fact, as seen in Figure 6, with the exception of the relatively smaller cold-leg diameter (19 vs. 76 cm) and downcomer gap (13 vs. 26 cm) dimensions, the *HDR is essentially a full-scale representation* of a PWR. Another unique aspect of these tests is the stress (strain) measurements on the vessel wall.

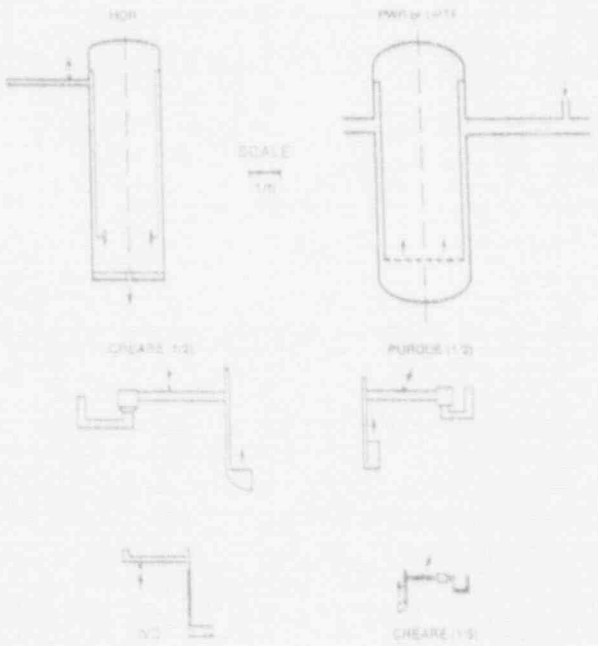

Figure 6. Schematic scaled representation of the HDR in relation to the world integral thermal mixing facilities for PTS.

As already mentioned, the complete TEMB series tests have been very favorably compared with the REMIX predictions; indeed, blind pretest calculations of the first two tests provided excellent predictions of the test data. As we will see in section 3, with accurate thermal boundary conditions the measured stress fields are also easily predictable by a full 3D finite element model. Application of these tools to reactor geometries indicate considerably different trends with regard to the issues mentioned in the introduction. The purpose of this section is to provide the thermal-hydraulic similarity considerations necessary to understand some of the origins of these differences. Structural considerations enter this understanding also; these are developed in section 3.

Table 1. Geometric data of HDR full-scale test facility.
Injector diameter: 5.0 cm

	Cold Leg	Vessel/ Downcomer	Lower Plenum	Pump	Loop Seal	Core Barrel	Thermal Shield
Inner Diameter (cm)	18.70	296.00	---	---	---	266.00	---
Length (cm)	600.00	694.26	---	---	---	694.26	---
Base Metal Wall Thickness (cm)	1.52	11.20	17.10	---	---	2.30	---
Clad Thickness (cm)	---	0.80	0.80	---	---	---	---
Insulation Thickness (cm)	10.00	10.00	10.00	---	---	---	---
Wall Heat Transfer Area to Water (cm^2) x 10^{-4}	3.52	64.56	23.35	---	---	58.02	---
Fluid Volume (cm^3) x 10^{-3}	1.65	78.47	129.80	---	---	---	---

Table 2. Geometric data of a US PWR.+
Injector diameter: 25.7 cm

	Cold Leg	Vessel/ Downcomer	Lower Plenum	Pump	Loop Seal	Core Barrel	Thermal Shield
Inner Diameter (cm)	76.2	436.9	---	---	76.2	375.9	---
Length (cm)	623.7	685.3	---	---	456.1	685.3	---
Base Metal Wall Thickness (cm)	6.35	21.9	11.1	---	6.35	4.45	---
Clad Thickness (cm)	0.318	0.794	0.794	---	0.318	---	---
Insulation Thickness (cm)	0.30	0.30	0.30	---	0.30	---	---
Wall Heat Transfer[a] Area to Water [(cm^2) x 10^{-5}]	1.49	2.35	0.745	[b]	1.09	2.02	---
Internal structures: Heat Transfer Area [(cm^2) x 10^{-5}]	---	---	---	3.08[b]	---	---	---
thickness (cm)	---	---	---	6.35	---	---	---
Fluid Volume [(cm^3) x 10^{-6}]	2.84	5.76	5.46	3.17	2.08	---	

[a] Per cold leg.
[b] Pump casing and internal structures have been lumped to 33,700 lb equivalent of stainless steel
+ Calvert Cliffs Unit 1

Table 3. Test conditions of HDR full-scale experiments

Test #	HPI nozzle #	T_{loop} (°C)	T_{HPI} (°C)	$\dot{m}_{HPI}$ (kg/s)	Fr_{HPI}
T32.11	1	300	20	0.12	0.1
T32.12		300	20	0.24	0.3
T32.13		300	20	0.37	0.5
T32.14		300	20	0.49	0.6
T32.15		300	20	0.99	1.3
T32.18		300	20	1.49	2.0
T32.19		300	20	2.37	3.2
T32.20		150	20	2.30	5.9
T32.21		300	20	5.56	7.4
T32.22		300	20	2.37	3.2
T32.31	2	300	20	0.12	0.1
T32.32		300	20	0.24	0.3
T32.33		300	20	0.37	0.5
T32.34		300	20	0.49	0.6
T32.36		300	20	0.99	1.3
T32.41		300	20	1.48	2.0
T32.51	3	300	20	0.49	0.6
T32.52		300	20	0.99	1.3
T32.57		300	20	1.48	2.0
T32.58		225	20	0.74	1.3
T32.61		150	20	0.52	1.3

The stratification behavior has been shown to be universally represented by two dimensionless groups (Theofanous & Yan 1991), namely*

$$Fr_{HPI,CL} = \frac{Q_{HPI}}{A_{CL}} \left\{ g D_{CL} \frac{\Delta\rho}{\rho_{HPI}} \right\}^{-1/2} \quad \text{and} \quad D^* = D_{CL}/D_{HPI} \tag{4}$$

When they are matched (in two different systems with the same T_m and T_{HPI}) the difference in cold stream and hot stream temperature is also matched. The actual solution is embodied in the intersection of two plots such as those shown in Figures 7 and 8. Figure 7 represents the entrainment in the HPI plume (MR1 in Figure 1), and it is parametrized by D^*, the value of 3.8 being appropriate for the HDR geometry. For a PWR with $D^* = 2.9$ the result is shown in Figure 9 (similar plots for D^* values in the range $2 < D^* < 10$ can be found elsewhere, Theofanous & Yan 1991). Figure 8 represents the counter-current flow requirement at the cold-leg downcomer junction expressed by

$$Fr_c^2 + Fr_h^2 = 1 \tag{5}$$

This figure is parametrized by $\rho^* = \rho_h/\rho_c$ and β. For reactor (and HDR) conditions $0.8 < \rho^* < 1$, and the results vary insignificantly in this range. The parameter β expresses whether the system geometry allows back-flow of the cold stream, towards the pump and loop seal volumes. When back-flow is possible and the pump and loop seal volumes represent a significant fraction of the total volume of the system, the $\beta = 1/2$ is appropriate. When such back-flow is not allowed, we set $\beta = 1$, and the result is shown in Figure 10. Returning now to the solution, the intersection (choose the one with the lower value) at the same value of $Fr_{HPI,CL}$, yields the dimensionless entrainment rate, in the plume region, i.e., $Q^* = Q_e/Q_{HPI}$. From Q^* the

* Note that with these definitions, $Fr_{HPI} = Fr_{HPI,CL} D^{*5/2}$.

cold stream temperature, T_c, and the downcomer plume "source" temperature, T_j, can be simply obtained from

$$T_c \simeq \frac{\rho_{HPI} T_{HPI} + \rho_m T_m Q^*}{\rho_{HPI} + \rho_m Q^*} \tag{6}$$

$$T_j \simeq \frac{1}{2}(T_c + T_m) \tag{7}$$

Applying this procedure to HDR test T32.18 ($Q_{HPI} = 1.49$ kg/s, T_{HPI} =20 °C) we find $Fr_{HPI,CL} = 0.07$ and from Figures 7 and 8 we read $Q^* = 1.1$. With $T_m \sim T_m(0) = 300$ °C, i.e., early in the transient, we thus obtain $T_c = 143$ °C and $T_j = 221$ °C; that is $T_m - T_j = 79$ °C. Using an IPTS plant (Calvert Cliffs as an example with $Q_{HPI} = 13.5$ kg/s, $T_{HPI} = 32$ °C) on the other hand we obtain $Fr_{HPI,CL} = 0.022$ and $Q^* = 3.8$ ($\beta = 1/2$, Figures 8 and 9). For $T_m \sim T_m(0) = 277$ °C, this translates to $T_c = 201$ °C and $T_j = 239$ °C; that is $T_m - T_j = 38$ °C. Even for $Q_{HPI} = 20$ kg/s, the Q^* decreases only slightly to 2.4, which yields $T_c = 190$ °C, $T_j = 234$ °C and $T_m - T_j = 43$ °C. A major discrepancy on the severity of stratification between the plant and the HDR "simulation" is evident. In fact, a much better simulation is provided by another HDR test, the T32.34 ($Q_{HPI} = 0.49$ kg/s, $T_m \sim T_m(0) = 308$ °C, $T_{HPI} = 20$ °C). From Figures 7 and 8 we read $Q^* = 2.5$, which yield $T_c = 203$ °C and $T_j = 256$ °C; that is $T_m - T_j = 52$ °C. Incidentally, ignoring the back-flow in the Calvert Cliffs calculation ($\beta = 1$) would yield (for $Q_{HPI} = 13.5$ kg/s) $Q^* = 3.5$, $T_c = 210$ °C and $T_j = 244$ °C, i.e., the sensitivity to this parameter is not great.

Turning next to the downcomer plume, its "strength" and hence the degree of departure from symmetric behavior are strongly related to how cold the plume is at its source (T_j) in relation to its surroundings (at T_m). From Equations (6) and (7) above we have

$$T_m(t) - T_j = \frac{1}{2}\frac{T_m(t) - T_{HPI}}{1 + \tilde{\rho} Q^*}, \qquad \tilde{\rho} = \frac{\rho_m}{\rho_{HPI}} \tag{8}$$

During a cooldown transient $\tilde{\rho}$ increases slowly from 0.76 to 1 and Q^* decreases very slowly from its initial value to less than 1 (note that the Q^* change is due to the ρ^* change). In fact, actual computations (with REMIX) indicate that the two variations compensate each other such that the plume "strength" remains nearly a constant fraction of $T_m(t) - T_{HPI}$. Specifically, this factor is 0.27, 0.19, and 0.15 for HDR/T32.18, HDR/T32.34, and the Calvert Cliffs example mentioned above, respectively. The nature of the thermal stress transient, and the role of the plume in inducing significant departures from the approximate 1D treatment, must therefore be understood in terms of the time constant that characterizes the $T_m(t)$ transient itself.

The global cooldown transient, $T_m(t)$, is characterized, primarily by the system volume (V) and the injection flow rate (Q_{HPI}), combined into a system time constant, τ_s

$$\frac{T_m(t) - T_{HPI}}{T_m(0) - T_{HPI}} \sim e^{-t/\tau_s}, \qquad \tau_s = \frac{V}{Q_{HPI}} \tag{9}$$

where Q_{HPI} is the total injection rate in all the loops. The HDR tests involved only one-loop injection; hence, the τ_s is rather large: 1.4×10^4 s and 4.3×10^4 s for T32.18 and T32.34, respectively, as compared to a value for the Calvert Cliffs example of 1.3×10^3 s for $Q_{HPI} = 13.5$ kg/s and 9.6×10^2 s for $Q_{HPI} = 20$ kg/s. This means that even test T32.34, which, as discussed above, provides a good simulation of the stratification, badly misses (to simulate) the thermal

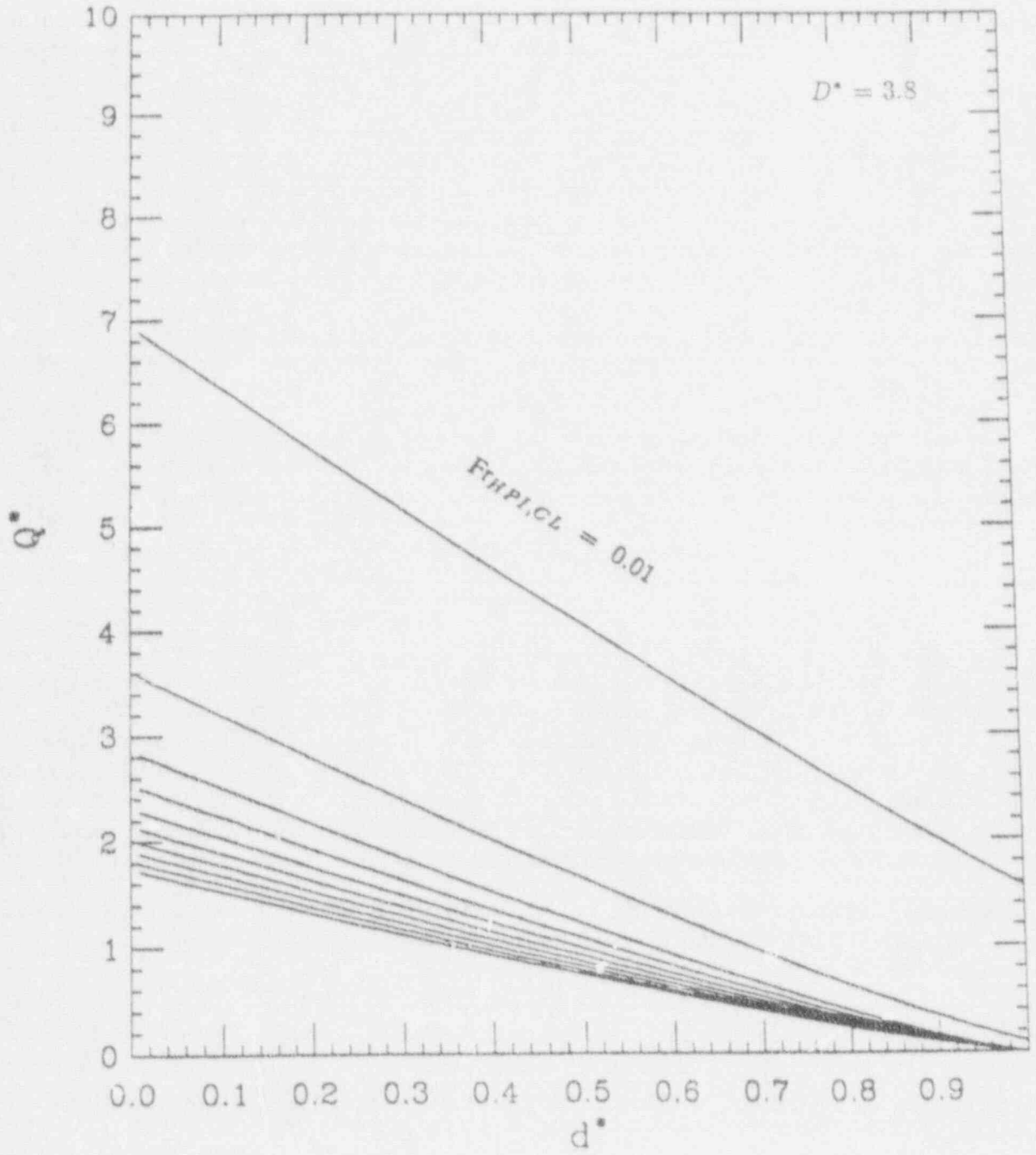

Figure 7. Illustration of plume entrainment for $D^* = 3.8$. $Fr_{HPI,CL}$ is ranging from 0.01 to 0.10 in increments of 0.01.

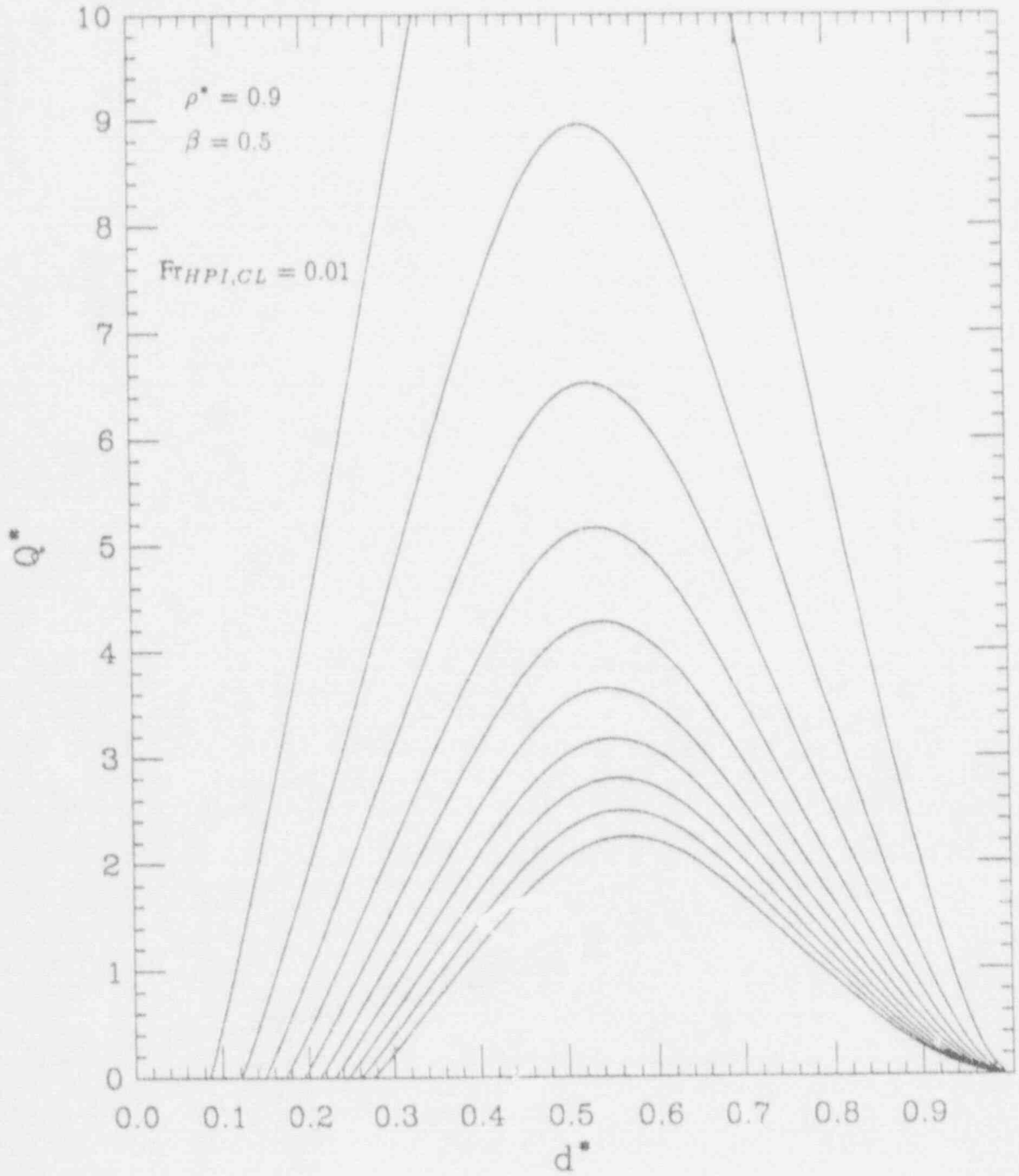

Figure 8. Illustration of counter-current flow-limited entrainment for $\rho^* = 0.9$ and $\beta = 1/2$ $Fr_{HPI,CL}$ is ranging from 0.01 to 0.10 in increments of 0.01.

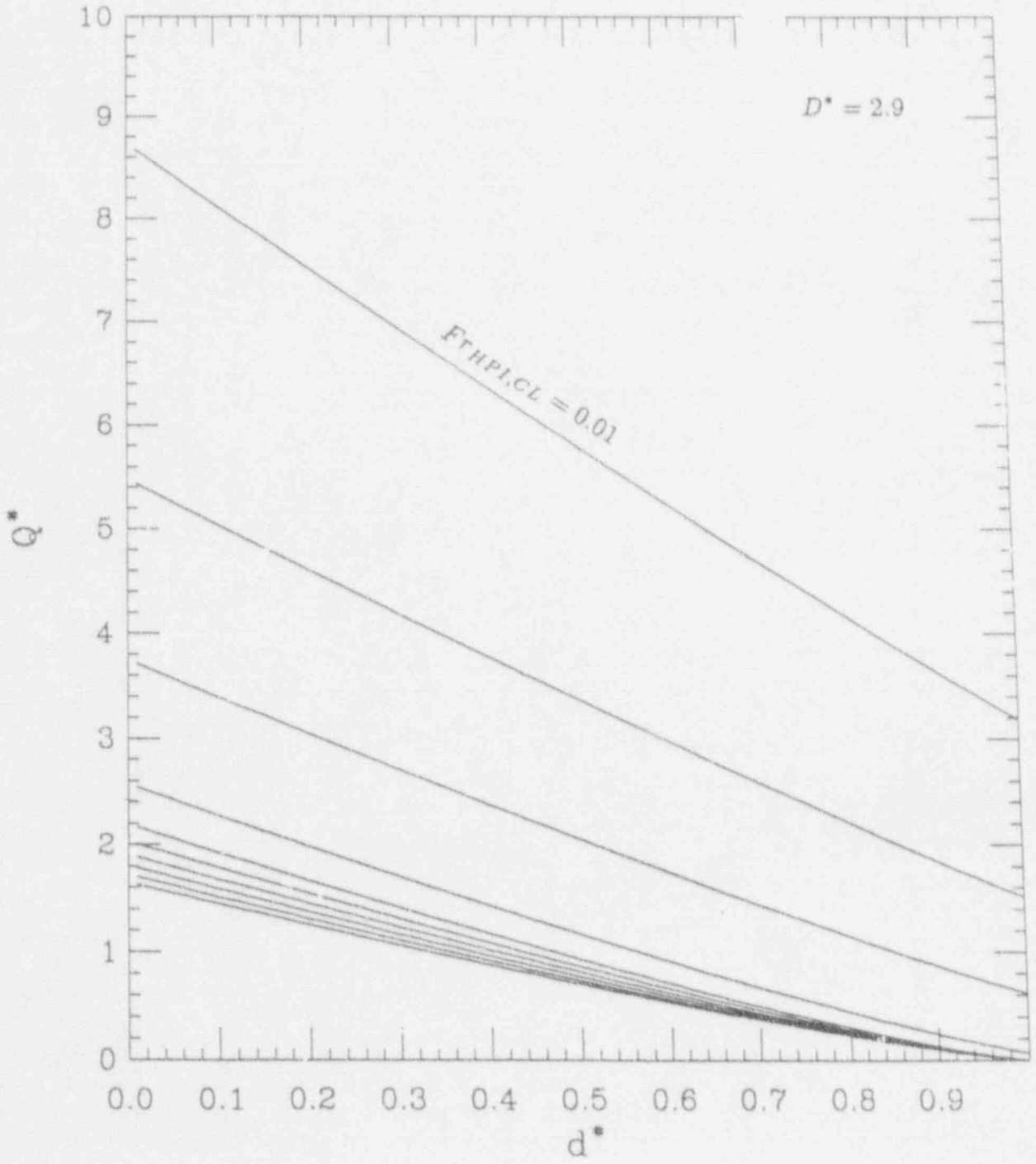

Figure 9. Illustration of plume entrainment for $D^* = 2.9$. $Fr_{HPI,CL}$ is ranging from 0.01 to 0.10 in increments of 0.01.

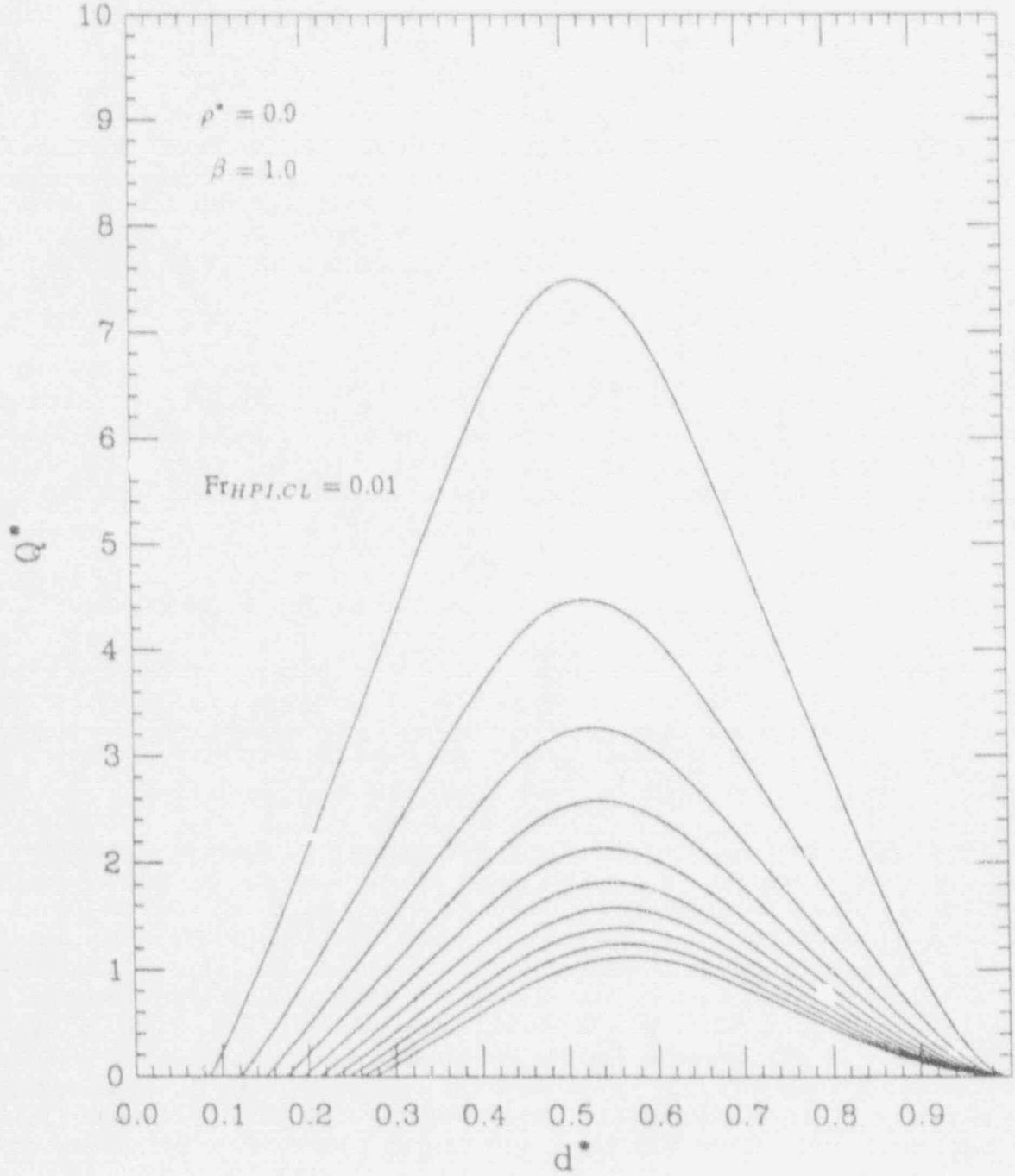

Figure 10. Illustration of counter-current flow-limited entrainment for $\rho^* = 0.9$ and $\beta = 1.0$ $Fr_{HPI,CL}$ is ranging from 0.01 to 0.10 in increments of 0.01.

stress behavior.* Specifically, in HDR we obtain relatively steady plumes in extremely slowly varying surroundings and the measured stresses are essentially all due to these plumes; while in Calvert Cliffs (or similar reactors) we obtain plumes of rapidly (in time) diminishing strength in relatively rapidly varying surroundings, i.e., the plume-induced stresses diminish in comparison to stresses due to the global cooldown — the latter being uniform and hence more in line with a 1D treatment. This suggests that an effective screening for multi-dimensional effects could be made on the basis of the interplay between plume strength and global cooldown; the details are presented in section 4.

For the stress analyses of section 3 we also need the shape of the downcomer plumes. From the data, it appears that the HDR plumes are well-behaving (i.e., steady, straight-down descent) and well-characterized (a lot of measuring points); hence, they are ideal for our purposes. Note also that since T32.34 provides a good simulation of stratification in a PWR, the plume behavior in it is also most appropriate. It turns out that when the local plume temperatures are normalized by the plume "strength," $T_m - T_j$, discussed above, even the very severe T32.18 plume takes on a quite similar form. These two experimental plumes are shown in Figures 11 and 12. In terms of stresses, and the discussion in the introduction, we expect that the plume of T32.18 is slightly more severe than that of T32.34, and both are well bounded (in severity) by the plume of Figure 3, used in conjunction with REMIX.

In closing this section, it may be worth remarking that both the stratification and transient cooldown solutions utilized above are in excellent agreement with the more detailed REMIX results, and the quality of comparisons with the HDR experiments T32.18 and T32.34 at the locations of interest (the elevations in Figures 4 and 5) are shown in Figures 13 and 14, respectively.

3. THERMAL STRESSES AND SIMILARITY CONSIDERATIONS

The thermal stress computations were carried out with the computer code ABAQUS (Version 4.8) using a three-dimensional finite element model, in a planar geometry, as illustrated in Figure 15. The fine-mesh regions can adequately represent the "hole" corresponding to the cold-leg nozzle as well as the thermal gradients within the plume beneath it. The large-mesh zones were incorporated so as to add an adequate amount of wall material surrounding the plume as is the case for the intended simulation. This plate model was fully encastered in all its four sides. As such, it is applicable to situations where the plume remains in steady surroundings (as in the HDR tests) with minimal restrictions on the duration of the transient. For transients involving also global cooldown, the applicability is restricted to short (conduction) penetration times. In both cases the idea is that thermal stresses in the cooled regions are accurately developed (in the model) as long as there is sufficient material in the initial state ("hot") to resist motion. Under these conditions a plate model free on all its four sides actually yielded the same results. Comparisons with the HDR data (at 7 and 14 minutes) justify this position for the plumes-only case. To judge the effect of global cooldown time (on the model accuracy) we compared the plate model prediction with a cylindrically symmetric full-vessel model, both driven with a sudden change on the inside wall temperature. The results for a reactor vessel wall of 22 cm in thickness are shown in Figure 16, indicating that the plate representation is quite adequate for

* This is exacerbated by the considerably thinner HDR wall (12 cm) compared to that of a large PWR (22 cm).

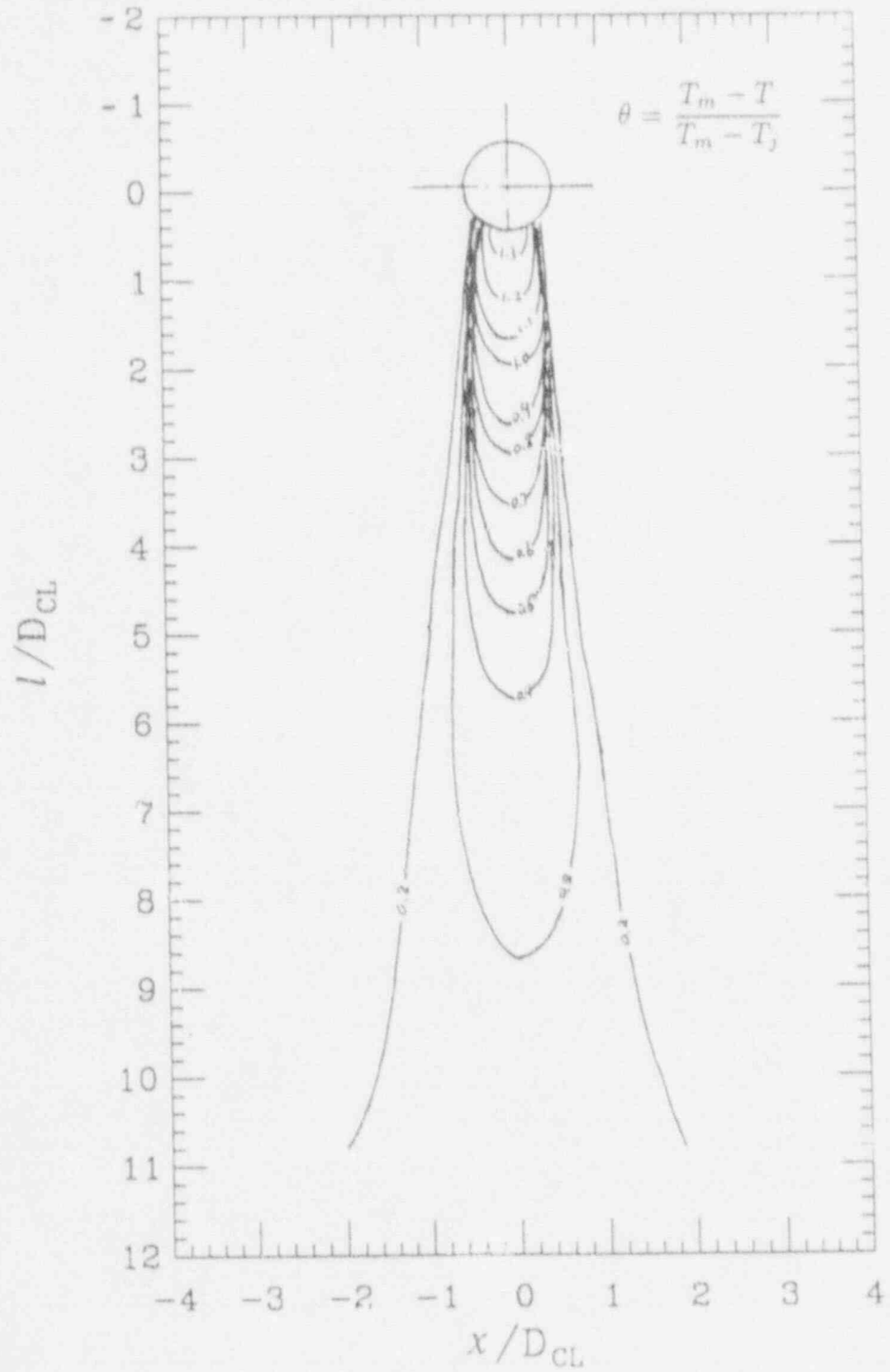

Figure 11. Rough representation of downcomer plume from HDR (test T32.18) data at 420 s.

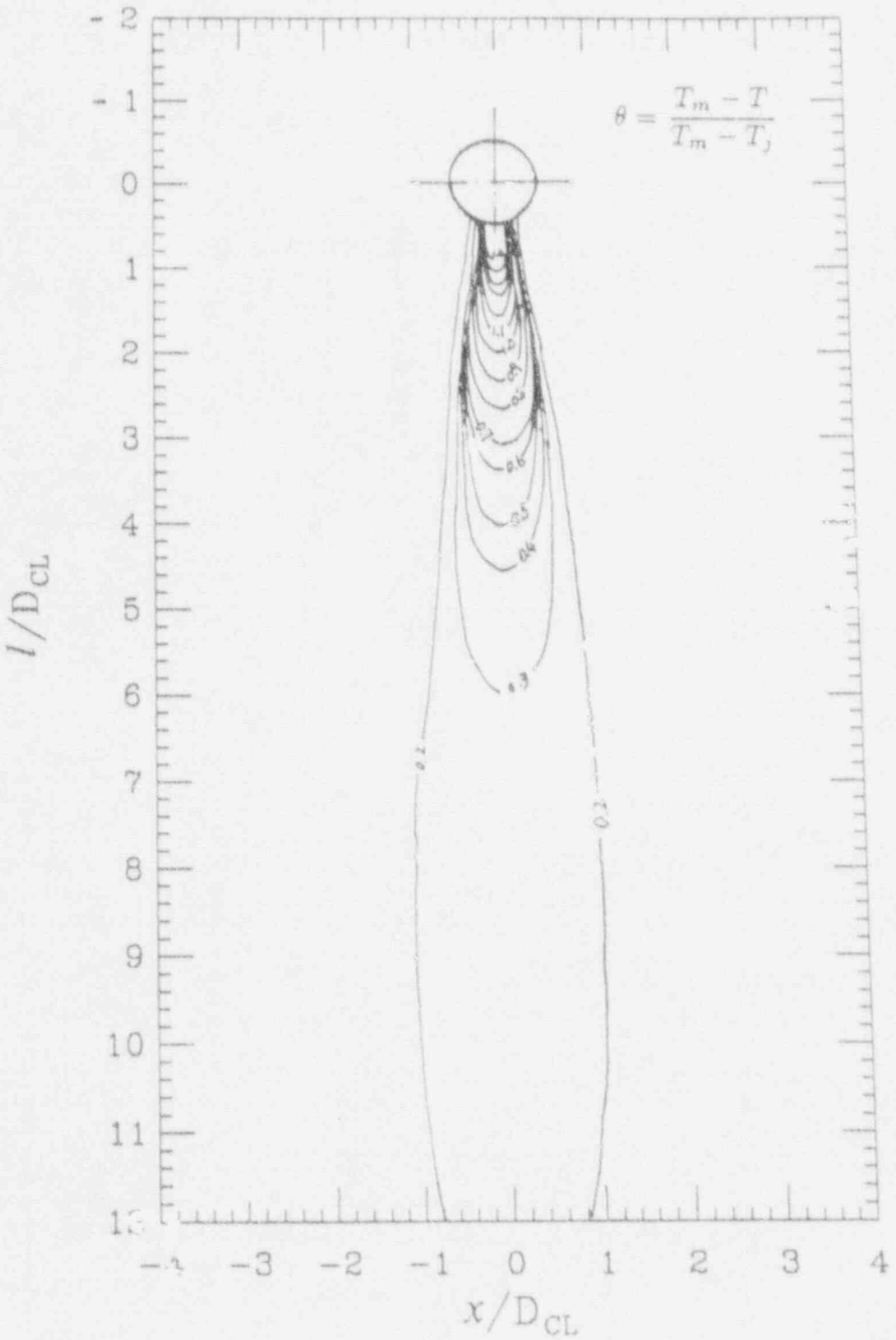

Figure 12. Rough representation of downcomer plume for HDR (test T32.34) data at 420 s.

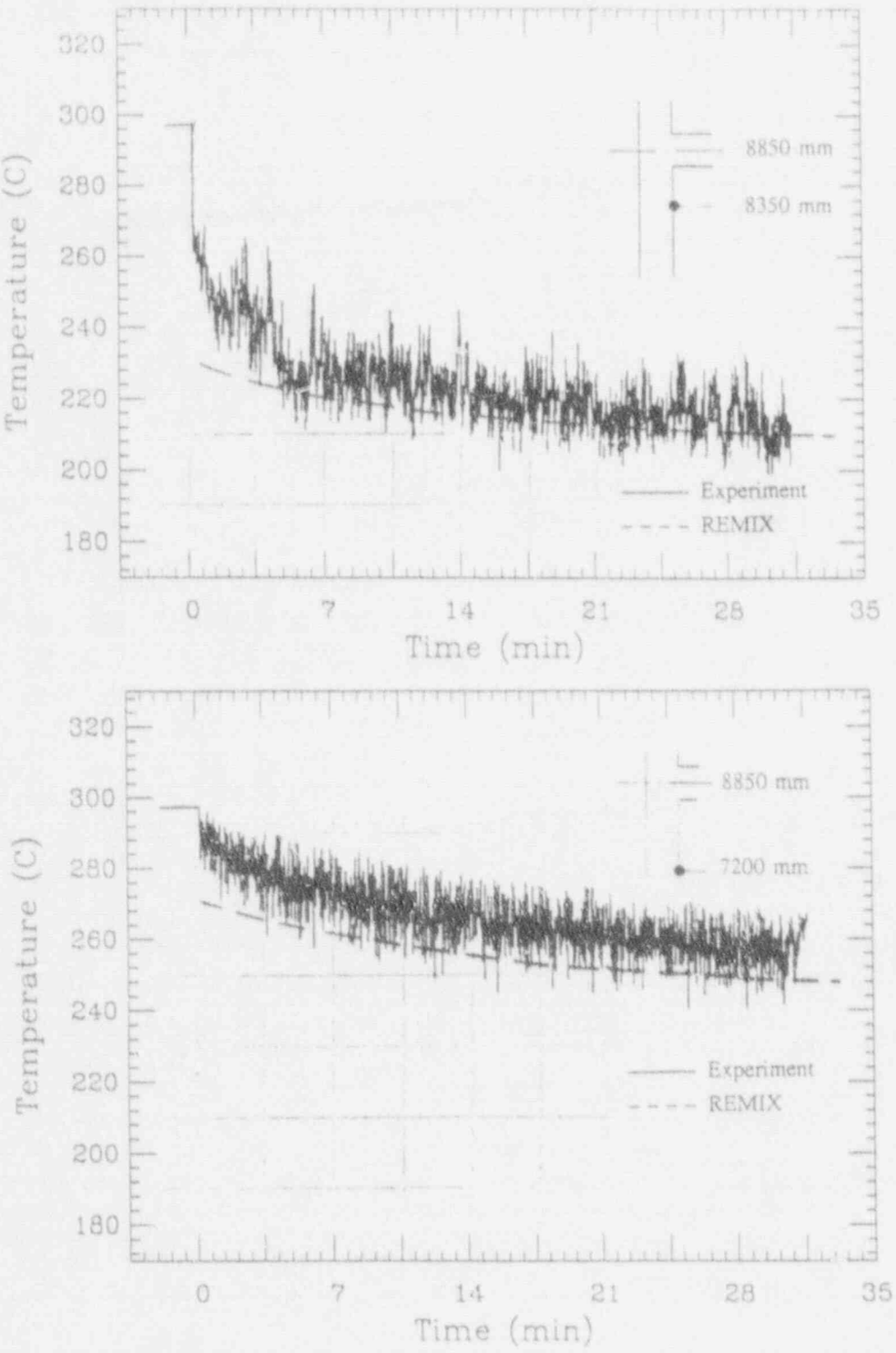

Figure 13. The vessel wall temperature transients measured in HDR (test T32.18) at positions 50 and 165 cm below the cold leg; compared with REMIX predictions.

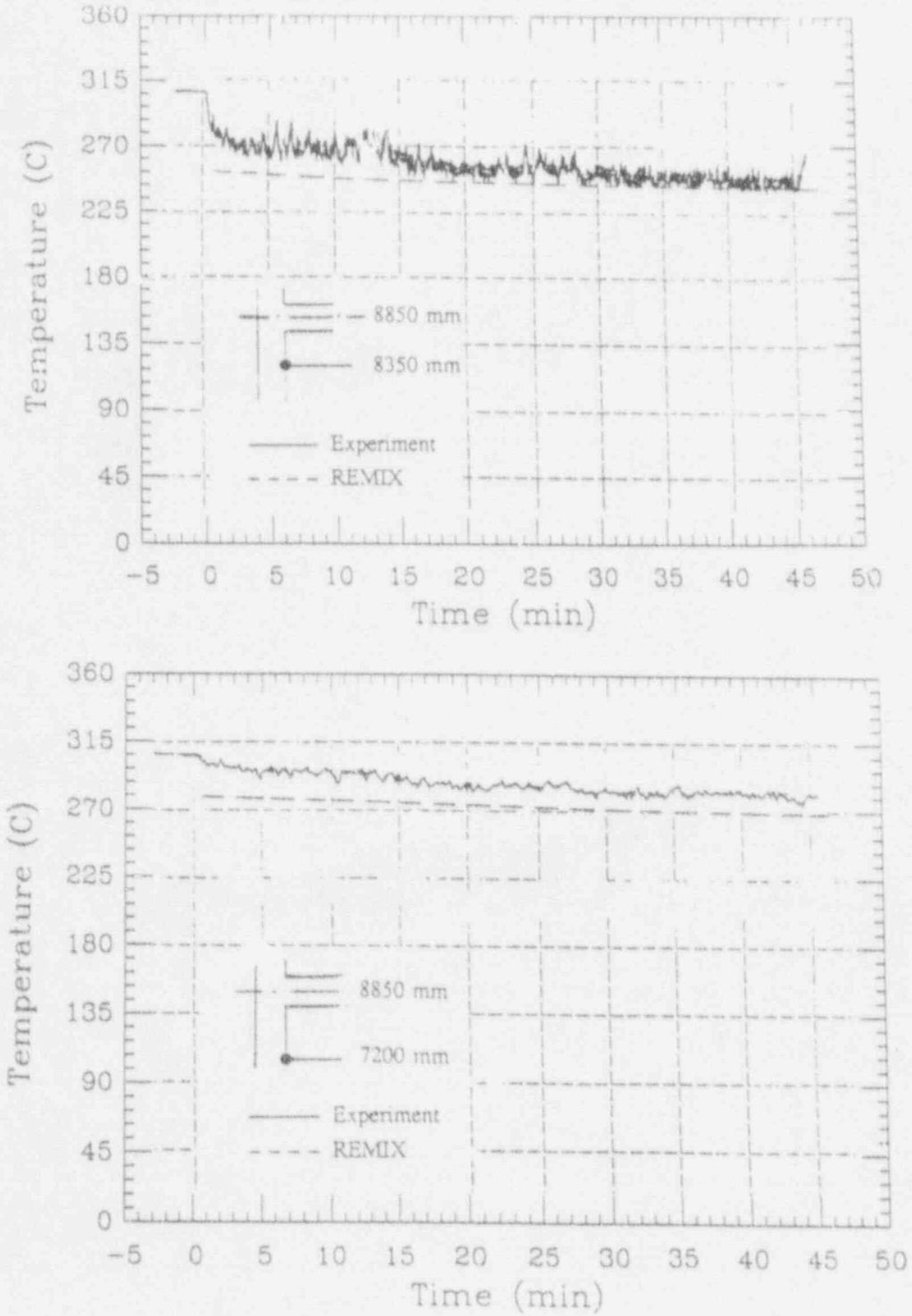

Figure 14. The vessel wall temperature transients measured in HDR (test T32.34) at positions 50 and 165 cm below the cold leg; compared with REMIX predictions.

at least up to 100 s. At this time, the thermal penetration ($\delta \sim 2\sqrt{\alpha t}$) corresponds to 32% of the wall thickness. The full-vessel, cylindrical finite element model is used, below, to compute stresses in the 1D approximation. According to the IPTS procedure, these calculations are based on a global cooldown referred to the $T_j(t)$ transient. Thus, as a matter of nomenclature in the following, 1D results refer to the cylindrical model and 3D results refer to the plate model. Note that the 1D model does not contain the cold-leg "hole." As illustrated in Figure 17, this results in an overprediction of stresses in the immediate vicinity of the "hole."

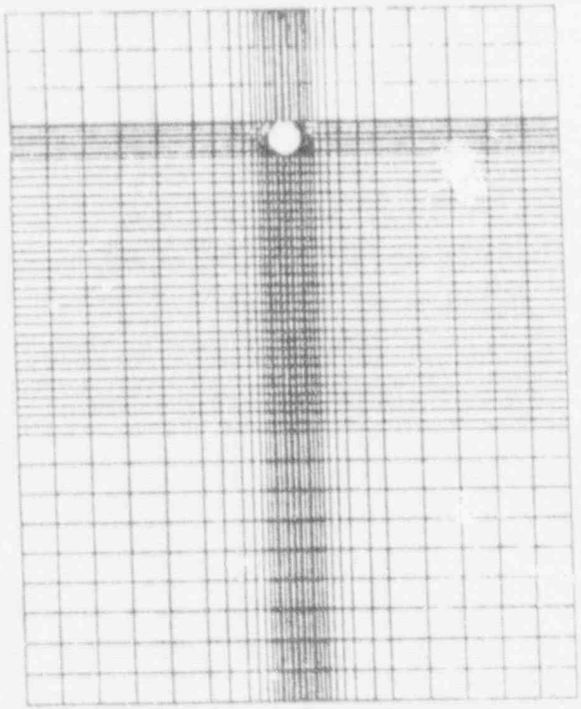

Figure 15. The finite element mesh utilized in the plate (3D) model. There are 7 equal-sized elements along the wall thickness.

A first set of results is contained in Figures 18(a), (b) and (c). All these results are for 7-min transients in HDR test T32.18 (18a), test T32.24 (18b), and a hypothetical Calvert Cliffs transient (18c) run in the manner of the HDR tests, i.e., with only 1 nozzle injection and negligible global cooldown in 7 minutes. For the HDR calculations we used the respective experimental plumes (Figures 11 and 12), while for the reactor example we used the plume of Figure 12. The experimental data from T32.18 are shown in Figure 18a, and are found to be in reasonable agreement with the computations. Note that the error in σ_x is larger than in σ_y. This is attributed to the larger uncertainty in the assessed plume widths (in Figure 11) as compared to their lengths. What is clear from Figure 18 is that the area of non-conservative quantification (for brevity we will call it the "area of non-compliance" or ANC), in the 1D approximation depends not only on plume strengths but also on certain additional parameters. We see that due to the increased strength of T32.18 relative to T32.34 the ANC expands from $\sim 4\ell/D$ to $\sim 5.5\ell/D$. On the other hand, for the reactor case it shrinks to $\sim 2.5\ell/D$ even though a plume similar to T32.34 was used. Otherwise, the distributions are similar and strongly non-uniform, giving the impression that the 1D approximation is truly inappropriate, i.e., either strongly conservative (lower part)

or strongly non-conservative (upper part). A global view of the stress pattern for the cases of Figure 18 is given in Figure 19.

One of the interesting features of the experimental data (Figures 4 and 5) is that stresses vary only very slowly with time. This indicates that they are primarily the consequence of plumes — only slight cooldown in the time period covered — and a mechanism similar to that discussed in analytical terms in the introduction. This behavior is also borne out by the finite element results. This is illustrated in Figure 20 depicting both calculations and data at 14 minutes into the transient. As another example in the other time direction, Figure 21 depicts the stress fields at 1 minute into the hypothetical HDR-like transient in Calvert Cliffs. It is interesting that although the stress levels for very early times are higher overall, the ANC remains relatively unchanged.

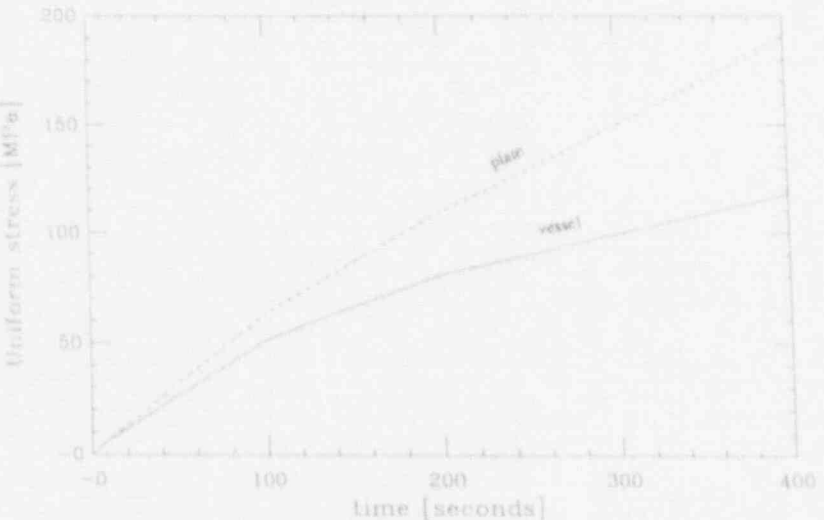

Figure 16. Deviations of the approximate plate model from a cylindrically symmetric full-vessel model as a function of conduction times.

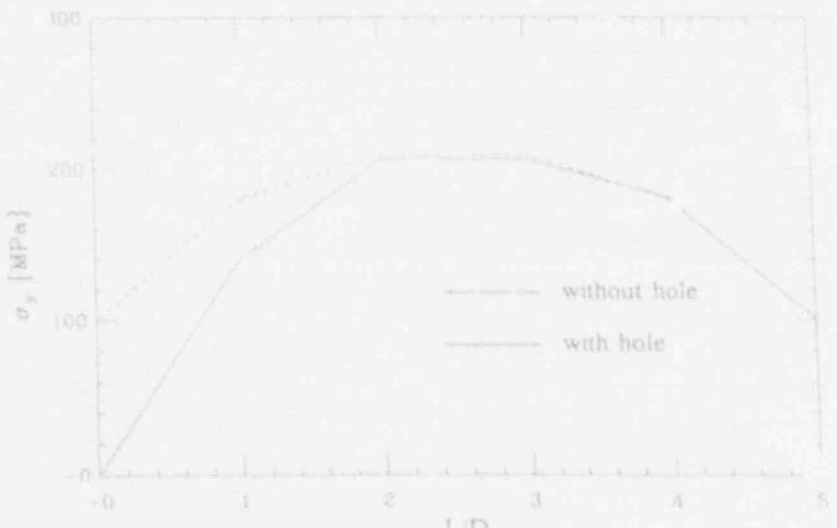

Figure 17. The range of influence of the cold-leg "hole" in the plate model. This sample calculation is for a rectangular plume below the hole of similar size as that in Figure 11, and uniform temperature.

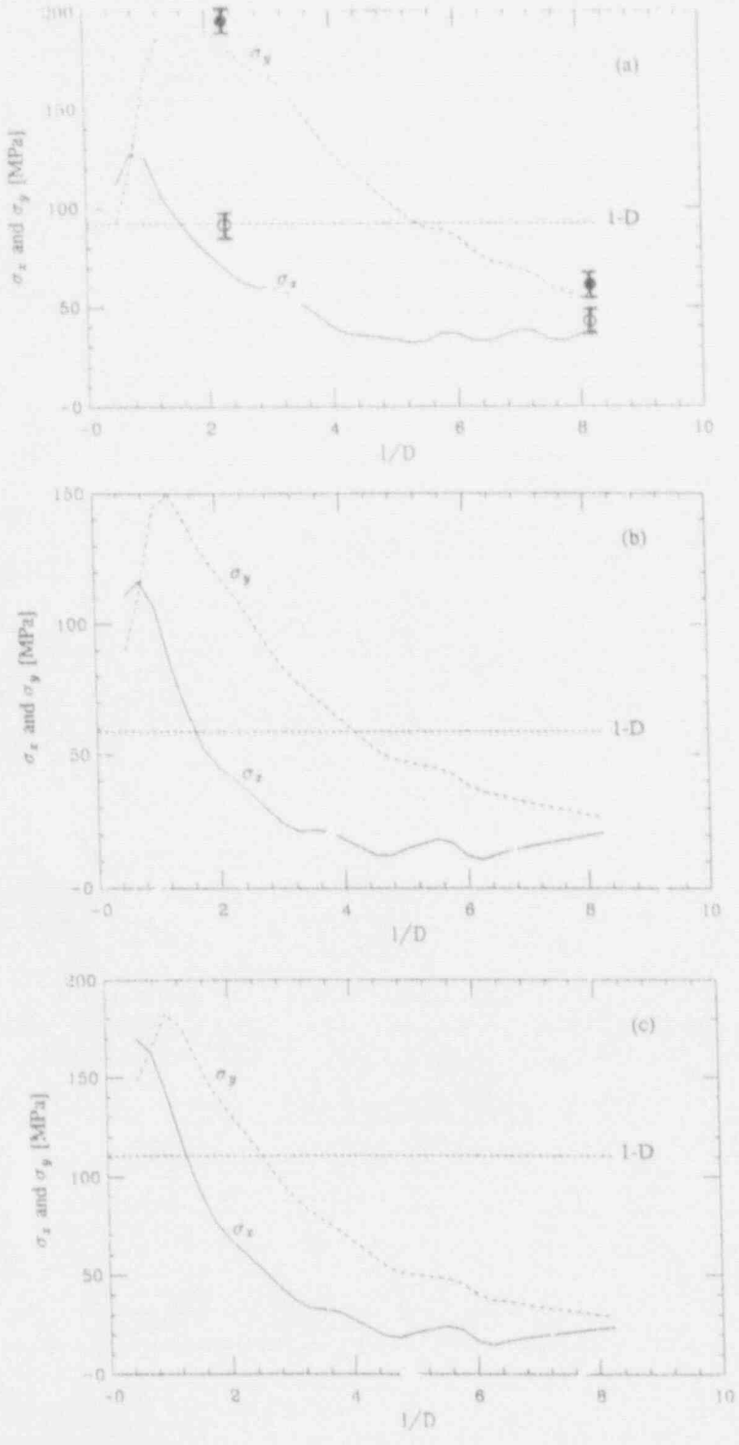

Figure 18. Stress distributions predicted by the plate model compared to the 1D IPTS prescription. (a) HDR test T32.18 at 7 min. (experimental points, ϕ σ_y, ϕ σ_z). (b) HDR test T32.34 at 7 min. (c) Calvert Cliffs geometry with T32.34 conditions (plume, T_m, T_y) at 7 min.

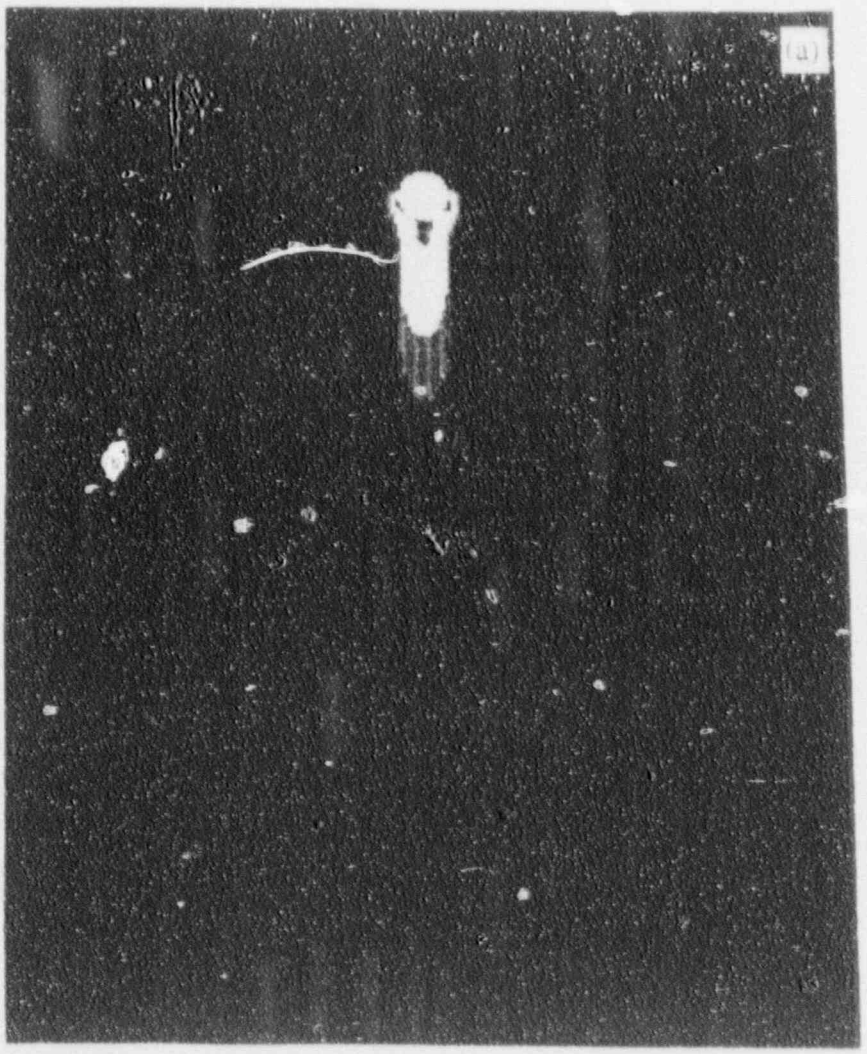

Figure 19. Stress distributions on the inside face of the RPV wall predicted by the plate model cases (a), (b), (c) correspond to those of Figure 18.

Figure 19. Continued.

Figure 19. Continued

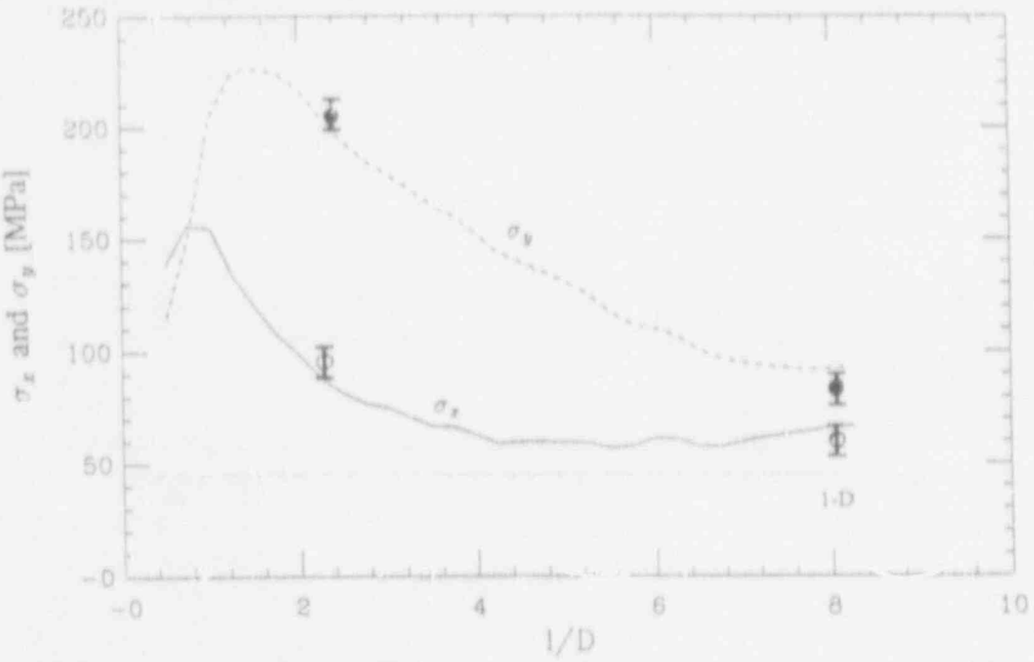

Figure 20. Stress distributions predicted by the plate model compared to the 1D IPTS prescription. HDR test T32.18 at 14 min. (experimental points, ϕ σ_y, ϕ σ_x).

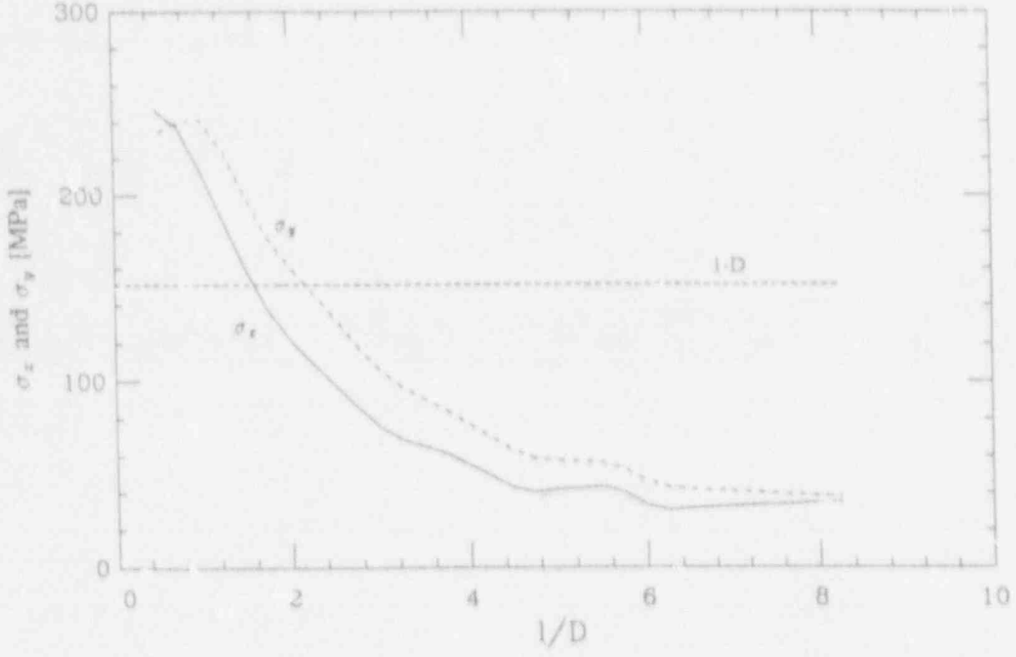

Figure 21. Stress distributions predicted by the plate model compared to the 1D IPTS prescription. Calvert Cliffs geometry with T32.34 conditions (plume, T_m, T_j) at 1 min.

Finally, to assess the role of global cooldown in combination with the plume stresses a representative reactor case was run, with all four HPI nozzles activated. The cooldown and stratification (from REMIX) are those of Figures 2 and 3. The predicted stress distribution at 60 and 100 seconds are shown in Figures 22 and 23, respectively. Note that the ANC is restricted to less than $\sim 2.5\ell/D$ and the real (3D) stress levels as they rise with time yield an increasingly more uniform distribution approaching, in the region of PTS interest, the 1D result. As the core mid-height is typically at $\sim \ell/D$, the region $0 < \ell/D < 2.5$ is comparatively less irradiated and hence of no interest for [illegible] analysis.

4. GENERALIZATION OF RESULTS

The transient conduction/stress problem is characterized by four length scales, the imposed cooldown time and temperature scales, the structural and thermal properties of the wall material, and the time scale for conduction to be limiting (beyond this time the wall surface temperature is essentially equal to the fluid temperature). In the following we discuss each one of these items (in reverse order) for the purpose of deducing the basic scaling criteria for reactor simulations, be they experimental (as in HDR) or analytical (as in those made in this paper).

The time scale, τ_c, for the onset of the conduction-limited regime can be estimated from

$$\tau_c \sim 10\frac{k\rho c_p}{h^2} \tag{10}$$

The heat transfer coefficients in the upper and middle plume regions (these are the regions of higher stresses as seen above) are quite high (Iyer & Theofanous 1991a), with typical values around 5000 W/m^2 K; thus the τ_c is of the order of only 70 s. The role of this extremely short, initial portion of the transient is to moderate the thermal stresses in the wall, and this role is strongly interactive with that of the cladding (both in structural material and thermal resistance). Focusing on the main theme of this paper, we will ignore this role—this is conservative.

The structural and thermal properties of the wall material in HDR are typical of reactor pressure vessels, and there is no need to be included in this scaling analysis. In the analytical simulations we will take them to be fixed at the nominal values utilized for the HDR test comparisons above.

The imposed temperature scale is defined by the initial system temperature, $T_m(0)$, and the "cold" safety injection temperature, T_{HPI}; that is, $T_m(0) - T_{HPI}$. From Equation (9) this overall temperature scale translates to the instantaneous temperature scale, through the system cooldown time constant, τ_s, i.e.,

$$T_m(t) - T_{HPI} = (T_m(0) - T_{HPI})e^{-t/\tau_s} \qquad \tau_s = \frac{V}{Q_{HPI}} \tag{11}$$

or

$$T_m(0) - T_m(t) = (T_m(0) - T_{HPI})(1 - e^{-t/\tau_s}) \tag{12}$$

With reference to Figure 24, this instantaneous temperature scale is seen to control the thermal gradients in the wall material outside the plume. The instantaneous temperature scale within the plume, $T_m(t) - T_j$, can be derived in a similar way from Equation (8)

$$T_m(t) - T_j(t) = \frac{1}{2}\frac{T_m(t) - T_{HPI}}{1 + \tilde{\rho}Q^*} \qquad \tilde{\rho} = \frac{\rho_m}{\rho_{HPI}} \tag{13}$$

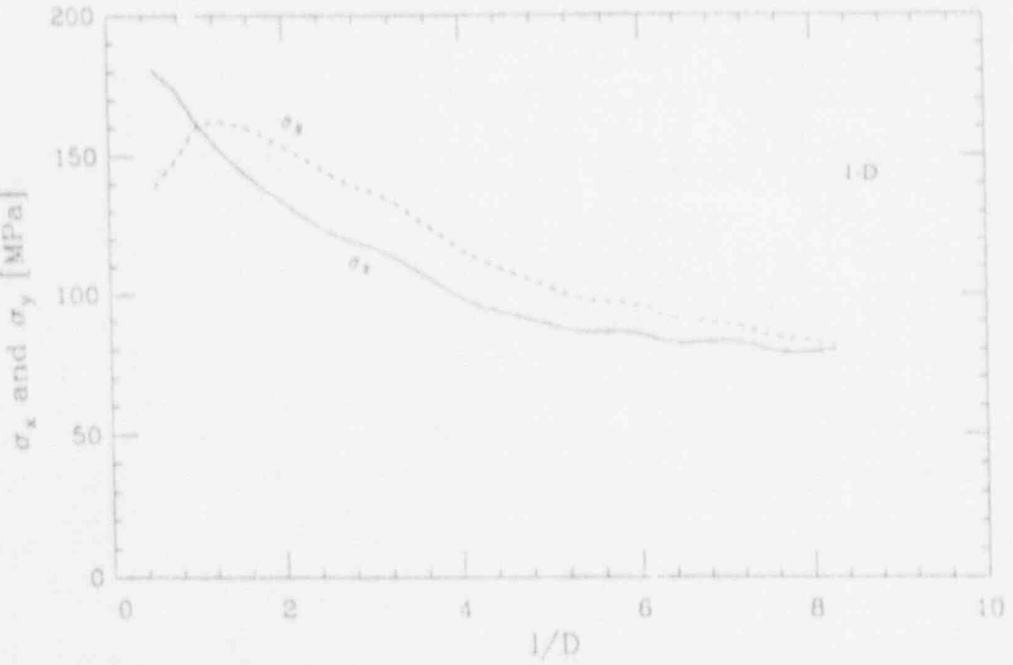

Figure 22. Stress distribution at 60 s for a full (4-nozzle injection) Calvert Cliffs simulation: $Q_{HPI} = 13.5$ kg/s per nozzle, $T_{HPI} = 32$ °C, and $T_m(0) = 277$ °C.

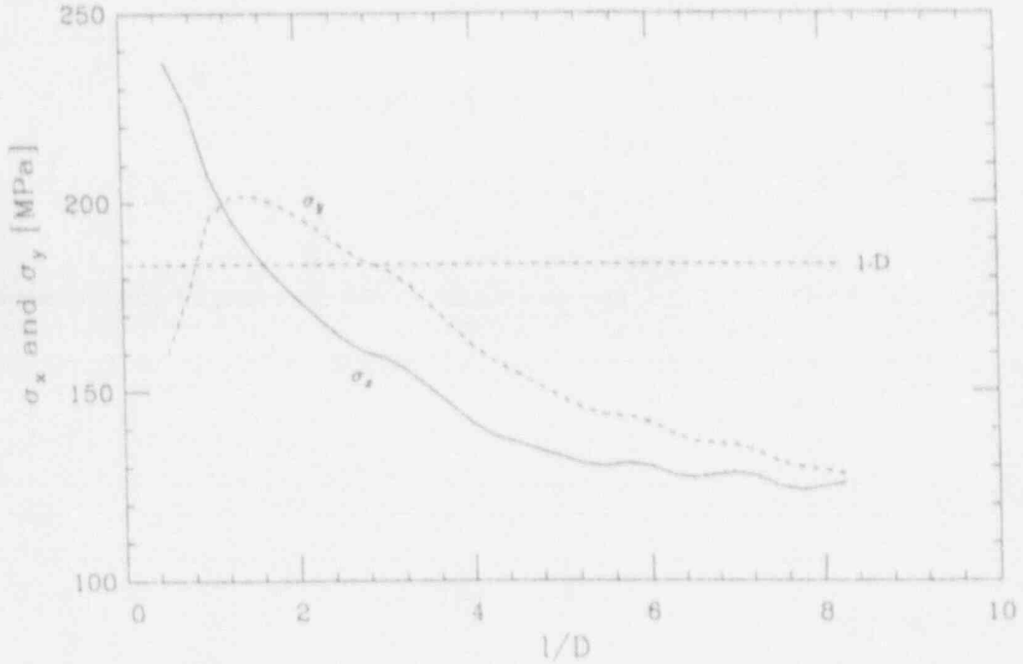

Figure 23. Stress distribution at 100 s for a full (4-nozzle injection) Calvert Cliffs simulation: $Q_{HPI} = 13.5$ kg/s per nozzle, $T_{HPI} = 32$ °C, and $T_m(0) = 277$ °C.

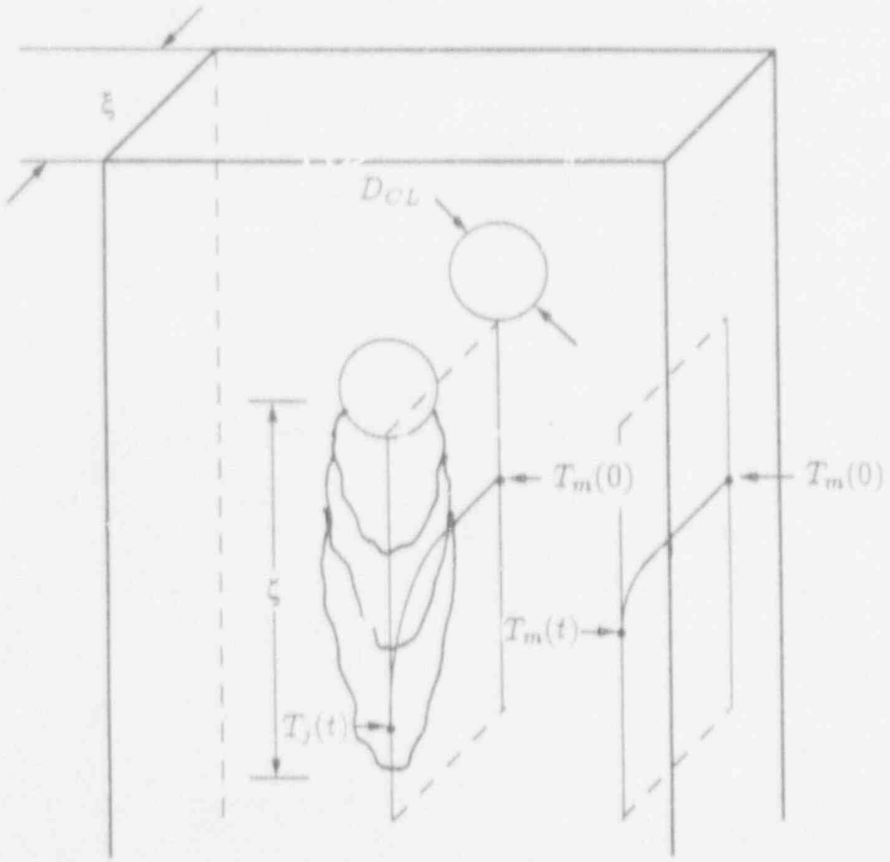

Figure 24. Illustration of thermal gradients and related length scales.

and in combination with Equations (11) and (12) we have

$$T_m(0) - T_j(t) = (T_m(0) - T_{HPI}) \left\{ (1 - e^{-t/\tau_s})^{-1} e^{-t/\tau_s} + 2(1 + \tilde{\rho} Q^*) \right\} \frac{1 - e^{-t/\tau_s}}{2(1 + \tilde{\rho} Q^*)} \quad (14)$$

Again, as seen in Figure 24, this controls the temperature gradients inside the plume region. Now, besides the system time constant, τ_s, we also have the normalized entrainment rate, Q^*, and the density ratio, $\tilde{\rho}$. But already we know that Q^* scales with the Froude number and the injection-to-cold-leg diameter ratio, i.e.,

$$Q^* = Q^*(Fr_{HPI,CL}, D^*) \quad (15)$$

while for the same initial and safety injection temperatures the $\tilde{\rho}$ transient will also scale with the system time constant, τ_s. Moreover, as we have seen, the two-dimensional plume structure can be represented by

$$\theta = \frac{T_m(t) - T(t)}{T_m(t) - T_j(t)} = f(x/D_{CL}, \ell/D_{CL}; Q^*) \quad (16)$$

where the Q^* dependency is weak. Thus we conclude that all internal-instantaneous temperature scales (i.e., those that control the stress-generating gradients) are scaled, on the basis of the overall, imposed, temperature scale, $T_m(0) - T_{HPI}$, through the following dimensionless groups

$$t/\tau_s \,, \qquad Fr_{HPI,CL} \,, \qquad D^* \tag{17}$$

the positional mapping, in the downcomer, being simply on the basis of x/D_{CL} and ℓ/D_{CL}.

Finally, the four length scales (see Figure 24) can be identified as the vessel wall thickness, ξ, the cold leg diameter, D_{CL}, some characteristic scale for the plume elongation, ζ, and the thermal penetration length scale $\sim\sqrt{\alpha t}$. They yield three dimensionless groups:

$$\xi/D_{CL}, \qquad \zeta/D_{CL} \quad \text{and} \quad \xi/\sqrt{\alpha t} \tag{18}$$

The first of these groups can be considered as fixed, the second is only weakly dependent on the plume strength (i.e., $Fr_{HPI,CL}$ and D^*), while the third group plays an essential role in the development of the stress field. It can also be written in terms of the penetration time constant, τ_p, as:

$$\tau_p/t \quad \text{where} \quad \tau_p = \xi^2/\alpha \tag{19}$$

expressing the extent of thermal gradient in the wall at any particular time, t, in the cooldown transient.

From the above, for geometric and Froude number similarity, the whole cooldown/stress problem can be scaled with only two parameters; namely, τ_p/τ_s and τ_p/t.

Regarding the behavior in relation to the τ_p/t group, the plate model, valid only for up to $\tau \sim 100$ s as already discussed, became rather restrictive. Thus a full-vessel, three-dimensional, finite element model was set up as shown in Figure 25. Benchmarking of this model with the measured stresses in HDR was even better than found for the simpler plate model (Figure 26 vs. Figure 18a). This model was then exercised, in conjunction with REMIX predictions of temperature histories applied as boundary conditions on the inside surface of the vessel, to cover a wide range of the τ_p/τ_s and τ_p/t scaling groups developed above. Starting with the Calvert Cliffs characteristics variations in system volume, and transient time were made to cover the range of potential interest in these scaling groups. A listing of all computational runs made is given in Table 4.

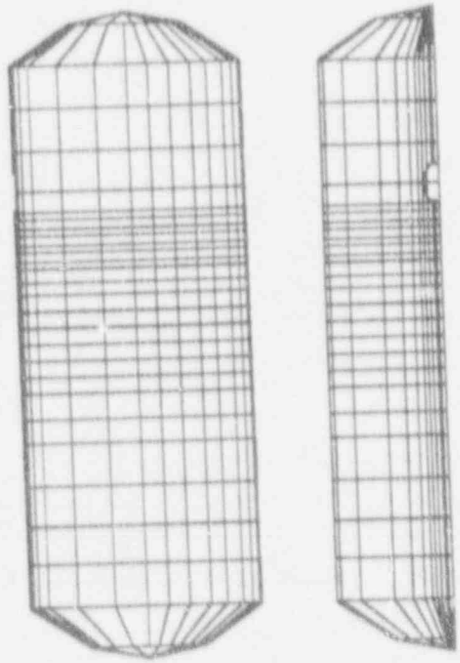

Figure 25. Mesh for full-vessel finite element model.

Qualitatively, the results can be distinguished in three classes, as illustrated in Figures 27(a), (b) and (c). Figure 27(a) represents a strongly non-conservative behavior of the 1D

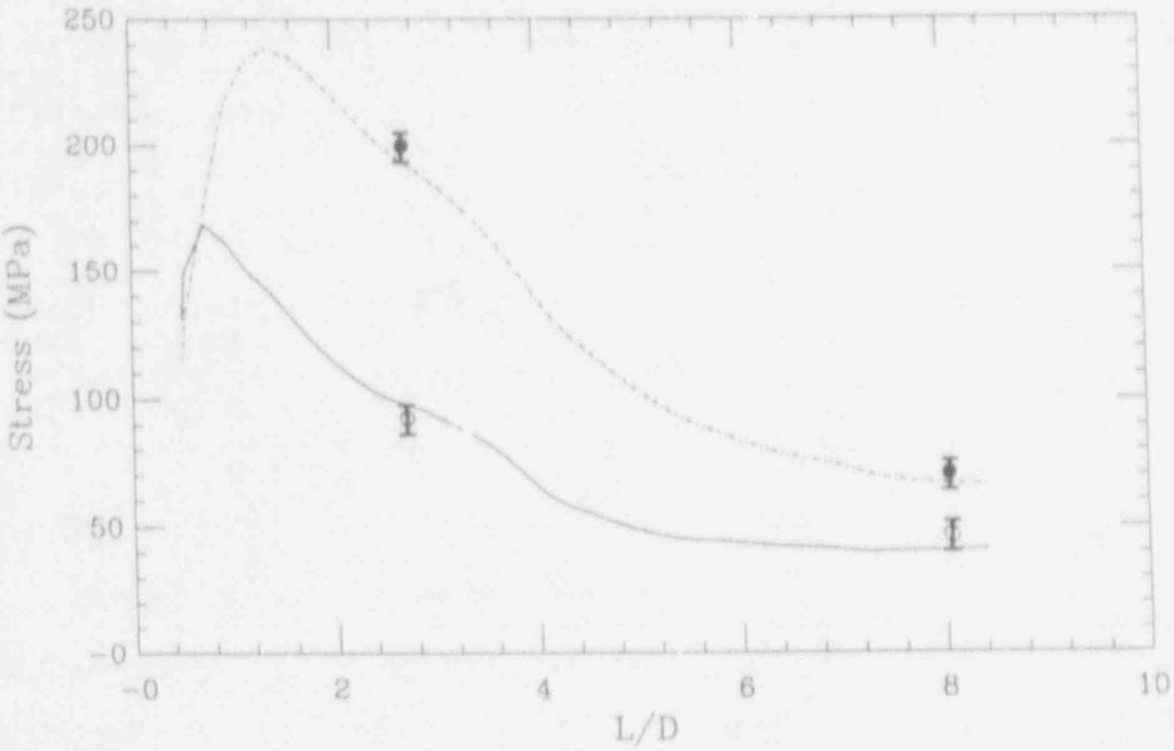

Figure 26. Stress distributions in the HDR wall test T32.18 at t = 7 min. - - - - - predicted σ_y, ϕ measured σ_y, —— predicted σ_x, ϕ measured σ_x.

approximation, Figure 27(b) shows a strongly conservative one, and Figure 27(c) shows a case where the 3D results are very close to the 1D approximation. Quantitatively, the "figures of merit" in assessing the impact of the 1D approximation can be summarized in terms of four parameters:

(a) ANC: The downcomer length (in ℓ/D's) for which the 3D stresses are higher than the 1D

(b) $\Delta_1 = \frac{\sigma_{max} - \sigma_{1D}}{\sigma_{max}} \times 10^2$: A measure of peak discrepancy between the 3D and 1D results

(c) $\Delta_2 = \frac{\sigma_{max} - \sigma(\ell/D=5)}{\sigma_{1D}} \times 10^2$: A measure of the deviation of the 3D result from the flat 1D one, over the upper half of the downcomer

(d) $\Delta_3 = \frac{\sigma_{max} - \sigma(\ell/D=10)}{\sigma_{1D}} \times 10^2$: A measure of the deviation of the 3D results from the flat 1D one, over the whole $10\ell/D$'s of the downcomer

For example, these parameters, for the three comparisons of Figure 26, in the order given above are:

Figure 27(a): $\Delta_1 = 50$, $\Delta_2 = 45$, and $\Delta_3 = 57$

Figure 27(b): $\Delta_1 = 15$, $\Delta_2 = 60$, and $\Delta_3 = 79$

Figure 27(c): $\Delta_1 = 4$, $\Delta_2 = 10$, and $\Delta_3 = 13$

Table 4. List of computational runs

Runs from 2-1 to 2-10 are for Calvert Cliffs reactor.
Others are obtained by varying the system volume only.

Run #	τ_s (s)	τ_p (s)	t	T_m °C	T_j °C
1-1	3572	5095	20	275.0	220.8
1-2	3572	5095	60	272.4	248.0
1-3	3572	5095	120	268.3	244.2
1-4	3572	5095	240	260.7	237.0
1-5	3572	5095	420	250.0	228.0
1-6	3572	5095	600	241.6	218.5
1-7	3572	5095	1200	217.5	195.0
1-8	3572	5095	1800	199.4	177.5
1-9	3572	5095	2400	185.3	163.9
1-10	3572	5095	3000	174.0	152.6
2-1	1324	5095	30	270.9	246.6
2-2	1324	5095	60	265.3	241.3
2-3	1324	5095	120	254.9	231.2
2-4	1324	5095	240	236.7	213.8
2-5	1324	5095	420	214.2	191.8
2-6	1324	5095	600	195.7	174.0
2-7	1324	5095	1200	152.3	131.4
2-8	1324	5095	1800	125.0	107.7
2-9	1324	5095	2400	106.7	92.5
2-10	1324	5095	3000	94.2	81.9
3-1	637	5095	30	265.0	241.0
3-2	637	5095	60	255.0	231.3
3-3	637	5095	120	238.5	215.6
3-4	637	5095	240	213.9	191.5
3-5	637	5095	420	188.6	167.1
3-6	637	5095	600	171.4	150.1
3-7	637	5095	1200	140.2	120.4
3-8	637	5095	1800	126.2	108.7
3-9	637	5095	2400	119.0	102.7
3-10	637	5095	3000	114.9	99.3
4-1	12016	5095	30	276.2	251.6
4-2	12016	5095	60	275.5	215.0
4-3	12016	5095	120	274.2	249.7
4-4	12016	5095	240	271.8	247.4
4-5	12016	5095	420	268.3	244.2
4-6	12016	5095	600	265.0	241.1
4-7	12016	5095	1200	255.3	231.6
4-8	12016	5095	1800	246.8	223.5
4-9	12016	5095	2400	239.3	216.3
4-10	12016	5095	3000	232.5	209.8

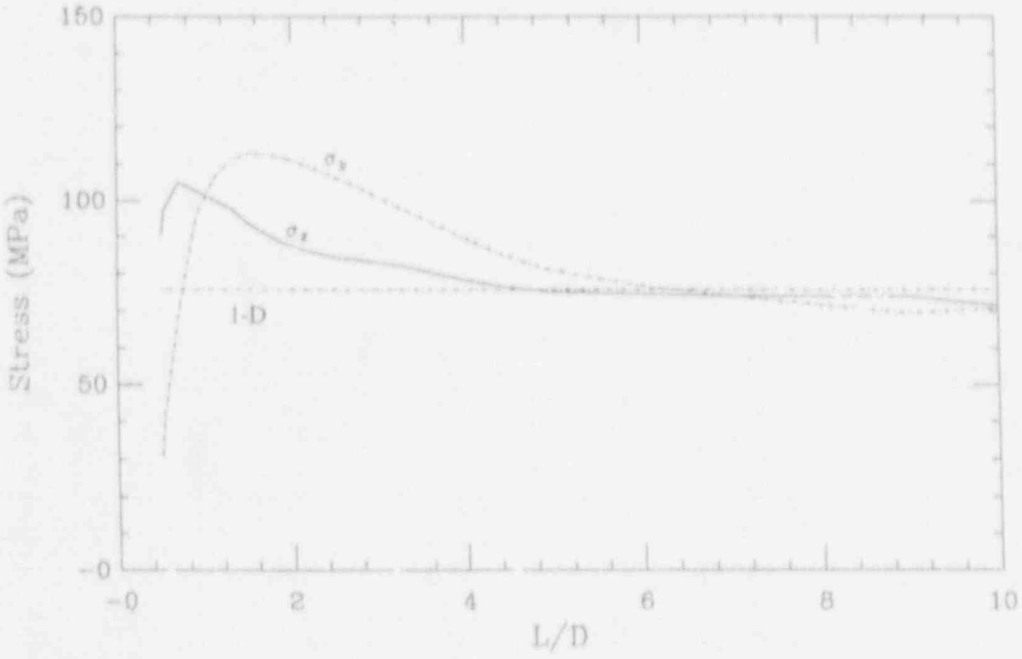

Figure 27(a). Stress distributions predicted by the vessel model compared to the 1D IPTS prescription. $\tau_s = 12016$ s, $\tau_p = 5095$ s and $t = 3000$ s.

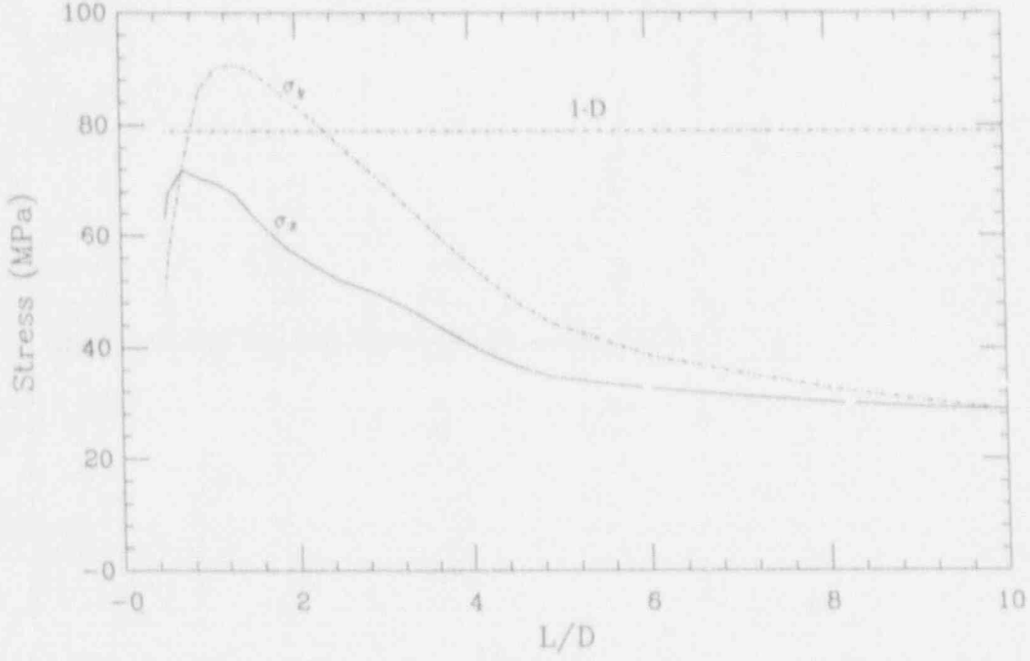

Figure 27(b). Stress distributions predicted by the vessel model compared to the 1D IPTS prescription. $\tau_s = 12016$ s, $\tau_p = 5095$ s and $t = 240$ s.

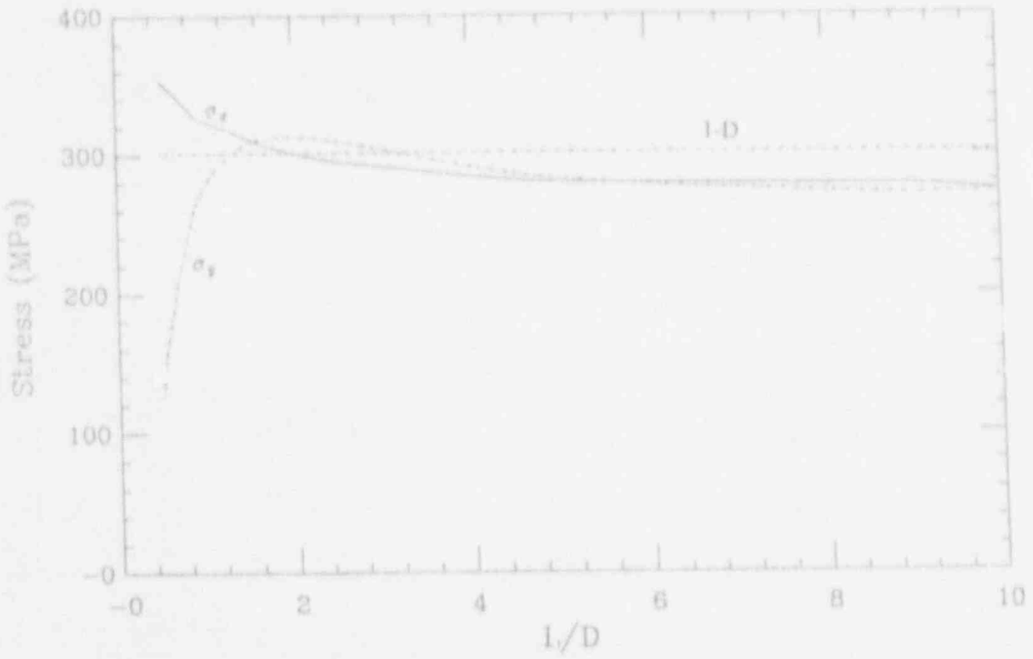

Figure 27(c). Stress distributions predicted by the vessel model compared to the 1D IPTS prescription. $\tau_s = 637$ s, $\tau_p = 5095$ s and $t = 600$ s.

The results from all computational runs are summarized in Figures 28, 29, 30 and 31. From the following explanation of the trends and meaning of these maps, it should become evident how they are to be used for particular applications. Note that for such applications in addition to figuring out the pertinent τ_p and τ_s values one will need to decide the duration of the transient of interest (t) and also the extent of the downcomer area of non-interest (ANI), because of lack of welds, or embrittlement, expressed as ℓ/D's from the cold-leg centerline.

Starting from Figure 28, we first note that the ANC is roughly independent of τ_p/τ_s. As seen in Table 4, for a normal vessel wall τ_p ~5,000 s and for a typical transient of interest t ~2,500 s we are looking at τ_p/t values in the range $2 < \tau_p/t < 100$; thus the ANC is seen to increase with time, getting as large as 4 to 6. Such large values may in fact begin to approach or even exceed the ANI.

Turning now to Figure 29, we note that Δ_1 is strongly dependent on τ_p/τ_s; as τ_p/τ_s increases Δ_1 decreases, approaching zero for $\tau_p/\tau_s \rightarrow 10$. We also see that the τ_p/t dependence has a minimum, going back up again as the τ_p/t decreases below a value of ~10. Typical values for reactors are $\tau_p/\tau_s = 4$. For the HDR test T32.18, $\tau_p/\tau_s = 0.1$; thus the strongly non-conservative trend in Figure 4 can be attributed to the atypically low value of τ_p/τ_s in the HDR. For $\tau_p/\tau_s < 1$, the bahavior expresses a very slow cooldown in relation to conduction across the vessel wall, and as may be expected, the 1D approximation fails completely. In fact, at this limit the behavior is very much like the analytical ellipse results given in the introduction, i.e., high anisotropic stress levels (within the plume) which are much higher than those computed in the 1D approximation. At the other extreme, $\tau_p/\tau_s >> 1$, anisotrophy is strongly disfavored as the rapid (in relation to conduction) global cooldown drags T_j down with it as the transient continues; thus the 1D stress field follows closely that developed in the plume region. To get into the τ_p/τ_s range of lower than 2 for a reactor, the cooldown time constant must be over 2,000 s,

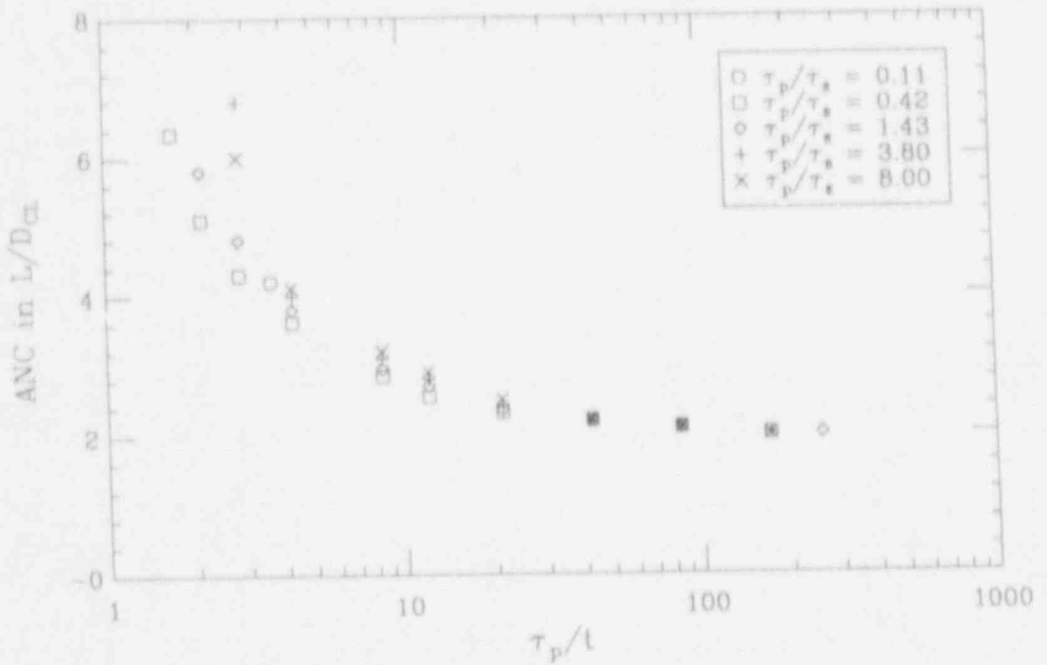

Figure 28. The downcomer length in L/D for which the prediction of the vessel model is higher than the 1D IPTS.

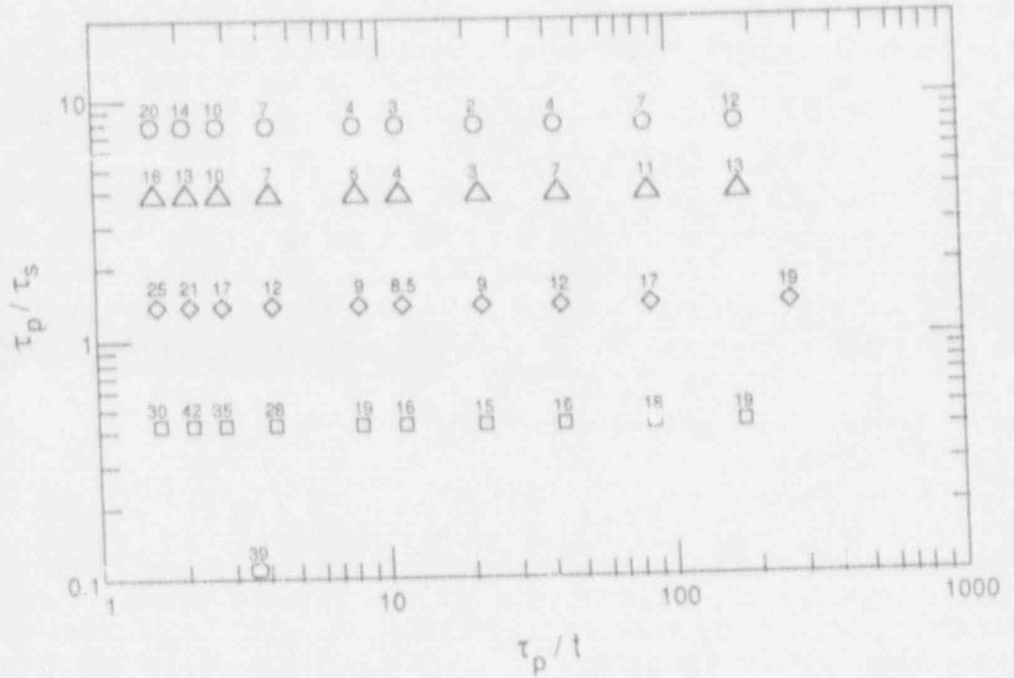

Figure 29. Map showing the extent of peak discrepancy between the 3D and 1D IPTS results.

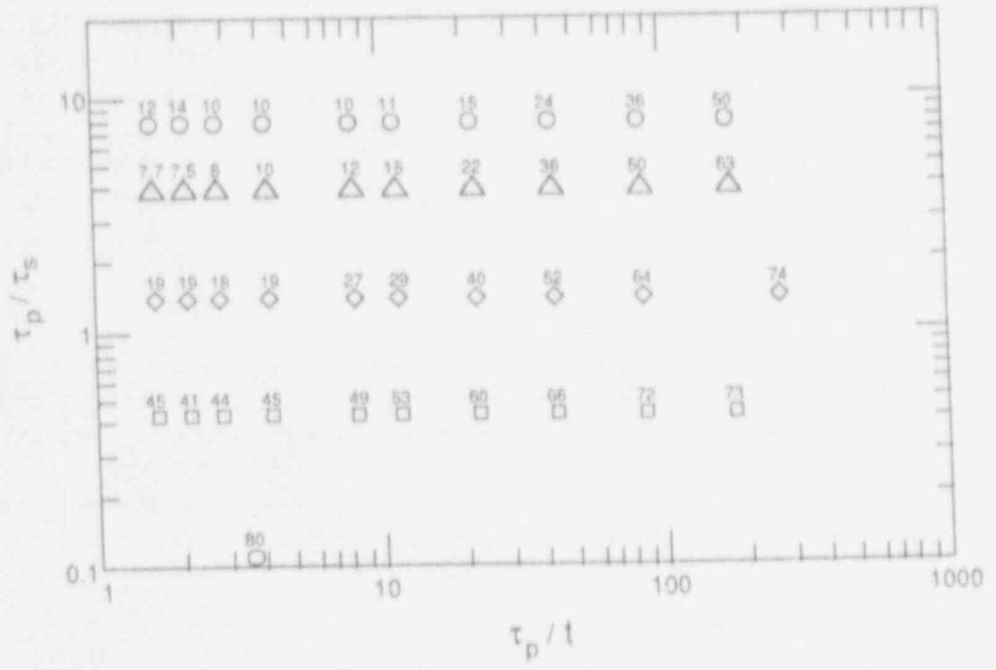

Figure 30. Map showing the deviation of the 3D results from the 1D IPTS one, over the upper half of the downcomer.

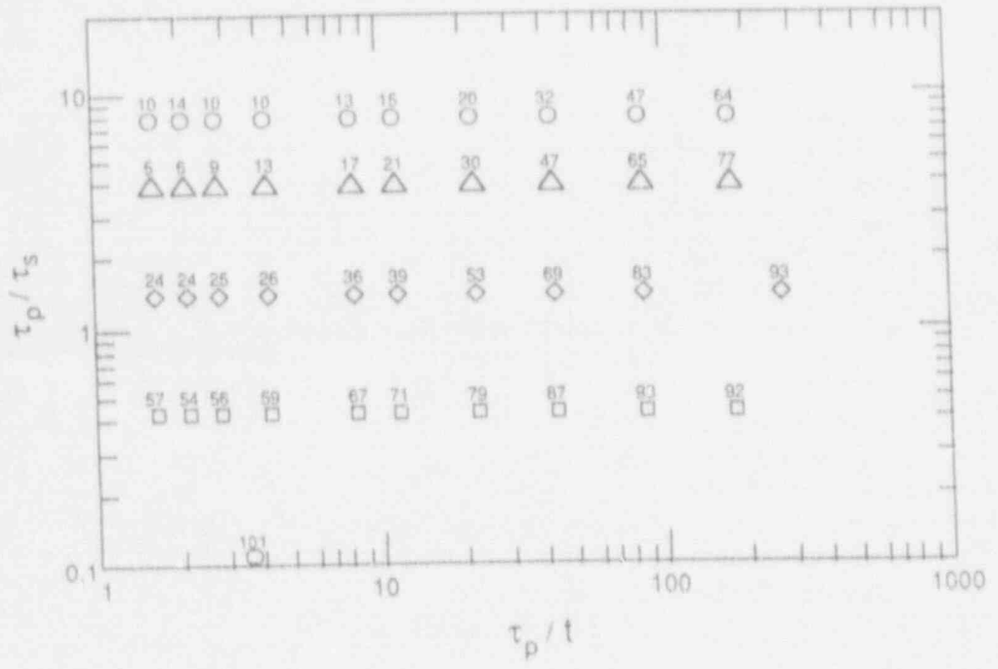

Figure 31. Map showing the deviation of the 3D results from the 1D IPTS one, over the whole 10ℓ/Ds of downcomer.

i.e., the injection rate must be so slow that there would hardly be any plumes! Thus the region of "difficulty" cannot be approached under any circumstances with all HPI nozzles injecting. These trends are exactly analogous for the Δ_2 and Δ_3 indices, as shown in Figures 30 and 31. In a combined use of these figures we note that a large value of Δ_2 or Δ_3 in combination with a small value of Δ_1 means that the 1D approximation is highly conservative for most of the area of the downcomer, while when all Δ_1, Δ_2, Δ_3 are small the actual behavior is very much like 1D (as in Figure 27(c)).

7 CONCLUSIONS

The applicability of the HDR tests to RPV wall stress behavior is shown to be remote in a subtle way. The primary reason for it is the 1-nozzle injection employed in these tests, but also the higher, than appropriate, injection rates contribute. The generalized regime maps together with the universal stratification solutions presented allow an *a priori* assessment of the possible area of difficulty in the 1D IPTS prescription. Also, these maps can be used to predict the general behavior of the 3D stress level on the basis of 1D stress results.

ACKNOWLEDGMENTS

The thermal mixing aspects of this work derive from previous work sponsored by the U.S. Nuclear Regulatory Commission.

NOMENCLATURE

A_i	cross-section area of system component i
a	minor ellipse semiaxis
b	major ellipse semiaxis
c_p	specific heat
D	diameter of cold leg
D^*	$= D_{CL}/D_{HPI}$ diameter ratio
D_i	diameter of fluid stream, or system component i
d^*	$= d_c/D_{CL}$
d_i	depth of fluid stream i
E	Young's modulus
Fr_i	$= U_i\{D_i g\Delta\rho/\rho\}^{-1/2}$, Froude number of stream i
$\mathrm{Fr}_{HPI,CL}$	$= (Q_{HPI}/A_{CL})\left\{gD_{CL}\frac{\Delta\rho}{\rho}\right\}^{-1/2}$, superficial Froude number in the cold leg
g	acceleration due to gravity
h	heat transfer coefficient
k	thermal conductivity
L, ℓ	vertical distance from cold-leg centerline in downcomer toward lower plenum
$\dot{m}_{HPI}$	HPI mass flow rate
Q_i	volumetric flow rate of stream i
Q^*	$= Q_e/Q_{HPI}$ dimensionless entrainment rate
T	temperature
t	time
U_i	velocity of fluid stream i
V	volume of the whole system
x	horizontal distance from the cold-leg centerline in downcomer

NOMENCLATURE (continued)

Greek

α	coefficient of thermal expansion, or thermal diffusivity
β	fraction of entrainment from downcomer side
ΔT	temperature difference
$\Delta\rho$	$\rho_i - \rho_j$ where i,j the two streams to which Fr is referred to
δ	thermal penetration length
ζ	elongation of the plume
θ	$= \frac{T_m - T}{T_m - T_j}$, dimensionless temperature
ξ	thickness of vessel wall
ρ_i	density of the fluid stream i
ρ^*	$= \rho_h / \rho_{HPI}$
$\tilde{\rho}$	$= \rho_m / \rho_{HPI}$
σ	stress
τ	characteristic time scale

Subscripts

c	cold stream, or conduction
CL	cold leg
e	entrainment
HPI	high pressure injection
h	hot stream
j	the position of $2D_{CL}$ from cold leg centerline down into the downcomer
m	well mixed or "ambient"
o	initial
p	thermal penetration
s	system
x	horizontal coordinate
y	vertical coordinate

REFERENCES

1. Cheverton, R.D. & D.G. Ball 1984. "OCA-P, A Deterministic and Probabilistic Fracture-Mechanics Code for Application to Pressure Vessels," NUREG/CR-3618, ORNL-5991, Oak Ridge National Lab.

2. Geiß, M. 1987. "Verification of OCA-P and VISA-II on Behalf of Strains and Stresses Induced During HDR-TEMB Thermal Mixing Tests," *Proc. 9th SMIRT Conf.*, Lausanne, August 1987.

3. Iyer, K. & T.G. Theofanous 1985. "Decay of Buoyancy Driven Stratified Layers with Applications to PTS: Reactor Predictions," *ANS Proceedings 1985 National Heat Transfer Conference*, Denver, CO, August 4–7, 1985, Vol. 1, p. 358, American Nuclear Society (1985). *Nuclear Science & Engineering* **108** 184–197 (1991).

4. Iyer, K., & T.G. Theofanous 1991a. "Decay of Buoyancy Driven Stratified Layers with Applications to Pressurized Thermal Shock: Reactor Predictions," *Nuclear Science & Engineering* **108** 184–197.

5. Iyer, K. & T.G. Theofanous 1991b. "Flooding-Limited Thermal Mixing: The Case of High Froude Injection," *Nuclear Science & Engineering* **108**, 198–207.

6. Neubrech, G.E., G. Katzenmeier & L. Wolf 1988. "Crack Initiation and Crack Growth during Therma' Shock Tests in the Reactor Pressure Vessel of the HDR under Corrosive Medium Conditions," *Int. J. Pres. Ves. & Piping*, **34**, 187-205.

7. Selby, D.L. et al. 1985a. "Pressurized Thermal Shock Evaluation of the Calvert Cliffs, Unit 1 Nuclear Power Plant," NUREG/CR-4022, ORNL/TM-9408, Oak Ridge National Lab.

8. Selby, D.L. et al. 1985b. "Pressurized Thermal Shock Evaluation of the H.B. Robinson Unit 2 Nuclear Power Plant," NUREG/CR-4183, ORNL/TM-956, Oak Ridge National Lab.

9. Theofanous, T.G. & K. Iyer 1987. "Mixing Phenomena of Interest to SBLOCAs," *Nuc. Eng. Des.*, **102**, 91–103.

10. Theofanous, T.G., J.L. La Chance & K.A. Williams 1989. "The Thermal Hydraulics of Small-Break Loss-of-Coolant Accidents Relative to Pressurized Thermal Shock," *Nuclear Science & Engineering* **102**, 74–100.

11. Theofanous, T.G. & H.P. Nourbakhsh 1982. "PWR Downcomer Fluid Temperature Transients Due to High Pressure Injection at Stagnated Loop Flow," *Proc. Joint NRC/ANS Meeting on Basic Thermal Hydraulic Mechanisms in LWR Analysis*, Bethesda, Maryland, Sept. 14–15, 1982, NUREG/CP-0043, 583–613.

12. Theofanous, T.G. & H. Yan 1991. "Interpretation of Thermal Mixing Experiments from One-Fifth to Full Scale," NUREG/CR-5677, U.S. Nuclear Regulatory Commission.

13. Turner, J.S. 1973. **Buoyancy Effects in Fluids**, Cambridge University Press, New York.

LIQUEFACTION INDUCED BY MODERN EARTHQUAKES AS A KEY TO PALEOSEISMICITY: A CASE STUDY OF THE 1988 SAGUENAY EVENT

Martitia Tuttle and Patience Cowie
Lamont-Doherty Geological Observatory
Palisades, New York 10964

Lorraine Wolf[1]
Phillips Laboratory (AFGL)
Earth Sciences Division
Hanscom Air Force Base, Massachusetts 01731

Abstract

Liquefaction features, including sand dikes, sills, and sand-filled craters, that formed at different distances from the epicenter of the 1988 (Mw 5.9) Saguenay earthquake are compared with one another and with older features. Modern liquefaction features decrease in size with increasing distance from the Saguenay epicenter. This relationship suggests that the size of liquefaction features may be used to determine source zones of past earthquakes and to estimate attenuation of seismic energy. Pre-1988 liquefaction features are cross-cut by the 1988 features. Although similar in morphology to the modern features, the pre-1988 features are more weathered and considerably larger in size. The larger pre-1988 features are located in the Ferland area, whereas the smallest pre-1988 feature occurs more than 37 km to the southwest. This spatial distribution of different size features suggests that an unidentified earthquake source zone (in addition to the one that generated the Saguenay earthquake) may exist in the Laurentide-Saguenay region. Structural relationships of the liquefaction features indicate that one, possibly two, earthquakes induced liquefaction in the region prior to 1988. The age of only one pre-1988 feature is well-constrained at 340 ± 70 radiocarbon years BP. If the 1663 earthquake was responsible for the formation of this feature, this event may have been centered in the Laurentide-Saguenay region rather than in the Charlevoix seismic zone.

Introduction

The Saguenay earthquake (mb 5.9, Mw 5.9) occurred on November 25, 1988, at a depth of 29 km beneath the Laurentide Mountains of Quebec Province, between the Saguenay River graben and the St. Lawrence River rift system (Figure

[1] Currently at the National Research Council, Board of Earth Sciences, 2101 Constitution Avenue, Washington, DC 20418

1; North et al., 1989). In the past 70 years, the Laurentide-Saguenay region has experienced only a few small earthquakes, and therefore, was thought to be relatively aseismic. In contrast, the Charlevoix seismic zone, located about 80 km southeast of the 1988 epicenter, has been very active during the period of instrumental seismic monitoring. Because of recent activity, the Charlevoix seismic zone has been thought to be the source of several other large historic earthquakes including the 1534, 1663, 1791, 1860, 1870, and 1925 (mb 6.7, Mw 6.8) events. The occurrence of the Saguenay earthquake in the Laurentide-Saguenay region, however, raises the possibility that some of these historic events may have occurred in this region instead of the Charlevoix area. The occurrence of the Saguenay earthquake in an "aseismic" region suggests that the pattern of recent and historic seismicity may not delineate all potential earthquake sources and underscores the need for paleoseismic techniques to help define seismic hazard in eastern North America.

During the past twenty years, liquefaction features preserved in Quaternary sediments have been used to expand the earthquake record in the eastern United States into the prehistoric past (e.g., Obermeier et al., 1990, 1991; Amick and Gelinas, 1991; and Tuttle and Seeber, 1991). These studies have relied on examples of liquefaction features that formed during historic earthquakes of uncertain location and magnitude. Unlike these previous events, the 1988 Saguenay, Quebec, earthquake has provided a unique opportunity in eastern North America to study modern liquefaction features that formed during a well-recorded earthquake of known magnitude and location.

The 1988 Saguenay earthquake induced liquefaction at seven known sites in the Laurentide-Saguenay region (Figure 1). Six of these sites are located in the sparsely populated Ferland-Boilleau valley 25 to 30 km northeast of the epicenter (or 38 and 41 km from the hypocenter). These sites were documented within six months of the earthquake (Tuttle et al., 1989, 1990). The seventh site is located about 11 km west of the epicenter and was discovered in September 1991 during reconnaissance in the uninhabited epicentral area. During the 1991 reconnaissance, no evidence of liquefaction was found between Ferland and the epicenter even though more than 20 km of terrain, similar to that where liquefaction occurred in Ferland, was searched. In this paper, characteristics of liquefaction features that formed during the Saguenay earthquake are documented. In addition, liquefaction features that formed during past earthquake(s) are compared with modern features. These findings are especially relevant for paleoseismic studies in glaciated areas. Because many types of soft-sediment deformation structures not related to earthquakes occur in glacial sediments, it is often difficult to distinguish earthquake-induced liquefaction features from structures of other origins (Coates, 1975; Thorson et al., 1986; and Schafer et al., 1987).

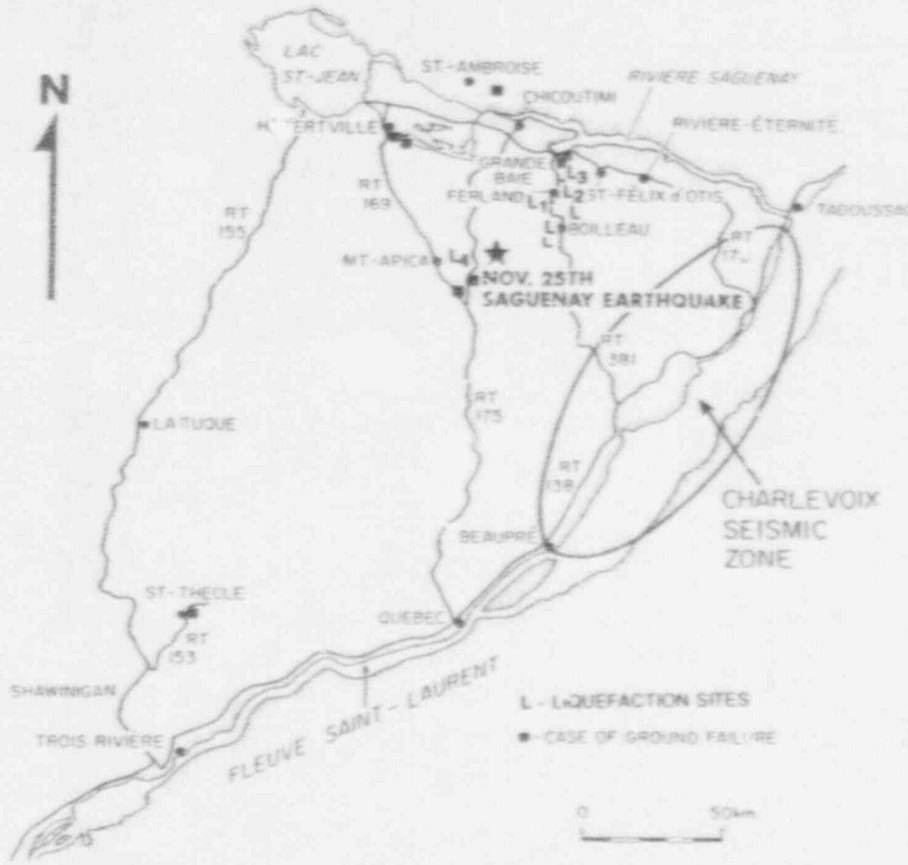

Figure 1. The November 25, 1988 Saguenay earthquake occurred in the Laurentide Mountains of Quebec Province between the Saguenay River Graben and the St. Lawrence River Rift System. Liquefaction occurred between 25 to 30 km northeast of the epicenter in the Ferland-Boilleau valley and also about 11 km west of the epicenter. In sharp contrast to the active Charlevoix Seismic zone located between 60 and 120 km southeast of the Saguenay earthquake, the Laurentide-Saguenay region was thought to be relatively aseismic. Study sites are denoted by L# and other liquefaction sites by L.

Liquefaction Features In the Meizoseismal Area of the Saguenay Earthquake

Liquefaction of subsurface sediments during the Saguenay earthquake was manifested at the surface as sand boils and ground cracks. Ground cracks ranged up to 20 m in length and exhibited about 1 to 3 cm of separation. Sand boil deposits were flat to slightly convex in section, circular to elliptical in plan view, and range in size from a few centimeters to 16 meters across. Homes at several sites of liquefaction were damaged as a result of differential settlement of their foundations (Tuttle et al., 1989).

Since the Saguenay earthquake, seven sand boils at four different sites have been excavated and liquefaction features, both young and old, have been documented. In this paper, features observed below sand boils at three liquefaction sites are discussed in order of decreasing distance from the epicenter of the Saguenay earthquake. Sites 3 and 1 are located 30 and 26 km northeast of the epicenter, respectively, in the community of Ferland; Site 4 is located 11 km west of the epicenter in the Laurentide Park. Site and sand boil designations as they appear in other papers and reports are maintained for consistency.

Liquefaction features 30 km from Saguenay earthquake epicenter: Site 3

Site 3 is located on the modern floodplain of Rivière des Ha! Ha! (Figure 2). Seven sand boils occurred in the mapped area (Figure 3), and at least four more formed elsewhere on the floodplain. Sand boil G formed in a swale or cut-off channel about 140 m west of Rivière des Ha! Ha! (Figure 3). This sand boil deposit is 10 m long and 5 m wide and ranges up to 10 cm in thickness. Within the organic-rich topsoil, the 1 to 3 cm wide feeder dike splits to form other smaller dikes and sills, which commonly follow surfaces of woody material (Figure 4). The feeder dike could be traced through the sandy and pebbly subsoil to a depth of 1.2 m, where the water-table was encountered. No evidence of previous liquefaction events was observed in excavations of this sand boil, probably because sediments within this active cut-off channel are fairly young.

Sand boil J is 10 m in length and 5 m in width and formed on a point bar deposit about 30 m west of Rivière des Ha! Ha! (Figure 3). The deposit of vented material was 9 cm thick and ranged in grain-size from fine sand along its base to silty, very fine sand near the surface. Several small dikes, less than 1 cm in width, could be traced downward from the vented deposit through the soil (Figure 5). Within 0.2 m of the surface, two of these dikes joined, forming one continuous U-shaped dike. This dike was connected to a more steeply dipping dike below, which cross-cuts a wider and weathered dike about 0.25 m below the surface. Two other modern dikes intersected another branch of the same weathered intrusion between 0.75 and 1 m depth. These dikes had clearly been emplaced along the margin of, as well as within, the more weathered and older structure.

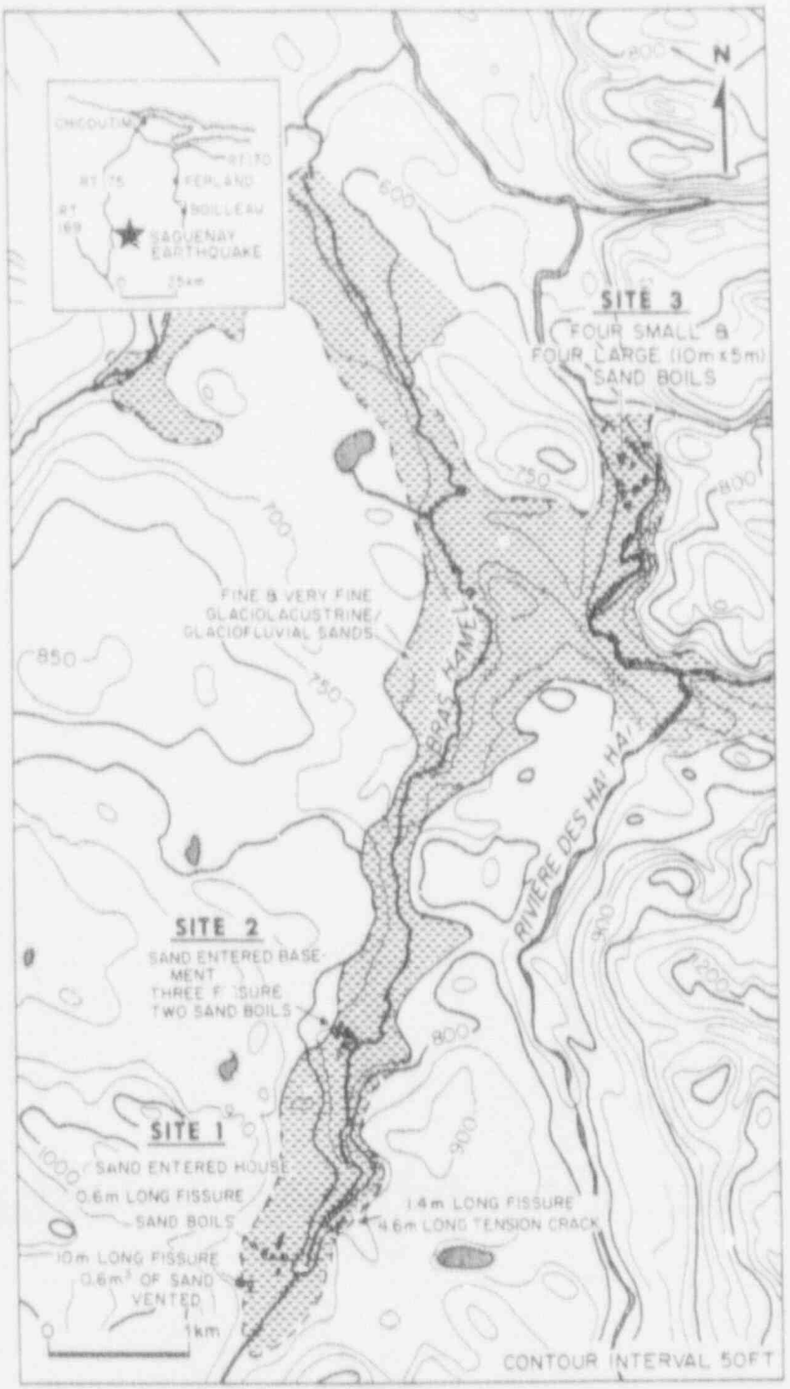

Figure 2. Topographic map of the Ferland area showing the locations of the three study sites and the distribution of a glaciolacustrine deposit thought to have liquefied during the 1988 Saguenay earthquake.

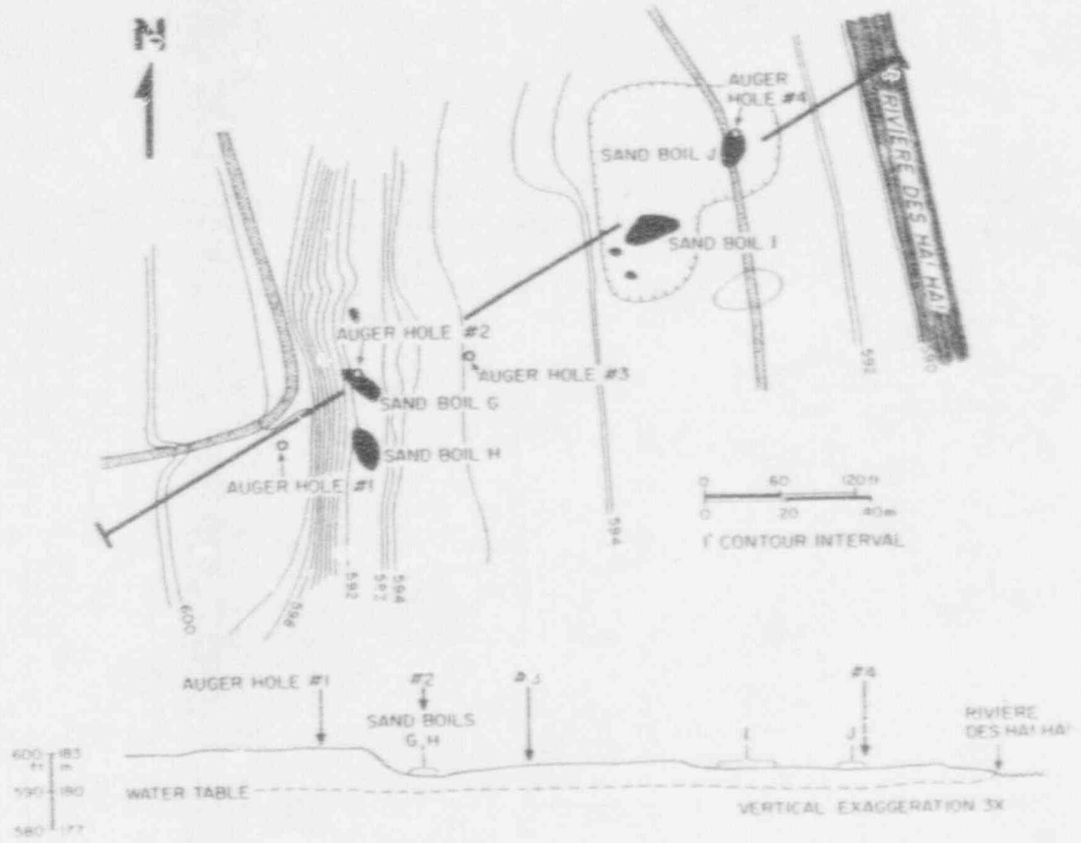

Figure 3. Topographic map and profile of Site 3, 30 km from the epicenter of the 1988 Saguenay earthquake. This site is located along the western bank of Rivière des Ha! Ha!. Eleven sand boils formed in low-lying areas on a river terrace, seven of which are located in the mapped area and are indicated by shading.

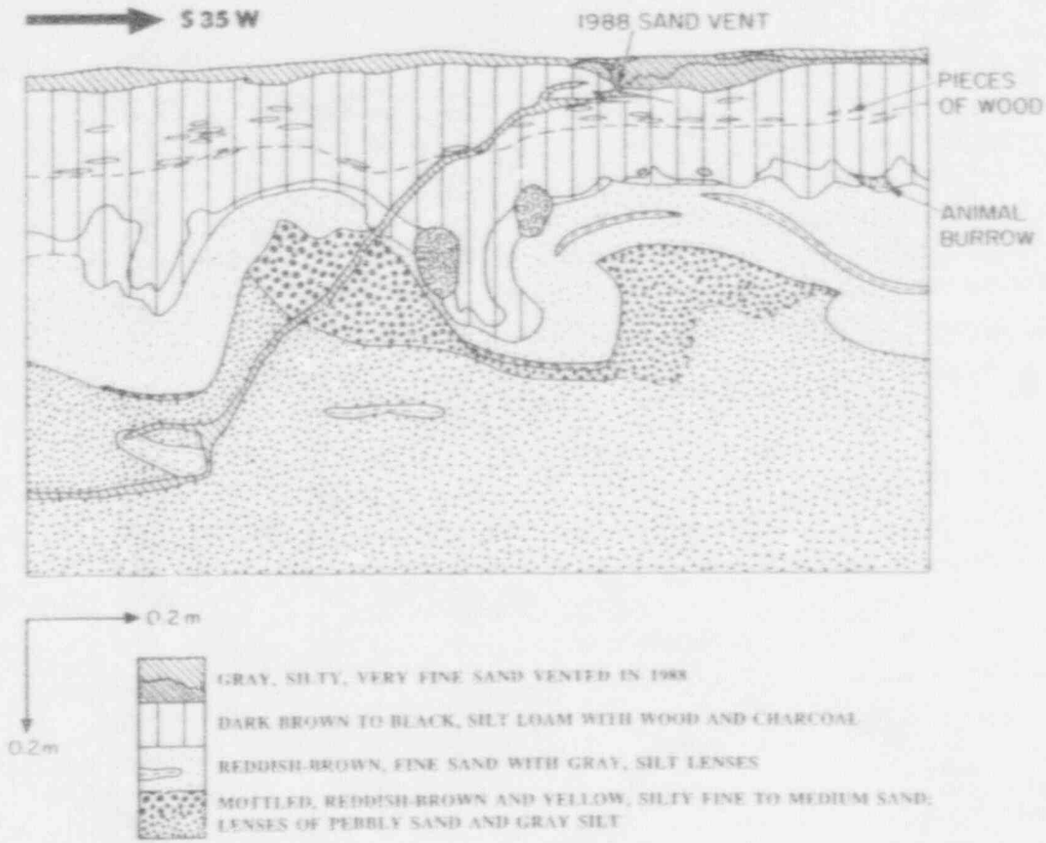

Figure 4. Diagram of excavation across the northwestern end of sand boil G. The feeder dike of this sand boil cross-cuts the coarse-grained subsoil and organic-rich topsoil to form only a narrow vent at the surface. The topsoil is the dark-colored surface soil or A horizon and is represented by the widely spaced, vertically lined pattern. No evidence of previous liquefaction events were present in any of the trenches in sand boils G and H. Deformation structures including paired lobes of topsoil and diapirs of subsoil are probably due to mixing of the soil combined with a small component of downslope movement as the result of freezing and thawing.

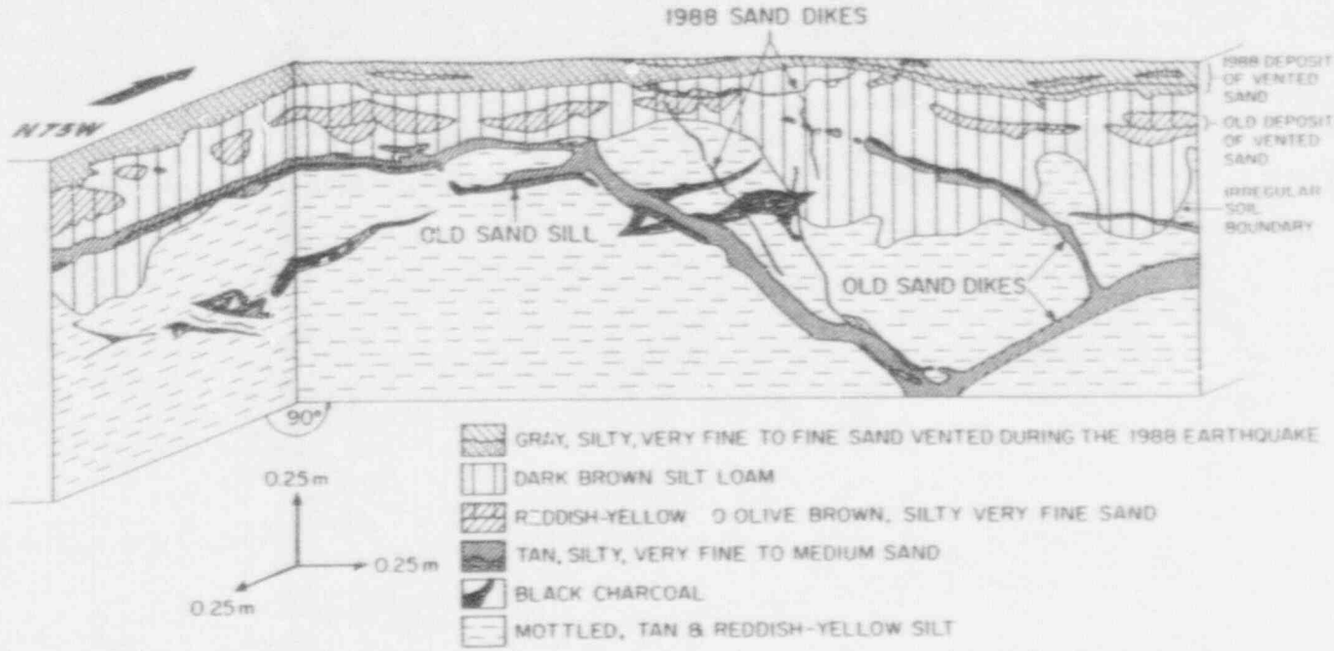

Figure 5. Diagram of trench excavated across the eastern margin of sand boil J which formed on a terrace 30 m from Rivière des Ha! Ha!. Small sand dikes, less than 1 cm in width, could be traced downward from the 1988 sand boil deposit through the topsoil where they cross-cut a large, weathered sand dike and into the subsoil where they joined another weathered dike. The two weathered dikes were two branches of a pre-1988 liquefaction feature. Sand and water that liquefied during the 1988 earthquake appear to have been injected along this old feature. One of the old dikes fed sills below and along the base of the topsoil. Lenses of weathered sand within the topsoil may represent vents and sand boil deposit that formed at the same time as the old dikes and sills.

The main feeder dike of the older structure below sand boil J was observed in the bottom of the excavation and branched up-section to form several smaller dikes (Figure 5). In contrast to the 1-cm-wide sand dikes that formed in 1988, these older dikes ranged up to 8 cm in width. One of these dikes formed sills below and along the base of the silty loam topsoil. Partitioning of fine- and coarse-grained fractions, similar to that in a 1988 sand dike at Site 1, was evident in the old dikes and sills. In addition, discontinuous lenses of weathered, silty, very fine sand occurred within the silty loam topsoil. These lenses are interpreted to be thicker portions of an old sand boil deposit that has since been buried and subjected to soil forming processes.

In several instances, near-surface dikes observed at Site 3 exhibited U-shaped morphology. Similar U-shaped, sand-filled dikes that occur in the meizoseismal area of the 1886 Charleston, South Carolina, earthquake have been identified as incipient sand-blow craters (Obermeier et al., 1990). The similarity of the U-shaped dikes in Ferland with those in the Charleston area is striking. If the upward hydraulic force had been greater at this site in 1988, then perhaps larger sand-filled craters similar to those at Site 1 would have formed.

The upper 1 m of soil below sand boils G and J, is intensely deformed (Figures 4 and 5). Lobes of the topsoil extend down into the subsoil. These lobes are coupled with asymmetrical diapirs of the subsoil. The lower part of the lobes appear to have been slightly folded in a direction away from the river. Vergence of the structures is consistent with downslope movement of the topsoil over the subsoil. Features similar to these referred to as plications have been attributed to congellipedoturbation or to the mixing of soils by freezing and thawing (Bryan, 1946; Hole, 1961; Buol et al., 1973). Given the cold continental climate of Quebec, this seems to be a reasonable mechanism for the formation of these structures. The organic-rich topsoil is not likely to liquefy itself, and liquefaction of the subsoil would probably result in fissuring and brecciation of the topsoil as occurred during the 1988 earthquake.

Subsurface data from augering at Site 3 show that a coarse-grained deposit comprised of fining-upward sequences of cobbles, pebbles, and sand is underlain by a fine-grained deposit of gray, laminated silt and sand (Figure 6). There is a sharp boundary between the two deposits. The fine-grained material was probably deposited in a late Pleistocene lake and subsequently buried by coarse-grained deposits of the Rivière des Ha! Ha! (LaSalle, 1968; Rondot, 1979). An especially loose, sandy layer was encountered within the glaciolacustrine deposit at about 3.5 m depth below sand boils G and J. This layer is identified as the probable source of the 1988 vented sand.

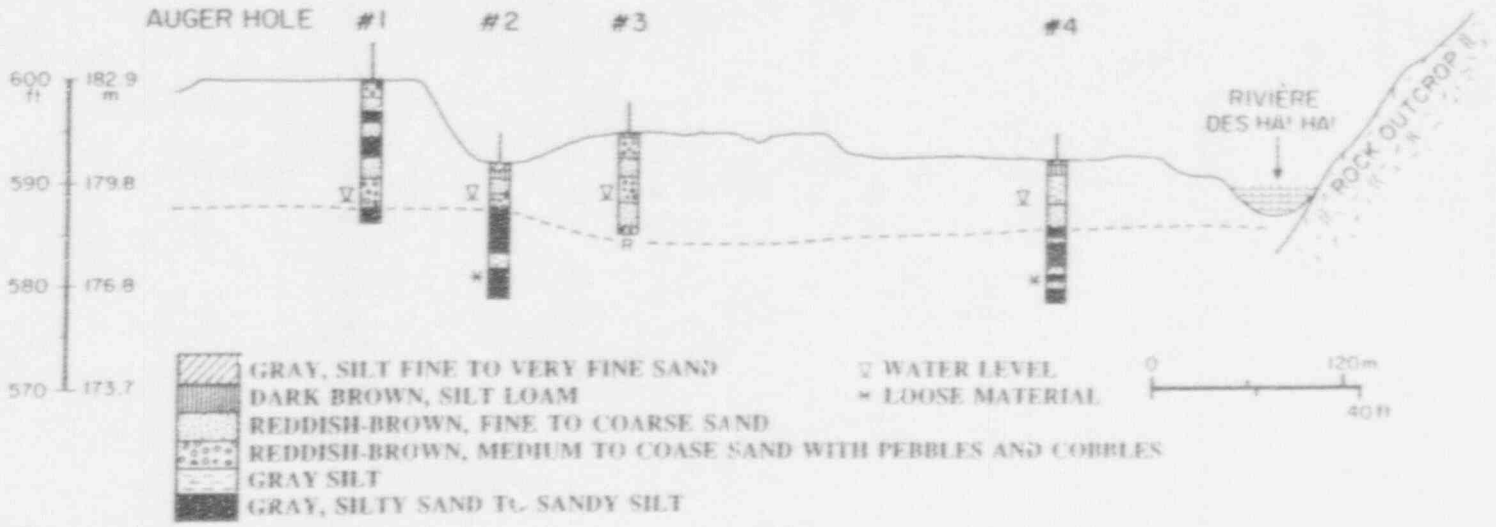

Figure 6. Cross-section of Site 3 showing topographic profile and subsurface stratigraphy. Coarse-grained fluvial deposit overlies fine-grained glaciolacustrine deposit. A loose sandy layer (marked by *) about 3.5 m below the surface and within the glaciolacustrine deposit is thought to be the layer that liquefied in 1988.

Liquefaction features 26 km from Saguenay earthquake epicenter: Site 1

Site 1 is located on a terrace about 30 m above a tributary to Rivière des Ha! Ha!, Bras Hamel, which is incised into glaciolacustrine deposits (Figure 2). It is the fine sand and silty, very fine sand of the mid- to lower-delta foresets that appear to have liquefied during the 1988 earthquake. Composed of very fine, sandy silt, sand boil A, about 0.5 to 1 m in diameter and 7.5 cm thick, was located close to a house that suffered differential settlement as the result of liquefaction (Figure 7). Excavation of the sand boil exposed a well-developed system of subsurface dikes and faults (Figure 8). The dikes could be followed along a northeast-trending, linear zone just below the modern soil for a distance of 4 m. At a depth of 1 m below the sand boil, a prominent planar and subvertical dike could be clearly identified as the feeder dike. Above this depth, where the host sediment becomes coarser-grained and therefore more permeable, the dike splits into a family of thin and discontinuous dikes. The passageway of the sand through the thin topsoil was marked by a very small sand vent not more than 1 cm in diameter. Several subsidiary dikes branched upward from the main dike, occurring along faults exhibiting centimeters of displacement. Where dikes encountered pebbles or stones, sand had accumulated below the obstacles. Dikes injected along normal faults terminated at the contact between silty, very fine sand below and medium sand above.

Several weathered dikes and sills are also exposed in the excavation of sand boil A at Site 1 (Figure 8). These features are suggestive of a pre-1988 liquefaction events. Some of the weathered features are intruded by 1988 dikes, including the main feeder dike. Exposed was a much larger structure comprised of a 10 cm wide, weathered sand dike at depth that merges upward into a 2 m wide, iron-stained sand-filled crater. Clasts of host sediment, as well as organic material, occur within the crater. Several reverse faults with up to 20 cm of separartion exist within 0.5 m of the crater and root into the dike associated with the crater. This structure is similar in morphology to, but larger than, the 1988 sand-filled crater beneath sand boil B and exhibits many of the characteristics of liquefaction features in the New Madrid seismic zone (Obermeier et al., 1990). The relationship of the reverse faults to the sand dike is not clear. However, the reverse faults do not cut the dike and therefore may have formed prior to or concurrently with the dike. The iron-stained sand crater and its feeder dike are distinctly older than the 1988 liquefaction features. The age of the crater is fairly-well constrained by radiocarbon dating of organic material as discussed later.

Sand boil B at Site 1 formed adjacent to an intermittent creek that drains into Bras Hamel (Figure 7). This creek was filled with gray, silty sand during the 1988 earthquake (Tuttle et al., 1989). Sand boil B is about 10 m in diameter, 22 cm thick, and is made up of alternating laminae of gray, fine sand and silty, very fine sand, that exhibit ripple cross-bedding. Excavation of the sand boil revealed that it had

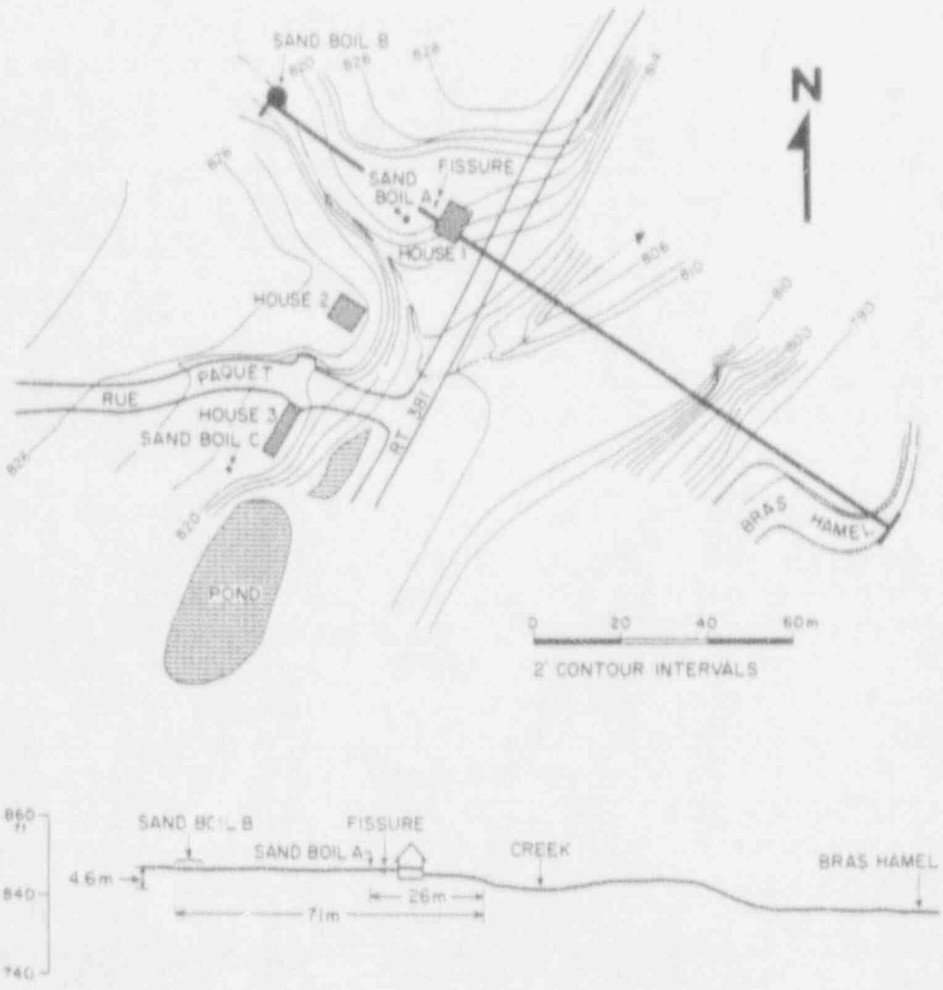

Figure 7. Topographic map and profile of Site 1, 26 km from the epicenter, with locations of sand boils and ground cracks induced by the Saguenay earthquake. Sand boils A and B were excavated. Pre-1988 liquefaction features, as well as those that formed in 1988, are described in the text. The house along the line of section suffered damages due to the earthquake. Houses are indicated by a hachured pattern.

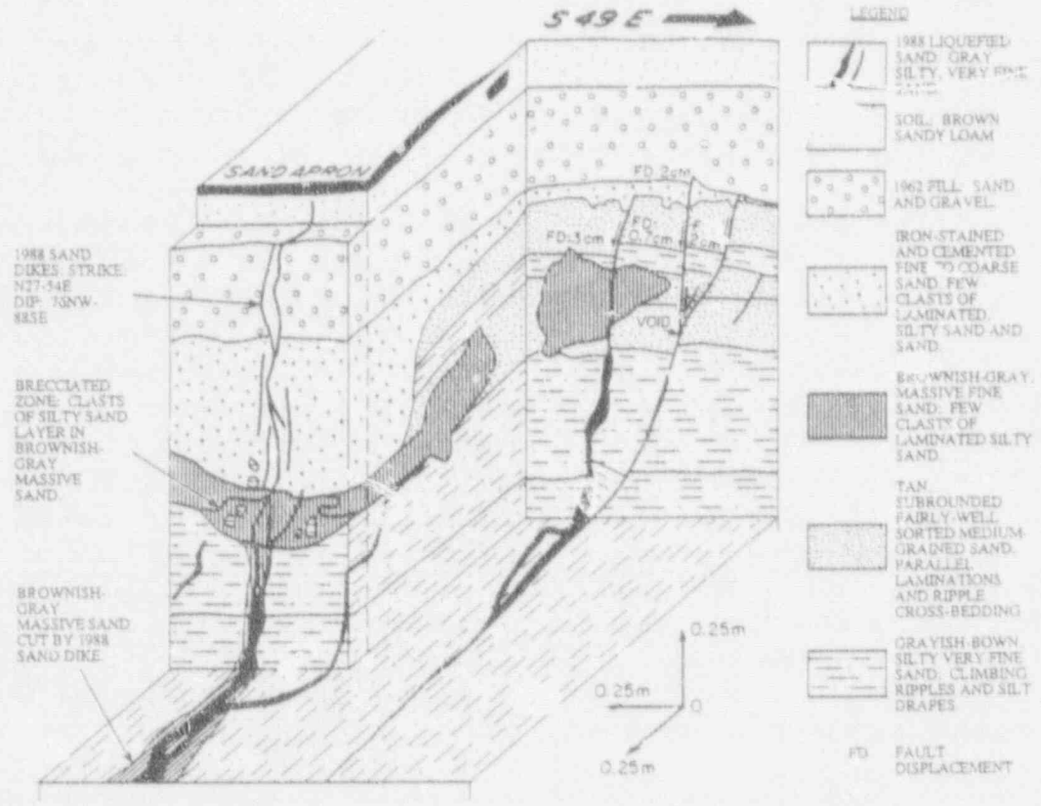

Figure 8. Diagram of the excavation of sand boil A at Site 1. Sand liquefied during the 1988 earthquake intruded along a steeply dipping dike directly below the sand boil and also along several subsidiary dikes that are associated with normal faults. In this section, the feeder dikes are visible but the small vent to the surface has been cut away. Subsidiary dikes are sub-parallel to the feeder dikes. Older liquefaction structures include weathered sand dikes, sills, and a crater filled with clasts of host sediment and iron-stained sand (only a small portion of the crater is present in figure). Radiocarbon analysis of organic material associated with the sand-filled crater indicates that it formed about 340 ± 70 radiocarbon years BP.

been fed through at least four vents, including a 30-cm-wide crater and 5 cm-wide dike (Figure 9). Both are considerably larger than the 1988 dikes observed at Site 3. Sand within the crater is normally graded. Directly above the crater, the laminae of the sand boil deposit are truncated by vent deposits. Also present in this section are a domain of iron-stained, medium sand adjacent to the modern sand-filled crater and a discontinuous sill of silty fine sand. Both features are weathered and are penetrated by roots, indicating that they predate the modern liquefaction features.

In another section perpendicular to the last, a portion of one of the 1988 vents and its associated feeder dike are exposed (Figure 10). Low in the section, the 1988 dike is actually comprised of two branches, one filled with silty, very fine sand, the other with fine sand. Higher in the section, the finer-grained dike truncates the coarser-grained dike, and forms a much wider dike filled with silty, very fine sand containing domains of the coarser-grained material. The structural and sedimentological characteristics of these dikes suggest a change from an initial transport of fine sand to silty, very fine sand. This may have been due to a reduction in the flow rate, and therefore, the carrying capacity of escaping fluids or to a change in the source layer from which fluids were derived.

Other features of interest beneath sand boil E include domains of reddish-brown (iron-stained), medium- to coarse-grained sand within the modern soil, as well as two distinct sills occurring along the base of the modern soil (Figure 10). A large area of the coarse material within the soil is cross-cut by one of the 1988 vents. This area widens towards the ground surface and is interpreted to be an old sand boil or vent deposit. The lower of the two sills is comprised of the same material as that within the old vent. Directly below the old vent deposit, the lower sill becomes a dike and cross cuts the overlying sill. This dike, in turn, is cross-cut by the 1988 sand dike. The upper sill is comprised of greenish-gray, sandy silt. Weathered and discontinuous domains of this material also occur in the overlying soil, suggesting that dikes of this material had extended into the soil. At depth, the modern feeder dike was observed to have been injected along the margin of a more weathered and, therefore, older dike of finer-grained material. It is hypothesized that the older, finer-grained dike had fed the fine-grained sill at the base of the soil as well as dikes extending into the soil.

A second trench excavated in sand boil B reveals a pre-1988 sand dike and associated structures within the modern soil (Figure 11). These features are filled with reddish-brown, medium to coarse sand, similar to the material within the old vent deposit in the excavation described above. The dike widens upward to form a wedge-shaped structure and at depth is connected to a discontinuous layer of massive sand occurring along the base of the soil. Material extending laterally away from the upper part of the wedge-shaped structure or vent may be part of an old sand boil deposit that was buried subsequent to its formation. Sand within the massive layer below the base of the soil is only slightly coarser-grained than the

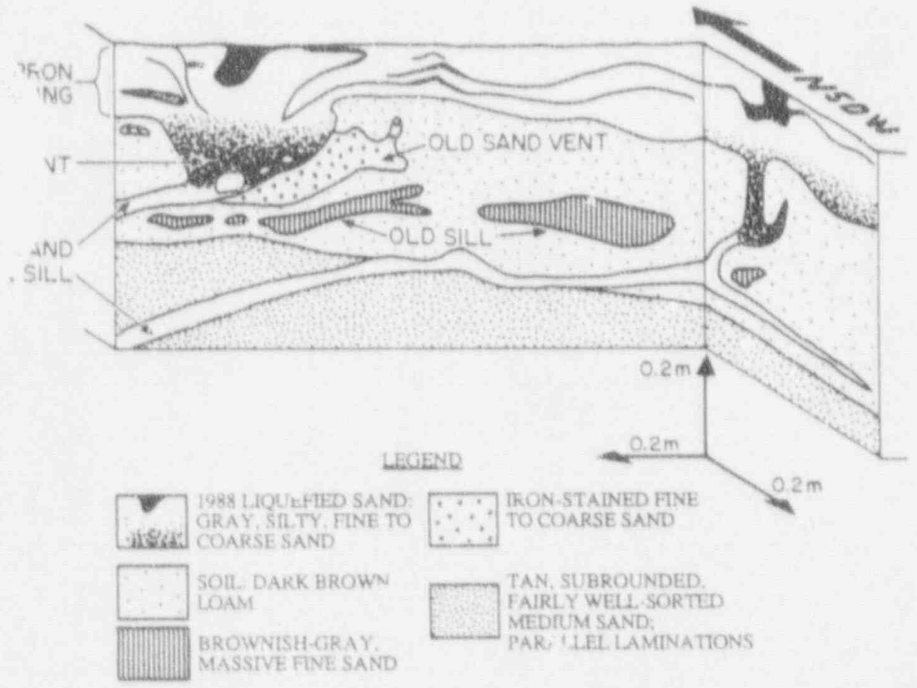

Figure 9. Diagram of excavation of sand boil B at Site 1 interpreted from photographs. The large sand boil deposit is about 10 m in diameter and up to 22 cm in thickness. The sand boil had been fed from below through at least 4 dikes and crater-shaped vents, two of which are illustrated in this figure. Pre-1988 sand dikes, sills and vents can be differentiated from 1988 features by the degree of weathering and the presence of roots.

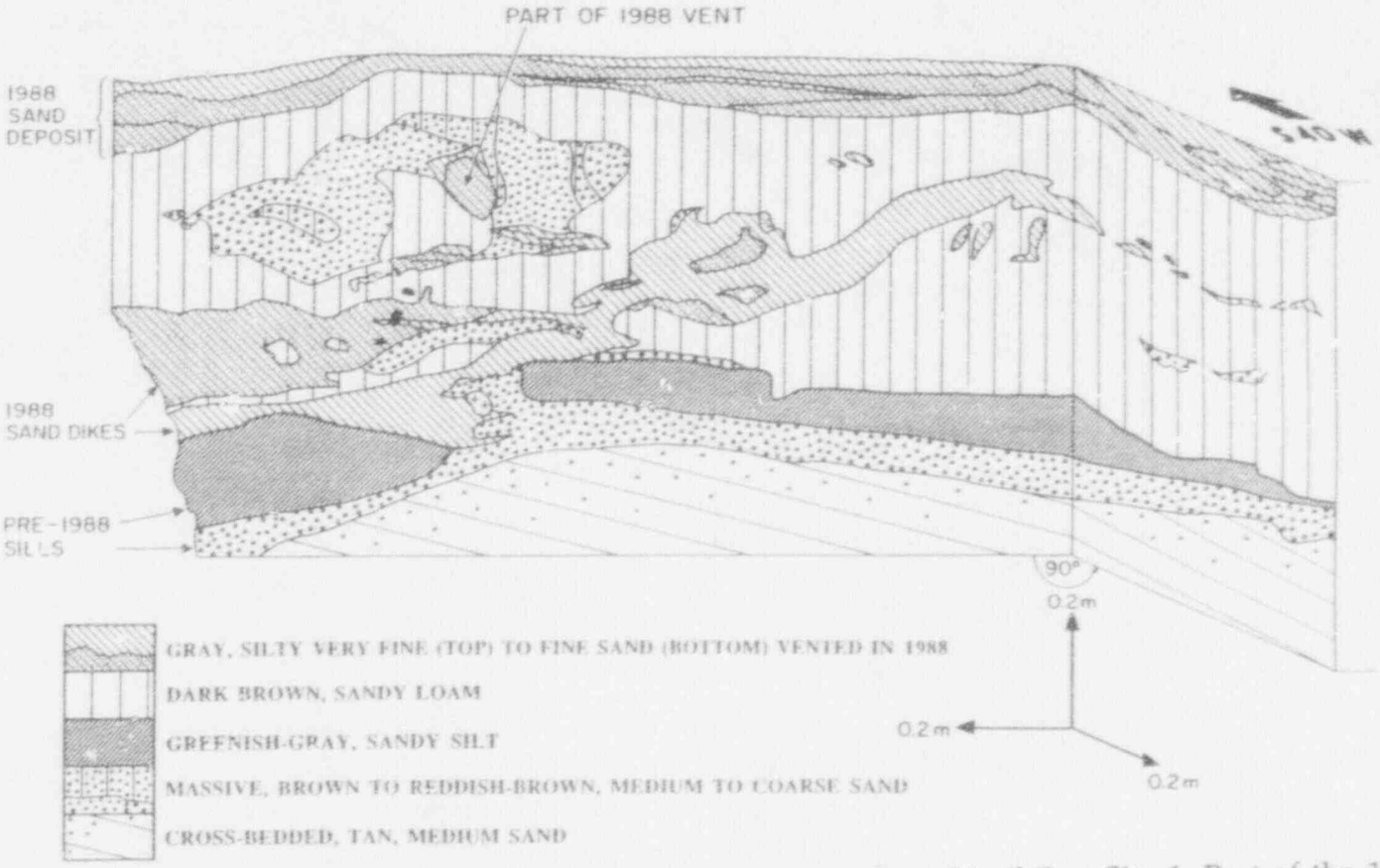

Figure 10. Diagram of excavation across the southern margin of sand boil B at Site 1. Part of the 1988 sand-filled crater or vent is exposed high in the section. The 1988 feeder dike within the topsoil exhibits partitioning of sediment by grain-size. Pre-1988 liquefaction features include the large domain of iron-stained, medium to coarse sand in the topsoil, interpreted as a crater or vent, and both the silty and sandy sills that occur along the base of the topsoil. The lower of the two sills is filled with material similar to that in the old vent. A dike of this sand cross-cuts the overlying sill, suggesting that the features filled with coarse sand are younger in age than the fine-grained sill.

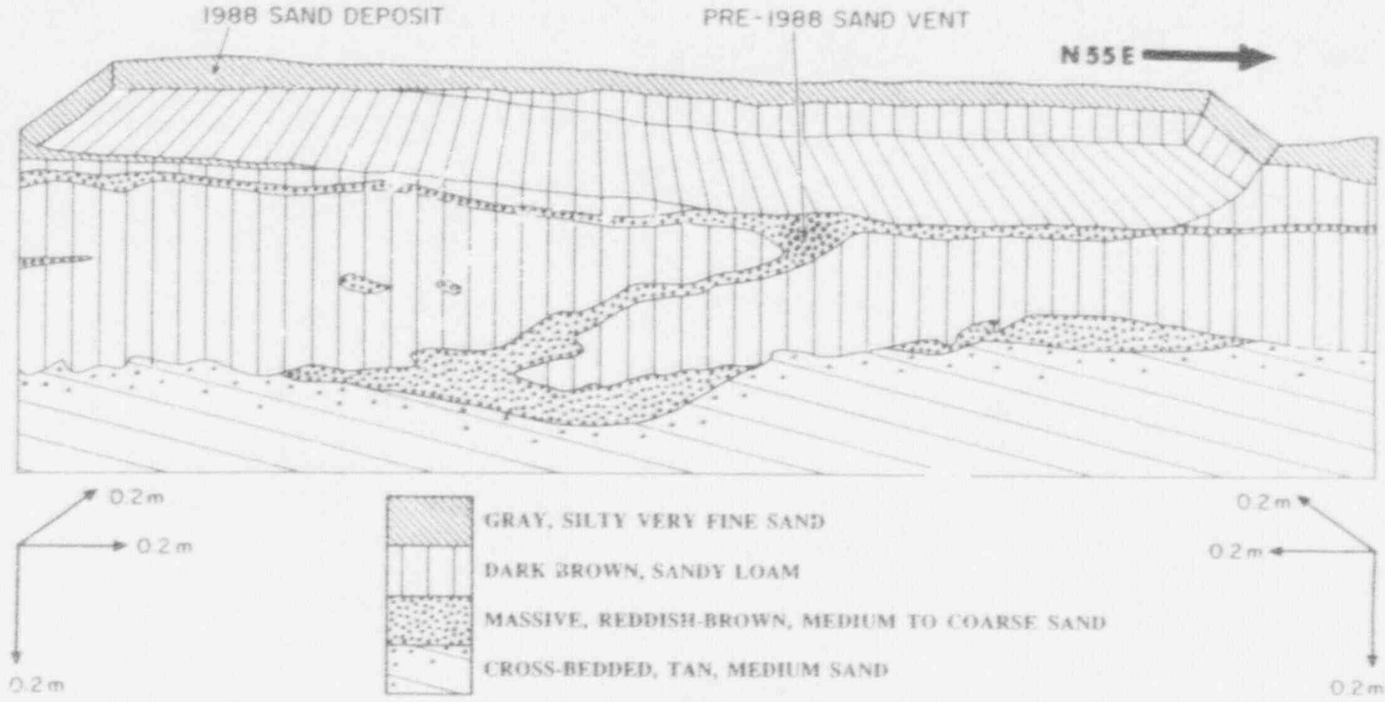

Figure 11. Diagram of trench excavated across the center of sand boil B at Site 1. A pre-1988 liquefaction feature complete with dike, crater, and buried sand boil deposit are filled with iron-stained medium to coarse sand, similar to that filling old liquefaction features in Figure 10. The related layer of sand occurring along the base of the topsoil may reflect the formation of a water interlayer during the liquefaction process.

underlying deposit of tan, medium sand that exhibits primary bedding. Clasts of the overlying soil occur within the massive sand layer, suggesting bearing strength failure involving the soil. No feeder dike of the medium to coarse sand that filled these old liquefaction features appears to cross-cut the underlying deposit of tan, medium sand. It is possible that the material filling the liquefaction features was derived from the upper portion of the deposit underlying the soil.

During the earthquake, liquefaction of the layer of tan, medium sand may have resulted in the formation of a water interlayer at the base of the relatively impermeable soil. This sort of phenomenon has been observed in laboratory experiments (Elgamal et al., 1989). The formation of such a water interlayer could have destroyed bedding in the upper few centimeters of the deposit and led to foundering of the overlying soil as observed. As the overpressurized water found routes of escape through the soil, it may have erupted at the ground surface forming vents and sand boils. As the rate of flow decreased, the finer-grained material could have been preferentially removed from the top of the source layer, resulting in the concentration of the coarser-grained material immediately below the soil.

Liquefaction features 11 km from Saguenay earthquake epicenter: Site 4

During the 1991 reconnaissance in the heavily wooded and uninhabited Laurentide Park, numerous sand boils ranging up to 10 m by 15 m in size were discovered about 11 km west of the epicenter. They formed on the modern floodplain of the nearby Rivière Pikauba (Site 4; Figure 1). Recently jackstrawed and downed trees in the vicinity of the sand boils are suggestive of lateral movement towards the river at the time of the event. Since then, the sand boils have been buried by leaf litter and are not now obvious except for the unusually flat topography they lend to the ground surface. Beneath the leaf litter, gray, silty fine sand overlies dark brown, sandy loam.

In exploratory excavations of one of the sand boils at Site 4, a large feeder dike striking southeasterly is seen coming up from below, branching to form sills near the base of the topsoil, and then intruding the organic-rich topsoil (Figure 12). The dike ranges from about 0.5 to 1 m in width and is considerably larger than any of the 1988 dikes observed at Sites 1 and 3. In fact, this feature is at least 10 times larger than the feeder dikes at Site 1, located 26 km from the epicenter, and 20 times larger than the feeder dikes at Site 3, located 30 km from the epicenter. Conventional wisdom that the size of liquefaction features decreases with distance from the epicenter holds true, despite differences in conditions at the three sites.

In another exploratory excavation at Site 4, where there was no evidence of liquefaction during the 1988 earthquake, a weathered sand dike about 2 cm in width was visible within the subsoil. This feature suggests that a previous liquefaction

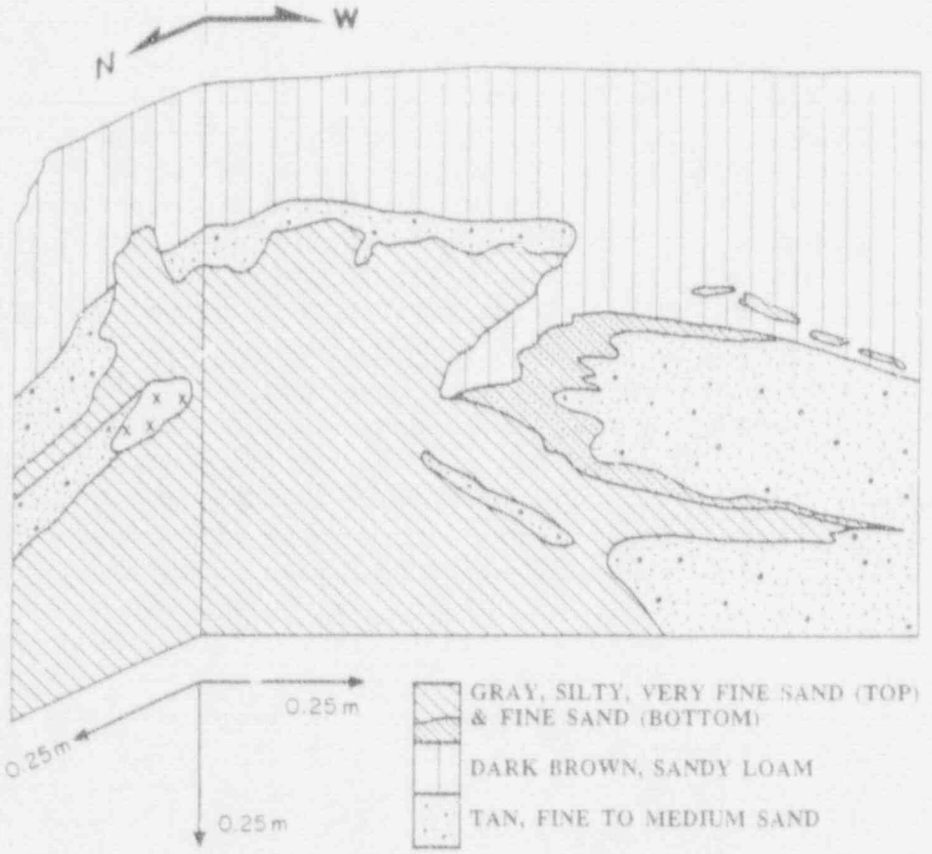

Figure 12. Diagram of exploratory trench excavated in sand boil at Site 4. A 0.5 to 1 m wide feeder dike is the most prominent modern liquefaction feature observed at any of the study sites. Sills branch off of the dike as they near the base of the topsoil.

event may be recorded in sediments at this site. Additional subsurface investigations are needed at Site 4 to study this and other pre-1988 features and to determine their relationships to liquefaction features at other sites.

Past Liquefaction Events

Radiocarbon dating of organic material associated with old, weathered liquefaction features at Site 1 (this paper) and Site 2 (Tuttle et al., 1990) are summarized in Table 1. Analysis of multiple samples collected from the sand-filled crater below sand boil A at Site 1 suggests that the crater formed about 340 ± 70 radiocarbon years before 1950, or roughly between 1540 and 1680. Two large historic earthquakes, the 1638 and the 1663 events, occurred during this time period. The 1663 earthquake, which triggered landslides about 90 km to the southeast of Ferland along the St. Lawrence River, is thought to have occurred in the Charlevoix seismic zone. The 1638 event is thought to have been smaller than the 1663 event and to have occurred near Trois Rivière about 240 km from Ferland (Figure 1). The 1663 earthquake, because of its proximity to the study area, is the more likely of the two to have induced liquefaction in Ferland. The 1925 event of m_b 6.7, like the 1663 earthquake, is thought to have occurred in the Charlevoix seismic zone. So far, no evidence of liquefaction in Ferland that could have been induced by the 1925 event has been found. Therefore, whatever event was responsible for liquefaction and the formation of the old sand-filled crater at Site 1 was probably larger than or located closer to Ferland than the 1925 event. In addition, the large size of the old crater compared to that of the 1988 crater, located at the same site, suggests that ground shaking was more intense during this earlier event than during the 1988 Saguenay earthquake.

Samples associated with various weathered sills yield only maximum ages for those features (Table 1). The youngest maximum age derived for the fine-grained sill below sand boil B is 2,240 ± 120 radiocarbon years BP. At Site 2, the youngest maximum age for another weathered sill is 1,245 ± 65 radiocarbon years BP. Unfortunately, the ages of the weathered sills are not well enough defined to determine whether or not the features formed contemporaneously with one another and with the sand-filled crater. At all four study sites, sills were emplaced at similar depths below the ground surface. This emplacement may have been due to frozen ground conditions at the time of the event. If so, it suggests that the sills formed at the same time as one another, but at a different time from the old sand crater. Cross-cutting relations of the features indicate that the crater formed after the sills.

The most likely interpretation of the available data is that two earthquakes large enough to induce liquefaction occurred in the region prior to the Saguenay earthquake. If this interpretation is correct, then three moderate to large earthquakes, including the 1988 event, occurred in the Laurentide-Saguenay region

Table I: Ferland Radiocarbon Analysis

Site	Event	Feature	C^{14}Age*
1	1?	sill	≤2240±120
		sill	≤ 2640 ±80
		sill	≤ 3040 ±70
	2	sand-filled crater	≥ 40 ±75
			340 ±70
			≤ 520 ±90
			≤ 1350 ±70
			≤ 1390 ±65
		fault	≤ 1615 ±70
2	1?	sill	≤ 1245 ±65
		sill	≤ 1910 ±70
		sill	≤ 2240 ± 90

* Years before 1950.

during the past 1,300 radiocarbon years. Alternatively, if all the old liquefaction features formed at the same time, then two events occurred in the region in the past 400 radiocarbon years. Additional radiocarbon dating of samples collected at Sites 3 and 4, as well as Site 1, may help resolve the ages of the various liquefaction features and their causative events.

Discussion and Conclusions

Because the location of the Saguenay earthquake is well known, it is possible to compare liquefaction features that formed at different distances from the epicenter. Liquefaction features that formed 11 km from the epicenter are at least 20 times larger than features that formed at 30 km from the Saguenay epicenter, while those at 26 km are more than 2 times larger than those that formed at 30 km. Despite differences in site conditions, liquefaction features increase markedly in size with decreasing distance from the epicenter. In previous studies of liquefaction features that formed during historic and prehistoric earthquakes, this relationship has been assumed. With additional data drawn from modern case studies, empirical relationships can be developed that may be useful in determining the location and magnitude of past earthquakes.

In addition to the features clearly related to liquefaction in 1988, weathered dikes, sills, and sand-filled craters were also present in the excavations of the 1988 sand boils. These weathered features were similar in morphology to the modern features and are therefore interpreted to be earthquake-induced liquefaction features. Intense deformation of the soil horizons, characterized by paired lobes and diapirs, is probably the result of mixing of the soil by freezing and thawing and not related to liquefaction.

Cross-cutting relationships of liquefaction features suggest that there was one, possibly two, liquefaction events prior to 1988. At this time, only the age of the weathered sand-filled crater at Site 1 is well-constrained. According to radiocarbon analysis, this feature formed 340 $\pm$ 70 radiocarbon years BP. No evidence of liquefaction related to the 1925 Charlevoix earthquake of mb 6.7 has yet been found in Ferland. Therefore, it is postulated that the earthquake, possibly the 1663 event, responsible for the formation of the sand-filled crater was larger than or located closer to Ferland than the 1925 event. Since this feature is considerably larger than the sand-filled crater that formed in 1988 at the same site, the past event may also have been larger than or located closer to Ferland than the 1988 earthquake.

Although structural relationships suggest that weathered sills pre-date the old sand-filled crater, their ages of formation cannot be differentiated with the available radiocarbon data. Two possible interpretations are that either (1) two earthquakes large enough to induce liquefaction occurred in the Laurentide-Saguenay region during the 1,300 radiocarbon years prior to the Saguenay event or

(2) one such earthquake occurred in the region in the 400 radiocarbon years before 1988. Future subsurface investigations at these and other sites will hopefully continue to unravel the earthquake history of the Laurentide-Saguenay region.

It is interesting to note that at Sites 1 and 3 the old dikes and sills in Ferland are larger than the equivalent features that formed during the 1988 earthquake; yet at Site 4 the old dike is much smaller than the modern dike. In addition, the pre-1988 dike at Site 4 is also smaller than the old dikes at Sites 1 and 3. If the old dikes and sills at the three sites formed at the same time, their sizes would suggest that the source of the earthquake responsible for their formation was located closer to Ferland and was probably different from the source that generated the Saguenay earthquake. If so, then at least one and possibly more earthquake sources capable of generating damaging earthquakes have yet to be identified in the region.

The seven known sites where liquefaction resulted from ground shaking during the 1988 Saguenay event occur fairly close in orientation to the surface projections of the two nodal planes of the earthquake focal mechanism. It is possible that the distribution of liquefaction sites may be related to the radiation pattern of seismic energy during the earthquake. Both the amplitude and duration of shear waves are often greater along the direction of the earthquake nodal planes. Shear wave energy may have contributed significantly to the occurrence of liquefaction at these sites. To what extent this and other factors such as site conditions, liquefaction susceptibility of sediments, and attenuation characteristics of the country rock contribute to the spatial distribution of liquefaction features needs to be determined.

Acknowledgements

This work was supported by the Atomic Energy Control Board of Canada contracts 3.144.1, 3.144.2, and 3.144.3 and the National Center for Earthquake Engineering Research contracts 88-1303 and 88-1508. Many thanks to Caroline Moseley, Nano Seeber, and Jo Wallach who provided valuable assistance and discussion in the field and to Nick Christie-Blick and Gerard Bond for their reviews of the manuscript.

References

Amick, D. and Gelinas, R., 1991, The search for evidence of large prehistoric earthquakes along the Atlantic seaboard, Science, 25, 655-658.

Bryan, K., 1946, Cryopedology - The study of frozen ground and intensive frost-action with suggestions on nomenclature, American Journal of Science, 244, 622-642.

Buol, S.W., Hole, F.D. and McCracken, R.J., 1973, Soil genesis and classification, Iowa State University Press, Ames, Iowa, 360pp.

Coates, D.R., ed, 1975, Quaternary deformed sediments of the St. Lawrence Lowland as an index of seismicity, Report to New York State Atomic and Space Development Authority, Binghamton, New York, 267pp.

Elgamal, A. -W., Dobry, R. and Adalier, K., 1989, Study of effect of clay layers on liquefaction of sand deposits using small-scale models, *in* O'Rourke, T.D. and Hamada, M., eds., Proceedings from the Second U.S.-Japan Workshop on Liquefaction, Large Ground Deformation and their Effects on Lifelines, National Center for Earthquake Engineering Research, Tech. Rept. NCEER-89-0032, 233-245.

Hole, F.D., 1961, A classification of pedoturbations and some other processes and factors of soil formation in relation to isotropism and anisotropism, Soil Science, 91, 375-377.

LaSalle, P., 1968, Field trip of Quaternary geology, Saguenay River-Lac St. Jean, Contribution to the ACFAS Congress, Quebec Department of Natural Resources, 31pp.

North, R.G., Wetmiller, R.J., Adams, J., Anglin, F.M., Hasegawa, H.S., Lamontagne, M., Duberger, R., Seeber, L. and Armbruster, J., 1989, Preliminary results of the November 25, 1988 Saguenay, Quebec earthquake, Seismological Research Letters, 60, 89-94.

Obermeier, S.F., Bleuer, N.R., Munson, C.R., Munson, P.J., Martin, W.S., McWilliams, K.M., Tabaczynski, D.a., Odum, J.K., Rubin, M., and Eggert, D.L., 1991, Evidence of strong earthquake shaking in the lower Wabash Valley from prehistoric liquefaction features, Science, 251, 1061-1063.

Obermeier, S.F., Jacobson, R.B., Smoot, J.P., Weems, R.E., Gohn, G.S., Monroe, J.E. and Powars, D.S., 1990, Earthquake-induced liquefaction features in the coastal setting of South Carolina and in the fluvial setting of the New Madrid seismic zone, U.S. Geological Survey, Professional Paper 1504, 44pp.

Raymond, R., 1969, Carte de la pedologique: region d' Chicoutimi, Ministere de l'Agriculture, Ferland 22D2, 1:50,000.

Schafer, J.P., Obermeier, S.F., and Stone, J.R., 1987, On the origin of wedge structures in southern New England, Geological Society of America, 22nd Annual Meeting of the Northeastern Section, Abstracts with Programs, 55.

Thorson, R.M, Clayton, W.S., and Seeber, L., 1986, Geologic evidence for a large prehistoric earthquake in eastern Connecticut, Geology, 14, 463-467.

Tuttle, M.P., Such, R., and Seeber, L., 1989, Ground failure associated with the November 25th, 1988 Saguenay earthquake in Quebec Province, Canada. *in* Jacob, K., ed., The Saguenay earthquake of November 25, 1988, Quebec, Canada: Strong motion data, ground failure observations, and preliminary interpretations, Buffalo, New York, National Center for Earthquake Engineering Research, 23pp.

Tuttle, M.P., Law, T., Seeber, L., and Jacob, K., 1990, Liquefaction and ground failure in Ferland, Quebec triggered by the 1988 Saguenay earthquake, Canadian Geotechnical Journal, 27, 580-589.

Tuttle, M., and Seeber, L., 1991, Historic and prehistoric earthquake-induced liquefaction in Newbury, Massachusetts, Geology, 19, 594-597.

HIGH-PRECISION ACCELERATOR-MASS-SPECTROMETER RADIOCARBON DATING OF BURIED TIDAL-MARSH SOILS--AN APPROACH TO ESTIMATING THE FREQUENCY AND COASTAL EXTENT OF SUBDUCTION ZONE EARTHQUAKES IN OREGON AND WASHINGTON

Alan R. Nelson[1], Yoko Ota[2], Thomas W. Stafford, Jr.[3], Masatomo Umitsu[4], Kaoru Kashima[5], and Yoshiaki Matsushima[6]

[1]U.S. Geological Survey, MS 966, PO Box 25046, Denver, CO 80225, U.S.A.
[2]Dept. of Geography, Yokohama National University, Hodogaya-ku, Yokohama, 240, Japan
[3]INSTAAR, University of Colorado, Boulder, Colorado, 80309-0450, U.S.A.
[4]Dept. of Geography, University of Nagoya, Chikusa-ku, Nagoya, 464-01, Japan
[5]College of General Education, Kyushu University, Ropponmatsu, Fukuoka, 810, Japan
[6]Kanagawa Prefecutural Museum, 5-60, Minaminaka-dori, Nakaku, Yokohama, 231, Japan

ABSTRACT

Accurate and precise radiocarbon dating of buried tidal-marsh soils in estuarine stratigraphic sequences in the Pacific Northwest can help distinguish soils submerged during regional plate-boundary earthquakes from soils submerged during local upper-plate earthquakes or by non-tectonic processes. More precise ages than those resulting from conventional methods of radiocarbon analysis can be obtained by averaging multiple accelerator-mass-spectrometer (AMS) ^{14}C ages of rigorously selected and pretreated plant macrofossils at the abrupt upper contacts of tidal-marsh soils. An initial test of this method in Coos Bay, Oregon, shows that standard deviations on AMS ages can be reduced to ±25-40 radiocarbon years. But consideration of the total analytical errors in AMS analysis and age differences due to variations in the rate of ^{14}C production in the atmosphere over time indicate that 95% confidence limits on calendar-corrected ages for submergence events range from 50 to 450 years.

INTRODUCTION

Has subduction of the Juan de Fuca plate beneath the North America plate (Fig. 1) produced great (magnitude, M>8) earthquakes during the late Holocene? Records of the past 200 years yield no evidence of great plate-boundary earthquakes in the Cascadia subduction zone (Heaton and Hartzell, 1987). But along the coasts of Washington (Atwater, 1987; Atwater and Yamaguchi, 1991; Atwater, in press), Oregon (Grant, 1989; Darienzo and Peterson, 1990; Peterson and Darienzo, in press; Nelson, in press a), and northern California (Vick, 1988; Valentine et al., 1990) peaty, tidal-wetland soils are interbedded with mud in estuarine stratigraphic sequences, and the submergence (relative rise of sea level) of some of these soils seems too widespread (>100 km), too large (>1 m), and too sudden (<10 yr) to be attributed to any process except coseismic subsidence. How large were the earthquakes that could have produced this coastal subsidence, and how often did they occur? Such questions are critical for earthquake hazard assessement in the Pacific Northwest, and radiocarbon dating of buried tidal-wetland soils can help answer these questions.

Buried tidal-wetland soils in the Pacific Northwest may have been submerged by sudden coastal subsidence during any of three types of earthquakes. First, great earthquakes (M>8) on one or more segments of the interface between the subducting and overriding plates may have produced a regional zone of coastal subsidence hundreds of kilometers long (Fig. 2). Tidal-wetland soils similar to those in southern Washington and northern Oregon were submerged and buried along hundreds of kilometers of coast following historic great subduction earthquakes in Alaska and Chile (Plafker, 1972; Atwater, 1987). Second, deformation on faults and folds in the overriding North America plate during great earthquakes on the plate-interface may have produced local areas of coseismic coastal subsidence (Fig. 3; McInelly and Kelsey, 1990; Valentine et al., 1990). And third, some localized subsidence may have occurred during smaller earthquakes (M 6-7¼) in the overriding plate independent of plate-interface events (Nelson and Personius, in press; e.g., Berryman et al., 1989).

At least some buried tidal-wetland soils, however, may have been submerged by non-tectonic processes. Peaty soils are commonly interbedded with mud in intertidal sequences of mid-latitude passive continental margins (e.g., Tooley, 1978; van de Plassche, 1982; in press; Shennan, 1986; Strief, 1987). Examples of non-tectonic processes that can produce such sequences include rapid changes in the rate of regional sea-level rise combined with changing sedimentation rates, or changes in the configuration of bars and channels in tidal inlets that led to local changes in tidal range. Tidal-wetland soils can be assumed to have been submerged by coseismic subsidence only where the abrupt upper contact of a widely-mapped, peaty soil gives strong evidence of a sudden, substantial change (>0.5 m) in water depth (Nelson, in press a).

Accurate and precise radiocarbon dating can help distinguish soils submerged during regional plate-interface earthquakes from soils submerged during local upper-plate earthquakes or by non-tectonic processes. Synchronous ages for soils submerged along hundreds of kilometers of coast would be consistent with great plate-interface earthquakes, some perhaps as large as M 9 (Heaton and Hartzell, 1987; Atwater, 1987; Rogers, 1988; Adams, 1990). Non-synchronous ages would indicate lower magnitude plate-interface earthquakes with coseismic subsidence of much more limited extent, moderate-magnitude earthquakes on shallow structures in the upper plate, or soil submergence by non-tectonic processes (Nelson and Personius, in press).

Each of the above processes may have submerged tidal-marsh soils in the Coos Bay region of southern Oregon. Coos Bay is near the eastern edge of the active accretionary wedge of the North America plate (Figs. 1 and 3; Clarke et al., 1985). Analogies with deformation measured in Chile, Japan, and Alaska indicate that regional uplift of as much as several meters and/or differential movements across folds and faults may occur in the accretionary wedge during great plate-interface

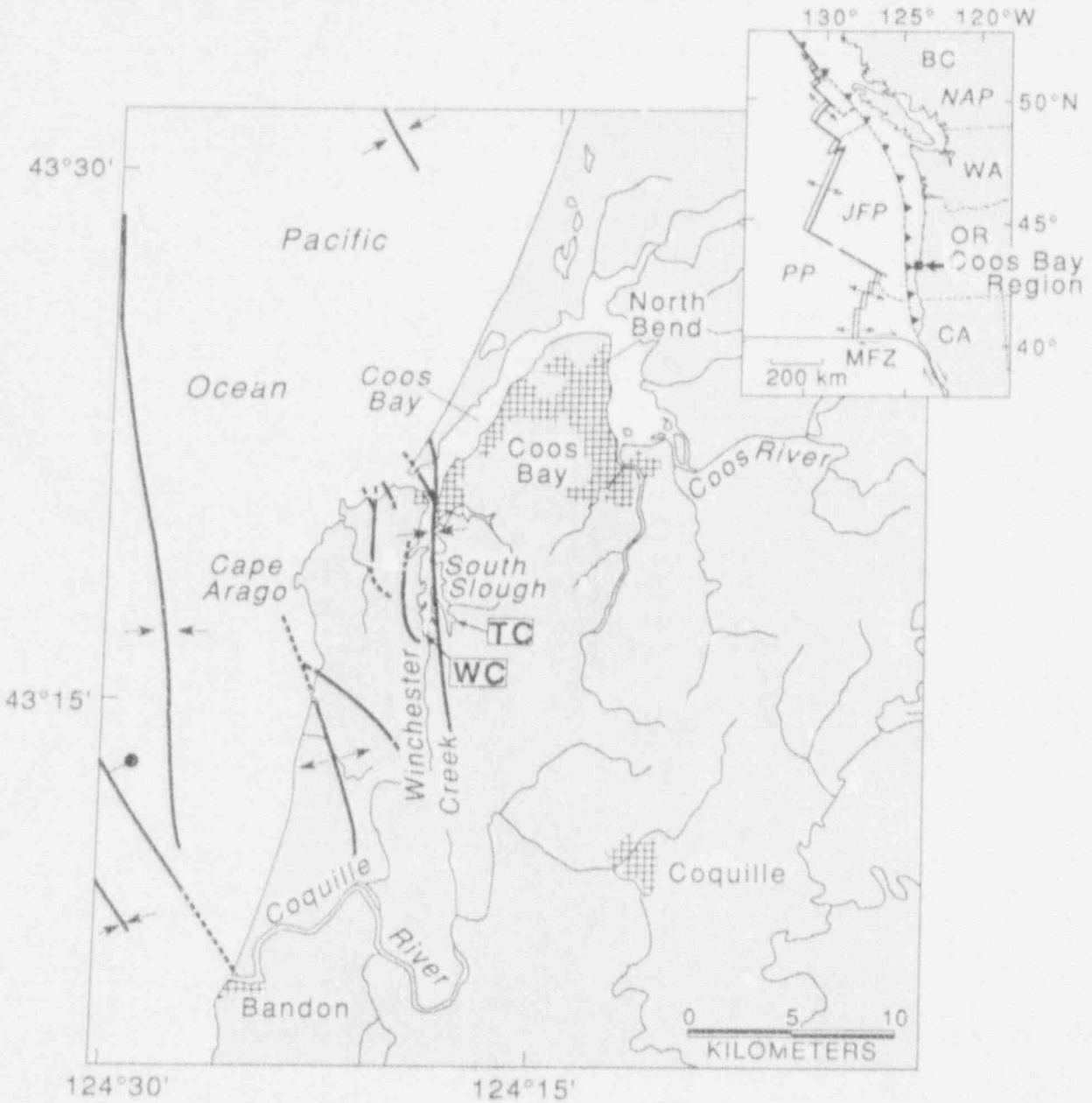

FIGURE 1.--The Coos Bay region in the southern part of the Cascadia subduction zone showing location of sites at Winchester Creek (WC) and Talbot Creek (TC) in the South Slough arm of the western part of the Coos Bay estuary. Urban areas shown by cross-ruled pattern. Anticlines, synclines, and faults that produce relief on the sea floor or deform Pleistocene marine or fluvial terraces are shown by thick lines (from Clarke et al., 1985; McInelly and Kelsey, 1990, fig. 13). Labels on inset map: NAP, North America plate; JFP, Juan de Fuca plate; PP, Pacific plate; MFZ, Medocino fracture zone; BC, British Columbia; WA, Washington; OR, Oregon; CA, California. In inset, double lines are spreading ridges, solid lines are transform fault zones, and dashed lines are other faults or political boundaries; trace of the Cascadia thrust fault (barbed line, barbs point down-dip) is placed at the boundary between the continental slope and abyssal plain.

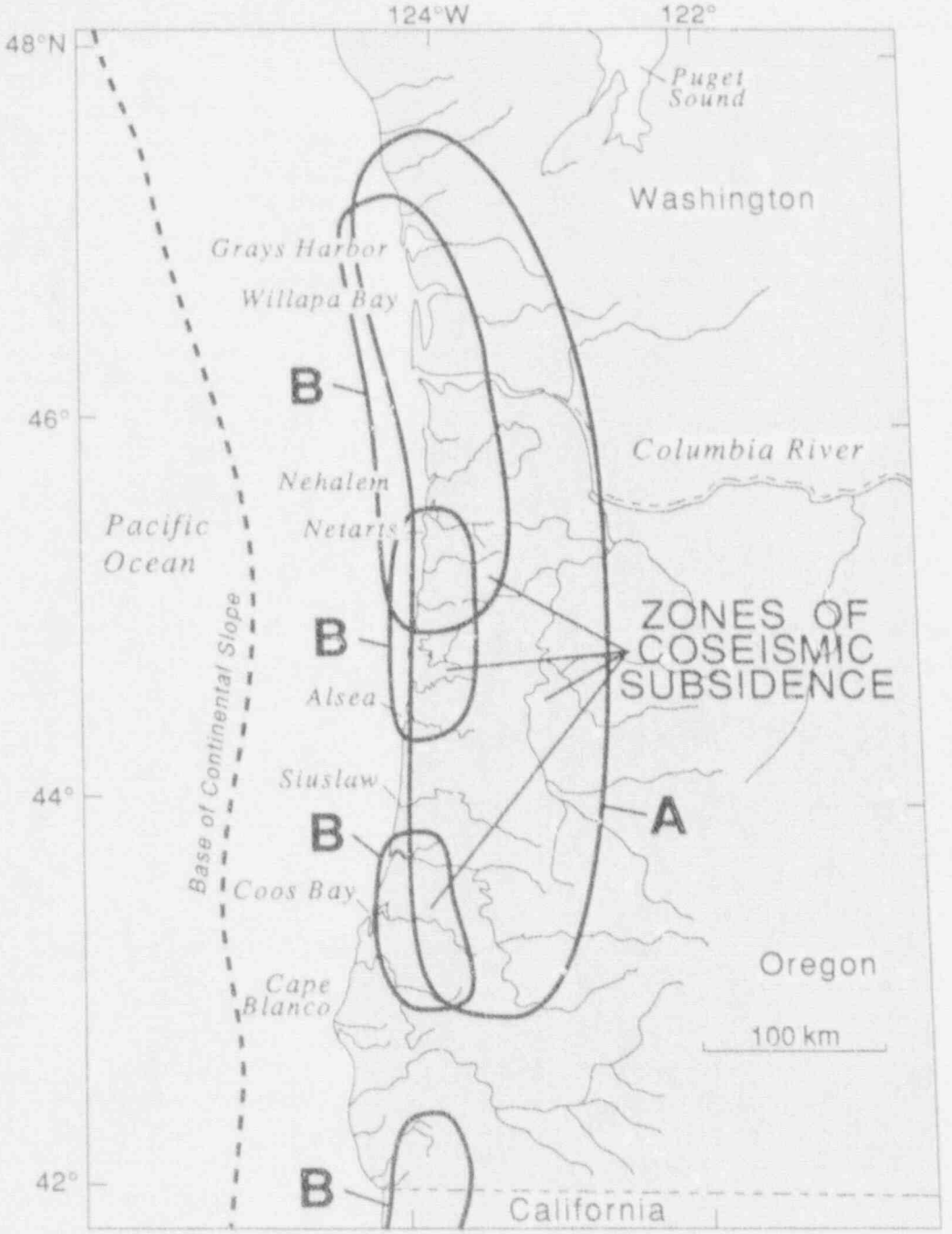

FIGURE 2.--Possible models of coseismic subsidence during plate-interface ruptures in the central part of the Cascadia subduction zone in Oregon and Washington. A rupture of two or more segments of the Cascadia zone along 300-600 km of the plate boundary during an earthquake of M 8¼-9 (model A) could produce a 50-to-120-km-wide zone of coseismic subsidence along the Oregon or Washington coasts. If only single Cascadia segments or portions of segments ruptured in events of less than M 8¼, then much smaller zones of coseismic subsidence less than 250 km long could be produced (model B). Some of these smaller earthquakes might not produce significant (>0.5 m) permanent subsidence of tidal wetlands in the region. Deformation on local (<30 km long) structures in the upper plate during either plate-interface or upper plate earthquakes (Fig. 3) could produce only small, localized areas of permanent subsidence (not shown).

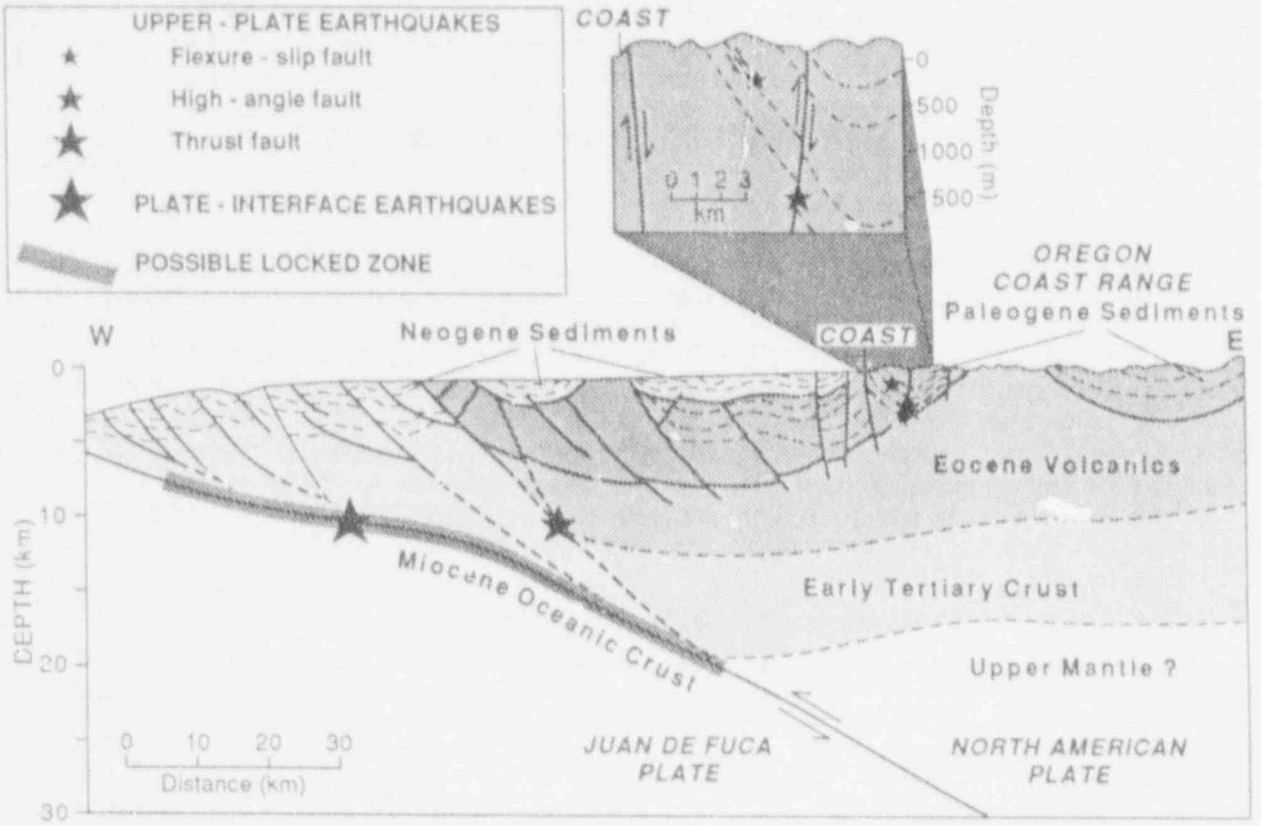

FIGURE . 3.-- Crossection through part of the Cascadia subduction zone in the Coos Bay region of south-central Oregon (based on figures in Newton, 1980; Snavely et al., 1985; Clarke et al., 1985; Keach et al., 1989; McInelly and Kelsey, 1990; and Kelsey, 1990). Stars show the locations of epicenters of four types of earthquake sources. Great earthquakes (M>8) could be produced by slip on the locked part of the plate interface; large earthquakes (M 6½-7¾) could be produced by slip on major thrust faults in the accretionary wedge of the upper plate, either independently or during plate-interface earthquakes; smaller earthquakes (M<7) could be produced by slip on high-angle faults that cut shallow structures in the upper plate, either independently or during plate-interface earthquakes; and small earthquakes (M<6) could be produced by slip on flexure-slip faults during folding in the upper plate during larger earthquakes (e.g., McInelly and Kelsey, 1990). Width of possible locked zone along the plate interface is a speculative maximum value for this earthquake source.

earthquakes (e.g., Plafker, 1969; 1972; Matsuda et al., 1978). In southern Oregon, late Holocene coseismic deformation has been inferred on shallow, upper plate faults and folds in the South Slough area of western Coos Bay (Figs. 1 and 3; McInelly and Kelsey, 1990; Nelson, in press a). Surface deformation associated with these structures might be reflected as submergence or emergence events of 0.5-2 m in the tidal-marsh stratigraphic record. Many localized deformation events in southern Oregon are probably coincident with plate-interface earthquakes, but shallow earthquakes of moderate to large magnitude (M 6-7¼) on smaller structures (<30 km long) in the upper plate might also produce localized areas of coseismic subsidence or uplift.

The frequency of submergence events and the accuracy and precision with which suddenly submerged soils can be radiocarbon dated determine if submergence events can be correlated from site to site. But in the Coos Bay region, the precision of conventional ^{14}C ages on peaty tidal-marsh soils is too low and the recurrence intervals between events are too short to distinguish local from regional submergence events (Nelson, in press b). High-precision conventional ^{14}C ages have been obtained by dating selected tree rings from stumps rooted in buried soils in southern Washington (Atwater et al., 1991), but outcrops that expose similar buried spruce-swamp soils have not been found in southern Oregon. However, the precision of age estimates for events throughout the Pacific Northwest can be improved through accelerator mass spectrometer (AMS) ^{14}C analysis of rigorously selected macrofossils at the abrupt upper contacts of tidal-marsh soils.

DATING THE TIMES OF TIDAL-MARSH SOIL SUBMERGENCE

Problems With Conventional ^{14}C Dating

A key assumption in initial paleoseismic studies in the Pacific Northwest was that conventional radiocarbon dating could provide accurate estimates of great earthquake recurrence through analysis of organic materials found at or just above the upper contact of abruptly submerged, peaty, tidal-marsh soils. It also was hoped that the times of peaty soil submergence were separated by enough time to allow the soils to be correlated from one estuary to another by using conventional ^{14}C ages. However, studies with over a hundred conventional ^{14}C ages in Washington (Grant and others, 1989; Atwater, in press, table 1) and Nelson's (in press b) comparative dating study in southern Oregon shows that conventional ^{14}C samples from the upper parts of the same buried soils contain materials that differ in age by many hundreds of years. In the Coos Bay region of south-central Oregon, errors on soil ages represent about the same length of time as recurrence times for submergence events (150-500 years) and therefore preclude the use of conventional ^{14}C ages in correlating buried soils along the coast of the Pacific Northwest.

Advantage of AMS ^{14}C Dating

Small sample size is the major advantage that AMS analysis has over conventional radiocarbon analysis for obtaining ages for the times of marsh soil submergence and burial. In AMS analysis, the percentage of ^{14}C in a sample is measured directly: carbon isotopes (including ^{14}C) in a graphite target made from the sample are accelerated in a high-energy mass spectrometer and their relative proportions measured (Elmore and Phillips, 1987). Conventional ^{14}C analysis measures ^{14}C only indirectly by recording the number of beta particles emitted by the ^{14}C isotopes in a sample during radioactive decay to ^{14}N in a highly shielded Geiger counter (Taylor, 1987). Because AMS analysis actually counts all ^{14}C atoms, not just those that decay radioactively during the short period of time when the sample is in the Geiger counter, only very small samples (containing as little as 0.2 mg of carbon) are required for analysis. Conventional ages require samples containing 500 times (about 1 gram) more carbon.

The sample-size advantage of AMS analysis allows us to be much more rigorous in selecting sample materials. Conventional dating of buried peaty soils usually requires analysis of bulk peat samples. In some areas, where the peaty surface horizons of buried soils are well-exposed in outcrop, only the upper 1 cm of peat in a soil has been sampled in an attempt to obtain an age that is close to the time of soil submergence and burial (e.g., Atwater, in press; table 1). However, like material from the organic-rich horizons of most soils (e.g., Matthews, 1980), bulk samples from buried marsh soils are mixtures of different types of organic material containing carbon of different ages. The ages of the different components of the soils depend on the many factors involved in marsh soil development, burial, and decay (e.g., Allen, 1978; Frey and Basan, 1985; Mook and van de Plassche, 1986; Allen, 1990). Examples of such factors include the type of marsh vegetation, the amount of woody detrital material deposited in the marsh, the extent and rate of mixing of the soil by animals and plant roots, the rate of peat accumulation, and the rate of sedimentation between soil burial events. In addition, buried tidal-marsh soils commonly contain the herbaceous and woody roots of younger plants that were rooted in higher, younger marsh soils (e.g., Kaye and Barghoorn, 1964; Mook and van de Plassche, 1986; Peterson and Darienzo, in press). But with AMS analysis we can sample only the *above-ground* parts of plants to avoid contamination by younger roots. We can also limit our sampling to delicate pieces of a single identifiable species; because of the rapid decay and tidal removal of organic material on the surface of a marsh, the delicate, non-woody parts of plants are unlikely to have been reworked from older deposits. Most importantly, plant parts can be collected from the upper surface of buried peaty soils, rather than from within the soils, to insure that the parts date from the time when the soil was submerged and buried.

Above-ground plant parts sampled for AMS analysis may be either detrital or rooted, but the bases of individual rooted marsh plants are preferred. In southern Washington, Atwater and Yamaguchi (1991) described marsh plant fossils rooted in the top of a high-marsh soil buried by intertidal mud and sand about 300 years ago. The delicate leaves and stems of the plants project several centimeters into the overlying sand and mud indicating sudden subsidence and burial of the marsh surface, as might occur during a great subduction zone earthquake and accompanying tsunami. Such rooted plant fossils are ideal for AMS analysis because it seems nearly impossible for them to be more than a few years older than the time of soil burial.

Unfortunately, rooted plant fossils extending into overlying sediment have not been found at the tops of most buried marsh soils in the Pacific Northwest, so AMS dating of the submergence times of these soils must rely on carefully selected samples of detrital material from the top of the soil. Detrital samples should be parallel to bedding, and lie either on the surface of the buried soil or on bedding planes within the lower few millimeters of the overlying mud or sand. The best detrital samples are the identifiable, above-ground parts of marsh plants, trees, or shurbs that grow in and around the marsh. The delicate, non-woody parts of plants, such as conifer needles or tree leaves, are preferred because they are much less likely to have been reworked from older deposits than woody materials such as large twigs, bark, or cones. In marsh sequences fringing the thick forests of the Pacific Northwest, some woody detrital material in buried marsh soils probably predates the time of soil burial by several hundred years (Nelson, in press b).

An Initial Test of High-precision AMS ^{14}C Dating

An initial test using multiple AMS ages to improve the precision of estimates of the times of soil-submergence events involved sampling probable correlative buried soils at sites near Winchester Creek (WC) and Talbot Creek (TC) in the South Slough arm of western Coos Bay (Fig. 1). The sites are less than 2 km apart near the upper (southern) end of the slough, but they lie in separate arms of the slough, which have different tidal characteristics. Continuous, large-

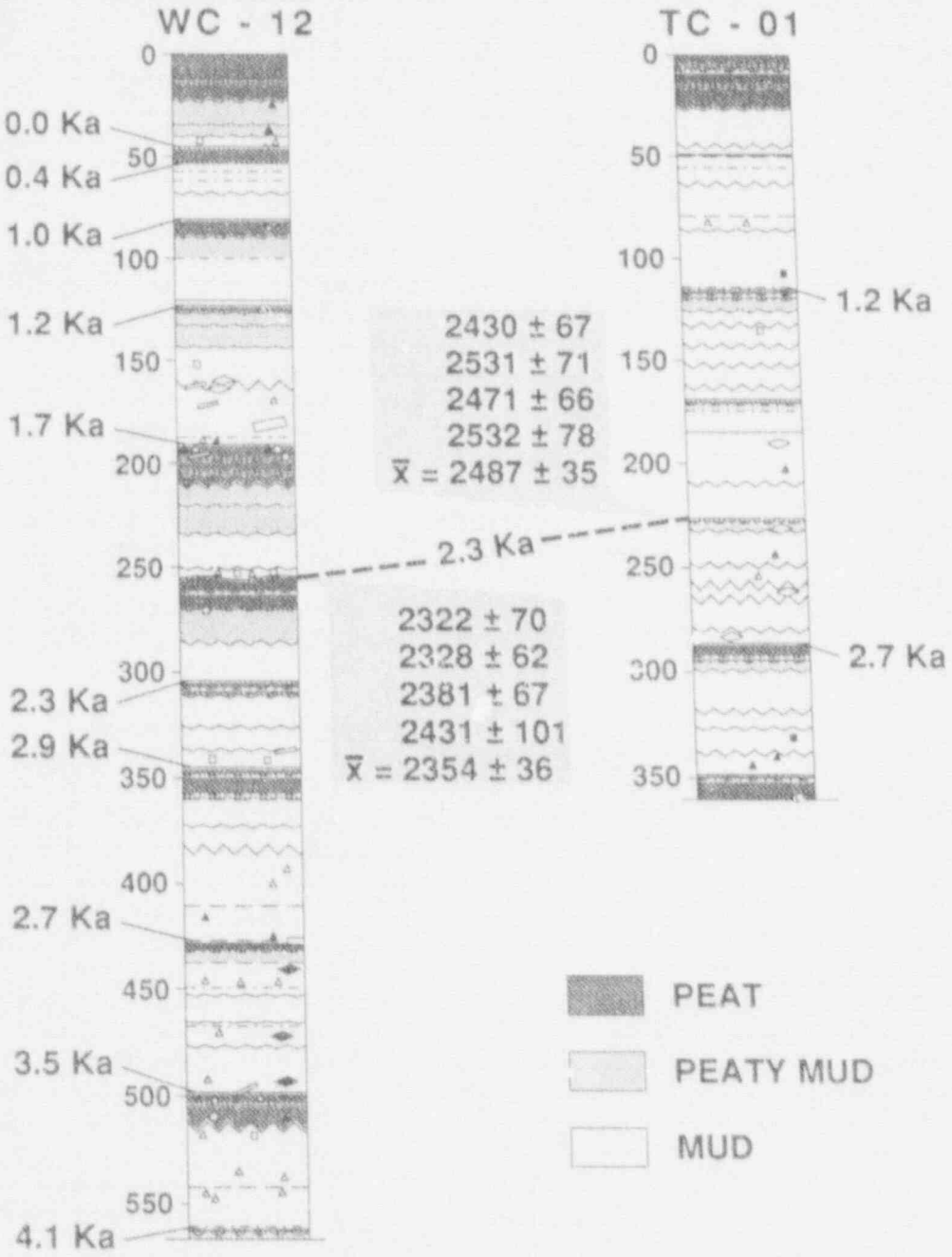

FIGURE . 4.-- General lithologies and ages (in thousands of ^{14}C years before A.D. 1950) for the tops of peaty soils in cores from sites near Winchester Creek (WC-12) and Talbot Creek (TC-01) in separate arms of South Slough, Coos Bay (location on Fig. 1). Contacts and symbols within shaded stratigraphic units show boundaries between lithologic subunits and fossils in more detail than discussed here. Approximate age estimates shown to left of core WC-12 are based on 20 conventional ^{14}C ages and seven AMS ages from that core (Nelson, in press b); approximate age estimates shown to right of core TC-01 are based on single AMS ages. Four ages from carefully selected and pretreated samples collected from the same soil (marked "2.3 ka") in both cores are shown with the mean age (x) and combined standard deviation of the mean age (Table 1).

Table 1.--Radiocarbon data for AMS samples from cores WC-12 and TC-01, South Slough, Coos Bay

Radiocarbon Laboratory No.	Sample depth (mm)[a]	Dry sample wt. (g)	No. hours cleaned[b]	Laboratory-reported age (^{14}C yr B.P. at 1σ)	Calibrated age (cal yr B.P. at 2σ)[c]	Description of dated material
Soil at 211 cm depth in core WC-12, Winchester Creek, South Slough, Coos Bay -- 43° 16' 45" N, 124° 19' 6" W						
AA-6964	+5	0.0047	1.0	2322±70		One half of leaf fragment, probably salal (*Gaultheria shallon*)
AA-6965	+3	0.0114	1.5	2328±62		Leaf fragment, probably salal (*Gaultheria shallon*)
AA-6966	-1	0.0044	1.0	2381±67		Two and a half western hemlock needles (*Tsuga heterophylla*)
AA-6967	+5	0.0034	1.0	2431±101		Other half of leaf fragment, probably salal (*Gaultheria shallon*)
			Mean age	2354±36	2710-2300	
Soil at 160 cm depth in core TC-01, Talbot Creek, South Slough, Coos Bay -- 43° 17' 20" N, 124° 17' 58" W						
AA-6960	-1	0.0069	0.5	2430±67		Douglas fir (*Pseudotsuga menziesii*) twig with leaf scars
AA-6961	0	0.0036	0.5	2531±71		Western hemlock (*Tsuga heterophylla*) twig with leaf scars
AA-6962	-2	0.0049	1.0	2471±66		Tips of two Port Orford cedar (cf. *Chamaecyparis lawsoniana*) bracts
AA-6963	-1	0.0025	0.5	2532±78		Western hemlock (*Tsuga heterophylla*) twig with leaf scars
			Mean age	2487±35	2740-2360	

[a] Depth of sample above (+) or below (-) the upper contact of the buried peaty soil.

[b] Time spent scraping AMS samples in distilled water at 20-50X.

[c] Ages calculated using method B of Stuiver and Reimer (1986) using decadal data set, error multiplier of 2, and age spans of 10 yr. Ages include time intervals of >95% probability distribution at 2σ.

diameter (7 cm) cores from each site showed a similar sequence of abruptly buried peaty soils (Fig. 4). However, the close vertical spacing of the soils and differences in their thicknesses and peat contents made stratigraphic correlation between the two sites uncertain. As discussed by Nelson (in press a), the soils at each site were probably submerged during either (1) tectonic subsidence of the axis of the South Slough syncline during great earthquakes on the plate interface or smaller earthquakes in the upper plate, or (2) sudden rises in tide levels due to the breaching of bars in the central and northern parts of the slough or to changes in the position of the mouth of the Coos River.

The correlated soils were selected on the basis of their peat-rich surface horizons with abrupt upper contacts. No rooted plant fossils were found at the tops of the sampled soils in the cores, so horizontally bedded, detrital plant material was carefully picked from the upper 2 mm of the soils or from bedding planes within the lower 5 mm of the mud overlying the sampled soils. Our samples consisted of hemlock needles, the small tips of fir and hemlock twigs and cedar bracts, and pieces of deciduous tree leaves (Table 1). All samples were identified at least to genus level, and then each part was scraped with a needle in distilled water under a binocular microscope (20-50X) to remove rootlets and any other foreign material.

Chemical pretreatment of the physically cleaned samples was similar to the acid-base-acid procedure used in pretreating conventional radiocarbon samples (e.g., Mook and van de Plassche, 1986) except that the procedure was repeated 5-8 times to be certain that no contaminants remained in the sample. All acid and base soluble components were removed from the samples by repeatedly rinsing with HCl and NaOH until no color change in the acid or base solutions was observed (e.g., Stafford and Tyson, 1988). Preparation of graphite targets and analysis of the targets in the accelerator at the NSF-Arizona Accelerator Facility for Radioisotope Analysis in Tuscon followed standard procedures for AMS ^{14}C samples (Linick et al., 1986; Donahue et al., 1990).

Results of Initial AMS Analyses

The results of the intial test of multiple AMS analyses are encouraging--the four ages from the tops of the soils in the two cores are not identical, but they are very similar (shaded boxes on Fig. 4). The greatest difference between two ages from the same soil was for two pieces of the same leaf. This difference is probably the result of the lower precision of AMS analysis on samples of less than 0.4 mg (note the standard deviation, σ, for sample AA-6967, Table 1). Our rigorous sample-selection procedures and the overlaps of the standard deviations of the four ages from each soil indicate that the samples from each soil are probably about the same age. A statistical test recommended by Ward and Wilson (1978, p. 21) also indicates that the four ages from each soil are probably from the same statistical populations and therefore can be averaged to give mean ages and standard deviations for the tops of each soil. Thus by averaging four or more AMS ages on samples of this type, standard deviations on mean AMS ages can be reduced to about ±25-40 radiocarbon years.

In order to compare the ages for the two soils at the two different sites the mean ages must be calibrated to allow for (1) variable ^{14}C production in the upper atmosphere (deVries effect; e.g., Stuiver and Pearson, 1986) and (2) total analytical errors in the radiocarbon analyses (Fig. 5). The estimated effects of total analytical errors in radiocarbon analysis (including pretreatment procedures) can be incorporated into a calibrated age by using an estimated *error multiplier* greater than 1 (Stuiver and Reimer, 1986). The shaded bands of figure 5 show how the mean ages in radiocarbon years (vertical axis) from Winchester Creek and Talbot Creek correspond with calibrated ages (horizontal axis). Initially considering only one standard deviation in the mean ages and an error multiplier of 1.0 (i.e., no additional analytical errors) the mean ages show how the shape of the calibration curve can affect the uncertainty in the resulting calibrated age. The

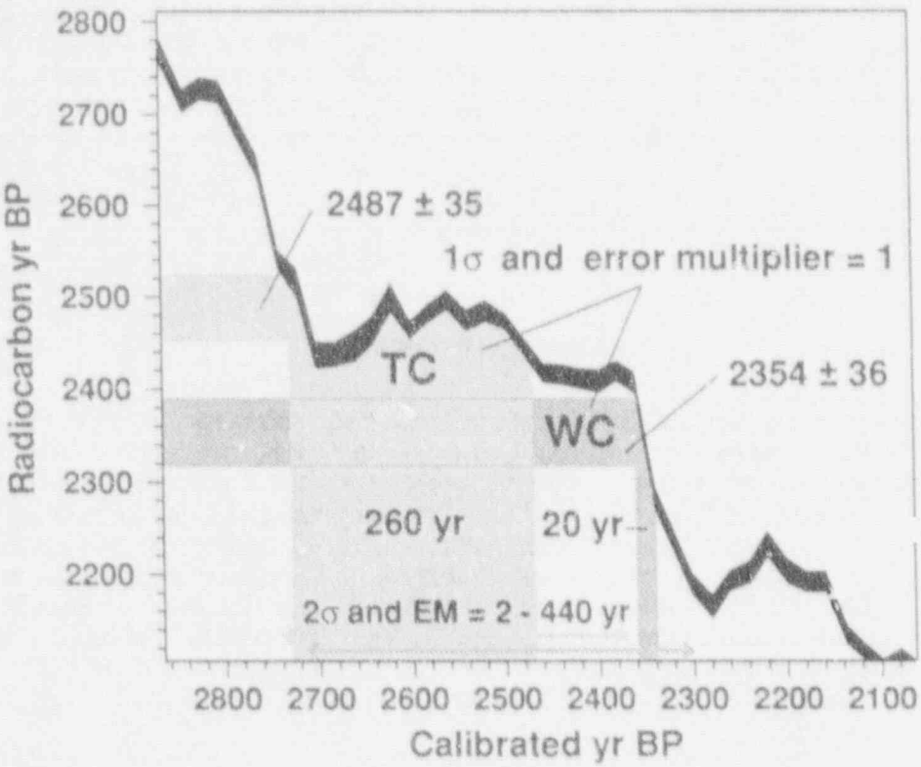

FIGURE . 5.-- Calibration of the mean AMS ages for the 2.3-ka soil in cores WC-12 and TC-01 from radiocarbon years to calibrated years (approximately calendar years before A.D. 1950). Heavy black line shows the calibration curve at one standard deviation from Stuiver and Pearson (1986). Shaded area shows how the mean age from core TC-01 (at one standard deviation with error multiplier of 1.0) corresponds to a calibrated-year time interval of 260 yr; the mean age from WC-12, which falls on a more favorable portion of the calibration curve, corresponds with a calibrated-year time interval of only 20 yr. Note that with an error multiplier of 1.0 at one standard deviation the calibrated age intervals do not overlap. However, if a more reasonable error multiplier of 2.0 is used (EM=2), the calibrated ages from the cores overlap considerably at two standard deviations (overlap shown by arrows above the horizontal axis). Because of this overlap we cannot infer that the soils in both cores were submerged at different times.

Winchester Creek mean age corresponds with a steep part of the calibration curve, resulting in a calibrated age interval of only 20 calibrated years (cal yr). In marked contrast, the Talbot Creek mean age corresponds with a subhorizontal part of the curve that contains multiple fluctuations, resulting in a calibrated age interval of 260 cal yr.

However, if a more realistic error multiplier of 2.0 is used (e.g., Scott et al., 1990) and two standard deviations in the mean ages are considered (95% confidence level), then the ages from both sites intersect longer parts of the calibration curve and the resulting calibrated-age intervals span much larger time intervals. The shaded arrows just above the horizontal axis of figure 5 show the range of the corresponding calibrated ages at 2σ if an error multiplier of 2.0 is used. These two larger calibrated age intervals (which span a total range of 440 cal yr) overlap considerably, and so the soils probably do not differ in age by more than this total age range. The soils may well have been submerged at exactly the same time, but from these two calibrated ages we can only conclude that they were submerged within the same 440 year period.

CONCLUSIONS

The precision of age estimates for times of tidal-marsh soil submergence in the Pacific Northwest can be improved by averaging multiple accelerator-mass-spectrometer (AMS) ^{14}C analyses of rigorously selected and pretreated plant macrofossils at the abrupt upper contacts of buried soils. An initial test of this method in the South Slough arm of Coos Bay shows that standard deviations on mean AMS ages can be reduced to ±25-40 radiocarbon years. However, consideration of the total analytical errors in AMS analysis and age differences due to changes in the rate of ^{14}C production in the atmosphere over time support the use of 95% confidence limits, which yield calendar-year-corrected ages for burial events of about 50-450 years. Events that occurred only 100 years apart may be distinguishable if their ages fall on favorable parts of the ^{14}C calibration curve. But in other cases we may not be able to distinguish events that occurred as much as 450 years apart.

Even greatly improved accuracy and precision in the dating of submergence times cannot prove that a soil submerged and buried about the same time along hundreds of kilometers of coastline was submerged during the same earthquake. However, more precise but discordant ages might show that soils at different sites are not the same age. Discordant ages from buried soils along much of the Washington and Oregon coasts would be inconsistent with the hypothesis that great plate-interface earthquakes as large as M 9 have ruptured several 150- to 300-km-long segments of the Cascadia subduction zone (e.g., Heaton and Hartzell, 1987; Rogers, 1988). Rather, discordant ages would suggest several alternatives: (1) great plate-inteface earthquakes were of lower magnitude (perhaps M 8-8 1/2) and did not cause regional coastal subsidence, (2) shallow, moderate to large (M 6-7 3/4), upper-plate earthquakes produced only localized coseismic subsidence, or (3) buried marsh soils were abruptly submerged by non-tectonic processes (Nelson and Personius, in press; Nelson, in press a).

ACKNOWLEDGEMENTS

This study was supported by the National Earthquake Hazards Reduction Program of the U.S. Geological Survey and by the U.S. Nuclear Regulatory Commission. Jan Hodder and other staff members of the Oregon Institute of Marine Biology, Charleston, Oregon, and Mike Graybill of the South Slough National Estuarine Research Reserve provided facilities, logistical support, and encouragement. Lee-Ann Bradley did the graphics. We thank Brian Atwater for discussions. Comments by Bob Bucknam and Steve Personius improved this paper. This is a contribution to IGCP Project 274.

REFERENCES

Adams, John (1990). Paleoseismicity of the Cascadia subduction zone--Evidence from turbidites off the Oregon-Washington margin. *Tectonics* 9, 569-583.

Allen, E.A.D. (1978). Petrology and stratigraphy of Holocene coastal-marsh deposits along the western shore of Delaware Bay. Ph.D. thesis, Dept. of Geology, Univ. of Delaware, Newark, Delaware, 287pp.

Allen, J.R.L. (1990). Salt-marsh growth and stratification--A numerical model with special reference to the Severn Estuary, southwest Britain. *Marine Geology* 95, 77-96.

Atwater, B. F. (1987). Evidence for great Holocene earthquakes along the outer coast of Washington state. *Science* 236, 942-944.

Atwater, B. F., and Yamaguchi, D.K. (1991). Sudden, probably coseismic submergence of Holocene trees and grass in coastal Washington State. *Geology* 19, 706-709.

Atwater, B.F., (in press). Earthquake-induced liquefaction about 1100 years ago in southern coastal Washington. *Journal of Geophysical Research*.

Atwater, B. F., Stuiver, Minze, and Yamaguchi, D.K. (1991). Radiocarbon test of earthquake magnitude at the Cascadia subduction zone. *Nature* 353, 156-158.

Berryman, K. R., Ota, Yoko, and Hull, A.G . (1989). Holocene paleoseismicity in the fold and thrust belt of the Hikurangi subduction zone, eastern North Island, New Zealand. *Tectonophysics* 163, 185-195.

Clarke, S. H., Jr., Field, M. E., and Hirozawa, C. A. (1985). Reconnaissance geology and geologic hazards of the offshore Coos Bay basin, Oregon. U.S. Geological Survey Bulletin 1645, 41 pp.

Darienzo, M. E., and Peterson, C. D. (1990). Episodic tectonic subsidence of late Holocene salt marshes, northern Oregon coast, central Cascadia margin, U.S.A. *Tectonics* 9, 1-22.

Donahue, D.J., Linick, T.W., and Jull, A.J.T. (1990). Isotope-ratio and background corrections for accelerator mass spectrometry radiocarbon measurements. *Radiocarbon* 32, 135-142.

Elmore, David, and Phillips, F.M. (1987). Accelerator mass spectrometry for measurement of long-lived radioisotopes. *Science* 236, 543-550.

Frey, R. W., and Basan, P. B. (1985). Coastal salt marshes. In "Coastal sedimentary environments" (R. A. Davis, Jr., Ed.). pp. 225-302. Springer-Verlag, New York.

Grant, W. C. (1989). More evidence from tidal-marsh stratigraphy for multiple late Holocene subduction earthquakes along the northern Oregon coast. *Geological Society of America Abstracts with Programs* 21, No. 5, pp. 86.

Grant, W. C., Atwater, B. F., Carver, G. A., Darienzo, M. E., Nelson, A. R., Peterson, C. D., and Vick, G. S. (1989). Radiocarbon dating of late Holocene coastal subsidence above the Cascadia subduction zone--Compilation for Washington, Oregon, and northern California. *EOS, Transactions of the American Geophysical Union* 70, No. 43, pp. 1331.

Heaton, T. H., and Hartzell, S. H. (1987). Earthquake hazards on the Cascadia subduction zone. *Science* 236, 162-168.

Kaye, C. A., and Barghoorn, F. S. (1964). Late Quaternary sea-level change and crustal rise at Boston, Massachusetts with a note on the autocompaction of peat. *Geological Society of America Bulletin* 75, 63-80.

Keach, R.W., Oliver, J.E., Brown, L.D., and Kaufman, S. (1989). Cenozoic active margin and shallow Cascades structure--COCORP results from western Oregon, *Geological Society of America Bulletin* 101, 783-794.

Kelsey, H. M. (1990). Late Quaternary deformation of marine terraces on the Cascadia Subduction Zone near Cape Blanco, Oregon. *Tectonics*, 9, 983-1014.

Linick, T.W., Jull, A.J.T., Toolin, L.J., and Donahue, D.J. (1986). Operation of the NSF-Arizona Accelerator Facility for Radioisotope Analysis and results from selected collaborative research projects. *Radiocarbon* 28, 522-533.

Matsuda, T., Ota, Yoko, Ando, M. and Yonekura, N. (1978). Fault mechanism and recurrence time of major earthquakes in southern Kanto district, Japan, as deduced from coastal terrace data. *Geological Society of America Bulletin* 89, 1610-1618.

Matthews, J. A. (1980). Some problems and implications of ^{14}C dates from a podzol buried beneath an end moraine at Haugabreen, southern Norway. *Geografiska Annaler* 62A, 185-208.

McInelly, G. W., and Kelsey, H. M. (1990). Late Quaternary tectonic deformation in the Cape Arago-Bandon region of coastal Oregon as deduced from wave-cut platforms. *Journal of Geophysical Research* 95, No. B5, 6699-6713.

Mook, W. G., and van de Plassche, Orson (1986). Radiocarbon dating. In "Sea-level research--A manual for the collection and evaluation of data" (Orson van de Plassche, Ed.), pp. 525-560. Geo Books, Norwich, U.K.

Nelson, A.R., (in press a). Constrasting styles of late Holocene relative sea-level change revealed by tidal-marsh stratigraphy, south-central Oregon coast, Cascadia subduction zone, In "Quaternary coasts of the United States--Lacustrine and marine systems" (Fletcher, C.P., and Wehmiller, J.F., Eds.) SEPM-IGCP Special Publication.

Nelson, A.R., (in press b). Discordant ^{14}C ages limit correlations of Holocene tidal-marsh soils in the Cascadia subduction zone, southern Oregon. *Quaternary Research.*

Nelson, A. R., and Personius, S. F., (in press). The potential for great earthquakes in Oregon and Washington--An overview of recent coastal geologic studies and their bearing on segmentation of Holocene ruptures, central Cascadia subduction zone. In "Assessing and reducing earthquake hazards in the Pacific Northwest" (Rogers, A. M., Kockelman, W. J., Priest, G. R., and Walsh, T. J., Eds.). U.S. Geological Survey Professional Paper 1560, (Director's approval pending; released in preliminary form as USGS Open-File Report 91-441-A).

Newton, V.C., Jr. (1980). Prospects for oil and gas in the Coos Basin, western Coos, Douglas, and Lane Counties, Oregon. Dept. of Geology and Mineral Industries, State of Oregon, Oil and Gas Investigation No. 6, 74pp.

Peterson, C. D., and Darienzo, M. E. (in press). Discrimination of climatic, oceanic, and tectonic forcing of marsh burial events from Alsea Bay, Oregon, U.S.A. In "Assessing and reducing earthquake hazards in the Pacific Northwest" (A. M. Rogers, W. J. Kockelman, G. R. Priest, and T. J. Walsh, Eds.). U.S. Geological Survey Professional Paper 1560, (Director's approval pending; released in preliminary form as USGS Open-File Report 91-441-F).

Plafker, George (1969). Tectonics of the March 27, 1964 Alaska earthquake. U.S. Geological Survey Professional Paper 543-I, 94 pp..

Plafker, George (1972). Alaskan earthquake of 1964 and Chilean earthquake of 1960--Implications for arc tectonics. *Journal of Geophysical Research* 77, 901-924.

Plassche, Orson, van de (1982). Sea-level change and water-level movements in the Netherlands during the Holocene. Mededelingen rijks geologische dienst 36-1, 93 pp.

Plassche, Orson van de (in press).Late Holocene sea-level fluctuations on the shore of Connecticut inferred from transgressive and regressive overlap boundaries in salt-marsh deposits. In "Quaternary coastal evolution of southern New England." (Gayes, P.T., Lewis, R.S., and Bokuniewicz, H.G., Eds.) *Journal of Coastal Research*, special issue no. 12.

Rogers, G. C. (1988). An assessment of the megathrust earthquake potential of the Cascadia subduction zone. *Canadian Journal of Earth Sciences* 25, 844-852.

Scott, E.M., Aitchison, T.C., Harkness, D.D., Cook, G.T., and Baxter, M.S. (1990). An overview of all three stages of the International Radiocarbon Intercomparison. *Radiocarbon* 32, 309-320.

Shennan, Ian (1986). Flandrian sea-level changes in Scotland. I--The geographical setting and evidence of relative sea-level changes. *Journal of Quaternary Science* 1, 119-154.

Snavely, P.D., Jr., Wagner, H.C., and Lander, D.L. (1985). Land-sea geologic cross section of the southern Oregon continental margin. U.S. Geological Survey Miscellaneous Investigations Series Map I-1463, 1:125,000 scale.

Stafford, T.W., Jr., and Tyson, R.A. (1988). Accelerator dates on charcoal, shell, and human bone from the Del Mar early Man site, California. *American Antiquity* 54, 389-395.

Streif, Hansjorg (1987). Barrier islands, tidal flats, and coastal marshes resulting from a relative rise of sea level in East Frisia on the German North Sea coast. In "Coastal lowlands--geology and geotechnology, Proceedings of the symposium on coastal lowlands" (W. J. M. van der Linden, S.

A. P. L. Cloetingh, J. P. K. Kaasschieter, W. J. E. Graff, J. Vandenberghe, and J. A. M. van der Gun, Eds.). pp. 213-223. Kluwer Academic Publishers, Dordrecht.

Stuiver, Minze, and Pearson, G. W. (1986). High-precision calibration of the radiocarbon time scale, AD 1950-500 BC. *Radiocarbon* 28, 805-838.

Stuiver, Minze, and Reimer, P. J. (1986). A computer program for radiocarbon age calibration. *Radiocarbon* 28, 1022-1030 (Rev. 2.0).

Taylor, R. E. (1987). "Radiocarbon dating--An archaeological perspective." 212 pp. Academic Press, Orlando.

Tooley, M. J., Ed. (1978). "Sea-level Changes in North-west England during the Flandrian Stage". 205 pp. Clarendon Press, Oxford, U.K.

Valentine, D.W., Carver, G.A., and Shivelle, Christine (1990). Late Holocene stratigraphic evidence for rapid episodic subsidence, Humboldt Bay, California. *Geological Society of America Abstracts with Programs* 22, No. 7, A23.

Vick, G.S. (1988). "Late Holocene paleoseismicity and relative sea level changes of the Mad River Slough, northern Humboldt Bay, California." Unpublished M.S. thesis. 87 pp. Dept. of Geology, Humboldt State University, Arcata, California.

Ward, G. K., and Wilson, S. R. (1978). Procedures for comparing and combining radiocarbon age determinations--A critique. *Archaeometry* 20, 19-31.

Soil/Structure Interactions of Eastern U. S. Type Earthquakes

Chang Chen, Ph.D., P.E.
Assistant Chief Engineer
and
Samir J. Serhan, Ph.D.
Senior Structural Engineer

Gilbert/Commonwealth, Inc.
P.O. Box 1498
Reading, Pa. 19603

ABSTRACT: This paper presents analyses and conclusions pertaining to the earthquake motions felt at Virgil C. Summer, Perry and Krsko nuclear power plants. Consideration is given to promote an improved understanding of these events, describe common characteristics, assess damage potential, and recommend operating procedures for similar future events. An easy-to-follow analytical investigation is performed to describe how the earthquakes recorded at Krsko may be influenced by soil/structure interaction including a few parametric studies to account for uncertainties in the soil properties. These consist of variations in the shear and compressional wave velocities and variations in the seismic wave environment in the form of arbitrarily oriented body waves and Rayleigh waves. The analysis takes into account nonlinearity of the soil material, radiation and hysteretic damping, ground-water table level, structural embedment, and structure/structure interaction. The analysis is based on state-of the-art computer software, elaborate analysis techniques and simpler engineering approximations. Results of analysis show clear evidence of soil/structure interaction, nonlinear softening of the soil material and encouraging qualitative and quantitative agreement with the recorded measurements. The structural response motions display high rocking mode.

1. INTRODUCTION

Several types of earthquakes have occurred in the eastern U. S. in the past. One type is the infrequent major events such as the 1811-1812 New Madrid Earthquakes, or the 1886 Charleston Earthquake. Another type is the frequent shallow earthquakes with high frequency, short duration and high accelerations. Two eastern U. S. nuclear power plants, V. C. Summer, and Perry, went through extensive licensing effort to obtain fuel load licenses after this type of earthquakes was recorded on sites and exceeded the design basis beyond 10-Hertz region.

Current NRC staff interim position [1] on this type of eastern earthquakes will prevent the operating plants from going tnrough unnecessary licensing efforts if the future recorded events are less than a magnitude of 5 1/4, within 25 km of the plants, and with acceleration spectrum exceedance beyond the 10 hertz region. EPRI [2] also suggests the Cumulative Absolute Velocity (CAV) of 0.3 g-sec as the non-exceedance criterion. This kind of short duration, high frequency, and high acceleration earthquakes is non-damaging for passive systems, components, or rugged active mechanical components. The possible engineering significance of this type of earthquakes is the impact on active electric or control systems equipment. Under certain circumstances, operator's actions will be able to correct spurious actuations of safety systems due to relay chattering caused by this type of eastern earthquakes. Soil/structure interaction of this type of earthquakes will assist to determine the need of operator's actions.

There were many soil/structure interaction analyses perfo. in the past. However, there was a lack of recorded data to ver: analysis results. For this reason, EPRI co-sponsored a seismic experiment [3] with 1/4 and 1/12 scale models constructed in Lotung, Taiwan. The previously mentioned seismic data recorded at V. C. Summer and Perry Nuclear Power Plants were not adequate to verify soil/structure interaction results. V. C. Summer data were recorded on an adjacent dam abutment but not inside the plant. Perry data was recorded inside the plant but not in the free field. However, Perry data was used to verify the structural model of dynamic analysis which successfully duplicated the high frequency responses on the steel containment as recorded.

On December 28, 1989, a magnitude 3.9 event occurred adjacent to Krsko Nuclear Power Plant, in the Republic of Slovenia, Yugoslavia. The plant is instrumented in accordance with USNRC Regulatory Guide 1.12. The strong motion instruments were activated. The records have the same characteristics of typical eastern U. S. earthquakes, namely, high frequency, short duration, and high accelerations. The recorded maximum horizontal compon t is 0.5g in the free field at the surface. However, the recorded acceleration in the same direction in the Reactor Building base mat is only 0.05g and that in the Diesel Generator Building is 0.1g. Traditionally, an earthquake of such a small magnitude was not analyzed because of its lack of damaging potential. However, since this is one of the few cases that strong motion data was recorded both inside and outside of an operating nuclear power plant, it is useful for verifying soil structural interaction analysis results. Furthermore this unusually high reduction factor from free surface to base mat needs investigation to determine whether the same kind of reduction can be expected for future earthquakes of larger magnitude.

Krsko Nuclear Power Plant is located in the Krsko block. In the geological past, regional tectonic conditions produced horizontal tension which caused the Krsko block to subside relative to boundary blocks. Thus, the plant is on top of about 700 m of soil deposit. At the current time the regional tectonics is under compression with maximum principal stress approximately in the North-South direction. The Reactor Building has about 16 meters of embedment. FLUSH [4] and Gilbert/Commonwealth vectorized version of SASSI program [5] on Cray computer was used to perform the soil/structure interaction analysis. Parametric study was performed to obtain the optimum parameters and assumptions in order to match not only the acceleration but also the frequency content of the responses. This paper describes the parametric studies, their results and conclusions with regard to future applications.

The seismic wave environment is assumed to consist of vertically propagating shear waves due to the low reduction of the high frequency portion of the measured structural response compared with the free field response counterpart. SASSI soil/structure interaction analysis of the December 1985 Earthquake resulted in encouraging qualitative and quantitative agreement with the recorded measurements for both horizontal East-West and North-South directions. Results of the analysis show clear evidence of strong soil structure interaction effects. The structural response motions displayed strong rocking mode participation due to irregular base mat shape in the vertical plane, and the high-frequency short-wave length input.

2. AUGUST 27 1978 and OCTOBER 16 1979 EVENTS AT MONTICLLLO [6]

The Virgil C. Summer Nuclear Station is located near Jenkinsville, South Carolina, approximately 26 miles northwest of Columbia. Numerous low-magnitude earthquakes occurred after South Carolina Electric & Gas began filling Monticello Reservoir to provide cooling water. On August 27 1978, an earthquake with a local magnitude of 2.8 occurred at a depth between 100m to 500m. The event triggered the strong-motion accelerometer, which was operated by The U.S. Geologic Survey. The accelerometer is located 3/4 mile northwest of the Virgil C. Summer Station and its foundation is underlain by 56 feet of saprolite soil. The plant was not operating and the installation of the plant earthquake-monitoring network was not completed. The event as shown in Figure 1 (parts b & c) has very high frequency content and short duration with a maximum acceleration of 0.25g.

On October 16 1979, another 2.8-magnitude event was recorded at the USGS strong motion accelerometer. This event has the same characteristics of high frequency and short duration as shown in Figure 1 (part a). Its maximum acceleration is 0.36g.

Both events were recorded in the free-field adjacent to the nuclear power plant. Since there was no record inside the plant, these data can not be used to verify soil/structure effects.

2. JANUARY 31 1986 EVENT at LEROY, OHIO [7]

On January 31, 1986, a 5.0-magnitude earthquake occurred near Leroy, Ohio at a depth between 5 km and 8 km along a strike-slip plane dipping near vertical. The epicenter area was estimated to be 17 km to the south of Perry Power Plant. Perry Power Plant was under pre-operational testing prior to fuel load at the time of the earthquake. The plant earthquake instrumentation was functional and recorded the event. The Perry site is approximately 35 miles northeast of Cleveland on the shore of Lake Erie.

This event was recorded at the base mat and the containment polar crane elevation of the Reactor Building. Figure 2 shows the recorded North-South motion at the base mat. Results display high amplitude, high frequency and short duration characteristics. The recorded motions were used to verify the original structural analysis model. Since the seismic motions were only recorded inside the building but not in the free field. Therefore, they can not be used to verify the soil/structure interaction effects.

3. DECEMBER 28 1989 EVENT at KRSKO, YUGOSLAVIA [8]

The Krsko Nuclear Power plant (KNPP) is located 2 km east of the town of Krsko on the northern bank of the Sava River in the Republic of Slovenia. It belongs geologically to the Krsko Depression. On December 28 1989, KNPP experienced a short-duration high-frequency earthquake with a magnitude of 3.9 that triggered plant seismic instrumentation. Acceleration records were obtained inside the buildings and a nearby free-field ground-motion recording station. Figure 3 Schematically shows the plan of KNPP, locations of earthquake instrumentation, and recorded peak acceleration.

This paper describes results of an analytical assessment of how the December 1989 Earthquake records measured at KNPP may be influenced by soil/structure interaction. Emphasis is placed to determine the causes behind the relatively high response of the Diesel Generator Building compared to the Reactor Building using the December 1989 Earthquake records.

This investigation is based on two-dimensional and three-dimensional models of the buildings and the surrounding soil medium and on using two different soil/structure analysis techniques- FLUSH and SHAKE/SASSI codes.

3.1 EARTHQUAKE SEISMIC MEASUREMENTS

Accelerometers were installed on the mats of the Reactor Building (A3) and Diesel Generator Building (A7), one free-field accelerometer (A1) in a small shelter located 50 m south of the Reactor Building and one downhole (A2) 10 m below A1 location. Each station contains three sensors capable of recording absolute acceleration time histories in the three orthogonal directions (Channel 1 for East-West direction, Channel 2 for Vertical direction and Channel 3 for North-South direction). A1 and A3 transmit data to the Control Room, but A7 is a self-contained instrument. Acceleration data is band-pass filtered between 0.05-0.5 Hertz and 33.0-35.0 Hertz.

Figures 4 through 5 show the recorded seismic free-field surface and Diesel Generator Building acceleration time history. The following observations are made:

Observation 1. Acceleration time histories display less than 1 sec of relatively strong motion, which leads to a short duration classification of the December 1989 earthquake.

Observation 2. The free-field peak ground acceleration at A1CH1 is 0.53 g, a relatively high value.

Observation 3. Reductions factors (RF) from free-field (FF) peak accelerations to Diesel Generator Building (DGB) and Reactor Building (RB) peak accelerations are:

Direction	FF	DGB	RF	RB	RF
E-W	0.53	0.19	2.8	0.05	10.5
N-S	0.45	0.14	3.9	0.08	5.4
Vertical	0.13	0.16	0.8	0.04	3.9

Results show reduction factors larger than unity, except for the response of the Diesel Generator Building in the vertical direction where amplification occurs. The Diesel Generator Building displays smaller reduction factors in all global directions compared to the Reactor Building.

3.2 FREQUENCY CONTENT

Response spectral comparisons of recorded free-field surface motions at A1 with recorded structural motions at A7 are presented in Figure 6. The dominant energy content for A1 motions is concentrated above 8 Hz which indicates a near-field event. The amplitude level, frequency content and shaking duration of surface ground motions caused by propagating seismic waves through the soil are significantly different from the motion in

the underlying bedrock. Some frequencies of propagating seismic waves experience soil amplification, but other waves having frequencies higher than the natural frequencies of the soil medium may experience de-amplification. However, the above modifying role of soil is not as effective for near-field events and this could explain the high-frequency content of the December 1989 Earthquake.

The recorded seismic motions of the Diesel Generator Building also display a dominant energy content above 8 Hz and demonstrate response amplification at about 12 Hz, compared to A1 records for the vertical direction. In both horizontal directions, a significant reduction in peak accelerations and amplitudes of acceleration response spectra exists for frequencies higher than 4 Hz. These observations could be explained by one or more of the following effects:

* Free-field soil de-amplification due to local soil and geologic conditions.

* Kinematic attenuation when the wavelength of propagating seismic waves is equal to or smaller than the embedded foundation dimension in the direction of wave propagation. Kinematic interaction is more significant for higher -frequency ground motions and non-vertical incident waves.

* Inertial interaction when input motions possess harmonic components that are far away from the lower vibration frequencies of the structure.

The overall soil/structure interaction consists of both kinematic and inertial effects.

3.3 COMPARISON WITH PLANT SEISMIC DESIGN BASIS

Comparisons of plant design response spectra with response spectra of recorded seismic measurements at the free-field surface are shown in Figures 7 for all three global directions. Design spectra were based on the USNRC Regulatory Guide 1.60 design spectra for seismic design of nuclear power plants. The USNRC Regulatory Guide 1.60 spectra are normalized to the peak ground acceleration measured in each direction and not to the plant OBE or SSE design accelerations. Recorded response spectra exceed design spectra at free-field surface for E-W, N-S and Vertical directions. The exceedance is at frequencies higher than 10 Hz. This suggests that The December 1989 Earthquake is similar to the eastern U.S. earthquakes which are usually of short duration and have high-frequency content. Based on earthquake experience at power and industrial facilities [2,6,7], high-frequency motions do not possess enough energy demand to cause damage or the need for plant shutdown. Additional conditions on maximum recorded displacement and velocity at foundation level are required before plant shutdown when OBE or SSE design spectra

are exceeded [7]. In Reference [2], it is concluded that only spectral ordinates below 10 Hertz need to be considered for damage potential and recommended a two-condition criterion for OBE exceedance.

First Condition: Recorded spectrum exceeds OBE design spectrum at 2-10 Hz frequencies or 0.2 g threshold value, whichever is greater, using 5% damping ratio.

Second Condition: The CAV of recorded motion is higher than 0.3 g.sec.

3.4 DYNAMIC SOIL PROPERTIES

The plant is located on an approximately 700-m thick pre-consolidated Pliocene sandy-clay alluvial material. The sub-surface conditions at the site were explored by borings. Cross-hole method was used to measure S and P wave velocities in a pair of holes up to 100 m in depth and gamma-gamma method to measure material density. Based on geoelectric borings in the range of 100 m to 300 m in depth, no lithological changes were found. At Depth 145.8 m, the compressional wave velocity is 1790 m/sec (higher than 1500 m/sec; seismic velocity of water), which suggests a completely saturated soil.

Laboratory tests were conducted to determine strain-dependent shear modulus and damping of the soil underlying the plant. The resulting curves are consistent with standard curves reported in literature. The strain-dependent curves are intended to simulate material nonlinearities of soil medium under cyclic loading with high-strain levels.

3.5 FREE-FIELD SOIL RESPONSE

Based on the dynamic soil properties, a free-field soil-column model is developed. The purpose of SHAKE [9] analyses is to obtain strain-compatible soil properties with the December 1989 Earthquake level and to construct dynamic characteristics of downhole data.

Several computer runs are made to check the stability and accuracy of results by varying layer thickness and depth of halfspace bottom layer.

The input motions for the soil-column analyses are the two-horizontal component recorded ground surface acceleration time histories at A1 station. A parametric study is performed to find the cut-off frequency for the soil-column analyses. Results display the high-frequency composition of the December 1989 Earthquake and a cut-off frequency of 33 Hz is required to obtain 0.53 g peak acceleration at the surface. Several SHAKE runs are

made to assure no erroneous results in the higher frequencies and to achieve a stable solution.

Results show a good match in the overall shape of Fourier spectra of deconvoluted motions and recorded motions at A3 and A7 stations. Response amplification of the Diesel Generator Building occurs at about 12.5 Hz.

3.6 PRELIMINARY SOIL/STRUCTURE INTERACTION ANALYSES

3.6.1 Two-Dimensional Analysis of the Diesel Generator Building Using FLUSH Code

A two-dimensional finite element model of the Diesel Generator Building is developed. Due to the symmetry, half of the East-West direction is considered. The model consists of quadrilateral elements to represent the massive embedded foundation block. The weight of the superstructure is included in the analysis but its stiffness is not accounted for at this stage of analysis assuming that the Diesel Generator Building superstructure responds rigidly.

A direct comparison of recorded spectrum at A7 station for East-West direction and analysis response spectrum using FLUSH soil/structure interaction technique demonstrates a poor correlation in terms of the zero-period acceleration and the overall shape of response spectrum.

	A7 (Recorded)	FLUSH Analysis (Predicted)
ZPA (g's)	0.19	0.35
Peak Frequency (Hz)	12.5	8.5
Pe Acceleration (g's) (5% damping)	0.56	1.13

3.6.2 Two-Dimensional Analysis of the Diesel Generator Building Using SASSI Code

A two-dimensional model of the Diesel Generator Building is developed to perform SASSI [5] analysis. The structural model only includes the 4-m deep base mat without the superstructure. The input control motion is the recorded acceleration time history at the free-field surface for East West direction. The seismic wave environment is assumed to consist of vertically propagating SV waves. This assumption is based on:

* The shear wave velocity generally increases with depth, which results in continuous refractions upward of seismic waves.

* The motion in the underlying rock formations has to go through a very deep soil deposit to reach the surface.

* The December 1989 Earthquake is a near-field event.

The two-dimensional SASSI analysis shows similar results to FLUSH analysis, but still a good correlation with the recorded seismic motions is not achieved.

	A7 (Recorded)	SASSI Analysis (Predicted)
ZPA (g's)	0.19	0.32
Peak Frequency (Hz)	12.5	7.7
Peak Acceleration (g's) (5% damping)	0.56	0.97

3.6.3 TWO-DIMENSIONAL MODEL OF THE DIESEL GENERATOR BUILDING INCLUDING SUPERSTRUCTURE

A two-dimensional model of the Diesel Generator Building is developed including the superstructure to account for inertial eccentricity. The roof is 7.6 m above the finished grade. The exterior walls and roof are made of reinforced concrete. The superstructure is modeled using beam and quadrilateral elements. The beam elements represent the walls and roof slabs that extend normal to the plane of the model. The quadrilateral elements represent the effective in-plane stiffness and mass of the three (3) transverse shear walls. The lower 13.5 ft of the Diesel Generator Building is embedded in the ground. The elastic halfspace of the soil medium is placed 83.5 ft from the base of the Diesel Generator Building.

The East-West component of the recorded surface motion is applied as the input control motion. Seismic wave environment consists of vertically propagating shear waves. SHAKE strain-compatible soil properties are used in this two-dimensional SASSI soil/structure evaluation.

Results display no significant changes in terms of the frequency content and ZPA value as a result of including the superstructure.

	A7 (Recorded)	SASSI Analysis Including the Superstructure (Predicted)
ZPA (g's)	0.19	0.31
Peak Frequency (Hz)	12.5	7.7
Peak Acceleration (g's) (5% damping)	0.56	0.95

3.7 PARAMETRIC STUDY: SEISMIC WAVE ENVIRONMENT

In the previous analyses, soil/structure interaction analyses assumed that there is no scattering of the impinging waves. This is the case for a foundation subjected to vertically propagating waves [10]. However, scattering effects can reduce the effective input motion to the structure. Scattering effects are a function of frequency content and incident angle of seismic motion, foundation geometry and dynamic properties of the supporting ground. Orientation and location of the source earthquake relative to the site (epicentral distance and focal depth) provide good prospects for predicting the incident angle. Lack of high-quality seismographic data of the December 1989 Earthquake precluded direct evaluations of the seismic wave environment.

Four SASSI runs are made to investigate the effects of variations in the wave types and incident angle. They are

(1) SV waves with 15 degrees incident angle
(2) SV waves with 30 degrees incident angle
(3) Vertically propagating P waves
(4) Rayleigh surface waves

Comparisons between the predicted results of 0-degree incident angle SV run and the results of these four (4) runs are presented below for East-West and Vertical directions.

X-ACC [East-West Direction]

	0° SV	15° SV	30° SV	0° P	Rayleigh
ZPA (g's)	0.21	0.27	0.24	0.00	0.13
Peak Freq. (Hz)	7.7	7.7	7	24.9	6.8
Peak Acc. (g's) (5% damping)	0.95	0.84	0.69	0.01	0.33

Z-ACC [Vertical Direction]

	0° SV	15° SV	30° SV	0° P	Rayleigh
ZPA (g's)	0.07	0.06	0.05	0.09	0.34
Peak Freq. (Hz)	13.8	13.8	12.3	10.9	7.7
Peak Acc. (g's) (5% damping)	0.25	0.39	0.25	0.32	1.18

This parametric study was conducted to improve the ZPA value and the shape of the frequency response curve. The former can be achieved by increasing the incident angle of the SV waves, however, the latter is not achieved yet. The frequency response curve still shows the calculated peak is at a lower frequency.

3.8 THREE-DIMENSIONAL SOIL/STRUCTURE INTERACTION ANALYSIS OF THE DIESEL GENERATOR BUILDING

A three-dimensional finite element model of the Diesel Generator Building is developed to investigate three-dimensional effects and to evaluate the results of the two-dimensional analyses. Due to the shallow embedment, the base mat is placed on the ground surface. The superstructure is modeled as a rigid beam with a concentrated weight at the end to account for inertial eccentricity. Three-dimensional solid elements (3 translational DOF) are used to model the excavated soil and the base mat, and rigid beam elements are used to model the longitudinal and transverse shear walls.

The deconvoluted SHAKE acceleration time history at Elevation -13 ft is used as the input control motion. The seismic wave environment consists of vertically propagating shear waves.

Results show good correlation between the two- and three-dimensional in terms of the overall shape of the frequency response curve. However, the two-dimensional analysis slightly underestimates the calculated acceleration values.

	2D Analysis	3D Analysis	Ratio
ZPA (g's)	0.18	0.2	1.11
Peak Frequency (Hz)	6.8	6.8	1.00
Peak Acceleration (g's)	0.42	0.5	1.19
CPU Time (sec) (5% damping)	50	1000	20

As clearly can be seen, the accuracy gained by the three-dimensional analysis is not enough to offset the associated high computational cost compared to the two-dimensional analysis.

3.9 PARAMETRIC STUDY: UNCERTAINTIES IN LOW-STRAIN SHEAR MODULUS VALUES

So far, numerous models were analyzed to improve the shape of the frequency response curve, but a satisfactory improvement is not yet achieved. This was the motivation behind the low-strain soil modulus parametric study to investigate variations in plant soil properties. The results of the recent Lotung experiment [11] indicate that the uncertainty range of in-situ measurements is about ±50% for low-strain shear modulus and is negligible for unit weight. A maximum variation factor of 2 is recommended in USNRC Standard Review Plan Revision 2. Generally, the softer the supporting soil relative to the supported structure the more significant are the effects of soil/structure interaction. The peak frequency of the frequency response curve is affected by a change in the low-strain shear modulus. It

should be noted that a change in the low-strain shear modulus has two major effects.

Effect 1: Shift in the fundamental vibration frequencies of the soil/structure system.

Effect 2: Variation in the frequency content of the input excitation to the structure.

Effect 3: Excite higher soil modes when input wave has high frequency content.

Two SHAKE runs are made to evaluate the effects of using reduced values of the in-situ low-strain shear moduli (Gmax). These are 60% and 30% of Gmax. The objective of this parametric study is to reduce Gmax to a point where the peak frequency of the deconvoluted free-field seismic motion at the base of the Diesel Generator Building (Elevation -13.5 ft) is around 12.5 Hz. This frequency corresponds to the recorded peak acceleration of the DGB in the East-West Direction.

	100% Gmax	60% Gmax	30% Gmax
Peak Frequency (Hz)	7.6	7.6	14.45
Peak Acceleration (g's) (5% damping)	0.90	0.68	1.09

This indicates that the free-field seismic motions, using 30% Gmax, possess a high-frequency content and should be used in the final analyses. For 30% Gmax, a peak frequency of 14.45 Hz is considered to be a higher mode of the site response. A 30% Gmax is a relatively low percentage in comparison with the current applicable range of _ 50%. A possible explanation is that the dynamic soil properties in Section 3.4 are based on pre-construction virgin soil and these properties are expected to be different for the existing soil inside the water proof membrane used for construction. Another reason could be that the higher soil modes are excited by the high frequency input.

3.10 SOIL/STRUCTURE INTERACTION ANALYSES OF THE DIESEL GENERATOR BUILDING USING 30% Gmax

This section covers three separate soil/structure interaction analyses of the Diesel Generator Building using 30% Gmax. They are:

(1) Two-dimensional analysis for East-West direction placing the base mat on the ground surface and including the effect of the superstructure inertial eccentricity. SHAKE deconvoluted seismic motion at Elevation -13.5 ft is used as the input control motion.

(2) Two-dimensional analysis for East-West direction including the effects of the base mat embedment and superstructure inertial eccentricity. Free surface recorded motion at A1CH1 is used as the input control motion.

(3) Two-dimensional analysis for North-South direction including the effect of the base mat embedment. Free surface recorded motion at A1CH3 is used as the input control motion.

The seismic wave environment consists of vertically propagating shear waves for all three analyses.

For East-West direction, results show that the recorded peak is at a higher frequency and is of larger magnitude. The calculated ZPA agrees well with the recorded ZPA at A7 station for East-West direction.

For North-South direction, Figure 8 shows a good agreement between the predicted and recorded results at A7 station in terms of the overall shape of the frequency response curve and ZPA. The calculated response displays a high-frequency content (around 12 Hz), but slightly underestimates the peak acceleration.

3.11 FINAL SOIL/STRUCTURE INTERACTION ANALYSIS OF A COMBINED MODEL OF THE DIESEL GENERATOR AND REACTOR BUILDINGS USING 30% Gmax

A two-dimensional combined model of the Diesel Generator and Reactor Buildings is developed to investigate the effects of structure/structure interaction and to reconstruct the spectral composition of the recorded seismic motion at A3 station. Reactor Building is modeled as a set of three (3) cantilever bears connected at the base to Node 141. These beams represent the Shield Building, Containment Vessel and Interior Concrete Structure.

In this analysis, the Diesel Generator Building is placed on the ground surface. SHAKE deconvoluted motion at Elevation -13 ft is used as the input control motion. The seismic wave environment consists of vertically propagating shear waves.

The predicted results display small variations in the ZPA values along the longitudinal dimension of the mats of the Diesel Generator and Reactor Buildings. Results of the analysis show clear evidence of strong soil/structure interaction and good correlation with the recorded motions.

	A3CH1		A7CH1	
	Analysis	Recorded	Analysis	Recorded
Peak Frequency (Hz) (5% damping)	22.2	25.0	12.3	12.5

The input control motion in this analysis is the deconvoluted horizontal East-West acceleration time history. However, the predicted results show significant response in both horizontal and vertical directions. This indicates that the high-frequency rocking mode contributes significantly to the overall response due to the high-frequency content of the input motion and the slant bottom surface of the base mat. Generally, stiffer and taller structures, such as the Reactor Building, exhibit more rocking participation.

The predicted results also show that the responses of the Shield Building and Containment Vessel are at high frequencies.

	Shield Building	Containment Vessel
Peak Frequency (Hz) (5% damping)	24.9	22.2

4. CONCLUSIONS AND RECOMMENDATIONS

The high frequency and low energy events occurred at the Monticello Reservoir, at Leroy and at Krsko are non-damaging for passive equipment and rugged active components. Traditionally, seismologists and engineers ignored magnitude 5 and lower earthquakes for their lack of damaging potential. However, they could cause chattering of sensitive electrical and control systems devices like relays, contactors, and switches. In order to assess its impact on this type of sensitive equipment, one needs to determine whether the high frequency content can be transmitted to the building at equipment locations especially at a soil site. This can be achieved by soil/structure interaction analysis. Since recorded data at Monticello Reservoir and Leroy, Ohio were not adequate to verify soil/structure interaction analysis, the strong motion data recorded at Krsko Nuclear Power Plant in Yugoslavia which have the same characteristics of eastern U.S. earthquakes were used to verify soil/structural interaction and assess the impact on sensitive relays.

SHAKE/SASSI soil/structure interaction analysis of the December 1989 Event at Krsko resulted in encouraging qualitative and quantitative agreement with recorded measurements for both horizontal East-West and North-South directions. Result of the analysis has shown clear evidence of strong soil/structure interaction. The structural response motions display strong rocking mode participation due to the high-frequency content of the free-field input seismic motions. Seismic wave environment is

assumed to consist of vertically propagating shear waves due to the high-frequency content of the structural seismic motions.

The conclusions of this soil/interaction analysis can be summarized as follows:

1. High frequency content can be transmitted to a nuclear power plant structure even at a soil site. Analytically, this can be simulated by vertical propagating shear wave.

2. Since this high frequency content is usually very far away from the dominant frequencies of the massive structures, large reduction of the response was observed and can be expected based on the classical theory of lack of resonance.

3 When a small structure is adjacent to a large structure at a soil site, the response of the small structure will be influenced by the large structure.

4. When the base mat has a irregular shape in the vertical plane, rocking mode can be anticipated from this kind of high frequency earthquakes.

5. This high frequency input also excited the higher modes of the site response.

REFERENCES

1. R. L. Rothman, Guidelines for Recommending Plant Shutdown Following an Earthquake, Proceedings of the 3rd Symposium on Current Issues Related to Nuclear Power Plant Structures, Equipment and Piping, Sponsored by North Carolina State University, December 1990.

2. EPRI NP-5930, A Criterion for Determining Exceedance of the Operating Basis Earthquake, Palo Alto, CA., 1988.

3. EPRI NP-6154, Proceedings EPRI/NRC/TPC Workshop on Seismic Soil-Structure Interaction Analysis Techniques Using Data From Lotung Taiwan, Volumes 1 and 2, 1989.

4. FLUSH, C.D.C. Version 2.420 -- NOS 2.43 + ECM, November 1986, University of California, Berkeley, CA.

5. SASSI, Version P.C.C.- CRAY-1.0, April 1989 Installation University of California, Berkeley, CA.

6. Robert B. Whorton, "High Frequency, High Amplitude and Low Energy Earthquake Study at V.C. Summer Nuclear Plant", Symposium on Current Issues Related to Nuclear Power Plant Structures, Equipment, and Piping, North Carolina State University, December 10-12, 1986.

7. C. Chen, C. Angstadt and M. Hayner," Studies of Equipment Response to Low Energy, Low Velocity, High Amplitude and High Frequency Seismic Events," Symposium on Current Issues Related to Nuclear Power Plant Structures, Equipment and Piping, Sponsored by North Carolina State University, December 1986. Also published in the Nuclear Engineering and Design 107, 127-139, 1988.

8. Gilbert/Commonwealth, Nonlinear Soil/Structure Seismic Evaluation of the December 1989 Earthquake, March 1991.

9. SHAKE, MS-DOS Version converted to IBM-PC, University of California, Berkeley, CA.

10. P. Jennings and J. Bielak," Dynamics of Building-Soil Interaction," Bulletin of the Seismological Society of America 63, 1973.

11. W. Tseng et al," Soil-Structure Interaction Analysis Guidelines Based on Lotung Experiment in Response to the Revised Standard Review Plan," Paper No. IX/3, Third Symposium on Current Issues Related to Nuclear Power Plant Structures, Equipment, and Piping, Orlando, Fl., 1990.

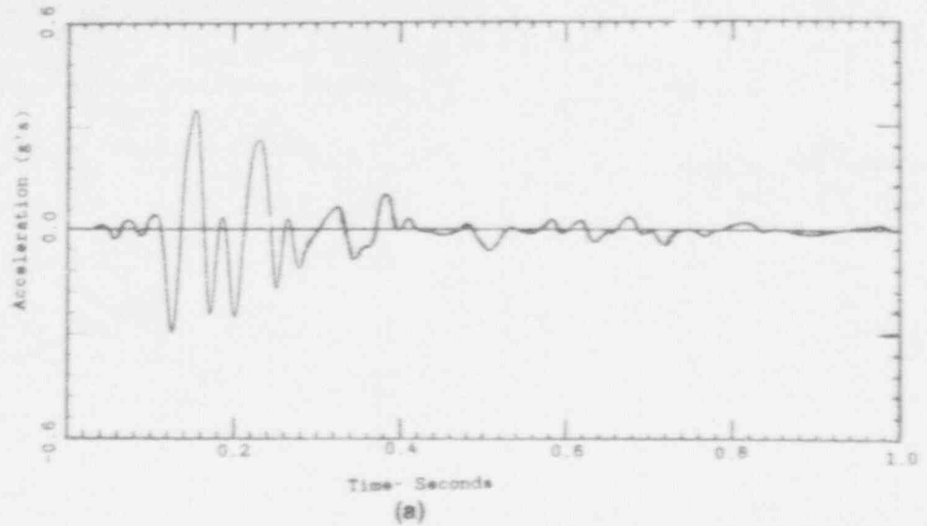

(a)

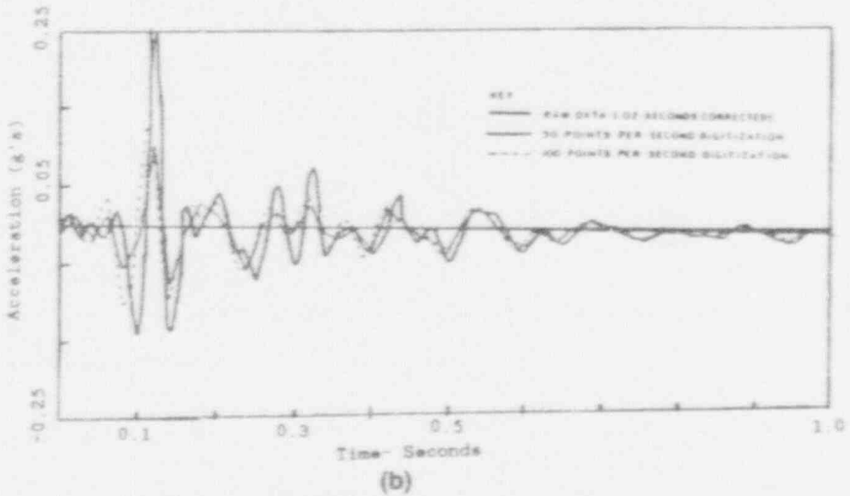

(b)

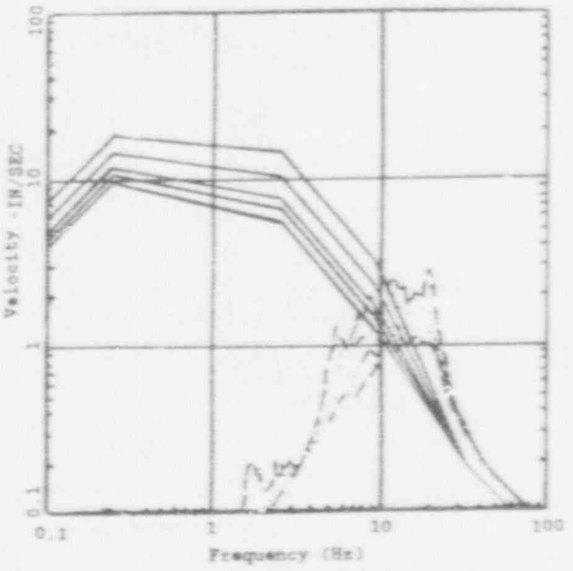

(c)

Figure 1 8/27/1978 and 10/16/1979 Events at Monticello [6]: (a) Acceleration Time History of the 10/16/1979 Event; (b) Acceleration Time History of the 8/27/1978 Event; (c) Comparison of the NRC R.G. 1.60 Response Spectra with the Recorded Velocity Response Spectra of the 8/27/1978 Event Using 0.5, 2.0, 5.0, 7.0 and 10.0% Damping.

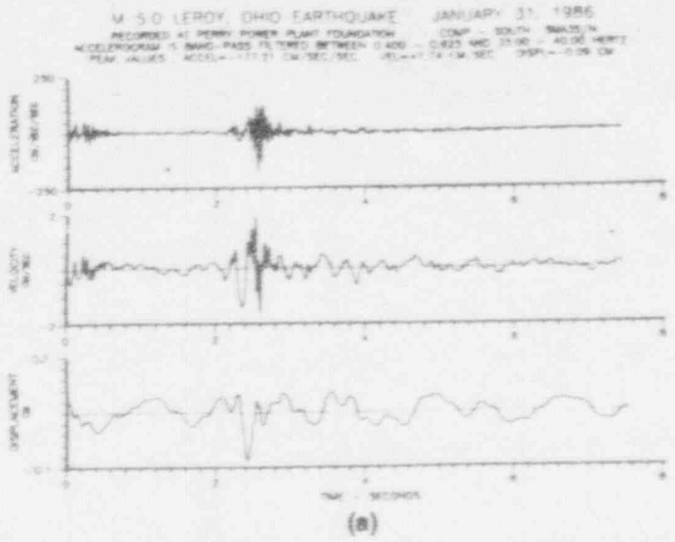

(a)

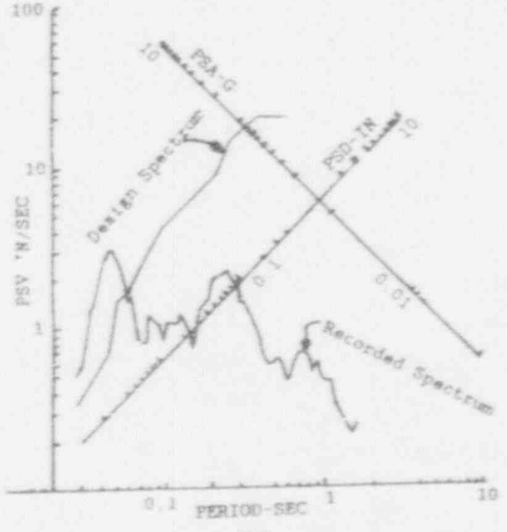

(b)

Figure 2. 1/31/1986 Event at Leroy [7]: (a) Acceleration, Velocity and Displacement Time History; (b) Comparison of the NRC R.G. 1.60 Design Spectrum with the Recorded Velocity Response Spectrum Using 2% Damping

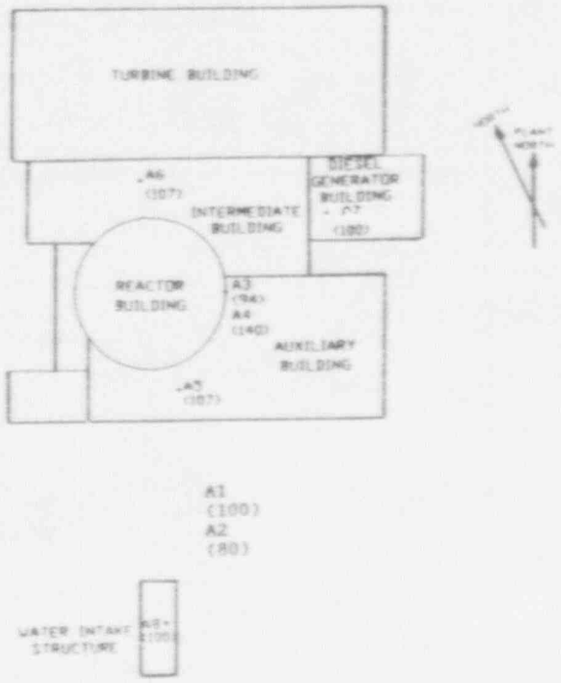

Accelerometer	Location	Peak Acceleration (g's) N-S	Vert.	E-W
A1	Free Field (EL. 100)	0.45	0.13	0.53
A2	Free Field (EL. 80)			
A3	R.B. Bldg. (EL. 94)	0.08	0.04	0.05
A4	R.B. Bldg. (EL. 140)	0.06	0.07	0.06
A5	Aux. Bldg. (EL. 107)			
A6	Int. Bldg. (EL. 107)			
A7	D.G. Bldg. (EL. 100)	0.14	0.16	0.19
A8	Int. Stru. (EL. 100)	0.10	0.06	0.06

Figure 3. Recorded Peak Accelerations (g's) of the NPP Krsko Seismic Instrumentation of the 12/28 '1989 Event [8].

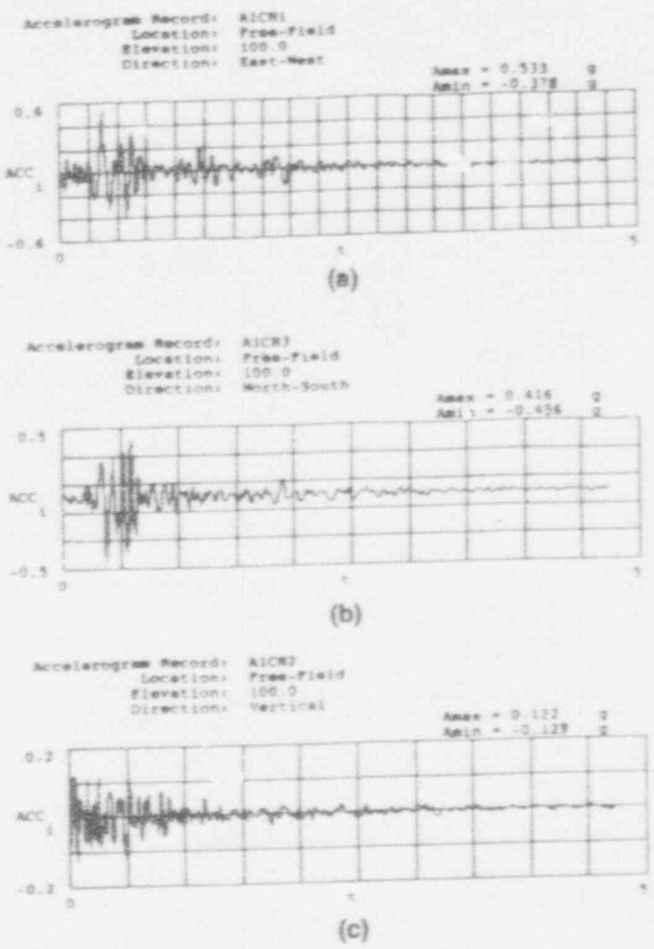

Figure 4. Recorded Free-Field Surface Acceleration Time History at NPP Krsko of the 12/28/1989 Event [8]: (a) East-West; (b) North-South; (c) Vertical.

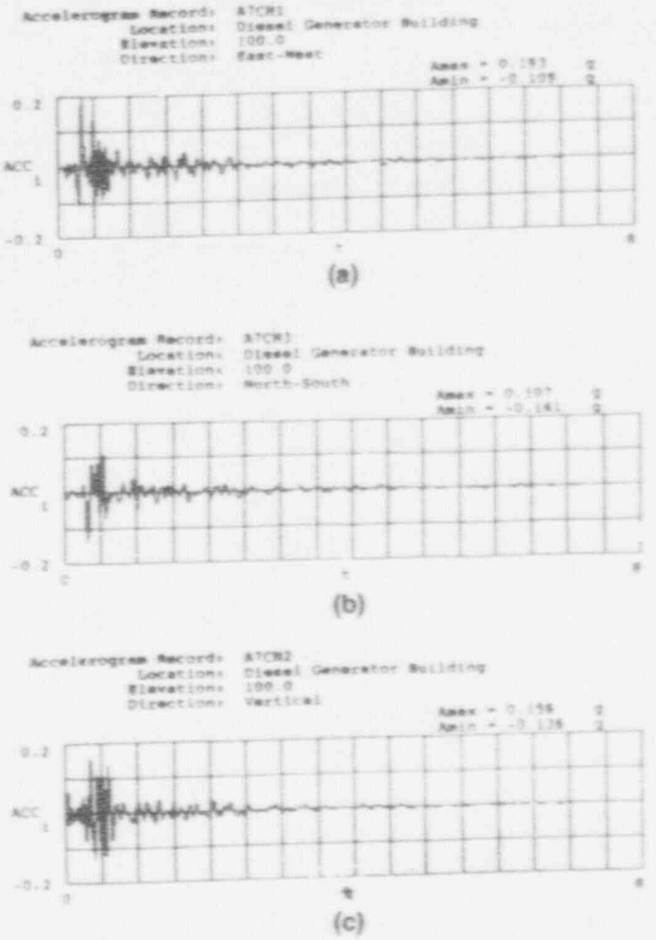

Figure 5. Recorded Acceleration Time History of the 12/28/1989 Event [8] at NPP Krsko Diesel Generator Building: (a) East-West; (b) North-South; (c) Vertical.

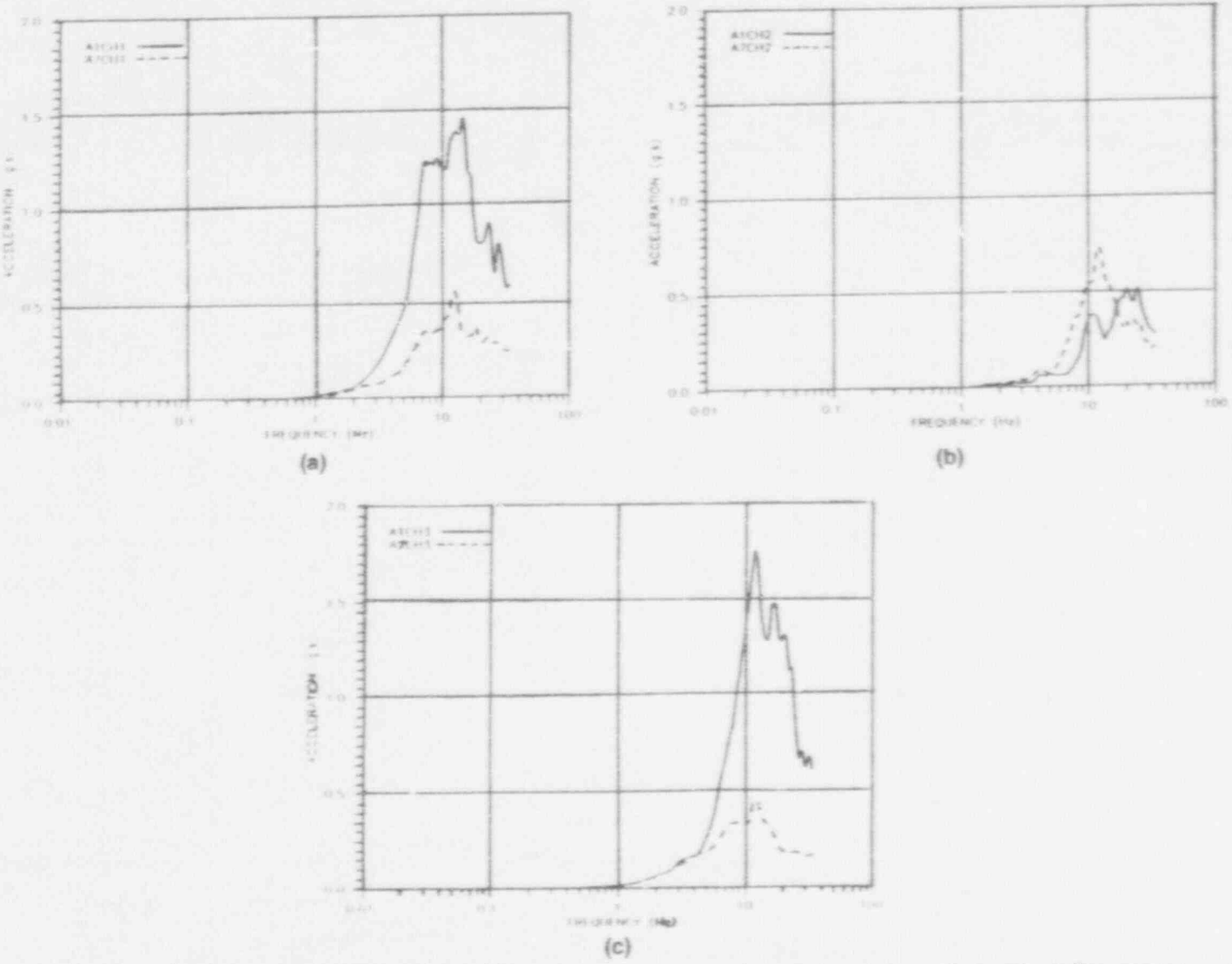

Figure 6. Comparison of the Recorded Free-Field Surface Response Spectra with the Diesel Generator Building Response Spectra of the 12/28/1989 Event [8] Using 5% Damping: (a) East-West; (b) Vertical; (c) North-South.

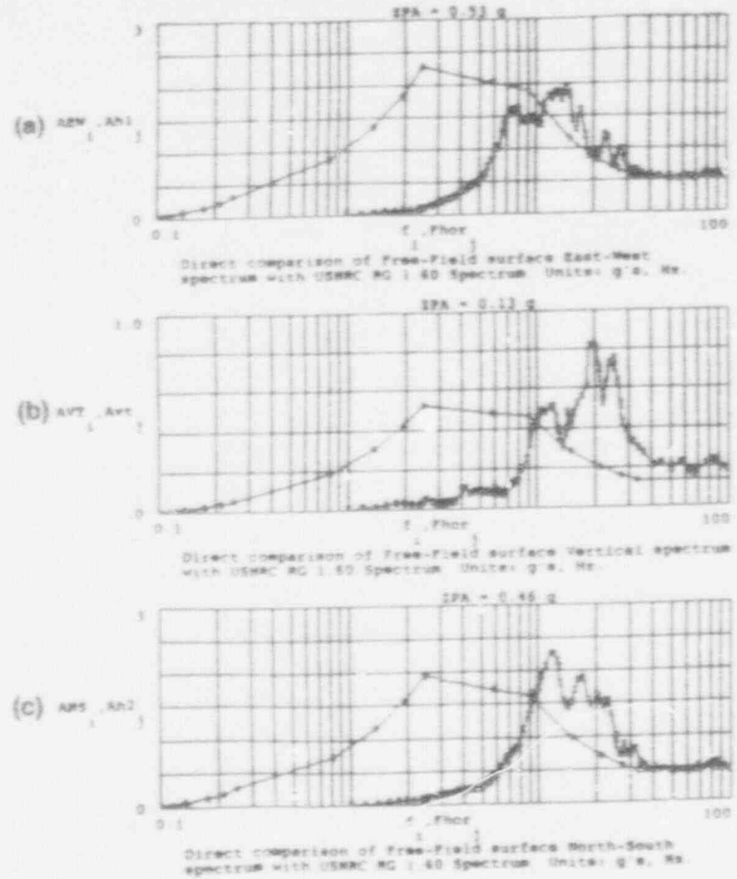

Figure 7. Comparison of the NRC R.G. 1.60 Design Spectra with the Recorded Free-Field Surface Response Spectra of the 12/28/1989 Event [8]: (a) East West; (b) Vertical; (c) North-South.

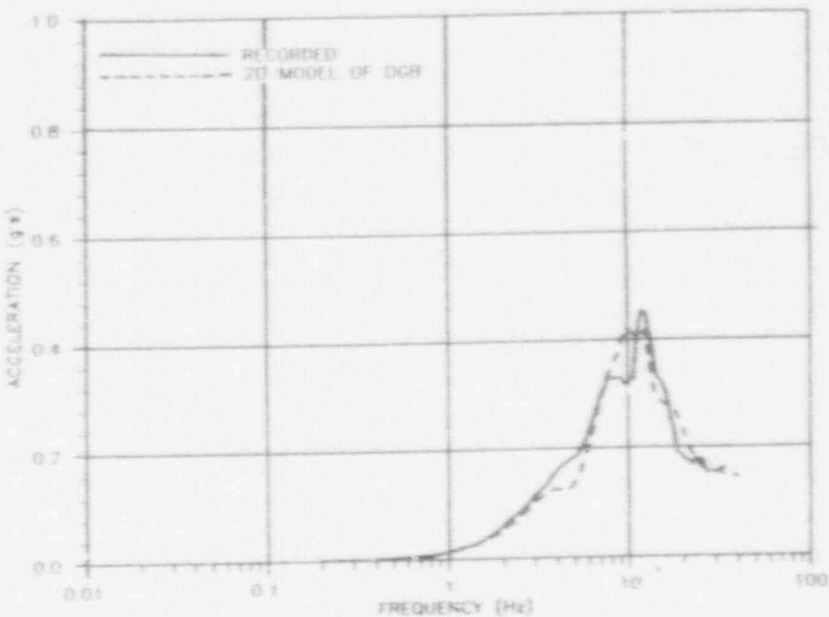

Figure 8. Comparison of the Analysis Response Spectrum with the Recorded Diesel Generator Building Response Spectrum of the 12/28/1989 Event [8] Using 5% damping, North-South.

A BASIS FOR STANDARDIZED SEISMIC DESIGN (SSD) FOR NUCLEAR POWER PLANTS

Thomas F. O'Hara, John P. Jacobson, Francis X. Bellini
Yankee Atomic Electric Company

Walter J. Brigs
Northeast Utilities

Yankee Atomic Electric Company
580 Main Street
Bolton, Massachusetts 01740, USA

1.0 Abstract

U.S. Nuclear Power Plants (NPPs) are designed, engineered, and constructed to stringent standards. Their seismic adequacy is assured by compliance with regulatory standards and demonstrated by both probabilistic risk assessments (PRAs) and seismic margin studies. However, present seismic siting criteria require fundamental changes in both the philosophy of how the rule should be written and in the actual application of a process to determine acceptable seismic design levels. Changes to siting criteria proposed here will provide a predictable licensing process and a stable regulatory environment.

Two recent state-of-the-art studies evaluate the seismic design for all eastern U.S. (EUS) NPPs: a Lawrence Livermore National Labs study (LLNL, 1989) funded by the NRC and similar research by the Electric Power Research Institute (EPRI, 1989) supported by the utilities. Both confirm that Appendix A 10CFR100 has not provided consistent seismic design levels for all sites.

Standardized Seismic Design (SSD) uses a probabilistic framework to accommodate alternative deterministic interpretations. It uses seismic hazard input from EPRI or LLNL to produce consistent bases for future seismic design. SSD combines deterministic and probabilistic insights to provide a comprehensive approach for determining a future site's acceptable seismic design basis. The essence of this approach is the calibration of a seismic hazard methodology to a common standard.

2.0 Background

Over the past ten years there has been extensive funding of seismic hazard research by both the electric utility industry and the Nuclear Regulatory Commission (NRC). The impetus for this effort can be traced to historical regulatory concerns associated with the licensing process given in Appendix A, "Seismic and Geologic Siting Criteria for Nuclear Power Plants", to 10CFR100, "Reactor Site Criteria." In fact, this research has resulted in a transition from the simple deterministic assumption that the Safe Shutdown Earthquake (SSE) could not be exceeded to the realization that the annual probability of exceeding the SSE varies considerably from site to site.

Appendix A originally addressed seismic siting criteria from a Western U.S. (WUS) perspective. This presumed that seismic activity could be assigned to structures, particularly faults exposed at the surface. In other words, given the distance to a fault and the expected rupture length, the ground shaking at some proposed site could be deterministically bounded. Of course for the eastern or central U.S. (EUS) such is not the case. Appendix A thus employed a concept of "tectonic provinces" (Hatheway and McClure, 1979) as a model to determine seismic design levels at nuclear power plant sites. The tectonic province approach is prescriptive, forcing adversaries to be placed into deterministic yes-no positions. This is particularly true with respect to determination of tectonic provinces and structures, maximum magnitude earthquake, conversion from Modified Mercalli Intensity (MMI) to Peak Ground Acceleration (PGA), and the appropriate spectral shape to anchor at the PGA. The fundamental problem with the deterministic approach (dramatically highlighted by both the LLNL (1989) and EPRI (1989) seismic hazard studies) is that there is no scientific consensus as to what are the correct provinces, structures, maximum magnitude earthquakes, etc. Furthermore, because contending viewpoints are framed in a legal context of an absolute yes-no question, the process usually ends up in court. This results in delays, increased costs, instability, and uncertainty in the overall licensing and regulatory process.

At present NRC is scheduled to complete their redraft of Appendix A and supporting regulatory guides in 1991. Fundamental to the goal of stabilizing the licensing process is the removal of interpretive details from Appendix A and placing them in regulatory guides. This is consistent with the philosophy defined in SECY-79-300 (Minogue, 1979). Furthermore, experience suggests that the existing treatment of significant siting factors such as meteorology and hydrology in 10CFR100 provide the appropriate model for the treatment of seismic licensing issues. In the present 10CFR100, it is specified that "consideration" of the site meteorology and hydrology are required when evaluating the suitability of a new site. However, all of the details of how an applicant may characterize and protect against extreme meteorological and hydrological phenomena are provided in supporting Regulatory Guides and Standard Review Plans. This approach has been proven to provide adequate protection against these external events for our current generation of plants. Consistent with this treatment of meteorological and hydrological concerns, it

is proposed that seismic concerns in a new Part 100 be addressed by the following statement "Consistent with General Design Criteria 2 of Appendix A to Part 50 of this chapter, geologic and seismic data analyses sufficient to determine site suitability and to provide reasonable assurance that a nuclear power plant can be constructed and operated at a proposed site without undue risk to the health and safety of the public shall be developed." This proposed simplification of the existing regulation should be accompanied by new regulatory guides which endorse acceptable methodologies in detail for deriving acceptable site seismic design levels and criteria for any site in question.

Our recent paper (O'Hara and Jacobson, 1990) discusses a method to determine acceptable site seismic design levels for future nuclear power plants that could be utilized in a regulatory framework. This paper is an application of the proposed methodology based upon seismic hazard results from both the LLNL and EPRI studies. We contend that state-of-the-art seismic hazard analyses represent a rational framework for the incorporation of the multitude of contending hypotheses concerning the cause of earthquakes, as well as for incorporation of new information. Furthermore, these analyses should be used to determine acceptable site seismic design levels. It should be noted that the SSD approach results in consistent acceptable site design levels from location to location in the EUS yet the actual design may be higher if the utility decides to adopt an enveloping 0.3g design level which is the present Advanced Light Water Reactor (ALWR) design level. The essence of this SSD approach is the calibration of a methodology (LLNL, 1989 or EPRI, 1989) to a common standard.

However, prior to describing this approach an awareness of some fundamental issues is needed to understand the basis for our approach. These issues are:

1. Evaluation of the Deterministic Licensing Process for Existing Plants.

2. Implications of Standardization.

3. Justification of a Deterministic Standard.

4. Calibration of a Hazard Methodology to a Common Standard.

The following sections discuss these issues with the objective of integrating the conclusions of each section into an overall method to standardize the seismic design licensing process.

3.0 Evaluation of the Deterministic Licensing Process for Existing Plants

Presently, both the Electric Power Research Institute (EPRI) and Lawrence Livermore National Labs (LLNL) have mature seismic hazard methodologies and both have calculated the seismic hazard at EUS NPP sites. Because the LLNL and EPRI methodologies are internally consistent, i.e., common attenuation

models, experts, and calculational procedures, the relative hazard between various NPP sites for each methodology is easily determined. In this context, the seismic hazard results from both the LLNL and EPRI studies can be used to independently evaluate the probability of exceeding the current licensing basis at existing NPPs. In particular, this comparison evaluates the consistency of the deterministic licensing process that has been used to define the current licensing basis at existing EUS NPP sites.

A fundamental licensing/engineering premise is that the seismic design basis (defined in Appendix A as the Safe Shutdown Earthquake, SSE) should be proportional to the expected seismic loadings; in other words, the higher the expected seismic loadings, the higher the seismic design basis. Figure 1 presents the SSEs determined for 61 EUS NPP sites. As can be seen these seismic design levels vary between 0.1g and 0.25g. Clearly, if the deterministic process used to determine these seismic design levels is consistent with the above premise (i.e., higher seismic loadings require a higher seismic design level) then it should follow that the probability of exceeding each plant's seismic design level should be about the same.

Figure 2 is a plot of the probability of exceeding the Safe Shutdown Earthquake (SSE) at 61 EUS NPP sites based upon **median** results from both LLNL and EPRI. Analyses have shown (NRC, 1990) that the median results (as compared to mean, 15th or 85th percentile results) are most consistent between LLNL and EPRI. As can be seen, the probability of exceeding the SSE from site to site is far from consistent within each methodology (LLNL or EPRI). These results cast doubt on the ability of the current deterministic approach to define consistent seismic design levels from site to site. However, what also can be seen from Figure 2, is that the trend from site to site between the LLNL and EPRI results is consistent in a relative sense, meaning that both studies consistently identify high and low hazard sites, albeit that the magnitude of the absolute probabilities vary significantly.

Figure 3 is a plot of the probability of exceeding the SSE for each of the 61 sites using the EPRI results. As can be seen, sites with an SSE of 0.15g vary by over two orders of magnitude in probability of exceedance. This figure further highlights the inability of the deterministic licensing process to define consistent design levels from site to site. Figures 2 and 3 are simply the probability of exceeding the PGA associated with the SSE at each site. Because the LLNL and EPRI results define the seismic hazard at the PGA, 25, 10, 5, 2.5, and 1 Hz, it is possible to convert SSE response spectra at each of these frequencies to probabilities and then plot the results. Figure 4 is such a plot and dramatically illustrates the inconsistency in probability of exceedance between sites not only at the PGA but at other frequencies as well. We thus conclude that across the current population of NPPs the deterministic process used to define the seismic design bases at existing NPPs has not resulted in consistent seismic design levels (as defined by similar probabilities of exceedance) and should not be used as the primary regulatory process for future plants.

This wide variation in probability of exceedance does not imply that those plants with the highest probability of exceeding their design basis are unsafe. PRAs and margins studies have shown that plant capacity exists well beyond the SSE and that the major contribution to seismically-induced core melt frequency for EUS plants come from earthquakes that are about 2 to 4 times the SSE (LLNL, 1985).

4.0 Implications of Standardization

A standardized seismic design level is a design level that is the same from location to location. This implies that the envelope of future site-specific seismic hazard characteristics should be determined such that standardized design may be repetitively applied at all sites. To allow repetitive applications, the standard design must be somewhat overdesigned to envelope the seismic hazard that varies from site to site. It is believed that standardization will result in savings in engineering, licensing, equipment and procurement, construction (learning curve), start up (standard procedures), and operation (standard procedures and spare parts) (Bechtel, 1986).

The standardized design approach is not without its inconsistencies. For example, assume that at locations A, B, and C the seismic hazard is that as shown on Figure 5, high, medium, and low, respectively. Because seismic hazard is not uniform across the EUS, standardization at a fixed design level will result in the probability of exceeding the fixed value to vary from location to location. This situation is exactly what has precipitated the protracted seismic reviews by the NRC for the current generation of NPPs. To avoid this problem it must be shown that the standardized design level is acceptable at the highest hazard site and therefore is acceptable at all other sites.

An alternative to the above approach is the standardization of the probability of exceeding the design level, in other words, because the hazard varies from location to location the design level should vary from location to location. Figure 6 illustrates this approach. As can be seen, if 2.0E-4 is considered to be an acceptable probability of exceeding the design level, then the design level at locations A, B, and C would be about 0.05g, 0.15g, and 0.30g, respectively. The advantage of varying the design level from location to location is that there will be a consistent probability of exceedance from site to site and also there is the potential for a reduction in cost at the low hazard sites. These acceptable site values if used as input ground motions for site geotechnical analyses such as liquefaction analyses would certainly result in cost savings. It should be noted, that if in fact Site A in Figure 5 represents the site with the highest hazard, and if in fact 0.3g is acceptable at that location, then the standardized probability of exceedance is defined by Site A.

As can be seen from the above discussion a standardized design value results in varying probabilities of exceedance from site to site while a standardized

probability of exceedance results in varying design levels from site to site. Advantages and disadvantages are associated with both methods of standardization, however, the task at hand is to take advantage of both approaches.

In its most fundamental sense, the establishment of standardized design criteria involves the balancing of benefits and costs. For seismic design, the benefit of providing additional reinforcement to withstand earthquake motion is a reduction in risk to the public posed by a facility. The enhanced seismic capacity associated with the standardized design is believed to be relatively inexpensive compared to total plant expenditures if incorporated into the original design and construction of a new plant. A follow-up to prior studies (Stevenson, 1981) by Stevenson (October 1991, personal communication) will show a 7% to 10% overall increase in cost by going from a 0.1g design to about a 0.3g design. Above about 0.3g costs increase more rapidly with design level. NPP licensing history has shown that licensing delays due to seismic design level issues and actual changes to the seismic design basis while construction is in progress have resulted in significant increases in cost and can no longer be tolerated.

Over time, as regulators require stricter and more costly so-called "safety" at newer facilities, they are assumed to be implementing the public's desire to pay more for incremental safety gains over similar previously licensed facilities. Within these arguments to standardize and increase safety, there must be an awareness of the bottom line cost to generate electricity, otherwise future plants may only exist on paper, and may not ever be built.

5.0 Justification of a Deterministic Standard

To avoid problems associated with the deterministic licensing process it has been recommended by EPRI (1989) that the SSE be standardized to 0.3g for all future plants. The basis for this recommendation was documented by Bechtel (1986) and was primarily based upon minimizing the increase in cost due to over design. In their analysis Bechtel deterministically evaluated 21 expected future sites. For these sites the 0.3g design value is equal to or greater than each site's Preliminary Safety Analysis Review (PSAR) seismic design value. For four sites the 1.0E-4, PGA based upon EPRI hazard results, was assumed to be the PSAR seismic design value.

Two additional arguments exist which support the 0.3g standardized design level. The first is an empirical argument. It follows that because the 0.3g value bounds all currently acceptable EUS design values, and because this sample of existing sites is representative of the population of future sites (i.e., future plants will be built where present plants exist or at locations similar in hazard to existing sites), the bounding value of 0.3g should surely be accept

The other argument is based on safety goals. The Advanced Light Water Reactor (ALWR) mean core damage frequency (MCDF) safety goal is 1.0E-5 (EPRI, 1989)

and the goal for the seismic contribution is 1.0E-6 (i.e., 10%). The safety goal approach is based upon meeting the seismic contribution to MCDF and has been applied by EPRI (1990) using only the EPRI hazard results to justify the 0.3g design level. Fundamental to the safety goal approach is the mean hazard curve for a given site and an assumed generic plant fragility of about 1.2g for the standard 0.3g plant. It is the convolving of the mean hazard curve and the plant fragility curve that defines the seismic contribution to MCDF. As shown on Figure 7, it is not unusual to have two to three orders of magnitude difference between the LLNL and EPRI mean hazard results at acceleration levels of interest (0.5g to 1.5g). A direct consequence of this situation is that justification of the 0.3g standardized design using safety goals appear to be satisfied using the EPRI results but it will certainly not be satisfied using the LLNL results for a typical site. Due to this, efforts are being made to resolve differences between the two studies. Also, it must be understood that the quantitative safety goal approach views these probabilities in an absolute context - that is as 'true' probabilities.

True probabilities, such as the probability of tossing a six in one throw of a fair die, are based on one's ability to define the sample space and the likelihood of each outcome. In seismic hazard analyses the process is not quite as simple. Figure 8 shows a logic tree which would typically be used to define the sample space (all possible outcomes) for a seismic hazard analysis. The figure illustrates how the "degree of belief" of each hypothesis (outcome) is calculated. First, weights are assigned to each parameter of the tree. The weights of the different zonations add to one, those of the different attenuation models add to one, and so on. These weights are typically subjective expert opinion. Second, the likelihood of each hypothesis (outcome) is obtained as the product of the weights of the various components that define that hypothesis. The point to be made here is that the sample space may be adequately covered but the likelihood of each outcome in the sample space is based upon subjective opinion unlike the classic die tossing problem. Because there are divergent opinions on all of the parameters that typically go into a seismic hazard analysis, use of these results in an absolute fashion (safety goal approach) will not prove to be feasible until all the significant differences are resolved.

The safety goals method is appealing because the acceptance criterion is apparently quantifiable. But, because the calculation to determine MCDF is based upon the convolving of both a mean hazard curve and an assumed generic plant fragility curve, and the half life of the hypotheses presented in seismic hazard analyses may be on the order of a few years (i.e., the length of time before new theories replace older ones), a meeting of the safety goals now may show otherwise in a few years. In addition, nothing prevents the safety goals or the value of the future-plant fragility curve from changing. Because of these issues, a safety goal approach, at present, cannot satisfactorily justify a 0.3g standardized design level. Conversely, deterministic arguments strongly support 0.3g as an acceptable value.

6.0 Calibration of a Hazard Methodology to a Common Standard

Acceptable probabilities must be defined relative to a common standard within a methodology. The relative use of subjective probabilistic results contrasts with the absolute safety goal approach. The relative approach is used because absolute approaches fail to recognize the inherent limitations in current EUS seismic hazard results. As discussed above, it is not unusual to find differences between EPRI and LLNL results of two orders of magnitude or more at a given acceleration. Because of these differences, there is a question as to whether these estimates of seismic hazard can be used in an absolute (safety goal) sense.

Justification of acceptable probabilities is empirical. The major problem associated with this approach is obviously that of calibrating the results from a seismic hazard methodology (LLNL or EPRI) to some realistic acceptance level. One approach is to calibrate these probabilities relative to existing NPPs. In other words, because design levels for currently operating NPPs are by definition acceptable the probabilities associated with these design levels must be acceptable. This approach ensures that acceptable site seismic design levels for future plants shall be consistent with current seismic designs. Also, consistent can be defined in such a manner that the population of future plants will have a higher seismic resistance than the current population of plants. Acceptable probabilities of exceedance (calibration) can be determined as follows:

1. Using the median seismic hazard results calculated by LLNL or EPRI for all existing EUS sites convert the existing SSEs (Figure 9) into probabilities at various frequencies (PGA, 25, 10, 5, 2.5, and 1 Hz). Figure 10 illustrates this process.

2. Define some target levels for future plants, and compute the acceptable probabilities. The acceptable probabilities could be, for example, the mean or median values of the probabilities of exceedance associated with current design spectra at the above defined frequencies.

An alternative and more objectively justifiable and consistent approach is based on use of the standardized 0.3g R.G. 1.60 spectrum. Because this spectrum exceeds all existing design spectra for EUS NPPs it can certainly be considered acceptable, if not excessive. Given this premise, an analysis similar to that described above can be performed except that rather than using existing SSEs, the 0.3g standardized spectrum is assumed to be the SSE at each site. Probabilities of exceeding the 0.3g spectrum can be calculated for each site and the enveloping probabilities are defined as acceptable. Using these approaches, interpretations of acceptable probabilities have been calculated consistent with both the LLNL and EPRI methodologies. Figure 11 shows the Figure 9 spectra converted to probabilities using the LLNL results. The dashed line defines acceptable probabilities based upon the assumption that the 0.3g spectrum is acceptable. Results of both approaches are shown on

Figure 12. As can be seen, even though the 0.3g spectrum approach envelopes all existing EUS spectra, its acceptable probabilities are consistent with the median probabilities for the current generation of NPPs.

Figure 12 also illustrates the basis for confusion that has typically been associated with the concept of acceptable probabilities. For example, in the Systematic Evaluation Program (SEP) the 1000-year spectra developed by LLNL were applied to the SEP sites. Given this information utilities assumed 1.0E-3 was acceptable and would then calculate seismic hazard at their sites using a different seismic hazard methodology and determine the PGA associated with the 1.0E-3 'acceptable' probability. As expected the 1.0E-3 PGA determined by the utility was significantly lower than the LLNL value. Obviously, the point to be made here is that the above defined acceptable probabilities are acceptable relative to the methodology. What will be shown in the next section is an application of the above defined acceptable probabilities and the use of these probabilities in a relative sense to define acceptable and consistent site seismic design values.

7.0 Standardized Seismic Design Process

This approach results in an acceptable site design level of less than 0.3g at typical EUS sites (excepting New Madrid, Missouri and Charleston, South Carolina) and a default standardized plant design level of 0.3g. A fundamental premise of this approach is that a utility should be given the option of building a plant to some standardized design (0.3g) or to some acceptable site design level less than or equal to 0.3g. Furthermore, using this approach, the probability of exceeding the acceptable site design level will be the same from site to site, while the probability of exceeding the actual plant design value will always be equal to or less than the acceptable site design value.

The essence of this approach is the calibration of a seismic hazard methodology relative to a standard (0.3g R.G. 1.60 spectrum) to determine acceptable probabilities, and then the use of these probabilities in an internally consistent manner. Figure 2 shows there is reasonable consistency between the LLNL and EPRI results in a relative sense but not in terms of the absolute value of the numbers. Given that the relative rankings of the hazard are consistent from site to site, it is only a matter of defining acceptable probabilities consistent with a methodology to determine acceptable site design levels.

As stated earlier, "consistent" is defined in terms of probabilities specific to a given methodology. Using these acceptable probabilities, standardized probabilistic methods (such as LLNL, EPRI, USGS, or the results of a resolution between LLNL and EPRI) can be used to determine acceptable site design levels that will be consistent in terms of probability of exceedance from location to location. The philosophy of this approach is similar to that of Short, et al (1990), except that in their paper they advocate the use of the mean probability of exceeding current SSE values. Based upon arguments

stated earlier, we conclude that the enveloping probabilities of exceeding the 0.3g spectrum at existing EUS sites should be used to define acceptable probabilities for future sites. Using the LLNL or EPRI hazard results for existing sites and these acceptable probabilities, it is possible to determine acceptable site seismic design spectra for future plants at these existing sites. The process is simply the reverse of the Figure 10 process. Figures 13 shows these proposed spectra relative to the 0.3g R.G. 1.60 spectrum. As can be seen Figure 13 looks very similar to Figure 9; however, the significant difference is that all of these spectra have exactly the same probability of exceedance which is defined by the dashed line on Figure 11. In other words, the probability of exceeding the spectra would be consistent across all sites. Similar results would be obtained if the EPRI hazard results were used. An important result of this approach is that it assures that a 0.3g standardized design is acceptable at any existing EUS site regardless of seismic hazard methodology.

Given an acceptable site design spectrum, it is extremely important that well defined, close in, seismological, and geological evidence around the proposed site be gathered to confirm the suitability of the site.

8.0 Conclusions

Two relevant issues have been discussed in this paper. The first is the basic philosophy as to how the rule for seismic design criteria for future plants should be written. The second is how the seismic design level for future plants should be determined.

As shown earlier, the existing treatment of significant siting factors such as meteorology and hydrology in 10CFR100 provides the appropriate model for how the issue of seismicity should be treated. In a similar manner, Part 100 should state that site geologic and seismicity data should receive appropriate consideration when assessing site suitability to ensure that General Design Criteria 2 of Appendix A to 10CFR50 can be satisfied. Details of how one ultimately demonstrates compliance with GDC 2 should be addressed only in the regulatory guidance documents.

Therefore, given the above philosophy, it is proposed that the existing subsection 10CFR100.10(c)(1) and 10CFR100, Appendix A be deleted from the rules and replaced with a new subsection 10CFR100.10(c)(1) reading:

"Consistent with General Design Criteria 2 of Appendix A to Part 50 of this chapter, geologic, and seismic data analyses sufficient to determine site suitability and to provide reasonable assurance that a nuclear power plant can be constructed and operated at a proposed site without undue risk to the health and safety of the public shall be developed."

An additional advantage of this recommended approach is that existing construction permit holders and licensees have already demonstrated appropriate compliance with GDC 2 and therefore should not be impacted by the

new rule. The issue of applicability of new detailed criteria and guidance can be addressed in the Implementation sections of the supporting Regulatory Guides.

The second issue discussed in this paper is that of defining a process to determine an acceptable site design level for future NPPs. Based upon a review of the issues and lessons learned with the determination of a seismic design basis for existing NPPs, the SSD methodology has been developed to stabilize the licensing and regulatory process. The SSD approach results in an acceptable site design level of less than 0.3g at typical EUS sites and a default standardized plant design level of 0.3g.

Three fundamental assumptions are used in this methodology. They are:

1. Multiple-hypotheses seismic hazard methodologies, such as LLNL or EPRI, represent rational methods to incorporate the diversity of expert opinion concerning earthquake prediction.

2. A conservative deterministic spectrum (0.3g R.G. 1.60 spectrum) assumed at existing NPP sites represents a common standard to calibrate seismic hazard methodologies.

3. Relative probabilities, based upon acceptable probabilities within a given methodology, will be stable and predictable.

The SSD methodology is important because it can be readily incorporated into the framework of regulatory guides. Furthermore, there is little reason as to why seismic design issues cannot be treated similar to meteorology and hydrology, in other words, for future sites, maps could be made defining acceptable site design levels for essentially all of the EUS. Even those utilities that choose to bound the acceptable site value with a 0.3g standardized value may find it beneficial to use the acceptable site values when performing liquefaction and other geotechnical analyses.

Lastly, there are those that see the existence of two or more seismic hazard methodologies as destabilizing to the licensing process for future NPPs or critical facilities. This concern merely becomes a distinction without a difference when our proposed SSD approach is used. Based upon use of the SSD approach in conjunction with conservative and consistent design standards, adequate seismic resistance will be provided at all future NPPs.

9.0 Bibliography

Bechtel Power Corporation, 1986, Site Parameter Envelope Study Report, prepared for Electric Power Research Institute, Page 43.

Electric Power Research Institute, 1989, "Probabilistic Seismic Hazard Evaluation at Nuclear Plant Sites in the Central and Eastern United States: Resolution of the Charleston Earthquake Issue," prepared by R. K. McGuire, et al, Electric Power Research Institute Report NP-6395-D.

Electric Power Research Institute, 1990, (Proprietary), "Advanced Light Water Reactor Utility Requirements Document," Volume III, ALWR Passive Plant, Chapter 1, Appendix A, PRA Key Assumptions and Ground Rules, Page 88.

Hatheway, A. W., and McClure, C. R., Jr, 1979, "Geology in the Siting of Nuclear Power Plants," Geological Society of America, Reviews in Engineering Geology, Volume IV, Page 256.

Lawrence Livermore National Laboratories, 1985, "An Approach to the Quantification of Seismic Margins in Nuclear Power Plants," prepared by R. J. Budnitz, P. J. Amico, C. A. Cornell, W. J. Hall, and R. P. Kennedy, USNRC NUREG/CR-4334.

Lawrence Livermore National Laboratories, 1989, "Seismic Hazard Characterization of 69 Nuclear Plant Sites East of the Rocky Mountains," prepared by D. L. Bernreuter, et al, USNRC, NUREG/CR-5250.

McCann, M. W., Jr., Reed, J. W., and Boissonnade, A. C., 1990, "Development of Seismic Hazard Input for the Advanced Light Water Reactor Seismic PRA," Revision 1, prepared for Electric Power Research Institute by Jack Benjamin Associates, Inc., Mountain View, California, Page 130.

Minogue, R. B., SECY-79-300, "Identification of Issues Pertaining to Seismic and Geologic Siting Regulation, Policy, and Practice for Nuclear Power Plants," USNRC, April 27, 1979.

O'Hara, T., and Jacobson, J. P., 1990, "Seismic Hazard Analyses - A Utility Perspective, Nuclear Engineering and Design," Volume 123, Pages 111 - 122.

Stevenson, J. D., 1981, "Evaluation of the Cost Effects on Nuclear Power Plant Construction Resulting from Increase in Seismic Design Level," USNRC NUREG/CR1508, Page 81.

Stevenson, J. D., October 1991, "Personal Communication Regarding Revised Estimates for Cost of Increased Seismic Design Levels for Nuclear Power Plants," USNRC NUREG in preparation.

US Nuclear Regulatory Commission, 1991, "Procedural and Submittal Guidance for the Individual Plant Examinations of External Events (IPEEE) for Severe Accident Vulnerabilities," USNRC NUREG-1407, Page 103.

Short, S. A., Murray, R. C., and Hill, J. R., 1990, "Deterministic Seismic Design and Evaluation Criteria to Meet Probabilistic Performance Goals," Third Symposium on Current Issues Related to Nuclear Power Plant Structures, Equipment, and Piping, Page 12.

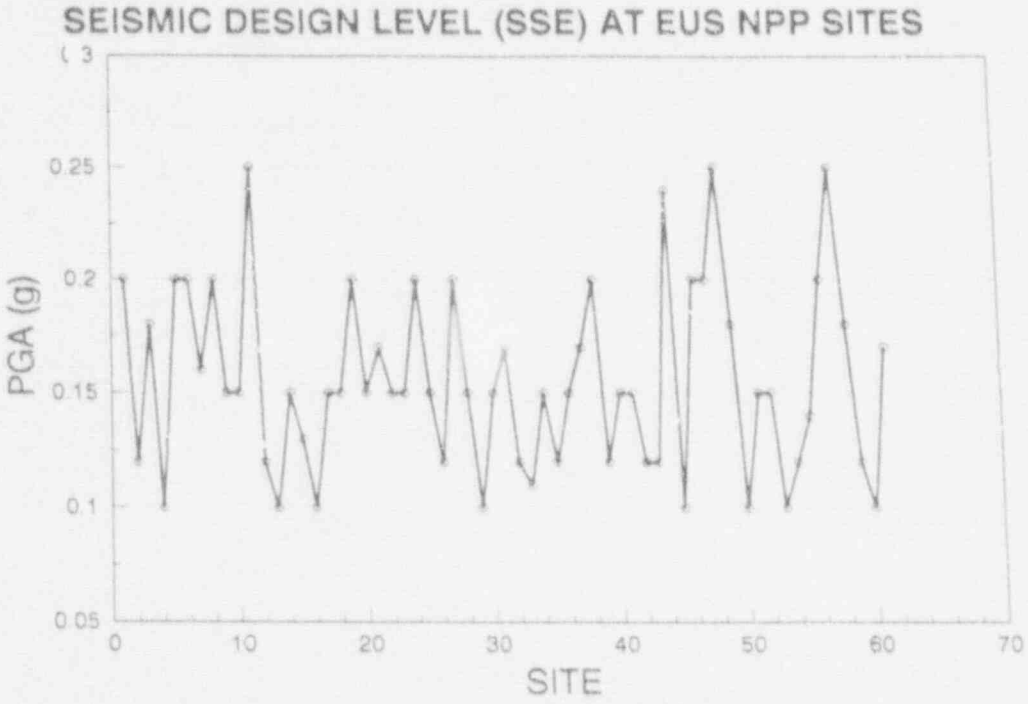

Figure 1. Distribution of seismic design levels (SSE) for EUS NPP's by sites

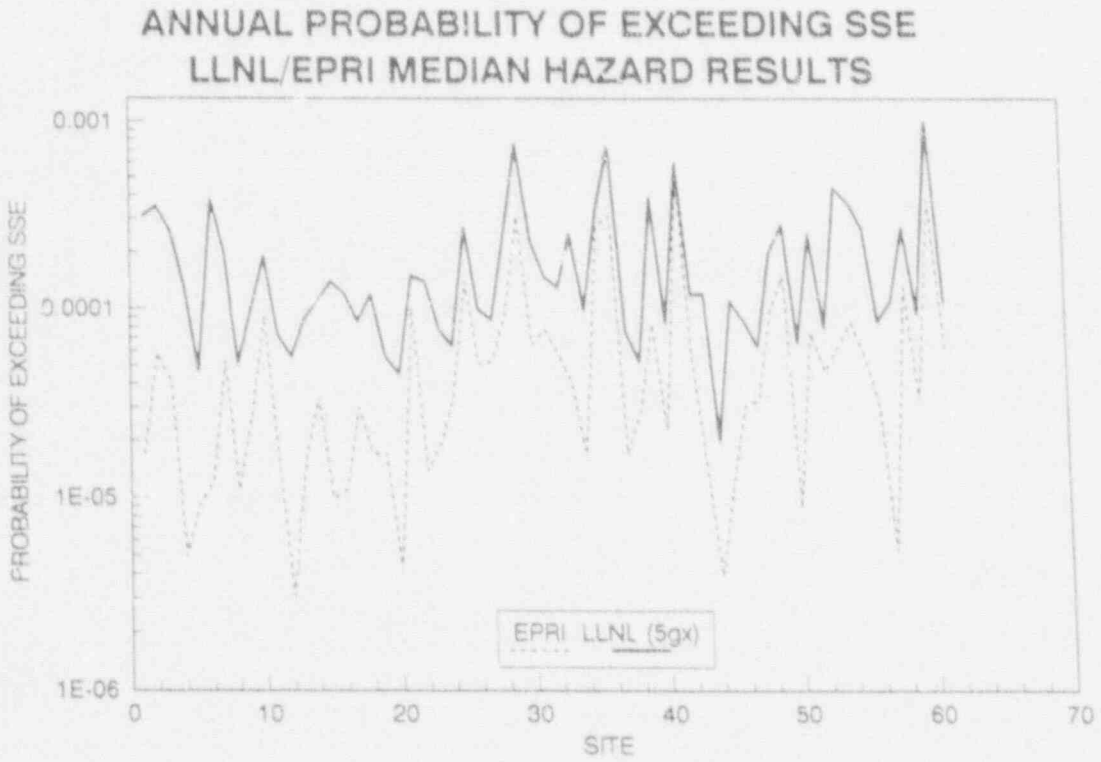

Figure 2. Annual probability of exceeding seismic design levels (SSE) based on median hazard results from EPRI (1989) and LLNL (1989).

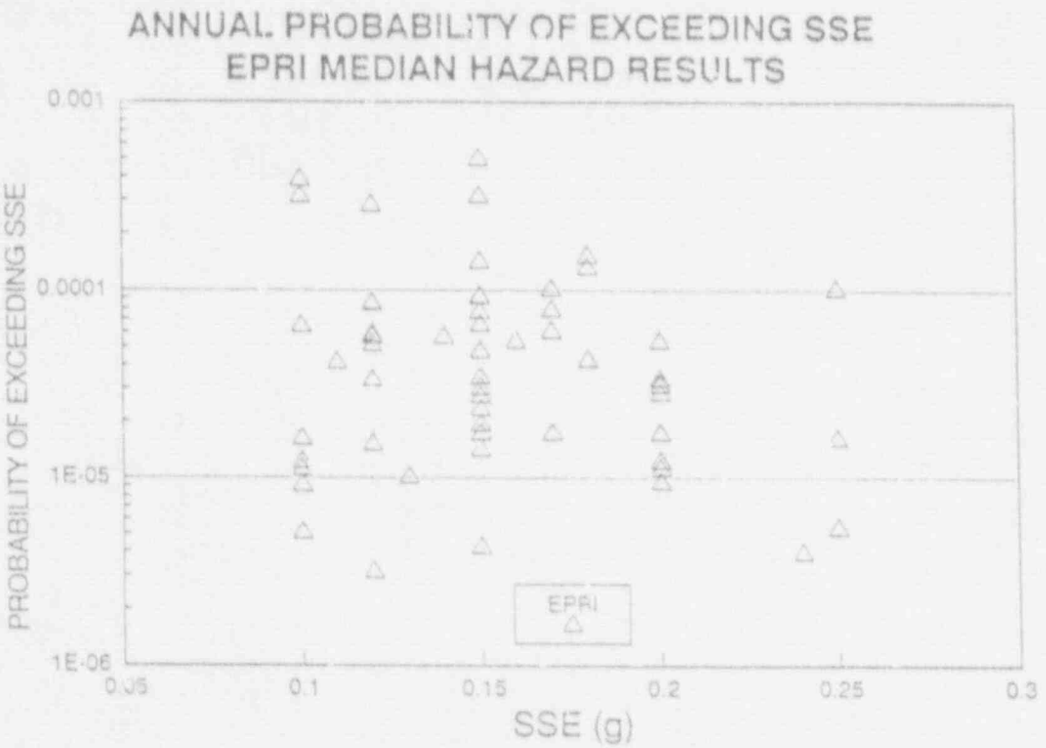

Figure 3. Annual probability of exceeding SSE by seismic design level.

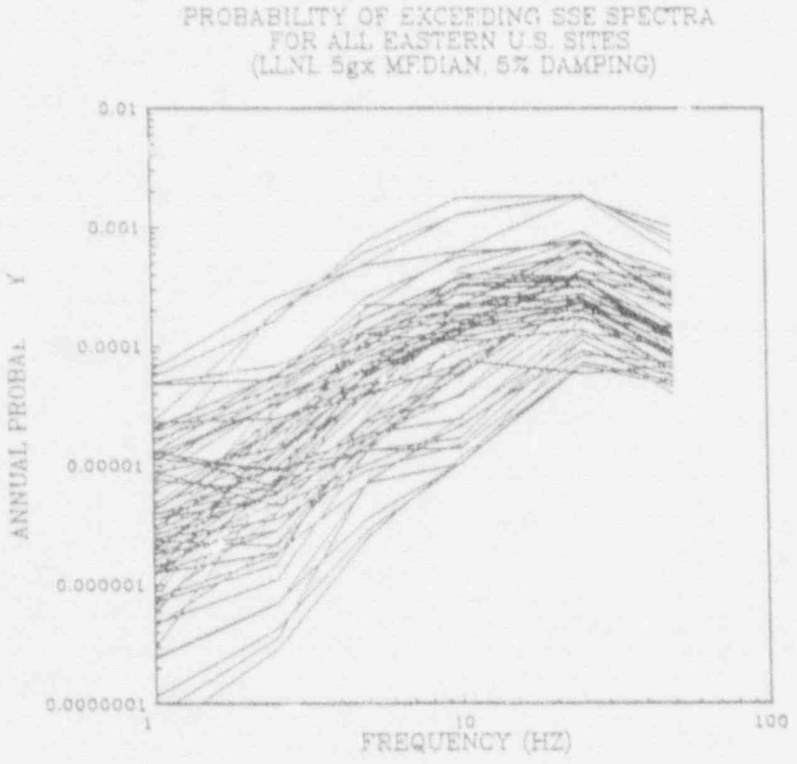

Figure 4. Probbability of exceeding SSE for all EUS sites based on LLNL (1989).

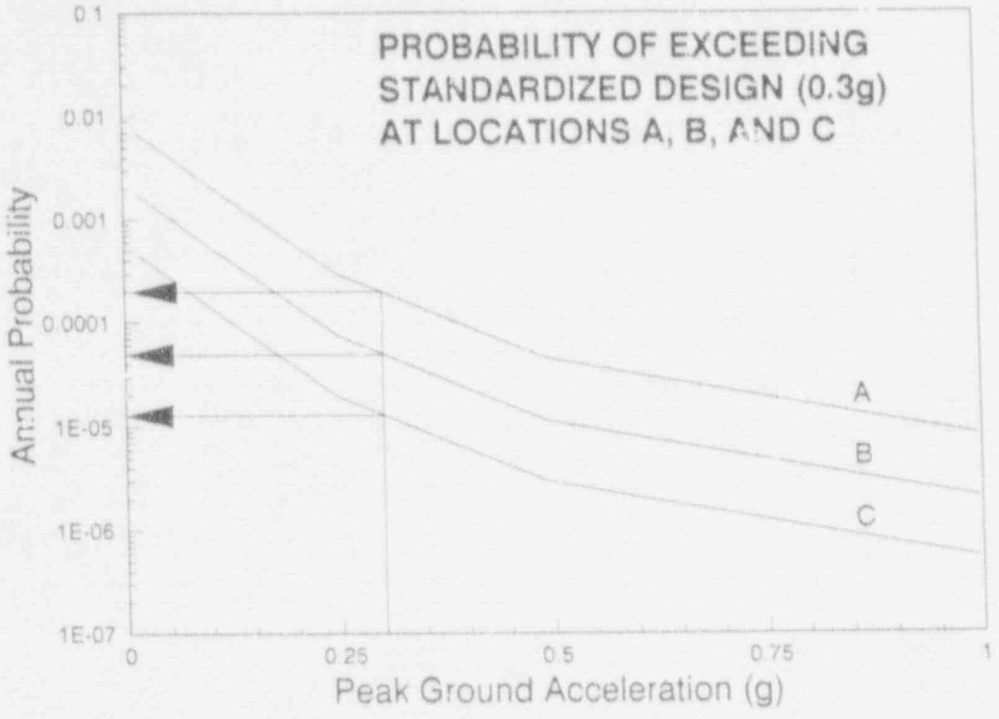

Figure 5. Probability of exceeding standardized design (0.3g) for hypothetical locations A, B and C. Choice of PGA is made to determine DBE.

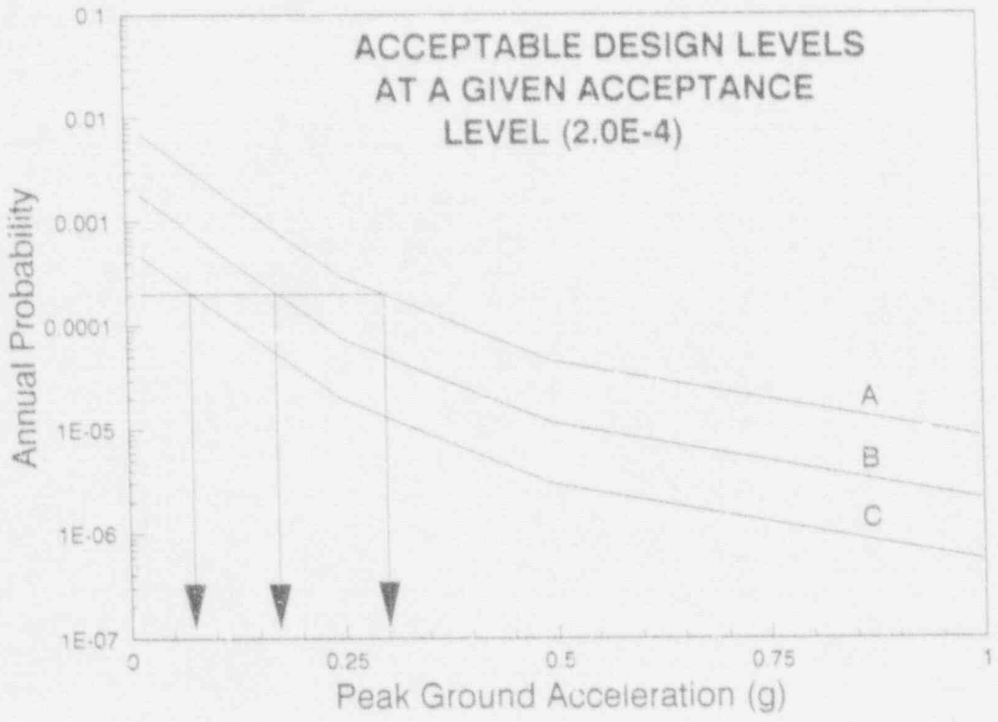

Figure 6. Acceptable design levels for a given acceptance level (2.0e-4). Choice of annual probability of exceedance is made to determine DBE.

COMPARISON OF MEAN HAZARD CURVES FOR TYPICAL NEW ENGLAND SITE

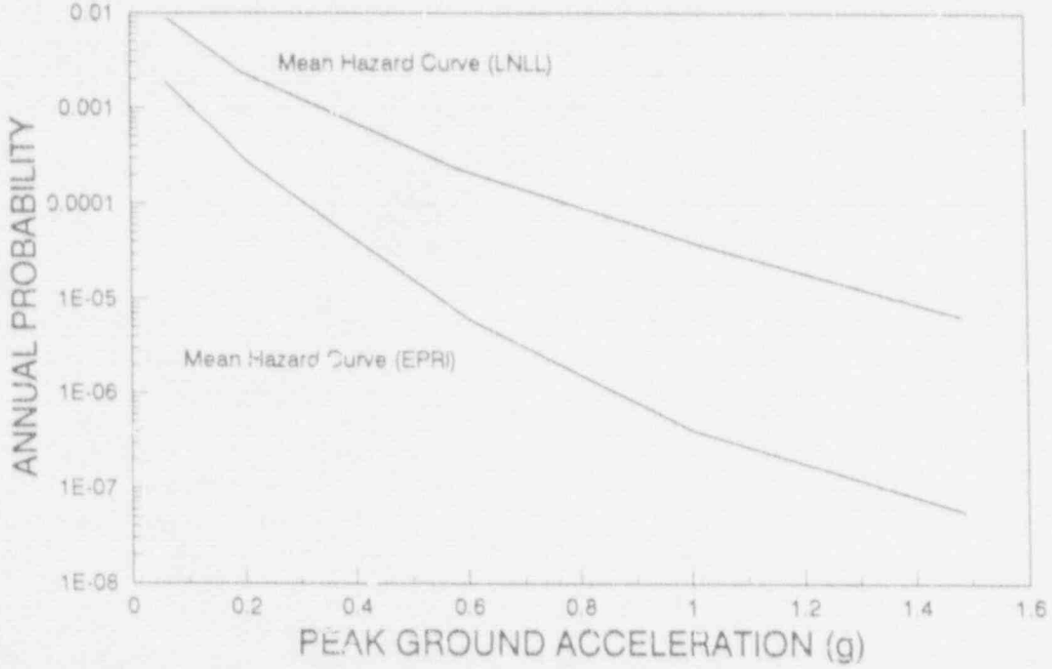

Figure 7. Mean hazard curves for data from EPRI (1989) and LLNL (1989) for an EUS site. Mean values are used for any "Safety Goals" approach.

PROCEDURE FOR GENERATION OF SEISMIC HAZARD HYPOTHESES AND THEIR PROBABILITIES

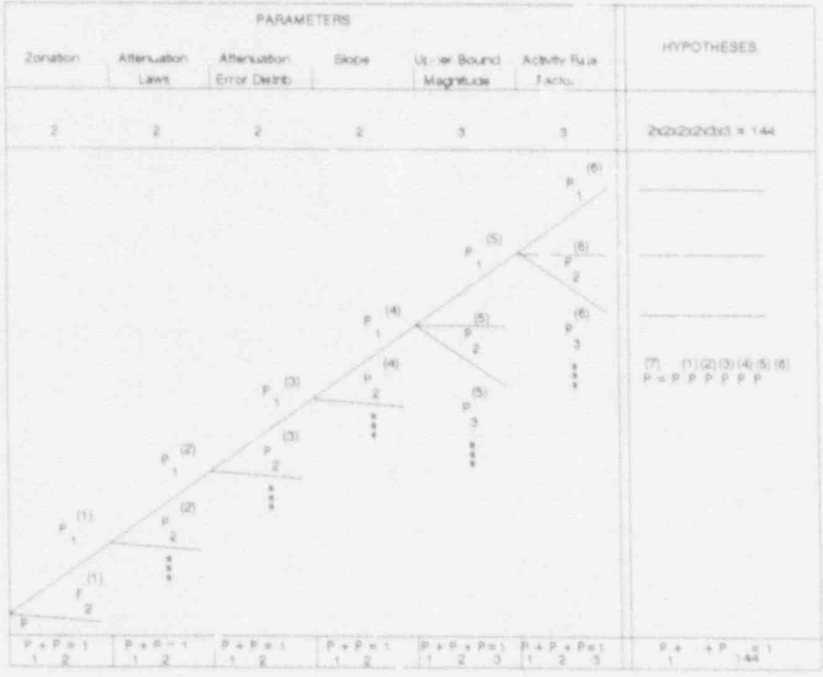

Figure 8. Illustration of procedures used to generate hypotheses and their probabilities for methodologies such as LLNL (1989) and EPRI (1989).

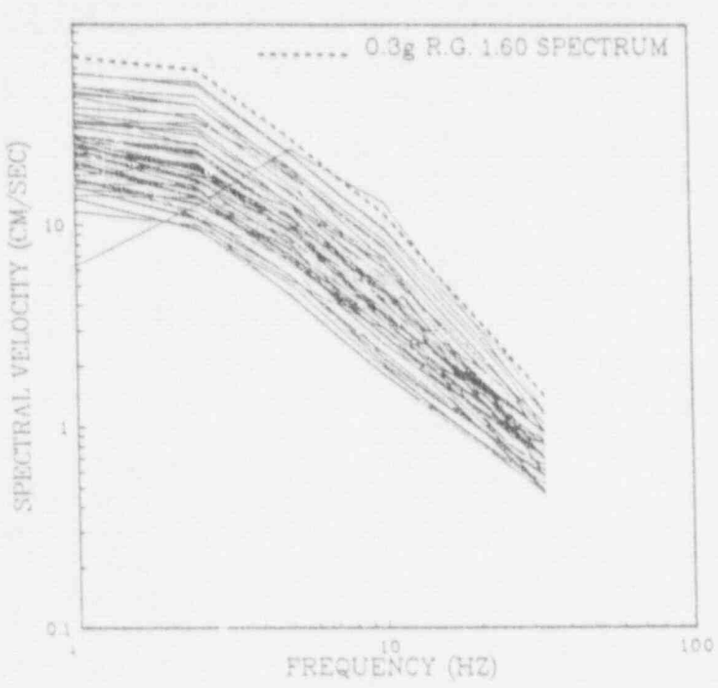

Figure 9. SSE design spectra for all EUS NPP's, and 0.3g R.G. 1.60 spectrum

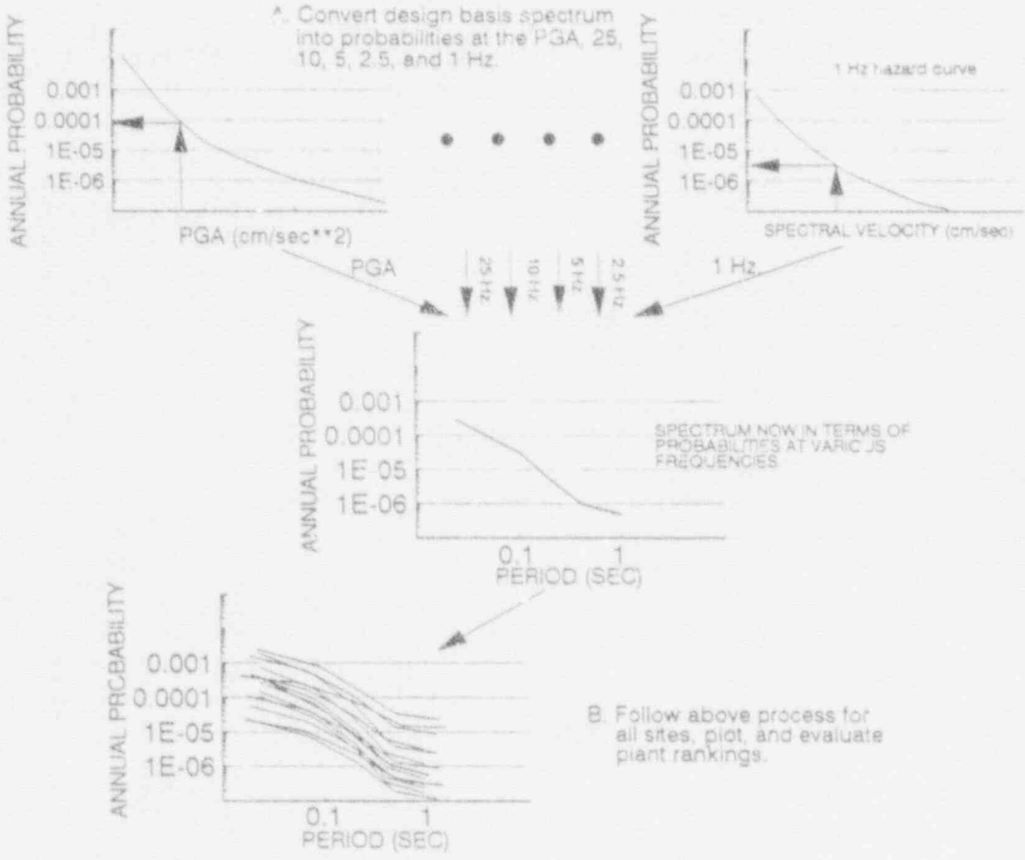

Figure 10. Procedure to illustrate relative comparisons among plants using design basis spectra and seismic hazard curves.

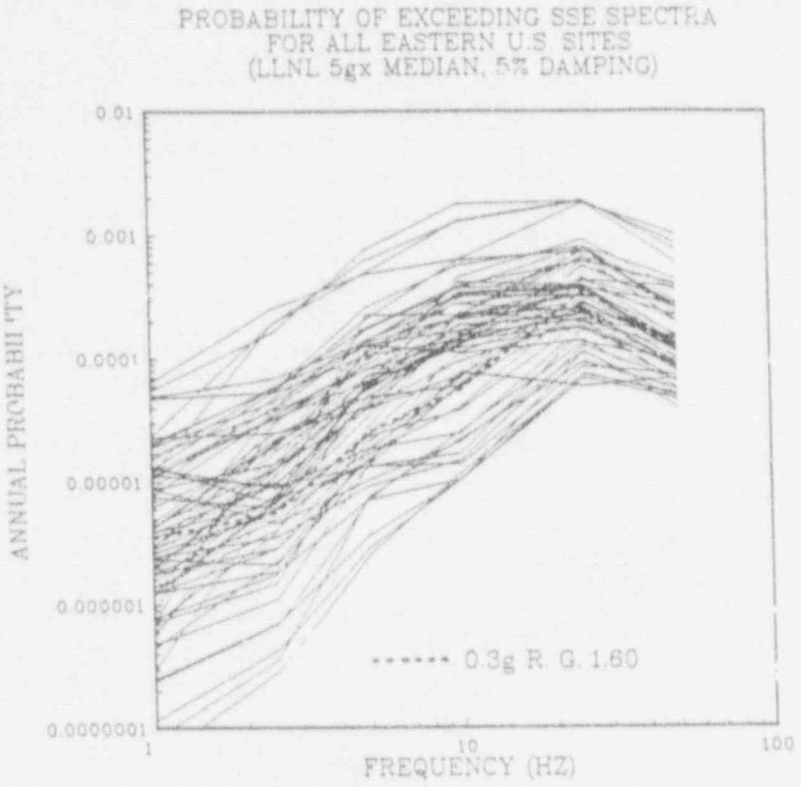

Figure 11. Probability of exceeding SSE spectra for all EUS NPP sites based on LLNL (1989) results, and the probability of exceeding spectrum from R.G. 1.60.

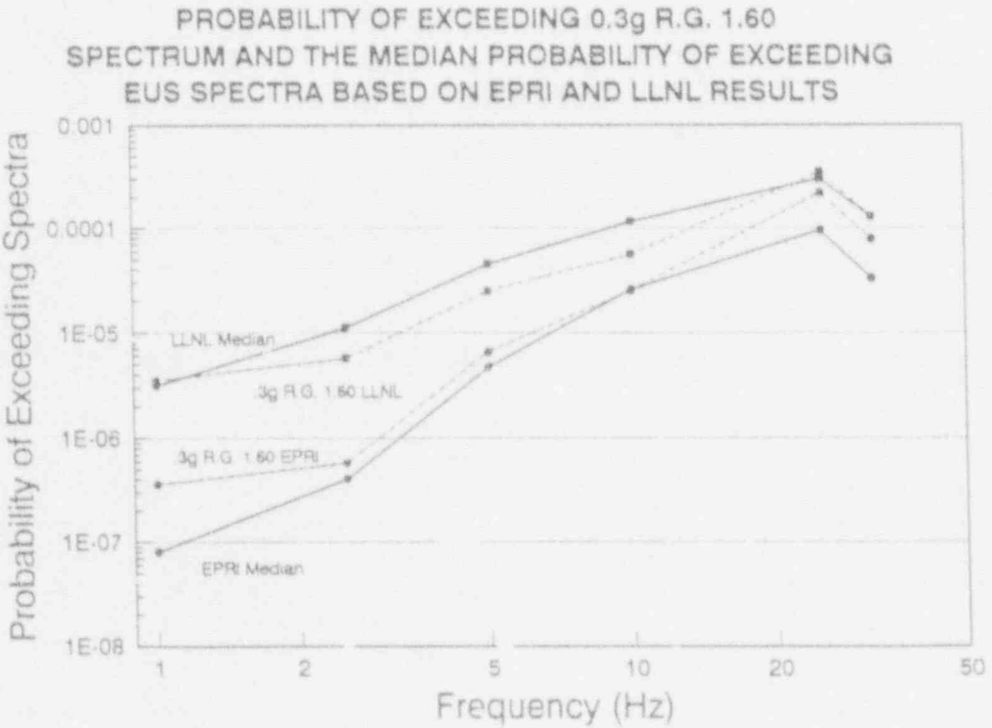

Figure 12. Probability of exceeding SSE spectra for all EUS NPP sites based on LLNL (1989) results, and the probability of exceeding spectrum from R.G. 1.60.

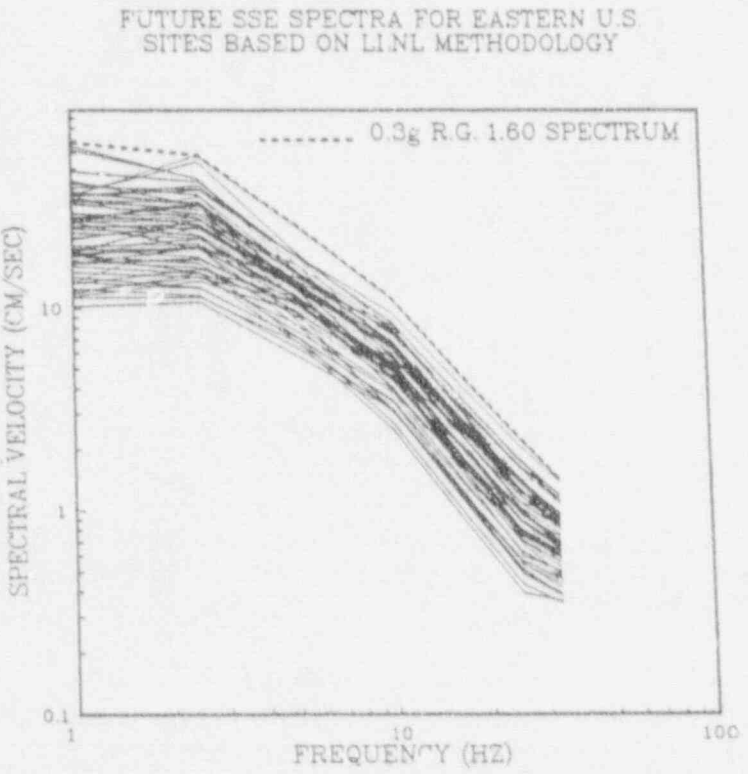

Figure 13. SSE spectra for future EUS NPP sites based on LLNL (1989).

NRC FORM 335 (2-89) NRCM 1102, 3201, 3202

U.S. NUCLEAR REGULATORY COMMISSION

BIBLIOGRAPHIC DATA SHEET

(See instructions on the reverse)

1. REPORT NUMBER (Assigned by NRC, Add Vol., Supp., Rev., and Addendum Numbers, if any.)

NUREG/CP-0119
Vol. 3

2. TITLE AND SUBTITLE

Proceedings of the Nineteenth Water Reactor Safety Information Meeting

3. DATE REPORT PUBLISHED

MONTH: April | YEAR: 1992

4. FIN OR GRANT NUMBER

A-3988

5. AUTHOR(S)

Compiled by Allen J. Weiss, BNL

6. TYPE OF REPORT

Proceedings of conference on safety research

7. PERIOD COVERED (Inclusive Dates)

October 28-30, 1991

8. PERFORMING ORGANIZATION – NAME AND ADDRESS (If NRC, provide Division, Office or Region, U.S. Nuclear Regulatory Commission, and mailing address; if contractor, provide name and mailing address.)

Office of Nuclear Regulatory Research
U.S. Nuclear Regulatory Commission
Washington, D.C. 20555

9. SPONSORING ORGANIZATION – NAME AND ADDRESS (If NRC, type "Same as above"; if contractor, provide NRC Division, Office or Region, U.S. Nuclear Regulatory Commission, and mailing address.)

Same as Item 8 above

10. SUPPLEMENTARY NOTES

Proceedings prepared by Brookhaven National Laboratory

11. ABSTRACT (200 words or less)

This three-volume report contains 83 papers out of the 108 that were presented at the Nineteenth Water Reactor Safety Information Meeting held at the Bethesda Marriott Hotel, Bethesda, Maryland, during the week of October 28-30, 1991. The papers are printed in the order of their presentation in each session and describe progress and results of programs in nuclear safety research conducted in this country and abroad. Foreign participation in the meeting included 14 different papers presented by researchers from Canada, Germany, France, Japan, Sweden, Taiwan, and USSR. The titles of the papers and names of the authors have been updated and may differ from those that appeared in the final program of the meeting.

12. KEY WORDS/DESCRIPTORS (List words or phrases that will assist researchers in locating the report.)

reactor safety - meetings, research programs - reviews, reactor accidents, reactor components, nuclear power plants - reliability, nuclear power plants - risk assessment, probabilistic estimation, loss of coolant, reactor accidents - management, human factors, systems analysis, leading abstract - proceedings, seismic effects, hydraulics - heat transfer, environmental engineering.

13. AVAILABILITY STATEMENT

Unlimited

14. SECURITY CLASSIFICATION

(This Page) Unclassified

(This Report) Unclassified

15. NUMBER OF PAGES

16. PRICE

NRC FORM 335 (2-89)

UNITED STATES
NUCLEAR REGULATORY COMMISSION
WASHINGTON, D.C. 20555

OFFICIAL BUSINESS
PENALTY FOR PRIVATE USE, $300

SPECIAL FOURTH-CLASS RATE
POSTAGE AND FEES PAID
USNRC
PERMIT NO. G-67

120556139531 1 1AN1R11R2IP31
US NRC-OADM
DIV FOIA & PUBLICATIONS SVCS
TPS-PDR-NUREG
P-211
WASHINGTON DC 20555